Talanta

The International Journal of Pure and Applied Analytical Chemistry

Publication information: *Talanta* (ISSN 0039-9140). For 2007, volumes 71–73 are scheduled for publication. Subscription prices are available upon request from the Publisher or from the Regional Sales Office nearest you or from this journal's website (http://www.elsevier.com/locate/talanta). Further information is available on this journal and other Elsevier products through Elsevier's website: (http://www.elsevier.com). Subscriptions are accepted on a prepaid basis only and are entered on a calendar year basis. Issues are sent by standard mail (surface within Europe, air delivery outside Europe). Priority rates are available upon request. Claims for missing issues should be made within six months of the date of dispatch.

Orders, claims, and journal enquiries: please contact the Customer Service Department at the Regional Sales Office nearest you:
Orlando: Elsevier, Customer Service Department, 6277 Sea Harbor Drive, Orlando, FL 32887-4800, USA; phone: (+1) (877) 8397126 [toll free number for US customers], or (+1) (407) 3454020 [customers outside US]; fax: (+1) (407) 3631354; e-mail: usjcs@elsevier.com
Amsterdam: Elsevier, Customer Service Department, PO Box 211, 1000 AE Amsterdam, The Netherlands; phone: (+31) (20) 4853757; fax: (+31) (20) 4853432; e-mail: nlinfo-f@elsevier.com
Tokyo: Elsevier, Customer Service Department, 4F Higashi-Azabu, 1-Chome Bldg, 1-9-15 Higashi-Azabu, Minato-ku, Tokyo 106-0044, Japan; phone: (+81) (3) 5561 5037; fax: (+81) (3) 5561 5047; e-mail: jp.info@elsevier.com
Singapore: Elsevier, Customer Service Department, 3 Killiney Road, #08-01 Winsland House I, Singapore 239519; phone: (+65) 63490222; fax: (+65) 67331510; e-mail: asiainfo@elsevier.com

USA mailing notice: *Talanta* (ISSN 0039-9140) is published monthly by Elsevier B.V. (P.O. Box 211, 1000 AE Amsterdam, The Netherlands). Annual subscription price in the USA US$ 3,818 (valid in North, Central and South America), including air speed delivery. Application to mail at periodical postage rate is paid at Rathway, NJ and additional mailing offices.
USA POSTMASTER: Send address changes to *Talanta*, Publications Expediting Inc., 200 Meacham Avenue, Elmont, NY 11003.
AIRFREIGHT AND MAILING in the USA by Publications Expediting Inc., 200 Meacham Avenue, Elmont, NY 11003.

Available online at www.sciencedirect.com
ScienceDirect
Talanta 73 (2007) 134–141
Talanta
www.elsevier.com/locate/talanta

A novel multi-element coprecipitation technique for separation and enrichment of metal ions in environmental samples☆

Funda Armagan Aydin [a,b], Mustafa Soylak [a,*]

[a] *Erciyes University, Faculty of Art and Science, Department of Chemistry, 38039 Kayseri, Turkey*
[b] *General Directorate of State Hydraulic Works, Technical Research and Quality Control Department, 06100 Ankara, Turkey*

Received 21 December 2006; received in revised form 18 February 2007; accepted 7 March 2007
Available online 14 March 2007

Abstract

A multi-element preconcentration–separation technique for heavy metal ions in environmental samples has been established. The procedure is based on coprecipitation of gold(III), bismuth(III), cobalt(II), chromium(III), iron(III), manganese(II), nickel(II), lead(II), thorium(IV) and uranium(VI) ions by the aid of Cu(II)–9-phenyl-3-fluorone precipitate. The Cu(II)–9-phenyl-3-fluorone precipitate was dissolved by the addition 1.0 mL of concentrated HNO_3 and then the solution was completed to 5 mL with distilled water. Iron, lead, cobalt, chromium, manganese and nickel levels in the final solution were determined by flame atomic absorption spectrometer, while gold, bismuth, uranium and thorium were determined by inductively coupled plasma mass spectrometer. The optimal conditions are pH 7, amounts of 9-phenyl-3-fluorone: 5 mg and amounts of Cu(II): 1 mg. The effects of concomitant ions as matrix were also examined. The preconcentration factor was 30. Gold(III), bismuth(III), chromium(III), iron(III), lead(II) and thorium(IV) were quantitatively recovered from the real samples. The detection limits for the analyte elements based on 3 sigma ($n = 15$) were in the range of 0.05–12.9 $\mu g\,L^{-1}$. The validation of the presented procedure was checked by the analysis of two certified reference materials (Montana I Soil (NIST-SRM 2710) and Lake Sediment (IAEA-SL-1)). The procedure was successfully applied to some environmental samples including water and sediments.

Keywords: Preconcentration; Separation; Heavy metals; Coprecipitation; 9-Phenyl-3-fluorone; Environmental samples

1. Introduction

Preconcentration–separation is a necessity for metal ions at trace levels prior to their instrumental detection due to lower analyte levels than the limit of quantitation of the instrument and interferic effects of high salt contents of the analyzed samples [1–3]. Until now, ion-exchange, liquid–liquid extraction, cloud point extraction, electrolytic deposition, electrophoretic separation, evaporation, flotation, sorption and adsorption on solid phases and membrane filtration have been reported as preconcentration and separation methods of trace metals in various samples [4–12]. While they have some advantages from each other, generally most of them are complicated and time-consuming and usage of the organic solvents is at high ratio [10–14].

Coprecipitation is a separation–preconcentration technique based on phase separation. Analyte ions could be precipitated in the procedure with the combination of a carrier element and a suitable chelating agent [15,16]. Some advantages of coprecipitation, as enrichment technique, is that pure inorganic reagents can be easily obtained and also the procedure is easily handled. In this work, generally a milligram quantity of carrier element was used [17–19]. As a carrier element, metals like copper and zinc are popular, because of their often low interferences in determination methods and their limited negative effects for environment.

For the coprecipitation of heavy metal ions at trace levels, organic coprecipitants are most popular due to good trace recovery and sufficient separation factors for alkali and alkaline earth metals. Organic coprecipitants like ditihiocarbamate, diethyldithiophosphate, dimethylaminobenzilidene-rhodanine, etc. are

☆ This study is a part of Ph.D. thesis of Funda Armagan Aydin.
* Corresponding author. Tel.: +90 352 4374933; fax: +90 352 4374933.
E-mail addresses: msoylak@gmail.com, soylak@erciyes.edu.tr (M. Soylak).

0039-9140/$ – see front matter © 2007 Elsevier B.V. All rights reserved.
doi:10.1016/j.talanta.2007.03.007

used by various researchers for the preconcentration and separation of traces of heavy metal ions in environmental samples, including natural waters [20–28].

Phenylfluorones are widely used organic chelating agent that has a larger formation constant with metal ions [29,30]. They are used in chemical enrichment–separation and spectrophotometric determination of some metal ions by various preconcentration techniques prior to their determination [31–34]. Uranium(VI) and thorium(IV) as 9-phenyl-3-fluorone chelates were preconcentrated on Duolite XAD761 prior to their inductively coupled plasma mass spectrometric determinations by our working group [34]. A solid phase extraction procedure was established. According to our literature review, until now Cu(II)–9-phenyl-3-fluorone combination has not been used for the coprecipitation of traces of heavy metal in environmental samples.

In the present work, a multi-element coprecipitation has been presented for some metal ions in environmental samples. In the determination step, flame atomic absorption spectrometer for iron, lead, cobalt, chromium, manganese and nickel levels and inductively coupled plasma mass spectrometer for gold, bismuth, uranium and thorium have been used.

2. Experimental

2.1. Apparatus

An Agilent model 7500a inductively coupled plasma mass spectrometer (Agilent Technologies, Palo Alto, CA, USA) and UNICAM 989 model flame atomic absorption spectrometer (Unicam 989, Thermo Elemental Corp., Franklin, MA, USA) were used for the determination of analytes. The instruments were optimized daily before measurement and operated as recommended by the manufacturers which is given in Table 1.

The pH values were measured using WTW inoLab Level 3 with terminal Level 3 (Weilheim, Germany). Rotina 38 Hettich model centrifuge (Buckinghamshire, UK) was used to centrifuge the solutions. The water that used all the experiments was purified in Millipore Synergy 185 (Billerica, MA, USA).

2.2. Reagents and solutions

High purity reagents from Sigma (St. Louis, MO, USA) and Merck (Darmstadt, Germany) were used for all preparations of the standard and sample solution. Stock solutions of analyte ions, 1000 mg L^{-1}, was diluted daily for obtaining reference and working solutions. The mono-elemental standard solutions (St. Louis) used for the calibration procedures were prepared before use by dilution of the stock solution with 1 mol L^{-1} HNO_3. Stock solutions of diverse elements were prepared from the high purity compounds (99.9%) (St. Louis).

A 0.5% (m/v) solution of 9-phenyl-3-fluorone (St. Louis) was prepared by dissolving of 0.5 g of 9-phenyl-3-fluorone in 1 mL of 0.1 mol L^{-1} NaOH and diluting to 100 mL with water.

The following buffer solutions were prepared for pH adjustment: (a) 3.79 g sodium dihydrogen phosphate and 9 mL of 85% phosphoric acid for pH 2; (b) 13.78 g sodium dihydrogen phosphate and 0.60 mL of 85% phosphoric acid for pH 3; (c) 77.0 g ammonium acetate and 413 mL acetic acid for pH 4; (d) 13.1 g sodium dihydrogen phosphate and 2.40 g disodium hydrogen for pH 5; (e) 58.5 g ammonium acetate and 2.5 mL acetic acid for pH 6; (f) 0.69 g sodium borate and 5 mL of 1 mol L^{-1} hydrochloric acid pH 7; (g) 53.5 g ammonium chloride and 4.0 mL ammonia for pH 8; (h) 500 mL of 0.1 mol L^{-1} of ammonium chloride and 250 mL of 0.1 mol L^{-1} of ammonia for pH 9; (i) 37.0 g ammonium chloride, 285 mL ammonia for pH 10 were taken

Table 1
Operating conditions for ICP-MS and FAAS

Agilent 7500a ICP-MS					
Nebulizer			Babington		
Spray chamber			Quartz, double pass		
RF power			1260 W		
Frequency			27.12 MHz		
Sampling depth			7.0 mm		
Plasma gas flow rate			15 L min^{-1}		
Auxiliary gas flow rate			1.0 L min^{-1}		
Carrier gas flow rate			1.15 L min^{-1}		
Sample uptake rate			0.3 mL min^{-1}		
Detector mode			Auto		
Integration time			0.10 s		
Analytical masses			^{238}U, ^{232}Th, ^{197}Au, ^{209}Bi		
Metal	Wavelength (nm)	Slit width (nm)	Lamp current (mA)	Flame type	Fuel flow rate (L s^{-1})
Unicam 989 FAAS					
Fe	248.3	0.2	15	Air/acetylene	1.0
Ni	232.0	0.2	15	Air/acetylene	1.0
Co	240.7	0.2	15	Air/acetylene	1.0
Mn	279.5	0.2	12	Air/acetylene	1.0
Cr	357.9	0.5	12	Nitrous oxide/acetylene	3.8
Pb	217.0	0.5	10	Air/acetylene	1.0

and the final volume was completed to 500 mL with distilled water.

2.3. Model working

The copper(II)–9-phenyl-3-fluorone coprecipitation procedure was tested with model solutions prior to its application to real samples. An aqueous solution containing 5 μg of Fe(III), Co(II), Mn(II), Ni(II); 10 μg of Pb(II), Cr(III); 0.5 μg of Au(III), Bi(III); 0.2 μg of U(VI), Th(IV) was placed in a centrifuge tube. One millilitre of 1000 mg L^{-1} of copper(II) as a carrier element was added. Then 1.0 mL of 0.5% (m/v) 9-phenyl-3-fluorone was added. The pH was adjusted to 7 by the addition of 2.0 mL of sodium borate buffer. After 10 min, the solution was centrifuged at 3500 rpm for 20 min. The precipitate adhering to the tube was dissolved with 1000 μL of concentrated HNO_3. Then the final volume was completed to 5.0 mL with distilled water. Fe, Pb, Co, Cr, Mn and Ni levels in the final solution were determined by flame atomic absorption spectrometer while Au, Bi, U and Th were determined by inductively coupled plasma mass spectrometer.

2.4. Analysis of real samples

The application of the presented procedure was performed with two certified reference materials (NIST-SRM 2710 Montana I Soil and IAEA-SL-1 Lake Sediment) and two sediment samples from Van Lake, Turkey. 0.1 g of certified reference material or 0.1 g of lake sediment was digested with 15 mL of aqua regia at room temperature and then, it was heated to 95 °C. When the evolution of NO_2 fumes had ceased, the mixture was evaporated almost to dryness on a sand-bath and mixed with 8 mL of aqua regia. Then the mixture was again evaporated to dryness. After evaporation, 8–9 mL of distilled water was added and the sample was mixed. The resulting mixture was filtered through a blue band filter paper. The filtrate was diluted to 25 mL with distilled water. The pH of this solution was adjusted to 7 by the addition of buffer solution. Then the coprecipitation procedure given above was applied.

The procedure was applied to two drinking water samples from Cubuk and Karagol villages, Ankara, Turkey and a lake water sample from Mogan Lake from Ankara, Turkey. The water samples analyzed were filtered through a cellulose membrane filter (Millipore) of 0.45 μm pore size. One hundred and fifty millilitres of water sample was transferred to a beaker. The pH of the sample was adjusted to 7 by the addition of buffer solution. Then the coprecipitation procedure given above was applied to this water sample.

3. Results and discussion

3.1. Influences of pH

The influences of pH of the solutions on the quantitative precipitation of gold(III), bismuth(III), cobalt(II), chromium(III), iron(III), manganese(II), nickel(II), lead(II), thorium(IV) and uranium(VI) on the copper(II)–9-phenyl-3-fluorone system were investigated in the pH range of 2–10. The studies were performed by using model solutions that include 1.0 mL of 1000 mol L^{-1} of copper(II) and 1.0 mL of 0.5% (m/v) 9-phenyl-3-fluorone. The pH adjustments were done by using buffer solution. Cu/9-phenyl-3-fluorone ratio was 1:2 [35]. Violet colored Cu(II)–9-phenyl-3-fluorone precipitate was formed at the pH range of 6–9. The precipitate was easy to handle without any problem. The results for influences of pH are depicted in Fig. 1.

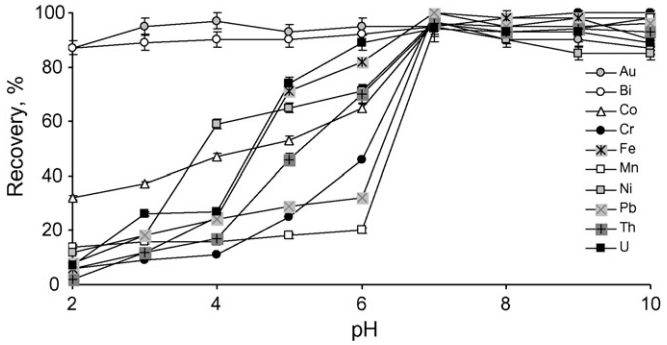

Fig. 1. The influences of pH on the recoveries of analytes on copper(II)–9-phenyl-3-fluorone system (amount of carrier element: 1 mg copper(II), amount of ligand: 5 mg 9-phenyl-3-fluorone, $N = 3$).

Nickel ion was quantitatively recovered at pH 7. Quantitative recoveries of iron(III), manganese(II), chromium(III), lead(II) and thorium(IV) were obtained at the pH range of 7–10. Cobalt(II), gold(III), bismuth(III) and uranium(VI) were quantitatively recovered in the pH range of 7–10, 3–7, 6–9 and 7–9, respectively. The recoveries in the pH range of 7–10 are generally quantitative. At pH higher than 7, the quantitative recoveries of some analytes may be sourced precipitate of their hydroxides. All further works were performed at pH 7 by adjusting with borate buffer.

3.2. Amount of 9-phenyl-3-fluorone

The influences of amount of 9-phenyl-3-fluorone on the quantitative coprecipitation of analyte ions were also investigated in the range of 0.0–10.0 mg of 9-phenyl-3-fluorone. The results are depicted in Fig. 2. Fe(III), U(VI) and Th(IV) were quantitatively recovered (>95%) at pH 7 without 9-phenyl-3-fluorone.

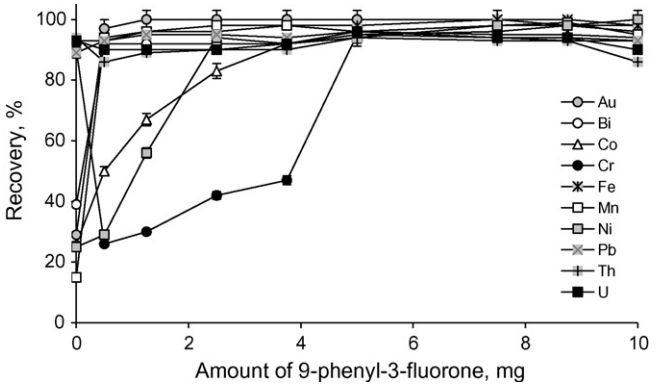

Fig. 2. The influences of the amounts of 9-phenyl-3-fluorone on the recoveries of analytes (pH 7, amount of ligand: 5 mg 9-phenyl-3-fluorone, $N = 3$).

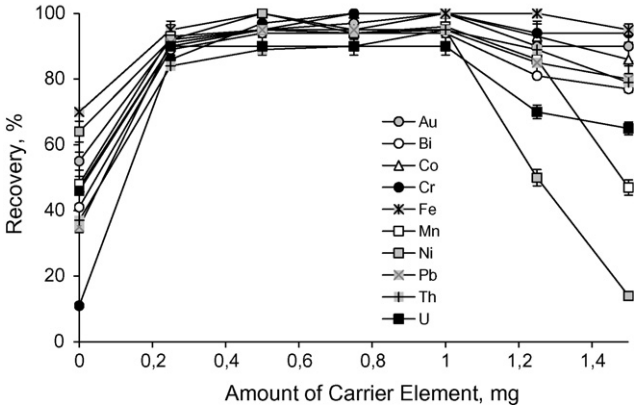

Fig. 3. The influences of amount of Cu^{2+} on the recoveries of analyte ions (pH 7, amount of ligand: 5 mg 9-phenyl-3-fluorone, $N = 3$).

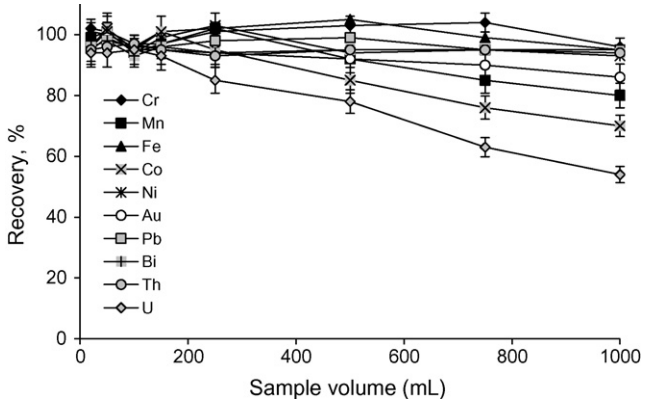

Fig. 4. The effects of sample volume on the recoveries of analytes (pH 7, amount of carrier element: 1 mg copper(II), amount of ligand: 5 mg 9-phenyl-3-fluorone, $N = 3$).

These recoveries for Fe(III), U(VI) and Th(IV) may be related to formation of the hydroxide precipitate of copper(II). The recoveries of other analytes were not quantitative without 9-phenyl-3-fluorone. Quantitative recovery values for Fe(II), Mn(II), Pb(II) and Au(III) were obtained in the range of 0.5–10.0 mg of 9-phenyl-3-fluorone. Cr(III) was quantitatively recovered 5.0–10.0 mg of ligand range. U(VI) and Th(IV) were recovered quantitatively in the range of 5.0–8.75 mg, while Ni, Co and Bi were recovered in the range of 5.0–10.0 mg of 9-phenyl-3-fluorone. These results show that 9-phenyl-3-fluorone is necessary for the quantitative recoveries of all of the 10 analytes at the optimal working conditions given in Section

Table 2
Influences of the matrix ions on the recoveries of analytes ($N = 3$)

	Added as	Concentration ($mg\,L^{-1}$)	Recovery (%)									
			Au	Bi	Co	Cr	Fe	Mn	Ni	Pb	Th	U
Na^+	NaCl	5000	94 ± 2[a]	94 ± 4	72 ± 2	104 ± 4	102 ± 3	77 ± 4	76 ± 4	99 ± 1	95 ± 3	85 ± 3
		10,000	88 ± 3	87 ± 3	69 ± 5	101 ± 1	104 ± 4	59 ± 4	57 ± 3	101 ± 2	95 ± 2	76 ± 2
		30,000	82 ± 5	69 ± 3	58 ± 3	101 ± 4	103 ± 5	54 ± 5	48 ± 5	99 ± 4	91 ± 4	65 ± 4
K^+	KCl	250	95 ± 2	95 ± 3	100 ± 2	98 ± 1	98 ± 1	95 ± 1	94 ± 3	100 ± 1	95 ± 4	85 ± 4
		500	97 ± 3	92 ± 1	98 ± 4	100 ± 2	100 ± 3	93 ± 2	93 ± 1	102 ± 3	95 ± 1	85 ± 2
Ca^{2+}	$CaCl_2$	500	95 ± 1	92 ± 3	70 ± 3	100 ± 1	98 ± 1	40 ± 3	21 ± 4	99 ± 1	95 ± 2	80 ± 3
		1000	95 ± 2	90 ± 1	60 ± 3	102 ± 3	101 ± 2	38 ± 2	13 ± 2	99 ± 1	96 ± 3	75 ± 2
Mg^{2+}	$MgCl_2$	500	96 ± 3	94 ± 2	75 ± 5	101 ± 2	100 ± 1	49 ± 2	40 ± 2	99 ± 1	95 ± 2	72 ± 4
		1000	80 ± 4	94 ± 2	65 ± 3	99 ± 1	100 ± 2	46 ± 4	21 ± 2	101 ± 1	100 ± 1	20 ± 2
SO_4^{2-}	Na_2SO_4	500	98 ± 1	95 ± 1	93 ± 1	102 ± 2	100 ± 2	90 ± 1	85 ± 1	98 ± 1	100 ± 2	90 ± 1
		1000	99 ± 2	98 ± 2	95 ± 1	100 ± 1	102 ± 4	70 ± 2	83 ± 5	101 ± 3	101 ± 4	85 ± 2
Al^{3+}	$Al_2(SO_4)_3{\cdot}18H_2O$	5	102 ± 1	104 ± 3	95 ± 1	100 ± 2	101 ± 1	90 ± 1	93 ± 2	100 ± 1	103 ± 3	96 ± 3
		10	95 ± 2	98 ± 1	80 ± 2	98 ± 1	100 ± 2	75 ± 1	90 ± 2	98 ± 1	100 ± 1	95 ± 2
Cr^{3+}	$Cr(NO_3)_3{\cdot}9H_2O$	5	100 ± 1	100 ± 2	95 ± 1	–	102 ± 1	92 ± 1	100 ± 3	101 ± 1	104 ± 1	94 ± 2
		10	98 ± 1	100 ± 1	90 ± 3	–	102 ± 3	80 ± 1	95 ± 1	98 ± 1	98 ± 2	92 ± 1
		20	95 ± 3	98 ± 2	81 ± 2	–	96 ± 1	66 ± 2	94 ± 1	94 ± 1	99 ± 1	89 ± 1
Fe^{3+}	$Fe(NO_3)_3{\cdot}9H_2O$	5	100 ± 1	100 ± 1	95 ± 1	100 ± 1	–	90 ± 1	96 ± 1	100 ± 1	101 ± 1	96 ± 1
		10	95 ± 3	102 ± 2	93 ± 1	99 ± 1	–	65 ± 3	95 ± 2	99 ± 2	100 ± 1	94 ± 2
Zn^{2+}	ZnI_2	5	98 ± 2	96 ± 2	80 ± 2	98 ± 1	104 ± 1	65 ± 1	93 ± 2	101 ± 2	98 ± 1	94 ± 2
		10	94 ± 1	99 ± 3	70 ± 1	100 ± 1	100 ± 1	50 ± 4	90 ± 1	100 ± 2	94 ± 1	96 ± 2
Ni^{2+}	$NiCl_2{\cdot}6H_2O$	5	101 ± 1	95 ± 1	90 ± 1	100 ± 1	98 ± 1	75 ± 1	–	104 ± 3	97 ± 2	96 ± 1
		10	99 ± 2	97 ± 3	80 ± 2	99 ± 1	98 ± 2	70 ± 2	–	101 ± 1	96 ± 1	96 ± 3
Pb^{2+}	$PbCl_2$	5	102 ± 1	95 ± 1	85 ± 2	103 ± 2	103 ± 2	75 ± 2	93 ± 1	–	95 ± 1	94 ± 1
		10	99 ± 1	96 ± 2	75 ± 3	102 ± 1	100 ± 1	70 ± 4	90 ± 1	–	96 ± 2	94 ± 2
Co^{2+}	$CoCl_2{\cdot}6H_2O$	5	100 ± 2	95 ± 1	–	101 ± 1	102 ± 2	102 ± 1	93 ± 1	102 ± 1	98 ± 1	96 ± 2
		10	98 ± 1	99 ± 2	–	98 ± 1	98 ± 1	98 ± 1	94 ± 1	100 ± 2	98 ± 3	94 ± 1

[a] Mean ± standard deviations.

Table 3
Tests of addition/recovery for two water samples (sample volume: 150 mL, final volume: 5 mL, $N = 4$)

Analyte	Added ($\mu g\,L^{-1}$)	Tap water from Ankara city center		Bottled mineral water	
		Found ($\mu g\,L^{-1}$)	Recovery (%)	Found ($\mu g\,L^{-1}$)	Recovery (%)
Au	0	<LOD	–	<LOD	–
	1.7	1.6 ± 0.1	94 ± 4	1.6 ± 0.1	94 ± 4
	3.3	3.2 ± 0.1	96 ± 3	3.2 ± 0.2	96 ± 3
	5.0	4.6 ± 0.2	92 ± 3	4.8 ± 0.2	96 ± 3
Bi	0	<LOD	–	<LOD	–
	1.7	1.6 ± 0.1	94 ± 3	1.6 ± 0.1	94 ± 4
	3.3	3.2 ± 0.1	96 ± 4	3.2 ± 0.1	96 ± 3
	5.0	4.8 ± 0.2	96 ± 4	4.7 ± 0.2	94 ± 3
Cr	0	<LOD	–	<LOD	–
	33.0	34.6 ± 0.6	104 ± 3	34.0 ± 1.3	103 ± 3
	66.0	64.0 ± 2.5	96 ± 4	64.3 ± 2.0	97 ± 4
	100.0	100.6 ± 2.0	101 ± 2	94.7 ± 1.0	96 ± 3
Fe	0	21.3 ± 2.7	–	23.7 ± 0.9	–
	33.0	55.3 ± 1.3	103 ± 4	59.3 ± 1.5	107 ± 5
	66.0	85.3 ± 2.7	97 ± 4	91.3 ± 1.0	102 ± 4
	100.0	116.7 ± 1.0	96 ± 3	118.3 ± 1.5	95 ± 3
Pb	0	6.7 ± 1.3	–	< LOD	–
	33.0	38.7 ± 2.0	97 ± 4	31.4 ± 1.5	96 ± 4
	66.0	72.0 ± 2.7	98 ± 4	64.0 ± 1.0	95 ± 3
	100.0	104.0 ± 3.3	97 ± 3	94.0 ± 2.0	94 ± 3
Th	0	<LOD	–	<LOD	–
	1.7	1.6 ± 0.1	95 ± 2	1.6 ± 0.1	94 ± 3
	3.3	3.2 ± 0.1	95 ± 2	3.1 ± 0.1	94 ± 3
	5.0	4.7 ± 0.1	94 ± 3	4.7 ± 0.2	93 ± 3

LOD: limit of detection.

2. For all further works, 5.0 mg of 9-phenyl-3-fluorone was used.

3.3. Effects of amount of Cu^{2+} as carrier element

The influences of amount of Cu^{2+} as carrier element on the recoveries of analyte ions were also investigated. The results are shown in Fig. 3. The recoveries were not quantitative without Cu^{2+}. After the addition of Cu^{2+}, the recoveries increased and reach to quantitative values for all the investigated analytes at 1.0 mg of Cu^{2+} due to the formation of Cu(II)–9-phenyl-3-fluorone precipitate. The recovery values were decreased with higher amounts of copper than 1.0 mg. This decrease on the recoveries may be source excess copper in the working media. In the light of these results, 1.0 mg of Cu^{2+} as carrier was used in all further works.

3.4. Influences of sample volume

The effects of sample volume on the quantitative coprecipitation of the analytes investigated were examined in the sample volume range of 20–1000 mL to possible application of the presented coprecipitation procedure for natural water samples. The results are depicted in Fig. 4. The recoveries of Fe, Cr, Pb, Ni, Bi and Th ions were found quantitative in the sample volume range of 20–1000 mL. Cobalt, manganese and gold ions were

Table 4
Application of the presented procedure for two certified reference materials and two sediment samples from Van Lake-Turkey ($N = 4$)

Analyte	Lake sediment (IAEA-SL-1)			Montana I Soil (NIST-SRM 2710)			Sediment from Van Lake	
	Certified value ($\mu g\,g^{-1}$)	Observed value ($\mu g\,g^{-1}$)*	Relative error (%)	Certified value ($\mu g\,g^{-1}$)	Observed value ($\mu g\,g^{-1}$)	Relative error (%)	74 m depth ($\mu g\,g^{-1}$)	115 m depth ($\mu g\,g^{-1}$)
Au	&	<LOD	–	0.6	0.6 ± 0.1	0	<LOD	<LOD
Bi	&	<LOD	–	&	<LOD	–	<LOD	<LOD
Cr	104	112 ± 11	+7.7	39	38 ± 4	−2.6	6 ± 1	8 ± 1
Fe	67,400	66,900 ± 1900	−0.7	33,800	33,682 ± 1066	−0.3	736 ± 59	1100 ± 248
Pb	37.7	39 ± 8	+3.5	5532	5576 ± 557	+0.8	6 ± 1	7 ± 1
Th	14	13 ± 1	−7.1	13	13 ± 3	0	0.2 ± 0.01	0.2 ± 0.01

&: Not certified; LOD: limit of detection.
* P: 0.95; $\bar{X} \pm ts/\sqrt{N}$.

Table 5
Analyte levels of water samples analyzed (sample volume: 150 mL, final volume: 5 mL, $N = 4$)

Analyte	Concentration ($\mu g\,L^{-1}$)		
	Lake water from Mogan Lake, Ankara	Tap water from Cubuk village	Tap water from Karagol village
Au	<LOD	<LOD	<LOD
Bi	<LOD	<LOD	<LOD
Cr	<LOD	<LOD*	<LOD
Fe	78 ± 9	46 ± 2	28 ± 0.4
Pb	9 ± 2	<LOD	<LOD
Th	0.3 ± 0.06	0.2 ± 0.02	0.2 ± 0.02

LOD: limit of detection.
* P: 0.95; $\bar{X} \pm ts/\sqrt{N}$.

quantitatively recovered in the sample volume range of 20–250 mL. Uranium(VI) can be recovered till 150 mL of sample volume. The high sample volumes may behave as eluent. The preconcentration factor is calculated by the ratio of the highest sample volume for the all together of the analytes (150 mL) and the lowest eluent volume (5 mL). The preconcentration factor was 30. The time required for the coprecipitation and determination was about 45 min.

3.5. Analytical performance of the procedure

The reproducibility of the presented procedure was evaluated by model solution containing analyte ions ($N = 7$). The relative standard deviations (R.S.D.) of these determinations were in the range of 0.8% (Fe)–2.7% (Ni).

The limits of detection (LOD) of the proposed procedure for the determination of analyte elements were studied under the optimal experimental conditions. The detection limits, defined as the concentration equivalent to three times the standard deviation of blank ($n = 15$, $X_L = X_b + 3s$, X_L: limit of detection, X_b: blank value) of the reagent blank [36], were 0.3 $\mu g\,L^{-1}$ for gold, 1.8 $\mu g\,L^{-1}$ for bismuth, 0.8 $\mu g\,L^{-1}$ for cobalt, 6.1 $\mu g\,L^{-1}$ for chromium, 12.9 $\mu g\,L^{-1}$ for iron, 2.6 $\mu g\,L^{-1}$ for manganese, 1.9 $\mu g\,L^{-1}$ for nickel, 3.6 $\mu g\,L^{-1}$ for lead, 0.07 $\mu g\,L^{-1}$ for thorium and 0.05 $\mu g\,L^{-1}$ for uranium.

3.6. Matrix effects

Matrix effects are important problem in the determination of heavy metals in real samples [37,38]. In order to assess the possible analytical applications of the recommended procedure, the effect of some foreign ions which interfere with the determination of metal ions by the presented method or/and often accompany analyte ions in various real samples, was examined with the optimized conditions as above. For these studies, a fixed amount of metal ions was taken with different amounts of foreign ions and recommended procedure was followed. Tolerable limit was defined as the highest amount of foreign ions that produced an error not exceeding 5% in the determination of investigated analyte ions. The results are summarized in Table 2. The recoveries of manganese, cobalt, nickel and uranium ions were affected by the matrix ions.

Table 6
Comparative data from some recent studies on preconcentration–separation of heavy metal ions

Technique	Analytes	System	Eluent	PF	Detection limit ($\mu g\,L^{-1}$)	R.S.D. (%)	Ref.
Coprecipitation	Pb	Manganese dioxide	HNO_3/H_2O_2	–	3.2	<5	[39]
Coprecipitation	Cd, Cu, Pb	Aluminum hydroxide	4 mol L^{-1} HNO_3	125	3–16	2–3	[40]
Coprecipitation	Fe, Pb, Bi	Yttrium phosphate	6 mol L^{-1} HNO_3		0.008–0.137 μg	1.2–4.1	[41]
SPE	Cd, Cu, Ni, Zn	Ammonium pyrrolidinedithiocarbamate impregnated activated carbon	1 mol L^{-1} HNO_3 in acetone	20	0.019–0.028	<0.6	[42]
SPE	Cu	Polyurethane foam/2-(6′-methyl-2′-benzo thiazolylazo) chromotropic acid	5×10^{-3} mol L^{-1} HCl	14.1	1.2	<6.3	[43]
SPE	Co, Ni	5,7-Dichloroquinone-8-ol embedded styrene–ethylene glycol dimethacrylate polymer	2.0 mol L^{-1} HCl	200	2.0–2.0	<3	[44]
SPE	Cd, Hg, Ni, Co, Cu, Zn	2-(Methylthio)aniline/functionalized Amberlite XAD-2	1 mol L^{-1} HCl	400	0.02–0.08	<10	[45]
CPE	Cr	Triton X-100/Cr(VI)/dibromophenylfluorone	1 mol L^{-1} HNO_3	50	0.01	2.6	[46]
Coprecipitation	Fe, Pb, Co, Cr, Mn, Ni, Cd, Au, Bi, U, Th	Cu(II)–9-phenyl-3-fluorone	HNO_3	30	0.05–12.9	<2.8	Present work

MF: membrane filtration, SPE: solid phase extraction, CPE: cloud point extraction, PF: preconcentration factor.

Gold(III), bismuth(III), chromium(III), iron(III), lead(II) and thorium(IV) ions were generally quantitatively recovered by the investigated matrix ions. As shown in Table 2, the recoveries of manganese(II), nickel(II), cobalt(II) and uranium(VI) were strongly effected and negatively affected. It may source the competition of recovery between matrix ions and these ions. This results show that the presented procedure could be applied to the multi-element separation and preconcentration of gold(III), bismuth(III), chromium(III), iron(III), lead(II) and thorium(IV).

3.7. Tests of addition/recovery

Tests of addition/recovery in the experiments for gold(III), bismuth(III), chromium(III), iron(III), lead(II) and thorium(IV) ions were performed in a tap water from Ankara city center and a bottled mineral water. The results are given in Table 3. A good agreement was obtained between the added and measured analyte amounts. The recovery values for the analyte ions were in the range of 92–107%. These values were quantitative and it shows that the presented procedure can be applied for the preconcentration of Cr, Fe, Au, Pb, Bi and Th ions in real samples.

3.8. Applications

The validation of the presented coprecipitation procedure is performed by the analysis of two certified reference materials (Montana I Soil (NIST-SRM 2710) and Lake Sediment (IAEA-SL-1)) for gold, bismuth, chromium, iron, lead and thorium values. The certified and observed values for certified reference materials are given in Table 4. The results found were in good agreement with the certified values of CRMs.

The presented procedure was applied to two different sediments from Lake Van, Van, Turkey. The results for lake sediments are given in Table 4. Another application of the presented coprecipitation procedure was performed for the analysis of three water samples. The water samples collected from Mogan Lake, Cubuk village and Karagol village of Ankara. The results are given for water samples in Table 5. The results given in Tables 4 and 5 have been calculated on the assumption of 100% recovery of investigated analyte ions.

4. Conclusions

The presented procedure for gold(III), bismuth(III), chromium(III), iron(III), lead(II) and thorium(IV) in real samples is simple and rapid with good precision and accuracy. Analyte ions were quantitatively recovered by the investigated matrix ions with some exceptions. The coprecipitated analyte ions can be sensitively determined by FAAS and ICP-MS without any influence of copper and 9-phenyl-3-fluorone. The comparative data from some recent studies on separation-enrichment of heavy metal ions are given in Table 6. The optimal conditions of presented preconcentration procedure are comparable for the procedure in literature [39–47] with quantitative recovery values and detection limits. The proposed procedure is superior to those reported heavy metal separation–preconcentration methods in literature in terms of no need to consumption of organic solvents and enrichment factor. The procedure has been successfully applied to gold(III), bismuth(III), chromium(III), iron(III), lead(II) and thorium(IV) ions with acceptable accuracy and precision. The developed procedure is successfully employed for analysis of agricultural and geological materials after successful validation.

Acknowledgements

F.A. Aydin would like to thank DSI, The Technical Research and Quality Control Department and Director of Testing Laboratory for taking the time to work in laboratory. The authors are grateful for the financial support of the Unit of the Scientific Research Project of Erciyes University (Project no.: EÜBAP-FBT 05 15).

References

[1] Y.D. Su, W.Y. Zhu, L. Qin, L.W. Chen, Spectrosc. Spect. Anal. 26 (2006) 959–962.
[2] E. Suren, S. Yilmaz, M. Turkoglu, S. Kaya, Environ. Monit. Assess. 125 (2007) 91–98.
[3] D. Afzali, A. Mostafavi, M.A. Taher, A. Moradian, Talanta 71 (2007) 971–975.
[4] Y. Wang, Chin. J. Anal. Chem. 33 (2005) 872–874.
[5] S.P. Quináia, M.C.E. Rollemberg, J.B.B. da Silva, Can. J. Anal. Sci. Spectros. 51 (2006) 225–233.
[6] J.L. Manzoori, M.H. Sorouradin, A.M. Haji Shabani, Microchem. J. 63 (1999) 295–301.
[7] H.K. Pandey, M. Vashistha, N. Bhojak, Asian J. Chem. 18 (2006) 3191–3193.
[8] P. Chiranjeevi, K. Suvardhan, K.S. Kumar, D. Rekha, S. Ramanaiah, Anal. Chem. Indian J. 2 (2006) 51–59.
[9] M. Soylak, Fresenius Environ. Bull. 7 (1998) 383–387.
[10] X.J. Zhu, Z.C. Jiang, B. Hu, J. Instrum. Anal. 24 (2005) 108–115.
[11] F.S. Rojas, C.B. Ojeda, J.M.C. Pavón, Ann. Chim. 97 (2007) 265–276.
[12] M.T. Kelly, A. Blaise, J. Chromatogr. 1134A (2006) 74–80.
[13] R.E.S. Froes, C.C. Windmöller, J.B.B. da Silva, Rev. Anal. 23 (2006) 32–43.
[14] Y.F. Li, W.J. Dong, J. Henan Normal Univ. 33 (2005) 94–97.
[15] T. Shimizu, H. Ito, H. Kawaguchi, Y. Shijo, Bull. Chem. Soc. Jpn. 72 (1999) 43–46.
[16] T. Akagi, H. Horaguci, Anal. Chem. 62 (1990) 81–85.
[17] B.K. Priya, P. Subrahmanayam, K. Suvardhan, K.S. Kumar, D. Rekha, A.V. Rao, G.C. Rao, P. Chiranjeevi, J. Hazard. Mater., in press.
[18] M. Soylak, G. Onal, J. Hazard. Mater. 137 (2006) 1130–1134.
[19] M. Soylak, B. Ozcan, L. Elci, Kuwait J. Sci. Eng. 31 (2004) 47–59.
[20] Y. Danzaki, Fresenius J. Anal. Chem. 356 (1996) 143–145.
[21] D. Atanassova, V. Stefanova, E. Russeva, Talanta 47 (1998) 1237–1243.
[22] M. Vircavs, V. Rone, D. Vircava, Fresenius J. Anal. Chem. 350 (1994) 650–651.
[23] Y.C. Sun, Anal. Chim. Acta 276 (1993) 33–37.
[24] S. Arpadjan, L. Jordenova, I. Karadjuva, Fresenius J. Anal. Chem. 347 (1993) 480–482.
[25] B. Welz, S. Xu, M. Sperling, Appl. Spectrosc. 45 (1991) 1433–1443.
[26] O.D. Sant'Ana, A.L.R. Wagener, R.E. Santelli, R.J. Cassella, M. Gallego, M. Valcarcel, Talanta 56 (2002) 673–680.
[27] I. Atsuya, K. Itoh, I. Ariu, Pure Appl. Chem. 63 (1991) 1221–1226.
[28] L. Elci, U. Sahin, S. Oztas, Talanta 44 (1997) 1017–1023.
[29] Z. Marczenko, Separation and Spectrophotometric Determination of Elements, Wiley, Chichester, 1986.
[30] W. Winkler, F. Buhl, A. Arenhövel-Pacuła, U. Hachuła, Anal. Bioanal. Chem. 376 (2003) 934–937.

[31] L. Zaijun, P. Jiaomai, T. Jian, Anal. Bioanal. Chem. 374 (2002) 1125–1131.
[32] Q. Gong, X.X. Li, X.L. Wei, X.Y. Li, J.J. Lu, K. Ouyang, Spectrosc. Spect. Anal. 26 (2006) 1162–1166.
[33] H.W. Gao, W.G. Liu, Bull. Korean Chem. Soc. 21 (2000) 1090–1094.
[34] F.A. Aydin, M. Soylak, Talanta, in press.
[35] K. Ueno, T. Imamura, K.L. Cheng, Handbook of Organic Analytical Reagents, second ed., CRC Press, London, 1992.
[36] IUPAC, Nomenclature, symbols, units and their usages in spectrochemical analysis, Pure Appl. Chem. 45 (1976) 105–111.
[37] S. Baytak, E. Kenduzler, A.R. Turker, Sep. Sci. Technol. 41 (2006) 3449–3465.
[38] H. Bag, A. Elci, L. Elci, Eurasian J. Anal. Chem. 1 (2006) 42–54.
[39] M.S. Bispo, E.S. da Boa Morte, M.G.A. Korn, L.S.G. Teixeira, M. Korn, A.C.S. Costa, Spectrochim. Acta 60B (2005) 653–658.
[40] G. Doner, A. Ege, Anal. Chim. Acta 547 (2005) 14–17.
[41] S. Kagaya, Y. Araki, N. Hirai, K. Hasegawa, Talanta 67 (2005) 90–97.
[42] P. Daorattanachai, F. Unob, A. Imyim, Talanta 67 (2005) 59–64.
[43] V.A. Lemos, A.A. de Jesus, E.M. Gama, G.T. David, R.T. Yamaki, Anal. Lett. 38 (2005) 683–688.
[44] R.S. Praveen, S. Daniel, T.P. Rao, Talanta 66 (2005) 513–518.
[45] Y. Guo, B. Din, Y. Liu, X. Chang, S. Meng, M. Tian, Anal. Chim. Acta 504 (2004) 319–324.
[46] X. Zhu, B. Hu, Z. Jiang, M. Ling, Water Res. 39 (2005) 589–595.
[47] S. Yao-Dong, Z. Wen-Ying, M. Hong-Mei, C. Long-Wu, Spectrosc. Spect. Anal. 26 (2006) 1732–1734.

Available online at www.sciencedirect.com
ScienceDirect
Talanta 73 (2007) 115–120
Talanta
www.elsevier.com/locate/talanta

Acidity of several polyprotic acids, amiodarone and quetiapine hemifumarate in pure methanol

Gemma Garrido, Vasco de Nogales, Clara Ràfols, Elisabeth Bosch *

Departament de Química Analítica, Universitat de Barcelona, Martí i Franquès 1-11, 08028 Barcelona, Spain

Received 29 November 2006; received in revised form 28 February 2007; accepted 7 March 2007
Available online 14 March 2007

Abstract

Methanol is the organic solvent closest to water and able to dissolve a huge amount of organic compounds. Therefore, it is a good candidate for pK_a determination of drugs sparingly soluble in water or a basic drug presented as a salt which pK_a is close to that of its counter-acid. In this work, the acidic dissociation constants in pure methanol of the most common acids used in pharmaceutical preparations (lactic, tartaric, fumaric, maleic and citric) were determined. In addition, the pK_a values of the antipsychotic quetiapine presented as hemifumarate (Seroquel) and the very insoluble antiarrhythmic amiodarone were also determined by potentiometry. From these values, the aqueous pK_a of these drugs were estimated by means of previously established equations. Estimated values are consistent with those from literature and show the interest of methanol for drug discovery pK_a measurements.

Keywords: pK_a in methanol; pK_a in water; Drugs; Potentiometry; Polycarboxylic acids; Amiodarone; Quetiapine hemifumarate; Seroquel

1. Introduction

Despite the fact that many drugs are sparingly soluble in water, the evaluation of the aqueous dissociation constants is an unavoidable requirement in drug discovery [1]. In these instances, experimental pK_a determination requires the use of an organic or hydroorganic solvent [2]. The first approach was the method proposed by Hall that relates the half neutralization potential in an organic solvent and aqueous pK_a values [3,4]. Nowadays, potentiometry is the preferred technique because of the excellent response of the glass electrode in many pure and binary solvents and the easy automation of the experimental measurements [5]. For aqueous pK_a ($^{w}_{w}$pK_a) determination purposes two main potentiometric approaches were developed. Both methods employ hydroorganic mixtures as sample solvents and require a suitable extrapolation equation to estimate the $^{w}_{w}$p$K_a$value, from the experimental constants in the binary solvent ($^{s}_{s}$pK_a). The first method involves the determination of $^{s}_{s}$pK_a in several hydroorganic mixtures and further extrapolation by means of the Yasuda–Shedlovsky equation [6–10]. The most employed solvent in these hydroorganic mixtures is methanol but, very recently, a mixture of equal volumes of methanol, dioxane and acetonitrile (MDM) has successfully proposed [6]. Good results are achieved using this method, particularly when mixtures with low organic content can be employed. The main limitation is again the solubility of the drug since the linearity of the Yasuda–Shedlovsky equation is kept until about 60% (w/w) of methanol or 50% (w/w) of MDM and it is not possible to use it at higher percentages. Therefore, this method hardly attains for the proper estimation of the $^{w}_{w}$pK_a values of very insoluble drugs. The second approach, developed for methanol/water mixtures, involves linear relationships to estimate the $^{w}_{w}$pK_a from a unique $^{s}_{s}$pK_a value determined in a suitable mixture. The slope and intercept of these linear equations can be easily calculated according to the methanol fraction of the binary solvent and the nature of the acid-base group of the drug. In this instance, it is possible to use a solvent with high methanol content although the precision of the extrapolated $^{w}_{w}$pK_a value is slightly lower than that achieved from poor methanol binary solvents [10–12].

Both approaches show a limitation in the determination of $^{w}_{w}$p$K_a$of drugs when they are presented as a salt formulation, which is very common. Thus, when the pK_a values in the working solvent of a basic drug and its counter-acid are close, the resolution of the concomitant equilibria involves a lost in the

* Corresponding author. Tel.: +34 934021284; fax: +34 934021233.
E-mail address: e.bosch@ub.edu (E. Bosch).

0039-9140/$ – see front matter © 2007 Elsevier B.V. All rights reserved.
doi:10.1016/j.talanta.2007.03.010

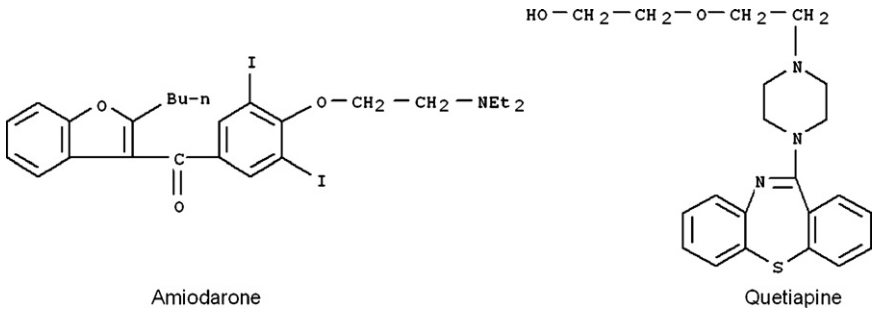

Fig. 1. The studied drugs.

accuracy and precision of the computed ${}^{s}_{s}pK_a$ values and, consequently, of the estimated ${}^{w}_{w}pK_a$. Stability considerations have led manufacturers to select counter-ions that show a minimum difference of three pK_a units between the ionizable groups of the drug and its counter-acid [13]. However, it is important to note that this difference can become much lower when the organic content of the solvent is high (>30%). This is a common feature since the pK_a values of neutral or anionic acids increase with the organic content in the solvent but the opposite behaviour should be expected for basic compounds (cationic acids) [6,10,11]. Calculations can be carried out using the ${}^{s}_{s}pK_a$values of the salt-forming acid as constant values, but very often these values are unknown. Recently, we have published ${}^{s}_{s}pK_a$ values of several common counter-acids in aqueous mixtures up to 60% (w/w) of methanol which can be used for these purposes [14]. As a working example, we determined the ${}^{s}_{s}pK_a$values of quetiapine formulated as hemifumarate using the suitable ${}^{s}_{s}pK_a$ of fumaric acid in various methanol/water mixtures. Further, the Yasuda–Shedlovsky model was used to estimate the ${}^{w}_{w}pK_a$values. The obtained ${}^{w}_{w}pK_{a1}(3.53 \pm 0.27)$ of quetiapine shows a high standard deviation due to the proximity between this pK_a and those of fumaric acid in the working binary solvents, whereas ${}^{w}_{w}pK_{a2}$ (6.92 ± 0.07), whose value is far from those of fumaric acid, shows a very good precision [14]. Alternatively, a look-up procedure can be used to iterate the experimental pH values and get all the involved equilibrium constants.

In this work, we propose pure methanol as a solvent to determine the ${}^{s}_{s}pK_a$ for very insoluble drugs because of all the organic solvents, methanol is the one closest to water and shows a high ability to dissolve organic compounds. We also propose methanol as suitable solvent to determine the ${}^{s}_{s}pK_a$ for drugs presented in salt form and whose aqueous pK_a is close to those of their salt-forming counterpart. This is because the ${}^{s}_{s}pK_a$ in methanol is well known to be about 5 pK units higher than ${}^{w}_{w}pK_a$for carboxylic acids, 4 units higher for phenols and only 1 unit or less for amines and pyridines, which are cationic acids (basic compounds) [15]. Since a salt is always composed by a base and an acidic compound, close pK_a values in water or water-rich binary mixtures become far away enough in methanol. Therefore, pure methanol could be a suitable option for this kind of salts.

Moreover, potentiometric measurements can be carried out with the glass electrode calibrated with standard aqueous buffers leading to ${}^{s}_{w}pH$ values, that is to say, to the pH values in the intersolvental pH scale. Since the δ quantity is well known (−2.34 in the molality scale and −2.24 in the molarity scale), easy change is allowed from the intersolvental pH scale (${}^{s}_{w}pH$) to the specific pH scale for pure methanol (${}^{s}_{s}pH$) [16–20], by means of

$$ {}^{s}_{s}pH = {}^{s}_{w}pH - \delta \quad (1) $$

and, therefore, experimental ${}^{s}_{w}pH$ measurements allow to get the ${}^{s}_{s}pH$ and also the ${}^{s}_{s}pK_a$ values. Since linear equations such as

$$ {}^{s}_{s}pK_a = a\,{}^{w}_{w}pK_a + b \quad (2) $$

were established for a variety of chemical families [11,15,21], these relationships can be used to estimate ${}^{w}_{w}pK_a$ from ${}^{s}_{s}pK_a$values obtained in pure methanol.

Two pattern drugs were selected for this study. The first one is an antianginal and antiarrhythmic drug used in treatments of heart diseases, amiodarone. This is a highly hydrophobic compound with a very small solubility in water (0.7 mg/mL) [22], which forms micelles with very low critical micelle concentration (0.5 mg/mL) [23]. Amiodarone requires, at least, 40% methanol/water [24] mixtures to prepare a solution of suitable concentration in a wide pH range. The other drug is the quetiapine hemifumarate, commercially named Seroquel, which belongs to the dibenzothiazepine derivatives. It is widely used to treat psychotic disorders and symptoms such as hallucinations, delusions and hostility [25]. Since ${}^{w}_{w}pK_{a1}(3.02)$ and ${}^{w}_{w}pK_{a2}(4.38)$ of fumaric acid [26] are very close to ${}^{w}_{w}pK_{a1}$ of quetiapine (3.30), three acid-base equilibria coexist in the moderately acidic pH range in aqueous solution [14]. Both drugs are shown in Fig. 1.

2. Experimental

2.1. Apparatus

- pH measurements were taken with a Ross combination electrode Orion 8102 (glass electrode and a reference electrode with a 3.0 M KCl solution in water as a salt bridge) in a Crison micropH 2002 potentiometer with a precision of ± 0.1 mV.
- Potentiometric titrations were carried out by means of a Methrom 665 Dosimat autoburet controled by the VALORA program specially designed for titrations in non-aqueous

media [27]. The resolution of the burette is ±0.001 and the absolute error is ±0.02 mL.

2.2. Chemicals

Lactic (>99%, Fluka), tartaric (>99.6%, Baker), fumaric (>99%, Fluka), maleic (>99.8%, Carlo Erba) and citric (>99.8%, Carlo Erba) acids, amiodarone hydrochloride (>98%, Aldrich) and quetiapine hemifumarate (>99%, Astra Zeneca) were titrated. Potassium hydroxide (>85%, Panreac); benzoic acid (>99.5%, p.a., Carlo Erba) and tris(hydroxymethyl) aminomethane (A.C.S., J.T. Baker) were also used. Methanol of chromatographic grade (p.a., >99.8%, Merck) was used in all experiments.

2.3. Procedure

- The electrode system was standardized with ordinary aqueous buffers of potassium hydrogen phthalate (pH 4.00), and potassium dihydrogen phosphate/disodium hydrogen phosphate (pH 7.02). The electrode was soaked for 15 min in methanol before the potentiometric measurements.
- Samples of acids in the range 5×10^{-4} M–1×10^{-2} M were dissolved in pure methanol and titrated with KOH 0.1 M or 0.01 M in the same solvent.
- Samples of amiodarone and quetiapine hemifumatate were dissolved in pure methanol and an excess of HCl in methanol was added in order to decrease the pH and assure that the drugs were completely protonated. In the case of amiodarone, this addition was not strictly necessary since the drug was presented as amiodarone hydrochloride and direct titrations without previous HCl addition were also carried out. Sample concentration was about 10^{-3} M. Titrant solution was KOH 0.1 M or 0.01 M in pure methanol. Four to nine titrations, at 25.0 ± 0.1 °C under a continuous stream of purified nitrogen, were done for each determination. Hydrochloric acid and potassium hydroxide were standardized potentiometrically.
- The hydrochloric acid solution used was prepared from aqueous 0.5 M HCl and the addition of the required amount of methanol to get a 0.05 M solution. The amount of HCl solution added to perform the titrations together with the water generated during the titration results in a percentage of water in the titrated solution that is lower than 0.6% in volume (calculated in the first equivalence point).
- Dissociation constants in methanol (${}^{s}_{s}pK_a$) were calculated using the following values: $\delta = -2.24$, the autoprotolysis constant $pK_{ap} = 16.7$ and the Debye-Hückel coefficients $A = 1.87$ and $a_oB = 2.31$ [20].

3. Results and discussion

In previous work, we have established linear equations that relate the ${}^{s}_{s}pK_a$ values in pure methanol to the thermodynamic ${}^{w}_{w}pK_a$ for different chemical families from two different approaches. Table 1 shows the coefficients for Eq. (2) derived for amines, nitrogen-protonated heterocycle derivatives and pyridines from different sets of substances and different approaches. Parameters from [11] were derived from a wide number of ${}^{s}_{s}pK_a$in different methanol/water mixtures whereas those from [15] and [21] were established from ${}^{s}_{s}pK_a$ values determined directly in pure methanol. The consistency between these parameters shows their robustness. Here, we have selected for calculations the coefficients from [15] for amines and from [21] for pyridines, since these were obtained from a greater number of compounds. It should be pointed out, however, that despite the fact of specific equations having been proposed for primary amines, for anilines, and for secondary and tertiary amines [15], in this study we used the parameters derived for the more general equation suitable for any kind of amino compounds. This is because of the molecular complexity of most drugs is very often far from those of the compounds used to build the specific equations, which were derived from substances with simpler structure and from a smaller number of compounds. In order to validate the proposed equations to estimate ${}^{w}_{w}pK_a$ values of basic drugs we tested these parameters using the values available in the literature for compounds with amino groups excluding those used in the coefficients derivation. As a matter of fact, the number of ${}^{s}_{s}pK_a$ of drugs in pure methanol found in the literature is low and they were determined by capillary electrophoresis in all instances. This technique is suitable for highly insoluble compounds because it requires very low concentration of the tested compound and, in addition, it is not necessary previous purification of the sample. However, it requires a significant number of

Table 1
Parameters for Eq. (2)

	Reference [11]					Reference [15]					Reference [21]				
	a	*b*	*r*[a]	*s*[b]	*n*[c]	*a*	*b*	*r*[a]	*s*[b]	*n*[c]	*a*	*b*	*r*[a]	*s*[b]	*n*[c]
Amines	0.968	1.171	0.987	0.48	30	0.94	1.23	0.981	0.58	55	–	–	–	–	–
Nitrogenated heterocycles and secondary and tertiary amines	–	–	–	–	–	0.94	0.67	0.994	0.24	40	–	–	–	–	–
Pyridines	0.951	0.520	0.996	0.12	11	0.93	0.67	0.916	0.20	15	1.02	0.30	0.991	0.45	23

a, slope; *b*, intercept.
[a] *r*, Correlation coefficient.
[b] *s*, Standard deviation.
[c] *n*, Number of compounds.

Table 2
Acidity constants of several basic compounds

	${}^{s}_{s}pK_a$	${}^{w}_{w}pK_a$ calc. Eq. (2)	${}^{w}_{w}pK_a$ literature
Desipramine	10.80 [28]	10.18	10.22 [25]; 10.2 [30]; 10.23 [31]
Nortriptyline	10.79 [28]	10.17	10.13 [1]; 10.14 [10]; 10.10 [25]; 9.73 [30]; 10.50 [31]; 9.7 [32]; 8.8 [33]; 10.19 [34]
Imipramine	10.38 [28]	9.73	9.30 [10]; 9.45 [25]; 9.5 [30]; 9.5 [32]; 9.21 [35]
Amitriptyline	10.33 [28]	9.68	9.41 [25]; 9.40 [31]; 9.32 [34]
Cyclohexylamine	11.33 [29]	10.74	10.79 [3]; 10.64 [26]; 10.63 [36]
Imidazole	7.97 [29]	7.17	6.95 [26]; 6.99 [36]; 7.0 [37]

buffer solutions to get reliable values. The ${}^{s}_{s}pK_a$ values of compounds studied by Cantu et al. [28] and Beckers et al. [29] are given with two decimal figures and throw them Eq. (2) leads to ${}^{w}_{w}pK_a$ values very close to those from literature, see Table 2. The ${}^{s}_{s}pK_a$ values determined by Porras et al. [38,39] for a variety of drugs were calculated from a small number of experimental points in a overmuch short pH range and, therefore, are given with lower precision, one decimal figure. Then, these values have been excluded in this study.

Amiodarone hydrochloride was titrated as described in the experimental part. Thus, the neutralization process involves water formation during the titration changing gradually the solvent composition but, in fact, the water content in the equivalence point is very low, about 5×10^{-3} M (0.01 vol.%). Thus, the water generated in the titration is low enough to be neglected in the ${}^{s}_{s}pK_a$ calculation. The studied chemical is amiodarone in its protonated form. However, many drugs require the addition of hydrochloric acid before titration to assure complete protonation and this step involves the addition of a fixed amount of water (see HCl solution preparation). To evaluate the effect of this added water in the reaction medium, titrations of amiodarone to which hydrochloric acid was added (initial water concentration about 10^{-2} M), were carried out too. Derived ${}^{s}_{s}pK_a$ value (9.16 ± 0.03) does not show significant difference with former result. Therefore, from a practical point of view, the presence of small amounts of water ($<10^{-2}$ M) do not affect the determined ${}^{s}_{s}pK_a$ in methanol. The final mean value is given in Table 3.

The potentiometric determination of ${}^{s}_{s}pK_a$ values of quetiapine is more complex because it is presented as a hemifumarate. Therefore, ${}^{s}_{s}pK_a$ values of fumaric acid in pure methanol were determined and are given in Table 4. In addition, the ${}^{s}_{s}pK_a$ of other common polyprotic counteracids used in pharmaceutical preparations [13] were also determined and are presented together with the values found in the literature. The effect of water generation in the titrations of these acids was tested in the way explained for amiodarone, and it can be concluded that the water effect on the final calculated ${}^{s}_{s}pK_a$ is negligible too. Then, the values reported in Table 4 can be used in acid-base equilibria studies in pure methanol. It should be pointed out that these acids are polyprotic and, thus, intramolecular interactions, mostly by hydrogen bond, could affect the ${}^{s}_{s}pK_a$ values. For instance, the ${}^{s}_{s}pK_{a1}$ of maleic acid is lower and the ${}^{s}_{s}pK_{a2}$ higher than those of its isomer, fumaric acid, and these differences are higher than those in aqueous solution since methanol shows lower solvating abilities than water, therefore favoring the internal hydrogen bond in the intermediate form. The titration curve of quetiapine hemifumarate is shown in Fig. 2 and the calculated ${}^{s}_{s}pK_a$ values are given in Table 3.

The calculated ${}^{w}_{w}pK_a$ value for amiodarone must be compared with those derived from different measurements in hydroorganic media since this value cannot be determined properly in aqueous solution, despite the fact we report some values from measurements in aqueous solutions (6.56 [43] and 6.09 [22]). The value obtained in this work is slightly lower than those previously published which were extrapolated from high methanol [24,41,42] content solutions. The ${}^{w}_{w}pK_{a2}$ of quetiapine agrees with the values experimentally determined in aqueous solution [14] despite the fact that the ${}^{s}_{s}pK_{a2}$ of quetiapine (7.90) and the ${}^{s}_{s}pK_{a1}$ (7.81) and ${}^{s}_{s}pK_{a2}$ (10.14) of fumaric acid are very close and that therefore three concomitant equilibria are involved in the basic part of titration curve (Fig. 2). Both, the pK_a of amiodarone and the pK_{a2} of quetiapine are attributable to protonated amino groups, and the ${}^{w}_{w}pK_a$ values were calculated using coefficients for amines from ref. [21]. The ${}^{w}_{w}pK_{a1}$ of quetiapine is due to the protonated nitrogen of a dibenzothiazepine ring and, therefore, there are no appropriate coefficients to use Eq. (2). However, coefficients derived for aromatic nitrogens, pyridines [21], were tested and results are given in Table 3. The calculated value is slightly lower than that determined in aqueous solution but it allows a good estimation of ${}^{w}_{w}pK_{a1}$ Thus, the procedure used leads to estimated ${}^{w}_{w}pK_a$ values of amiodarone and quetiapine consistent with those from various experimental approaches from only a single titration process using an electrode system standardized with common aqueous buffers.

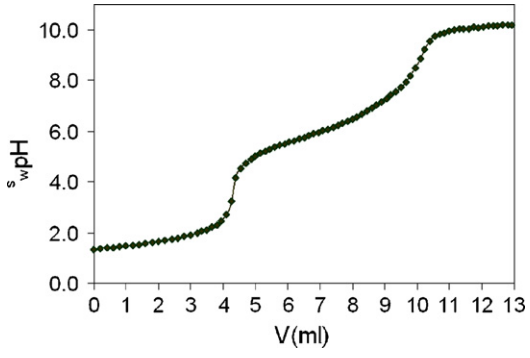

Fig. 2. Titration curve of quetiapine hemifumarate in pure methanol.

Table 3
Acidity constants of the studied drugs

	${}^{s}_{s}pK_{ai}$		${}^{w}_{w}pK_{ai}$ calc.		${}^{w}_{w}pK_{ai}$ literature	
	$i=1$	$i=2$	$i=1$	$i=2$	$i=1$	$i=2$
Amiodarone	9.22 ± 0.03	–	8.50 ± 0.03	–	8.85 ± 0.01[a]; 8.7 ± 0.5[b]; 8.73 ± 0.07[c]; 8.7 ± 0.2[d]; 6.56 ± 0.06[e]; 6.09[f]	–
Quetiapine	3.54 ± 0.12	7.90 ± 0.12	3.24 ± 0.12	7.09 ± 0.12	3.30 ± 0.05[g]; 3.53 ± 0.27[h]; 3.31 ± 0.04[i]	7.06 ± 0.03[g]; 6.92 ± 0.01[h]; 6.97 ± 0.01[i]

[a] Ref. [24]. From a measurement at 50 wt% MeOH/H_2O by CE.
[b] Ref. [40]. From interfacial air/water measurements.
[c] Ref. [41]. From measurements in MeOH/H_2O mixtures by potentiometry.
[d] Ref. [42]. From measurements in MeOH/H_2O mixtures by potentiometry.
[e] Ref. [22]. From spectrophotometric measurement in aqueous solution.
[f] Ref. [43]. From aqueous measurements by CE.
[g] Ref. [14]. From aqueous measurements by CE.
[h] Ref. [14]. From measurements in MeOH/H_2O mixtures by potentiometry.
[i] Ref. [14]. From aqueous measurements by potentiometry.

Table 4
${}^{s}_{s}pK_a$ values of several mono and polycarboxylic acids in methanol

	${}^{s}_{s}pK_{a1}$	${}^{s}_{s}pK_{a2}$	${}^{s}_{s}pK_{a3}$
Lactic acid	8.63 ± 0.07	–	–
Tartaric acid	7.67 ± 0.03	9.52 ± 0.05	–
Fumaric acid	7.81 ± 0.06	10.14 ± 0.07	–
	8.0 [44]	10.4 [44]	
	–	9.78 [45]	
Maleic acid	5.52 ± 0.07	12.64 ± 0.09	–
	5.9 [46]	13.0 [46]	–
Citric acid	7.58 ± 0.08	9.56 ± 0.07	11.14 ± 0.12

4. Conclusions

It has been demonstrated that the previously published linear equations with coefficients derived for amines and for nitrogenated heterocycles can be successfully applied to estimate the aqueous pK_a of several basic drugs from values determined in pure methanol by capillary electrophoresis or potentiometry. Potentiometry is the faster and simpler method because it requires solely the electrode standardization that can be carried out with ordinary aqueous buffers provided that we know the value of the δ parameter, which allows the transfer from the universal pH scale to the methanol pH scale. Two representative drugs were studied, the very insoluble amiodarone and quetiapine hemifumarate, a drug presented in salt form that required the determination of the pK_a values of fumaric acid in methanol. The pK_a in methanol of other mono and polycarboxylic acids used in drug salt preparations was also determined. The aqueous pK_a values of amiodarone and quetiapine were also successfully estimated by means of the determined values in pure methanol, as well as the proposed equations, including that for pK_{a1} of quetiapine whose nitrogen belongs to a dibenzothiazepine ring.

Acknowledgements

We would like to thank the AstraZeneca Firm for kindly donating a sample of Seroquel. We also thank the Ministerio de Ciencia y Tecnología of the Spanish Government and the Fondo Europeo de Desarrollo Regional of the European Union (Project CTQ2004-00633/BQU) for their financial support.

References

[1] H. Wang, J. Ulander, Exp. Opin. Drug Metab. Toxicol. 2 (2006) 139–155.
[2] B. Testa, H. van de Waterbeemd, G. Folkers, R. Guy (Eds.), Pharmacokinetic Optimization in Drug Research, Wiley, Weinheim, 2001.
[3] H.K. Hall Jr., J. Phys. Chem. 60 (1956) 63–70.
[4] A. Önen, A.S. Saraç, Z. Fres, Anal. Chem. 328 (1987) 663–664.
[5] E.P. Serjeant, Potentiometry and Potentiometric Titrations, Wiley, New York, 1984.
[6] G. Völgyi, R. Ruiz, K. Box, J. Comer, E. Bosch, K. Takács-Novák, Anal. Chim. Acta 583 (2007) 418–423.
[7] A. Avdeef, K.J. Box, J.E.A. Comer, S.J. Thomson, Anal. Chem. 65 (1993) 42–49.
[8] K. Takács-Novák, K.J. Box, A. Avdeef, Int. J. Pharm. 151 (1997) 235–248.

[9] A. Avdeef, K.J. Box, J.E.A. Comer, M. Gilges, M. Hadley, C. Hibbert, W. Patterson, K.Y. Tam, J. Pharm. Biomed. Anal. 20 (1999) 631–641.
[10] R. Ruiz, C. Ràfols, M. Rosés, E. Bosch, J. Pharm. Sci. 92 (2003) 1473–1481.
[11] F. Rived, I. Canals, E. Bosch, M. Rosés, Anal. Chim. Acta 439 (2001) 315–333.
[12] R. Ruiz, M. Rosés, C. Ràfols, E. Bosch, Anal. Chim. Acta 550 (2005) 210–221.
[13] M.J. Bowker, in: P.H. Stahl, C.G. Wermuth (Eds.), Handbook of Pharmaceutical Salts. Properties, Selection and Use, Wiley-VCH, Weinheim, 2002 (Chapter 7).
[14] G. Garrido, C. Ràfols, E. Bosch, Eur. J. Pharm. Sci. 28 (2006) 118–127.
[15] F. Rived, M. Rosés, E. Bosch, Anal. Chim. Acta 374 (1998) 309–324.
[16] C.L. De Ligny, M. Rehbach, Recl. Trav. Chim. 79 (1960) 727–730.
[17] R.G. Bates, M. Paabo, R.A. Robinson, J. Phys. Chem. 67 (1963) 1833–1838.
[18] R.G. Bates, Determination of pH: Theory and Practice, second ed., Wiley, New York, 1964.
[19] IUPAC, Compendium on Analytical Nomenclature. Definitive Rules 1987, second ed., Blackwell, Oxford, 1987.
[20] I. Canals, J.A. Portal, E. Bosch, M. Rosés, Anal. Chem. 72 (2000) 1802–1809.
[21] D. Augustin-Nowacka, M. Makowski, L. Chmurzynski, Anal. Chim. Acta 418 (2000) 233–240.
[22] M. Bonati, F. Gaspari, V. D'Aranno, E. Benfenati, P. Neyroz, F. Galleti, G. Tognoni, J. Pharm. Sci. 73 (1984) 829–830.
[23] L.J. Ravin, E.G. Shami, E.S. Rattie, J. Pharm. Sci. 64 (1975) 1830–1833.
[24] V. de Nogales, R. Ruiz, M. Rosés, C. Ràfols, E. Bosch, J. Chromatogr. A 1123 (2006) 113–120.
[25] R.G. Hendrickson, A.P. Morocco, J. Toxicol. 41 (2002) 105–108.
[26] G. Körtum, W. Vogel, K. Andrussow, Dissociation Constants of Organic Acids in Aqueous Solution, IUPAC, Butterworths, London, 1961.
[27] M. Rosés, Anal. Chim. Acta 276 (1993) 223–234.
[28] M.D. Cantu, S. Hillebrand, E. Carrilho, J. Chromatogr. A 1068 (2005) 99–105.
[29] J.L. Beckers, M.T. Ackermans, P. Bocek, Electrophoresis 24 (2003) 1544–1552.
[30] D.W. Newton, R.B. Kluza, Drug Intell. Clin. Pharm. 12 (1978) 546–554.
[31] F. Luan, W. Ma, H. Zhang, X. Zhang, M. Liu, Z. Hu, B. Fan, Pharm. Res. 22 (2005) 1454–1460.
[32] C.J. Drayton (Ed.), Comprehensive Medicinal Chemistry, vol. 6, Pergamon, Oxford, 1990.
[33] R.J.M. Vervoort, E. Ruyter, A.J.J. Debets, H.A. Claessens, C.A. Cramers, G.J. de Jong, J. Chromatogr. A 964 (2002) 67–76.
[34] S.M.C. Buckenmaier, D.V. McCalley, M.R. Euerby, J. Chromatogr. A 1026 (2004) 251–259.
[35] Z. Jia, Curr. Pharm. Anal. 1 (2005) 41–56.
[36] D.D. Perrin, Dissociation Constants of Organic Bases In Aqueous Solutions, Butterworths, London, 1965.
[37] J.J. Klicic, R.A. Friesner, S.Y. Liu, W.C. Guida, J. Phys. Chem. A 106 (2002) 1327–1335.
[38] S.P. Porras, P. Jyske, M.L. Riekkola, E. Kenndler, J. Microcol. Sep. 13 (2001) 149–155.
[39] S.P. Porras, M.L. Riekkola, E. Kenndler, J. Chromatogr. A 905 (2001) 259–268.
[40] J. Ferreira, R. Brasseur, P. Chatelain, J.M. Ruysschaert, J. Pharm. Pharmacol. 38 (1986) 561–566.
[41] F. Boury, J.C. Gautier, Y. Bouligand, J.E. Proust, Colloids Surf. B 20 (2001) 219.
[42] S.D. Krämer, J.C. Gautier, P. Saudemont, Pharm. Res. 15 (1998) 1310–1313.
[43] J.M. Miller, A.C. Blackburn, Y. Shi, A.J. Melzak, H.Y. Ando, Electrophoresis 23 (2002) 1833–2841.
[44] M.K. Chantooni, I.M. Kolthoff, J. Phys. Chem. 79 (1975) 1176–1182.
[45] V.A. Palm, Tables of rate and equilibrium constants of heterolytic reactions, vol. 1 (1), Proizbodstvenno-Izdatelckii Kombinat Biniti, Moscow, 1975, vol. 1 (Suppl. (3)), Tartuskii gosudarsvennii Universitet, Tartu, 1985.
[46] I.M. Kolthoff, M.K. Chantooni, Anal. Chem. 50 (1978) 1440–1446.

Available online at www.sciencedirect.com
ScienceDirect
Talanta 73 (2007) 95–102
Talanta
www.elsevier.com/locate/talanta

GC–MS identification of proteins in wall painting samples: A fast clean-up procedure to remove copper-based pigment interferences

Gwénaëlle Gautier*, Maria Perla Colombini

Dipartimento di Chimica e Chimica Industriale, Università di Pisa, Via Risorgimento 35, 56126 Pisa, Italy

Received 22 September 2006; received in revised form 12 February 2007; accepted 7 March 2007
Available online 14 March 2007

Abstract

A new approach was explored to purify proteins in a multi-step procedure for the characterisation of proteinaceous materials (casein, animal glue, and egg) in artwork samples by gas chromatography–mass spectrometry. High concentrations of inorganic salts, such as azurite, have been found to impair the determination of protein via amino acid analysis. The effect of varying concentrations of copper-based pigments on the quantification of amino acids was evaluated through the analysis of replica paintings prepared with the three types of proteinaceous materials. Glycine, aspartic and glutamic acids are the amino acids most affected by the presence of copper salts. In the case of high concentration of salts, this interference hampers the correct identification of the proteins. To eliminate the inorganic salts, a C18 pipette tip was used to clean-up the ammonia extracts before the acidic hydrolysis step. The clean-up procedure allows us to prevent the influence of the inorganic salts and thus allows correct protein identification, though the quantitative recovery of proteinaceous material is quite low. The effectiveness of the optimised procedure was evaluated by analysing samples from two Italian wall paintings from the 13th and the 14th centuries. Without the clean-up it would not have been possible to detect the presence of a mixture of egg and animal glue in one case, and that of egg in the other one.

Keywords: GC–MS; Clean-up; Protein; Wall painting; Azurite

1. Introduction

The importance of technical scientific support for the study and conservation of cultural heritage has long been recognised. The analysis of constituent materials remains one of the main concerns, not only to improve our knowledge of culturally significant objects, but also to understand the deterioration processes undergone by the materials and to choose suitable conservation treatments. Over the centuries, when producing pictorial works of art, artists have experimented with a vast range of natural organic substances (proteins, polysaccharide gums, siccative oils, resins, waxes, etc.) together with inorganic pigments on a variety of substrates [1–3]. A painting consists of several layers applied on a support (canvas, panel or wall): each of these layers may comprise one or more organic binders with inorganic pigments mixed together or not. The most common proteinaceous binders found in paintings are: animal glue, egg and milk or casein. In many cases, due to the very low amount of organic material present, the identification of these binding media is a difficult task. The latter is further complicated by the denaturation and aging processes that materials have undergone, the presence of complex mixtures of organic and inorganic substances, and the impossibility of physically separating different paint layers.

In the particular case of the wall paintings, the difficulty of protein identification is even greater due to the presence of the inorganic species in very high concentration. Pigments may continuously interact with the medium mainly through the formation of strong complexes [4–12]. For example, copper ions in pigments such as azurite[1] have a great affinity for complexing amino acids. Others metal ions, including Hg^{2+}, Fe^{3+}, Ni^{2+},

* Corresponding author. Tel.: +39 050 2219 305; fax: +39 050 2219 260.
E-mail addresses: ggautier@artic.edu, gwen_claire@hotmail.com (G. Gautier).

[1] Azurite is composed of basic carbonate copper [$Cu(OH)_2{\cdot}2(CuCO_3)$], and was an important natural blue pigment during the Middle Ages, the Renaissance, and later on.

0039-9140/$ – see front matter © 2007 Elsevier B.V. All rights reserved.
doi:10.1016/j.talanta.2007.03.008

Ca^{2+}, Mg^{2+}, from pigments that may be present in paintings, can act the same way as copper ions. In addition, amino acids differ in their susceptibility to forming metal complexes, and consequently proteins subjected to aging will react differently relative to the type of pigments present. The above-mentioned interactions with cations may selectively substract some amino acids from the analysis or give rise to interferences during the analytical pre-treatment and thus may hamper the correct identification of the proteinaceous binder [13,14]. In fact, a decrease in the total recovery of proteins from paint layers has been related to the presence of these inorganic cations and may be due to the reduced solubility of the organic materials because of cross-linking reactions where cations may be active as catalysts and the formation of stable complexes with the amino acids [2,6,8,10,12–19]. It has been reported that the recovery of egg protein significantly decreases when gypsum, calcium oxalate or both are present [18].

For the reasons discussed so far, the identification of organic paint constituents and in particular proteinaceous paint media is still a real challenge for chemists. One of the main difficulties in the protein analysis lies in the isolation of the proteins from a heterogeneous sample. Analytical procedures based on chromatographic techniques have been suggested for the suppression of interferences due to the presence of inorganic species. These include the extraction of the proteinaceous matter by an ammonia solution [10], the use of a cation-exchange resin [6,10,11,16], or a chelating agent [12,20]. However, some issues still need to be resolved. For example, the ammonia extraction is not suitable for all types of pigments, and generally the desalting procedures used are quite laborious, time-consuming, and may lead to sample contamination and loss of analytes.

This paper focuses on the optimisation of an analytical procedure for the characterisation of the proteinaceous materials in wall painting samples and principally on the suppression of the copper-based pigment interferences in the identification of these materials. To achieve this goal, a clean-up system using a C18 micro-column has been adopted to optimise the published GC–MS procedure [19]. This step is generally used in methods to purify and enrich very low levels of peptides and/or proteins in the proteomics field, usually before MALDI-TOF analyses [21–25], and seems well suited to our case. To study the influence of the copper-based pigments on the amino acid determination and to validate the optimised procedure, a set of painted replicas based on three proteinaceous binders (egg, casein, and animal glue) and different concentrations of azurite was prepared. Finally, to test the effectiveness of the procedure including the purification step, it was used to analyse a sample from pictorial cycles of the crypt of Siena's Cathedral (Siena, Italy) containing high amounts of the interfering pigment azurite. Although the procedure was only studied with azurite, a sample from the wall painting of the Magdalena's Chapel in the National Museum of Bargello (Florence, Italy) containing cinnabar was also analysed in order to test the reliability of the analytical procedure in the presence of other possible interfering ions. In fact, the settled procedure allowed the binder identification while without the purification of the proteinaceous materials it was not possible to obtain any results.

2. Experimental

2.1. Reagents

All the solvents were Baker HPLC grade. Hexadecane (80 μg/g in isooctane), used as an internal standard, and *N-tert*-butyldimethylsilyl-*N*-methyltrifluoroacetamide (MTBSTFA) with 1% trimethylchlorosilane (TBDMCS) were purchased from Fluka (USA) and used without any further purification. Pyridine hydrochloride (PyHCl, purity 98%) was purchased from Sigma–Aldrich (USA) and used subsequent to desiccation without any further purification. A standard solution of amino acids in 0.1N HCl, was purchased from Sigma–Aldrich (USA), containing 12.5 μmol/mL of proline (Pro) and Hydroxyproline (Hyp), and 2.5 μmol/mL of aspartic acid (Asp), glutamic acid (Glu), alanine (Ala), arginine, cysteine, phenylalanine (Phe), glycine (Gly), hydroxylysine, isoleucine (Ile), histidine, leucine (Leu), lysine (Lys), methionine (Met), serine (Ser), tyrosine (Tyr), threonine, valine (Val). A bi-distilled water solution 80 μg/g of norleucine (Sigma–Aldrich (USA), purity 99%) used as derivatisation internal standard for amino acids was prepared, and stored at 4 °C. Alimentary casein and dried whole egg were purchased from Sigma–Aldrich (USA), and animal skin glue from Lefranc (France). The azurite used as pigment for the standard samples came from Zecchi (Florence, Italy). Pasteurised whole milk and fresh whole egg were bought at a local market.

2.2. Equipment

The Omix tip (C18 pipette tip) was purchased from Varian (Milan, Italy). It consists of a 100 μL pipette tip containing a miniaturised solid phase extraction bed of functionalised monolithic sorbent, with a capacity of 79 μg, inserted inside the tip.

The Solarbox (1500e RH), purchased from Erichsen (Germany), was used for aging the painted replicas. The conditions of exposure were 572 h at 20 °C, 50% relative humidity (RH), and a wavelength range of 295–400 nm.

A microwave oven model MLS-1200 MEGA Milestone (FKV, Sorisole (Bergamo,) Italy) was used for hydrolysis.

A 5890-Series II gas chromatograph (Hewlett Packard, Milan, Italy), equipped with an on-column injection port and a mass spectrometric detector mod. 5971 (electron impact 70 eV, ion source temperature 180 °C, interface temperature 280 °C) was used for the amino acid analysis. Chromatographic separation was performed with a chemically bonded fused-silica capillary column HP-5MS (Agilent Technologies, Palo Alto, CA, USA), stationary phase 5% phenyl–95% methylpolysiloxane, 0.25 mm internal diameter, 0.25 μm film thickness, 30 m length, connected to 2 m × 0.32 mm internal diameter deactivated fused-silica pre-column. The carrier gas was helium (99.995% purity) at a constant flow of 1.2 mL/min. The chromatographic conditions for the separation of silylated amino acids were as follows: initial temperature 100 °C, isothermal for 2 min, then 4 °C/min ramp up to 280 °C, and isothermal for 15 min. Chromatograms were recorded both in TIC (Total Ion

Table 1
Composition of the painted replicas

Sample	Whole milk	Whole egg	Animal glue	Azurite	Ratio protein: azurite
Casein					
A1	×	–	–	–	1:0
A2	×	–	–	×	3:1
A3	×	–	–	×	1:5
Egg					
B1	–	×	–	–	1:0
B2	–	×	–	×	3:1
B3	–	×	–	×	1:5
Glue					
C1	–	–	×	–	1:0
C2	–	–	×	×	3:1
C3	–	–	×	×	1:5

Current, mass range 50–600) and SIM (Single Ion Monitoring) mode.

2.3. Painted replicas

The painted replicas were prepared by using commercial whole milk, fresh whole egg, and animal glue. These binders were mixed with the azurite powder in various ratios (w/w) as reported in Table 1 before application on glass slides. Animal glue was dissolved in warm water; whole milk and whole egg were used without any treatment. Before sampling, the replicas were kept at room temperature for 1 week in the laboratory. Samples removed from the replicas were stored in glass vials in the dark.

Subsequent to sampling, the painted replicas were artificially aged in the Solarbox for 3 weeks prior to the removal of an "aged" set of samples. The average weight of the samples analysed was 0.4 mg.

2.4. Italian wall painting samples

Samples of wall paintings were collected from the crypt of the Cathedral of Siena and from the Magdalena's Chapel in the National Museum of Bargello (Florence).

The wall paintings of the Cathedral of Siena, which date to 1285 and are attributed to the great local artist Duccio di Buoninsegna (1255–1319), were uncovered in 2001 during excavations of the cathedral foundations and represent 180 m^2 of scenes of the *Passion* and *Resurrection of Jesus*. Since the wall paintings were protected from damaging dampness and light, the fading of the brilliant gold, purple, red and blue pigments has not occurred. Sample 63, described in Table 2, was taken from the sky of the scene of the "Crucifixion".

The pictorial cycle of the Magdalena's Chapel in the National Museum of Bargello (Florence, Italy) is one of the last masterpieces of Giotto (1332–1337). The cycle was notably expansive, about 500 m^2, of which 300 m^2 remain. Degradation of Giotto's work is evident mainly due to the harmful effect of water infiltrations and the lime applied on the paintings during the past. Sample 30, described in Table 2, was taken from the scene of the Paradise in the entrance of the Magdalena's Chapel.

In order to isolate the paint layers for analysis, samples collected from the wall paintings were further processed with the aid of a stereomicroscope to remove as much plaster as possible and then divided into two sub-samples in order to run the analysis in duplicate. An un-pigmented sample from the plaster was used as field blank sample.

2.5. Procedure

The analytical method used is based on a GC–MS procedure [19] where a clean-up step and an optimised derivatisation step for the protein analysis have been added. This part is summarised as follows:

1. *Ammonia extraction* [200 μL of NH3 2.5 M are used twice for 2 h at 60 °C in an ultrasonic bath]: Proteins contained in the sample were dissolved and separated from most of the inorganic salts that may be present.
2. *Clean-up of the proteinaceous materials*: In order to eliminate the inorganic salts that may have been dissolved in ammonia solution, the extracts were purified prior to hydrolysis. The ammonia extracts were dried under a nitrogen flow and admixed with 1% trifluoroacetic acid (TFA) solution up to a volume of 100 μL (this volume corresponds to the volume of the tip). The tip was pre-conditioned with a wetting and then an equilibration solution (50% acetonitrile (ACN)/water and 0.1% TFA solution, respectively). After conditioning, the sample solution was carefully loaded on the C18 pipette tip. The organic salts and other unretained compounds present passed through the tip, and were thus removed and discarded. The residual contaminants that might be weakly bound to the sorbent material were washed later from the tip with a slightly acidic water rinse using a 0.1% TFA solution. The wash (100 μL) was repeated twice. Finally, the target proteinaceous material was eluted into a vial with a slightly acidic, aqueous-organic solvent (75% ACN/water/0.1% TFA). The complete purification procedure takes less than 5 min to perform.
3. *Hydrolysis*: The content of the vial was dried under nitrogen flow and the residue was subjected to microwave-assisted vapour-phase acidic hydrolysis [35 mL of HCl 6 M; T = 160 °C; time = 10 min at power 250 W, time = 30 min at

Table 2
Description of the wall painting samples

Sample	Provenance	Description	Pigment	Sample weight (mg)
63	Crypt of the Cathedral of Siena	Fragment of the blue sky on the right of the cross	Azurite, malachite [26]	1.4
30	Bargello's National Museum	Wall Paradise: Bright red cloche of an ecclesiastic	Cinnabar, red ochre [27]	0.6

power 500 W]. After the hydrolysis, 50 μL of bi-distilled water was added to the sample. The acidic solution contains free amino acids.

4. *Derivatisation*: An aliquot of the acidic solution was transferred to a clean vial. To this 5 μL of 80 μg/g norleucine solution, the derivatisation internal standard, was added. Contents were evaporated to dryness under a stream of nitrogen and were subjected to derivatisation with 50 μL of the silylating solution [300 μL of *N*-methyl-*N*-(*t*-butyldimethylsylil)trifluoroacetamide) (MTBSTFA) + 1% TBDMCS, 700 μL of pyridine (solvent), 28 mg of pyridine hydrochloride (PyHCl)]. The derivatisation was performed at 60 °C for 30 min. After the addition of 5 μL of an 80 μg/g hexadecane solution, to serve as the injection internal standard, 2 μL were analysed by GC–MS. Quantification of 14 amino acids (Ala, Gly, Val, Leu, Ile, Pro, Met, Ser, Phe, Asp, Hyp, Glu, Lys, Tyr) was performed by means of calibration curves. All data are expressed in mole percentages.
5. *Protein identification*: In order to characterise the proteinaceous binders, the data evaluation was based on the use of the multivariate statistical method principal component analysis (PCA) [6]. Relative percentage values of amino acids were processed using XLSTAT 6.0 (Addinsoft, France). The first two components account for 81.5% of the variance. The database used for the clustering, reported in the literature [6], considers the following eleven amino acids: Ala, Gly, Val, Leu, Ile, Pro, Ser, Phe, Asp, Hyp, Glu.

3. Results and discussion

3.1. Analysis of the painted replicas

In order to study the influence of the copper-based pigment azurite on the quantification of amino acids, samples from the set of painted replicas were analysed without performing the clean-up step. Fig. 1 reports the chromatograms of samples from egg-bound painted replicas with different concentrations of azurite. The interference of copper ions on amino acid recovery is evident from the decrease in peak intensities with increasing proportions of azurite. The internal standard, norleucine, is affected the same way. Its recovery in the presence of copper salts seems also dependent on the protein analysed: it is more likely that the concentration of free copper ions in solution changes as a function of the type of protein present so that different amounts of norleucine–copper complexes are formed even if the same concentration of copper salts is present in the reference painted replica. The behaviour of the internal standard highlights that copper ions strongly complex the amino acids in the acidic solution and that the subsequent derivatisation reaction with MTBSTFA is partially hampered: basically the norleucine concentration decreases with the increasing concentration of the pigment. The extent of norleucine recovery is an index of the pigment interference in the derivatisation reaction. Fig. 2 clearly shows that the presence of a high proportion of azurite relative to the proteinaceous binder causes a significant decrease in the norleucine recovery.

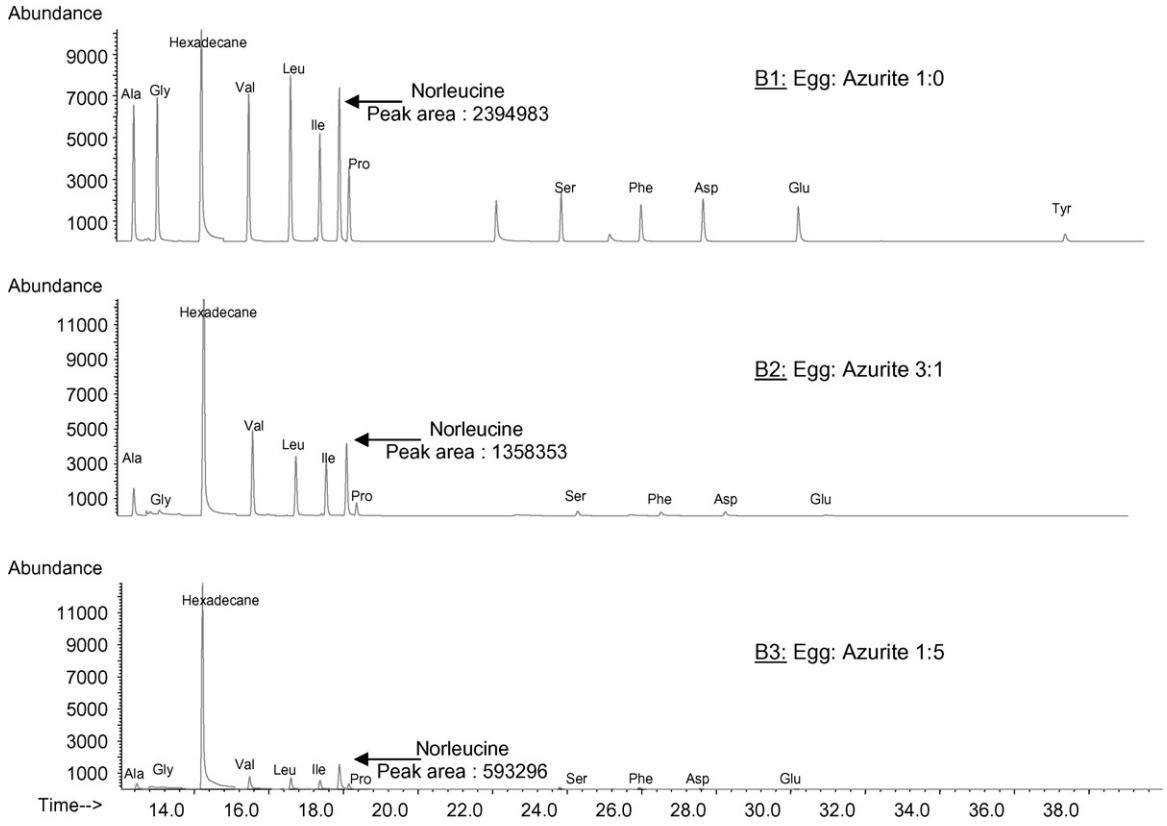

Fig. 1. Chromatograms, acquired in Single Ion Monitoring (SIM), of the painted replicas samples containing egg using the procedure without purification.

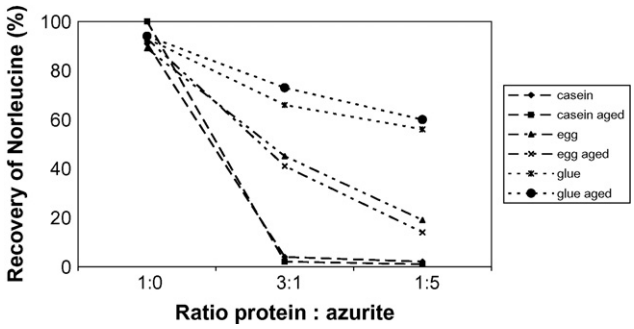

Fig. 2. Norleucine recoveries in the painted replicas samples using the procedure without purification.

An inspection of the relative mole percentages of amino acids in the painted replica samples allows the following conclusions to be drawn:

1. As far as the unaged and aged pure materials are concerned, the amino acid data are in agreement with those cited in the literature; however, in the aged binders, the most labile amino acids – lysine (Lys) and tyrosine (Tyr) – are highly depleted [28].
2. In the replica samples containing azurite, glycine (Gly), aspartic (Asp) and glutamic (Glu) acids are the amino acids most affected by the presence of the pigment. The intensities of chromatographic peaks for the above amino acids drastically decreased, if not disappeared, with an increase in the concentration of azurite. In samples from the aged replicas, Ser and Phe were also affected by the pigment interference in addition to Gly, Asp, and Glu. These amino acids are essential for the correct identification of the proteinaceous matter: Gly being present in high concentrations in collagen, and Asp and Glu being crucial to distinguishing between casein and egg proteins.

While aging itself does not influence the identification of a protein [13], a large amount of azurite may lead to incorrect conclusions using the suggested statistical data analysis. The PCA score plot (Fig. 3) shows the various effects that the increasing concentration of azurite may have on protein identification. Our observations are that:

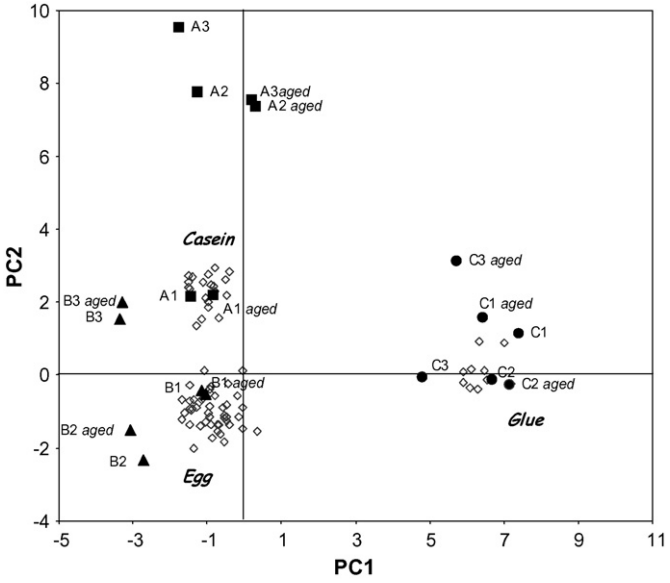

Fig. 3. PCA score plot of the painted replicas samples analysed using the procedure without purification (the white diamonds are the reference data base, and the solid diamonds are the actual data).

- The identification of the casein binder is possible only in absence of azurite; all the samples containing azurite are located far away from the casein cluster.
- The egg samples without azurite are perfectly located in the respective cluster. Even though 30% of azurite is present, the identification of egg protein is plausible based on their relative proximity to the reference cluster. However, higher concentrations of azurite clearly prevents proper identification.
- The glue binder may be correctly identified in all cases although the respective cluster results more scattered. This is mainly due to the presence of hydroxyproline (marker of the animal glue), which has a high loading value and PCA scores do not seem to suffer excessively due to interference from copper.

Table 3
Relative amino acid mole percentages of the set of samples containing egg

Sample	B1 omix	B2 omix	B3 omix	B1 aged omix	B2 aged omix	B3 aged omix
Ala	12.7	11.1	12.6	12.3	11.0	9.3
Gly	10.8	8.6	10.2	10.7	9.9	11.9
Val	11.8	11.4	11.5	9.2	10.0	10.8
Leu	14.9	12.3	11.8	11.6	11.3	13.4
Ile	8.3	8.6	8.3	7.5	7.9	9.2
Met	0.0	0.0	0.0	0.0	0.0	0.0
Ser	7.1	9.2	7.4	9.3	9.8	9.4
Pro	4.8	4.2	2.3	9.0	5.4	3.8
Phe	6.1	6.8	7.3	6.8	7.1	7.6
Asp	11.2	9.6	8.2	9.2	10.7	9.7
Glu	11.7	11.9	11.6	8.9	10.0	9.2
Lys	0.6	6.1	8.8	5.1	6.5	4.8
Hyp	0.0	0.0	0.0	0.0	0.0	0.0
Tyr	0.0	0.0	0.1	0.5	0.5	0.9

The same set of painted replica samples was analysed using the protocol that includes the clean-up step of the proteinaceous materials. The relative mole percentages of amino acids of samples from the egg-bound painted replicas are reported in Table 3 (the values are the average on three replicates). The amino acid profiles obtained are similar to the expected ones [28]. The amino acid percentages were subjected to the statistical method of the principal components analysis. Fig. 4 clearly shows that inclusion of the purification step results in the location of samples in their respective reference data clusters.

In conclusion, the analyses show that the incorporation of the purification step during sample preparation eliminates interferences from salts and pigments. A reliable identification of the proteinaceous matter is always achieved, even where there is extremely low protein content and high levels of inorganic salts. However, it should be noted that the recovery of proteinaceous materials tested in the absence of azurite is rather low under these experimental conditions. Inclusion of the purification step results in a decrease of recovery from about 80% to less than 10%. Experiments are in progress to increase the recovery rate.

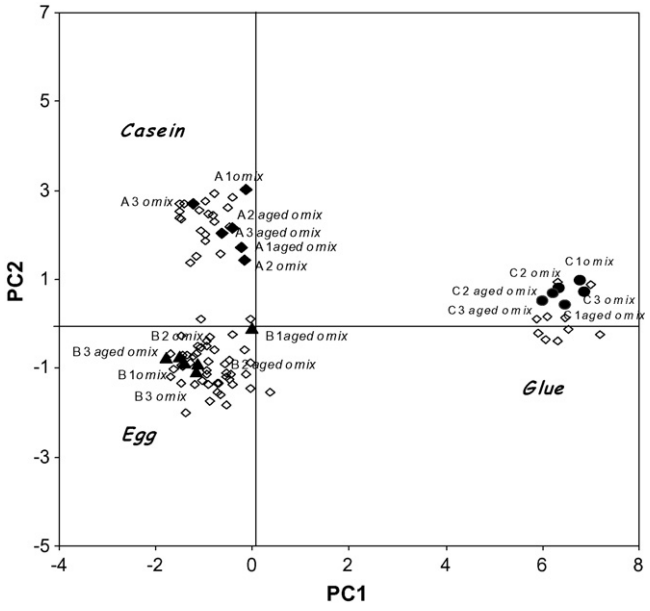

Fig. 4. PCA score plot of the painted replicas samples analysed using the optimised procedure (the white diamonds are the reference data base, and the solid diamonds are the actual data).

3.2. Analysis of Italian wall painting samples

The protocol involving the clean-up step was used to analyse samples from two Italian wall paintings: sample 63 from

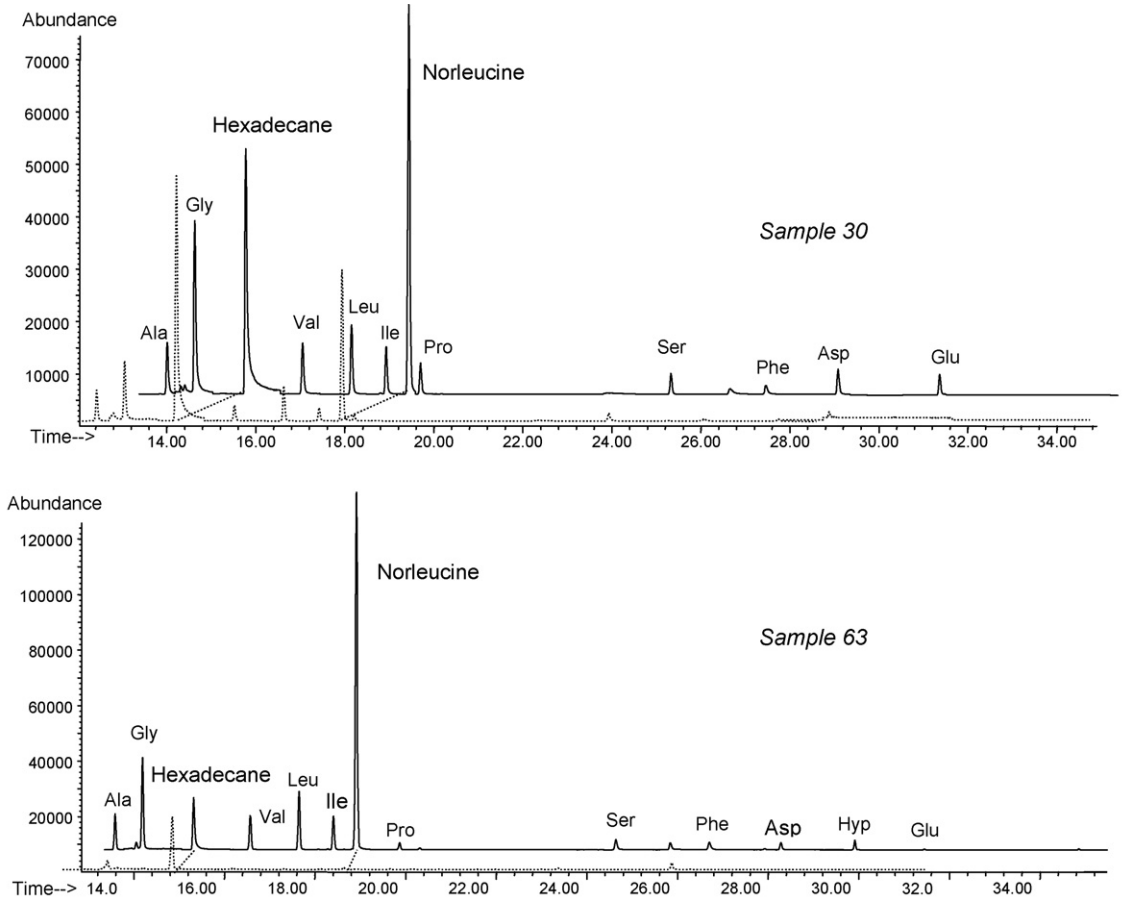

Fig. 5. Chromatograms, acquired in Single Ion Monitoring (SIM), of samples 63 and 30 analysed with the optimised procedure (solid line, above) and the not optimised one (dotted line, below).

Table 4
Relative amino acid mole percentages of the samples from the Italian wall paintings analysed with the optimised analytical procedure

Sample	63	30
Ala	26.1	11.0
Gly	24.8	19.3
Val	9.2	8.4
Leu	9.8	9.7
Ile	7.0	7.0
Met	0.0	0.0
Ser	8.5	10.0
Pro	1.4	8.5
Phe	2.8	4.5
Asp	3.2	11.6
Glu	6.1	9.8
Lys	0.5	0.0
Hyp	0.1	0.0
Tyr	0.5	0.2
Σ of the 14 amino acids recovered (μg)	0.46	0.38

the crypt of Siena's Cathedral and sample 30 from the National Museum of Bargello (Florence). Although sample 30 did not contain a copper-based pigment, it was included in this study since no result was obtained when analysed without the purification step, that is the derivatisation of its amino acid content was hampered. This was due to the high amount of mercury that may cause severe interferences.

Fig. 5 shows the chromatograms resulting from the analysis of samples prepared with (solid line) or without (dotted line) the purification step. Protein identification without the clean-up step was not possible for either sample due to the interference caused by the very high amounts of copper and mercury, as highlighted by the low recovery of norleucine. Table 4 reports the relative mole percentages of amino acids calculated for samples 63 and 30 analysed with the optimised analytical procedure and the protein content corresponding to the sum of the quantified amino acids expressed in μg.

The protein content recovered in the field blank sample (plaster sample) was less than 0.2 μg. Conversely, the protein content recovered from wall painting samples 63 and 30, as reported in Table 4, are 0.46 and 0.38 μg, respectively. Based on the analysis of laboratory blanks, the detection and quantitation limits of the protein content of the analytical procedure were determined to be 0.19 and 0.36 μg, respectively (at statistical significance levels of 0.05). Since the protein content of the field blank was the same as the detection limit, the proteinaceous material recovered was attributed to the environmental contamination. Since protein recovery from samples 63 and 30 exceeded the quantitation limit, the presence of proteinaceous matter may therefore be attributed to the sample. Examination of the amino acid percentages reported in Table 4 suggests the use of animal glue in sample 63 based on the presence of hydroxyproline (Hyp) along with a very high amount of glycine (Gly). However, relatively high amounts of valine (Val), leucine (Leu), and isoleucine (Ile) indicate the presence of another proteinaceous binder as well. The amino acid profile of sample 30 was very close to the profile of an egg protein, although with a notably high amount of Gly.

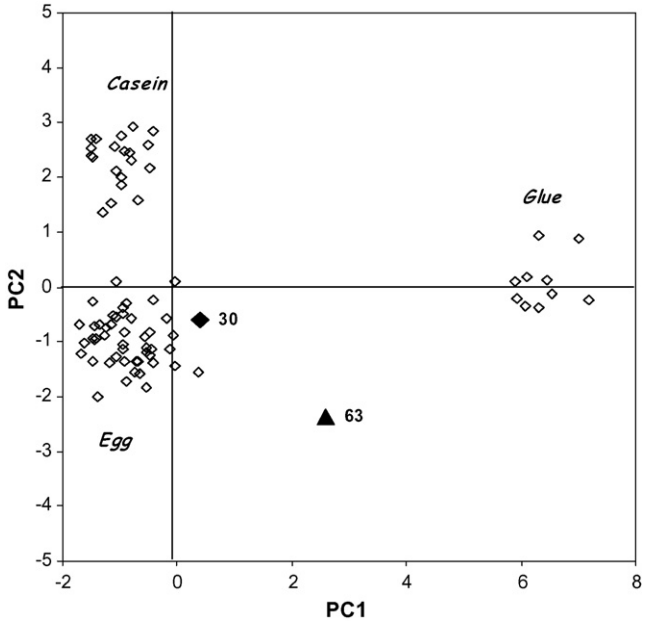

Fig. 6. PCA score plot of the two samples from the Italian wall paintings (the white diamonds are the reference data base, and the solid diamonds are the actual data).

PCA scores were calculated for both samples and compared with those of reference materials. The PCA score plot locates sample 63 between the clusters of glue and egg binders (Fig. 6). Again, this might be explained by the presence of both types of proteinaceous matter. As far as sample 30 is concerned, the PCA scores allow the classification of the binder as an egg protein. The recovery of a relatively high amount of protein and the absence of Hyp further help in ruling out the presence of glue binder.

The application of the clean-up step to the analysis of sample 30 allowed the identification of the proteinaceous binder. This result is very interesting as it highlights the effectiveness of the purification regarding other pigments as it was expected. In fact, the clean-up step is based on the fact that proteins are bound to the C18 stationary phase of the pipette tip whereas inorganic salts are un-retained. Nevertheless, experiments on samples containing different pigments is still in progress, the optimised procedure seems to be an excellent method to eliminate interferences from salts in the protein characterisation.

4. Conclusions

The study of works of art and cultural heritage frequently demands that conservation scientists develop and use advanced analytical procedures due to the small size of samples, their structural complexity and state of degradation. This paper fulfils the goal of reliably characterising proteinaceous media in wall paintings by overcoming interferences due to the presence of high concentration of azurite and the method appears very promising regarding other types of inorganic salts. The quantitative recovery of glycine, aspartic and glutamic acids has been found to suffer the most from the presence of azurite. As these amino acids are important in the calculation of PCA scores,

errors in their quantification hamper the correct identification of the proteinaceous binder.

Interference from pigments is eliminated by the introduction of a new step that purifies the proteinaceous materials by means of the C18 pipette tip. The clean-up step is quite rapid – it can be completed in less than 5 min – and is highly effective, considering that it allows the identification of proteins in samples from wall painting, even when the concentration of salts is extremely high. The optimised procedure was applied to the study of samples from historic wall paintings in Siena and Florence. It evidenced the presence of a mixture of egg and animal glue in the sample containing azurite, and egg in the sample containing mercury, showing the effectiveness of the procedure not only on samples containing copper-based pigments.

Acknowledgments

The authors would like to thank the Prof. Guasparri and Dr. Lanterna (Opificio delle Pietre Dure, Florence) for providing the wall painting samples from the crypt of the Cathedral of Siena and from the Magdalena's Chapel in the National Museum of Bargello (Florence).

References

[1] R.J. Gettens, G.L. Stout, "Painting Materials", A Short Encyclopaedia, Dover, New York, 1966.
[2] J.S. Mills, R. White, The Organic Chemistry of the Museum Objects, Butterworths, London, 1987.
[3] C. Cennini, Il Libro dell'Arte (XIV) sec., in: R. Simi, Barabba (Ed.), Lanciano, 1932.
[4] F. Ronca, Stud. Conserv. 39 (1994) 107–120.
[5] R. White, Natl. Gallery Tech. Bull. 8 (1984) 5–14.
[6] M.P. Colombini, R. Fuoco, A. Giacomelli, et al., Sci. Technol. Cult. Heritage 7 (1) (1998) 9–58.
[7] J. Wouters, M. Van Bos, K. Lamens, Stud. Conserv. 45 (2000) 169–179.
[8] M.P. Colombini, G. Gautier, A. Casoli, E. Campani, M. Schilling, J. Mazurek, Proceedings of the Organic Materials in Wall Paintings Workshop & Symposium, Turin, Italy, May 8th–12th, 2006.
[9] J.J. Boon, S.L. Peulvé, O.F. Van den Brink, et al., Proceedings of Early Italian Paintings Techniques and Analysis Symposium, Maastricht, October 9–10, 1996, pp. 35–56.
[10] M.P. Colombini, F. Modugno, A. Giacomelli, J. Chromatogr. A 846 (1999) 101–111.
[11] S.M. Halpine, Conserv. Res. 51 (1995) 28–69.
[12] J. De la Cruz-Cañizares, M.T. Doménech-Carbó, J.V. Gimeno-Adelantado, et al., J. Chromatogr. A 1025 (2) (2004) 277–285.
[13] M.P. Colombini, F. Modugno, J. Sep. Sci. 27 (2004) 147–160.
[14] M.R. Schilling, H.P. Khanjian, J. Am. Inst. Conserv. 35 (1996) 123–144.
[15] M.R. Schilling, H.P. Khanjian, L.A.C. Souza, J. Am. Inst. Conserv. 35 (1996) 45–59.
[16] E. Kenndler, K. Schmidt Beiwl, F. Mairinger, et al., Fresenius J. Anal. Chem. 342 (1992) 135–141.
[17] J. Wouters, M. Van Bos, K. Lamens, Stud. Conserv. 45 (2000) 106–116.
[18] L. Rampazzi, A. Andreotti, I. Bonaduce, et al., Talanta 63 (2004) 967–977.
[19] A. Andreotti, I. Bonaduce, M.P. Colombini, G. Gautier, F. Modugno, E. Ribechini, Anal. Chem. 78 (2006) 4490–4500.
[20] S.L. Vallance, B.W. Singer, S.M. Hitchen, LC–GC Int. 15 (1997) 48–53.
[21] R. Strong, "A comparative proteomic analysis of mitochondrial proteins from drug susceptible and drug resistant human MCF-7 breast cancer cells", University of Maryland, College Park (USA), PhD, 2005.
[22] T. Bączek, J. Pharm. Biomed. Anal. 34 (2004) 851–860.
[23] R. Tummala, P.A. Limbach, Anal. Chim. Acta 551 (2005) 137–141.
[24] D.E. Terry, E. Umstot, D.M. Desiderio, J. Am. Soc. Mass Spectrom. 15 (2004) 784–794.
[25] R.U. Halden, D.R. Colquhoun, E.S. Wisniewski, Appl. Environ. Microbiol. 71 (2005) 2442–2451.
[26] L. Rampazzi, F. Cariati, G. Tanda, et al., J. Cult. Heritage 3 (2002) 237.
[27] G. Lanterna, C. Lalli, M. Rizzi, I. Tosini, Proceedings of the Congress Scienza e Beni Culturali XXI: "Sulle pitture murali, Riflessione, Conoscenze, Interventi", Arcadia Ricerche Editions, Bressanone (Italy), July 12–15, 2005.
[28] M.P. Colombini, F. Modugno, E. Menicagli, et al., Microchem. J. 67 (2000) 291–300.

Available online at www.sciencedirect.com
ScienceDirect
Talanta 73 (2007) 37–45
Talanta
www.elsevier.com/locate/talanta

High selective SiO_2–Al_2O_3 mixed-oxide modified carbon paste electrode for anodic stripping voltammetric determination of Pb(II)

M. Ghiaci, B. Rezaei *, R.J. Kalbasi

Department of Chemistry, Isfahan University of Technology, Isfahan 84156, Iran

Received 28 October 2006; received in revised form 19 February 2007; accepted 20 February 2007
Available online 23 February 2007

Abstract

The main purpose of this study is to develop an inexpensive, simple, selective and especially highly selective modified mixed-oxide carbon paste electrode (CPE) for voltammetric determination of Pb(II). For the preliminary screening purpose, the catalyst was prepared by modification of SiO_2–Al_2O_3 mixed-oxide and characterized by TG, CHN elemental analysis and FTIR spectroscopy. Using cyclic voltammetry the electroanalytical characteristics of the catalyst have been determined, and consequently the modified mixed-oxide carbon paste electrode was constructed and applied for determination of Pb(II). The electroanalytical procedure for determination of the Pb(II) comprises two steps: the chemical accumulation of the analyte under open-circuit conditions followed by the electrochemical detection of the preconcentrated species using differential pulse anodic stripping voltammetry. During the preconcentration step, Pb(II) was accumulated on the surface of the modifier by the formation of a complex with the nitrogen atoms of the pyridyl groups in the modifier. The peak currents increases linearly with Pb(II) concentration over the range of 2.0×10^{-9} to 5.2×10^{-5} mol L^{-1} ($r^2 = 0.9995$).

The detection limit (three times signal-to-noise) was found to be 1.07×10^{-9} mol L^{-1} Pb(II). The chemical and instrumental parameters have been optimized and the effect of the interferences has been determined. The Proposed method was used for determination of lead ion in the real samples.

Keywords: Modified SiO_2–Al_2O_3 mixed-oxide; Organically modified carbon paste electrode; Voltammetry; Preconcentration; Lead(II)

1. Introduction

Among heavy metals, lead is the most commonly encountered toxic pollutant in the environment as a result of its current and previous use in batteries, gasoline, and paints. Lead is known to cause health problems, such as digestive, neurological, cardiac, and mental troubles. Several techniques have been employed for such a purpose [1]. The electrochemical techniques are considered to be low cost, simple, accurate and fast. Anodic stripping voltammetry (ASV) has been widely used for measurement of heavy metals in various samples because of its remarkably low (pg/mL) detection limits [2–4]. Other advantageous features of stripping voltammetry include the capability for simultaneous multi-element determination and instrumentation that is relatively inexpensive when compared to that required for many of the spectroscopic techniques used for trace metal analysis. In addition, the possibility of having portable and compact instruments for stripping analysis and their low power needs make them attractive for onsite monitoring of trace metals, such as lead.

Derivatization of inorganic solids with organofunctional groups was widely studied and successfully applied in many divergent areas of research [5,6]. This synthetic route is still the subject of considerable interest due to the numerous possibilities of designing new materials, especially by exploiting the versatility of sol–gel chemistry [7,8]. The covalent linkage of organic moieties to silica-based materials resulted in organic-inorganic hybrid solids which were so-called ormosils (organically modified silicates). In contrast to functional polymers, ormosils have several advantages such as better mechanical stability, higher concentration of the chelating groups at the substrate surfaces, higher specific surface area, and moreover inorganic materials are often cheaper than their organic counterparts. Various preparation methods of ormosils were reported. Basically they

* Corresponding author. Tel.: +98 311 3912351; fax: +98 311 3912350.
E-mail address: rezaei@cc.iut.ac.ir (B. Rezaei).

0039-9140/$ – see front matter © 2007 Elsevier B.V. All rights reserved.
doi:10.1016/j.talanta.2007.02.026

can be classified into two main categories: the direct grafting of the organofuctional groups onto the silica surface using silanol (or even siloxane) groups [9]; and one-pot synthesis of functionalized silicas from a mixture of tetraalkoxysilanes and organosilanes [7]. Of course these primary procedures can be completed by various secondary modifications (i.e. chemical or thermal treatments). The chemical modification of silicas was thoroughly reviewed by Vansant et al. [9]. Recently, substantial advances were achieved in this field after the discovery of a new family of mesoporous silicas (as well as aluminosilicates) featuring cylindrical regular mesopores of monodispersed diameter [10]. Especially, pure silica MCM-41s were prepared and further modifed by grafting organofunctional groups onto their internal surfaces [11,12]. More recently, the one-pot synthesis of functionalized MCM-type silicas was also reported [13,14]. Ormosils have provided numerous analytical applications as selective adsorbents [13], stationary phases in chromatography [15], electrochemical oxidation [16], hydrazine determination [17] or for preconcentration of trace metals [18], in heterogeneous catalysis [19], as well as in biochemistry as immobilization supports for enzymes [20,21].

Aminosilane is the most widely used compound of the organosilane family [13]. Among many other applications, polysiloxane-immobilized amine ligands were used for the preconcentration of trace metals from natural waters [22,23]. To date, most of the work in this field has been made on amine-grafted silica gel, and it has mainly applied to the uptake of copper species. The binding capacity of aminated silica gels for copper was related to the primary amine content [24]. In this case, however, the extent of metal preconcentration was limited either by the amount of grafted ligand or by the restricted accessibility to the chelating sites. It appears therefore interesting to investigate other aminated silicas displaying either higher ligand loadings (as those obtained from the condensation of tetraalkoxysilanes and trialkoxysilylpropylamine) or regular pore channels allowing unrestricted access of the analyte to all the functional sites (as aminated MCM-41).

In recent years, chemically modified electrodes (CMEs) were used for the voltammetric quantification of various organic and inorganic species after their open circuit accumulation [25,26]. Much of the work in this field was directed to exploit the chemical reactivity of the modifier towards a target analyte for electroanalytical purpose. Multitudes of modifying agents were used either as coatings on solid electrode surfaces or dispersed within a conductive matrix. It is noteworthy that this last approach is well suited when using electronically insulating modifiers requiring a direct contact to an electronically conducting substrate as used in connection with electrochemistry. The application of silicates and related mineral materials in electrochemistry is rather recent and was directed to combine their intrinsic properties to selected electrochemical reactions in order to improve the response of the electrode. In doing so, clay, zeolite and silica-modified electrodes were prepared, characterized and applied (sometimes tentatively) in various fields including for example electroanalysis and sensors, electrocatalysis, photochemistry, thin-film technology, fuel cells, molecular recognition. Many of these investigations are reported in several recent reviews and papers [27–31]. Silicates continue to stimulate attention from electrochemists, as expressed by many recent papers [32–34], indicating a marked actual tendency to exploit the versatility of sol–gel chemistry in designing new modified electrodes mainly based on organically modified silicates.

Chemically modified carbon paste electrodes (CMCPE's) are especially useful in the determination of traces of metal species and organic compounds. The analyte is first bound at the electrode surface via a non-electrochemical interaction with the embedded modifier, e.g. chemical reaction or adsorption process, so that a sensitive and/or a selective accumulation are achieved. Usually modifiers for the determination of metal cations are organic polymers [35], complexing agents [36,37], ion exchangers [38], crown ethers [39] or minerals [40,41]. Normally the modifier is directly embedded in the paste of the electrode, which consists of a homogeneous mixture of graphite and nujol [25].

A limited number of studies on the use of CMCPEs for voltammetric determination of Pb(II) have been reported. These are CPEs modified with dibenzo-18-crown-6 and cryptand [39], lichen [42], moss [43], benzoin oxime [44], 1-(2-pyridylazo)-2-naphthol and Nafion [45], and *N*-*p*-chlorophenylcinnamohydroxamic acid [46]. However, some of these modified CPEs require additional steps for their preparation [42,43,45] or require a medium exchange [46]. While the most modified CPE requires longer accumulation time (15 min) [43], lichen modified CPE requires longer renewal time (5 min) and has a high detection limit (2×10^{-5} mol L^{-1}) [42], dibenzo-18-crown-6 and cryptand modified CPEs [39] have higher detection limits (1×10^{-6} and 0.5×10^{-6} mol L^{-1}, respectively), and 1-(2-pyridylazo)-2-naphthol and Nafion modified CPE require longer accumulation times (8 min), suffer from leaching, and their regeneration requires recoating of the electrode surface [45]. Furthermore, no systematic interference studies have been made on some of these methods and have not been applied to the determination of lead in real samples [42,45].

This study proposed a new modified supported reagent on SiO_2–Al_2O_3 mixed-oxide. Among different application for this new catalyst, we would like to report a new modified carbon paste electrode which has been prepared by the supported catalyst. It has shown a selective preconcentration and quantization of Pb(II) by differential pulse anodic stripping voltammetry. This study has led to the development of a new modified electrode for the determination of Pb(II) with improved qualities compared to the previous studies [39,42,47–49] such as simplicity of electrode preparation, wider linear range, low detection limit, high selectivity and very good stability of modifier.

The TG, CHN and FTIR were employed to characterize the properties of the supported catalysts.

2. Experimental

2.1. Reagents

Di-2-pyridylketone (Aldrich), Aluminiumtri-*sec*-butylate, trimethoxy silyl propyl amine (both from Merck), 2,4-pentandione (Merck), tetraethyl orthosilicate (Acros), Spectral

carbon powder, nitric acid, lead nitrate (Merck) and paraffin oil (Fluka) were used as received. All other chemicals used were of analytical reagent grade (from Merck, Aldrich or Fluka) and deionized double distilled water was used throughout.

2.2. Instrumentation

A MCPE as working electrode and a standard Ag/AgCl (3 M NaCl) reference electrode, were used in selected experiments. A platinum wire auxiliary electrode and a 75 mL glass electrochemical cell were utilized in selected experiments. Electrochemical measurements were done with a galvanopotentiostat Behpajooh Co. model BHP2063+. A Metrohm pH-meter (model 691) was used for the pH measurements. Thermal gravimetric analysis (TGA) data for the organic compounds were obtained by a Mettler TGA-50 under air atmosphere at a rate of 10 °C/min. Elemental analysis was performed by a CHN-O-Rapid Heraeus elemental analyzer (Wellesley, MA). FT-IR spectra were recorded by an FT-IR spectrophotometer (Jasco-680, Japan). The spectra of solids were obtained using KBr pellets. The vibrational transition frequencies are reported in wave numbers (cm^{-1}).

2.3. CPEs and MCPEs preparation and analytical procedures

The unmodified CPEs were prepared as follows: 5 g of reagent-grade graphite powder was taken, washed with ethanol and dried under vacuum which was then mixed with 3 mL of Nujol. To modify the CPEs, the graphite powder was mixed with modifier in various composition ratios, which were 0.0, 2.0, 4.0, 6.0, 8.0, 10.0 and 14.0% (w/w) of modifier to graphite powder. Both unmodified and modified CPEs were packed into a 1 mL disposable polyethylene syringe (5.0 mm, i.d.) that had been cut off at the end. Electrical contact to the paste was established via a thin Pt wire passed through the syringe piston. The fresh surfaces were obtained by polishing the electrode on a clean paper until they showed a smooth and shiny appearance after every measurement.

2.4. Recommended procedure

SiO_2–Al_2O_3 (1/1) was used as the support. This support was prepared by the sol–gel method. Aluminum tri-*sec*-butylate (97%) and tetraethyl orthosilicate (98%) were used as the precursors, and 2,4-pentandione (H-acac) as the complexing agent. Appropriate amounts of Aluminum tri-*sec*-butylate and tetraethylorthosilicate were dissolved in the solvent, *n*-butanol. The solution was heated to 60 °C. The components were thoroughly mixed. Then the solution was cooled down to room temperature, and H-acac as the complexing agent was added. This clear solution was hydrolyzed with deionized water (11.0 mol H_2O/mol alkoxide). The solutions were left overnight to hydrolyze the alkoxides, yielding transparent gels. The transparent gels were dried at 110 °C to remove water and solvent, and then calcined at 500 °C for 5 h to remove the organics. The support is denoted as SiO_2–Al_2O_3 (1:1).

SiO_2–Al_2O_3 (1:1)-supported aminopropyl (compound **1**)was prepared by refluxing SiO_2–Al_2O_3 (1:1) (5.2 g) with various volumes of trimethoxysilylpropylamine (5.7 mL, 7.0 mL, 10.5 mL and 12.0 mL) in dry dichloromethane (100 mL) for 24 h. The solid was filtered off, washed with methanol and dried at 100 °C.

Then we added di-2-pyridyl ketone and a catalytic amount of acetic acid to a suspended solution of SiO_2–Al_2O_3 (1:1)-supported aminopropyl in dry methanol. The mixture was refluxed for 24 h to make a Schiff base (compound **2**) on the surface of the mixed-oxide (a bi-dentate ligand). This Schiff base introduces sites for interaction of the metal pollutants with the catalyst. On the other hand the Schiff base is active on the surface of the electrode, so it can attend in electrochemical reactions.

Consequently the mixed-oxide carbon paste electrodes were constructed using different ratio of mixed-oxide and carbon paste, and used for determination of Pb(II). The cyclic voltammetry has been applied from 0.000 to −1.100 V versus Ag/AgCl with scan rate of 100 mv/s. The instrumental and chemical conditions were optimized. The cyclic voltammograms were obtained in nitric acid solution (pH 3.05), the preconcentration time and accumulation potential were determined to be 360 s and −0.500 V versus Ag/AgCl reference electrodes, respectively.

3. Results and discussion

3.1. Characterization

In a part of this work we have investigated the reaction of di-2-pyridyl ketone with monolayer of trimethoxysilylpropylamine

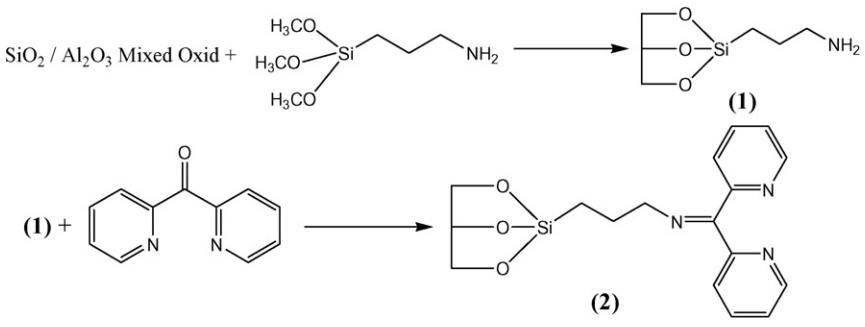

Scheme 1.

(TMSPA) formed on amorphous SiO_2–Al_2O_3 mixed-oxide (Scheme 1). Infrared spectroscopy serves as a main investigation tool, supported by TG, and elemental analysis.

It is shown that attachment proceeds by formation of imine at the di-2-pyridyl ketone (DPK) carbonyl group. Moreover, the thermal stability of resultant TMSPA-DPK monolayer was investigated by TG with view to identify routes for further applications.

Investigation of mid-IR spectra of aluminosilicate powder before modification, after modification with TMSPA, and after further reaction with DPK shows a notable changes associated with TMSPA modification including weakening of free silanol O–H stretch at 3744 cm^{-1}, consistent with formation of TMSPA–silicate siloxane bonds, and appearance of primary amine stretches at 3303 and 3370 cm^{-1}, C–H stretch bands in the 2800–3000 cm^{-1} region and, less prominently, NH_2 bend at 1600 cm^{-1}, CH_2 bend at 1470 cm^{-1}, and Si–CH_2 bend at 1412 cm^{-1}. Spectral features arising from subsequent powder modification with DNK are discussed below.

The attachment mechanism between DNK and TMSPA monolayer was investigated using IR spectroscopy. The –N–H stretch doublet became very week, signifying near complete absence of primary amines. This observation is attributed to their incorporation into imine bonds with DNK residues. The aromatic C–H stretching at 3100 and 3080 cm^{-1} and the band at 1580 cm^{-1} are attributed to the aromatic moieties of DNK residues. The band appeared at 1660 cm^{-1} is also attributed to the stretching vibration of the C=N bond.

Elemental analysis showed that the addition of DNK to surface amines was not stoichiometric; rather, DNK coverage was consistently less than that of TMSPA (the nitrogen content of the catalyst was 5.1 wt.% after loading the surface with TMSPA and 9.1 wt.% after formation of the Schiff base). From these data one can calculate that the luminosilicate support bearing 1.1×10^{-2} TMSPA residues/nm^2, and after reaction with sufficient DNK, creating 6.5×10^{-3} molecules of Schiff base/nm^2 of powder surface.

The DTG curves of the various samples have been investigated. The TMSPA–SiO_2–Al_2O_3 sample shows three separate weight loss steps. The first, small (around 6%, w/w) step appearing at temperature <150 °C corresponds to the release of water (i.e., adsorbed water on the inner and outer surface). The second step (about 150–350 °C) can be attributed to the water loss from the condensation of adjacent Si–OH groups to form siloxane bonds (around 5%, w/w). The third weight-loss (about 360–590 °C) amounts around 15% (w/w) is related to the decomposition of the TMSPA moiety. The main oxidative desorption of the TMSPA takes place in the range of 450–485 °C. The DTG curve of TMSPA–DPK–SiO_2–Al_2O_3 sample also shows three weight loss steps, however the heights of them are different. The first step amounts around 4% (w/w), which is about that for the sample TMSPA–SiO_2–Al_2O_3, discussed previously. From this it might be suggested that the organic template has not been released in this step. Probably the decomposition of the Schiff base starts at about 200 °C and the weight-loss from this temperature to 692 °C is around 30% (w/w).

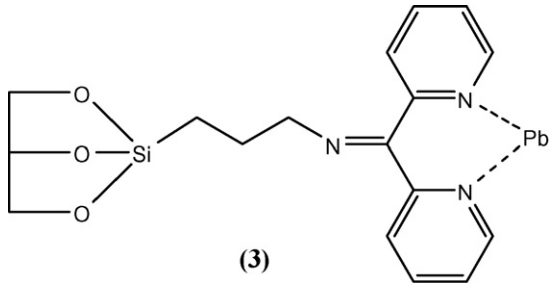

(3)

Scheme 2.

3.2. Adsorptive and voltammetric characteristics of the Pb(II)-modifier complex

The active sites for the interaction of the mixed-oxide with metals have been shown in Scheme 2. It is obvious that this substrate can react with metals and provide a fixed substrate for metals for the electrochemical redox reactions. Therefore the modified carbon paste electrode has been prepared and applied for electrocatalytic determination of Pb(II).

Construction of modified mixed-oxide electrode made an opportunity for determination of Pb(II) selectivity in optimal conditions mentioned in recommended procedure.

Cyclic voltammogram in nitric acid media (at the pH 3.05), under optimal conditions, shows cathodic and anodic peaks, which makes it possible to determine this cation. Although the cyclic voltammetry technique is limited for determination of near 10^{-6} mol L^{-1}, but in the presence of mixed-oxide modifier peak current rapidly increased and therefore the detection limit decreased. Finally the calibration curve was plotted and the influence of various substances as potential interference compounds on the determination of this pollutant was studied under the optimum conditions.

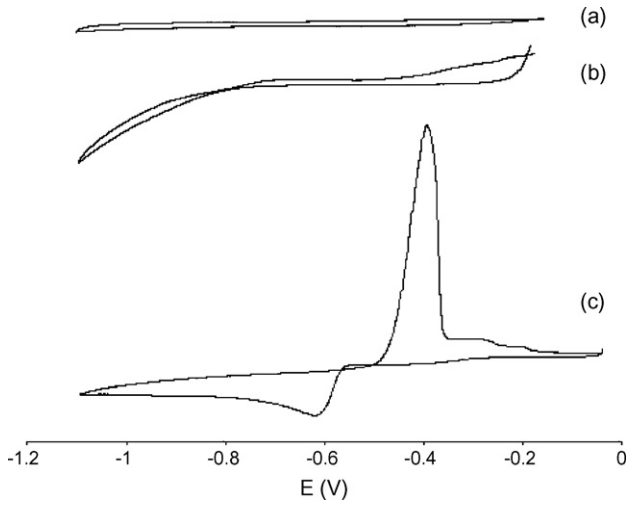

Fig. 1. Cyclic voltammograms of (a) modified carbon paste electrode without lead(II) preconcentration (b) unmodified carbon paste electrode with lead(II) preconcentration (c) modified carbon paste electrode with lead(II) preconcentration. Condition: 0.0010 mol L^{-1} HNO_3 (pH 3.05), lead(II) concentration, 5.0×10^{-7} mol L^{-1}; preconcentration time, 5.0 min; CVs scanned from −1.100 to 0.000 V vs. calomel reference electrode and scan rate, 100 mV s^{-1}.

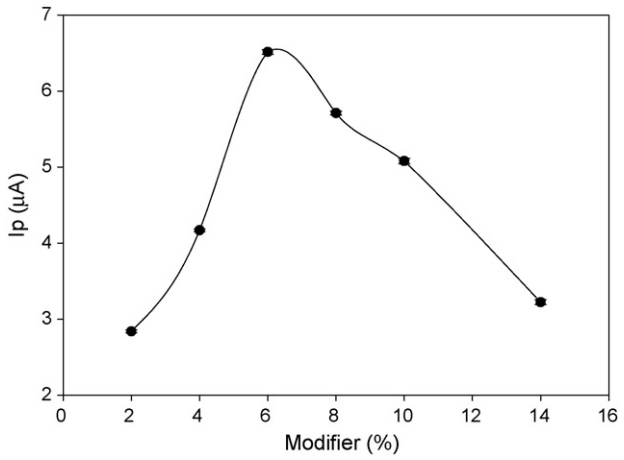

Fig. 2. Effect of percentage of modifier on the peak current. Conditions as Fig. 1.

The cyclic voltammograms were obtained for the unmodified CPE and the Modified CPE in the presence of lead(II) and without lead(II). There were no redox peaks in the CV of the modified CPE without Pb(II) (Fig. 1(a)) and unmodified CPE in the presence of 5.0×10^{-7} mol L^{-1} of lead(II) (Fig. 1(b)). The modified CPEs interacting with 5.0×10^{-7} mol L^{-1} of lead(II) showed an anodic peak at −0.408 V versus calomel reference electrode (Fig. 1(c)).

3.3. Optimization of the experimental conditions

3.3.1. Influence of percentage of modifier

The dependence of $I_{p,a}$ on the various volumes of trimethoxysilylpropylamine immobilized on SiO_2–Al_2O_3 (see compound (**1**)) was examined over the range of 5.7–12.0 mL (5.7 mL, 7.0 mL, 10.5 mL and 12.0 mL) The highest peaks were obtained with 10.5 mL of trimethoxysilylpropylamine immobilized on SiO_2–Al_2O_3 mixed-oxide and this optimal percentage used for electroanalysis of lead(II). Then the dependence of $I_{p,a}$ on the percentage of modifier (compound (**2**)) was examined over the range of 2–14% (Fig. 2). The highest peaks were obtained with 6% of modifier in the carbon paste.

It is shown that $I_{p,a}$ increases with increasing modifier percentage up to 6%, $I_{p,a}$ was increased because the pyridil sites for adsorption of lead were increased (see Scheme 2). Further increment of modifier concentration, resistance of MCPE increased, thus $I_{p,a}$ was decreased.

3.3.2. Influence of media and HNO_3 concentration

Preliminary experiments showed that a better peak shape and a higher peak current were obtained in $KClO_4$ as an electrolyte. Thus 0.13 mol L^{-1} $KClO_4$ was chosen as suitable electrolyte for further studies.

The modified CPE was found to work well in acidic solutions. The effect of nitric acid concentration (and pH) on the peak current of a 5.0×10^{-7} M Pb(II) solution was studied in the range 1.0×10^{-5} to 2.0×10^{-2} mol L^{-1} (Fig. 3(a)). The maximum peak current was observed for 0.0010 mol L^{-1} solution. As a result, $I_{p,a}$ is strongly dependent on the pH value. It is found from Fig. 3(a) that the greatest $I_{p,a}$ is produced at the pH 3.05 (=0.0010 mol L^{-1} HNO_3), because in the high acidic media (lower than pH 3.05) pyridil groups of modifier should be protonated and therefore $I_{p,a}$ was decreased. Therefore, a 0.0010 mol L^{-1} nitric acid solution was used for the fixed accumulation potential and voltammetric measurements of Pb(II) ions.

The anodic peak potential depends on nitric acid concentration (pH) of solution (Fig. 3(b)).

3.3.3. Influence of deposition time

The dependence of the variation of peak current on the changes in the deposition time was examined in a 5.0×10^{-7} mol L^{-1} Pb(II) solution (pH 3.05). Anodic currents increased rapidly as the deposition time increased from 0.0 to 5.0 min, afterward, the anodic currents decreased slowly, probably owing to the interaction sites between the Pb(II) ion and the active sites of the electrode surface should be saturated after 5.0 min.

3.3.4. Influence of accumulation potential

The dependence of I_p on the accumulation potential was examined over the range of (−0.800) to (−0.100) V versus calomel reference electrode. A maximum peak current is obtained at the accumulation potential of −0.500 V versus calomel reference electrode. An accumulation potential of −0.500 V versus calomel reference electrode was employed for all subsequent work (see Fig. 4).

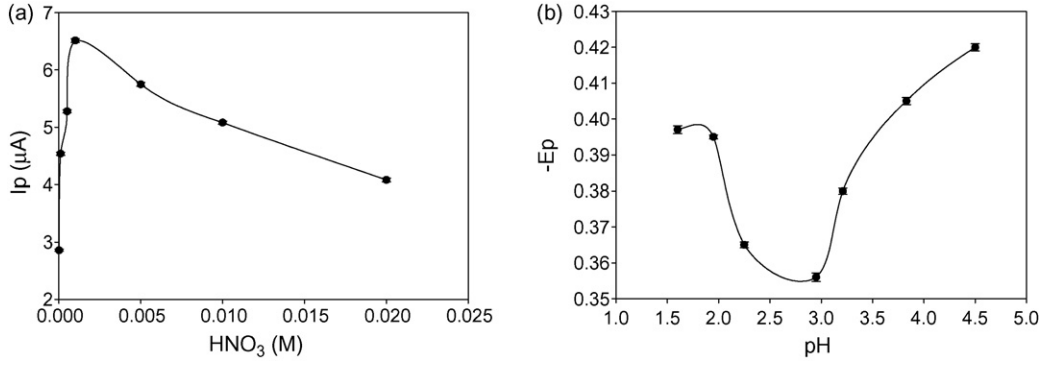

Fig. 3. The effect of (a) HNO_3 on the peak current and (b) pH on the potential. Other conditions as Fig. 1.

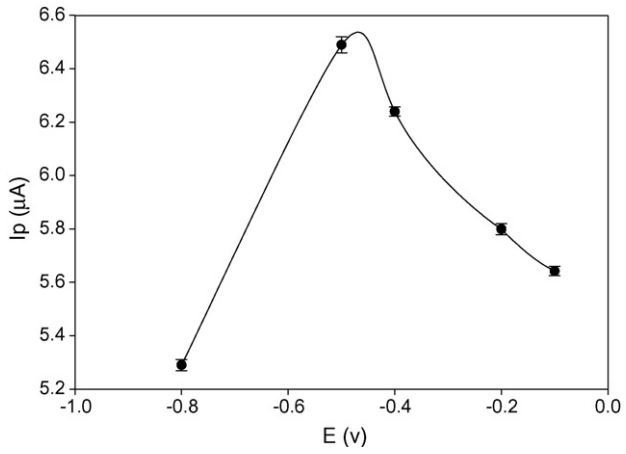

Fig. 4. The effect of accumulation potential on the peak current. Other conditions as Fig. 1.

3.3.5. Influence of scan rate

The scan rate was varied from 10 to 500 mV s^{-1}. The variation of the peak intensity with the scan rate was studied. An approximately linear relationship was found between the peak intensity and the square root of the scan rate ($r^2 = 0.9801$) from 10 to 100 mV s^{-1} (see Fig. 5). Therefore scan rate of 100 mV s^{-1} was used for further studies.

In summary, the optimum conditions for the analysis of Pb(II) ions were attained as follows: deposition solution of pH 3.05; composition of MCPE of 6% (w/w), deposition time of 5.0 min and accumulation potential of −0.500 V versus calomel reference electrode. In the CV, the scan rate was fixed at 100 mV s^{-1} with consideration of the sensitivity.

3.4. Calibration graph, reproducibility, detection limit and stability

The linear range for Pb(II) determination was evaluated under the optimum experimental conditions. The peak currents increases linearly with Pb(II) concentration over the range of 2.0×10^{-9} to 5.2×10^{-5} mol L^{-1} with the correlation equation:

$$I_p\,(\mu A) = (1.0204 \pm 0.09) \times 10^{-3}\, C_{Pb} - (1.0616 \pm 0.14) \times 10^{-4}$$

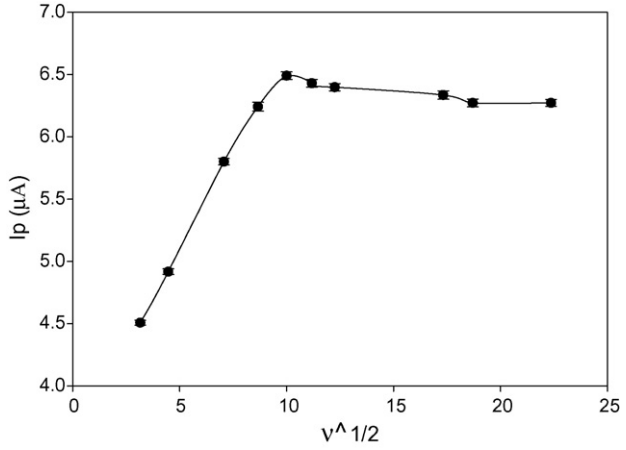

Fig. 5. Effect of scan rate on the peak current. Other conditions as Fig. 1.

with $r^2 = 0.9995$ where C_{Pb} is the molar concentration of Pb(II). The detection limit (three times signal-to-noise) was found to be 1.07×10^{-9} mol L^{-1} Pb(II). Statistical treatment of the results obtained by nine determinations of 1.0×10^{-5}, 1.0×10^{-6}, 1.0×10^{-7} mol L^{-1} of Pb(II) gave a relative standard deviation lower than 3.90%.

The stability of a single chemically modified carbon-paste electrode was tested by using of this electrode for reading peak current (after polishing the electrode surface in each determination) over a period of five months. Statistical treatments of the results show that by using the testing electrode, the maximum relative standard deviation for interday determination was 0.3% and after 5 months was1.5%.

3.5. Interference studies

The selectivity of the chemically modified carbon-paste electrode containing organically SiO_2–Al_2O_3 mixed-oxide evaluated by intentionally introducing concentrations of other metal ions as interferences into Pb(II) solutions during preconcentration. The experimental data are listed in Table 1. These ions were chosen because they might reasonably be expected to exhibit redox activity in roughly the same potential range as Pb(II)-organically SiO_2–Al_2O_3 mixed-oxide-CPE and existing in real samples. The results show that 1000-fold excess of these ions have not interferences on the determination of Pb(II).

Table 1
Change in ASV peak current of 5.0×10^{-7} mol L^{-1} Pb^{2+} in the presence of 5.0×10^{-4} mol L^{-1} of other ions

Interfering ion	Change in peak current (%)
Ag^{+}	+0.07
Hg^{2+}	−0.19
Cu^{2+}	−0.34
Cd^{2+}	−1.10
Fe^{3+}	−0.09
Ni^{2+}	−0.31
Mn^{2+}	+0.25
Zn^{2+}	−0.43
Na^{+}	+0.71
K^{+}	+1.02
Ba^{2+}	−0.11
Ba^{2+}	+0.08
Al^{3+}	−0.06
Li^{+}	−0.04
Ti^{3+}	+0.07
La^{3+}	−0.09
Sn^{2+}	+0.29
V^{3+}	−0.23
V^{5+}	−0.13
Fe^{2+}	0.03
Mo^{6+}	−0.02
Zr^{4+}	+0.01
Cr^{3+}	−0.09
S^{2-}	−0.21
Cl^{-}	+0.56
F^{-}	+0.18
SCN^{-}	−0.31
Br^{-}	+0.58

Table 2
Comparison of figure of merit of the present work with other studies

Detection limit	Linear range mol L^{-1}	Interferent	Reference
9.7×10^{-9}	2.4×10^{-8} to 4.8×10^{-6}	–	[43]
1.0×10^{-8}	2.0×10^{-8} to 2.4×10^{-5}	No	[46]
8.0×10^{-8}	1.0×10^{-7} to 1.0×10^{-6}	S^{2-}	[50]
4.8×10^{-9}	4.8×10^{-9} to 7.2×10^{-8}	NR[a]	[51]
5.0×10^{-9}	1.0×10^{-9} to 1.0×10^{-6}	NR	[52]
4.0×10^{-7}	$(0–15) \times 10^{-6}$	NR	[53]
2.0×10^{-6}	5.0×10^{-6} to 1.0×10^{-1}	no	[54]
4.0×10^{-7}	$(0–50) \times 10^{-6}$	NR	[55]
4.8×10^{-8}	4.8×10^{-7} to 4.8×10^{-3}	Al^{3+}, Ag^{+}, Cu^{2+}, Hg^{2+}	[56]
1.8×10^{-5}	5.8×10^{-5} to 1.0×10^{-2}	Hg^{2+}	[57]
7.0×10^{-8}	1.0×10^{-7} to 1.0×10^{-2}	Hg^{2+}	[58]
6.0×10^{-7}	1.0×10^{-6} to 1.0×10^{-1}	Hg^{2+}	[59]
NR	4.8×10^{-9} to 1.2×10^{-8}	Co^{2+}, Cd^{2+}, Hg^{2+}, Cu^{2+}	[60]
1.0×10^{-8}	1.0×10^{-7} to 1.5×10^{-5}	Hg^{2+}, Ni^{2+}	[61]
4.8×10^{-8}	9.6×10^{-8} to 3.8×10^{-7}	K^{+}, Na^{+}, Ba^{2+}, Hg^{2+}, Fe^{3+}, Cu^{2+}	[62]
1.0×10^{-10}	4.8×10^{-9} to 7.2×10^{-7}	no	[63]
1.0×10^{-9}	2×10^{-9} to 1.06×10^{-5}	Tl^{+}, Ag^{+}, Cu^{2+}, Mn^{2+}, Al^{3+}, Cd^{2+}, Zn^{2+}, Bi^{3+}, Ba^{2+}	[37]
1.2×10^{-7}	1.2×10^{-7} to 9.6×10^{-7}	Cd^{2+}, Cu^{2+}	[31]
–	4.8×10^{-6} to 7.2×10^{-5}	NR	[64]
1.8×10^{-8}	4.8×10^{-7} to 2.4×10^{-5}	Na^{+}, K^{+}, Cl^{-}, $NO_3{}^{-}$	[65]
2.4×10^{-8}	1.2×10^{-7} to 1.2×10^{-6}	Zn^{2+}, Ni^{2+}, Fe^{3+}, Cd^{2+}, Hg^{2+}, Cu^{2+}	[66]
1.78×10^{-8}	NR	Co^{2+}, Fe^{3+}, Ni^{2+}, Cu^{2+}, Mn^{2+}, Cr^{3+}	[67]
9.6×10^{-9}	$(0–2.5) \times 10^{-5}$	Mn^{2+}, Hg^{2+}, Zn^{2+}, Cu^{2+}, Ni^{2+}, Fe^{3+}, Cd^{2+}, $NO_2{}^{-}$, $PO_4{}^{3-}$, I^{-}, Br^{-}, F^{-}	[68]
8.6×10^{-9}	2.4×10^{-8} to 1.9×10^{-7}	NR	[69]
6.0×10^{-6}	1.0×10^{-5} to 1.0×10^{-2}	Ag^{+}, K^{+}, Li^{+}, Na^{+}, Fe^{3+}, Cu^{2+}, Ba^{2+}, Ni^{2+}, Cd^{2+}	[47]
2.5×10^{-6}	6.3×10^{-6} to 3.16×10^{-3}	Ag^{+}, Hg^{2+}	[70]
1.07×10^{-9}	2×10^{-9} to 5.15×10^{-5}	No	Present work

[a] NR means not reported

3.6. Response characteristics

In Table 2, response characteristics of the proposed method are compared with those obtained by recently reported methods. It can be seen from Table 2 that Ag^{+} [37,56,4,70], Hg^{2+} [56–62,66,68,70], Cu^{2+} [31,37,56,60,62,66–68,47], Cd^{2+} [31,37,60,66,68,47], Fe^{3+} [62,66–68,47], Ni^{2+} [61,67,68,47], Mn^{2+} [37,67,68], Zn^{2+} [37,66,68], Na^{+} and K^{+} [62,65,47], Ba^{2+} [62,47], Al^{3+} [37,56], Li^{+} [47], S^{2-} [50], Cl^{-} [65], Br^{-} and F^{-} [68] which strongly interfere with some other lead sensors have negligible interference with the present sensor (see Table 1). The results showed that this modified mixed-oxide is suitable for determination of the Pb selectively.

As shown in Table 2, the proposed method in this work has an excellent linear dynamic range and detection limit. However, there are a few reports in the literature [46,54,63] which have represented a good selectivity and detection limits in regard to measuring the Pb^{2+} without any interference, but the advantage of our method in comparison to those methods is the extension of the linear range and presenting a lower detection limit. Although Malakhova et al. [63] reported a better detection limit (1.0×10^{-10} mol L^{-1}) in comparison to proposed method (1.07×10^{-9} mol L^{-1}), but in the present work, the limit of quantitation is lower and the linear range is much broader.

3.7. Determination of lead(II) in the spiked and real water and waste water samples

In order to evaluate the performance of modified carbon paste electrode by practical analytical applications, the determination of lead(II) was carried out in tap and "zayande rood" river water

Table 3
Determination of Pb(II) in the spiked tap water sample

Sample	Added ($\times 10^{-7}$ mol L^{-1})	Found by proposed method by normal calibration method ($\times 10^{-7}$ mol L^{-1})	Found by proposed method by standard addition method ($\times 10^{-7}$ mol L^{-1})	Found by AAS method by standard addition method ($\times 10^{-7}$ mol L^{-1})
Tap water	0.0	–	–	–
	3.0	3.17 ± 0.057	3.10 ± 0.044	3.13 ± 0.114
	5.0	5.18 ± 0.024	5.12 ± 0.019	4.88 ± 0.173
	7.0	7.13 ± 0.043	7.01 ± 0.054	6.79 ± 0.084
	9.0	8.73 ± 0.076	8.90 ± 0.038	9.21 ± 0.128

Table 4
Determination of Pb(II) in the real water and waste water samples

Sample	Found by proposed method by normal calibration method ($\times 10^{-7}$ mol L^{-1})	Found by proposed method by standard addition method ($\times 10^{-7}$ mol L^{-1})	Found by AAS method by standard addition method ($\times 10^{-7}$ mol L^{-1})
River water	5.39 ± 0.08	5.03 ± 0.07	5.11 ± 0.170
Steel complex waste water	23.76 ± 0.128	21.81 ± 0.265	21.74 ± 1.011
Electroplating waste water	32.77 ± 0.320	30.49 ± 0.121	30.42 ± 1.075

sample without of any pretreatment. The lead(II) concentration was determined by the standard addition technique. It should be mentioned at this point that the reason for using the standard addition technique is to compensate the matrix effect from industrial wastes and river water samples that contain high concentrations of nitrate ions and other foreign ions as high as over thousand times of lead(II) concentration. Hence, for determination of lead(II) the these samples by calibration method the interferences of these ions impose errors on lead(II) determination. Moreover, it is clear that there is not such difficulties in determining lead(II) in tap water because of the simplicity of matrix in these samples. Table 3 shows comparative determination of lead(II) in tap water sample by the proposed method and atomic absorption spectrophotometric method. The mean percentage recoveries of the added lead(II) were found to be 102.03 ± 0.93, 101.19 ± 0.74 and $(100.32 \pm 2.45) \times 10^{-7}$ mol L^{-1} for calibration method, standard addition method (using the proposed method) and atomic absorption spectrophotometric method (using standard addition method), respectively. The results for other real water and waste water samples are summarized in the Table 4. The assessment by Student's *t*-test did not show a statistically significant difference between the methods used (95%). These observations and results have confirmed that the modified carbon paste electrode can be used for practical analysis.

4. Conclusions

Anodic stripping voltammetry analysis utilizing the modified carbon paste electrode for the determination of lead dissolved in aqueous solutions has been demonstrated. This CMCPE can also be used as a relatively simple, selective, sensitive and quick method to determine lead(II) in polluted and industrial waste water. Since there is no leaching out of the electrode because of insolubility of the supported reagent on SiO_2–Al_2O_3 mixed-oxide; in aqueous solution, a single electrode surface can be used for multiple analytical determinations over several weeks. The voltammetric response was linear in the concentration range of 2.0×10^{-9} to 5.2×10^{-5} mol L^{-1} for 5.0 min preconcentration time at fixed accumulation potential. The MCPE presented here has a wider linear range and a lower detection limit than the reported methods, and specially is not interfered significantly by other metal ions. The proposed MCPE was applied successfully to the analysis of tap and river water. The present work illustrates the interest of SiO_2–Al_2O_3 mixed-oxide, chemically modified with a Schiff base covalently attached to the backbone, for designing a new highly selective electrode modifier liable to be applied to chemical sensing.

Acknowledgements

The authors thank to Isfahan University of Technology (IUT) Research Council and Center of Excellence in Chemistry (IUT) for support of this work.

References

[1] J. Breen, C. Stroup (Eds.), Lead Poisoning, CRS Press, Boca Raton, FL, 1995.
[2] J. Wang, Stripping Analysis: Principles, Instrumentation and Applications, VCH, Deerfield Beach, FL, 1985.
[3] J. Wang, in: P.T. Kissinger, W.R. Heineman (Eds.), Laboratory Techniques in Electroanalytical Chemistry, 2nd ed., Marcel Dekker, New York, 1996, pp. 719–737.
[4] S.B. Saban, R.B. Darling, Sens. Actuators B 61 (1999) 128.
[5] E.P. Plueddemann, Silane Coupling Agents, Plenum Press, New York, 1991.
[6] T. Maschmeyer, Curr. Opin. Solid State Mater. Sci. 3 (1998) 71.
[7] R.J.P. Corriu, D. Leclercq, Angew. Chem. Int. Ed. Engl. 35 (1996) 1420.
[8] M. Rehahn, Acta Polym. 49 (1998) 201.
[9] E.F. Vansant, P. Van Der Voort, K.C. Vrancken, Characterization and chemical modification of the silica surface, in: Studies in Surface Science, Catalysis, vol. 93, Elsevier, Amsterdam, 1995.
[10] C.T. Kresge, M.E. Leonowicz, W.J. Roth, J.C. Vartuli, J.S. Beck, Nature 359 (1992) 710.
[11] J. Liu, X. Feng, G.E. Fryxell, L.-Q. Wang, A.Y. Kim, M. Gong, Adv. Mater. 10 (1998) 161.
[12] C.P. Jaroniec, M. Kruk, M. Jaroniec, A. Sayari, J. Phys. Chem. B 102 (1998) 5503.
[13] D.J. Macquarrie, D.B. Jackson, Chem. Commun. (1997) 1781.
[14] M.H. Lim, C.F. Blanford, A. Stein, Chem. Mater. 10 (1998) 4670.
[15] K.B. Sentell, D.M. Bliesner, S.T. Shearer, in: J.J. Pesek, I.E. Leigh (Eds.), Chemically Modified Surfaces, Royal Society of Chemistry, Cambridge, 1994, p. 190.
[16] S.T. Fujiwara, C.A. Pessoa, Y. Gushikem, Electrochim. Acta 48 (2003) 3625.
[17] S.T. Fujiwara, Y. Gushikem, C.A. Pessoa, S. Nakagaki, Electroanalysis 17 (2005) 783.
[18] P. Lessi, N.L. Dias Filho, J.C. Moreira, J.T.S. Campos, Anal. Chim. Acta 327 (1996) 183.
[19] T.J. Pinnavaia, J.G.-S. Lee, M. Abedini, in: D.E. Leyden, W.T. Collins (Eds.), Silylated Surfaces, Gordon and Breach, London, 1980, p. 333.
[20] J. Gun, O. Lev, Anal. Chim. Acta 336 (1996) 95.
[21] S. Sampath, O. Lev, J. Electroanal. Chem. 426 (1997) 131.
[22] A. Walcarius, M. Etienne, C. Delacote, Anal. Chim. Acta 508 (2004) 87.
[23] S. Sayen, A. Walcarius, J. Electroanal. Chem. 581 (2005) 70.
[24] I. Taylor, A.G. Howard, Anal. Chim. Acta 271 (1993) 77.
[25] K. Kalcher, J.M. Kauffmann, J. Wang, I. Svancara, K. Vytras, C. Neuhold, Z. Yang, Electroanalysis 7 (1995) 5–22.
[26] J. Li, S. Liu, X. Mao, P. Gao, Z. Yan, J. Electroanal. Chem. 561 (2004) 137.
[27] S.M. Macha, A. Fitch, Microchim. Acta 128 (1998) 1.
[28] A. Walcarius, Electroanalysis 10 (1998) 1217.
[29] A. Walcarius, Anal. Chim. Acta 384 (1999) 1.

[30] N.L. Dias Filho, D.R. do carom, Talanta 68 (2006) 919.
[31] W. Yantasee, Y. Lin, G.E. Fryxell, B.J. Busche, Anal. Chim. Acta 502 (2004) 207.
[32] Z.M. Hu, A.F. Slaterbeck, C.J. Seliskar, T.H. Ridgway, W.R. Heineman, Langmuir 15 (1999) 767.
[33] J. Li, L.S. Chia, N.K. Goh, S.N. Tan, J. Electroanal. Chem. 460 (1999) 234.
[34] A. Walcarius, Anal. Chim. Acta 388 (1999) 79.
[35] I. Svancara, K.I. Vytras, J. Barek, J. Zima, Crit. Rev. Anal. Chem. 31 (2001) 311.
[36] X. Lu, Z. Wang, Z. Geng, J. Kang, J. Gao, Talanta 52 (2000) 411.
[37] M.F. Mousavi, A. Rahmani, S.M. Golabi, M. Shamsipur, H. Sharghi, Talanta 55 (2001) 305.
[38] R. Agraz, M.T. Sevilla, J.M. Pinilla, L. Hernandez, Electroanalysis 3 (1991) 393.
[39] S.V. Prabhu, R.P. Baldwin, L. Kryger, Electroanalysis 1 (1989) 13.
[40] Z. Navratilova, P. Kula, Fres. J. Anal. Chem. 367 (2000) 369.
[41] P. Kula, Z. Navratilova, P. Kulova, M. Kotoucek, Anal. Chim. Acta 385 (1999) 91.
[42] M. Connor, E. Dempsey, M.R. Smyth, D.H.S. Richardson, Electroanalysis 3 (1991) 331.
[43] J.A. Ramos, E. Bermejo, A. Zapardiel, J.A. Perez, L. Hernandez, Anal. Chim. Acta 273 (1993) 219.
[44] T. Peng, Z. Tang, G. Wang, B. Shen, Electroanalysis 6 (1994) 597.
[45] Z. Hu, C.J. Seliskar, W.R. Heineman, Anal. Chim. Acta 369 (1998) 93.
[46] T.H. Degfa, B.S. Chandravanshi, H. Alemu, Electroanalysis 11 (1999) 1305.
[47] M.F. Mousavi, M. Barzegar, S. Sahari, Sens. Actuators B 73 (2001) 199.
[48] M.F. Mousavi, S. Sahari, N. Alizadeh, M. Shamsipur, Anal. Chim. Acta 414 (2000) 189.
[49] N. Tavakkoli, Z. Khojasteh, H. Sharghi, M. Shamsipur, Anal. Chim. Acta 360 (1998) 203.
[50] T. Molina-Holgado, J.M. Pinilla-Macias, L. Hernández-Hernández, Anal. Chim. Acta 309 (1995) 117.
[51] O. Bagel, E. L'Hostis, G. Lagger, M.D. Osborne, B.J. Seddon, H.H. Girault, D. Brack, U. Loyall, H. Schafer, J. Electroanal. Chem. 469 (1999) 189.
[52] G.S. Reeder, W.R. Heineman, Sens. Actuators B 52 (1998) 58.
[53] Y. Guo, A.R. Guadalupe, Sens. Actuators B 46 (1998) 213.
[54] M.M. Ardakany, A.A. Ensafi, H. Naeimi, A. Dastanpour, A. Shamlli, Sens. Actuators B 96 (2003) 441.
[55] S. Laschi, I. Palchetti, M. Mascini, Sens. Actuators B 114 (2006) 460.
[56] N.A. Yusof, M. Ahmad, Sens. Actuators B 94 (2003) 201.
[57] S.S.M. Hassan, M.H.A. Ghalia, A.E. Amr, A.H.K. Mohamed, Talanta 60 (2003) 81.
[58] M.R. Ganjali, M. Hosseini, F. Basiripour, M. Javanbakht, O.R. Hashemi, M.F. Rastegar, M. Shamsipur, G.W. Buchanen, Anal. Chim. Acta 464 (2002) 181.
[59] V.S. Bhat, V.S. Ijeri1, A.K. Srivastava, Sens. Actuators B 99 (2004) 98.
[60] W. Yantasee, C. Timchalk, G.E. Fryxell, B.P. Dockendorff, Y. Lin, Talanta 68 (2005) 256.
[61] C. Hu, K. Wu, X. Dai, S. Hu, Talanta 60 (2003) 17.
[62] W. Ouangpipat, T. Lelasattarathkul, C. Dongduen, S. Liawruangrath, Talanta 61 (2003) 455.
[63] N.A. Malakhova, E.G. Miroshnikova, N.Yu. Stojko, Kh.Z. Brainina, Anal. Chim. Acta 516 (2004) 49.
[64] H. Yao, G.J. Ramelow, Talanta 45 (1998) 1139.
[65] E.M. Gama, A. da Silva Lima, V.A. Lemos, J. Hazard. Mater. B 136 (2006) 757.
[66] M.S.D. Nezio, M.E. Palomeque, B.S.F. Band, Talanta 63 (2004) 405.
[67] M. Soylak, I. Narin, M.A. Bezerra, S. Luís Costa Ferreira, Talanta 65 (2005) 895.
[68] O.A. Zaporozhets, L.Ye. Tsyukalo, Talanta 58 (2002) 861.
[69] K. Pyrzynaska, M. Cheregi, Water Res. 34 (2000) 4215.
[70] X. Yang, D.B. Hibbert, P.W. Alexander, Anal. Chim. Acta 372 (1998) 387.

Available online at www.sciencedirect.com
ScienceDirect
Talanta 73 (2007) 166–171
Talanta
www.elsevier.com/locate/talanta

Sequential spectrophotometric determination of inorganic arsenic species by hydride generation from selective medium reactions and colour bleaching of permanganate

M. Hashemi *, P. Modasser

Department of Chemistry, Faculty of Sciences, Bu-Ali Sina University, Hamedan, Iran

Received 12 December 2005; received in revised form 8 March 2007; accepted 15 March 2007
Available online 24 March 2007

Abstract

A simple spectrophotometric method is presented for the sequential determination of inorganic arsenic (As) species in one sample. It is based on the sequential arsine generation from As(III) and As(V) using selective medium reactions, collection of the arsine generated in an absorbing solution containing permanganate and ethanol at 5 °C and subsequent reduction of permanganate by arsine. The decrease in permanganate absorbance at 524.2 nm is monitored for As determination. The acetic acid/sodium acetate and HCl mediums were used for selective arsine generation from As(III) and remaining As(V) in one solution, respectively. The effect of interferences and their possible mechanisms were discussed. Interferences from transition metal ions were removed by using a Chelex 100 resin. Under optimized conditions, the established method is applicable to the determination of 3–30 μg of each arsenic species. Good recoveries (96–102%) of spiked artificial sea water, tap water and standard mixtures of As(III) and As(V) were also found. The method is simple, accurate, precise and environmental friendly.

Keywords: Hydride generation; Spectrophotometry; Arsenic determination; Permanganate

1. Introduction

In recent years, there has been growing interest in the analysis and speciation of arsenic (As) species, owing to their high toxicity and abundance in the environment. Hydride generation (HG) is a well known technique for determination of As species in a wide range of samples, as has been highlighted by several reviews [1–4]. A number of analytical techniques based on the HG exist for As determination, such as atomic absorption spectrometry [5], atomic emission spectrometry [6], atomic fluorescence spectrometry [7], ICP-mass spectrometry [8], gas diffusion flow injection with electrochemical detection [9]. These methods benefit from high sensitivity and low detection limit, but need sophisticated instrumentation, optimization of different parameters and expert hands. On the other hand, the spectrophotometric method can be regarded as a simple method that can be used for most commercial laboratories. Two classic spectrophotometric methods have been described for determination of As using HG. These methods are based either on the colour reaction of arsine with silver diethyldithiocarbamate (SDDC) in an organic base-chloroform solution or trapping of arsine in an alkaline iodine solution in which As is determined by the molybdenum blue (MB) method [10,11]. These methods deal with expensive and toxic substances, involve several steps and suffer strong interferences from coexisting ions. In spite of disadvantages of the classic SDDC and MB methods, only a few attempts have been made to replace these methods. Recently Gosh and co-worker described a spectrophotometric method for total inorganic As determination based on the in situ colour bleaching of methylen blue in micellar medium by arsine in an one-pot system[12]. However, the use of micellar medium for absorbing of arsine cause a troublesome foaming in conventional HG system in which the generated hydride has been transported by a carrier gas. Also, Cardwell and co-worker used a pervaporation-flow injection (PFI) system for determination of As based on the transportation of arsine across a semi-permeable membrane into a static acidic permanganate solution [13]. In comparison with the conventional HG system, the PFI system

* Corresponding author. Tel.: +98 811 8228313; fax: +98 811 8272404.
E-mail address: mhashemi@basu.ac.ir (M. Hashemi).

0039-9140/$ – see front matter © 2007 Elsevier B.V. All rights reserved.
doi:10.1016/j.talanta.2007.03.026

has certain disadvantages. It requires optimisation of several parameters and the sensitivity of the measurements is limited by the lifetime and thickness of the membrane used. Also the pH range of HG reaction is limited, so that the efficiency of HG severely decreases in the pH range of grater than 2, therefore selective generation of arsine from different inorganic As species by exploiting the pH dependence is impossible [13,14]. Conventional HG has easier performance, however the trapping efficiency of arsine in permanganate is nearly zero in this system [11].

This study reports a simple colorimetric method for selective determination of inorganic As species based on the reduction of permanganate by the arsine generated in a conventional HG system. The decrease in colour intensity of permanganate is a direct measure of the arsenic concentration. Speciation of As(III) and AS(V) was carried out by selective HG from As(III) and As(V) from different reaction mediums. The interference effects and their possible mechanisms were investigated. The interferences from transition metal ions were overcome by separation with Chelex 100 resin. The method is simple and free from toxic reagents.

2. Experimental

2.1. Apparatus

A schematic diagram of the analytical system used is shown in Fig. 1. This system consists of a hydride generator and a thermostated arsine trapping U-tube, containing 2 mm diameter glass beads. A lead acetate scrubber was placed in the inlet arm of the U-tube for absorbing any hydrogen sulfide which may be generated during hydride generation. A peristaltic pump (Ismatec) furnished with tygon pumping tubes was used for introduction of the sample, acid and $NaBH_4$ solution into the hydride generator. A glass column (200 mm × 10 mm) packed with 100 mm height of Chelex 100 resin was used for off-line separation of transition metal ions. All spectrophotometric measurements were made with a Shimadzu UV-265 spectrophotometer.

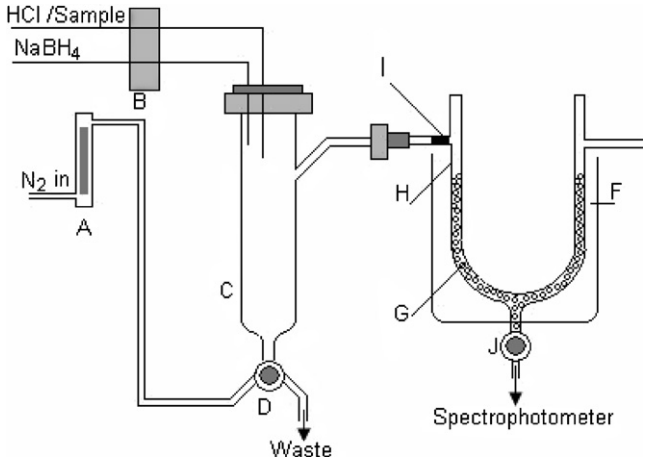

Fig. 1. The schematic diagram of the analytical system: (A) flow meter; (B) peristaltic pump; (C) hydride generator; (D) three-way valve; (E) waste; (F) thermostated ice bath; (G) glass beads; (H) absorbing U-tube; (I) lead acetate scrubber; (J) two-way valve.

2.2. Reagents

Analytical grade reagents and doubly distilled water were used throughout the analysis. Stock solutions (1.000 g/l) of As(III) and As(V) were prepared by dissolving appropriate amounts of As_2O_3 in 0.1 M NaOH and Na_3AsO_4 in 0.1 M HCl. Potassium permanganate stock solution (1×10^{-2} M) was prepared by dissolving 0.1584 g of $KMNO_4$ in 100 ml of distilled water. This solution was kept on a steam bath for about an hour, cooled, filtered and stored in the dark. The working solutions were freshly prepared by appropriate dilution of the stock solutions. The $NaBH_4$ solution was prepared daily as 1% (m/v) solution in 0.1 M NaOH. A sodium acetate (0.1 M)–acetic acid buffer solution was used for the adjustment of sample pH to 5.

2.3. Procedure

For determination of As(III), the pH of sample solution was adjusted to 5 with sodium acetate/acetic acid buffer and introduced into the generator flask. The absorber U-tube immersed in the ice bath was filled with 8 ml of 0.8 mM $KMNO_4$ and after 1 min, 2 ml ethanol was added to it. Then 1 ml of 1% (m/v) $NaBH_4$ was introduced into the generator. The arsine formed from As(III) was purged by a stream of N_2 gas at a flow rate of 20 ml/min and transported into the absorber U-tube, in which arsine reduces the permanganate. After 5 min, the decrease in the absorbance of the permanganate solution was monitored at 524.2 nm. Then, for determination of remaining As(V), the absorber U-tube was refilled with permanganate and ethanol and 5 ml of 5 M HCl introduced into the generator followed by a further 2 ml of 1% (m/v) $NaBH_4$. After 5 min the decrease of the permanganate absorbance was monitored at 524.2 nm.

3. Results and discussion

3.1. Indicator reaction

The spectrophotometric methods for determination of As using conventional HG involve trapping of the arsine generated in an absorbing medium containing spectrophotometric indicator and other species for increasing the efficiency of the arsine trapping and/or catalysing the indicator reaction. Due to reducing property of arsine, the reaction of arsine with redox indicators can be used for colorimetric determination of As. Permanganate is an inexpensive and standard oxidant which has self indicating quality. A concentration of only about 2×10^{-6} M permanganate is sufficient to form a perceptible colour in solution. When it is completely reduced by arsine, becomes colourless. Then, the decrease in the permanganate absorbance can be a direct measure of As. The preliminary examination has shown that the absorbance of MnO_4^- solution has a linear calibration range up to 10^{-3} M. Thus a concentration of 10^{-3} M MnO_4^- was selected for subsequent studies. With introduction of the arsine generated from 5, 10 and 20 μg of As(III)

into MnO_4^- solution, no considerable and reproducible changes in absorbance were observed. This is in line with the finding of Neto and co-workers who demonstrated that the absorption efficiency of arsine in MnO_4^- solution is nearly zero [11]. The spot test by filter impregnated with $AgNO_3$ showed that an amount of arsine escape from absorber U-tube. This may be due to either low solubility of covalent arsine in aqueous medium at room temperature or slow reaction rate of arsine with MnO_4^-. Decreasing the flow rate of carrier gas and addition of different surfactants (TX-100, SDS and CTAB) for increasing the solubility of covalent arsine in aqueous absorbing medium had no beneficial effects. Furthermore, addition of surfactant caused a troublesome foaming. Also, addition of common redox catalysers such as iodine monochloride (ICl) and KI and decreasing the pH of MnO_4^- solution for catalysing the indicator reaction were found ineffective. Ethanol can also increase the solubility and reactivity of arsine in aqueous mediums [15,16]. In present case, addition of different amounts of ethanol to absorbing solution at room temperature was found to be an impractical alternative, because the methodological blank enhanced due to the fast oxidation of ethanol by MnO_4^-. Since the oxidation rate of ethanol can be reduced at low temperatures, the absorber U-tube was immersed in the thermostated ice bath and ΔA values for blank measurements were studied at different temperatures ranging from 0 to 25 °C. The results of this study showed that the ΔA value of 10^{-3} M MnO_4^- in 20% ethanol after 10 min was nearly zero up to 5 °C and then increased slightly up to 10 °C and finally increased sharply at higher temperatures. Therefore, the absorber U-tube was kept at 5 °C for subsequent investigations. Also the effect of the ethanol on the possible shift of the maximum absorbance wavelength of the MnO_4^- (λ_{max}) was studied. The results showed that the λ_{max} of MnO_4^- did not alter in the presence of ethanol.

3.2. Effect of the ethanol concentration

Ethanol concentration can affect the blank and sample measurements. Preliminary experiments showed that the ΔA values for blank measurements were negligible up to 30% (v/v) ethanol concentration. Therefore, the effect of ethanol concentration in the range of 5–30% (v/v) on the ΔA value for 10 μg As(III) was investigated (Fig. 2). Results show that the ΔA value increases with increasing ethanol concentration up to 20% (v/v) and then leveled off with further increases in ethanol concentration. Therefore a 20% (v/v) ethanol concentration was selected for subsequent studies.

3.3. Effect of MnO_4^- concentration

MnO_4^- concentration can affect the blank and sample measurements. Preliminary studies showed that the ΔA value for the blank measurements was nearly zero up to 10^{-3} M MnO_4^- and then increased with increasing of MnO_4^- concentration, indicating that ethanol oxidized by MnO_4^-. Therefore the effect of MnO_4^- concentration was studied in the range 1×10^{-4} to 1×10^{-3} M (Fig. 3). The results show that the sensitivity increases with increasing MnO_4^- concentration up to 8×10^{-4} M and maximum sensitivity is obtained over the range 8×10^{-4} to 1×10^{-3} M. Therefore this concentration was selected for further studies.

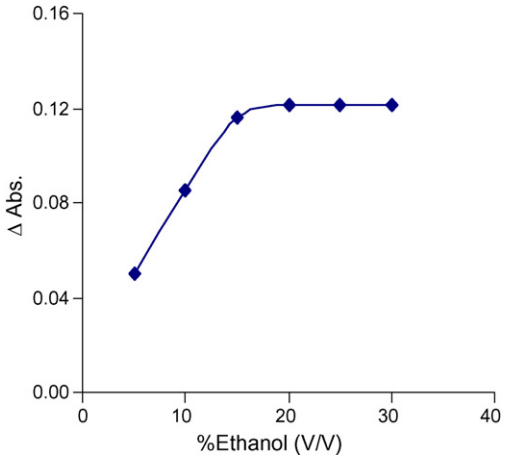

Fig. 2. The effect of ethanol concentration on the ΔA value of 10 μg of As(III). Conditions: MnO_4^-, 1 mM; reaction time, 10 min; indicator volume, 8 ml; temperature, 5 °C; N_2 flow rate, 20 ml/min; sample acidity, 0.02 M, $NaBH_4$, 1% (w/v); sample volume, 30 ml.

3.4. Indicator volume and reaction time

The effect of indicator volume was examined in the range 4–12 ml. The maximum sensitivity was obtained over the range 8–12 ml. At lower indicator volumes, the efficiency of the arsine trapping decreased. The effect of reaction time was also investigated in the range of 4–12 min. It was found that a reaction time of 5 min was sufficient to obtain maximum sensitivity.

3.5. Sample volume and N_2 gas flow rate

The effect of sample volume was investigated in the range 10–50 ml. The sensitivity was constant in the range 10–30 ml and then decreased at higher sample volumes, indicating that the efficiency of hydride separation from generator was incomplete.

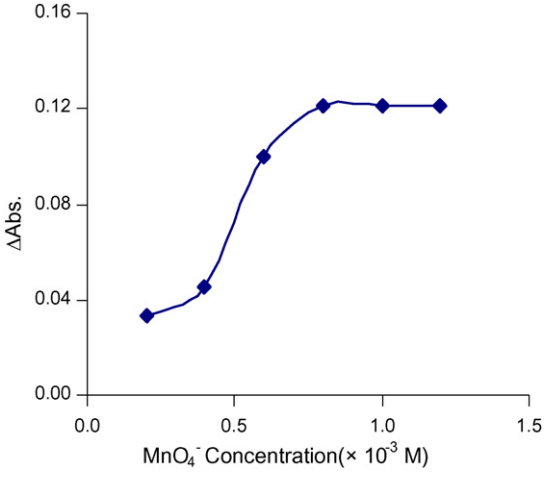

Fig. 3. The effect of MnO_4^- concentration on the ΔA value of 10 μg of As(III). All other conditions are as in Fig. 2.

Also, the effect of N_2 flow rate was investigated in the range of 10–30 ml/min. The optimum N_2 flow rate was found to be 20 ml/min. This flow rate was sufficient to ensure that the transfer of reaction mixtures to absorption U-tube did not occurred. At higher flow rates, the pressure increased significantly and caused leakage.

3.6. Sample acidity

HCl is generally used for arsine generation, in most HG systems. The effect of the HCl concentration on the arsine generation from 10 μg of As(III) was investigated in the range 2×10^{-5} to 2×10^{-2} M. The sensitivity increased with increasing HCl concentration up to 2×10^{-4} M and maximum sensitivity was obtained over the range 2×10^{-4} to 2×10^{-2} M.

3.7. Analytical figures of merit

A linear calibration graph was obtained over the range 3–30 μg of As(III) with the linear regression equation $\Delta A = 0.009C + 0.0221$ (C, μg As) and correlation coefficient $r = 9991$. An absolute detection limit ($3S_b$) of 0.34 μg and a concentration detection limit of 0.034 μg ml^{-1} were obtained using a 10 ml sample volume. The precision (R.S.D.) for five replicate determination of 10 μg As(III) was 1.3%.

3.8. Speciation study

There are few papers about the speciation of As(III) and As(V) using different reaction mediums [16–20]. The most common procedures are based on the selective generation of arsine from As(III) and total inorganic As in the separate samples. Then As(V) can be determined by difference [16–19]. As(III) and As(V) can be converted to arsine in HCl and/or thiogloycollic acid mediums with high chemical yield [16–20]. Furthermore, the use of dimethylformamide [21], acetic acid/sodium acetate buffer solution (pH 5) [16–20] and masking agents such as F^- [22] and Zr(II) [23] were proposed to suppress the evolution of arsine from As(V). In this study the possibility of sequential determination of As(III) and As(V) using acetic acid/sodium acetate buffer solution (pH 5) for selective arsine generation from As(III) in the presence of As(V) and HCl medium for arsine generation from remaining As(V) in a single sample was examined. Preliminary experiments showed that the sensitivity of As(III) measurements in HCl mediums (pH < 2) and acetic acid/sodium acetate buffer solution (pH 5) under same experimental conditions were same and there was no difference in the performance of two mediums for arsine generation. When As(V) solution was used in place of As(III) solution, no discernible changes in absorbance were observed in acetic acid/sodium acetate buffer medium (pH 5). Investigation of the presence of As(V) on the determination of As(III) showed that As(V) did not affect the determination of 10 μg As(III) within 100-fold excess. Therefore, this medium was used for selective generation of arsine from As(III) in the presence of As(V). Investigation of arsine generation from remaining As(V) showed that addition of 5 ml of 5 M HCl and 2 ml of 1% (w/v) $NaBH_4$, respectively, was sufficient to ratio of the ΔA value for 10 μg As(V) to that of 10 μg As(III) reach to unite. The efficiency of the sequential HG from As(III) and As(V) by different mediums in a single analysis was compared with replicate measurements ($n = 5$) of ΔA values for 10 μg of each As species. The *t*-test showed that there was no significant difference ($p = 0.05$) between ΔA values and therefore sequential hydride generation efficiencies from As(III) and As(V). The results of this study showed that the sensitivity of the sequential determination of As(III) and As(V) is the same and the kinetic problem in arsine generation from different inorganic species is not important. This indicates that arsenic in both states have similar response and can be determined by single calibration curve in one sample solution. Table 1 shows the results of selective determination of As(III) and As(V) in the mixture of standard solutions. The average recoveries of As(III) and As(V) were found to be 101 and 96%, respectively. Achieved sampling rate for selective determination of As(III) and As(V) was 8 samples h^{-1}.

Table 1
Selective determination of As(III) and As(V) in standard mixtures

Mixture (μg)	Determined (μg)		Recovery (%)	
As(III) + As(V)	As(III)	As(V)	As(III)	As(V)
15 + 0	14.7 ± 0.2	–	98	–
10 + 5	10.2 ± 0.2	4.7 ± 0.3	102	94
5 + 10	5.2 ± 0.2	9.6 ± 0.3	104	96
0 + 15	–	14.6 ± 0.2	–	98
–	–	–	99[a]	97[a]

All results: mean ± S.D. based on five replicate analyses.
[a] Mean recovery.

3.9. Interference effects

The effect of various ions on the determination of 10 μg of As(III) and As(V) were investigated. Alkaline and alkaline earth ions and common anions such as Cl^-, Br^-, I^-, PO_4^{3-}, SO_4^{2-}, CH_3COO^- and tartarate did not interfere up to and possibly grater than 100-fold excess. The interferences of transition metal ions on HG based on $NaBH_4$ reduction is well known [2]. The results of interference study from transition metal ions are shown in Table 2. Except for Hg(II), the investigated metal ions gave a

Table 2
Effect of interferences on the determination of 10 μg As(III) and As(V) in the presence of 1000 μg foreign ions

Ion	Recovery (%)	
	As(III)	As(V)
Ag(I)	20	60
Cd(II)	92	101
Co(II)	96	99
Cu(II)	0	36
Fe(III)	40	88
Hg(II)	>400	>486
Mo(VI)	96	103
Mn(II)	91	100
Ni(II)	56	80
Zn(II)	89	100

Table 3
Results (mean ± S.D. based on five replicate analysis) of determination of As(III) and As(V)

Sample	Added (μg)		Found (μg)		Recovery (%)	
	As(III)	As(V)	As(III)	As(V)	As(III)	As(V)
Tap water[a]	0	0	nd	nd	--	--
	5	5	4.7 ± 0.3	4.6 ± 0.4	94	92
	10	10	9.6 ± 0.2	9.4 ± 0.3	96	94
	15	15	14.7 ± 0.2	14.4 ± 0.3	98	96
Artificial sea water[b]	5	5	4.9 ± 0.2	4.7 ± 0.3	98	94
	10	10	9.8 ± 0.2	9.6 ± 0.3	98	96
	15	15	15.2 ± 0.2	14.6 ± 0.3	101	97

[a] Collected at the Bu-Ali Sina University.
[b] Composition of artificial sea water [10]: NaCl, 0.4266 mol/kg; KCl, 0.0105 mol/kg; $CaCl_2$, 0.0107 mol/kg; $MgCl_2$, 0.0551 mol/kg.

sever suppressing effect. The positive interference of Hg(II) is due to generation of Hg vapors under the experimental conditions and bleaching of permanganate by Hg vapors that increases the apparent recovery of the As species. The mechanism of the other interfering ions can be explained by interaction of arsine generated with reduced form of the metals or corresponding metal borides. Also, the catalytic effect of interfering metal ions on the decomposition of tetrahydroborate can be considered as another possible mechanism. There are differences in interference pattern and therefore interference magnitude for As(III) and As(V). Generally, As(V) is more vulnerable to interferences than As(III) in most common procedures. However, Table 2 shows that the interference magnitude for As(V) is smaller than As(III). This is due to more solubility of transition metal precipitates in HCl medium in which arsine generation from As(V) is carried out. On the other hand, the rate of $NaBH_4$ hydrolysis is significantly enhanced in the presence of transition metal ions at pH 5 [24] in which arsine is generated from As(III). The separation of transition metal ions with Chelex 100 is well known. The ability of Chelex 100 to remove metal ions depends on the sample pH and has a maximum value above pH 4 [25]. Since this ability is well consistent with experimental conditions of speciation procedure, the off-line separation of transition metal ions with Chelex 100 prior to HG was selected as the most straightforward way to overcome transition metal interferences. For removal of transition metal ions, the pH of sample solution was adjusted to 5 and passed through the Chelex 100 column at a flow rate of 1 ml/min. The pH of collected sample was adjusted to 5 again and analysed by presented procedure. The results showed that the absolute errors in As(III) and As(V) recoveries were less than 3% in all cases. Although, the adjustment of the sample pH to 5 with acetate buffer appears to be a limitation, but it offers the possibility of chemical speciation and increases the performance of Chelex 100 for removal of the transition metal ions. For providing the same ability of the column for all experiments and also in order to avoid the column saturation, it is better to regenerate the column for each experiment by passing a solution of 0.1N HNO_3 and distilled water from column. Also, the interferences from hydride forming elements were investigated. Sb(III), Sn(II), and Se(IV) for As(III) and Sb(V) and Se(VI) for As(V) gave significant positive errors when present at an equivalent concentration. On the other hand Pb(II) and Bi(III) could be tolerated (<5% interference) within 25- and 10-fold excess, respectively. These interferences may be due to generation of related hydrides under experimental conditions and reaction of them with permanganate. Investigation of the prior cleanup of sample with Chelex 100 showed that the tolerance level (<5% interference) of Pb (II), Bi(III) and Sn(II) increased up to 100-, 100- and 10-fold excess, respectively. No improvement was found for Sb(III), Sb(V) and Se (II).

3.10. Application to water analysis

Since there are no interferences from major consistent of water samples and interferences of transition metal ions can be overcome by separation with Chelex 100, this method is, specially, suitable for water analysis by simple standard calibration. Since no standard reference material with certified values for As(III) and As(V) are currently available, the spiked artificial see water and tap water were prepared to demonstrate the reliability of the method for determination of As(III) and As(V). The results summarized in Table 3 show the high selectivity and excellent recovery for sequential determination of As (III) and As(V).

4. Conclusion

A new spectrophotometric method has been developed for sequential determination of inorganic arsenic species in μg level. It is based on the arsine generation and colour bleaching of permanganate in the presence of ethanol at low temperature. The decrease in colour intensity of permanganate is a direct measure of the arsenic concentration. The arsenic speciation can be performed by sequential HG using selective medium reactions. Acetic acid/sodium acetate (pH 5) buffer medium has been used to achieve a selective arsine generation from As(III) in the presence of As(V). Then, the remaining As(V) has been converted to arsine in HCl medium. The main advantage of the presented method is that the selective determination of As(III) and As(V) can proceed in the same solution. The mutual interferences between two arsenic species are insignificant and interferences from transition metal ions were removed by using Chelex 100

resin. The method is simple, precise, accurate and environmental friendly which can be used for most commercial laboratories. Future work in this area will concentrate on adoption of the presented procedure to a flow injection arrangement. Considerable advantages may result form this, including increased sample throughput, improved precision and extended range of tolerable concentration from interfering ions.

References

[1] K.A. Franceconi, D. Kuehnlet, Analyst 129 (2004) 373.
[2] A.D. Yan, Z.-M. Ni, Anal. Chim. Acta 292 (1994) 890.
[3] A.D. Campbell, Pure. Appl. Chem. 64 (1992) 227.
[4] J. Dedina, Prog. Anal. Spectrosc. 11 (1988) 251.
[5] A.G. Howard, M.H. Arbab-Zavar, Analyst 106 (1981) 213.
[6] J.M. Costa-Fernandes, F. Junzer, R. Pereiro-Garcia, A. Sanaz-Medel, J. Anal. At. Spectrom. 10 (1995) 1019.
[7] F. El-Hadri, A. Morales-Rubio, M. de-la Guardia, Talanta 52 (2000) 653.
[8] Y.-L. Feng, H.-Y. Chen, L.-C. Tian, H. Narasaki, Anal. Chim. Acta 375 (1998) 67.
[9] J.R. Farrell, P.J. Iles, Y.J. Yan, Anal. Chim. Acta 334 (1996) 193.
[10] M.H. Arbab-Zavar, M. Hashemi, Talanta 52 (2000) 1007.
[11] J.A.G. Neto, R. Montes, A.A. Cadoso, Talanta 50 (1999) 959.
[12] S. Kundu, S.K. Ghosh, M. Mandal, T. Pal, Talanta 58 (2002) 935.
[13] T. Rupasinghe, T.J. Cardwell, R.W. Cattrall, I.D. Potter, S.D. Kolev, Anal. Chim. Acta 510 (2004) 225.
[14] T. Rupasinghe, T.J. Cardwell, R.W. Cattrall, M.D. Luque de Castro, S.D. Kolev, Anal. Chim. Acta 445 (2001) 229.
[15] S.S. Michael, Anal. Chem. 49 (1979) 337.
[16] M.H. Arbab-Zavar, M. Hashemi, J. Sci. I. R. Iran 4 (1993) 255.
[17] P. Bermejo-Barrera, J. Moreda-Pinerio, A. Moreda-Pinerio, A. Bermejo-Barrera, Anal. Chim. Acta 374 (1998) 231.
[18] R.K. Anderson, M. Thompson, E. Culbard, Analyst 111 (1986) 1143.
[19] R.K. Anderson, M. Thompson, E. Culbard, Analyst 111 (1986) 1153.
[20] A.G. Howard, M.H. Arbab-Zavar, Analyst 105 (1980) 338.
[21] W.H. Clement, S.D. Faust, Environ. Lett. 5 (1973) 155.
[22] H. Bombach, E. Weinhold, Mikrochim. Acta, I. (1989) 229.
[23] S. Nakashima, Analyst 104 (1979) 172.
[24] J. Agget, G. Boyes, Analyst 114 (1989) 1159.
[25] Bio.RAD Laboratories,Chemical Division, Produce Information 2020, separating metal using Chelex 100 chelating resin, July 1978. Printed in USA, 78-0422.

Available online at www.sciencedirect.com
ScienceDirect
Talanta 73 (2007) 62–67
Talanta
www.elsevier.com/locate/talanta

Sensitive determination of *S*-nitrosothiols in human blood by spectrofluorimetry using a fluorescent probe: 1,3,5,7-tetramethyl-8-(3′,4′-diaminophenyl)-difluoroboradiaza-*s*-indacene

Ke-Jing Huang [a,b], Wan-Zhen Xie [b], Hong Wang [a], Hua-Shan Zhang [a,*]

[a] *Department of Chemistry, Wuhan University, Wuhan 430072, PR China*
[b] *Department of Chemistry, Xinyang Normal University, Xinyang 464000, PR China*

Received 4 January 2007; received in revised form 25 February 2007; accepted 25 February 2007
Available online 1 March 2007

Abstract

S-Nitrosothiols (RSNO) have been proved to be potent smooth muscle relaxants and inhibitors of platelet aggregation. It has been reported as the best candidate for the endogenous storage and transport of nitric oxide (NO) *in vivo*. Sensitive determination of RSNO in biosamples seems to be of great significance. In this work, a novel spectrofluorimetric method is proposed to determine RSNO. An excellent fluorescence probe 1,3,5,7-tetramethyl-8-(3′,4′-diaminophenyl)-difluoroboradiaza-*s*-indacence (DAMBO) is used to label RSNO. The derivatization reaction performs in aqueous medium at 30 °C for 15 min in the presence of 1.0×10^{-4} mol L^{-1} Hg^{2+}. The derivative is detected by fluorescence at an emission wavelength of 507 nm with excitation at 498 nm. The response is a linear function of concentration in the range of 6.0–400.0 $\times 10^{-9}$ mol L^{-1}. The detection limit is 1.2×10^{-10} mol L^{-1} (S/N = 3). The method is applied to determine RSNO in the blood of healthy persons and patients suffering from cardiovascular diseases. Recoveries of RSNO from spiked blood samples are between 97.52 and 102.81%. The studies indicate that the method presented here is rapid, simple, sensitive and feasible.

Keywords: *S*-Nitrosothiols; Spectrofluorimetry; Cardiovascular diseases; 1,3,5,7-Tetramethyl-8-(3′,4′-diaminophenyl)-difluoroboradiaza-*s*-indacence

1. Introduction

S-Nitrosothiols (RSNO), which can be formed from nitrosating agents derived from acidic nitrite [1], have been suggested to mediate certain aspects of signal transduction [2]. These compounds exhibit NO-like biological actions such as vasodilation and inhibition of platelet aggregation. They also have been proved to be key intermediates in the action of various nitrovasodilating compounds such as sodium nitroprusside and nitroglycerin [3,4]. Furthermore, report shows that *S*-nitrosothiol proteins might serve as a circulating source of NO [5]. Further studies reveal that *S*-nitrosoproteins are produced during various phases of the immune response [6]. Therefore, *S*-nitrosothiols constitute an important class of compounds, whose analysis may aid in understanding the biology of RSNO.

However, because RSNO is an intermediate of NO metabolites, its process of metabolizability is very complex and easy to be influenced by many factors *in vivo*. So it is very difficult to sensitively and selectively determine RSNO in biosamples by common methods. Some analytical methods for the determination of RSNO are developed. These mainly include spectrophotometry [7,8], chemiluminescence [9], electrometric methods [10,11], chromatography [12–14] and spectrofluorimetry [8,15], etc. Due to its good sensitivity and selectivity, spectrofluorimetry for RSNO determination have been rapidly developed. In spectrofluorimetric methods, RSNO is either chemically reactive or a catalyst for several types of chemical reactions on products, with a subsequent effect on the fluorescence properties (development, inhibition, or enhancement) in either a direct or an indirect way.

In 1958, Saville had reported that mercury ion displaces NO from *S*-nitrosothiols [16].

$$2\mathrm{RSNO} \xrightarrow{Hg^{2+}} 2\mathrm{NO} + \mathrm{RSSR}$$

* Corresponding author. Tel.: +86 27 68762261; fax: +86 27 68754067.
E-mail address: hshzhang@whu.edu.cn (H.-S. Zhang).

0039-9140/$ – see front matter © 2007 Elsevier B.V. All rights reserved.
doi:10.1016/j.talanta.2007.02.031

Many people have successfully determined *S*-nitrosothiol in a number of biological systems according to this strategy [5,6]. It is reported that the fluorescence probes containing vicinal aromatic diamines, such as diaminonaphthalene (DANs), diaminofluoresceins (DAFs) and diaminorhodamine (DARs), can rapidly trap NO to form triazole and fluoresce strongly [17,18]. Some researchers have used DANs to successfully determine RSNO in biosamples [19,20]. However, the emission wavelength of DAN is about 450 nm which will be influenced greatly by the self-fluorescence of biosamples in the determination of RSNO.

As one kind of important fluorescent probes, difluoroboradiaza-*s*-indacenes (BODIPY) has advantages of high extinction coefficients, high fluorescence quantum efficiency, stability to light and availability in a wide range of pH [21–24]. It has been demonstrated that *o*-phenylenediamine with electron-donating substituents causes greater inhibition of the fluorescence increase and *o*-phenylenediamine derivatives with high electron density are essential for improvement of the probe's sensitivity [25]. It also has been reported that 1,3,5,7-tetramethyl BODIPYs exhibit highest fluorescence in BODIPY analogues [26]. In these views, 1,3,5,7-tetramethyl-8-(3′,4′-diaminophenyl)-difluoroboradiaza-*s*-indacene (DAMBO) will exhibit very low fluorescence but its derivative may fluoresce highly in BODIPY analogues. Although DAMBO has been synthesized and its reactivity with NO has been studied [25], it has not been used in analysis of RSNO in blood. Therefore, in this work, DAMBO is chosen and firstly used to detect RSNO in human blood by spectrofluorimetry.

2. Experimental

2.1. Apparatus

A RF-5000 spectrofluorimeter (Shimadzu, Japan) equipped with a 1 cm × 1 cm quartz cell was employed for the fluorescence intensity measurements. Absorption spectra were recorded with a Shimadzu (Kyoto, Japan) UV-1601 spectrophotomerer. pH value of solutions was measured using a Mettler Toledo DELTA 320 meter (Mettler-Toledo, Greifensee, Switzerland).

2.2. Chemicals and reagents

Glutathione (GSH) (reduced form, free acid 98–100%) and cysteine (CYS) (hydrochloride monohydrate) were obtained from Sigma Chemical Company (St. Louis, MO, USA). DAMBO was synthesized in our lab according to the ref. [25]. The stock solution of 1×10^{-4} mol L^{-1} DAMBO was prepared in methanol. Phosphate buffered saline (PBS) consisted of 10.0 g L^{-1} NaCl, 0.25 g L^{-1} KCl, 1.44 g L^{-1} Na_2HPO_4, 0.25 g L^{-1} KH_2PO_4 and adjusted to pH 7.4.

All other reagents were of analytical reagent grade and obtained from Shanghai Chemical Reagent Co. (Shanghai, China) and all solutions were stored in the dark at 4 °C. The water used was purified in a Milli-Q water purification system (Millipore, Billerica, MA, USA).

2.3. Preparation of RSNO

RSNO was prepared fresh for each experiment by incubating 100 mM thiol (GSH or CYS) with 100 mM sodium nitrite in the presence of 250 mM HCl and 0.1 mM EDTA for 30 min at room temperature. The solutions rapidly turned red upon exposure to water, forming the corresponding RSNO. Previous studies have established that essentially no nitrite remains in the nitrosothiol solutions using this synthetic method [27]. These stock solutions were stored on ice. The final concentrations were determined using the reported extinction coefficients at 334–338 nm for GSNO ($\varepsilon_{334\,nm} = 780\ mol^{-1}\ cm^{-1}$), CYSNO ($\varepsilon_{334nm} = 900\ mol^{-1}\ cm^{-1}$) [16,28].

2.4. Determination of RSNO

Two milliliters of 2.5×10^{-5} mol L^{-1} DAMBO was transferred to a 10 mL volumetric flask. Two milliliters of PBS, 0.05 mL of 4×10^{-4} mol L^{-1} GSNO and 1 mL of 1×10^{-3} mol L^{-1} Hg^{2+} were added and the solution was diluted to the mark with water. The mixture was kept at 30 °C for 15 min. The fluorescence intensity was measured at $\lambda_{ex}/\lambda_{em}$ = 498/507 nm against a reagent blank carried through the same procedure except for the addition of RSNO.

2.5. Preparation of samples

0.5 mL of blood samples were collected from healthy volunteers and patients treated at the Hospital of Wuhan University, respectively. Six healthy persons, six hypertension patients and six hyperlipidemia patients were included in this study. All the blood samples were obtained by venipuncture using sodium citrate as an anticoagulant (3.15%, final concentration) and kept on ice in the dark. The experiments showed that nitroso compounds did not decomposed within 1.5 h during storage. After bubbling oxygen to exclude NO for 5 min, the blood samples were added into the solutions that contained 2 mL of DAMBO (2.5×10^{-5} mol L^{-1}) and 2 mL of PBS. Then 1 mL of Hg^{2+} (1×10^{-3} mol L^{-1}) solution was transferred into the above mixture and diluted to 10 mL with water and stood for 15 min at 30 °C. The whole solution was centrifuged for 10 min at 3000 rpm for removing deposit. The supernatant was taken out and determined with the proposed method.

3. Results and discussion

3.1. Fluorescence properties of DAMBO and its RSNO derivative

GSNO reacts with DAMBO and yielded an intensely fluorescent triazole derivative DAMBO-T is shown in Fig. 1. The maximum excitation wavelength of DAMBO is at 496 nm and its emission wavelength is at 505 nm. The maximum excitation wavelength of the DAMBO-T is at 498 nm following the emission wavelength at 507 nm.

It has been reported that the probe which contains two vicinal diamines nitrosated by N_2O_3 at its vicinal amino moi-

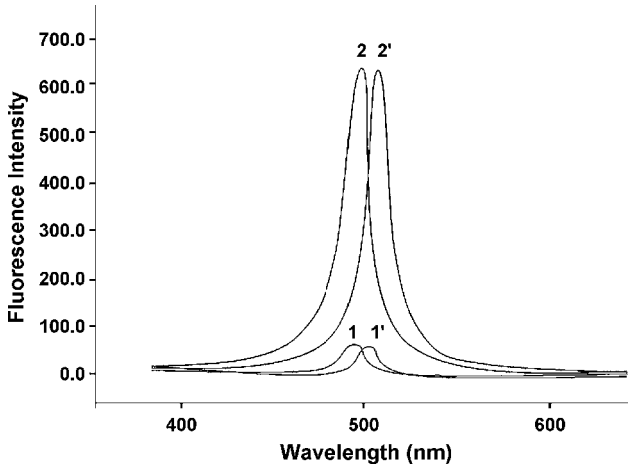

Fig. 1. Fluorescence spectra of DAMBO and the triazole $C_{DAMBO} = 5 \times 10^{-6}$ mol L^{-1}, $C_{GSNO} = 2 \times 10^{-6}$ mol L^{-1}, 1: is excitation spectrum of DAMBO at 505 nm emission wavelength; 1′: is emission spectrum of DAMBO at 496 nm excitation wavelength; 2: is excitation spectrum of the triazole at 507 nm emission wavelength; 2′: is emission spectrum of the triazole at 498 nm excitation wavelength. The slit of excitation and emission are 3 and 3 nm, respectively.

eties, an internal diazotation reaction takes place that leads to formation of the corresponding triazole, the reaction is associated with a lowering of the energetic charge-transfer state below the ground state of the fluorophore, and it removes the quenching effect of the benzoic structure and allows the fluorophore to fluoresce efficiently. DAMBO is a probe that contains two vicinal diamines. In comparison with highly fluorescent 1,3,5,7-tetramethyl-8-phenyl-difluoroboradiaza-*s*-indacene, the fluorescence of DAMBO becomes very weak ($\Phi_{fl} = 0.001$) because the two neighboring electron-donating groups, -NH_2, attached to the phthalic ring of 1,3,5,7-tetramethyl-8-phenyl-difluoroboradiaza-*s*-indacene cause a great inhibition of the fluorescence. However, when the electrondonating groups are transformed into less electron-donating groups, the fluorescence will recover. In fact, when DAMBO reacts with NO, the formation of the triazole, DAMBO-T increases the fluorescence intensity remarkably ($\Phi_{fl} = 0.40$) [25]. This phenomenon has also been observed by Munkholm et al. in the conversion of fluoresceinamine from amine to amide [29].

When mercury ion displaces NO from RSNO, the NO rapidly reacts with O_2 to form N_2O_3. Then DAMBO captures N_2O_3 to form high fluorescence triazole. The reaction process is shown as Fig. 2. A sensitive spectrofluorimetry of RSNO can be developed based on the reaction.

Because the stability of DAMBO and its derivative may greatly influence the reproducibility and sensitivity of RSNO determination, the stability of DAMBO and its RSNO derivative at room temperature has been investigated. DAMBO and DAMBO-T solution were placed at room temperature for 60 h, respectively. The results showed that the fluorescence intensity of DAMBO and its RSNO derivative decreased by only 0.48 and 0.36%.

Furthermore, DAMBO has been reported to have high sensitivity and to selectively react with NO [25], so it also can be used to sensitively and selectively detect RSNO in complex

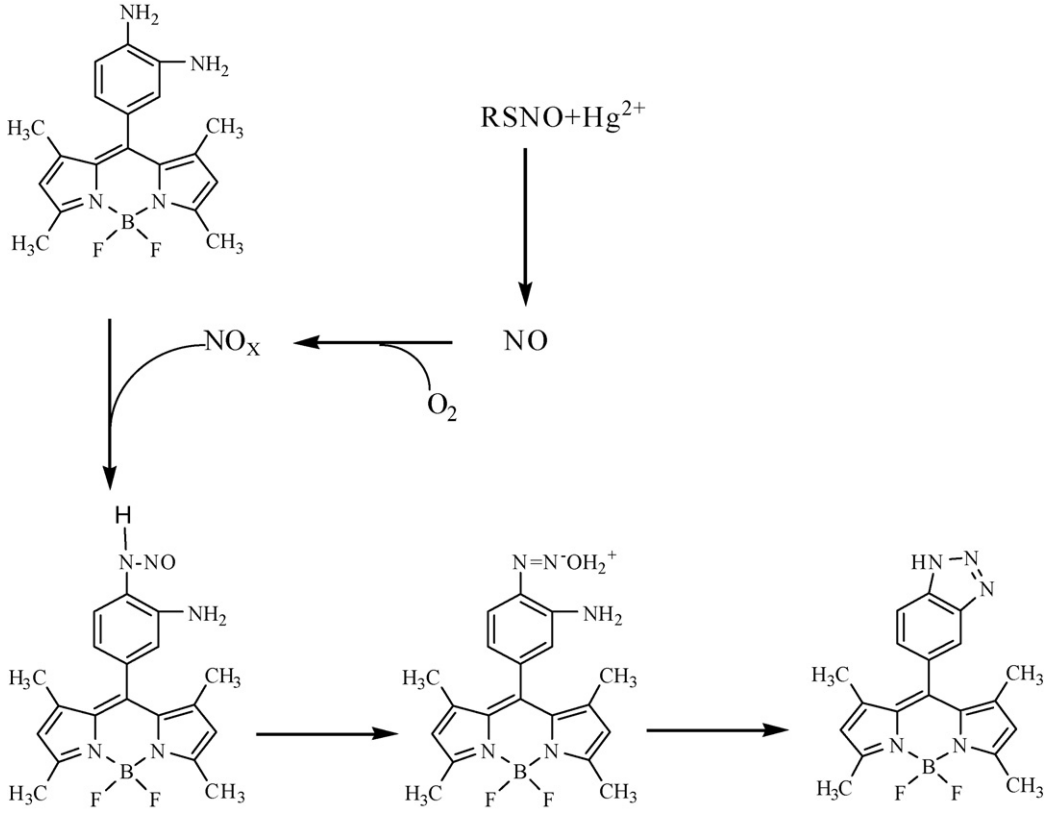

Fig. 2. Reaction of RSNO with DAMBO.

Table 1
Effect of different metal ions on fluorescence intensity

Metal ions (0.1 mM)	Fluorescence intensity (with metal ion)	Fluorescence intensity (without metal ion)
Hg(II)	618.28	12.15
Cu(II)	548.54	12.12
Pb(II)	12.49	12.15
Zn(II)	18.76	12.15
Fe(II)	12.91	12.18
Fe(II)	14.68	12.12
Co(II)	12.99	12.12
Mn(II)	14.11	12.15
Cd(II)	25.89	12.15

biosamples. All these properties made DAMBO preferable in the determination of RSNO.

3.2. Optimization of derivatization conditions

3.2.1. Effect of metals

It has been reported that some metals can decompose RSNO [29]. A variety of metal ions were exposed to the solutions that contained 2×10^{-6} mol L^{-1} GSNO and 5×10^{-6} mol L^{-1} DAMBO. Table 1 showed that no other metals except Cu(II) and Hg(II) ions caused obvious increase of fluorescence of the above solution at 507 nm. Trace amounts of copper ion and mercury ion can catalyze the decomposition of *S*-nitrosothiols [30,31]. Although Cu^{2+} was less toxic than Hg^{2+}, Hg^{2+} was more efficient in displacing NO from GSNO. In order to improve the sensitivity of the method, Hg(II) ion was selected for further experiments.

3.2.2. Effect of DAMBO concentration

DAMBO concentration had effect on the fluorescence intensity (Fig. 3). The maximum of fluorescence intensity appeared at the DAMBO concentrations of $4.0–6.0 \times 10^{-6}$ mol L^{-1}. For reducing the eventual interference, 4×10^{-6} mol L^{-1} of DAMBO solution was chosen for the following experiments.

3.2.3. Effect of Hg(II) ion concentration

Hg(II) ion was an important factor to effectively decompose RSNO. When its concentration was too low, it cannot completely decompose RSNO. However, when its concentration was too high, it was superfluous and then may be dangerous to the health of human. Therefore, its effect on the fluorescence intensity has been investigated in detail. It was found that the fluorescence intensity reached the maximum in a concentration that ranged from 0.8 to 1.2×10^{-4} mol L^{-1} (Fig. 4). Then 0.8×10^{-4} mol L^{-1} Hg(II) ion concentration was chosen.

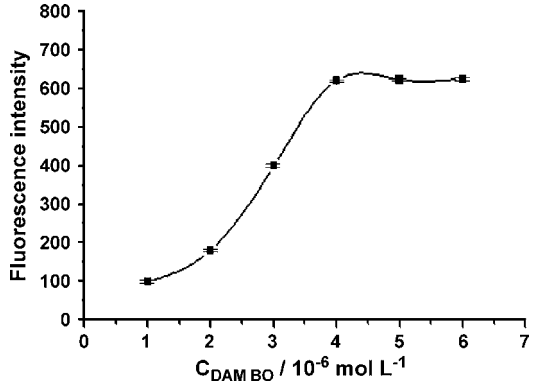

Fig. 3. Effect of DAMBO concentration $C_{GSNO} = 2 \times 10^{-6}$ mol L^{-1}; $C_{Hg^{2+}} = 1 \times 10^{-4}$ mol L^{-1}; reaction time, 15 min; reaction temperature, 30 °C.

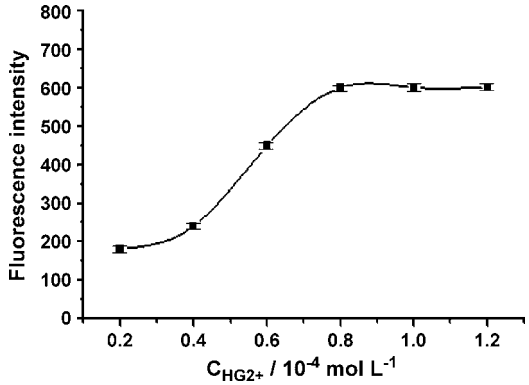

Fig. 4. Effect of Hg^{2+} concentration $C_{GSNO} = 2 \times 10^{-6}$ mol L^{-1}; $C_{DAMBO} = 5 \times 10^{-6}$ mol L^{-1}; reaction time, 15 min; reaction temperature, 30 °C.

3.2.4. Effect of reaction time and temperature

Time and temperature were both critical factors in the reaction of DAMBO and RSNO. The effect of time and temperature on the fluorescence intensity is shown in Fig. 5. When the reaction was carried out at 30 °C, the fluorescence intensity reached the maximum. The reaction temperature at 30 °C was used. The fluorescence intensity was stable after 15 min. The reaction time of 15 min was selected for further experiments.

3.3. Effect of foreign ions

To evaluate the selectivity of the proposed method, the effect of diverse ions on the determination of GSNO has been studied. Known quantities of the diverse ions were added to a fixed amount of GSNO, and then the fluorescence intensity of the mixture was determined. The ions that cause an

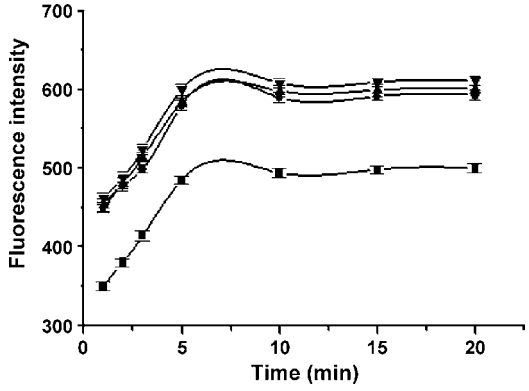

Fig. 5. Effect of reaction time and temperature $C_{GSNO} = 2 \times 10^{-6}$ mol L^{-1}; $C_{DAMBO} = 5 \times 10^{-6}$ mol L^{-1}; $C_{Hg^{2+}} = 1 \times 10^{-4}$ mol L^{-1}; (■), 10 °C; (●), 20 °C; (▼), 30 °C; (▲), 40 °C.

Table 2
Effect of foreign ions

Foreign ion	Tolerance ($\mu g\,L^{-1}$)
Ca^{2+}	40000
Mg^{2+}	30000
Zn^{2+}	20000
BSA	24000
Cys	21000
GSH	20000
NO_3^-	100000
NO_2^-	40000
SO_4^{2-}	40000
CO_3^{2-}	50000
EDTA	150000
PO_4^{3-}	100000

error less than ±5% in the determination of 2×10^{-6} mol L^{-1} GSNO are given in Table 2. When present in relatively large to moderately large mass excess, 12 cations, anions and complexing agents had negligible interference in the determination of GSNO. The study revealed that the tolerance limits for these ions were larger than their concentrations in real samples.

3.4. Method validation

Under the optimized conditions, the analytical quantitation of GSNO with proposed method has been carried out. According to the fluorescence intensity of analytes, a linear relationship was observed in the range of 6.0–400.0 $\times 10^{-9}$ mol L^{-1} ($\gamma = 0.9995$). The linear regression equation was $Y = 14.78X + 18.07$ (Y was the fluorescence intensity and X was the concentration of GSNO (1×10^{-9} mol L^{-1})). The limit of detection (S/N = 3) was found to be 0.12 nmol L^{-1}. The inter-day and intra-day precision (relative standard deviation, R.S.D.) and accuracy (relative error, R.E.) of the proposed method for spiked samples were studied at four quality control levels. The results (Table 3) showed that the R.S.D.s and R.E.s were all below 2.38 and 1.80%, respectively. The results showed that the proposed method was more sensitive than other known methods (Table 4).

Table 3
Precision and accuracy for the determination of GSNO in intra- and interday analysis

Concentration known (nM)	Concentration found (nM)	R.S.D. (%)	R.E. (%)
	Intra-day analysis ($n = 6$)		
6.0	6.09	1.42	1.45
30.0	30.24	1.36	0.80
180.0	178.58	1.22	−0.79
400.0	396.72	1.12	−0.82
	Inter-day analysis ($n = 6$)		
6.0	6.11	2.38	1.80
30.0	30.37	2.05	1.24
180.0	181.66	1.90	0.92
400.0	403.44	1.85	0.86

Table 4
Comparison of detection limits for determinations of RSNO

Method/reagent(s) used	Detection limit (nM)	References
Chemiluminescence	10	[9]
HPLC	200	[10]
HPLC	1	[37]
HPLC	500	[38]
HPLC/*o*-phthalaldehyde	3	[39]
Electrometry	20	[40]
Electrometry	50	[41]
Spectrofluorimetry/2,3-diaminonaphthalene	100	[42]
Spectrofluorimetry/2,3-diaminonaphthalene	150	[43]
Spectrofluorimetry/DAMBO	0.12	This paper

Table 5
Analytical results of the samples

Sample	Added (10^{-7} mol L^{-1})	Found (10^{-7} mol L^{-1})	R.S.D (%) ($n = 6$)	Recovery (%)
Healthy human				
(1)	0.00	11.23	2.42	
	10.00	20.98	2.75	97.52
(2)	0.00	11.20	2.46	
	10.00	20.95	2.70	97.59
(3)	0.00	11.26	2.53	
	10.00	21.13	2.78	98.74
(4)	0.00	11.24	2.31	
	10.00	21.38	2.56	101.42
(5)	0.00	11.32	1.94	
	10.00	21.55	2.61	102.30
(6)	0.00	11.18	1.89	
	10.00	21.09	3.04	99.12
Hypertension				
(1)	0.00	4.24	1.89	
	4.00	8.35	2.10	102.81
(2)	0.00	4.26	1.94	
	4.00	8.36	2.70	102.41
(3)	0.00	4.20	2.56	
	4.00	8.11	2.67	97.68
(4)	0.00	4.16	2.35	
	4.00	8.14	3.01	99.62
(5)	0.00	4.12	1.98	
	4.00	8.05	2.46	98.32
(6)	0.00	4.24	2.15	
	4.00	8.28	2.60	100.89
Hyperlipidemia				
(1)	0.00	4.28	2.89	
	4.00	8.22	3.12	98.42
(2)	0.00	4.26	2.36	
	4.00	8.21	2.87	98.78
(3)	0.00	4.28	2.46	
	4.00	8.24	3.10	99.12
(4)	0.00	4.32	2.48	
	4.00	8.23	2.54	97.64
(5)	0.00	4.24	2.31	
	4.00	8.34	2.64	102.41
(6)	0.00	4.26	1.89	
	4.00	8.21	2.72	98.74

3.5. Application to blood

It was reported that the number of deaths caused by cardiovascular diseases could reach more than 1.5 million every year in China [32]. Obviously, cardiovascular diseases would be the greatest threat to the human health. Human blood obtained from the healthy individuals and patients were chosen as the targets for the proposed method analysis.

The proposed method was applied to the determination of trace RSNO in the blood samples including healthy persons, hypertension patients and hyperlipidemia patients. After all the blood samples were obtained, bubbling oxygen was performed to exclude NO from the samples. The experiments showed that 5 min of bubbling oxygen was enough to remove the interference of NO. Then all samples were analyzed for six times using the same recommended procedure and conditions. The results of samples unspiked and spiked with standard solutions are shown in Table 5. The recoveries ranged from 97.52 to 102.81% and the R.S.D. from 1.89 to 3.12%, which was satisfactory.

The results in Table 5 showed that the amounts of RSNO in blood samples of patients with cardiovascular diseases were less than that in healthy individuals, and it was the lowest in that of hypertension patients. Many studies [33–36] have demonstrated that vascular endothelial cells were impaired in cardiovascular diseases, and then NO synthesization is depressed accordingly. Therefore, the synthesization of RSNO also decreased. Our results confirm these conclusions.

4. Conclusion

A novel spectrofluorimetric method has been developed for analysis of RSNO. 1,3,5,7-Tetramethyl-8-(3′,4′-diaminophenyl)-difluoroboradiaza-*s*-indacence (DAMBO), a sensitive fluorescent labeling reagent was successfully used for the first time to label and assay these compounds by use of spectrofluorimetry. The derivatization reaction was performed in aqueous medium at 30 °C for 15 min. The changes of fluorescence intensity were linear in the concentration range 6–400 nmol L^{-1} of RSNO. The detection limit reached 0.12 nmol L^{-1} (S/N = 3). The proposed method was successfully applied to the determination of RSNO in blood samples that included healthy persons, hypertension patients and hyperlipidemia patients with satisfactory recoveries varying from 97.52 to 102.81%. Mainly because of the favorable labeling chemistry of DAMBO, the method has advantages of good specificity and sensitivity.

Acknowledgement

The research presented in this manuscript was supported by the National Natural Science Foundation of China (No. 20575047).

References

[1] D.L.H. Williams, in: D.H.L. Williams (Ed.), Nitrosation, Cambridge University Press, New York, 1988.
[2] J.S. Stamler, Cell 78 (1994) 931.
[3] L.J. Ignarro, B.K. Barry, D.Y. Gruetter, J.C. Edwards, E.H. Ohlstein, C.A. Gruetter, W.H. Baricos, Biochem. Biophys. Res. Commun. 94 (1980) 93.
[4] L.J. Ignarro, Pharmacol. Res. 6 (1989) 651.
[5] J.S. Stamler, O. Jaraki, J. Osbourne, D.I. Simon, J. Keaney, J. Vita, D. Singel, R. Valeri, J. Loscalzo, Proc. Natl. Acad. Sci. U.S.A. 89 (1992) 7674.
[6] B. Gaston, J. Reilly, J.M. Drazen, J. Fackler, P. Ramdev, D. Arnelle, M.E. Mullins, D.J. Sugarbaker, C. Chee, D.J. Singel, J. Loscalzo, J.S. Stamler, Proc. Natl. Acad. Sci. U.S.A. 90 (1993) 10957.
[7] C.M. Padget, Arch. Biochem. Biophys. 358 (1998) 232.
[8] J.A. Cook, S.Y. Kim, D. Teague, Anal. Biochem. 238 (1996) 150.
[9] A. Samouilov, J.L. Zweier, Anal. Biochem. 258 (1998) 322.
[10] R.K. Goldman, A.A. Vlessis, D.D. Trunkey, Anal. Biochem. 259 (1998) 98.
[11] A.S. Vidwans, S. Kims, D.O. Coffin, J. Neurochem. 72 (1999) 1843.
[12] J.S. Stamler, J. Loscalzo, Anal. Chem. 64 (1992) 779.
[13] A. Vliet, P.A.C. Hoen, P.S.Y. Wong, Am. Soc. Biochem. Mol. Biol. 273 (1998) 30255.
[14] D. Nikitovic, A. Holmgren, Am. Soc. Biochem. Mol. Biol. 271 (1996) 19180.
[15] K. Shibuki, Neurosci. Res. 9 (1990) 69.
[16] Saville, Analyst 83 (1958) 670.
[17] H. Kojima, N. Nakatsubo, K. Kikuchi, Anal. Chem. 70 (1998) 2446.
[18] H. Kojima, M. Hirotani, N. Nakatsubo, Anal. Chem. 73 (2001) 1967.
[19] K.G. Robert, A.V. Angelo, D.T. Donald, Anal. Biochem. 259 (1998) 98.
[20] A.C. John, Y.K. Sungmee, T. Diane, C.K. Murali, P. Roberto, B.M. James, V. Yoram, W.N. Raymond, C. Danae, M.M. Allen, B.G. Matthew, A.W. David, Anal. Biochem. 238 (1996) 150.
[21] F. Li, S.L. Yang, Y. Ciringh, J. Seth, C.H. Martin, D.L. Singh, D. Kim, R.R. Birge, D.F. Bocian, J. Am. Chem. Soc. 120 (1998) 10001.
[22] J. Arolin, L.B. Johansson, L. Strandberg, T. Ny, J. Am. Chem. Soc. 116 (1994) 7801.
[23] J.S. Li, H. Wang, L.W. Cao, H.S. Zhang, Talanta 69 (2006) 1190.
[24] K.J. Huang, H. Wang, Y.H. Guo, R.L. Fan, H.S. Zhang, Talanta 69 (2006) 73.
[25] Y. Gabe, Y. Urano, K. Kikuchi, H. Kojima, T. Nagano, J. Am. Chem. Soc. 126 (2004) 3357.
[26] M. Kollmannsberger, K. Rurack, U. Resch-Genger, J. Daub, J. Phys. Chem. A 102 (1998) 10211.
[27] D.R. Arnelle, J.S. Stamler, Arch. Biochem. Biophys. 318 (1995) 279.
[28] L. Field, R.V. Dilts, R. Ravichandran, P.G. Lenhert, G.E. Carnahan, J. Chem. Soc. Chem. Commun. 1157 (1978) 249.
[29] A.M. Munkholm, D.R. Parkinson, D.R. Walt, J. Am. Chem. Soc. 112 (1990) 2608.
[30] J. McAninly, D.H.L. Williams, S.C. Askew, A.R. Butler, C. Russell, J. Chem. Soc. Chem. Commun. 93 (1993) 1758.
[31] A.F. Vanin, Biochemistry (Moscow) 80 (1995) 441.
[32] R.T. Hui, X.H. Fan, J. Clin. Intern. Med. 22 (2005) 1.
[33] J.A. Panaza, P.R. Casino, D.M. Badar, Circulation 87 (1993) 1468.
[34] T.F. Luscher, C.M. Boulanger, Z. Yang, Circulation 87 (1993) 36.
[35] A.P. Davenport, E.R. Kuc, J.J. Maguire, J. Cardiovasc. Pharmacol. 26 (1995) 265.
[36] T.M. Ian, J. Todd, M. Anderson, Am. J. Cardiol. 72 (1993) 27.
[37] O. Tashimo, T. Ishibashi, J. Yoshida, H. Tsuchida, M. Nishio, Nitric Oxide 9 (2003) 148.
[38] D. Tsikas, K. Denker, J. Chromatogr. A 915 (2001) 107.
[39] D. Tsikas, J. Sandmann, D. Holzberg, P. Pantazis, M. Raida, Anal. Biochem. 273 (1999) 32.
[40] J. Vitecek, J. Petrlova, J. Petrek, V. Adamb, D. Potesil, L. Havel, R. Mikelova, L. Trnkova, R. Kizek, Electrochimica. Acta. 51 (2006) 5087.
[41] S. Pfeiffer, A. Schrammel, K. Schmidt, B. Mayer, Anal. Biochem. 258 (1998) 68.
[42] J.H. David, H. Katarina, F. Martin, B.G. Matthew, Free Radic. Biol. Med. 28 (2000) 409.
[43] M. Marzinzig, A.K. Nussler, J. Stadler, E. Marzinzig, W. Barthlen, N.C. Nussler, H.G. Beger, S.M. Morris, Nitric Oxide 2 (1997) 177.

Available online at www.sciencedirect.com
ScienceDirect
Talanta 73 (2007) 1–11
Talanta
www.elsevier.com/locate/talanta

Review

Atomic spectrometric methods for the determination of metals and metalloids in automotive fuels – A review

Maria das Graças Andrade Korn [a,*], Denilson Santana Sodré dos Santos [a], Bernhard Welz [a], Maria Goreti Rodrigues Vale [b], Alete Paixão Teixeira [a], Daniel de Castro Lima [a], Sérgio Luis Costa Ferreira [a]

[a] *Grupo de Pesquisa em Química Analítica, Instituto de Química, Universidade Federal da Bahia, 40170-290 Salvador – BA, Brazil*
[b] *Instituto de Química, Universidade Federal do Rio Grande do Sul, A. Bento Gonçalves 9500, 91501-970 Porto Alegre – RS, Brazil*

Received 9 February 2007; received in revised form 13 March 2007; accepted 13 March 2007
Available online 24 March 2007

Abstract

Gasoline, diesel, ethanol and more recently also biodiesel are the four types of fuel used for automobile, truck and other transportation vehicle. The presence of metallic and metalloid species in automotive fuels is undesirable, except in the form of additives in order to improve specific characteristics of the fuel. Metallic or metalloid elements may derive from the raw product, such as nickel and vanadium in petroleum-based fuel or phosphorus in biodiesel, or they may be introduced during production and storage, such as copper, iron, nickel and zinc in case of petroleum-based fuel and alcohol or sodium and potassium in the case of biodiesel. The most famous additive to fuel is undoubtedly lead, the use of which has been banned or drastically reduced now in many countries of the world. The problems related to the trace element content may be economic, such as fuel degradation and poisoning of automotive catalysts, and/or environmental, such as the emission of metal compounds to the atmosphere. The analytical methods that have been developed for metal and metalloid quantification in automotive fuel are reviewed in this article. The main atomic spectrometric techniques used for trace metal and metalloid determination in fuels, particularly atomic absorption spectrometry with flames, graphite furnaces and with chemical vapor generation, and inductively coupled plasma coupled with optical emission and mass spectrometry are presented, including the different sample preparation procedures proposed for these techniques.

Keywords: Automotive fuels; Biodiesel; Metallic and metalloid elements; Atomic spectrometry; Sample preparation

Contents

* Corresponding author. Tel.: +55 71 32636830; fax: +55 71 32355166.
E-mail address: korn@ufba.br (M. das Graças Andrade Korn).

0039-9140/$ – see front matter © 2007 Elsevier B.V. All rights reserved.
doi:10.1016/j.talanta.2007.03.036

1. Introduction

Fuel is any material that is capable of releasing energy when its chemical or physical structure is changed or converted. The important property of a fuel is that its energy can be stored to be released only when needed, and that the release is controlled in such a way that the energy can be used to produce work. Different types of automotive fuel are available and their energy is released through chemical means, i.e. by burning [1]. The automotive fuels most commercialized worldwide nowadays are: gasoline, diesel, ethanol and biodiesel.

Gasoline is a volatile liquid that is used in internal combustion engines. It is formed by a complex mixture of hydrocarbons, between 4 and 12 carbons, such as paraffins, naphthenes, olefins, and aromatic hydrocarbons derived from petroleum crude plus a small amount of additives to improve its stability, control deposit formation in engines, improve performance and modify other characteristics [2,3]. The most well-known additive to gasoline is without any doubt lead in the form of tetramethyl lead (TML) and tetraethyl lead (TEL).

Diesel fuel is a blend of petroleum-derived compounds called middle distillates, heavier than gasoline but lighter than lubricating oil, and may or may not contain metal additives. Diesel fuel consists mostly of hydrocarbons ranging from 10 to 24 carbons, with boiling points between about 150 and 400 °C. It is designed to operate in a diesel engine where it is injected into the compressed, high-temperature air in the combustion chamber and ignites spontaneously. This differs from gasoline, which is ignited in an Otto engine by spark plugs [4,5]. The most notorious contaminant in diesel fuel is sulfur, which, however, is not usually determined by atomic spectrometric methods.

Ethanol derived from crops (bio-ethanol) is a demonstrably sustainable energy resource that might offer environmental and long-term economic advantages over fossil fuel (gasoline and diesel). It is readily obtained from the sugar or starch in crops such as maize and sugarcane. Ethanol can be used as fuel for automobiles either alone in specially designed engines or as an additive to gasoline. Nowadays essentially all car manufacturers produce engines that can use ethanol, gasoline or any mixture of these fuels without any modification. Ethanol can be blended with gasoline in varying quantities to reduce the consumption of petroleum fuels, as well as to reduce air pollution. Ethanol is also increasingly used as an oxygenate additive for standard gasoline to replace methyl *t*-butyl ether (MTBE), which has been responsible for considerable groundwater and soil contamination [1,6]. Among the elements that have to be controlled in fuel ethanol are sodium, potassium and copper.

Biodiesel is a renewable, biodegradable and non-toxic fuel derived from biological sources such as vegetable oil or animal fat through transesterfication reaction in the presence of potassium hydroxide as a catalyst. It can be used in diesel engines and can supplement fossil fuels as the world's primary transport energy source. Conventional diesel engines can seamlessly run up to 20% biodiesel blends (B20) with 80% petroleum diesel; minor modifications are necessary to the engine to run 100% biodiesel. Besides not being refined from crude oil, biodiesel offers other attractive characteristics, such as better lubricity than diesel fuel because of its higher viscosity, and a significantly lower emission of carbon monoxide (CO), carbon dioxide (CO_2), sulfur dioxide (SO_2) and hydrocarbons (HC). It also eliminates the cloud of dense, black smoke normally associated with diesel vehicles and other particulate matter (PM) emissions that cause respiratory damage [7]. Among the elements that have to be controlled in biodiesel are sodium and potassium (maximum permissible concentration 5 mg kg^{-1}), which originate from the catalyst used in its production and phosphorus (maximum permissible concentration 10 mg kg^{-1}), which originates from the raw material.

Although metal-organic species are present in fuels only in low concentration, the overall emission relative to its burning contributes significantly to environmental pollution, particularly in densely populated areas. This automotive emission has an adverse environmental impact, contributing to a decline in air quality, which can have an effect on human health [8]. According to energy information administration (EIA) the total worldwide consumption of automotive fuels has been growing rapidly during the past 15 years and is expected to continue to do so in the future, as shown in Fig. 1 [9]. Since the consumption of fuels has become an indispensable part of modern life, the monitoring of

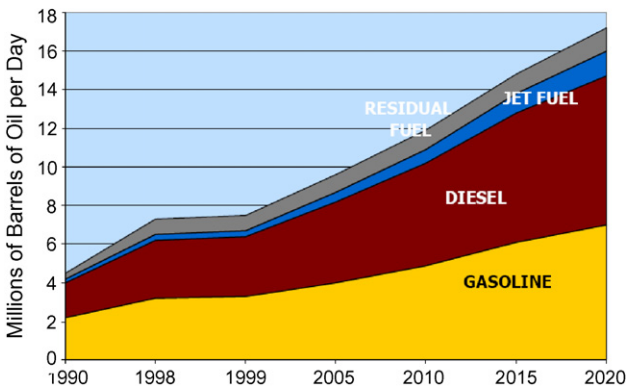

Fig. 1. Worldwide fuel consumption (from Ref. [8] with permission).

its environmental impact and the implementation of fuel quality control programs is an urgent requirement.

The development of analytical techniques for the quantification of metals in fuel hence is driven by environmental and economic interests. However, several problems are associated with the analysis of this kind of samples due to their high complexity and organic nature of their matrix. A variety of analytical procedures have been proposed for quantification of metallic and metalloid species in fuels. In this review the main spectroscopic techniques used for this purpose are presented, including different sample preparation procedures proposed for these techniques.

2. Presence of metals in fuels

Some metals, such as nickel and vanadium are natural constituents of petroleum, and consequently they are found in all its derived products, although in significantly lower concentration [10,11]. Iron and zinc are the main construction materials for fuel tanks, this way, they might be transferred to the fuel during transport and/or storage [12,13]. Copper may be introduced during the distillation and refinement process [14]. Other metallic species can also be introduced deliberately into fuels as additives in order to promote specific characteristics. Additives for gasoline, diesel, fuel oil, kerosene, and jet fuel can contain such metals as aluminum, calcium, cerium, chromium, cobalt, copper, lanthanum, lead, lithium, magnesium, manganese, molybdenum, nickel, silicon, silver, sodium, thallium, tin, tungsten, vanadium, zinc and zirconium [15–19].

2.1. Lead in gasoline

Lead is undoubtedly the metallic element most frequently determined in gasoline due to the fact that, for more than half a century, this element was blended to automotive fuels as metal-organic tetramethyl lead (TML) and tetraethyl lead (TEL), with the purpose of suppressing uncontrolled ignition in the internal combustion engine [20]. Burning of these leaded fuels resulted in lead deposits in the motor parts, which caused corrosion. The solution for this problem was the addition of dibromo- and dichloro-ethylene which resulted in the formation of volatile lead compounds that were removed from motor parts and released into the environment through the vehicle exhaust system. These volatile products were oxidized in the atmosphere under the influence of the solar light forming lead oxide (PbO), which stayed in the atmosphere in the form of aerosol particles for hours or even days [21] before it was deposited in the environment.

The emission from vehicle was for several decades the main source of lead in human blood. It entered the human body through the inhalation of air or the alimentary chain, since the soluble lead, which deposited on soil, plants and in water, was absorbed by plants and animals and ended up in the food chain. Lead has long been known to be toxic; it can cause neurological dysfunctions, renal damage, and at high doses death [22]. In addition, it is also known that lead even in small concentrations can poison hydrocarbon reforming and car catalysts [23]. For these reasons, legislation in many countries has fixed the maximum permissible concentration of lead in gasoline or removed it definitely from the use as an additive for fuel. The introduction of unleaded gasoline is considered an important event for environmental quality.

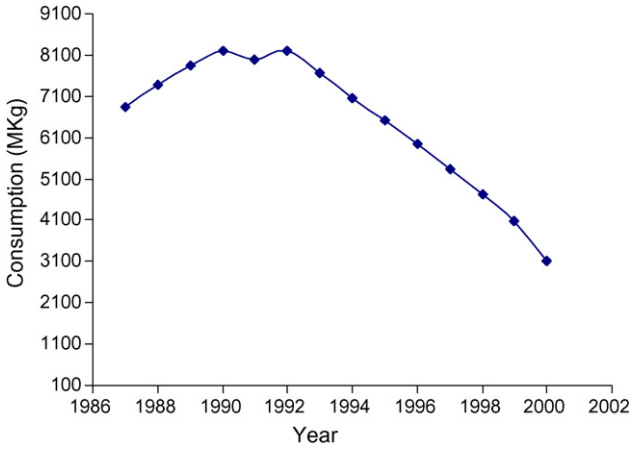

Fig. 2. Annual consumption of leaded gasoline in accordance to ASERPETROL (according to data from Ref. [25]).

From the 1960s up to well into the 1980s, a significant increase in the consumption of leaded gasoline was observed, mainly in economically developed countries [24]. In consequence, the lead concentration in the environment increased to the same proportion. At the end of the 1980s, with the introduction of unleaded gasoline, a gradual decrease of environmental lead contamination and health problems was recorded [25–28]. Fig. 2 shows the consumption of leaded fuels, as provided by the Spanish Association of Petroleum Refining Companies (ASERPETROL), the Association of Petroleum Operators (AOP) and the Corporation of Strategic Reserves of Petroliferous Products (CORES). However, lead poisoning due to leaded gasoline remains a topic of concern in many third-world countries.

2.2. Other trace elements in fuel

Besides lead, other elements, such as As, Cd, Hg, Se and Tl are released into the environment due to combustion of fuel in automobiles, which are an important source of atmospheric pollution [11]. Micrometer and sub-micrometer particles (PM10 to PM0.1) derived from fossil fuel combustion have direct and indirect impact on human health especially that of young children [29–35]. Studies carried out to assess the characteristics and significance of metals released into the atmosphere suggest that the emission of some metals in vehicle exhaust, such as barium, could be fully explained by their presence in the fuel [36].

Gasoline contains some unsaturated hydrocarbons that introduce a certain degree of instability to the fuel. This molecular instability is responsible for an oxidation process that begins soon after gasoline production and continues throughout the storage period. In these oxidation reactions the hydrocarbons present in gasoline react with oxygen and with each other, promoting changes in its physical and chemical properties due to formation of gums, which cause deposits in filters and distribu-

tion lines. Metals, such as Cu catalyze these oxidation reactions and increase significantly the gum content of gasoline leading to fuel decomposition and poor engine performance [37,38]. In addition, the presence of Ni and Pb compounds in fuel reduces the efficiency of catalytic reactors used in vehicle exhaust systems, increasing the emission of exhaust gases such as carbon monoxide and oxides of sulfur and nitrogen [39,40].

Corrosion problems are more severe with alcohol than with hydrocarbon fuels due to its chemical composition [37]. The presence of metals such as Cu, Fe and Na in alcohol may be associated with corrosion of engine parts. Therefore, the quantification of these metals is quite important due to their effect on the fuel performance and for fuel quality [14]. The presence of Na and K in biodiesel, which originate from the potassium hydroxide catalyst may equally cause corrosion problems and are therefore limited to 5 mg kg^{-1}. Phosphorus, which originates from the raw products of biodiesel production, i.e., vegetable oils or animal fat, is a poison for the catalytic converters in the exhaust system of diesel engines [41] and increases the emission of CO, CO_2, SO_2, HC and PM.

The presence of metallic elements in fuel is usually undesirable, even in low concentration, and their quantification is necessary to evaluate fuel quality and to control atmospheric pollution. In the case of additives, the quantification of metals is indispensable for the control of physical and chemical properties of the fuel [42].

The concentration of metals in fuels is generally low and requires the use of highly sensitive analytical techniques. Nowadays these determinations are mainly accomplished by electrothermal atomic absorption spectrometry (ET AAS), and inductively coupled plasma mass spectrometry (ICP-MS). Flame atomic absorption spectrometry (FAAS), flame emission spectrometry (FAES) and inductively coupled plasma optical emission spectrometry (ICP OES) do not offer sufficient sensitivity for the direct determination of most elements of interest. Chemical vapor generation (CVG) combined with AAS or atomic fluorescence spectrometry (AFS) is one of the most sensitive techniques available, but it is limited to a few analytes and requires complete destruction of the organic matrix. Techniques such as X-ray fluorescence spectrometry, spectrophotometry, polarography, titrimetry, and anodic stripping voltammetry are used less frequently.

3. Sample pretreatment procedures

Sample pretreatment is probably the most critical stage of fuel analysis and consists of submission of the sample to a procedure in which it becomes more appropriate for analysis. This is the stage of an analysis, where most errors occur, which is most time consuming and which increases the cost of the analysis; therefore all stages of a pretreatment procedure have to be carefully considered [43]. The various pre-treatment procedures employed for the determination of metals in fuel exhibit advantages and disadvantages. Among the factors that have to be taken into account are: (i) the analytical technique employed; (ii) the nature of the sample; (iii) the analyte and its concentration; (iv) the degree of accuracy and precision required; (v) the availability of equipment, materials and reagents and (vi) cost of the analysis.

3.1. Direct analysis of fuels

There are only a few examples of fuel analysis without any previous treatment in the literature [44–46]. The direct introduction of fuel samples for the determination of trace metals presents some general problems, such as volatility, flammability and immiscibility with water, and a number of specific problems, depending on the analytical technique used, such as: (i) production of flames that are very rich in fuel and unstable in the case of FAAS, a problem that can be solved relatively easily by simply reducing the acetylene supply or increasing the flow rate of air; (ii) difficulty of sample introduction due to the low viscosity and surface tension in ET AAS; (iii) excessive spreading of the fuel during thermal pretreatment in ET AAS due to the temperature gradient when longitudinally heated atomizers are used; (iv) deposition of carbon residues on components of the spectrometer and de-stabilization or extinction of plasma in ICP methods [39,47]; (v) interferences due to carbon-based polyatomic species in ICP-MS.

In addition to problems related to the complexity of the matrix, organic standards, which are indispensable in case of direct sample introduction, are unstable and there are no certified reference materials available for these samples. For this reason the accuracy of the developed methods has to be accomplished by comparison with results obtained with independent techniques, particularly with respect to sample preparation. To overcome these problems, depending on the technique used and the element to be determined, several procedures of fuel sample preparation have been proposed, from dilution with organic solvents over emulsification to total mineralization [48].

3.2. Dilution with organic solvents

Dilution with organic solvents, in spite of its simplicity, has several inconveniences: (i) the stability of the solutions depends on the container material and the analyte concentration may change rapidly after dilution due to adsorption at the walls of the recipients [47]. This applies for the analyte in the sample and/or in the calibration solution. Analyte concentration may also increase due to evaporation of the solvent. (ii) Handling of some organic solvents with conventional laboratory equipment is difficult due to their high vapor pressure and/or low viscosity. (iii) The problems of plasma destabilization or extinction in case of the ICP techniques and contamination of the instrument with carbon residues persist, as the organic load is not reduced with dilution. (iv) The toxicity of many organic solvents requires special care to avoid any health hazard for laboratory personnel. (v) Different metal-organic compounds often exhibit different sensitivity, and the sensitivity depends on the composition of the fuel and the diluent used [10,20]. In addition it is necessary to use organic standards for calibration, which are not only relatively expensive, but might also show a sensitivity different from that of the metal-organic compounds present in the fuel [49]. Examples of solvents typically used in dilution procedures

are xylene, isobutyl methyl ketone (IBMK), octane, propan-2-ol, and toluene [10,20,50].

3.3. Preparation of emulsion/micro-emulsion

Alternatively, a fuel sample might be modified by formation of an emulsion or micro-emulsion (three-component system). Whenever two immiscible liquids are stirred, a macro emulsion is obtained, either oil-in-water (O/W, droplets of oil in water) or water-in-oil (W/O, droplets of water in oil), depending on the dispersed phase. In emulsions and micro-emulsions the fuel is dispersed in the aqueous phase as micro-drops stabilized by micelles or vesicles generated by the addition of a detergent. The kind of emulsion that is formed is mainly related to the formulation and to a lesser degree to the O/W ratio. In the case of micro-emulsions without detergent a co-solvent allows the formation of a homogeneous and long-term stable three-component solution containing the aqueous and organic phase [51,52]. Such approach allows the use of aqueous standards for calibration without the need of sample mineralization. The thermodynamic stability of these systems is influenced by several variables such as the chemical nature and the relative amounts of the components, as well as the technique used for mixing the components [53–59]. Generally, in the preparation of emulsions a surfactant with a suitable hydrophilic–lyophilic balance (HLB) is used that permits relatively high solubility between the immiscible phases and in the case of detergentless micro-emulsions the co-solvent is an alcohol of low molecular weight [60]. Emulsions and micro-emulsions have been successfully applied for the preparation of fuel samples, due to the homogeneous dispersion and stabilization of the oil micro-droplets in the aqueous phase, which brings the viscosity close to that of an aqueous solution and reduces the organic load of the system.

3.4. Analyte extraction

Extraction of the analyte from the fuel is another way of sample preparation that combines the advantages of separating the analyte from the matrix, transferring it to an aqueous phase and making at the same time a pre-concentration. Liquid–liquid extraction procedures present as main advantage their simplicity. In the most common configuration a separation funnel is used; alternately, several extractors are available. On the other hand, this technique has a series of disadvantages: (i) the enrichment factor (EF) depends directly on the volume ratio of the two liquids, which implies the need of relatively large sample volumes to obtain a good EF; (ii) the analytes may become adsorbed at recipient walls, resulting in measurement errors; (iii) the process is difficult to automate [61].

Solid phase extraction is a useful separation/pre-concentration procedure for determination of trace metals in fuel by atomic spectrometric methods. It is based on the partition between a liquid (sample) and a solid phase (sorbent), which can be unloaded, loaded or chemically modified with organo-functional groups [62]. After pre-concentration the analyte is recovered by elution with an appropriate solvent or directly determined in the solid phase, e.g., in the case of X-ray methods or ET AAS. Experimental parameters, such as shaking time in batch technique, loading and elution flow rate in flow systems, concentration of the eluent and the amount of solid phase and eluent have to be optimized [63]. This approach has several advantages such as easy automation, use of smaller amounts of sample and reagents and removal of potentially interfering concomitants, which could improve the method of analysis considerably and extend the limit of detection to significantly lower concentrations [64–66].

3.5. Complete mineralization

Among the procedures that involve complete mineralization of the organic constituents, dry ashing in open crucibles is the most rigorous approach and one of the cheapest sample preparation procedures. Large quantities of sample may be used and the analytes could be concentrated once the residue might be reconstituted in a small volume of a dilute mineral acid (HCl or HNO_3), which obviously makes possible the use of aqueous standards for the calibration. The main disadvantages of the dry ashing procedure of fuel samples are the risks of contamination and/or analyte loss by formation of volatile compounds, and the low analytic frequency because of the time involved in this procedure [67,68].

The Wickbold apparatus has also been employed for fuel mineralization. In this procedure the sample is burned in an oxygen-hydrogen flame and the combustion products are dissolved in an acid solution. As the combustion is in a semi-closed system, this method minimizes the loss of volatile analytes. In addition, the Wickbold apparatus allows the use of a greater sample mass. However, the large inner surface with which the sample is in contact can provoke analyte losses by adsorption and/or contamination problems. In spite of the extreme conditions to which the sample is submitted, the combustion product might contain some organic compounds that could interfere in the determination of the metallic species, depending on the analytical technique used [69].

Wet digestions assisted by microwave radiation have been demonstrated to be safer and more efficient than conventional procedures. In addition these procedures minimize contamination and reduce the amount of reagents necessary for sample preparation [70,71].

3.6. Addition of an oxidant solution

The conversion of metal-organic compounds in the fuel to an inorganic form by addition of an oxidant solution is another procedure to overcome the incompatibility of the organic sample with aqueous standard solutions. The oxidant solutions commonly used in this procedure are inorganic oxygen acids and halogen saturated solutions such as chlorine, iodine and bromine solutions [72–74]. This is also a way to overcome the difference in response caused by the presence of different analyte compounds in the fuel by their conversion to water soluble salts by the reaction with an oxidant such as iodine or iodine monochloride and stabilization with the addition of a liquid

anion exchanger, such as trioctyl-methylammonium chloride (Aliquat 336) [20,75].

4. Determination of metals and metalloids in automotive fuels

As it was pointed out earlier, a variety of atomic spectrometric techniques has been used for the determination of metals and metalloids in automotive fuels. The exhaustive description of these techniques is not within the scope of this revision, instead a retrospect of the most significant contributions to trace metal and metalloid determination in fuel samples, particularly with flames, graphite furnaces, chemical vapor generation, and with inductively coupled plasma optical emission and mass spectrometry are presented.

4.1. Flame atomic absorption and emission spectrometry (FAAS and FAES)

Due to their inherently low sensitivity FAAS and FAES only a few reports are found in the literature involving the direct analysis of automotive fuels using these techniques. Nowka [76] proposed a method for the determination of Na and K in biodiesel by FAES after a simple dilution with kerosene. The 'optical background' due to the emission from non-combusted sample constituents could be controlled easily by an increase of the air supply to the flame. This problem is much more pronounced and much more difficult to control in ICP OES due to the inert atmosphere of the argon plasma. The results were in good agreement with those obtained by FAAS after microwave-assisted acid digestion of the samples.

Several procedures for metal pre-concentration from automotive fuels have been developed for quantification by flame methods. Of particular interest are those using solid sorbents modified with chelating groups, some of which are presented in Table 1.

In the method proposed by Universal Oil Products Company (UOP) for the determination of Fe, Ni, V, Cu, Na and K in petroleum derivatives, including gasoline, by FAAS, the sample pre-treatment consists in a digestion with sulfuric acid and the oxidation of the residue in a muffle furnace. For the determination of V, Na and K a cesium solution is added as ionization buffer [67]. Obviously this kind of procedure is more suited as a reference technique for validation purposes than as a routine procedure, as it is rather labor-intensive and time consuming. Cardarelli et al. [60] developed an FAAS method for lead determination in gasoline. The samples were prepared as emulsions stabilized with propan-2-ol or a mixture of ethanol and a surfactant. The results showed good reproducibility and accuracy, although the sensitivity was not sufficient for the determination of low lead levels.

4.2. Electrothermal atomic absorption spectrometry (ET AAS)

Electrothermal AAS with a graphite furnace is one of the most useful analytical techniques for metal determination in fuels due to its high sensitivity and capability to deal with high organic loads. The graphite furnace technique makes possible a direct analysis of fuel samples, since it allows complete elimination of the organic matrix if an appropriate heating program and a suitable chemical modifier are used. These characteristics result in a series of advantages, such as a significant decrease of sample preparation time and a dramatically reduced risk of contamination and/or analyte loss. In addition, ET AAS requires only very small amounts of sample. However, special attention has to be given to the low surface tension of organic liquids, particularly when fuel samples are introduced without sample preparation or after simple dilution with an organic solvent. In case of a temperature gradient within the graphite tube these samples migrate rapidly to the coolest part. In the case of a longitudinally heated graphite furnace this could mean that the sample is migrating to the very ends of the tube and into the contacts, and significant analyte losses and memory effects might be encountered. This problem is minimized when platform atomization and a transversely heated graphite tube are used.

Nakamoto [77] described the determination of arsenic compounds in thermally cracked gasoline using ET AAS. Nickel nitrate was employed as chemical modifier, and there was no effect observed of the kind of thermally cracked gasoline or from other metals. The same author [73] proposed a method for the direct determination of lead in thermally cracked gasoline using ET AAS. The organic lead was treated with iodine to reduce its volatility and this way it was possible to use inorganic lead standards for calibration.

De Oliveira et al. [72] described a method for the simultaneous determination of Al, As, Cu, Fe, Mn, and Ni in fuel ethanol by ET AAS using a transversely heated graphite atomizer with longitudinal Zeeman-effect background correction. The sample was diluted with nitric acid (10 mL ethanol + 10 mL of 0.28 mol L^{-1} HNO_3) and dispensed into the graphite tube. The method presented good recoveries and a paired *t*-test showed that the results were in agreement at the 95% confidence level with those obtained by single-element ET AAS. The same authors [45] evaluated $Pd(NO_3)_2 + Mg(NO_3)_2$; W/Rh and W + co-injection of $Pd(NO_3)_2 + Mg(NO_3)_2$ as chemical modifiers for this application and the modifier W + co-injection of $Pd(NO_3)_2 + Mg(NO_3)_2$ showed the highest recovery level, and was therefore selected.

Aucelio et al. [53] proposed a method for the determination of V in diesel and asphaltene fractions based on ET AAS. Diesel samples were stabilized as detergentless micro-emulsions by mixing with propan-1-ol and nitric acid; aqueous solutions could be used for calibration. Campos et al. [47] developed a procedure for the determination of Cu, Fe, Pb and Ni in gasoline at $\mu g\,L^{-1}$ levels, by ET AAS. The sample was stabilized by formation of a three-component solution, prepared by mixing appropriate volumes of water, gasoline and n-propanol. Calibration was performed using analytical solutions prepared in the same three-component medium or by the analyte addition technique. The palladium and magnesium nitrates modifier in aqueous solution proved to be efficient for iron and lead determination, while no modifier was necessary for copper and nickel.

Table 1
Selected solid sorbents used for metal pre-concentration from automotive fuels

Sample	Solid phase	Analyte	LOD ($\mu g\,L^{-1}$)	Refs.
Gasoline	Silica gel modified with 2-aminothiazole groups	Cu	0.8	[63]
		Zn	0.1	
		Ni	2.0	
		Fe	3.0	
Fuel ethanol	Silica gel modified with 2-aminothiazole groups	Cu	1.7	[64]
		Ni	2.3	
		Zn	0.34	
Fuel ethanol	Amberlite XAD-4 functionalized with 3,4-dihydroxybenzoic acid	Cu	2.3	[37]
		Fe	5.0	
		Ni	7.8	
		Zn	0.1	
Fuel ethanol	Silica gel modified with 2,5-dimercapto-1,3,4-thiadiazole	Zn		[66]
		Cd		
		Ni	–	
		Pb		
		Co		
Fuel ethanol	Silica gel modified with benzimidazole	Cd		[88]
		Cu	–	
		Mn		
		Ni		
		Fe		
		Zn		
Fuel ethanol	Silica gel modified with 5-amino-1,3,4-thiadiazole-2-thiol	Cd		[89]
		Co		
		Cu	–	
		Fe		
		Ni		
		Pb		
		Zn		
Fuel ethanol	Acid carboxymethyl-cellulose	Cd		[90]
		Cu		
		Cr	–	
		Fe		
		Ni		
		Zn		
Fuel ethanol	Silica gel modified with niobium oxide	Cu	1.4	[91]
		Cd	0.2	
		Co	1.4	
		Zn	1.0	

Good agreement was obtained between the results obtained by the proposed and independent methods.

Aucelio and Curtius [18] developed an ET AAS method for determination of trace concentrations of As, Sb and Se in gasoline and kerosene using micro-emulsion sample introduction. The platform atomization technique was used together with chemical modification (ruthenium permanent modifier or Pd and Mg nitrates chemical modifier). Better results were obtained when samples were introduced as micro-emulsions prepared with a surfactant (Triton X-100) compared to detergentless micro-emulsions (three-component solution). Laboratory-prepared samples were analyzed with good precision and recovery.

Reyes and Campos [56] proposed an ET AAS method for quantification of Ni and Pb in diesel and gasoline samples stabilized as micro-emulsions using conventional (Pd-Mg) and permanent (Ir) modifiers. The calibration was possible using aqueous or organic standard solutions prepared as micro-emulsions with a single organic solvent. Good agreement was obtained between the results using the proposed and independent procedures (UOP).

Ozcan and Akman [70] described a determination of Cu, Co and Pb in gasoline by ET AAS using aqueous standard addition in a gasoline-ethanol-water three-component system. Good agreement was found between the results of this method and those obtained by digesting gasoline in a microwave oven with nitric acid. Brandão et al. [78] developed a procedure for the determination of As in diesel, gasoline and naphtha by ET AAS. The samples were prepared as micro-emulsions by mixing appropriate volumes of the sample, propan-1-ol and nitric acid. Palladium was used as the modifier added in the conventional manner. The optimum micro-emulsion composition as well as

the temperature program was optimized by Central Composite multivariate design, and the method has been validated by the analysis of a set of commercial samples using independent procedures.

Anselmi et al. [44] proposed the determination of Cd, Cr, Cu, Pb and Ni in gasoline and diesel fuel samples by ET AAS using the Transverse Heated Filter Atomizer (THFA) designed by Katskov et al. [79]. Metal-organic standards were used for calibration and gasoline samples were analyzed directly, while diesel fuel samples were diluted 1:4 with n-heptane. The THFA has several advantages for the analysis of organic solutions, such as: (i) analysis of volatile elements is possible without the need of chemical modifiers; (ii) improved sensitivity and limits of detection because of the reduced absorption volume and the injection of higher sample volumes is possible; (iii) background absorption should not play an important role in the vaporization of hydrocarbon blends due to the filtering action of the furnace.

A number of selected applications of ET AAS to the analysis of fuels are summarized in Table 2

4.3. Chemical vapor generation for AFS and AAS

Some elements, such as Hg, As and Sb are present in fuel samples in concentrations that are lower than even the detection limits of ET AAS. For these elements, chemical vapor generation (CVG) techniques can be used to provide the required sensitivity. However, CVG when applied to the analysis of fuels is susceptible to spectral interferences, mostly due the presence of aromatic organic compounds in the gas stream. There is also a high risk of analyte loss due the high volatility of some compounds and their property to adsorb on many surfaces at the ng g^{-1} level [80]. In addition, CVG techniques such as the cold vapor (CV) technique for mercury and the hydride generation (HG) technique for As and Sb require that the analyte is present as inorganic ion in a defined oxidation state. Therefore the application of CVG techniques to the analysis of fuels generally requires complete mineralization of the metal-organic compounds and their separation from the organic phase.

Liang et al. [61] developed a simple sample preparation method for the determination of Hg in gasoline and other petroleum products by CV AFS. The organo-mercury compounds were oxidized and extracted into the aqueous phase using BrCl/HCl as oxidant/acid solution. The ionic mercury extracted into the aqueous phase was reduced to metallic Hg by $SnCl_2$ before its determination. Gasoline samples and other petroleum based materials, such as kerosene, diesel and heating oil of different origin were analyzed and satisfactory results were obtained. The recoveries for mercury in a certified reference material were close to 100%. Brandão et al. [59] proposed a similar procedure for the determination of mercury in gasoline by CV AAS.

Trindade et al. [71] proposed a method for the determination of As in gasoline by HG AAS. The method involved a microwave-assisted sample digestion; calibration was carried out using aqueous standards.

Table 2
Selected publications about trace element determination in fuels using ET AAS

Sample	Sample treatment	Analytes	LOD ($\mu g\,L^{-1}$)	Refs.
Gasoline and kerosene	Detergentless micro-emulsion	As	2.0	[18]
		Sb	4.0	
		Se	3.0	
Gasoline	Water-in-oil-in-water emulsions	Mo	0.9	[39]
		V	4.7	
Gasoline and diesel fuel	Gasoline: direct analysis. Diesel fuel: dilution with *n*-heptane	Cd	0.13	[44]
		Cr	0.4	
		Cu	0.9	
		Pb	1.5	
		Ni	2.5	
Fuel alcohol	Dilution with nitric acid (0.28 mol L^{-1})	As	2.5	[72]
		Al	1.2	
		Cu	0.22	
		Fe	1.6	
		Mn	0.2	
		Ni	1.1	
Gasoline	Micro-emulsion	Cu	0.4	[43]
		Fe	3.0	
		Ni	0.8	
		Pb	1.8	
Diesel and asphaltene	Detergentless micro-emulsion	V	5.0 for diesel and 4.0 for asphaltene	[54]
Diesel and gasoline	Micro-emulsion	Ni	4.5	[57]
		Pb	3.6	
Gasoline	Micro-emulsion	Co	1.5	[70]
		Cu	2.5	
		Pb	4.0	

De la Guardia [81] developed a CVG AAS method for the determination of lead and manganese additives in gasoline. The analytes in samples and standards were volatilized using a pre-heated Pyrex reactor, and introduced into the flame in the vapor phase by a nitrogen carrier gas flow. Results obtained for the analysis of commercial gasoline samples by the proposed procedure were compared with a reference method.

Obviously, because of the rather complex sample preparation required for CVG in the case of fuel samples, this technique is only second choice, i.e., only if more direct techniques such as ET AAS do not provide sufficient sensitivity. This is most frequently the case in the determination of mercury, where CV AAS and particularly CV AFS provide significantly better LOD. In addition, this element has often to be determined at extremely low concentrations because of its importance as global pollutant. In contrast, ET AAS often provides sufficient sensitivity for the hydride-forming elements, so that CVG might be used only as a reference method for validation.

4.4. Inductively coupled plasma optical emission spectrometry (ICP OES)

Inductively coupled plasma OES has as main advantage the multi-element detection capability, while AAS, with a few exceptions is a one-element-at-a-time technique. However, only a few examples of ICP OES analyses of automotive fuels are found in literature, mostly because trace elements are usually not present in fuel samples at a sufficiently high concentration that allow their direct determination without pre-concentration. In addition, the introduction of organic solvents, such as fuels, cause plasma destabilization or even plasma extinction, so that the use of special ICP accessories is necessary, such as direct injection nebulizer, ultrasonic nebulizer with microporous membrane desolvator, a thermostated condenser between the spray chamber and the plasma torch or a chilled spray chamber [42]. An obvious solution for these problems is a digestion of the organic material in order to obtain aqueous solutions.

Onyeso et al. [42] developed a method for the determination of Mn in gasoline and diesel fuel by ICP OES after a digestion in a microwave oven and dilution with water before direct aspiration into the plasma. De Souza et al. [57] proposed a method for quantification of Mo, Cr, V and Ti in diesel and in used fuel oil by ICP OES using sample preparation as emulsions and the addition of HNO_3, which allowed the use of inorganic standards for calibration. Detergent and detergentless emulsion sample preparation procedures were evaluated and better results were obtained for detergent emulsions with recoveries ranging from 90.1–106.5%.

Borszeki et al. [58] developed a method for the quantification of Al, Cr, Cu, Fe, Mg, Ni, and Pb in oil and petroleum products, such as gasoline, by ICP OES using a minitorch. The samples were stabilized as aqueous emulsions prepared by using two kinds of emulsifiers, one with low sulfur content and the other sulfonated. Calibration was made with aqueous standards and the results were in good agreement with those obtained using oil standard solutions.

Uden et al. [82] proposed a method for the determination of Mn, which was present as methyl-cyclopentadienyl-manganesetricarbonyl in gasoline utilizing gas chromatographic separation interfaced with detection by ICP OES. Samples were injected into the gas chromatograph with a micro-syringe, and chromatograms could be repeated every 3 min. Preheated argon sheath gas was required in addition to the argon supplied to sustain the plasma, in order to optimize spectral sensitivity.

Brenner et al. [83] proposed a method for the determination of lead in gasoline by ICP OES using argon and argon–oxygen as plasma gas. In this work the intensity variations of inorganic and organic lead species in aqueous solution and in gasoline emulsions were studied using a sequential spectrometer. Although detection limits of lead in gasoline emulsions were significantly degraded relative to an aqueous solution, they were adequate for the direct determination of lead at the $mg\,kg^{-1}$ level.

Both, the US ASTM D-4951 method [84] and the European method CEN, EN 14 107 [85] for the determination of phosphorus in biodiesel propose a method based on the direct determination after a 1:10 dilution with an organic solvent such as toluene or xylene using ICP OES. This is kind of surprising as it is well established that such procedure causes significant problems regarding plasma stability. In addition it has been shown in yet unpublished work that the LOD of ICP OES in the case of direct determination after a 1:10 dilution is too close to the threshold limit of $10\,mg\,kg^{-1}$ level in undiluted biodiesel to allow an accurate determination. Hence a reliable method for this kind of analysis has yet to be developed.

4.5. Inductively coupled plasma mass spectrometry (ICP-MS)

Inductively coupled plasma MS is a very sensitive multi-element technique, but the introduction of organic solvents into the plasma – similar to ICP OES – requires special care, as the organic load may de-stabilize or extinguish the plasma. Additional problems that appear in ICP-MS are formation of carbon deposits on the sampler and skimmer cones and in the ion lens of the mass spectrometer and spectral interferences due to carbon-based polyatomic species [39].

Howard et al. [46] developed an ICP-MS method for the determination of TEL and TML in gasoline using direct analysis of the fuel samples. The results obtained by the proposed method were in good agreement with results of ASTM Method D-526. Al Swaidan [54] accomplished the determination of Pb and Cd in petroleum products, including gasoline and diesel by ICP-MS using a micro-emulsion procedure for sample preparation while the analyte addition technique was used for calibration. Recoveries of added lead and cadmium as oil soluble salts were found to be in the 99–103% and 100–101% ranges, respectively. However, this result is not surprising as analyte addition was used for calibration, and in this case any spike recovery (which is another form of analyte addition) by definition has to be around 100% even in the presence of severe interference.

Lord [86] developed a method for lead in gasoline converting TEL and TML into water-soluble species that were extracted into dilute nitric acid. Lead concentrations in the

Table 3
Selected publications about trace element determination in fuels using ETV-ICP-MS

Sample	Sample treatment	Analytes	LOD ($\mu g\,L^{-1}$)	Refs.
Gasoline	Oil-in-water emulsions	Cd	0.3	[14]
		Cu	2.0	
		Fe	5.0	
		Pb	0.4	
		Tl	3×10^{-3}	
Gasoline	Oil-in-water emulsions	Cu	0.22	[39]
		Mn	0.02	
		Ni	0.38	
		Sn	0.03	
Fuel alcohol	Addition of 0.3% (v/v) nitric acid	Ag	0.02	[87]
		Cd	0.08	
		Cu	0.1	
		Pb	0.05	
		Tl	0.001	
Fuel alcohol	Addition of 0.3% (v/v) nitric acid	Ag	0.015	[92]
		Co	0.002	
		Cu	0.22	
		Fe	0.72	
		Mn	0.025	
		Ni	0.026	
		As	0.02	
		Cd	0.07	
		Pb	0.02	
		Sn	0.010	
		Tl	0.0008	

nitric acid extracts were determined by ICP-MS using bismuth as internal standard. Reimer and Miyazaki [55] proposed a method for the determination of Ni and V in commercial gasoline by ICP-MS. The samples were prepared as oil-in-water micro-emulsions. The results showed that internal standardization and a standard calibration curve method were equivalent.

A very useful approach for the analysis of organic samples is the technique of electrothermal vaporization (ETV). With this sample introduction system, the matrix components are previous volatilized by employing an appropriate temperature program, very similar to ET AAS, before introducing the analyte into the plasma. This way, the problems related to the complexity of fuel samples can be minimized and the determination of metals accomplished satisfactorily [39,87]. In addition, ETV improves sample introduction efficiency compared to direct solution nebulization, making possible the use of small and discrete sample volumes and rapid sample changeover. The main limitation with ETV sample introduction is the transient nature of the generated signal, which reduces the number of elements that can be determined simultaneously by ICP-MS to five or six [39]. The sample preparation procedures for the determination of metals in fuels using ETV-ICP-MS depends of the sample matrix and can reach from a simple acidification to the formation of emulsions. Table 3 summarizes some publications using ETV-ICP-MS for fuel analysis.

5. Conclusion

Considering the importance of the determination of metallic and metalloid species in automotive fuels and the low concentration of these elements there appears to be a significant lack of reliable methods. Electrothermal AAS with a graphite furnace and ETV-ICP-MS appear to be the most appropriate techniques; however the lack of certified reference materials is one of the greatest problems in method development and validation. Complete mineralization of the metal-organic compounds is still the only reliable sample preparation technique in order to validate less labor-intensive methods. It should be pointed out that spike recovery, although frequently applied in the literature, is not a valid technique to demonstrate the accuracy of a method. To add a certain metal-organic compound, often an oil-soluble salt of an organic acid, to a fuel sample, and to determine its recovery using the same compound in an organic solvent as the standard does not mean anything. The analyte in the sample, which might be present as a completely different organic compound (or several different compounds) might behave in a completely different way. Hence, really independent techniques, typically including complete mineralization, are the only way of method validation for trace element determination in fuel.

Acknowledgement

The authors are grateful to Fundação de Amparo a Pesquisa do Estado da Bahia (FAPESB), Conselho Nacional de Desenvolvimento Científico e Tecnológico (CNPq) and Coordenação de Aperfeiçoamento de Pessoal de Nível Superior (CAPES) for financial support. M.G.A.K., M.G.R.V., A.P.T., D.C.L. and S.L.C.F. have research scholarships from CNPq, D.S.S.S has a research scholarship from CAPES and B.W. has a research scholarship from FAPESB.

References

[1] Wikipedia, The Free Encyclopedia, http://en.wikipedia.org/wiki/Ethanol_fuel.
[2] R.C.C. Pereira, V.M.D. Pasa, Energy Fuels 19 (2005) 426.
[3] American Petroleum Institute, http://www.api.org.
[4] Oahu Trans 2K, http://www.oahutrans2k.com.
[5] Exxon, http://www.exxon.com.
[6] Michigan Departmen of Agriculture (MDA), http://www.michigan.gov.
[7] M. Bowman, D. Hilligoss, S. Rasmussen, R. Thomas, Hydrocarbon Process. (February 2006) 103.
[8] L. Kiuru, Proceedings of the Regional Workshop on Better Air Quality in Asia and Pacific Rim Cities, Hong Kong, 16–18 December, 2002.
[9] Energy Information Administration (EIA), http://www.eia.doe.gov.
[10] M.G.R. Vale, I.C.F. Damin, A. Klassen, M.M. Silva, B. Welz, A.F. Silva, F.G. Lepri, D.L.G. Borges, U. Heitmann, Microchem. J. 77 (2004) 131.
[11] M. Turunen, S. Peraniemi, M. Ahlgren, H. Westerholm, Anal. Chim. Acta 311 (1995) 85.
[12] Z.D. Kalitchin, M.I. Boneva, S.K. Ivanov, P.T. Georgiev, S.K. S Tanielyan, Proceedings of the International Conference on Stability and Handling of Liquid Fuels, Rotterdam, 5th October 1994.
[13] A. Falahi-Ardakani, Ecotoxicol. Environ. Saf. 8 (1984) 152.
[14] T.D. Saint'Pierre, L.F. Dias, S.M. Maia, A.J. Curtius, Spectrochim. Acta, Part B 59 (2004) 551.
[15] R.T.J. Russell. European Patent WO2005087901 (2005).
[16] C. Ignacio, U.S. Patent 5308553 (2004).

[17] N.I. Butenko, S.I., Butenko, V.I. Nikitenko, V.A. Drozdenko, P.I. Lyubenko, N.P. Kitsenko, European Patent RU2187541 (2002).
[18] R.Q. Aucelio, A.J. Curtius, J. Anal. Atom. Spectrom. 17 (2002) 242.
[19] B. Du, Q. Wei, S. Wang, W. Yu, Talanta 44 (1997) 1803.
[20] C.G. Taylor, J.M. Trevaskis, Anal. Chim. Acta 179 (1986) 491.
[21] C. Baird, Cann F.M., Environmental Chemistry, third ed., W.H. Freeman, New York, 2004.
[22] A. Lofgren, H. Hammar, Transport. Res. Part D 5 (2000) 419.
[23] Z. Aneva, M. Iancheva, Anal. Chim. Acta 167 (1985) 371.
[24] P.L. McCalla, K.C. Land, Soc. Sci. Res. 33 (2004) 339.
[25] R.A. Ligero, M. Casas-Ruiza, M. Barrera, F. Lopez-Aguayo, D. Sales, D. Garcia, Environ. Int. 30 (2004) 99.
[26] X. Yin, X. Liu, L. Sun, R. Zhu, Z. Xie, Y. Wang, Sci. Total Environ. 371 (2006) 252.
[27] V. Nichani, W. Li, M.A. Smith, G. Noonan, M. Kulkarni, M. Kodavor, L.P. Naeher, Sci. Total Environ. 363 (2006) 95.
[28] Y.H. Hwang, Y. Ko, C.D. Chiang, S.P. Hsu, Y.H. Lee, C.H. Yu, C.H. Chiou, J.D. Wang, H.Y. Chuang, Environ. Res. 96 (2004) 274.
[29] D.D. Cohena, B.L. Gulsonb, J.M. Davisc, E. Stelcera, D. Gartona, O. Hawasa, A. Taylord, Atmos. Environ. 39 (2005) 6885.
[30] H. Ozaki, I. Watanabe, K. Kuno, Water, Air, Soil Pollut. 157 (2004) 209.
[31] D. Lee, A. Miller, D. Kittelson, M.R. Zachariah, J. Aerosol Sci. 37 (2006) 88.
[32] Y.F. Wang, K.L. Huang, C.T. Li, H.H. Mi, J.H. Luo, P.J. Tsai, Atmos. Environ. 37 (2003) 4637.
[33] S. Hlawiczka, Z. Kowalewska, Archiwum Ochrony Srodowiska 28 (2002) 119.
[34] S. Okada, C.B. Kweon, J.C. Stetter, D.E. Foster, M.M. Shafer, C.G. Christensen, J.J. Schauer, A.M. Schmidt, A.M. Silverberg, D.S. Gross, Jpn. Soc. Automotive Eng. Special Publ. (2003) 59.
[35] K. Lombaert, S. Morel, L. Le Moyne, P. Adam, J.T. de Maleissye, J. Amouroux, Plasma Chem. Plasma Process. 24 (2004) 41.
[36] S. Chellam, P. Kulkarni, M.P. Fraser, J. Air Waste Manage. Assoc. 55 (2005) 60.
[37] L.S.G. Teixeira, M.A. Bezerra, V.A. Lemos, H.C. dos Santos, D.S. de Jesus, A.C.S. Costa, Sep. Sci. Technol. 40 (2005) 2555.
[38] D.S.S. dos Santos, A.P. Teixeira, M.G.A. Korn, L.S.G. Teixeira, Spectrochim. Acta Part B 61 (2006) 592.
[39] T.D. Saint'Pierre, L.F. Dias, D. Pozebon, R.Q. Aucélio, A.J. Curtius, B. Welz, Spectrochim. Acta Part B 57 (2002) 1991.
[40] A.C. Campos, E. Leontsinis, Petróleo & Derivados, Editora Técnica Ltda, São Paulo, 1990.
[41] US Department of Energy, Biodiesel Handling and Use Guidelines, National Renewable Energy Laboratory DOE/GO-102004-1999, 2004, p. 13.
[42] C.C. S Onyeso, Abstracts of 57th Southeast/61st Southwest Joint Regional Meeting of the American Chemical Society, Memphis, November 1–4, 2005.
[43] E. Oliveira, J. Braz. Chem. Soc. 14 (2003) 174.
[44] A. Anselmi, P. Tittarelli, D.A. Katskov, Spectrochim. Acta Part B 57 (2002) 403.
[45] A.P. de Oliveira, J.A. Gomes Neto, M.M.C. Ferreira, Eclet. Quim. 31 (2006) 7.
[46] H.E. Howard, W.C. Ferguson, L.R. Snyder, Anal. Chem. 32 (1960) 1814.
[47] R.C. Campos, H.R. Santos, P. Grinberg, Spectrochim. Acta Part B 57 (2002) 15.
[48] Z. Kowalewska, A. Ruszczynska, E. Bulska, Spectrochim. Acta Part B 60 (2005) 351.
[49] E. Teserovsky, S. Arpadjan, J. Anal. Atom. Spectrom. 6 (1991) 487.
[50] J.W. Robinson, Anal. Chim. Acta 24 (1961) 451.
[51] D.G. Smith, J. Colloid Interface Sci. 60 (1977) 488.
[52] E. Pelizzeti, E. Pramauro, Anal. Chim. Acta 169 (1985) 1.
[53] R.Q. Aucelio, A. Doyle, B.S. Pizzorno, M.L.B. Tristão, R.C. Campos, Microchem. J. 78 (2004) 21.
[54] H.M. Al-Swaidan, Sci. Total Environ. 145 (1994) 157.
[55] R.A. Reimer, A. Miyazaki, Anal. Sci. 9 (1993) 157.
[56] M.N.M. Reyes, R.C. Campos, Spectrochim. Acta Part B 60 (2005) 615.
[57] R.M. de Souza, B.M. Mathias, I.S. Scarminio, C.L.P. da Silveira, R.Q. Aucelio, Microchim. Acta 153 (2006) 219.
[58] J. Borszeki, G. Knapp, P. Halmos, L. Bartha, Microchim. Acta 108 (1992) 157.
[59] G.P. Brandão, R.C. Campos, A.S. Luna, Spectrochim. Acta Part B 60 (2005) 625.
[60] E. Cardarelli, M. Cifani, M. Mecozzi, G. Sechi, Talanta 33 (1986) 279.
[61] L. Liang, M. Horvat, P. Danilchik, Sci. Total Environ. 187 (1996) 57.
[62] M.G.A. Korn, J.B. Andrade, D.S. de Jesus, A. Valfredo, M.L.S.F. Lemos, W.N.L. Bandeira, M.A. dos Santos, F.A.C. Bezerra, A.S. Amorim, S.L.C. Souza, Ferreira, Talanta 69 (2006) 16.
[63] P.S. Roldan, I.L. Alcântara, C.C.F. Padilha, P.M. Padilha, Fuel 84 (2005) 305.
[64] P.S. Roldan, I.L. Alcantara, G.R. Castro, J.C. Rocha, C.C.F. Padilha, P.M. Padilha, Anal. Bioanal. Chem. 375 (2003) 574.
[65] P.M. Padilha, A.F. Oliveira, F.V. Moraes, F.A. Silva, C.C.F. Padilha, J.C. Rocha, South. Braz. J. Chem. 8 (2000) 113.
[66] P. Lessi, J.C. Moreira, N.L. Filho, J.T.S. Campos, Anal. Chim. Acta 327 (1996) 183.
[67] Universal Oil Products Company (UOP), UOP Method 391-91.
[68] E.J. Ekanem, J.A. Lori, S.A. Thomas, Bull. Chem. Soc. Ethiop. 2 (1998) 9.
[69] K. Hoppstock, M. Michulitz, Anal. Chim. Acta 350 (1997) 135.
[70] M. Ozcan, S. Akman, Spectrochim. Acta Part B 60 (2005) 399.
[71] J.M. Trindade, A.L. Marques, G.S. Lopes, E.P. Marques, J. Zhang, Fuel 85 (2006) 2155.
[72] A.P. Oliveira, M. Moraes, J.A. Gomes Neto, E.C. Lima, At. Spectrosc. 23 (2002) 39.
[73] Y. Nakamoto, Bunseki Kagaku 53 (2004) 13.
[74] B.E. Gordon, R.A. Burdett, Anal. Chem. 19 (1947) 137.
[75] S.T. Holding, J. Palmer, Analyst 109 (1994) 507.
[76] R. Nowka, GIT Labor-Fachzeitschrift 47 (2003) 518.
[77] Y. Nakamoto, Bunseki Kagaku 49 (2000) 43.
[78] G.P. Brandão, R.C. Campos, A.S. Luna, E.V.R. Castro, H.C. Jesus, Anal. Bioanal. Chem. 385 (2006) 1562.
[79] D.A. Katskov, P.J.J.G. Marais, P. Tittarelli, Spectrochim. Acta Part B 51 (1996) 1169.
[80] Ph. Quevauviller, E.A. Maier, Quality Assurance for Environmental Analysis: Method Evaluation within the Measurement and Testing Programme (BCR), Elsevier, Amsterdam Belgium, 1995.
[81] M. de La Guardia, A.R. Mauri, C. Mongay, J. Anal. Atom. Spectrom. 3 (1988) 1035.
[82] P.C. Uden, R.M. Barnes, F.P. DiSanzo, Anal. Chem. 50 (1978) 852.
[83] I.B. Brenner, A. Zander, S. Kim, J. Shkolnik, J. Anal. Atom. Spectrom. 11 (1996) 91.
[84] American Society of Testing Materials, ASTM D-4951.
[85] European Committee for Standardization, CEN-EN 14 107.
[86] C.J. Lord III, J. Anal. Atom. Spectrom. 9 (1994) 599.
[87] T.D. Saint'Pierre, V.L.A. Frescura, A.J. Curtius, Talanta 68 (2006) 957.
[88] N.L. Dias Filho, Y. Gushikem, W.L. Polito, J.C. Moreira, E. Ehirim, Talanta 42 (1995) 1625.
[89] L.A.M. Gomes, P.M. Padilha, J.C. Moreira, N.L. Dias Filho, Y. Gushikem, J. Braz. Chem. Soc. 9 (1998) 494.
[90] P.M. Padilha, C.C.F. Padilha, J.C. Rocha, Quimica Analítica 18 (1999) 299.
[91] E.L. Silva, D. Budziak, E. Carasek, Anal. Lett. 37 (2004) 1909.
[92] T.D. Saint'Pierre, T.D. Maranhão, V.L.A. Frescura, A.J. Curtius, Spectrochim. Acta Part B 60 (2005) 605.

Available online at www.sciencedirect.com
ScienceDirect
Talanta 73 (2007) 46–53
Talanta
www.elsevier.com/locate/talanta

A simple and green analytical method for determination of iron based on micro flow analysis

Senee Kruanetr [a], Saisunee Liawruangrath [a,*], Napaporn Youngvises [b]

[a] Department of Chemistry, Faculty of Science, Chiang Mai University, Chiang Mai 50200, Thailand
[b] Department of Chemistry, Faculty of Science and Technology, Thammasat University, Pathum Thani 12121, Thailand

Received 24 December 2006; received in revised form 23 February 2007; accepted 23 February 2007
Available online 7 March 2007

Abstract

A simple, inexpensive and reagent-less colorimetric micro flow analysis (μFA) system was implemented in a polymethyl methacrylate (PMMA) micro fluidic manifold. A T-shaped micro channel on a PMMA chip was fabricated by laser ablation and topped with molded polydimethylsiloxane (PDMS). The fabricated μFA system was integrated with the optical components as detector and applied to the determination of iron in water samples. It is based on the measurement of Fe(III)–nitroso-R salt complex at 720 nm formed by the reaction between Fe(III) and nitroso-R salt in an acetate buffer solution pH 5. The proposed μFA consumed very small amount of reagent and sample, it released waste of less than 2.0 mL h^{-1}. The relative standard deviation (R.S.D.) was less than 2% ($n = 11$) with the recovery of 98.7 ± 0.12 ($n = 5$). The linear range for the determination of iron in water samples was over the range of 0.05–4.0 μg mL^{-1} with a correlation coefficient (r^2) of 0.9994. The limit of detection (3σ) and limit of quantitation (10σ) were 0.021 μg mL^{-1} and 0.081 μg mL^{-1}, respectively with a sample throughput of 40 h^{-1}.

Keywords: Simple; Green analytical method; Micro flow analysis; Iron

1. Introduction

In recent years, various chemical analysis techniques have distinct advantages in sensitivity, reproducibility, simplicity, cost effectiveness, flexibility and rapidity. However, a paradoxical situation has emerged because most of the analytical methodologies employed to analysis of various samples generate a large amount of chemical wastes, resulting in an environmental and human impact. In some circumstances, the chemicals employed are even more toxic than the species being monitored. As a consequence, the work of some analytical chemists has been focused on the development of methodologies, which are less harmful to human and to the environment. In the development of a new analytical procedure, the amount and toxicity of wastes are as important as any other analytical feature [1]. The micro total analytical system, μTAS (also called lab on a chip or micro flow analysis), is one of analytical techniques that is rapid, high sensitivity and low waste produced. It involves the miniaturization of all function in chemical analysis, including sampling, removal of interferences, small amount of chemical consumption, and small size of mixing and reaction chamber. The entire chemical measurement device could be miniaturized onto a few square centimeters [2].

Iron is one of the important elements in plants and animals. Several spectrometric procedures have been used for analysis of iron in various samples using various reagents including ion chromatography with spectrometric detection [3,4], UV–vis spectrophotometry [5–13] atomic absorption spectrometry [14–17], ICP [18,19], flow injection analysis [13,20–27], chemiluminescence [27], stop flow analysis [28] and voltammetry [29]. Unfortunately these analytical techniques consumed a large amount of reagent volumes, and generated a large amount of hazardous chemical wastes. Some of analytical techniques required more analysis time, and they also required complicated system operation and maintenance. Various flow-based methods for iron determination in water have been reported based on FIA [13,20–27], Stop flow analysis [28] and SIA [30–32] with spectrometric detection. There are wide choices of complexing agents for determining iron in water spectrophotometrically. For examples, Pascual-Reguera et al. [13] developed normal FIA and

* Corresponding author. Tel.: +66 53943341–5x126; fax: +66 53892277.
E-mail address: scislwrn@chiangmai.ac.th (S. Liawruangrath).

0039-9140/$ – see front matter © 2007 Elsevier B.V. All rights reserved.
doi:10.1016/j.talanta.2007.02.032

reversed FIA for determination iron using ferrozine. The proposed method was sensitive with detection limit of 0.012 and 0.010 μg mL^{-1} for normal FIA and reversed FIA, respectively. The method was satisfactorily applied to the determination of iron in waste water at a sampling rate of 90 and 50 samples h^{-1} for normal FIA and reversed FIA, respectively, Asan et al. [20] developed the FIA method for determination of iron. This method is based on the measurement of the absorbance of the complex formed between Fe(III) and *N*,*N*-dimethylformamide (DMF) at 310 nm. The method was successfully applied to determination of iron in river water with detection limit and sampling rate of 0.1 ng mL^{-1} and 60 h^{-1}, respectively. Nabivanets et al. [33] determined iron by measuring the absorbance of its complex with nitroso-R salt at 720 nm in NH_4OH buffer. The sensitivity of the method is very high. The reagent itself does not absorb at the same wavelength nor do the complexes of other metals possibly present in the exits.

Disodium-1-nitroso-2-naphthol-3,6-disulphonate (nitroso-R salt) was introduced in 1921 by Klooster for the detection of cobalt [34] and subsequently used for determination of small quantities of this metal in various samples. Other metals such as iron [33,35–37], copper [35,38] and nickel [39–41] were reported based on complexation reaction between each metal ions with nitroso-R salt under suitable experimental conditions. Selectivity for determining these metal ions were achieved by adjustment of pH valves with suitable buffer solution and measurement of the absorbance of each metal complex at its λmax which was characteristic of each metal ions. Because different metal-nitroso-R salt complexes gave different λmax values. For example, Fe(III), Co(II), Cu(II) and Ni(II) complexes gave the maximum absorption wavelengths at 710, 425, 480 and 480 nm, respectively [35,39].

Among the cited spectrophotometric methods, many papers used nitroso-R salt as complexing agent for iron determination only in batch wise process [17,33,35–37], which consumed rather large amounts of reagents and samples (>1000 mL per day). There are also generated a large amount of waste. To our present knowledge, no previous articles based on flow injection spectrometric determination of iron using nitroso-R salt have been published in the literature. Although traditional FIA procedures consume less reagents than those consumed by the batch-wise ones, they still consume rather large amounts of reagents and waste generation. Micro flow injection analysis seems promising to satisfy with these purposes. It has been employed for some environmental analysis namely nitrite [42,43], nitrate [44], orthophosphate [45], phosphorous [46], nitrogen dioxide [47] and uric acid [48]. However, no published articles have been mentioned about iron determination based on such a micro flow manifold using nitroso-R salt.

In this paper a simple and greener colorimetric micro flow analysis (μFA) system was specially designed and fabricated using easily available materials equipment in Thailand and in the laboratory. The fabricated μFA system was integrated with the optical components as detector to achieve the greener analytical method for determination of iron in water samples. It is based on the complexation between Fe(III) with nitroso-R salt in an acetate buffer. Optimum conditions for determining iron were investigated.

2. Experimental

2.1. Chemicals

All reagents used were of analytical reagent grade (unless otherwise specified) and used without any further purification. All solutions were prepared and/or diluted with deionized reverse osmosis water (resistivity ≥ 10 M cm).

A standard stock solution of iron 10 μg mL^{-1} was prepared from a standard iron solution (AAS standard, 1000 μg mL^{-1} Merck, Germany). Working standard solutions were prepared by appropriate dilution of this stock standard solution.

A stock reagent 2.0% w/v nitroso-R salt (Merck, Germany) solution was prepared by dissolving 2.0 g nitroso-R salt in deionized water and adjusting volume to 100 mL.

Buffer solutions of pH 3–7 and pH 7–10 were prepared by mixing an appropriate ratio of 0.5 mol L^{-1} acetic acid with 0.5 mol L^{-1} sodium acetate, and 0.5 mol L^{-1} ammonium hydroxide with 0.5 mol L^{-1} ammonium acetate, respectively.

2.2. Apparatus

The micro flow analysis (μFA) system (Fig. 1.) consisted of a planar T-shaped poly methyl methacrylate (PMMA) μFA topped with a poly dimethyl siloxane (PDMS) plate (MF), a computer controlled selection valves (VICI, Valco Instruments) (SV) and a computer controlled peristaltic pump (ISMATEC) (P). The PMMA μFA was fabricated by using Laser ablation (Mercury Laser source 25 W); the channel was 200 μm wide, 50 μm deep and 20 mm long. The PDMS top plate was prepared by mixing the ratio 9:1 of silicone elastomer and silicone curing agent (Sylgard 184, Dow Corning, USA), subsequently

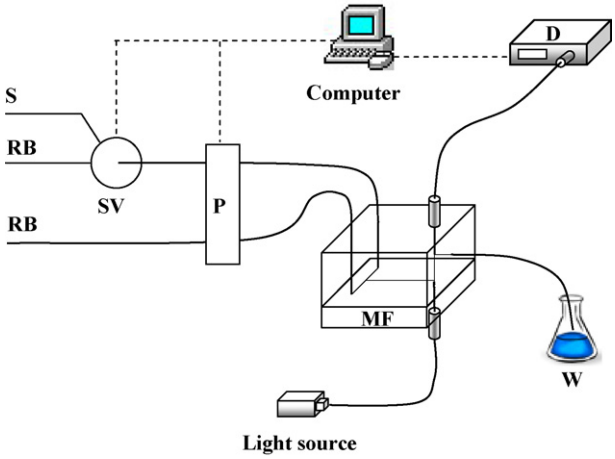

Fig. 1. A micro flow analysis system for Fe(III) determination. S, sample; RB, nitroso-R reagent (0.40%) adjusted pH 5 with acetate buffer; SV, selection valve (VICI Valcol Instrument, Co., Inc.); P, peristaltic pump (Reglo digital ISM 834, IMATEC Co., Inc.); MF, a PMMA T-shaped (0.2 mm wide, 0.05 mm deep and 20 mm long) micro flow analyzer; D, UV–vis spectrophotometer (USB2000 UV–vis spectrophotometer, Ocean Optics, Inc.); W, waste.

the mixture was poured into the mold with appropriate design and cured at 60 °C for 6 h. The PDMS top plate obtained was clear cubic with three small channels. The first and the second channel are used for delivering sample and reagent to the μFA. The third one is used as flow cell (0.8 mm i.d., 10 mm path length) where the absorbance of the complex was measured, and the solution passed out. The μFA flow cell was integrated with two fiber optic probes. The first fiber optic probe is connected to USB2000 spectrophotometer, Ocean Optics, FL. as detector (D) and the second one is connected to tungsten light source. FIAlab Software Version 5.0 (FIAlab Instruments, Medina, WA) was used to control fiber optic spectrometer and also used for data collection. A ten-port selection valves, VICI, Valco Instruments, USA (SV) and a peristaltic pump, ISMATEC peristaltic pump 0.001–68 mL min^{-1} per channel with Tygon pump tubing 0.19 mm i.d. (P), controlled by using computer program were used for injecting accurate volume of samples (S) and delivering appropriate flow rate of reagent (RB). PTFE tubings (0.19 mm i.d.) were used as flow lines connected with the μFA.

2.3. Sample collection and pretreatment

Water samples were collected from rainwater, Ang-Keaw water reservoir, Ang-Karset water reservoir, Chiang Mai Canal, and Mae Ping River in Chaing Mai and Lumpun provinces, Thailand. The water samples were filtered through a 0.45 μm membrane filter at the selected sampling sites and stored in polyethylene containers that had been previously washed with 10% nitric acid and rinsed with deionized water for several times. After filtration, a 5 mL of concentrated hydrochloric acid was added in each liter of water. Water sample (100 mL) was treated with 2.0 mol L^{-1} hydrochloric acid and heated to 200 °C. It was allowed to cool to room temperature, filtered and diluted to appropriate concentration. The treated water samples were used for analysis of iron using the proposed method.

2.4. Procedure

The μFA system (Fig. 1) integrated with a fiber optic spectrometer to obtain a micro flow manifold for determining of Fe(III). The method involved the injection 5 μL of standard or sample solution containing Fe(III) by switching the selection valve into a reagent stream of 0.4% w/v nitroso-R salt adjusted to pH 5 with 0.5 mol L^{-1} acetate buffer with an appropriate flow rate of 30 μL min^{-1} using peristaltic pump with the specially desired software to control flow system (sample injection volume calculated from aspiration time and flow rate). Nitroso-R salt and Fe(III) were reacted on T-junction of the μFA (MF) resulting in a green Fe(III)–nitoso-R complex and then passed through the flow cell fixed in PDMS top plate, where the fiber optic probe was placed to measure the absorbance at 720 nm.

3. Results and discussion

The fabricated μFA was used as a basis for development of a greener method for analysis of trace iron. Appropriate micro flow analysis conditions for the quantitative analysis of iron were achieved. The method is based on the measurement of absorbance arising from Fe(III)–nitroso-R complex in an acetate buffer solution pH 5 medium, formed by the reaction of Fe(III) with nitroso-R on the T-shaped micro channel in micro flow analyzer. The Fe(III)–nitroso-R complex was measured at 720 nm. This complexing agent has not been previously applied to Fe(III) determination using μFA system. The analyte was introduced into the reagent and buffer stream by using a computer controlled selection valve and peristaltic pump. As a sequence, they were mixed completely on the T-shaped micro channel in micro analyzer. Under optimum conditions other species did not interfere.

3.1. Designed of the micro flow system

The developed micro flow manifold is shown in Fig. 1. It was designed with two flow lines. The flow line with a ten-port selection valves (SV) was used for delivering sample or standard solution (S) and the other flow line was used for delivering reagent (RB) into the μFA system (MF). A T-shaped micro channel (0.2 mm wide, 0.05 mm deep and 20 mm long) of the PMMA μFA was topped with a PDMS plate (MF), where a flow through cell (5 μL) was fixed. A flow through cell was connected with two fiber optic probes. The first probe, placing at the vertical axis on PDMS top Plate 10 mm from the PMMA chip was connected to USB2000 spectrophotometer (D). The second one, placing at the vertical axis under the PMMA chip was connected to tungsten light source. Sample or standard solutions (S) were introduced with accurate volume into the system by timed based injection using a ten-port selection valves (SV) controlled by the specially designed software developed in our laboratory termed "SIA". This software is also used for controlling the peristaltic pump (P) with small pump tubing to deliver the reagent at an appropriate flow rate through the μFA system. By this design, reproducible signal with low noise can be achieved. The network as a T-shape reactor planar on PMMA chip is suitable for producing Fe(III)–nitroso-R complex. The system consumed less reagents volume and released less waste than the traditional FI system (less than 2.0 mL h^{-1}).

3.2. Selectivity of the Fe(III)–nitroso-R salt complex

Preliminary investigation indicated that the micro flow system for iron determination using nitroso-R salts had been formed to give a selective means as well as copper(II) because they could be determined in the presence of each other at different absorption wavelengths (720 and 495 nm of Fe(III) and Cu(II)-complexes respectively). In addition, selectivity of the nitroso-R salt for Fe(III) and Cu(II) determinations could be achieved by adjustment of pH of the reaction medium using appropriate buffer solution. The sensitivity for Fe(III) determination is five times as sensitive as that of Cu(II) using nitroso-R salt under identical experimental conditions (see Fig. 4). As mentioned earlier in the introduction, selectivity for the metal-nitroso-R salt complexes could be obtained by pH adjustment and the maximum absorption wavelength for each metal. Therefore, further investigation was carried out to study the λmax of Fe(III),

Cu(II), Co(II) and Ni(II) under the given conditions; 1 μg mL^{-1} of each studied metals, 5 μL injection volume, 30 μL min^{-1} flow rate and 0.40% w/v nitroso-R salt. It was found that the maximum absorption for the four metal ions were 720, 495, 485, and 530 nm, respectively. The effects of various pH on the absorbance of each metal-complex at its λmax were also examined and plotted in Fig. 4a. It was clear that for Fe(III), Cu(II), Co(II) and Ni(II) could be selectively determined at 720, 495, 485 and 530 nm, respectively, in order to investigate the selectivity of the reagent for iron over copper and other metals (Co and Ni) effects of various pH valves (3.0–10.0) on the absorbances of Fe, Cu, Co and Ni complexes at 720 nm were carried out. Results are plotted in Fig. 4b. It was seen that Fe(III)–nitroso-R salt complex exhibited the greater sensitivity (at pH 5) than those obtained by Cu(II), Co(II) and Ni(II) complexes. The sensitivity for Fe(III) determination is 5 times, 5.5 times and 4 times as high as those of Cu(II), Co(II) and Ni(II) complexes, respectively. It is seen that the maximum absorption wavelengths obtained by this investigation are rather different from those reported in the literature for Fe, Cu, Co, and Ni (710, 480, 425 and 480 nm, respectively) [34–41]. Bathochromic shift (red shift) was obtained in the experimental results (λmax for four metals studied) probably owing to the used of different buffer solution to control the pH level. The present experiment employed HOAc/NaOAc buffer (pH 5) where as the reported experiment used NH_4OH/HOAc (pH 4) to control the pH of the reaction medium.

3.3. Optimization of the experimental conditions

The proposed micro flow analysis device was developed and optimized by a univariate method, to select the optimum conditions for the highest absorbance of Fe(III)–nitroso-R complex. The value of one variable was changed while keeping the other variables at their constant values. Then, by maintaining that variable at its optimum value, another was studied. The optimum values were selected from the maximum absorbance with low background and standard deviation. The optimizations of the experimental conditions were carried out by using standard Fe(III) solution. In all experiments, five replicate measurements were performed for each studied parameter. The analytical signal comparing between four standard Fe(III) solutions of this proposed μFA is shown in Fig. 2

3.3.1. Selecting the absorption wavelength

The optimum absorption wavelength for determining Fe(III) by complexing with nitroso-R salt was studied over the range of 600–800 nm. It was found that the Fe(III)–nitroso-R complex had a maximum absorption with low noise at 720 nm. Therefore, the absorption wavelength of 720 nm was chosen as the optimum wavelength and used for subsequent experiments.

3.3.2. Effect of flow rate

Reagent and/or carrier flow rates can be more or less affected on the FI signals due to dispersion. A high flow rate leads to a shorter time for each sample passing through the system, a low precision of the peak height and a high rate of reagent consumption. With a low flow rate, the residence time for each sample is long and the dispersion is large which can reduce the sensitivity and the sample throughput. Therefore, the effects of total flow rates on absorption signal of Fe(III)–nitroso-R complex in the micro flow analysis system were investigated for determining iron. The total flow rate was varied over the range of 10.0–100.0 μL min^{-1}. It was found that, the absorbance increased with increasing flow rate up to 30.0 μL min^{-1}, above this flow rate the absorbance decreased. As a result, the optimum flow rate was 30.0 μL min^{-1} (Fig. 3).

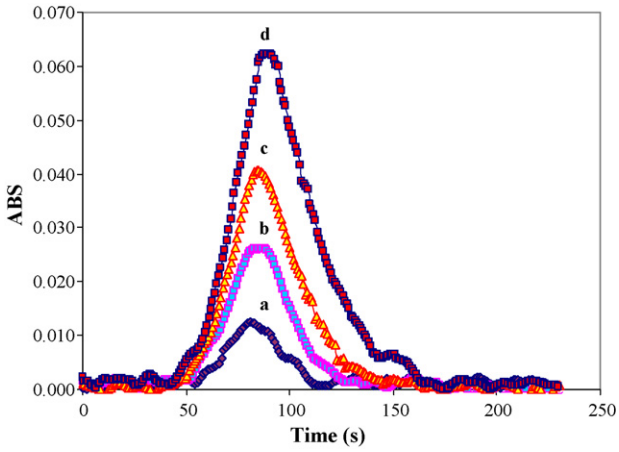

Fig. 2. Analytical signal for determination of Fe(III) by a T-shaped PMMA μFA system. Fe(III) concentration:(a) 0.1 μg mL^{-1};(b) 0.5 μg mL^{-1};(c) 1.0 μg mL^{-1}; and (d) 1.5 μg mL^{-1}.

3.3.3. Effect of sample introduction volume

The influence of sample introduction volume on Fe(III)–nitroso-R complex absorption was studied by controlling pump flow rate and changing the switching time of selection valve at sample line over the range between 2.0 μL and 10.0 μL. Results showed that initially, the absorbance increased rapidly with increasing sample volume up to 5.0 μL, above which the absorbance slightly decreased with boarding

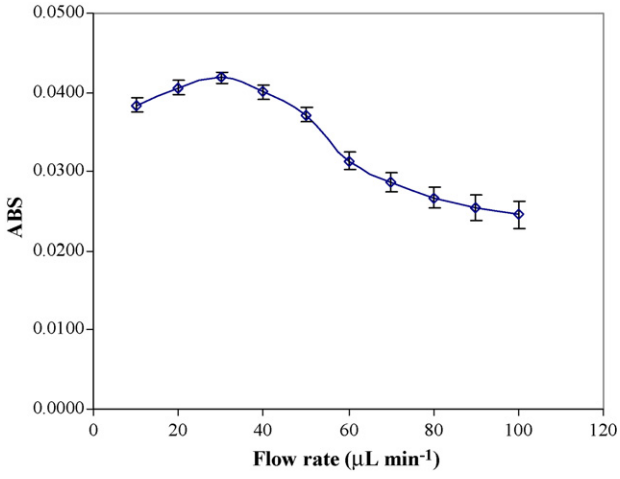

Fig. 3. Effect of fow rate on the absorbance of Fe(III)–nitroso-R complex. Iron(III) concentration 1.0 μg mL^{-1}; injection volume 5.0 μL, pH 5.

peak probably owing to the effect of dispersion. Hence, the injection volume of 5.0 μL was considered to be optimum sample introduction volume for the proposed micro flow system, which was used throughout the experiments.

3.3.4. Effect of pH

Normally, all complexation reactions between metal ions and any organic reagents as ligands are pH dependent. Selectivity for spectrophotometric determination of each metal ion can be obtained by adjusting the pH level of the reaction medium as mentioned earlier. The pH of solution is not only affecting on the selectivity but also influenced on the stoichiometry of the complexes resulting in hypsochromic shift and/or bathochromic shift of the maximum absorption wavelength (λmax) depending on the reaction concerns. Therefore, it is necessary to investigate the effect of pH on the absorbance of the Fe(III)–nitroso-R salt complex.

The absorbance of Fe(III)–nitroso-R complex was studied at various pH values in the range of 3.0–10.0. The pH values were adjusted with acetic acid/sodium acetate buffer solution (pH 3–7) and ammonium hydroxide/ammonium acetate buffer solution (pH 7–10). As a consequence, the absorbance of Fe(III)–nitroso-R complex was increased while increasing pH up to about 4.0–6.0 (Fig. 4), above this the absorbance decreased significantly. Hence, pH 5.0 was chosen as the optimum pH value and was used for further investigations.

3.3.5. Effect of nitroso-R salt concentrations

In general, the amount of reagent (as ligand) greater than required stoichiometry of the complex (Fe(III): nitroso-R salt = 1:3) is required for complete color development. The effects of nitroso-R salt concentrations (0.1–1.0% w/v) on the absorbance of Fe(III)–nitroso-R complex were studied. The absorbance increased with increasing concentrations of nitroso-R from 0.1 to 0.4% w/v, above which the absorbance slightly decreased (Fig. 5). As a result the optimum concentration of nitroso-R salt was 0.4% w/v.

3.4. Analytical figures of merit

Regarding to the proposed micro flow analysis system for determination of iron(III) in water sample illustrated in Fig. 1, the linear calibration ranges, the detection limits (LOD) and the limits of quantitation (LOQ) for iron were investigated. The LOD was determined as the concentration of the analyte leading to a signal that was three times of the blank standard deviation (3σ) as reported by Miller and Miller [49]. Similarly, the LOQ was determined as the concentration of analyte leading to a signal that was 10 times of the blank standard deviation (10σ). The calibration graph was linear over the range 0.05–4.0 μg mL^{-1}, which was expressed by the regression equation $Y = 0.0328X + 0.0097$ ($r^2 = 0.9994$). Where Y is absorbance of Fe(III)–nitroso-R complex and X is iron concentration (μg mL^{-1}). The LOD and LOQ were 0.021 and 0.081 μg mL^{-1}, respectively. The precision of the method based on repeatability was performed, by 11-replicates of three standard solutions covering different concentration levels: low,

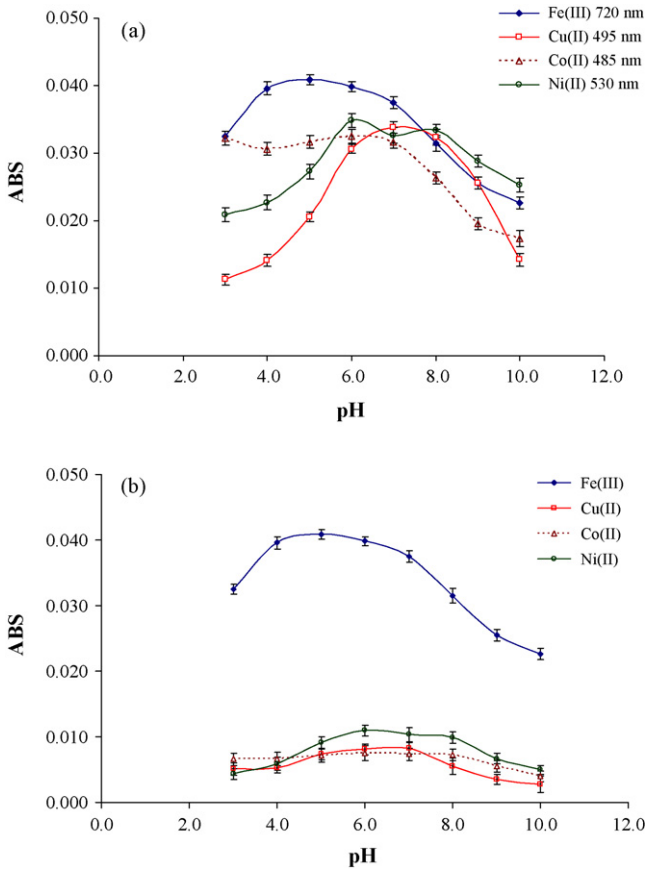

Fig. 4. (a) Effect of pH on the absorbances of Fe(III) and some major interferences (Co(II), Cu(II) and Ni(II)) as their metals-nitroso-R complexes (1.0 μg mL^{-1} of Fe(III), Co(II), Cu(II) and Ni(II)) measured at each maximum wavelength (720, 485, 495 and 530 nm, respectively), 5 μL injection volume, 30 μL min^{-1} flow rate and 0.4% w/v nitroso-R salt. (b) Effect of pH on the absorbance of the metal-nitroso-R complexes as in (a) but their absorbances were measured at 720 nm under the same experimental conditions as in (a).

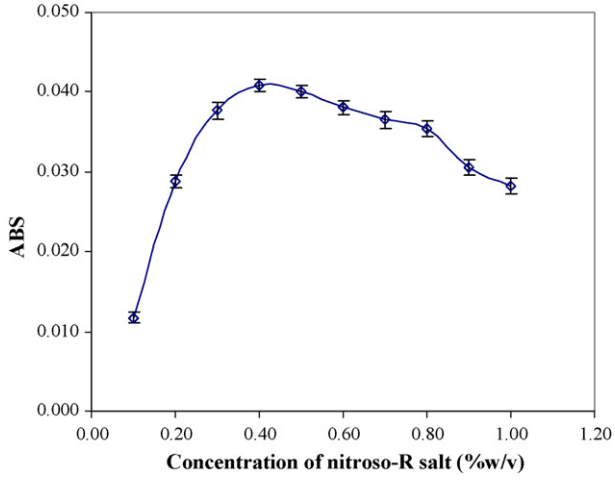

Fig. 5. Effect of nitroso-R salt concentrations on the absorbance of Fe(III)–nitroso-R complex. Iron(III) concentration 1.0 μg mL^{-1}; flow rate 30.0 μL min^{-1}; injection volume 5.0 μL; buffer pH 5.

medium and high (0.1, 1.0 and 3.0 μg mL^{-1}), and the peak heights (as absorbance) of which were measured. Statistical evaluation revealed that the relative standard deviation of each concentration of iron(III) solution was estimated to be 1.25, 0.74 and 0.58%, respectively. The percentage recovery was studied by spiking 1.0 μg mL^{-1} of iron (III) standard solution into water samples. The results showed that the percentage recovery was estimated to be 98.7 ± 0.12% ($n = 5$),

The LOD of the proposed method (21 ng mL^{-1}) far more higher than that reported by Hirata et al. [25] (0.02 ng mL^{-1}) based on FIA with column preconcentration of chelating resin functionalized with *N*-hydroxyethylethylenediamine ligands and chemiluminescence detection, with a rather long analysis time of 7.5 min $sample^{-1}$. However, the proposed method was operated without any preconcentration micro column leading to poor sensitivity and hence high LOD was obtained. The main objective of this work is aim at development of a green analytical procedure for Fe(III) determination in natural water that containing rather high amounts of Fe(III). Therefore, in this case extremely high sensitivity is unnecessary. Further improvement of this method will be performed to achieve a highly sensitive micro flow method for analyzing any species in biological samples. Although the proposed method was not as sensitive as the reported one described above, the proposed method was simple, cost effective and rapid with a sample throughput of 40 samples h^{-1} which was five times as rapid as that reported (8 samples h^{-1}) by Hirata et al. [25]. Considering the sample volume, the proposed method used 5 μL of sample volume which was >1000 times less than that reported (5.6 mL) by Hirata et al. [25]. The advantages of the proposed μFA system over the traditional FI system were minimum sample and reagent consumption, minimum waste generation, small size of instrumentation, simple and cost effective.

In contrast to examples of some previous reports found in the literature on various analytical methods for Fe(III) determination including FIA [13], AAS [17], SIA [31] and spectroscopy [11] and some hyphenated methods (SIA-FAAS) [30,32] as shown in Table 2. Several analytical methods provided higher sensitivity and/or lower LOD values than that obtained by the proposed μFA procedure, but they consumed large amount of reagent and sample. In a traditional flow based method (FIA and SIA), the amounts of sample volumes were in the range of 0.187–27 mL whereas that consumed by the μFA was 0.005 mL (5 μL). The average amounts of waste generation by some reported methods was more than 300 mL h^{-1} whereas 2.0 mL h^{-1} of waste was produced by the μFA. The SIA method was also required complicated system operation, indicating that using the μFA the sample and reagent consumption can be reduced more than 50 and 100 times as much as some traditional flow-based methods. The developed provided by the μFA procedure was also simple and cost effective. The sensitivity and LOD provided by AAS and spectroscopy are similar to those obtained by the recommended μFA method, the proposed method is simple, rapid and inexpensive with low reagent and sample consumptions, minimum waste generation and no flame gases are required (compared to AAS).

3.5. Effects of interfering ions

The effect of some possible interferences (foreign species) on the determination of Fe(III) in water sample was undertaken for the maximum concentration ratio of foreign species (μg mL^{-1}) to Fe(III) up to 200:1. The tolerance is defined as the foreign species concentration causing error smaller than ±10% for determining the analyte of interest. The tolerance concentrations of the studied species to 1.0 μg mL^{-1} Fe(III) under the optimum conditions were >200 μg mL^{-1} for Na^+, K^+, Ca^{2+}, NO_3^-, NO_2^- and SO_4^{2-}; 100 μg mL^{-1} for Pb^{2+}, Cr^{3+}, Mg^{2+}, Cd^{2+}, Cl^- and PO_4^{3-}; 70 μg mL^{-1} for Mn^{2+} and Zn^{2+}; 30 μg mL^{-1} for Co^{2+} and Cu^{2+} and 25 μg mL^{-1} for Ni^{2+}.

3.6. Sample analysis

Following the procedure described in the previous sections, the proposed method was applied to the determination of Fe(III) in natural water samples. The water samples were collected from rainwater, Ang-Keaw water reservoir, Ang-Karset water reservoir, Chiang Mai Canal, and Mae Ping River in Chaing Mai and Lumpun provinces, Thailand. The results are given in Table 1 compared with those obtained by atomic absorption spectrophotometry. It is shown that the results obtained by the proposed device agreed well with those obtained by AAS, because the calculated student *t*-value (0.26, $n = 11$) was less than the theoretical value (2.23) at confident level of 95%. The

Table 1
Concentrations of iron(III) in water sample (μg mL^{-1}) analyzed by using the proposed μFA

Sample	Iron contents (μg mL^{-1}), $n = 5$			
	The proposed μFA		FAAS	
	a	b	a	b
Rain water	0.27 ± 0.02	0.28 ± 0.03	0.25 ± 0.02	0.30 ± 0.05
Tap water	1.80 ± 0.15	1.76 ± 0.20	1.70 ± 0.25	1.83 ± 0.10
Ang-Keaw water reservoir	3.33 ± 0.22	3.61 ± 0.30	3.70 ± 0.20	4.09 ± 0.25
Ang-Karset water reservoir	4.09 ± 0.30	5.04 ± 0.21	4.57 ± 0.28	5.10 ± 0.32
Chiang Mai canal	9.80 ± 0.25	9.60 ± 0.12	10.01 ± 0.33	10.70 ± 0.27
Mea-Ping river (Chiang Mai province)	8.50 ± 0.20	9.02 ± 0.25	9.50 ± 0.31	8.30 ± 0.17
Mea-Ping river (Lumpun province)	20.01 ± 1.73	19.20 ± 1.11	18.60 ± 1.50	19.40 ± 1.06

a, calibration method; b, standard addition method.

Table 2
Comparison of the analytical characteristics of various analytical techniques for analysis of iron(III) with those obtained by the proposed.

Analytical methods	Speed (sample h^{-1})	Sample volume (mL)	Flow rate (mL min^{-1})	Waste (mL h^{-1})	Detection limit ($\mu g\,mL^{-1}$)
The proposed method	40	0.005	0.030	<2.0	0.021
Spectroscopy [11]	No report	>1.0	–	>500	0.010
FIA ferrozine [13]	90	0.600	4.6	300	0.012
FI-CL hydrogen peroxide [25]	8	5.6	2.8	>250	2.0×10^{-5}
AAS [17]	No report	>1.0	–	>300	0.0196
SIA [31]	40	0.187	2.8	200	0.018
SIA-FAAS [30]	18.5	1.83	1.0–5.5	>600	0.03
SIA-FAAS [32]	8, 10	9, 27	1.4–6.5	>500	0.012, 0.006

amounts of Fe(III) in water samples analyzed by the proposed method were in the range of 0.2–20 $\mu g\,mL^{-1}$. With respect to the amounts of chemical and reagents consumption, the proposed micro flow analysis method consumed smaller amount of chemical and reagent than those consumed by other methods; it also released smaller waste than those produced by other methods as shown in Table 2. Since the proposed micro-flow system employs miniaturized components (selection valve, peristaltic pump and fiber optic spectrometer) and a laptop for data manipulation that seem promising for adoption to being portable. The laptop can be replaced by a micro computer or personal digital assistant (pocket PC or palm) which makes the device become more portable and suitable for field monitoring. These have been studied in details, which will be described in subsequent publication.

4. Conclusions

It can be concluded that, the proposed method has been satisfactorily applied to the determination of Fe(III) in water samples with the relative standard deviation (%R.S.D.) in the ranges of 0.58–1.25% and the percentage recovery of 98.7 ± 0.12 ($n = 5$). In addition, the use of nitroso-R salt as complexing agent using the proposed micro flow device has proven to be highly precise (R.S.D. of less than 2%) sensitive, (LOD = 0.021 $\mu g\,mL^{-1}$ and LOQ = 0.081 $\mu g\,mL^{-1}$), accurate (%recovery of 98.7 ± 0.12, $n = 5$) and rapid with a sample throughput of 40 h^{-1}. The proposed micro analysis method also consumed very small amount of chemicals and reagents (less than 2.0 mL h^{-1}), with minimum waste production. It is also simple and inexpensive. Hence, it is considered to be a green analytical technique and environmental friendly technique.

Acknowledgements

The authors would like to express their sincere thanks to the Bureau of Personnel Administration and Development, Commission on Higher Education, The Ministry of Education, Thailand for fully financial support. We also would like to thank Mahasarakham University and the Center for Innovation in Chemistry: Postgraduate Education and Research Program in Chemistry (PERCH-CIC) for their partial financial support. Finally, we would like to thank the Department of Chemistry, Faculty of Science, Chiang Mai University for providing all laboratory facilities and the Alpha Flow Analysis Group for excellent guidance.

References

[1] R.P. Rocha, J.A. Nobrega, O. Fatibello-Filho, Green. Chem. 3 (2001) 216.
[2] P.A. Greenwood, G.M. Greenway, Trends Anal. Chem. 21 (11) (2002) 726.
[3] B. Divjak, M. Franko, M. Novic, J. Chromatogr A 829 (1998) 167.
[4] S. Sylvia, R. Stefan, J.K. Heinz, Environ. Sci. Technol. 32 (1998) 1530.
[5] J.L.F.C. Lima, C. Delerue-Mates, M. Carmo, V.F. Vazt, Food Chem. 62 (1) (1998) 117.
[6] E. Viollier, P.W. Inglett, K. Hunter, A.N. Roychoudhury, P.V. Cappellen, Appl. Geochem. 15 (2000) 785.
[7] Komadel, Stucki, Clays Clay Miner. 36 (1988) 379.
[8] G.S.R. Krishnamurti, P.M. Huang, Talanta 37 (7) (1990) 745.
[9] P.L. Croot, K.A. Hunter, Anal. Chim. Acta. 406 (2) (2000) 289.
[10] B. Klein, L.B. Lucas, Clin. Chem. 17 (12) (1971) 1196.
[11] Z. Moldovan, E. Neagu, J. Serb. Chem. Soc. 67 (10) (2002) 510–669.
[12] K. Sözegen, E. Tütem, Anal. Sci. 17 (2001) i861.
[13] M.I. Pascual-Reguera, I. Ortega-Carmona, A. Molina-Díaz, Talanta 44 (1997) 1793.
[14] M. Feng, Y. Yang, P. He, Y. Fang, Spectrochim. Acta Part A 56 (2000) 581.
[15] S. Saracoglu, M. Soylak, L. Elci, Acta Chim. Slov. 50 (2003) 807.
[16] I.I. Naqvi, Q. Saeed, M.A. Farrukh, Pak. J. Biol. Sci. 7 (8) (2004) 1355.
[17] J. Miura, S. Arima, M. Satake, Analyst 115 (9) (1990) 1191.
[18] C.J. Park, J.K. Suh, JAAS 12 (1997) 573.
[19] K. Pomazal, C. Prohaska, I. Steffan, G. Reich, J.F.K. Huber, Analyst 124 (1999) 657.
[20] A. Asan, M. Andac, I. Isildak, Anal. Sci. 19 (2003) 1033.
[21] F.R.P. Rocha, B.F. Reis, J.J.R. Rohwedder, Fresenius J. Anal. Chem. 370 (2001) 22.
[22] T. Imato, H. Ohura, Anal. Sci. 17 (2001) i395.
[23] H. Hwang, J. Kim, J. Korean Chem. Soc. 46 (5) (2002) 419.
[24] M. Novič, NovičF M., CCACAA 75 (2) (2002) 531.
[25] S. Hirata, H. Yoshihara, M. Aihara, Talanta 49 (1999) 1059.
[26] D.A. Weeks, K.W. Bruland, Anal. Chim. Acta 453 (2002) 21.
[27] D. Lannuzel, J.d. Jong, V. Schoemann, A. Trevena, J. Tison, L. Chou, Anal. Chim. Acta 556 (2006) 476.
[28] S.H. Lee, M.S. Nam, J. Korean Chem. Soc. 46 (6) (2002) 509.
[29] P. Ugo, L. Moretto, D. Rudello, E. Birrel, J. Chevalet, Electroanalysis 13 (8–9) (2001) 661.
[30] R.C.C. Costa, A.N. Araújo, Anal. Chim. Acta. 438 (2001) 227.
[31] Z.O. Tesfaldet, J.F. van Staden, R.I. Stefan, Talanta 64 (2004) 1189.
[32] E. Rubí, M.S. Jiménez, F. Bauzá de Mirabó, R. Forteza, V. Cerdà, Talanta 44 (1997) 553.
[33] B.I. Nabivanets, N.V. Chernaya, V.G. Matyashev, Yu.A. Omel'chenko, Vestn. Kiev. Politekhn. In-ta. Khim. Mashinostr. i Tekhnol. 22 (1985) 35.
[34] H.S.V. Klooster, J. Am. Chem. Soc. 43 (1921) 746.
[35] B.K. Purl, S. Balani, Talanta 42 (3) (1995) 337.
[36] Makitie, Osmo, Ann. Agr. Fenn. 7 (2) (1968) 117.

[37] H. OH, H. Choi, Anal. Sci. 16 (2000) 183.
[38] B. Purachat, S. Liawruangrath, P. Sookamiti, S. Rattanaphani, D. Buddhasukh, Anal. Sci. 17 (2001) 443.
[39] R.M. Issa, S.E. Zayan, T.M. El-shamy, G.B. El-Hefnawey, Monatshefte füer Chemie. 111 (6) (1980) 1413.
[40] G. Her, H. Choi, J. Korean Chem. Soc. 49 (2) (2005) 145.
[41] M.A. Taher, Talanta 50 (1999) 559.
[42] T. Odake, M. Tabuchi, T. Sato, H. Susaki, T. Koreaga, Anal. Sci. 17 (2001) 535.
[43] S. Fujii, T. Tokuyama, M. Abo, A. Okubo, Anal. Sci. 20 (2004) 209.
[44] P.H. Petsul, G.M. Greenway, S.J. Haswell, Anal. Chim. Acta 428 (2001) 155.
[45] G.N. Doku, S.J. Haswell, Anal. Chim. Acta 382 (1–2) (1999) 1.
[46] M. Bowden, M. Sequeira, J.P. Krog, P. Gravesen, D. Diamond, Analyst 127 (2002) 1.
[47] Y. Wei, M. Oshima, J. Simon, S. Motomizu, Talanta 57 (2002) 355.
[48] D. He, Z. Zhang, Y. Huang, Y. Hu, H. Zhou, D. Chen, Luminescence 20 (4–5) (2005) 271.
[49] J.C. Miller, J.N. Miller, Statistics for Analytical Chemists, third ed., Ellis Harwood, London, 1994, p. 115.

Available online at www.sciencedirect.com
ScienceDirect
Talanta 73 (2007) 76–80
Talanta
www.elsevier.com/locate/talanta

Liquid chromatography/tandem mass spectrometric method for the simultaneous determination of tobacco-specific nitrosamine NNK and its five metabolites

Hui-Ling Lee, Chiying Wang, Susana Lin, Dennis Paul Hsientang Hsieh *

Division of Environmental Health and Occupational Medicine, National Health Research Institutes, Miaoli County350, Taiwan

Received 30 January 2007; received in revised form 3 March 2007; accepted 3 March 2007
Available online 12 March 2007

Abstract

A sensitive and robust high-performance liquid chromatography–electrospray ionization tandem mass spectrometry method to analyze 4-(methylnitrosamino)-1-(3-pyridyl)-1-butanone (NNK) and its five metabolites in one passage was developed and validated. The method achieved excellent reproducibility and accuracy. Linearity was observed for all six compounds ($R^2 = 0.999$) with detection limits (S/N $\geq$ 3) ranging from 0.2 to 2.4 pg on column and 0.01–0.12 ng ml^{-1} in samples injected. Average intra-day and inter-day variations (% R.S.D.) were 1.2 and 3.5%, respectively. A sample preparation method involving C8 and C18 solid phase extraction provided satisfactory recovery of the analytes in mouse urine. Each NNK metabolite was identified by its chromatographic retention time and specific fragmentation pattern. Since the carcinogenicity of NNK is related to its metabolism, the method described in this report should facilitate toxicological investigations into the carcinogenesis due to NNK exposure in the environment.

Keywords: 4-(Methylnitrosamino)-1-(3-pyridyl)-1-butanone (NNK); LC–MS/MS; Metabolite

1. Introduction

Epidemiological data have shown an increased risk of lung cancer in nonsmokers exposed to environmental tobacco smoke (ETS) [1,2]. Tobacco-specific nitrosamine 4-(methylnitrosamino)-1-(3-pyridyl)-1-butanone (NNK) is believed to play a significant role in lung cancer in smokers. It is a potent carcinogen in rodents, inducing primarily adenocarinoma of the lung, the most common type of lung cancer observed in nonsmokers [3–5]. In humans, rodents, and primates, NNK is extensively and rapidly metabolized to 4-(methylnitrosamino)-1-(3-pyridyl)-1-butanol (NNAL). NNAL, like NNK, is also a potent pulmonary carcinogen in rodents. The major pathways of NNK and NNAL metabolic activation to DNA adducts formation involve α-hydroxylation of the terminal carbons adjacent to *N*-nitroso groups. This metabolic activation pathway occurs for a wide range of nitrosamines [6,7]. The α-hydroxylation of NNK and NNAL can proceed at either the methyl or methylene carbon, producing the secondary products 4-hydroxy-1-(3-pyridyl)-1-butanone (HPB), 4-oxo-4-(3-pyridyl)-butyric acid (keto acid), 1-(3-pyridyl)-1,4-butanediol (PBD) and 4-hydroxy-4-(3-pyridyl)-butyric acid (hydroxy acid) as shown in Fig. 1.

NNK metabolites are useful biomarkers for metabolic activation or detoxification of NNK in an exposed individual. Because epidemiological studies showed that lung cancer risk was increased in arseniasis-endemic areas in Taiwan, an interac-

Abbreviations: As, arsenic; CAD, collision-assisted dissociation; CE, collision energy; $^{13}C_6$-NNK, [1′,2′,3′,4′,5′,6′-$^{13}C_6$]-NNK; CXP, cell exit potential; d_3-NNAL, 4-(methyl-d_3-nitrosamino)-1-(3-pyridyl)-1-butanol; DP, declustering potential; ESI-MS/MS, electrospray ionization tandem mass spectrometry; ETS, environmental tobacco smoke; FP, focusing potential; GC, gas chromatography; GC–TEA, GC with thermal-energy analyzer; HPB, 4-hydroxy-1-(3-pyridyl)-1-butanone; HPLC, high performance liquid chromatography; Hydroxy acid, 4-hydroxy-4-(3-pyridyl)-butyric acid; IS, internal standards; Keto acid, 4-oxo-4-(3-pyridyl)-butyric acid; LC–MS/MS, (liquid chromatography/tandem mass spectrometry); LOD, limit of detection; LOQ, limit of quantification; MRM, multiple reaction monitoring; NNAL, 4-(methylnitrosamino)-1-(3-pyridyl)-1-butanol; NNK, 4-(methylnitrosamino)-1-(3-pyridyl)-1-butanone; PBD, 1-(3-pyridyl)-1,4-butanediol; RSD, relative standard deviation; SPE, solid phase extraction

* Corresponding author at: Division of Environmental Health and Occupational Medicine, National Health Research Institutes, No 35 Keyan Road, Zhunan Town, Miaoli County 350, Taiwan. Tel.: +886 37 246166x36500; fax: +886 37 587406.
E-mail address: dphsieh@nhri.org.tw (D.P.H. Hsieh).

0039-9140/$ – see front matter © 2007 Elsevier B.V. All rights reserved.
doi:10.1016/j.talanta.2007.03.001

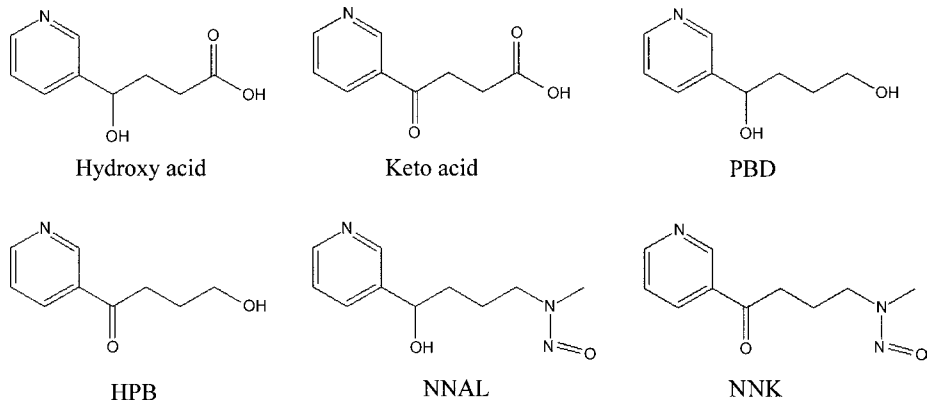

Fig. 1. Structures of NNK and its metabolites.

tion between cigarette smoke and arsenic (As) was proposed [8] to test the hypothesis that As exposure may enhance the NNK carcinogenicity by altering its metabolism. To further examine this metabolic modulation of NNK carcinogenicity in laboratory animals, a sensitive and rapid analytical method is needed to monitor the profiles of NNK metabolites. To date, the most widely used approach for the detection/separation/identification of NNK and its metabolites has been high performance liquid chromatography (HPLC) [9,10], followed by gas chromatography (GC) being less commonly used [11,12]. The use of high-performance liquid chromatography–electrospray ionization tandem mass spectrometry (LC–MS/MS) [13–15] instead of GC with thermal-energy analyzer (GC–TEA) [16–19] provides higher throughput with analyte-specific detections based on both retention time and structurally specific analyte fragmentation information.

As part of our study on the NNK carcinogenicity in non-smoking females in Taiwan, we have developed and validated a LC–MS/MS method that takes advantage of the specificity and sensitivity of tandem mass spectrometry. We also demonstrated the utility of this method in analyzing NNK, conjugated NNAL, free NNAL and several metabolites in the urine samples of mice that had been dosed NNK. Quantification was achieved by the use of trideuterated NNAL and $^{13}C_6$-NNK as internal standards. The urinary metabolites were collected by solid phase extraction (SPE) with C18 and C8 columns. This analytical procedure has greatly facilitated our study on the metabolism of NNK in relation to its carcinogenicity in animals.

2. Experimental

2.1. Chemicals

All the solvents and salts used in this study were of analytical grade from Merck (Darmstadt, Germany). Water used was purified by a Millipore (Bedford, MA, USA) Milli-Q water system. β-Glucuronidase type IX-A (product G 7396) from Sigma–Aldrich (St. Louis, MO, USA), 4-(methylnitrosamino)-1-(3-pyridyl)-1-butanone (NNK), 4-(methylnitrosamino)-1-(3-pyridyl)-1-butanol (NNAL), 4-oxo-4-(3-pyridyl)-butyric acid, 4-hydroxy-1-(3-pyridyl)-1-butanone (HPB), 1-(3-pyridyl)-1,4-butanediol (PBD), and 4-hydroxy-4-(3-pyridyl)-butyric acid were purchased from Toronto Research Chemicals Inc. (North York, Canada). 4-(methyl-d_3-nitrosamino)-1-(3-pyridyl)-1-butanol (d_3-NNAL) and [1′,2′,3′,4′,5′,6′-$^{13}C_6$]-NNK ($^{13}C_6$-NNK) were obtained for use as internal standards from Toronto Research Chemicals Inc. (North York, Canada) and Cambridge Isotope Laboratories (Andover, MA), respectively.

2.2. Sample preparation

All of the reference analytes were prepared as 1 mg ml^{-1} standard stock solutions in methanol and stored at 4 °C. Then the standard solutions were diluted to 0.03–150 ng ml^{-1} with 5% methanol containing 10 mM ammonium acetate, pH 6.5 and spiked with a fixed amount of 1 ng ml^{-1} d_3-NNAL as internal standards (IS) for NNAL, PBD and hydroxy acid, and $^{13}C_6$-NNK for NNK, HPB and keto acid.

Each 0.25 ml A/J mouse urine sample was spiked with NNK and its metabolites at 3 and 15 ng ml^{-1}, respectively. For determination of recoveries, the spiked samples were loaded onto SPE Waters C18 or C8 (100 mg × 1 ml, Milford Massachusetts, Ireland) cartridges preconditioned with 1 ml of methanol followed by 1 ml of Milli-Q water. After loading the sample, the cartridge was washed with 1 ml of Milli-Q water. The analytes in samples were eluted with 1 ml of 5% methanol containing 10 mM ammonium acetate (pH 6.5) and 1 ml of 50% methanol. The eluates were dried under vacuum (Thermo SpeedVac, Waltham, MA, USA, 1200 rpm, 40 °C, 180 min) and reconstituted with 0.25 ml of 5% methanol containing 10 mM ammonium acetate, pH 6.5 for LC–MS/MS analysis.

The enzyme hydrolysis and SPE procedure for urine samples of A/J mice treated with NNK was performed according to the method of Byrd and Ogden [15] with a slight modification. Each 0.5 ml mouse urine sample was spiked with 50 μl of 10 ng ml^{-1} d_3-NNAL and $^{13}C_6$-NNK and divided into 0.25 ml used for free NNAL determination and 0.25 ml for total NNAL determination. For total NNAL determination, the urine samples were acidified to precipitate proteins, centrifuged, and were added 25,000 units of β-glucuronidase enzyme in 1 ml of the 50 mM phosphate buffer (pH 7.0). The mixture was incubated at 37 °C with shaking at 250 rpm for 20 h. Preparation of the metabolites freed up for LC–MS/MS analysis was as described in the preceding paragraph.

Table 1
Operation parameters of simultaneous analysis of six tobacco-specific nitrosamine metabolites by LC–MS/MS in MRM mode.

Analyte	Precursor ions (*m/z*)	Product ions (*m/z*)	DP[a] (V)	FP[b] (V)	CE[c] (V)	CXP[d] (V)
(A) Hydroxy acid	182	164	46	290	23	24
(B) Keto acid	180	134	46	330	29	22
(C) PBD	168	108	46	330	47	18
(D) HPB	166	106	41	310	25	18
(E) NNAL	210	93	36	270	29	16
(F) NNK	208	122	36	260	17	20
(G) d_3-NNAL	213	93	41	240	29	16
(H) $^{13}C_6$-NNK	214	128	36	290	19	22

[a] Declustering potential.
[b] Focusing potential.
[c] Collision energy.
[d] Cell exit potential.

2.3. Liquid chromatography

HPLC analysis was performed with a PE series 200 binary pump and auto-sampler (PE series 200, Perkin-Elmer, Norfolk, CT, USA) system and 20 μl injections of each sample. Analytes were separated on a C18 column (Thermo Electron Corporation, 2.1 mm × 150 mm, 3 μm, Waltham, MA, USA) at a flow rate of 200 μl min^{-1}. The optimized mobile phase gradient involved the following alternation of mobile phase A (5% methanol containing 10 mM ammonium acetate) and mobile phase B (95% methanol containing 10 mM ammonium acetate): 92:8 mobile phase A/mobile phase B (v/v) from 0 to 6 min; 30:70 mobile phase A/mobile phase B (v/v) from 6 to 10 min, holding this composition until 16 min, then quickly returning to 100% mobile phase B and then 100% mobile phase A to finish a 20 min cycle of analysis before the next sample was injected.

2.4. Electrospray ionization tandem mass spectrometry (ESI-MS/MS)

The separated analytes eluted from the HPLC system were introduced into a triple-quadrupole mass spectrometer, API 3000 (Applied Biosystem/MDS SCIEX, Concord, Ontario, Canada), operating with a TurboIonSpray source. The mass spectrometer coupled with electrospray ionization (ESI) interfaces was operated in positive ion mode and ion spray voltage at 5500 V. Turbospray settings were as follows: nebulizer and curtain gas at 12 l min^{-1}, collision-assisted dissociation (CAD) at 12 l min^{-1}, turbo gas at 8 l min^{-1}, and the source heater probe temperature at 400 °C. For the most sensitive quantitative analysis of NNK metabolites, measurements were taken in the multiple reaction monitoring (MRM) mode, which included precursor ions, product ions, declustering potential (DP), focusing potential (FP), collision energy (CE), and cell exit potential (CXP) as listed in Table 1.

3. Results and discussion

3.1. Method development

Our goal in the present study was to develop a simple and rapid method with demonstrated validity for the detection/identification/quantification of NNK and its metabolites. Many variables affect the separation performance and signal intensities, such as column, organic solvent, pH and buffer solution. To achieve maximum sensitivity and optimize peak shape, we evaluated different types of solvents, including methanol and acetonitrile both containing ammonium acetate. The presence of ammonium acetate strongly facilitated the retention of NNK and its metabolites on the HPLC column and also enhanced chromatographic selectivity and reproducibility.

Experiments using a mobile phase A (5% methanol containing 10 mM ammonium acetate) and mobile phase B (95% methanol containing 10 mM ammonium acetate) with different pH values yielded an optimal pH of 6.5, which produced peaks for the NNK metabolites with the best resolution. Under the starting condition of 92:8 mobile phase A and mobile phase B (v/v), separation of all of the compounds with well-defined peak shapes and maximum sensitivity were observed, as shown in Fig. 2. In the positive ionization mode, the most abundant ions observed were the single-charged molecular cations of NNK and all its metabolites. The turbo ion spray source features a heated probe that directs hot nitrogen gas toward the spray aerosol; the optimal temperature was 400 °C.

The fragmentation patterns of each compound are described in the Table 1. One major advantage of MS–MS for trace analysis is its added identity confirmation for analytes due to their characteristic product ions from selected precursors ions. Fragmentation studies and optimization of MRM conditions were realized by infusions of standard solutions of each analyte.

3.2. Calibration curve and limit of quantification

One important consideration in the development of any analytical method is the linearity range and sensitivity of the method. Our calibration curves ranged from 0.03 to 150 ng ml^{-1}. Excellent linearity was obtained with correlation coefficient values between 0.998 and 0.999.

Calibration curves were obtained by analyzing a series of blank mice urines spiked with reference standards over a concentration range, with $^{13}C_6$-NNK and d_3-NNAL used as internal standards. Calibration curves were constructed by plotting peak area ratio of the reference standard and internal standard against concentration.

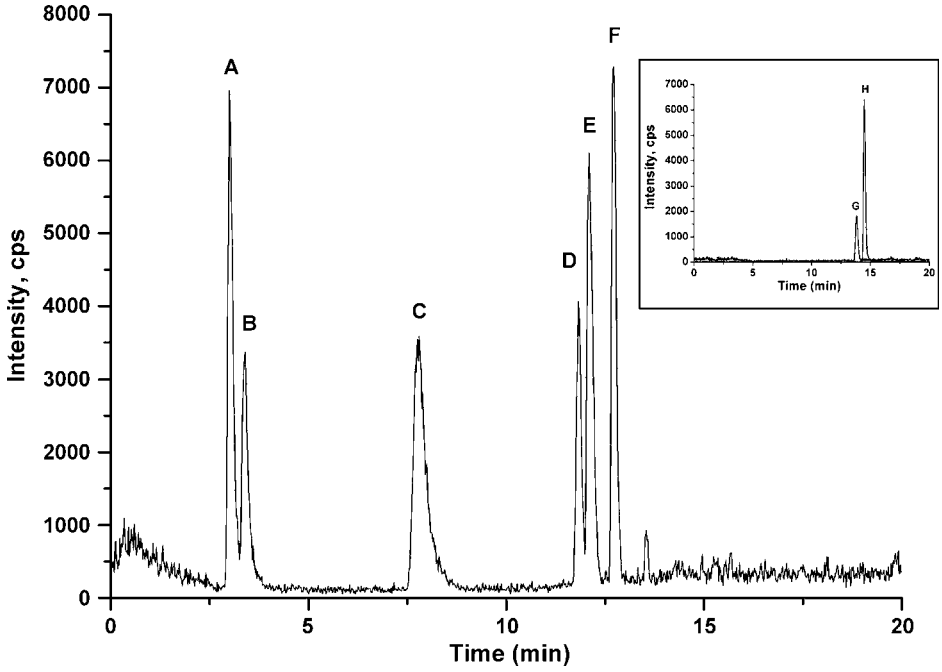

Fig. 2. LC–MS/MS chromatogram of reference compounds using MRM (multiple reaction monitor) mode. (A) 1.5 ng ml^{-1} hydroxy acid, (B) 1.5 ng ml^{-1} keto acid, (C) 1.5 ng ml^{-1} PBD, (D) 1.0 ng ml^{-1} HPB, (E) 1.0 ng ml^{-1} NNAL and (F) 0.5 ng ml^{-1} NNK. All compounds were dissolved in [5% methanol + 10 mM ammonium acetate].

Table 2
Precision and limit of detection (LOD) and limit of quantification (LOQ) of the LC–MS/MS method developed for NNK and its metabolites

Analyte	Intra assay precision[a]	Inter assay precision[a]	LOD (ng ml^{-1})[b]	LOQ (ng ml^{-1})[c]
Hydroxy acid	2.0	3.5	0.12	0.41
Keto acid	1.6	3.0	0.09	0.29
PBD	1.2	3.2	0.02	0.07
HPB	1.7	3.4	0.05	0.17
NNAL	1.3	2.1	0.01	0.03
NNK	1.5	2.5	0.02	0.06

[a] R.S.D. (%), $n = 5$, concentration of analyzed samples = 1.5 ng ml^{-1}.
[b] S/N ≥ 3.
[c] S/N ≥ 10.

The limit of detection (LOD) and limit of quantification (LOQ) were defined by peak heights, respectively, 3 and 10 times higher than the maximum baseline height of blank. As shown in Table 2, the LOD and LOQ for the concentrations of the six NNK metabolites were between 0.01–0.12 ng ml^{-1} and 0.03–0.41 ng ml^{-1}, respectively. The precision of the method was determined by calculating the relative standard deviation (R.S.D.) of the replicate measurements. All R.S.D. were less than 3.5% for intra and inter-assay precision. Precision and recovery could be improved by using a better internal standard for the secondary metabolites, such as a stable isotope-labeled analog when it becomes available commercially.

3.3. Recovery of metabolites in urine

The recovery rates of NNK and its metabolites in 0.25 ml of A/J mouse urine determined for SPE using C8 and C18 cartridges at two different concentrations (3 and 15 ng ml^{-1}) are shown in Table 3. The recovery rates using C18 cartridges were greater than those using C8 cartridges. The mean recovery rates of NNK and metabolites using C18 cartridges at 3 and 15 ng ml^{-1} were 78.2–95.5% and 80.5–98.7%, respectively.

Table 3
Recoveries of NNK and its metabolites in A/J mouse urine from C8 and C18 extraction

Mean recovery (%)[a]				
Analyte	C8 SPE		C18 SPE	
	3 ng ml^{-1}	15 ng ml^{-1}	3 ng ml^{-1}	15 ng ml^{-1}
Hydroxy acid	75.2 ± 5.5	80.7 ± 4.5	78.2 ± 5.6	80.5 ± 4.2
Keto acid	80.1 ± 4.6	85.9 ± 3.2	82.3 ± 5.2	90.1 ± 3.1
PBD	89.1 ± 3.5	96.1 ± 2.5	89.1 ± 3.7	95.3 ± 2.6
HPB	90.2 ± 3.5	98.6 ± 2.8	90.1 ± 3.0	97.4 ± 2.5
NNAL	87.2 ± 3.3	88.8 ± 2.4	95.5 ± 2.8	98.7 ± 2.3
NNK	89.5 ± 2.5	90.3 ± 2.0	94.7 ± 2.5	97.2 ± 2.1

[a] $n = 5$.

Table 4
Limit of detection (LOD) and limit of quantification (LOQ) of some comparable analytical methods

Method	Analyte	LOD (ng ml^{-1})	LOQ (ng ml^{-1})	Reference
LC–MS/MS	NNK, NNAL	0.05, 1.23	ND[a]	[13]
LC–MS/MS	NNAL	ND[a]	0.02	[15]
LC–MS/MS	NNK, NNAL, keto acid, hydroxy acid, HPB, PBD	0.01–0.12	0.03–0.41	This study
GC–TEA	NNAL	ND[a]	0.02	[16]
HPLC	NNK, NNAL, keto acid, hydroxy acid, HPB, PBD	20–250	ND[a]	[9]

[a] ND = no data given.

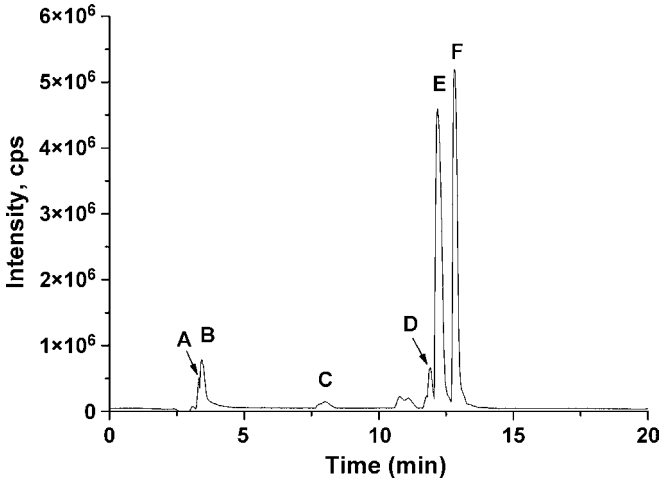

Fig. 3. LC–MS/MS chromatogram of NNK metabolites in A/J mouse urine using MRM (multiple reaction monitor) mode. (A) Hydroxy acid, (B) keto acid, (C) PBD, (D) HPB, (E) NNAL and (F) NNK. All compounds were redissolved in [5% methanol + 10 mM ammonium acetate] for LC–MS/MS analysis.

Thus, C18 is the cartridge of choice in the sample preparation process. The developed method was applied to the analysis of the urine samples of mice treated with NNK (0.5 mg/mice/day). The results are shown as in Fig. 3. From urine analysis, the amount of total NNAL was about 10-fold greater than the free NNAL. The method was used to demonstrate the influence of other chemicals on the kinetic and metabolism of NNK in A/J mice (results to be published elsewhere). This method is useful in a wide range of samples including those from smoke-exposed animals, if samples are properly concentrated. Our method is favorably compared with some known methods in terms of analytes applicable, LOD and LOQ as shown in Table 4.

4. Conclusion

A rapid LC–MS/MS method combined with an off-line SPE step has been developed for detection//identification/quantification/ of NNK and its primary and secondary metabolites in A/J mouse urine. Satisfactory recoveries and precision were obtained ranging from 78.2 to 98.7% at trace levels in all cases, with relative standard deviations lower than 3.5%. The selectivity and sensitivity of this method to measure six NNK metabolites simultaneously would greatly facilitate studies of the metabolism of NNK in relation to its carcinogenicity in animals.

Acknowledgements

This study was supported by a grant DOH95-TD-G-111-018 from the Department of Health, Taiwan, ROC. The authors gratefully acknowledge the helpful discussions given by Dr. Louis W. Chang and Dr. Pin-Pin Lin of this Division.

References

[1] S.S. Hecht, Chem. Res. Toxicol. 11 (1998) 559.
[2] IARC monographs on the evaluation of carcinogenic risks to humans, Monographs programme finds smokeless tobacco is carcinogenic to humans, International Agency for Research on Cancer, 2004.
[3] S.S. Hecht, J. Natl. Cancer Inst. 91 (1999) 1194.
[4] G.N. Wogan, S.S. Hecht, J.S. Felton, A.H. Conney, L.A. Loeb, Semin. Cancer Biol. 14 (2004) 473.
[5] S.S. Hecht, Mutat. Res. 424 (1999) 127.
[6] J.R. Jalas, S.S. Hecht, S.E. Murphy, Chem. Res. Toxicol. 18 (2005) 95.
[7] S.S. Hecht, Nat. Rev. Cancer 3 (2003) 733.
[8] C.L. Chen, L.I. Hsu, H.Y. Chiou, Y.M. Hsueh, S.Y. Chen, M.M. Wu, C.J. Chen, JAMA 292 (2004) 2984.
[9] W.M. Mullett, K. Levsen, J. Borlak, J. Wu, J. Pawliszyn, Anal. Chem. 74 (2002) 1695.
[10] P. Upadhyaya, E.J. McIntee, S.S. Hecht, Chem. Res. Toxicol. 14 (2001) 555.
[11] S.S. Hecht, N. Trushin, S.K. Chhabra, L.M. Anderson, P.V. Nerurkar, Drug Metab. Dispos. 28 (2000) 5.
[12] S.G. Carmella, A. Borukhova, S.A. Akerkar, S.S. Hecht, Cancer Epidemiol. Biomarkers Prev. 6 (1997) 113.
[13] W. Wu, D.L. Ashley, C.H. Watson, Anal. Chem. 75 (2003) 4827.
[14] K.A. Wagner, N.H. Finkel, J.E. Fossett, I.G. Gillman, Anal. Chem. 77 (2005) 1001.
[15] G.D. Byrd, M.W. Ogden, J. Mass Spectrom. 38 (2003) 98.
[16] J.D. Adams, K.D. Brunnemann, D. Hoffmann, J. Chromatogr. 256 (1983) 347.
[17] H. Begutter, H. Klus, I. Ultsch, J. Chromatogr. 321 (1985) 475.
[18] M.V. Djordjevic, K.D. Brunnemann, D. Hoffmann, Carcinogenesis 10 (1989) 1725.
[19] S.S. Hecht, S.G. Carmella, M. Ye, K. Le, J.A. Jensen, C.L. Zimmerman, D.K. Hatsukami, Cancer Res. 62 (2002) 129.

Available online at www.sciencedirect.com
ScienceDirect
Talanta 73 (2007) 172–177
Talanta
www.elsevier.com/locate/talanta

Short communication

Voltammetric determination of catechol using a sonogel carbon electrode modified with nanostructured titanium dioxide

Suzanne K. Lunsford [a,*], Hyeok Choi [b], Jelynn Stinson [a], Amber Yeary [a], Dionysios D. Dionysiou [b]

[a] *Department of Chemistry, Wright State University, Dayton, OH 45435-0001, USA*
[b] *Department of Civil and Environmental Engineering, University of Cincinnati, Cincinnati, OH 45221-0071, USA*

Received 12 December 2006; received in revised form 5 March 2007; accepted 6 March 2007
Available online 12 March 2007

Abstract

In this study, we investigate highly efficient sonogel carbon electrode (SGC/TiO_2) modified with nanostructured titanium dioxide synthesized *via* sol–gel method employing surfactant template for tailor-designing the structural properties of TiO_2. The stable SGC/TiO_2 electrode detects catechol, a neurotransmitter, in the presence of ascorbic acid, a common interferent, using cyclic voltammetry. A possible rationale for the stable catechol detection of SGC/TiO_2 electrode is attributed to most likely the adsorption of catechol onto highly porous TiO_2 (surface area of 147 $m^2\ g^{-1}$ and porosity of 46.2%), and the formation of $C_6H_4(OTi)_2$ bond between catechol and TiO_2. The catechol absorbed onto TiO_2 rapidly reaches the SGC surface, then is oxidized, involving two electrons (e^-) and two protons (H^+). As a result, the surface of TiO_2 acts as an electron-transfer accelerator between the SGC electrode and catechol. In addition to the quantitative and qualitative detection of catechol, the SGC/TiO_2 electrode developed here meets the profitable features of electrode including mechanical stability, physical rigidity, and enhanced catalytic properties.

Keywords: Carbon electrode; Catechol; Cyclic voltammetry; Electrochemistry; Nanostructure; Neurotransmitters; Sensor; Sol–gel; Titanium dioxide

1. Introduction

Recently, electrochemical detection of neurotransmitters using smart sensors has attracted neuroscientists' attention since the altered levels of such chemicals have been associated with mental and behavioral disorders such as schizophrenia, attention deficient disorder, Alzheimer's disease, Parkinson's disease, eating disorders, epilepsy, amphetamine addiction, and cocaine addiction [1]. One of the major challenges in assessing their environmental fate and distribution in the human body is to measure them *in situ* in a more effective way. As a result, there is an urgent need to develop innovative sensors to detect catechol and its derivatives, a class of neurotransmitters (1,2 dihydroxybenzenes) [2].

In synthesizing inorganic materials with reactivity and functionality, sol–gel process is among the most promising methods. Sol–gel method refers to the formation of solid inorganic material from its liquid molecular precursors through room temperature wet chemistry-based procedures [3–7]. The application of sol–gel chemistry in fabricating carbon-based electrode has attracted great attention in developing a new type of sensors [8–10]. Recently, solid graphite composite electrode was synthesized *via* sonocatalysis, where high energy ultrasonic cavitation is applied directly to the silica alkoxide precursors for their prompt hydrolysis [11]. Furthermore, the deliberate chemical modification of the electrode surface with a suitable reagent results in the control of the rates and selectivities of electrochemical reactions at the solid/liquid interface [12,13]. One of popular approaches for the chemical modification is to use electroactive polymeric films onto the electrode surface [14–16]. Chitosan-modifed electrode has also been reported to be effective for the detection of phenolic compounds [17]. However, due to the real challenges of achieving successful analysis of clinical and environmental samples in the presence of common interferents, it is believed that the properties of the electrode, such as mechanical stability, physical rigidity, surface renewability, and selectivity, should be significantly improved before the electrode can become

* Corresponding author. Tel.: +1 937 775 2480; fax: +1 937 775 2717.
E-mail address: suzanne.lunsford@wright.edu (S.K. Lunsford).

0039-9140/$ – see front matter © 2007 Elsevier B.V. All rights reserved.
doi:10.1016/j.talanta.2007.03.002

competitive for full-scale applications in developing such sensors.

In this study, we have synthesized a sonogel carbon electrode modified with highly active nanostructured titanium dioxide (denoted as SGC/TiO_2) as a new class of sensors. The synthesis of nanostructured TiO_2 is of great interest because of its attractive optical, electrical, chemical, and catalytic properties [18,19]. Fabrication of well-defined nanostructured TiO_2 or other inorganic oxides has been achieved *via* sol–gel methods employing self-assembly of surfactant molecules as pore templates in the inorganic networks with high surface area [20–22]. Surfactants added in the TiO_2 sol can self-assemble into micelles, which can incorporate the titanium alkoxide around the micellar corona, forming surfactant organic core/TiO_2 inorganic shell composites. After heat treatment to remove the surfactant templates, the final TiO_2 has continuous phase porous inorganic network and tunable pore size similar to the micellar size. Applying such a nanotechnological approach, we can fabricate TiO_2 material with tailor-designed porous structure, which can enhance adsorption of molecules of interest at the TiO_2 surface. The nanostructured TiO_2 shows high adsorption capacity and catalytic activity toward organic molecules [20].

In addition to new nanotechnological and new materials chemistry procedures for the synthesis of SGC/TiO_2 electrode, this paper investigates the detection of catechol in the presence of ascorbic acid, a common interferent, with the SGC/TiO_2 electrode using cyclic voltammetry (CV), where the oxidation peaks for catechol and ascorbic acid are too close to allow their resolution [23,24]. A possible rationale for the stable catechol detection of SGC/TiO_2 electrode and the role of TiO_2 in facilitating adsorption of catechol and thus in accelerating charge transfer between catechol and SGC electrode are discussed. The SGC/TiO_2 electrode developed here meets the profitable features of electrode including the quantitative and qualitative detection of catechol, mechanical stability, physical rigidity, and enhanced catalytic properties.

2. Experimental

2.1. Sonogel carbon electrode

For the fabrication of sonogel carbon (SGC) electrode, 1.5 ml of methyltrimethoxysilane (MTMOS, Fluka) was added into 0.3 ml of 0.2 M HCl solution [11]. This mixture was sonicated in an ultrasonicator (2510R-DH, Bransonic) for 15 s. Then, 3 g of graphite carbon powder (Alfa Aesar, 99.999%) was added into the MTMOS solution and mixed thoroughly for 10 min, where the total volume of the reactants was significantly reduced up to 20%, condensing the SGC. A 0.25 mm copper wire (Alfa Aesar) was installed inside 0.69 mm I.D. capillary glass tube (Sutter Instrument) used as the bodies of the SGC electrode. The glass tube was filled with the SGC, and dried at 40 °C for 24 h. Finally, the tip of the SGC electrode was polished with a fine sand paper, followed by wiped with a soft tissue. Adherence between copper wire and SGC was stable at more than 180 g cm^{-1} of tensile strength.

2.2. Modification with nanostructured TiO_2

The TiO_2 was synthesized *via* sol–gel method. In order to control the structural properties of TiO_2 at the nano-level, the approach introduced in this study involved the use of a surfactant for the precise orchestration of the titanium precursor in the sol and the synthesis of the final TiO_2 material with high porosity [20–22]. Polyoxyethylenesorbitan monooleate (Tween 80, Aldrich) surfactant was selected as a pore directing agent in TiO_2 sol [20]. A suitable amount of Tween 80 was homogeneously dissolved in isopropanol (iPrOH, Fisher). Acetic acid (Fisher) was added into the solution for the esterification reaction with iPrOH to generate water [25]. When adding titanium tetraisopropoxide (TTIP, Aldrich) as TiO_2 precursor into the solution, hydrolysis and condensation reactions of TTIP occurred, forming a stable TiO_2 sol. The molar ratio of the ingredients was optimized at Tween 80:iPrOH:acetic acid:TTIP = 1:45:6:1.

The tip of SGC electrode was dipped into the TiO_2 sol for 3 s and taken out. After coating, the SGC/TiO_2 electrode was dried at room temperature for 1 h and calcined in a multisegment programmable furnace (Paragon HT-22-D, Thermcraft) to remove the surfactant templates and obtain a desirable crystal phase of TiO_2. The temperature was increased at a ramp rate of 3 °C min^{-1} to 500 °C, maintained at this temperature for 20 min, and cooled down naturally. Due to the difficulty to directly characterize the properties of TiO_2 materials on the SGC electrode, easy-to-remove TiO_2 coating was prepared on borosilicate glass (Micro slide, Gold Seal), assuming that if the substrate changes, the porous structure and crystal phase of TiO_2 reported here are similar since those properties originate from the surfactant addition and heat treatment rather than the substrate properties [26]. For comparison, control SGC electrode without TiO_2 was synthesized and SGC electrode modified with conducting polymer, poly(3-methylthiophene) (denoted as P3MT) was also fabricated, based on the method described elsewhere [1,27].

2.3. Characterization of SGC/TiO_2

In order to determine the crystallographic structure of TiO_2, X-ray diffraction (XRD) analysis using a Kristalloflex D500 diffractometer (Siemens) with Cu Kα (λ = 1.5406 Å) radiation was employed. A porosimetry analyzer (Tristar 3000, Micromeritics) was used to determine structural characteristics of TiO_2 including Brunauer, Emmett, and Teller (BET) specific surface area, porosity, and pore size distribution in the mesoporous range, using nitrogen adsorption and desorption isotherms. The structure of TiO_2 materials at the nano-level was visualized using a JEM-2010F (JEOL) high resolution-transmission electron microscope (HR-TEM) with a field emission gun at 200 kV. The TiO_2 sample scratched from the easy-to-remove TiO_2 coating on glass substrate was dispersed in methanol and fixed on a carbon-coated copper grid (LC200-Cu, Electron Microscopy Sciences). An environmental scanning electron microscope (ESEM, Philips XL 30 ESEM-FEG) was used to investigate the electrode surface at the micro-level. An elemental composition analysis of TiO_2 was per-

formed using an energy dispersive X-ray spectroscope (EDAX, Oxford Isis) connected to the HR-TEM and ESEM.

2.4. Detection of catechol

Electrochemical measurement of catechol was carried out with an Electrochemical Workstation (Epsilon, Bioanalytical Systems), based on CV employing three electrodes: Pt auxiliary electrode (Bioanalytical Systems), Ag/AgCl reference electrode (Bioanalytical Systems), and SGC/TiO_2 working electrode developed here. Catechol of 5 mM solution ($C_6H_4(OH)_2$, Fluka) as a target compound to detect and ascorbic acid of 5 mM solution ($C_6H_8O_6$, Aldrich) as an interferent compound to resolve were prepared in 10 mM sulfuric acid (Aldrich) at pH 1.7 with deionized water. The scan rate of CV was 100 mV s^{-1}. In order to investigate the relation between current in CV and catechol concentration, catechol concentration was varied from 0.1 to 1.0 mM. The chemical bondings between TiO_2 and catechol during the experiment were monitored using Fourier transform infrared spectroscope (FTIR, Perkin-Elmer 1610). In comparison to the conditions above, (i) 1 mM dopamine ($C_8H_{11}NO_2HCL$, Aldrich), another neurotransmitter in 0.1 M phosphate buffer with 0.1 M NaCl at pH 7.4, and (ii) 10 mM catechol and 10 mM acetaminophen ($CH_3CONHC_6H_4OH$, Aldrich), another common interferent in 0.1 M phosphate buffer and 0.1 M NaCl solution at pH 7.4 were tested.

3. Results and discussion

3.1. Catechol detection in the presence of ascorbic acid

Cyclic voltammograms shown in Fig. 1(a) illustrate the selectivity principle in the electrochemical detection of catechol in the presence of ascorbic acid, a common interferent. Ascorbic acid exhibits irreversible behavior while catechol does reversible behavior. The oxidation peaks of catechol at (i) E_{pa} = 518 mV (anodic potential) and ascorbic acid at (iii) E_{pa} = 246 mV are exceptionally resolved and the reduction peak of catechol at (ii) E_{pc} = 445 mV (cathodic potential) is detected with the SGC/TiO_2 electrode. However, the bare SGC electrode does not respond to the presence of catechol and ascorbic acid, making flat line at current of around zero. These results imply the presence of TiO_2 onto SGC electrode surface is crucial to detect catechol electrochemically. Another neurotransmitter, dopamine at a neutral pH 7.4 was also detected with the SGC/TiO_2 electrode, as shown in Fig. 1(b). Detection of neurotransmitters can be inhibited by the presence of common inteferents such as acetaminophen and ascorbic acid since they are also oxidized at around the same potential as the target compound catechol. However, with the SGC/TiO_2 electrode, catechol and acetaminophen at pH 7.4 were simultaneously detected at different positions, as demonstrated in Fig. 1(c).

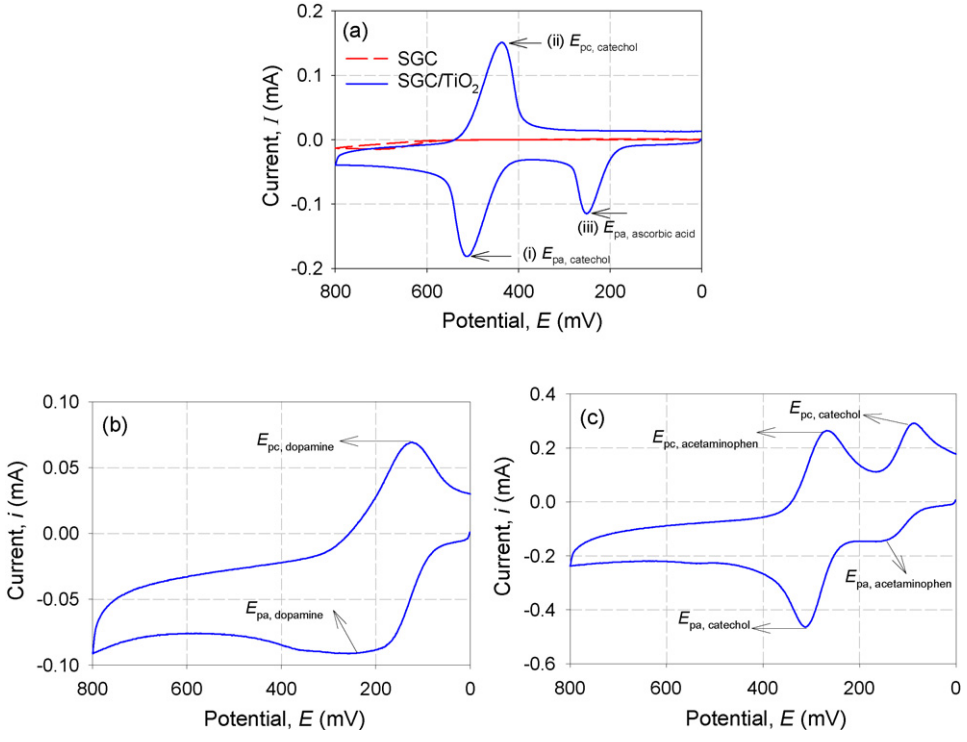

Fig. 1. Cyclic voltammograms of (a) 5 mM catechol and 5 mM ascorbic acid in 10 mM sulfuric acid (pH 1.7); (b) 1 mM dopamine in 0.1 M phosphate buffer + 0.1 M NaCl (pH 7.4); and (c) 10 mM catechol and 10 mM acetaminophen in 0.1 M phosphate buffer + 0.1 M NaCl solution (pH = 7.4). Red line in the middle is for bare sonogel carbon electrode (SGC) and blue line in the outer is for titanium dioxide-modified sonogel carbon electrode (SGC/TiO_2) developed in this study. (For interpretation of the references to colour in this figure legend, the reader is referred to the web version of the article.)

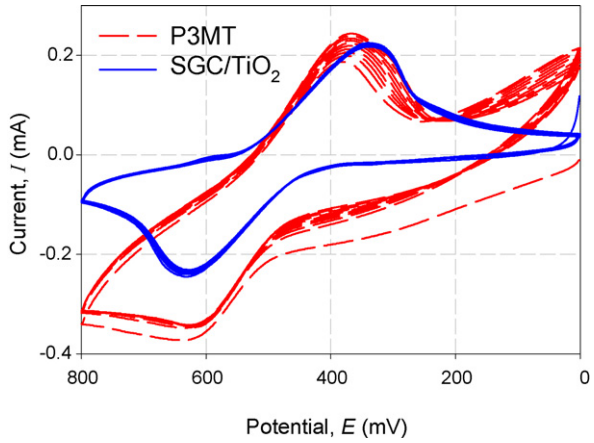

Fig. 2. Cyclic voltammograms of 5 mM catechol in 10 mM sulfuric acid during 25 scans. Red line is for P3MT electrode and blue line is for SGC/TiO_2 electrode. (For interpretation of the references to colour in this figure legend, the reader is referred to the web version of the article.)

3.2. Comparison with conducting polymer-modified carbon electrode

Typically, conducting polymers such as P3MT are an alternative to the detection of catechol in the presence of common interferents [1,27]. The P3MT electrode improves the reversibility of catechol oxidation and thus detects catechol and ascorbic acid simultaneously. However the problem with the P3MT electrode, like other modified electrodes, is poor reproducibility, mechanical instability, and electrode fouling. CV signal stability of the SGC/TiO_2 electrode is compared with that of the P3MT electrode during over 25 scans to detect catechol, as shown in Fig. 2. CV signal for the P3MT electrode started to be more and more diverged from the initial, which indicates P3MT conducting polymer comes off from the electrode surface and thus the CV signal is unstable. On the other hand, the SGC/TiO_2 shows good stability and reproducibility for the detection of catechol. In addition, the SGC/TiO_2 electrode has a more positive potential shift to detect catechol in CV *via* oxidation, allowing better resolution for the ascorbic acid peak and thus simultaneous analysis without prior separation of ascorbic acid.

3.3. Properties of SGC/TiO_2 electrodes

The SGC/TiO_2 electrode exhibits so far improved electrocatalysis and selectivity towards catechol compared to the neat SGC and P3MT modified electrodes, indicating that the TiO_2 in the electrode played a crucial role in detecting catechol electrochemically. In order to investigate what properties of TiO_2 affected the stable detection of catechol, various materials characterization techniques are introduced to the SGC/TiO_2 electrode. Fig. 3 shows ESEM images of the surface of the SGC/TiO_2 electrode. The tip of the electrode was packed well with condensed graphite powder due to the chemical bonding of carbon in the graphite and silicon in MTMOS. Fig. 3(b) shows the smooth surface of the SGC electrode incorporated with nanostructured TiO_2. There were no serious micro-cracks and defect structures. Even though it was difficult to identify

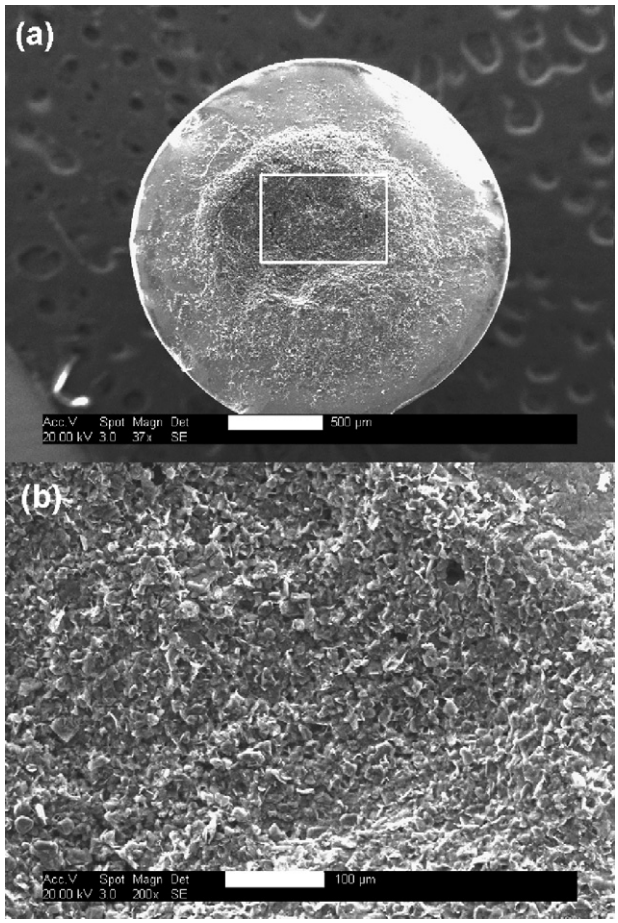

Fig. 3. (a) ESEM images of SGC/TiO_2 electrode: (a) the tip (scale bar = 500 μm) and (b) the surface of area highlighted in (a) (scale bar = 100 μm).

TiO_2 inorganic spots in the ESEM images as expected, it is believed that TiO_2 is uniformly coated and distributed on the graphite powders present at the tip of the SGC electrode since EDX analysis at various spots showed a relatively similar elemental composition for Ti. The representative EDX elemental composition at the tip of the SGC/TiO_2 electrode is shown in Fig. 4. Carbon, silicon, titanium, and oxygen were identified as major elements, and their sources were obviously graphite powder, MTMOS, TTIP, and oxides and surface hydroxyl groups, respectively.

XRD analysis showed that the TiO_2 heat-treated at 500 °C is active anatase crystal phase with crystallite size of approximately 9 nm. It should be noted that the nanosize TiO_2 particles exhibit good mechanical stability on substrate and resistance to abrasion [28]. In order to investigate structural properties of TiO_2, collected powder from the easy-to-remove TiO_2 on glass substrate was analyzed using HR-TEM and porosimetry analyzer. Fig. 5 shows the morphology of the nanostructured TiO_2. The TiO_2 was highly porous and a distinct pore structure was observed with average diameter of 5 nm. The synthesized films had bicontinuous structure with highly interconnected network, indicating the surfactant template used in this synthesis method effectively acted as a pore directing agent [26,29]. The mesoporous structure is important for the accessibility of the

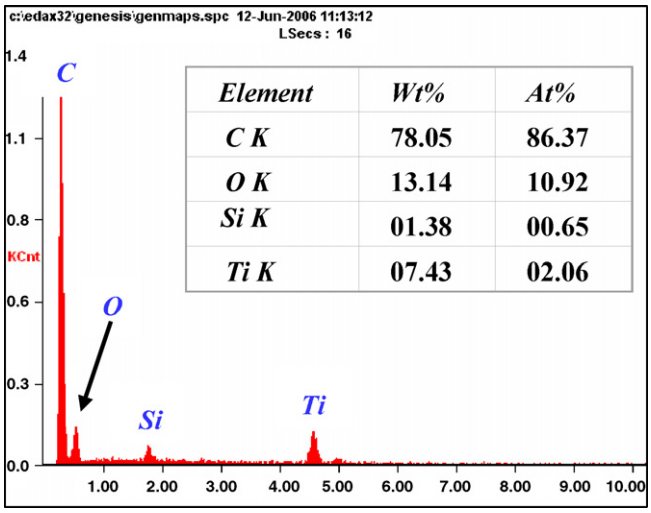

Fig. 4. Elemental analysis of SGC/TiO_2 electrode using EDX connected to ESEM.

reactants to or from the active sites in TiO_2 [20]. Nitrogen adsorption–desorption isotherms were typical IV type, characteristic of well-developed mesoporous materials. The pore size distribution was significantly narrow, ranging from 2 to 8 nm. The BET surface and porosity were significantly high at 140 $m^2\,g^{-1}$ and 45%, respectively. The porous structure was reported to exhibit high adsorption ability for the reactants and following enhanced chemical reaction [20].

3.4. Detection route and mechanisms

A possible rationale for the stable catechol detection of SGC/TiO_2 electrode is attributed most likely to the adsorption of catechol onto highly porous TiO_2 and the formation of bonding

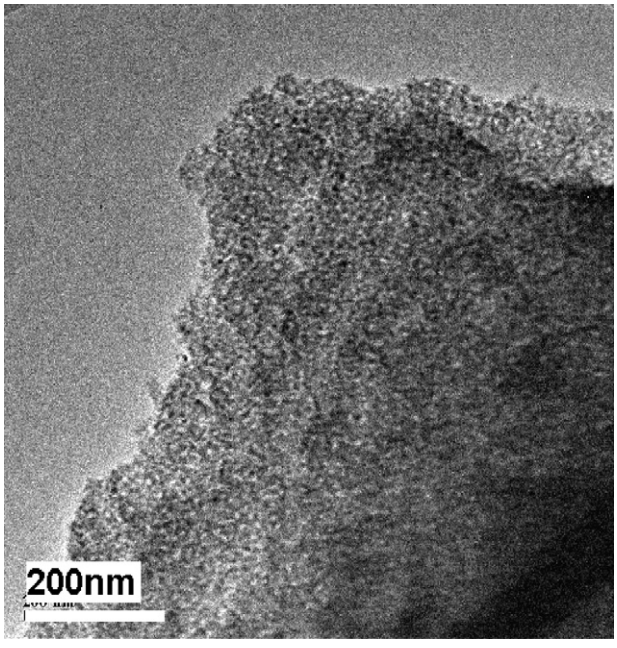

Fig. 5. HR-TEM image of TiO_2 with mesoporous structure, taken from TiO_2 particles scrapped from the SGC/TiO_2 electrode.

Table 1
Summarized IR results showing possible bondings between TiO_2 and catechol at pH 7.0[a]

Frequencies (cm^{-1})		Assignment
Catechol + TiO_2 [Ref. 30]	Catechol adsorbed on nanostructured TiO_2 in this study	
1068	1058	γC–H in plane
1486	1491	ν(–C–C–)
1450	1451	ν(–C=C–)
1263	1258	ν(C–O)
1215; 1105	1208; 1095	γ(C–H) in plane

[a] This test was performed with nanostructured titanium dioxide thin film immobilized on glass substrate. The titanium dioxide film was dipped into the catechol solution (pH = 7.0) and washed with super quality water several times.

between catechol and SGC/TiO_2 electrode [30–32]. The important IR peaks and their designation are summarized in Table 1 and compared with findings by Martin et al. [30]. The main bands and their assignment are as follows: 1491 cm^{-1}, stretching (C–C); 1451 cm^{-1}, stretching (C=C); 1258 cm^{-1}, stretching (C–O); 1208 and 1095 cm^{-1}, bending (C–H). The 1198 cm^{-1} –OH wag is absent for the doubly deprotonated species and the 1353 cm^{-1} in-plane –OH bending is not seen (only a weak and broad feature centered at 1208 cm^{-1} was seen). As a result, a possible mechanism for the efficient detection catechol on SGC/TiO_2 electrode is suggested in Scheme 1 [31]. The TiO_2 acts as an electron-transfer accelerator between SGC and catechol [32]. This nanostructured TiO_2 exhibits the electrocatalytic properties for the redox of catechol. Catechol absorbed onto TiO_2 rapidly reaches the SGC surface, then is oxidized, involving two electrons (e^-) and two protons (H^+). Similar observation on the enhanced adsorption of the electroactive species and acceleration of the proton transfer step was reported [33,34]. As a result, the surface of TiO_2 acts as a redox mediator for the electron transfer between the SGC electrode and catechol [35,36].

3.5. Calibration curve

For quantitative analysis of catechol at low concentration using the SGC/TiO_2 electrode, ΔI (difference in reduction cur-

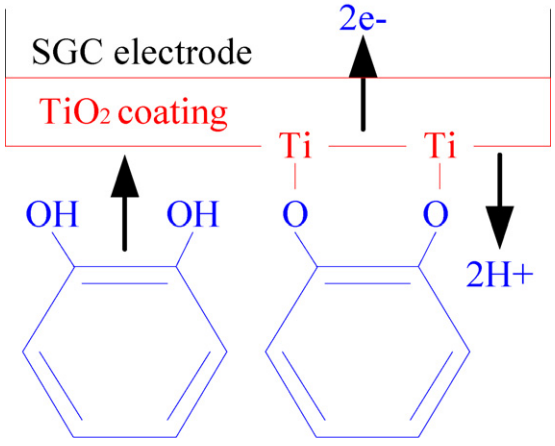

Scheme 1. Bonding and electron transfer in sonogel carbon electrode modified with titanium dioxide (SGC/TiO_2).

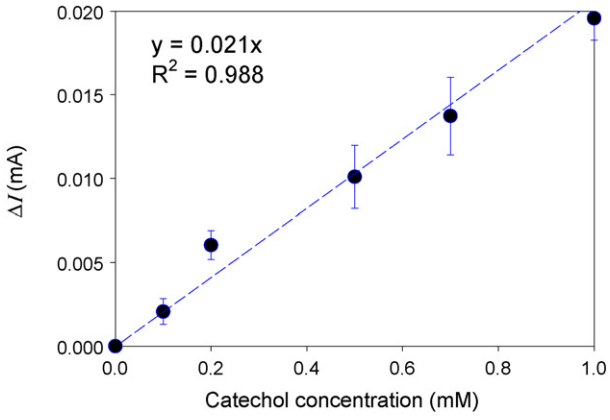

Fig. 6. Relation between current in cyclic voltammetry and catechol concentration. Error bars indicate the standard deviation of cyclic voltammetry result for three SGC/TiO_2 electrodes.

rent, I_{pc} and oxidation current, I_{pa} in unit of mA) in CV was monitored upon varying concentration of catechol ranging from 0 to 1.0 mM and presented in Eq. (1). As shown in Fig. 6, linear relation between ΔI and catechol concentration was observed with $R^2 = 0.988$. This result implies that the SGC/TiO_2 electrode can detect catechol both quantitatively and qualitatively.

$$\text{Catechol concentration(mM)} = 47.62 \times (I_{pc} - I_{pa}) \quad (1)$$

4. Conclusions

The deliberate chemical modification of carbon electrode surface with nanostructured TiO_2 made it possible to control the rates and selectivities of electrochemical reactions at the solid/liquid interface. The SGC/TiO_2 electrode detected catechol efficiently in the presence of ascorbic acid, a common interferent, using cyclic voltammetry. Due to the high surface area of porous TiO_2, catechol was easily adsorbed onto TiO_2 and formed a chemical bonding, $C_6H_4(OTi)_2$, where the surface of TiO_2 acted as an electron-transfer accelerator between the SGC electrode and catechol. The SGC/TiO_2 electrode developed here met the profitable features of electrode including quantitative and qualitative detection, mechanical stability, physical rigidity, and enhanced catalytic properties. We anticipate this new modified sonogel carbon electrode with nanostructured titanium dioxide could be used in several chemical sensor applications for environmental and biological molecules of interest.

Acknowledgements

The authors acknowledge financial support for this research by the Wright State University Research and Sponsored Programs and the National Science Foundation through a CAREER Award (BES-0448117) to D.D. Dionysiou and a REU Program to support Ms. Amber Yeary, a 2006 summer research fellow.

References

[1] H.B. Mark, N.F. Atta, Y.L. Ma, L.L. Petticrew, H. Zimmer, Y. Shi, S.K. Lunsford, J.F. Rubinson, A. Galal, Bioelectrochem. Bioenerg. 38 (1995) 229.
[2] N. Atta, I. Marawi, K. Pettricrew, H. Zimmer, H.B. Mark Jr., A. Galal, J. Electroanal. Chem. 408 (1996) 47.
[3] S. Alegret, Analyst 121 (1996) 1751.
[4] P. Ugo, M. Moretto, Electroanalysis 10 (1998) 1217.
[5] O. Lev, M. Tionsky, L. Rabinovich, V. Glezer, S. Sampath, I. Pankratov, J. Gun, Chem. Mater. 9 (1997) 2354.
[6] F. Tian, G. Zhu, Sens. Actuators B 86 (2002) 266.
[7] M. Ahkim, W.Y. Lee, Anal. Chim. Acta 479 (2003) 143.
[8] L. Rabinovich, O. Lev, Electroanalysis 13 (2001) 265.
[9] M.M. Collinson, A.R. Howells, Anal. Chem. 72 (2000) 702A.
[10] J. Wang, P.V.A. Pamidi, K.R. Rogers, Anal. Chem. 70 (1998) 1171.
[11] M. del Mar Cordero-Ro, J.L.H.-H. Cisneros, E. Blanco, I.I. Naranjo-Rodríguez, Anal. Chem. 74 (2002) 2423.
[12] R.F. Lane, A.T. Hubbard, J. Phys. Chem. 77 (1973) 1401.
[13] P.R. Moses, L. Wier, R.W. Murray, Anal. Chem. 47 (1975) 1882.
[14] L. Su, L. Mao, Talanta 70 (2006) 68.
[15] L.M. Zen, P.J. Chen, Anal. Chem. 69 (1997) 5087.
[16] J. Wang, S.P. Chen, M.S. Lin, J. Electroanal. Chem. 273 (1989) 231.
[17] A. Liu, I. Honma, H. Zhou, Biosens. Bioelectron. 21 (2005) 809.
[18] K. Yoo, H. Choi, D.D. Dionysiou, Chem. Comm. (2004) 2000.
[19] F. Caruso, Adv. Mater. 13 (2001) 11.
[20] H. Choi, E. Stathatos, D.D. Dionysiou, Thin Solid Films 510 (2006) 107.
[21] M. Antonelli, J.Y. Ying, Angew. Chem. Int. Ed. Engl. 34 (1995) 2014.
[22] H. Yoshitake, T. Sugihara, T. Tatsumi, Chem. Mater. 14 (2002) 1023.
[23] R.C.S. Luz, F.S. Damos, A.B. Oliveira, J. Beck, L.T. Kubota, Sens. Actuators B: Chem. 117 (2006) 274.
[24] R.M. Carvalho, C. Mello, L.T. Kubota, Anal. Chim. Acta 420 (2000) 109.
[25] C. Wang, Z.X. Deng, Y. Li, Inorg. Chem. 40 (2001) 5210.
[26] H. Choi, A.C. Sofranko, D.D. Dionysiou, Adv. Funct. Mater. 16 (2006) 1067.
[27] J.G. Redepenning, Anal. Chem. 6 (1987) 18.
[28] A. Mills, S.L. Hunte, J. Photochem. Photobiol. A 108 (1997) 1.
[29] F. Bosc, D. Edward, N. Keller, V. Keller, A. Ayral, Thin Solid Films 495 (2006) 272.
[30] S.T. Martin, J.M. Kesselman, D.S. Park, N.S. Lewis, M.R. Hoffmann, Environ. Sci. Technol. 30 (1996) 2535.
[31] S. Mu, Biosens. Bioelectron. 21 (2006) 1237.
[32] F.S. Damos, M.D.T. Sotomayor, L.T. Kubota, S.M.C.N. Tanaka, A.A. Tanaka, Analyst 128 (2003) 225.
[33] S. Dong, T. Kuwana, J. Electrochem. Soc. 6 (1994) 617.
[34] J. Wang, P. Pamidi, M. Jiang, Anal. Chem. Acta 360 (1998) 171.H.
[35] Razmi, M. Agazadeh, B. Habibi, J. Electroanal. Chem. 547 (2003) 25.
[36] H. Qi, C. Zhang, Electroanalysis 17 (2005) 832.

Available online at www.sciencedirect.com
ScienceDirect
Talanta 73 (2007) 121–126
Talanta
www.elsevier.com/locate/talanta

Factorial design for Fe, Cu, Zn, Se and Pb preconcentration optimization with APDC and analysis with a portable X-ray fluorescence system

F.L. Melquiades [a,b,*], P.S. Parreira [b], M.J. Yabe [c], M.Z. Corazza [c], R. Funfas [c], C.R. Appoloni [b]

[a] *State University of Center-West, Department of Physics, P.O. Box 3010, 85015-430 Guarapuava, PR, Brazil*
[b] *State University of Londrina, Department of Physics, P.O. Box 6001, 86051-990 Londrina, PR, Brazil*
[c] *State University of Londrina, Department of Chemistry, PR, Brazil*

Received 30 November 2006; received in revised form 6 March 2007; accepted 7 March 2007
Available online 12 March 2007

Abstract

Preconcentration of heavy metals in water with ammonium pyrrolydine dithiocarbamate (APDC) is a common practice in analytical chemistry. A literature review on this topic showed that several authors use this precipitation agent, but in different preconcentration conditions, conducting to divergent results. The objective of this work is to use factorial design to optimize the factors involved in the preconcentration process of heavy metals using APDC. Five factors were studied: sample volume, solution pH, APDC concentration, APDC volume and stirring time. The assays were performed by energy dispersive X-ray fluorescence (EDXRF). The values for detection limits within 95% confidence level, in $\mu g\,L^{-1}$, were: Fe (6.0 ± 0.1), Cu (4.0 ± 0.1), Zn (2.0 ± 0.1), Se (4.0 ± 0.1) and Pb (5.0 ± 0.1). The value for quantification limit for the five elements was $20\,\mu g\,L^{-1}$, with 3% deviation. Multi-element standard solutions were prepared. Precipitation procedure was applied in the spiked solutions and the samples were filtered in cellulose ester membrane for quantification measurements. The optimum values obtained were 300 mL of sample solution, pH 4, 1 mL of 2% APDC and 10 min of stirring time. The concentration results obtained for the validation measurements were satisfactory for *in situ* survey employing a portable instrument.

Keywords: Water; Metal; Preconcentration; Ammonium pyrrolydine dithiocarbamate; Energy dispersive X-ray fluorescence

1. Introduction

One of the most dangerous kinds of pollution in aquatic systems is due to the dumping of heavy metals. Their increasing use in industries and other activities considered to be essential for modern human life has resulted in modifications in the natural geochemical cycle of these elements, generating several environmental problems [1].

Various techniques have been applied for the determination of trace heavy metals in aqueous samples. Among them, the most common are atomic absorption spectrometry (AAS), inductively coupled plasma mass spectrometry (ICP-MS), liquid chromatography (LC) and instrumental neutron activation analysis (INAA) [2,3]. The necessity of a nuclear reactor for INAA and the exhaustive sample preparation for AAS, ICP and LC, stimulate the interest towards energy dispersive X-ray fluorescence (EDXRF) in environmental investigations [4,5].

X-ray fluorescence (XRF) technique is indicated for inorganic chemical elements identification and quantification in different kinds of samples and for a wide range of atomic numbers and concentrations.

A current tendency is the development of new analytical techniques and methods capable of identifying and quantifying complex sample constituents such as those related to food and environmental problems, as well as giving fast analytical response and/or enabling *in situ* analysis [6]. When EDXRF is employed for in natural water analysis, the methodology does not have enough sensitivity to reach the concentration level required by regulatory agencies. For this reason, the majority of the water analysis methods require a preconcentration step [7]. These methods can reduce the matrix effect, improving detection limits and providing accurate results.

* Corresponding author at: State University of Center-West, Department of Physics, P.O. Box 3010, 85015-430 Guarapuava, PR, Brazil.
Tel.: +55 43 33714736; fax: +55 43 33714166.
E-mail address: fmelquiades@unicentro.br (F.L. Melquiades).

0039-9140/$ – see front matter © 2007 Elsevier B.V. All rights reserved.
doi:10.1016/j.talanta.2007.03.004

Various preconcentration methods were considered, namely, evaporation, ion-exchange resin columns, ion-collecting filters, precipitation with chelating agents and the use of passive monitors [8–12].

The intention of this work is to quantify the total amount of metal present in water using a portable EDXRF system, so the sample preparation must be as minimum as possible. Dissolved metals, normally found in trace level, are not retained by common filters. Therefore, preconcentration through direct precipitation with organic reagents and posterior membrane filtering is the most appropriate technique for this analysis system. In this case, the preconcentration of metals is achieved by the addition of a chelating agent to an aqueous sample and extraction of formed metal complexes into an organic phase [13].

In precipitation methods, carbamates are very popular and attractive reagents due to the low aqueous solubility of its chelating metals [9]. The most common reagents are NaDDTC, DDTC, APDC and PAN [10]. Ammonium pyrrolydine dithiocarbamate (APDC) is a non-specific chelating agent, which reacts with metallic ions forming a very stable complex with the majority of the transition metals [14]. Due to these properties and its good performance, APDC was chosen in this study as the best option for the objective of this work.

Basically, preconcentration with APDC consists of adding a quantity of APDC in a specific concentration to a liquid sample volume with corrected pH; after that, the solution is stirred for some time and, in the sequence, filtered in membrane filter with a vacuum pump.

Literature shows several works that deal with APDC as a precipitation agent, but with differences in the parameter values used in the preconcentration methodology, as shown in Table 1.

Although APDC has been used in many works as a metal co-precipitation agent, a multivariate analysis of the influence of the involved factors on each different procedure step was not found in any one. Two different works, Alvarez et al. [16] and Narin and Soylak [20], present a detailed study of the factor that influences APDC precipitation, but the results diverge and univariate analysis was applied.

The objective of this work is to accomplish a factorial design for the optimization of heavy metal preconcentration methodology with APDC chelating agent, aiming to obtain conclusive information about the factor conditions for APDC usage. At the same time, it also aims at evaluating the performance of a portable EDXRF system to analyze the samples.

Generally, studies that deal with the optimization of experimental variables are realized through procedures that evaluate the variable effect individually, which in general, impedes optimum true value establishment. The univariate optimization does not consider the interaction of variables [21]. In the last years, systems of multivariate optimization have demonstrated their use in several knowledge fields. The observation of the effects of the variables and the interactions between them are of great importance to understand the process that has been tested or monitored in an experiment [22].

2. Experimental

2.1. Factorial design

Factorial design is a simple and important statistic tool, but not very much explored in spectrometry. It is one of the multivariate methods capable of evaluating simultaneously a great number of variable effects, through a reduced number of experimental assays [23].

In this study, five factors were considered: pH, sample volume, APDC concentration, APDC solution volume and stirring time. It is necessary to vary the level of each factor to study its effect on the element concentration. For K factors, a two level complete design requires 2^K different assays. Three factorial designs were necessary for the optimization process, with the factors analyzed in two levels, as shown in Table 2.

The first test was a 2^5 factorial design which require 32 samples plus 32 blanks. It was opted for a fractional factorial design, $2^{(5-1)} = 2^4 = 16$ samples, plus 16 blanks, to reduce the preparing time and cost. The fractional factorial design is an option to obtain the desired information and involve all the factors with a smallest number of assays, corresponding to a fraction of the number of assays from a complete design.

Interactions among variables are evaluated by calculating the interaction effects [22]. An effect will be significant when its absolute value is bigger than the standard deviation of the effect, at 95% confidence level.

The effect interpreted with normal graphics is a technique that facilitates distinguishing the values that really correspond

Table 1
Abstract of APDC preconcentration methodologies in the literature

Reference	Sample volume (mL)	pH	APDC concentration	APDC volume (mL)	Stirring time (min)
[10]	100	4	1%	1	15
[14]	200	3	1%	4	20
[15]	200	3	1%	4	20
[16]	1000	3–7	1%	4–25	30
[17]	100	3	2%	1	20
[18]	200	4	1%	2	15
[19]	50	4	0.01 g	2	30
[20]	250	2	5 mg		10

Table 2
Factorial design sequence for optimization procedure determination

Design number	Factor number	Factor	Level (−)	Level (+)
Design 1	1	pH	3	5
	2	Sample volume	100 mL	200 mL
	3	APDC concentration	1%	2%
	4	APDC volume	1 mL	4 mL
	5	Stirring time	5 min	20 min
Design 2	1	pH	5	6
	2	Sample volume	200 mL	250 mL
	5	Stirring time	5 min	10 min
Design 3	1	pH	4	5
	2	Sample volume	300 mL	250 mL

to significant effects in the results of the planning. These graphics are based on cumulative probability where y-axis correspond to the standard normal distribution (Z). Therefore, points far away from the tendency do not belong to the population of the central region.

With the first result, a complete factorial design with the three more relevant factors (2^3 factorial = 8 samples + 8 blanks) was accomplished. After this analysis, another complete design with the two factors that influenced the result (2^2 factorial) the most was necessary.

An univariate design was performed using the established conditions for a pH curve construction of the preconcentration procedure to finalize the optimization process, seeking to establish the best pH for each element individually. This factor is highly important in the process.

2.2. Sample preparation

Multi-element solutions from stock mono-element solutions (Sigma Aldrich Inc.) were prepared. The multi-element solutions consisted of the following elements, with concentrations in mg L^{-1}: Mn (0.5), Fe (0.3), Cu (0.5), Zn (0.3), Se (0.3) and Pb (0.5). The dilution was in Milli-Q water.

For pH adjustment, HNO_3 and NaOH were used. The APDC solution (Sigma Aldrich Inc.) was freshly prepared. After the pH adjustment, the APDC solution was added to the sample, stirred for chelating and filtered with a vacuum pump in cellulose ester membranes with 0.45 μm pore size. According to Alvarez et al. [16] the pore diameter does not influence the procedure and likewise Narin and Soylak [20], quantitative results are better with cellulose nitrate or acetate membranes. The membranes were dried at room temperature for 24 h.

To obtain the calibration curves, mono-element membranes with concentrations from 0.01 to 2.0 mg L^{-1} of Mn, Fe, Cu, Zn, Se and Pb were prepared.

A standard reference material SRM1643e from NIST (National Institute of Standards and Technology) was analyzed for validation. It was prepared using 200 mL of the standard with 100 mL of Milli-Q water to obtain the optimized volume of 300 mL for preconcentration.

Also, three multi-element standard solutions with higher concentrations were analyzed for methodology certification: multi-element standard solution Sigma Aldrich 70002, multi-element standard solution Sigma Aldrich 70006 for analysis of drinking and sewage water and multi-element standard solution High Purity Inc.: drinking water primary standard (DWPS) and drinking water secondary standard (DWSS). They were prepared with the optimized preconcentration methodology.

2.3. Instrumentation

The EDXRF system was consisted of a Si-PIN X-ray detector (FWHM 221 eV for Mn 5.9 keV line, 25 μm Be window) (Amptek Inc.) [24], with standard electronics for data acquisition. In the detector, an Ag collimator of 3 mm diameter aperture was used. For excitation, a mini X-ray tube (Ag target, 4 W) (Moxtek Inc.) [25] with 50 μm thickness Ag filter was employed. The measurements were realized with the system operating at 28 kV and 10 μA, with acquisition time of 500 s. Two measurements of each filter in different positions were conducted.

2.4. Quantification procedure

The concentrations were determined by the fundamental parameter equation for thin films (Eq. (1)) [26]:

$$I_i = C_i S_i \tag{1}$$

where I_i is the net intensity of the characteristic X-ray (cps), C_i represents the concentration (μg L^{-1}), and S_i is the elementary sensitivity (cps mg^{-1} L) of the analyzed element.

Detection limits (DL) were obtained using Eq. (2) [27]:

$$\mathrm{DL} = \frac{3\sqrt{Bg_i}}{S_i t} \tag{2}$$

where Bg_i is the background counts for the element and t is the measurement time.

Quantification limits were also calculated according to Eq. (3) [27]:

$$\mathrm{DQ} = \frac{10\sqrt{Bg_i}}{S_i t} \tag{3}$$

3. Results and discussion

Calibration curves are presented in Fig. 1 and the values for detection limits within 95% confidence level, in μg L^{-1}, are as follows: Fe (6.0 ± 0.1), Cu (4.0 ± 0.1), Zn (2.0 ± 0.1), Se (4.0 ± 0.1) and Pb (5.0 ± 0.1). The value for quantification limit for the five elements is 20 μg L^{-1}, with 3% deviation.

Fig. 2 presents the normal graphics for $2^{(5-1)}$ factorial design, in which it can be noticed that the effects of factors 1 and 2 move away from the tendency. That indicates that the values should be higher than the ones tested. This is confirmed by analyzing the values starting from the ones in which the effects have a real meaning. The values for significant effect are in the lower right corner of each graphic of Fig. 2. This behavior was verified for all elements except Se, whose pH value must be reduced. From this analysis, the values of 1 mL APDC solution with 2% concentration were fixed, since these factors do not have a significant influence on the final results.

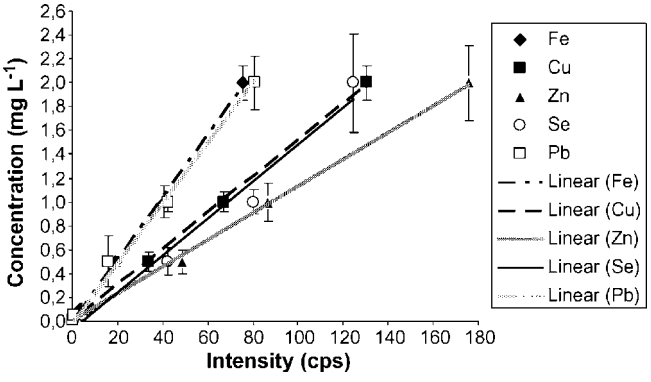

Fig. 1. Calibration curves obtained from the mono-element standards.

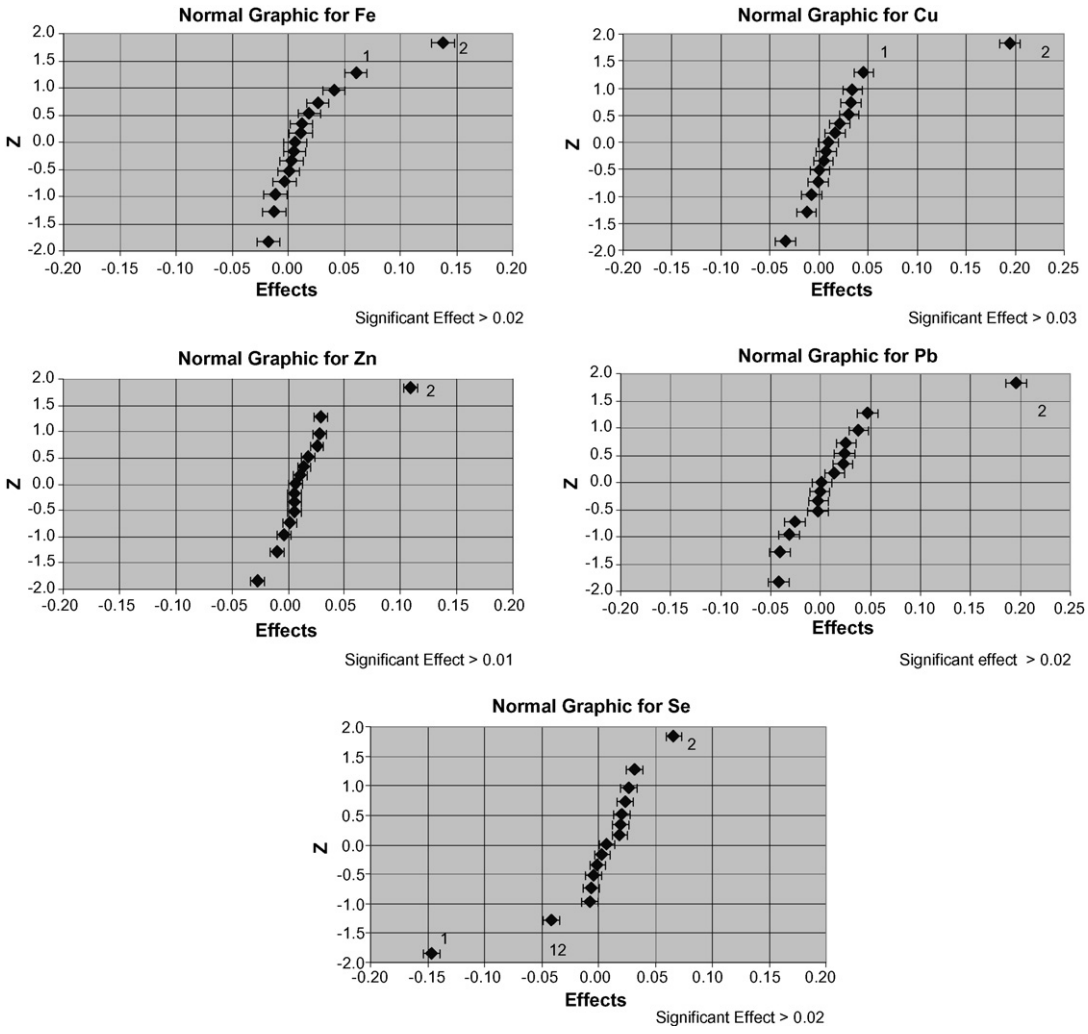

Fig. 2. Normal graphic with $2^{(5-1)}$ factorial design result.

For the 2^3 factorial design, the values for factors 1 and 2 were higher, as shown in Table 2. The results are in Fig. 3, where it can be seen that the same factors still influence the result. Here, factor 1 must be reduced and factor 2 increased. Again, the behavior for Se is different, hindering its determination in these conditions.

Table 3 shows the results for the 2^2 factorial design. It was chosen the L assay, in which the five elements were determined with 10% deviation. This assay corresponds to 300 mL sample volume at pH 4.

Fig. 4 shows the univariate design results, in which a pH curve was plotted for each studied element. In the individual analysis it was perceived that, for Fe and Cu, the best pH value was 5, for Zn and Se it was 4, and for Pb it was 3.

Concentrations for the interest elements in the SRM1643e are near the system quantification limits and some concentrations were not recovered. For Fe and Zn, the measured concentrations were 0.179 ± 0.012 and 0.028 ± 0.03, and the certified values were 0.065 ± 0.01 and 0.052 ± 0.01, in mg L^{-1}, respectively.

The measurement results for the three multi-element standards aiming at the methodology validation are listed in Table 4. In this case, standard deviation within 95% confidence was around 15%.

Table 3
Results of concentrations for the 2^2 factorial design (mg L^{-1})

	Factor		Fe (0.3)[a]	Cu (0.5)[a]	Zn (0.3)[a]	Se (0.3)[a]	Pb (0.5)[a]
Assay	pH	*V* (mL)					
I	5(+)	250(+)	0.32 ± 0.03	0.46 ± 0.01	0.27 ± 0.01	0.02 ± 0.01	0.47 ± 0.02
J	4(−)	250(+)	0.26 ± 0.01	0.41 ± 0.01	0.19 ± 0.01	0.27 ± 0.01	0.38 ± 0.01
K	5(+)	300(−)	0.25 ± 0.02	0.49 ± 0.01	0.24 ± 0.01	0.01 ± 0.01	0.44 ± 0.01
L	4(−)	300(−)	0.25 ± 0.01	0.46 ± 0.04	0.25 ± 0.02	0.32 ± 0.03	0.42 ± 0.05

[a] Concentration in the multi-element solution.

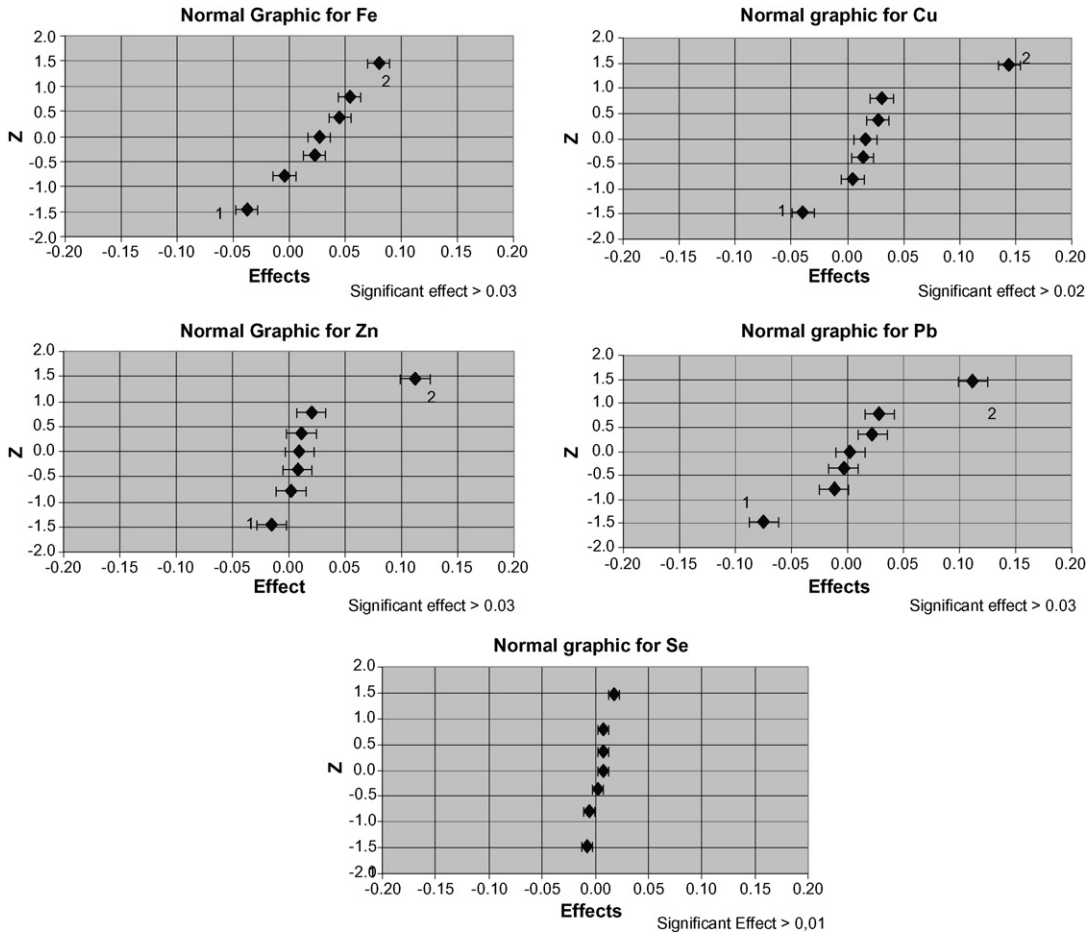

Fig. 3. Normal graphic with 2^3 factorial design result.

Table 4
Results of the multi-element standard solutions

Standard	Element	Membrane concentration	Measured membrane concentration
70002 Sigma Aldrich	Fe	0.09–0.12	0.07–0.09
	Cu	0.09–0.12	0.07–0.09
	Zn	0.09–0.12	0.11–0.13
	Pb	0.85–1.15	0.76–0.94
70006 Sigma Aldrich	Fe	0.78–1.06	0.73–0.85
	Cu	0.15–0.21	0.13–0.15
	Zn	0.78–1.06	0.52–0.60
	Se	0.78–1.06	0.48–0.56
	Pb	0.31–0.43	0.07–0.21
DWPS + DWSS	Fe	0.085–0.115	0.089–0.097
	Cu	0.425–0.575	0.041–0.046
	Zn	0.425–0.575	0.046–0.064
	Se	0.026–0.035	0.012–0.018
	Pb	0.026–0.35	0.061–0.067

Values at 95% confidence level, in mg L^{-1}.

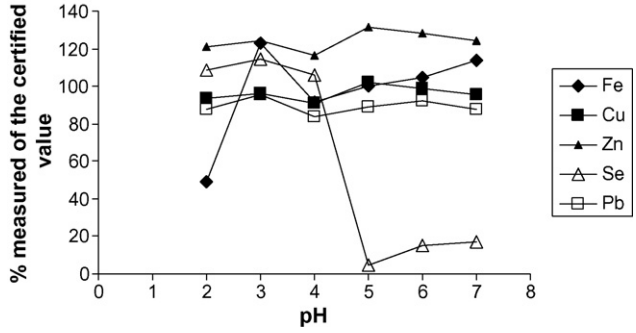

Fig. 4. pH curve from the univariate design.

However, these results are satisfactory for a portable instrument, in which a standard deviation around 30% is accepted [28].

4. Conclusions

Manganese was not measured with significance in the range of the levels from the tested factors, making it necessary to find another pH range or another chelating agent.

In spite of the stirring time, a significant influence on the results was not verified. The measurements with 10 min show that the concentration values were around the certified ones.

From the results of the three stages of factorial design and one univariate design, it was concluded that the best optimized situation for Fe, Cu, Zn, Se and Pb preconcentration in a multi-element sample, using APDC precipitation methodology, is the following: 300 mL sample volume at pH 4 and 1 mL APDC 2% solution with 10 min of stirring time.

The concentration results obtained are satisfactory for *in situ* measurements employing a portable instrument.

Using these optimized conditions for APDC preconcentration methodology and considering a wide range for standard deviation, a portable XRF equipment is very useful for *in situ* analysis of effluents and liquid environmental samples.

Acknowledgments

We are grateful to Fundação Araucária de Apoio ao Desenvolvimento Científico e Tecnológico do Paraná (009/2005-5402) and to the Conselho Nacional de Desenvolvimento Tecnológico, CNPq (470662/2004-2), for the financial support.

References

[1] A.C.M. Costa, M.J. Anjos, R.T. Lopes, C.A. Perez, C.R.F. Castro, X-ray Spectrom. 34 (2005) 183.
[2] P. Daorattanachai, F.F. Unob, A. Imyim, Talanta 67 (2005) 59.
[3] M. Balcerzak, Anal. Sci. 18 (2002) 737.
[4] V. Orescanin, L. Mikelic, V. Roje, S. Lulic, Anal. Chim. Acta 570 (2006) 277.
[5] X. Hou, B.T. Jones, Microchem. J. 6 (2000) 115.
[6] F.L. Melquiades, C.R. Appoloni, J. Radioanal. Nucl. Chem. 262 (2004) 533.
[7] I. Komjarova, R. Blust, Anal. Chem. Acta 576 (2006) 221.
[8] R. Van Grieken, K. Bresseleers, J. Smiths, B. Vanderborht, M. Vanderstappen, Adv. X-ray Anal. 19 (1976) 435.
[9] R. Van Grieken, Anal. Chim. Acta 143 (1982) 3.
[10] A.T. Ellis, D.E. Leyden, W. Wegscheider, B.R. Jablonski, W.B. Bodnar, Chim. Acta 142 (1982) 73.
[11] H. Kingston, P.A. Pella, Anal. Chem. 53 (1981) 223.
[12] M.E. Mccomb, H.D. Gesser, Talanta 49 (1999) 869.
[13] V. Camel, Spectrochim. Acta, Part B 58 (2003) 1177.
[14] M.J. Salvador, G.N. Lopes, V.F. Nascimento Filho, O.L.A.D. Zucchi, X-ray Spectrom. 31 (2002) 141.
[15] S.M. Simabuco, V.F. Nascimento Filho, G.R. Inácio, III Encontro Nacional de Aplicações Nucleares, 1995.
[16] A.M. Alvarez, J.R.E. Alvarez, R.P. Alvarez, J. Radioanal. Nucl. Chem. 245 (2000) 485.
[17] E. Almeida, V.F. Nascimento Filho, E.P.E. Valencia, R.M. Cunha, J. Radioanal. Nucl. Chem. 252 (2002) 541.
[18] N.A. Nkono, O.I. Asubiojo, J. Radioanal. Nucl. Chem. 227 (1998) 117.
[19] M. Necemer, P. Kump, Spectrochim. Acta B 54 (1999) 621.
[20] I. Narin, M. Soylak, Anal. Chim. Acta 493 (2003) 205.
[21] P. Peralta-Zamora, J.L. Morais, N. Nagata, Eng. Sanit. Ambient. 10 (2005) 106.
[22] B. Barros Neto, I.S. Scarmínio, R.E. Burns, Como fazer experimentos, 2nd ed., Editora da Unicamp, Campinas, SP, 2003.
[23] E.R. Pereira-Filho, R.J. Poppi, M.A.Z. Arruda, Quim. Nova 25 (2002) 246.
[24] Operating manual—XR-100CR x-ray detector system and PX2CR power supply/shaper, Amptek Inc., 1998.
[25] Operating Manual—Miniature Bullet X ray Tube, Moxtek Inc., 2003.
[26] E.P. Bertin, Principles and Practice of X-ray Spectrometric Analysis, Plenum Press, London, 1975, p. 1079.
[27] L.A. Currie, Anal. Chem. 40 (1968) 586.
[28] P. Kump, M. Nècemer, P. Rupnik, Development of the Quantification Procedures for *in situ* XRF Analysis, Report IAEA-TECDOC-1456, 2005.

Available online at www.sciencedirect.com
ScienceDirect
Talanta 73 (2007) 23–29
Talanta
www.elsevier.com/locate/talanta

Fidelity genotyping of point mutation by enhanced melting point difference using DNA ligase

Xiangxian Meng [a], Huimin Li [a], Kemin Wang [a,*], Weihong Tan [a], Jun Li [a], Qiuping Guo [a], Xiaohai Yang [a], Qiuhua Mo [b], Xiangmin Xu [b]

[a] *State Key Laboratory of Chemo/Biosensing and Chemometrics, Institute of Biological Technology, Biomedical Engineering Center, College of Chemistry and Chemical Engineering, Hunan University, Changsha 410082, PR China*
[b] *Department of Medical Genetics, Southern Medical University, Guangzhou 510515, PR China*

Received 19 October 2006; received in revised form 25 January 2007; accepted 26 January 2007
Available online 12 February 2007

Abstract

Melting curve analysis is a powerful tool for detecting single-base mutations that may be linked to genetic diseases. Current existing methods provide insignificant melting point difference for some point mutations with the risk of wrong genotyping results, causing great limitations to their applications in clinic diagnosis. Here, we have developed an enhanced melting point difference approach to genotype single-base mutations using DNA ligase. Ligase covalently joins an allele-specific discriminating probe and a signal probe flanked the mutation site to form a long duplex, resulting in an enhanced melting temperature. CD17 and Ivs-2-654 point mutations of β-globin gene in *thalassemia* disease were identified by using this approach, and the homozygotes and heterozygotes were scored accurately and conveniently. To the best of our knowledge, the use of ligase to improve the differences of melting temperature between various genotypes has not been reported. This method will provide a promising tool for clinical diagnosis of gene-mutant diseases.

Keywords: Fidelity; Genotyping; Melting curve analysis; DNA ligase; β-Globin gene

1. Introduction

Single nucleotide polymorphisms (SNPs) are the most abundant and simple form among many variations of the human genome and occur one every 100–300 bases [1,2]. Many genetic diseases are associated with single-base mutations of particular genes. Identification of these mutations has great applications in prevention, clinic genetic testing and molecular diagnosis of these diseases [3–7]. Up to now, there have been many approaches to identify and visualize point mutations. Conventional assay is usually performed by gel electrophoresis and autoradiography that are time-consuming and stringent [8,9]. In recent years, there have been efforts to develop methods for allele-specific discrimination. These methods can be broadly classified into two categories: enzyme-based methods and hybridization-based methods [10,11]. Typical examples of enzyme-based methods include specific primer extension [12], dye-labeled oligonucleotide ligation [13], solution-phase homogeneous assay [14] and ligase-mediated colorimetric method [15]. Typical examples of hybridization-based methods include dynamic allele-specific hybridization [16,17], molecular beacon assay [18], hybridization probe assay [19] and induced fluorescence resonance energy transfer (iFRET) [20]. Among these methods, hybridization-based melting analysis approaches have attracted increasing interest because of its simple procedures and low cost [21]. For example, Howell [16,20] and Jobs et al. [17] used an allele-specific probe and a standard heating step of probe/target duplex, resulting in melting temperature peaks directly related to genotypes. Gundry et al. [22] used labeled PCR primers and amplicon melting temperature to rapidly score polymorphisms in the HTR2A, β-globin and cystic fibrosis genes. Housni et al. [23] conveniently performed genotyping for the factor V Leiden and prothrombin 20210A mutations by melting curve analysis of single dual-labeled probes. These assays perfectly discriminated genotyping for investigative polymorphisms. However, these methods might

* Corresponding author. Tel.: +86 731 8821566; fax: +86 731 8821566.
E-mail address: kmwang@hnu.cn (K. Wang).

0039-9140/$ – see front matter © 2007 Published by Elsevier B.V.
doi:10.1016/j.talanta.2007.01.067

be difficult to discriminate these point mutations that exhibited insignificant melting temperature difference [15]. Boyd and Bruns [24] found that the discriminations of heterozygotes and homozygotes for UGT1A gene variant in gilbert syndrome were difficult because of their undistinguishable melting temperatures, which was possible to produce wrong genotyping results. So, it is very important to develop a new approach that can enhance melting point difference to genotype single-base mutations with high fidelity.

In this paper, we have proposed an enhanced melting point difference assay to detect point mutations using DNA ligase. An allele-specific discriminating probe and a signal probe flanked the mutation base are joined covalently by DNA ligase to form a long duplex with template, bringing to an enhanced melting temperature. Compared with two alternative melting analysis fluorescence methods, namely, the using SYBR Green I alone and the iFRET methods, this proposed method successfully provided more significant melting point difference between various genotypes. This method has also been validated with the genotyping of two common point mutations [CD17 (A → T) and Ivs-2-654 (C → T)] of β-globin gene in *thalassemia* disease, which is an inherited hemoglobin disorders characterized by reduced production of β-globin chain [25]. Owing to its simple procedures, easy interpretation and high fidelity, this method is expected to hold great promise in practical clinic diagnosis of gene-mutant diseases.

2. Experimental

2.1. Oligonucleotides and reagents

Oligonucleotides (Table 1) were synthesized by Takara Biotechnology Co., Ltd. (Dalian, China). N1 and N2 are 43-nt oligos, representing two alleles of the CD17 mutation in the β-globin gene; a 50/50 mixture of N1 and N2 symbolizes the heterozygous [16]. N3 and N5 are signal probes, labeled with 6-carboxy-X-rhodamine (ROX) at the 5′-end and terminate one base upstream from the mutant site. N4 and N6 are allele-specific discriminating probes, containing an allele base at the 5′-end and are 5′-phosphorylated. T4 DNA ligase, TakaRa Ex taq, 10 × Ex Taq buffer and dNTP mixture were purchased from Takara Biotechnology Co., Ltd. ATP and $MgCl_2$ were purchased from Amresco (Solon, OH). Acrylamide and *N*,*N*,*N*′,*N*′-tetramethylethylenediamine were purchased from Sigma Chemical Co. (St. Louis, MO). SYBR Green I was purchased from Shanghai ope technology development company, China. *N*′,*N*-methylene-bis-Acrylamide and urea were purchased from Bebco (Kansas, AZ). Deionized water was obtained through a Nanopure Infinity™ ultrapure water system (Barnstead/thermolyne Corp, Dubuque, IA) and had an electric resistance >18.3 MW.

2.2. Ligation reaction

Ligation reaction was performed in a total volume of 150 μL at 37 °C by incubating 100 nM template (N1/N2 or PCR-amplified product) with 100 nM signal probe and 115 nM discriminating probe in a basal solution (consisted of 1.2 U T4 DNA ligase, 0.1 M Tris–HCl (pH7.6), 10 mM $MgCl_2$, 10 mM DTT, 0.1 mM ATP, 2 mM spermidine and 1:10,000 dilution of SYBR Green I). The time of ligation reaction was 35 min. Then ligation solution was heated to inactivate DNA ligase at 85 °C for 5 min. The concentrations of signal probe and SYBR Green I were adjusted while their influences on detection signal were investigated.

2.3. Gel image

We used denaturing polyacrylamide gel electrophoresis to confirm the ligation reaction. To perform denaturing polyacrylamide gel electrophoresis, ligation mixtures similar to that mentioned above, but containing 500 nM N1/N2, 450 nM signal probe and discriminating probe, were prepared [27]. Five microlitre ligation solutions were removed separately from these mixtures before adding T4 DNA ligase, and after the ligation process had taken place for 35 min with the addition of ligase. The samples were then electrophoresed on 20% denaturing polyacrylamide gels with 7 M urea. After fixing and silver staining, gels were scanned using an ImageMaster VDS-CL (Amersham).

Table 1
Oligonucleotides

Name	Sequence(5′→3′)
Template (N1)	CTGCCGTTACTGCCCTGTGGGGCTAGGTGAAGAAGGATGAAGT
Template (N2)	CTGCCGTTACTGCCCTGTGGGGCAAGGTGAAGAAGGATGAAGT
Probe CD17 (N3)	ROX- AACTTCACCT
Probe CD17 (N4)	p-AGCCCCACAG
Probe Ivs-2-654 (N5)	ROX- AGTTGCTATT
Probe Ivs-2-654 (N6)	p-ACCTTAACCC
Probe (N7)	AACTTCACCTAGCCCCACAG
Probe (N8)	ROX-AACTTCACCTAGCCCCACAG

Templates and probes used in this paper were designed according to ref.[26] with some modifications. These designed sequences were used to detect CD17 (A → T) and Ivs-2-654 (C → T) point mutations of β-globin gene associated with *thalassemia* disease. The circled base in N1 indicates the mutant base. P in N4 and N6 represent 5′-phosphorylation. ROX is 6-carboxy-X-rhodamine. N3 and N5 probes have 2-base at 5′-end as extending arm to link ROX. N7 and N8 are probes for the using SYBR Green I alone and iFRET methods, respectively, which have the same bases as the ligation product of N3 and N4.

2.4. Fluorescence measurement and melting curve

The fluorescence measurements were carried out on a Fluorolog Tau-3 spectrofluorometer (Jobin Yvon, Inc., Edison, NJ, USA) equipped with thermostat accuracy to 0.1 °C. Slits for both the excitation and the emission were set at 5 nm. The emission spectra were obtained at 37 °C by exciting the samples at 491 nm and by scanning the emission from 500 to 700 nm in steps of 1 nm. The time scan was recorded with the addition of 1.2 U T4 DNA ligase. When the fluorescence intensity became steady, T4 DNA ligase was added into ligation solution and after stirring for ~4 s, the fluorescence intensity was recorded over time [27].

Plotting fluorescence versus temperature generated melting curves. The fluorescence of ligation solution was monitored by exciting at 491 nm and an emission of 605 nm was recorded, when the sample temperature rose at 1 °C interval with a holding time of 10 s/° from 7 to 85 °C. Plotting the derivative of fluorescence versus temperature revealed melting temperature peaks that were more convenient for allele discrimination. In this paper, we compared this method with the using SYBR Green I alone and the iFRET methods. For using SYBR Green I alone, fluorescence measurements were carried out at excitation at 491 nm and emission at 520 nm. For iFRET method, fluorescence measurements were carried out at excitation at 491 nm and emission at 605 nm similar to the proposed method.

2.5. Determination genotypes by reverse dot-blot assay and DNA extraction

Patients, who originated from guangzhou city, guangdong province in South China, had classic β-*thalassemia* trait. Their genotypes were investigated using a reverse dot-blot (RDB) method established in the laboratory of department of medical genetics, Southern Medical University, China [25]. Here, we chose two common point mutations [CD17 (A → T) and Ivs-2-654 (C → T)] of β-globin gene to investigate. Genomic DNAs were isolated from leucocytes in peripheral blood of normal subjects and patients with CD17 or Ivs-2-654 point mutation using standard DNA extraction method [28].

2.6. Preparation of PCR-amplified product

2.6.1. Symmetric PCR

The primers for PCR were designed according to the Oligo 5.0 software (Molecular Biology Insights). The PCR was performed on a GeneAmp™ PCR System 2700 (Applied Biosystems). The PCR reaction mixture (50 μL) was consisted of 0.5 U TakaRa Ex taq, 1 × Ex Taq buffer, 0.2 mM each dNTP, 0.5 μM of the positive primer and negative primer and 50 ng genomic DNA. A 55-bp fragment that included the CD17 mutation was amplified with the positive primer 5′-AGTCTGCCGTTACTGCCCTG-3′ and negative primer 5′-TCACCACCAACTTCATCC-3′. A 69-bp fragment that included the Ivs-2-654 mutation was amplified with the positive primer 5′-TCTAAAGAATAACAGTG-3′ and negative primer 5′-GCAGAAATATTTATATGC-3′. The conditions of PCR were the following: initial denaturation at 94 °C for 5 min, followed by 25 cycles of denaturation at 94 °C for 30 s, annealing at 57 °C (for CD17) or 50 °C (for Ivs-2-654) for 35 s and extension at 72 °C for 10 s, then a final extension at 72 °C for 1 min. To confirm the fidelity of the reaction, PCR products were electrophoresed on 20% polyacrylamide gels. Gels were scanned after ethidium bromide staining.

2.6.2. Asymmetric PCR

Two microlitre symmetric PCR products were subjected to the asymmetric PCR. Except for only 0.5 μM positive primer and 5 nM negative primer, the asymmetric PCR reaction mixture was the same as the symmetric PCR. The PCR reaction was performed on a GeneAmp™ PCR System 2700 with the following conditions: initial denaturation at 94 °C for 5 min, fol-

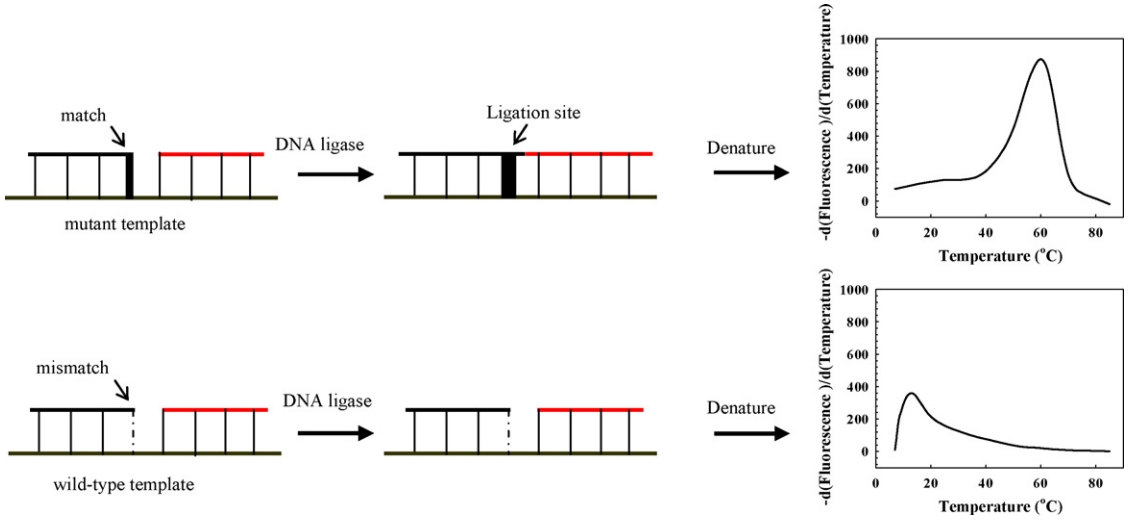

Fig. 1. Schematic representation of this assay. Allele-specific discriminating probe and signal probe flank the mutation site of the template. DNA ligase covalently joins the two adjacent probes to form a long duplex when perfectly matched to the template, resulting in a high melting temperature. Conversely, for the unligated probes, a low melting temperature is observed. According to ref. [20], detection signal of the method was provided by FRET.

lowed by 40 cycles of 94 °C for 30 s, annealing at 57 °C (for CD17) or 50 °C (for Ivs-2-654) for 30 s and extension at 72 °C for 10 s, then a final extension at 72 °C for 1 min. PCR products were detected and purified on 20% polyacrylamide gels [28]. They then were quantified by measuring the OD_{260} on DU-800 spectrofluorometer (Beckmann, Germany).

3. Results and discussion

3.1. Principle

The detection principle is illustrated in Fig. 1. This method uses a DNA ligase, a template, an allele-specific discriminating probe and a signal probe flanked the mutation site. A perfect match between the base at the 3′-end of the discriminating probe and the template allows the ligase to covalently join the two adjacent probes to form a long duplex, resulting in a high melting temperature, while a mismatch remains unaltered and produces a low melting temperature. In order to increase specificity and reduce the background [20], detection signal of this method was provided by FRET (SYBR Green I as donor and ROX affixed to signal probe as acceptor).

3.2. Assay refinement

3.2.1. Optimization of reagent concentration

Detection signal in this method was provided by FRET. In order to obtain sufficient FRET signal, the concentration of donor and acceptor had to be selected. As shown in Fig. 2, the FRET signal kept rise with the increase of the concentration of signal probe and achieved a higher signal when the concentration of signal probe was close to that of the template. The influence of SYBR Green I on detection signal was also studied and it was found that SYBR Green I at 1:10,000 dilutions had optimal detection signal (data not shown).

3.2.2. Ligation reaction

It is clear from Fig. 1 that the method is based on ligation reaction to enhance melting point difference between genotypes. The perfect ligation reaction is essential to ensure fidelity genotyping. Therefore, it is necessary to confirm appropriate ligation time. Fig. 3 (left) is real-time monitoring of ligation process, which is useful in determining the optimal ligation time. For a perfect match between the template and two adjacent probes (curve A), there was a rapid fluorescence rise after the addition of DNA ligase, with the slope of the curve decreasing gradually as time lapsed. The fluorescence intensity became steady at 33 min after adding DNA ligase. This indicated that the adjacent probes were joined by ligase to produce FRET signal and the ligation reaction accomplished in 33 min ligation time. For a mismatch

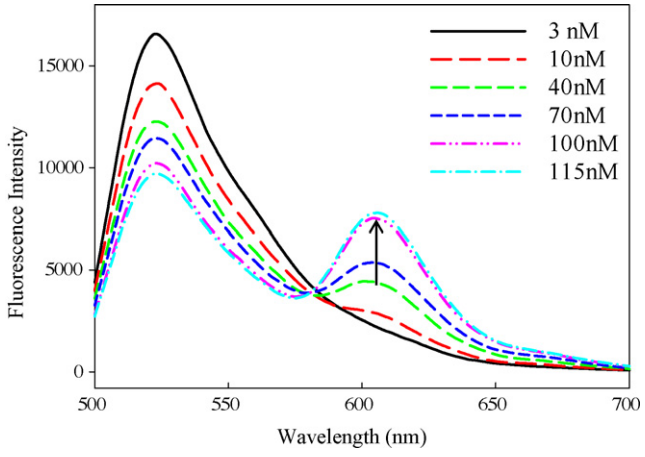

Fig. 2. The effect of the concentration of signal probe on the detection signal at 605 nm. The curves from bottom to top are obtained with different signal probe concentrations: 3 nM, 10 nM, 40 nM, 70 nM, 100 nM and 115 nM.

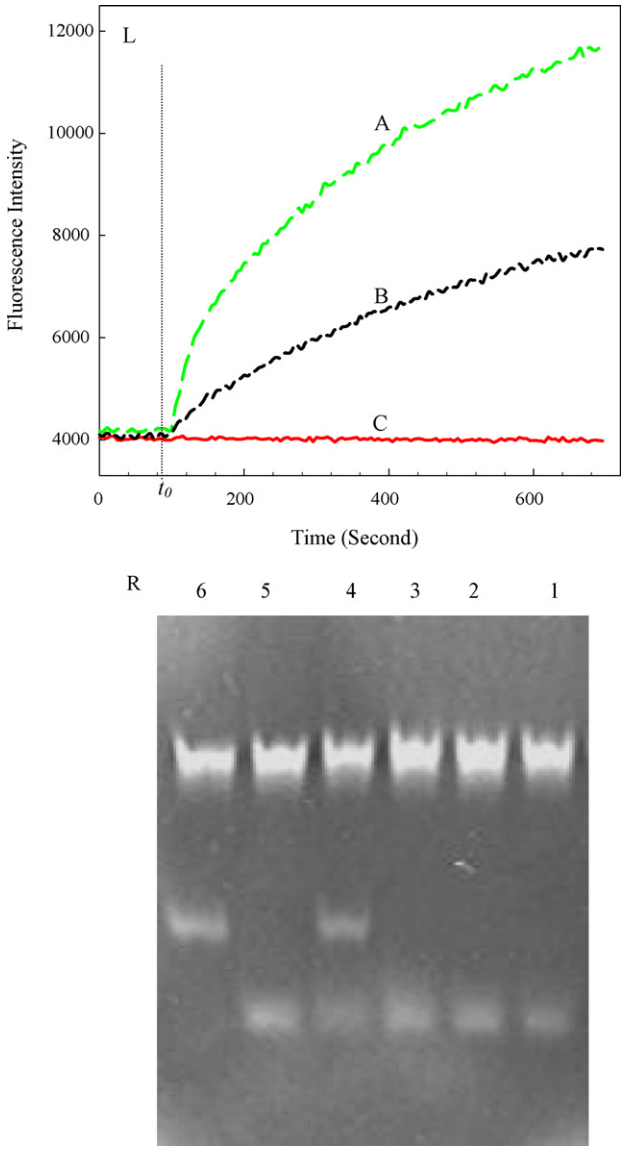

Fig. 3. Real-time scans of ligation reaction and corresponding gel electrophoresis. (Left) Curves A—C represent time scans of fluorescence intensity of matched template, heterozygous type and mismatched template, respectively. T4 DNA ligase is added into the reaction solution at time t_0. The fluorescence intensity A and B became steady at 33 and 19 min after adding DNA ligase, respectively. (Right) Gel electrophoresis image. Lanes 1 and 2 are for curve C; 3 and 4 for curve B; 5 and 6 for curve A. Lanes 1, 3, 5 represent samples C, B and A before the addition of T4 DNA ligase, while lanes 2, 4 and 6 represent corresponding samples obtained at 35 min after the addition of ligase.

between the template and two adjacent probes (curve C), the fluorescent intensity had no obvious change after adding the ligase. This showed that ligation did not occur, indicating high ligation specificity in the provided buffer. For the heterozygous (curve B), the fluorescence also had an obvious rise with the addition of ligase, but less than that of curve A. The fluorescence intensity became steady at 19 min after adding DNA ligase, indicating the completion of ligation reaction. In experiments, 35 min was chosen as the ligation time to ensure a sufficient ligation reaction.

3.2.3. Gel image

We carried out gel electrophoresis assay to obtain direct evidence to confirm the above ligation process. As shown in Fig. 3 (right), all the odd number lanes were for the samples before the ligation process started, and the even numbers represented the samples that had a 35 min ligation time. It is clear that obvious difference exists between these lanes (lane 3 versus 4, 5 versus 6), except for lane 1 versus 2. This is in agreement with the time scan results shown in Fig. 3 (left, lane 1 versus 2 for C, 3 versus 4 for B, 5 versus 6 for A). Moreover, there appeared a new band in lane 4 (lane 3 versus 4) that suggested the ligation product of two adjacent probes. In lane 6 (lane 5 versus 6), there emerged a new ligation product band similar to that of in lane 4, at the same time, the band of two adjacent probes was invisible. This suggested the two adjacent probes were efficiently joined to become ligation products.

3.3. Melting analysis of homozygous or heterozygous duplex

Fluorescence versus temperature data for the homozygous or heterozygous duplexes is presented in Fig. 4L. The derivative of the fluorescence versus temperature (Fig. 4R) is shown beside the primary fluorescence curves. Melting temperature peaks revealed in Fig. 4R are more convenient and direct for allele discrimination and genotype calling [16]. It was clear in Fig. 4R that a perfect match between template and two adjacent probes represented a single melting peak at high temperature (60 °C) and a mismatch represented a single melting peak at low temperature (15 °C). The heterozygote produced two well-separated peaks (15 and 58 °C, respectively). It is shown that value of the match peak was larger than that of the mismatch peak. The reason for this difference may be that the two adjacent probes are covalently joined to form a longer duplex with template in the matched. So more SYBR Green I molecules insert into the long DNA duplex, and more energy transferred from SYBR Green I to ROX results in stronger fluorescence.

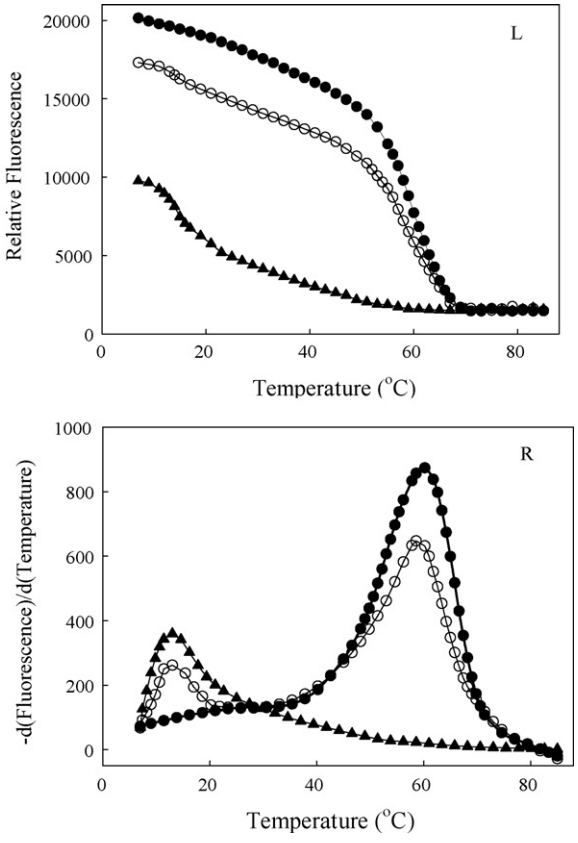

Fig. 4. Melting curves for matched duplex and single-base mismatched duplex. The graph L (left) depicts fluorescence versus temperature, and the graph R (right) is the derivative fluorescence versus temperature. Solid circles are corresponded to the matched duplex, hollow circles are corresponded to the heterozygous and solid triangles are corresponded to the mismatched duplex.

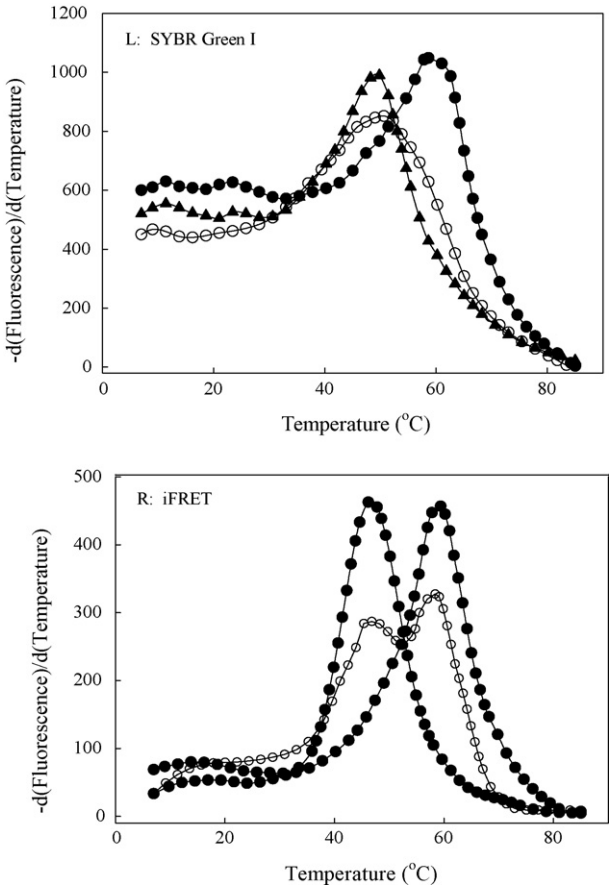

Fig. 5. Melting curves of using SYBR Green I alone (L) and iFRET (R) methods. Solid circles are corresponded to the matched duplex, hollow circles for the heterozygous and solid triangles for the mismatched duplex.

We compared this method to two alternative fluorescence SNP methods, namely, the using SYBR Green I alone and the iFRET method. Two probes (N7 and N8 in Table 1) were synthesized for the two methods, respectively. Reaction conditions of the three methods were kept the same except that the probes used were different and no ligase was used in the using SYBR Green I alone and the iFRET method. All three detection systems were more than sufficient to discriminate two homozygozes (Figs. 4R and 5). The melting temperature differences between match and mismatch duplexes are readily derived from the observed peak temperatures. The proposed method gave the largest difference, with a mismatch peak at 15 °C and a match peak at 60 °C, resulting in a 45 °C separation between match and mismatch peaks. Using SYBR Green I alone gave a mismatch peak at 50 °C and a match peak at 59 °C, resulting in a difference in melting temperature of 9 °C. For iFRET method, the values were 47 °C, 60 °C and 13 °C, respectively. The heterozygote type underwent two phases of denaturation, so theoretically it will produce two peaks in melting curve [16]. As shown in Fig. 4R, the proposed method provided two significantly separated peaks (15 °C and 58 °C) for the heterozygote, while the using SYBR Green I alone method provided only single peak (Fig. 5L). The small melting point difference for the using SYBR Green I alone method and iFRET method is probably due to single-base weak hybridization stability difference between the oligonucleotide probe and template, while the proposed method provides 10-base hybridization stability difference, and thus produces a big melting difference.

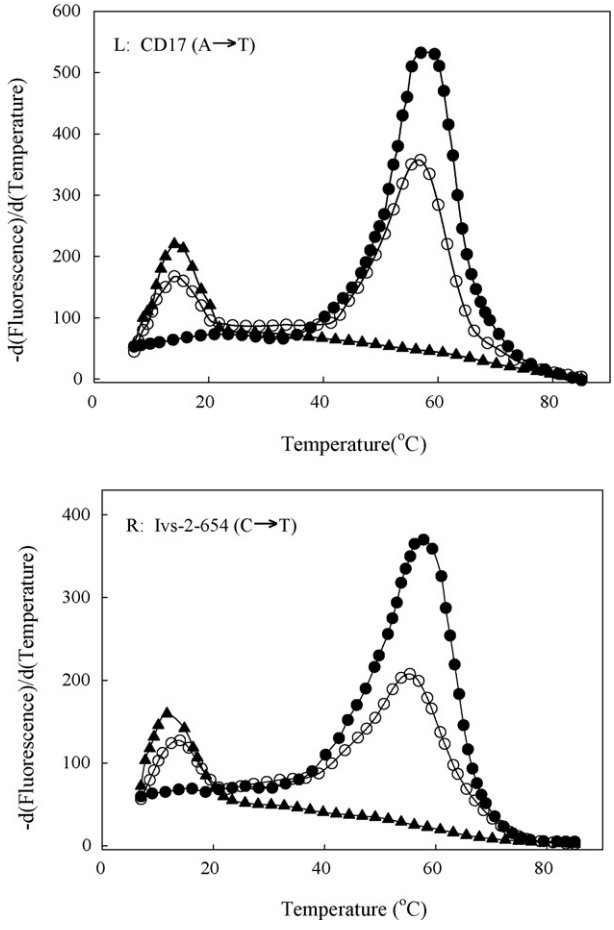

Fig. 6. Melting curve of CD17 and Ivs-2-654 point mutants of β-globin gene in *thalasseamia* disease. (L) represents CD17 (A → T) mutation and (R) represents Ivs-2-654 (C → T) mutation, respectively. Solid circles are corresponded to mutant homozygosity, hollow circles for the heterozygous and solid triangles for wild-type homozygosity.

3.4. Analysis of genetic DNA

In order to show the developed method was applicable to real samples, two common mutant sites [CD17 (A → T) and Ivs-2-654 (C → T)] of β-globin gene in *thalassemia* subjects were investigated. The PCR products of these genomic DNAs were detected under the aforementioned optimized conditions. PCR Primers were designed according to human β-globin gene (GenBank Version: M34058. GI: 183814). The gel electrophoresis image of the two PCR products confirmed the lengths of these two sequences are 55 bp for CD17 and 69 bp for Ivs-2-654 mutation, respectively. Analysis of these two point mutation samples using the developed method gave melting curves shown in Fig. 6. For CD17 mutant, it was clear in Fig. 6L that a single melting peak presented in both homozygous mutant (59 °C) and wild-type (15 °C). Heterozygoze presented two significantly separated peaks (15 °C, 57 °C, respectively), resulting in a difference of 42 °C in melting temperature. For Ivs-2-654 mutant, there had similar results as CD17 mutant (shown in Fig. 6R). By observing obvious melting point peaks, three genotypes were discriminated accurately and conveniently.

4. Conclusion

The method employs ligase to seal the nick of signal probe and discriminating probe, resulting in a long duplex and an enhanced melting temperature. It provides a significant melting point difference for detection point mutation accurately and conveniently. The method is easy to implement, avoiding complex steps such as stringent washing, separation and centrifugation after the discrimination is set up initially. Moreover, this assay is not restricted to a particular homogeneous format. It is possible to use it in high-throughput strategy by immobilizing many kinds of allele-specific discriminating probes on a chip to type many mutations at one time, which could bring even faster and cheaper genotyping possibilities in the relatively near future.

Acknowledgements

This work was supported by the National Key Basic Research Program (2002CB513110, 2004CB520804), Natural Science Foundation of China (20505007, 20305006, 20475015) and Key Project of International Technologies Collaboration Program of China (2003DF000039).

References

[1] N. Patil, A.J. Berno, D.A. Hinds, W.A. Barrett, J.M. Doshi, C.R. Hacker, C.R. autzer, D.H. Lee, C. Marjoribanks, D.P. McDonough, Science 294 (2001) 1719.

[2] R. Sachidanandam, D. Weissman, S.C. Schmidt, J.M. Kakol, L.D. Stein, G. Marth, S. Sherry, J.C. Mullikin, B.J. Mortimore, D.L. Willey, Nature 409 (2001) 928.
[3] A.D. Roses, Nature 405 (2000) 857.
[4] A. Vrie, E.R. Flores, B. Miranda, H.M. Hsieh, C.T. Oostrom, J. Sage, T. Jacks, PNAS 99 (2002) 2948.
[5] Y. Michikawa, F. Mazzucchelli, N. Bresolin, G. Scarlato, G. Attardi, Science 286 (1999) 774.
[6] R.E. Davis, S. Miller, C. Herrnstadt, S.S. Ghosh, E. Fahy, L.A. Shinobu, D. Galasko, L.J. Thal, M.F. Beal, N. Howell, Proc. Natl. Acad. Sci. U.S.A. 94 (1997) 4526.
[7] M.B. Wabuyele, H. Farquar, W. Stryjewski, R.P. Hammer, S.A. Soper, Y.W. Cheng, F. Barany, J. Am. Chem. Soc. 125 (2003) 6937.
[8] A. Ganguly, D.J. Prockop, Electrophoresis 16 (1995) 1830.
[9] M. Orita, H. Iwahana, H. Kanazawa, K. Hayashi, T. Sekiya, Proc. Natl. Acad. Sci. U.S.A. 86 (1989) 2766.
[10] B.W. Kirk, M. Feinsod, R. Favis, R.M. Kliman, F. Barany, Nucleic Acids Res. 30 (2002) 3295.
[11] A.C. Syvanen, Nat. Rev. Genet. 2 (2001) 930.
[12] K. Takatsu, T. Yokomaku, S. Kurata, T. Kanagawa, Nucleic Acids Res. 32 (2004) e60.
[13] X. Chen, K.J. Livak, P.Y. Kwok, Genome Res. 8 (1998) 549.
[14] T.M. Hsu, X. Chen, S. Duan, R.D. Miller, P.Y. Kwok, Biotechniques 31 (2001) 560.
[15] J.S. Li, X. Chu, Y.L. Liu, J.H. Jiang, Z.M. He, Z.W. Zhang, G.L. Shen, Y.Q. Yu, Nucleic Acids Res. 33 (2005) e168.
[16] W.M. Howell, M. Jobs, U. Gyllensten, A.J. Brookes, Nat. Biotechnol. 17 (1999) 87.
[17] M. Jobs, W.M. Howell, L. Stroqvist, T. Mayr, A.J. Brookes, Genome Res. 13 (2003) 916.
[18] S. Tyagi, D.P. Bratu, F.R. Kramer, Nat. Biotechnol. 16 (1998) 49.
[19] E. Schutz, N. Ahsen, M. Oellerich, Clin. Chem. 46 (2000) 1728.
[20] W.M. Howell, M. Jobs, A.J. Brookes, Genome Res. 12 (2002) 1401.
[21] K. Takatsu, T. Yokomaku, S. Kurata, T. Kanagawa, Nucleic Acids Res. 32 (2004) e156.
[22] C.N. Gundry, J.G. Vandersteen, G.H. Reed, R.J. Pryor, J. Chen, C.T. Wittwer, Clin. Chem. 49 (2003) 396.
[23] H.E. Housni, P. Heimann, J. Parma, G. Vassart, Clin. Chem. 49 (2003) 1669.
[24] J.C. Boyd, D.E. Bruns, Clin. Chem. 47 (2001) 1331.
[25] Q.H. Mo, H. Zhu, L.Y. Li, X.M. Xu, Genet. Testing 8 (2004) 257.
[26] G. Wu, L. Hua, J. Zhu, Q.H. Mo, X.M. Xu, Br. J. Haematol. 122 (2003) 1.
[27] Z.W. Tang, K.M. Wang, W.H. Tan, J. Li, L.F. Liu, Q.P. Guo, X.X. Meng, C.B. Ma, S.S. Huang, Nucleic Acids Res. 31 (2003) e148.
[28] J. Sambrook, D.W. Russell, Molecular Cloning: A Laboratory Manual, third ed. (P.T. Huang, Trans.), Science Press, Beijing, 2002, pp. 426–429, 483–485.

Available online at www.sciencedirect.com
ScienceDirect
Talanta 73 (2007) 103–114
Talanta
www.elsevier.com/locate/talanta

Chromatographic methods applied in the monitoring of biodesulfurization processes – State of the art

Milagros Mezcua [a,*], Amadeo R. Fernández-Alba [b], Antonio Rodríguez [a], Karina Boltes [a], Pedro Leton [a], Eloy García-Calvo [a]

[a] *Department of Analytical Chemistry and Chemical Engineering, University of Alcala, Spain*
[b] *Pesticide Residue Research Group, University of Almería, 04120 Almería, Spain*

Received 1 November 2006; received in revised form 20 February 2007; accepted 7 March 2007
Available online 14 March 2007

Abstract

Analytical methodologies employed in biodesulfurization processes have been reviewed; attention is primarily focused on the use of analytical techniques in the identification of degradation products and on the monitoring of degradation processes in which microbial sulphur-specific transformations take place. This is the first review of analytical techniques applied to biodesulfurization processes. Methodologies based on gas chromatography (GC) are the most frequently employed, in tandem with various detectors, mainly with the mass spectrometry (MS) detector, and the flame ionization detector (FID). High performance liquid chromatography (HPLC) coupled with ultra violet (UV) detection has also been widely employed. Different sulphurated compounds are used as model in biodesulphurization processes, naphtothiophene (NTH), benzothiophene (BTH), alkilated BTH, dibenzothiophene (DBT), alkilated DBT and their transformation products has been reviewed. DBT is the most frequently employed.

Keywords: Biodesulfurization; Dibenzothiophene; GC–MS; GC–FID; HPLC–UV; Polycyclic aromatic sulfurated hydrocarbons (PASHs); Alkilated dibenzothiophenes

1. Introduction

Crude oil and its distillates contain significant amounts of low-molecular-mass organosulphur compounds such as alkyl- and cycloalkyl thiols, alkyl- and arylthioethers and aromatic heterocycles based on thiophene. This last group of polycyclic aromatic sulfurated hydrocarbons (PASHs) includes thiophene itself, benzothiophene, dibenzothiophene, and their alkylated derivatives. These compounds have been of concern for decades because they constitute a major class of ubiquitous environmental contaminants found in both air and sea areas [1–3]. In order to mitigate the consequences of this contamination, such as acid rain [4,5] and air pollution caused by sulphur dioxide released from the combustion of oils, more and more regulations on sulphur content in petroleum are being established. The current specification in Europe and USA calls for a maximum sulphur content of 50 ppm in gasoline and diesel oil by 2005, and this level will be reduced to below 10 ppm by the year 2010 [6]. The current industrial method used for the removal of sulphur from fuels is hydrodesulfurization (HDS), which requires high temperature and high pressure. HDS is costly energy-intensive for deep desulfurization. Furthemore, HDS is not effective for removing heterocyclic sulphur compounds such as DBT and DBT derivatives [7]. Biodesulfurization has attracted attention owing to its application to the desulfurization of petroleum due to its mild conditions, lower energy consumption and lower emission of CO_2. Thus biodesulfurization (BDS), which operates under room temperature and pressure conditions, is expected to be a complementary as well as promising alternative to HDS. BDS is a process which removes sulphur from fossil fuels using a series of enzyme-catalyzed reactions. It leads to the development of highly efficient reactions and environmentally friendly technologies. Numerous attempts have been made to develop BDS processes. A few strains which can desulfurize DBT and DBT derivatives have been isolated, such as *Rhodococcus erythropolis* IGTS8 [8], *Gordona* sp. CYKD1 [9] *Peanibacillus* sp. A11-2 [10] and *Rodococcus* sp. Strain P 32C1 [11], *Mycobacteium* sp. [12], and *Pseudomonas* sp.[13].

* Corresponding author. Tel.: +34 950015531; fax: +34 950015483.
E-mail address: mmezcua@ual.es (M. Mezcua).

0039-9140/$ – see front matter © 2007 Elsevier B.V. All rights reserved.
doi:10.1016/j.talanta.2007.03.011

The desulfurization activity of naturally occurring bacterial cultures is low in comparison to the requirements of a commercial process and genetic manipulation has been used to achieve higher desulfurization rates [14].

Due to the complexity of the system to studying, the biodesulfurization has been conducted preferably in model reactions media in presence or not of water-immiscible organic solvents. Until now, there have been few reports concerning the biodesulfurization of crude oil, hydrodesulfurization-treated diesel oil and gasoline [15–17]. These studies published in 2006 represent a great advance for industrial process implementation.

When a degradation process is performed, the use of analytical techniques to identify and quantify the degradation products is an aspect of interest. Subsequently, analytical techniques which give structural information of intermediates have special interest when a pathway is required. Different analytical techniques have been used with this aim when the degradation of organic compounds under different conditions has been studied. As examples, GC–MS, gas chromatography coupled to atomic emission detector (GC–AED) or liquid chromatography–time of flight–mass spectrometry (LC–ToF–MS) techniques have been used in the determination of transformation products of Imidacloprid (a pesticide), Methyl *tert*-butyl ether (and additive of gasoline) and Bisphenol A (an industrial chemical) in degradation processes such as advanced oxidation processes or sunlight photo-alteration [18–22].

When only monitoring of the process is required more simple analytical techniques can be used, such as, GC–FID, HPLC–UV.

In most cases the concentration of the transformation products in degradation processes is low, so, preconcentration techniques must be employed [18] in order to increase the analytical signal of the transformation products. Besides, sometimes the media in which the degradation is performed is not adequate for analysis under chromatographic techniques; so, a change in the solvent is required before gas or liquid chromatography analysis. All these sample treatments which need to be performed after the biodesulfurization processes will be reviewed in this paper.

When a biodesulfurization process is developed it is necessary to choose a model compound which will be degraded under controlled conditions, the parent compounds used traditionally in biodesulfurization studies will be reviewed in this paper and this revision will focus on the interesting that lies in selecting these compounds in biodesulfurization processes, the analytical techniques employed in the monitoring of the process and the problems concerning the identification of compounds.

Analytical techniques employed in the identification of degradation products in biodesulfurization processes will also be reviewed in the present paper. By using different analytical techniques two pathways for the DBT metabolism are now recognized, namely, the ring-destructive pathway, represented by the Kodama pathway and the sulphur-specific pathway, the know as 4S pathway [23–26]. This review will focus on degradation products of the 4S pathway.

2. Sample treatment

Preconcentration steps after a degradation process are a very important aspect when intermediate products have to be determined, since normally the concentration of unknowns is very low, the extraction procedure is typically optimized for the compounds that will be degradated and for some others which are expected to form if analytical standards are available [17,21,22], then, the application of the method is performed in order to detect all of the transformation products generated in the degradation process. Even when a preconcentration is not necessary, a change of the solvent is normally required, before injection in chromatographic system.

In a biodesulfurization process two phases are typically involved, a watery phase and an organic phase, normally the organic phase is a long chain hydrocarbon such as dodecane. These two phases should be separated and analysed in a different way; the organic phase can be directly analysed by GC or LC or can be extracted by solid phase extraction, and the watery phase can be directly analysed by LC or can be extracted by liquid-liquid extraction if GC analysis is required.

Solid phase extraction sorbents are normally chosen by the nature of their primary interaction or retention mechanisms with the analyte in question. In that case non polar or moderately polar compounds should be extracted from a non polar organic solvent. Sorbents like silica, animopropyl, cyanopropyl are specially indicated to extract compounds with functioanal groups such as hydroxyls, amines and heteroatoms (S, O, N) from non polar matrices.

In fact, the solid phase extraction methods used for the extraction of biodesulfurization compounds (pattern compounds or degradation products) developed by various authors, involve the use of silica packing for the separation and concentration of DBT, 2-HBP (2-hydroxy biphenyl), 2,2′-biphenilol and DBT-sulfone [27], alkylated dibenzothiophenes and its transformation products [24,28].

Different solvents have been used to perform liquid-liquid extraction, ethyl acetate [29–34,26], *n*-hexane [35] methylene chloride [36]. The culture broth is normally acidified before liquid-liquid extraction at pH 2 [26,34].

3. Model compounds used in biodesulfurization processes

3.1. Dibenzothiophene

It is well know that some polycyclic aromatic sulphur heterocycles (PASH) are more recalcitrante than aliphatic sulphur compounds in the catalytic hydrodesulfurization because the sulphur atom is embedded in an aromatic system and furthermore it can be shielded by alkyl groups.

Dibenzothiophene (DBT), is a polycyclic aromatic sulfurated hydrocarbon (see structure in Fig. 1a), which is a representative compound of organic sulphur compounds in fossil fuels. This compound has been the mostly used as a model compound in biodesulfurization processes [29,30,36–39].

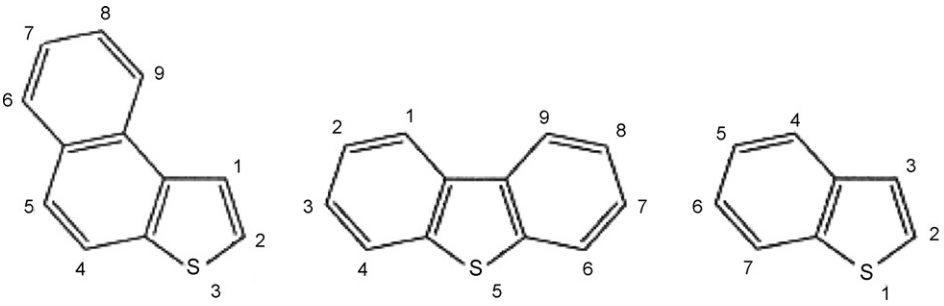

Fig. 1. Chemical structure of naphtho [2,1-*b*] thiophene, dibenzothiophene, and benzo [*b*] thiophene.

DBT concentration in biodesulfurization processes has been determined by different analytical techniques based on gas and liquid chromatography.

In gas chromatography, non polar cross-linked wall coated open tubular (WCOT) analytical columns, are normally employed. The composition of the stationary phases normally employed are 5% phenyl, 95% dimethylpolysiloxane (e.g. HP-5) or 100% dimethylpolysiloxane (e.g. DB-1), SE-54 and DB17 (see Tables 2–4).

An isotherm analysis is used by some authors, fixing the oven temperature at 250 °C [33,37,39,40]. A temperature program has been chosen by other authors [35,36,38].

Different detectors coupled to gas chromatography have been employed to determine DBT. Flame ion detection and mass spectrometry are the most commonly used. Flame photometric detector (FPD) is employed only in a few applications (see Tables 1–4).

Flame ion detection coupled to gas chromatography (GC–FID) has been used to detect and to quantify dibenzothiophene in biodesulfurization processes (see Table 4). This system of detection has a very low noise level. It has a linear response over a very wide range, its sensitivity is high and the optimized response varies very little with factors such as detector temperature, flow-rates of hydrogen and carrier gas or other parameters. FID works by burning carbon compounds which produce ions [41]. When a carbon compound is eluted from the GC column into the hydrogen flame of the detector, a current intensity will pass between electrodes placed near the flame and held at a suitable potential, thus producing a recordable signal. This technique does not provide structural information of analysed compounds; an analytical standard is always required in order to identify and quantify dibenzotiophene using this technique [30,31,35,37,38,40].

Mass selective detection coupled with gas chromatography (GC–MS) is widely used for the separation and determination of such volatile PASHs as DBTs [30,31,36–38]. This technique has been used to identify DBT in biodesulfurization processes, of all the ionization techniques for the production of ions for MS analysis, electron ionization (EI) is the most widely applied in the identification of dibenzotiophene. This ionization technique often produces both molecular and fragment ions. In EI, gas analyte molecules are bombarded by energetic electrons (typically 70 eV), which leads to the generation of a molecular radical ion (M^+) which can subsequently generate ionised fragments. This technique generally allows for the determination of both relative molecular mass and the structure of the molecule.

The mass spectrum of dibenzothiophene under electron impact ionization show as base peak the ion at *m*/*z* 184 corresponding with the molecular ion of dibenzothiophene, *m*/*z* 139 and *m*/*z* 152.

High resolution liquid chromatography coupled to UV detection has been used to determine the concentration of DBT during biodesulphurization processes (see Table 1). The analytical columns normally employed are filled with C18 as stationary phase. The composition of the mobile phases normally used is as follows, AcN:water [26,29,42–44], AcN:THF:water [29,42], MeOH:water [45,46], AcN:10 mM phosphate buffer (pH6) [36], the analysis typically have been performed in isocratic mode. The UV detection is carried out at a wavelength of 232 nm [36], 254 nm [29,42], 240 nm [43] and 280 nm [26,43,45,46].

3.2. Alkylated dibenzothiophenes

Although DBT is generally taken as the model compound of heterocyclic organosulphur present in diesel oil, alkylated DBTs represent a high proportion of these molecules. Crude oil contains a large number of molecules which contain sulphur; however, the major sulphur-containing molecules in the middle distillate fraction diesel fuel are alkilated dibenzothiophenes. Furthermore, a sterilally-hindered sulphur molecule such as 4,6-dimethyl DBT is quite representative of the compounds recalcitrant to HDS which should be removed to obtain ultra-low sulphur diesel oils.

Alkylated DBT compounds typically employed as a model in biodesulfurization processes are, 1-methyl DBT, 2-methyl DBT, 3-methyl DBT and 4-methyl DBT [30], 4,6-dimethyl DBT [30,36,37], 4,6-diethyl DBT [30,37], 4,6-dipropyl DBT [30,37,47], 4,6-dibutyl DBT [30,47] and 4,6-dipentyl DBT [47].

Analytical methods, based on gas and liquid chromatography, developed to analyse DBT and its transformation products have been applied to identify alkylated DBTs and its transformation products. When an alkylated DBT is chosen to

Table 1
Liquid chromatography–UV detection based method applied in the analysis parents compounds (in bold) in biodesulfurization processes and its degradation products

Compound	Column	Mobile phase	Detector/Ynm	Purpose	Reference
NTH	Puresil C18	AcN:Water (1:1) or AcN:THF:water (1:1:3)	UV (254 nm)	Quantification (standard calibration curves)	[29]
$NTHO_2$	Puresil C18	AcN:water (1:1) or AcN:THF:water (1:1:3)	UV (254 nm)	Quantification (standard calibration curves)	[29]
BTH	Puresil C18	AcN:water (1:1) or AcN:THF:water (1:1:3)	UV (254 nm)	Quantification (standard calibration curves)	[29]
3-Methyl BTH	Puresil C18	AcN:water (1:1) or AcN:THF:water (1:1:3)	UV (254 nm)	Quantification (standard calibration curves)	[29]
5-Methyl BTH	Puresil C18	AcN:water (1:1) or AcN:THF:water (1:1:3)	UV (254 nm)	Quantification (standard calibration curves)	[29]
DBT	Puresil C18	AcN:water (1:1) or AcN:THF:water (1:1:3)	UV (254 nm)		[29,42]
	Hipersil C18	AcN:10 mM phosphate buffer (pH6) (3:1)	UV (232 nm)	Quantification (standard calibration curves)	[36]
	Zorbax C18	MeOH:Water (9:1)	UV (280 nm)		[45]
	Cosmosil C18	AcN:Water (1:1)	UV (280 nm)		[26,34]
	Zorbax C18	MeOH:Water (9:1)	UV (280 nm)		[46]
	NOVA.PAK C18	AcN:Water (4:6)	UV (280 nm)		[43]
	Kromasil C8	AcN:Water (1:1)	UV (240 nm)		[44]
$DBTO_2$	Puresil C18	AcN:water (1:1) or AcN:THF:water (1:1:3)	UV (254 nm)	Quantification (standard calibration curves)	[29]
	Cosmosil C18	AcN:water (1:1)	UV (280 nm)		[26]
2-HBP	Puresil C18	AcN:water (1:1) or AcN:THF:water (1:1:3)	UV (254 nm)		[29,42]
	Zorbax C18	MeOH:water (9:1)	UV (280 nm)	Quantification (standard calibration curves)	[45]
	Cosmosil C18	AcN:water (1:1)	UV (280 nm)		[26,34]
	Zorbax C18	MeOH:water (9:1)	UV (280 nm)		[46]
HBP	Hipersil C18	AcN:10 mM phosphate buffer (pH6) (3:1)	UV (207 nm)	Quantification (standard calibration curves)	[36]
	NOVA.PAK C18	AcN:water (4:6)	UV (280 nm)		[43]
	Kromasil C8	AcN:water (1:1)	UV (240 nm)		[44]
4,6-Dimethyl -DBT	Puresil C18	AcN:water (1:1) or AcN:THF:water (1:1:3)	UV (254 nm)	Quantification (standard calibration curves)	[29]
	Hipersil C18	AcN:10 mM phosphate buffer (pH6) (3:1)	UV (232 nm)		[36]
	Zorbax C18	MeOH:water (9:1)	UV (280 nm)		[45]
4,6-Dimethyl-HBP	Hipersil C18	AcN:10 mM phosphate buffer (pH6) (3:1)	UV (207 nm)	Quantification (standard calibration curves)	[36]
	Zorbax C18	MeOH:water (9:1)	UV (280 nm)	Identification.	[45]

study a biodesulfurization process, problems may be found identifying and quantifying transformation products, since no analytical standard can be commercially acquired. Gas chromatography is the technique of choice to separate alkylated DBTs from the matrix, since they are non polar and volatile compounds. The analytical columns typically used to determine alkylated dibenzothiophenes by gas chromatography are those used to determine DBT, DB-5 [30], DB-1 [36], and DB-17 [47,39].

A detailed study into the gas chromatography behaviour of alkylated dibenzothiophenes (several of which were synthesized for the purpose) on two non polar stationary phases have been performed by Sachade et al. [48]. The influence of the subtituents was described. A strong retention was observed for isomers methylated in the 1-position. In contrast, the retention time is shortened for isomers which posses a methyl group in the 4- or 6-position. Furthermore, a pronounced ortho effect is shown by this class of compounds: with two methyl groups in ortho position to each other, the retention time increase significantly. With the aid of multiple linear regressions, an equation is derived to describe the gas chromatographic behaviour of the polymethylated dibenzothiophenes in a quantitative way and to predict the behaviour of further isomers.

Detectors employed with gas chromatography to determine alkylated DBTs are FID, MS and FPD (see tables), the use of FPD is not very common, although a few applications have been performed using this technique [30,39].

Flame ion detection has been employed to quantify alkylated DBTs by using external calibration, and determination of concentration of alkylated DBTs at different stages of the degradation process allow monitoring of the process [26,30,33,37].

Table 2
Gas chromatography–mass spectrometry detection based method applied in the analysis parents compounds (in bold) in biodesulfurization processes and its degradation products

Compound	Column	Temperature program	Ions (*m/z*)	Purpose	Reference
NTH	HP5-MS	40 °C (3 min) 280 °C (10 °C/min)	184 (M^+), 135	Structural determination	[29]
	DB5				[30]
$NTHO_2$	HP5-MS	40 °C (3 min) 280 °C (10 °C/min)	216 (M^+), 187, 168, 115	Structural determination	[29]
	DB5				[30]
HNE	HP5-MS	40 °C (3 min) 280 °C (10 °C/min)	170 (M^+), 141, 115	Structural determination	[29]
	DB5				[30]
NFU	HP5-MS	40 °C (3 min) 280 °C (10 °C/min)	168 (M^+), 139	Structural determination	[29]
	DB5				[30]
BTH	HP5-MS	40 °C (3 min) 280 °C (10 °C/min)	134 (M^+), 89, 67, 63	Structural determination	[29]
	DB5			Structural determination	[32]
$BTHO_2$	HP5-MS	40 °C (3 min) 280 °C (10 °C/min)	137, 106, 166 (M^+), 63	Structural determination	[29]
	DB5				[30]
BcOTO	HP5-MS	40 °C (3 min) 280 °C (10 °C/min)	118, 89, 166 (M^+), 63	Structural determination	[29]
$BcOTO_2$	HP5-MS	40 °C (3 min) 280 °C (10 °C/min)	89, 118, 182 (M^+), 63	Structural determination	[29]
	DB5				[32]
o-Hydroxystyrene	HP5-MS	40 °C (3 min) 280 °C (10 °C/min)	91, 120 (M^+), 69, 66	Structural determination	[29]
	DB5				[32]
HPEal	HP5-MS	40 °C (3 min) 280 °C (10 °C/min)	107, 136 (M^+), 77, 51, 89, 63	Structural determination	[29]
BFU	HP5-MS	40 °C (3 min) 280 °C (10 °C/min)	118 (M^+), 89, 63	Structural determination	[29]
	DB5				[30]
DBT	DB5	Not reported	Not reported	Structural determination	[30]
	DB1	from 50 to 310 (10 °C/min)	Not reported		[36]
	SE-54	Not reported	184 (M^+), 139, 152		[31]
	DB17	250 °C	Not reported		[38]
	DB17	From 200 °C to 280 °C (5 °C/min), held 14 min	Not reported		[38]
$DBTO_2$	DB5	Not reported	Not reported	Structural determination	[30]
2-HBP	DB5	Not reported	Not reported	Structural determination	[30]
	SE-54	Not reported	170 (M^+), 141, 115		[31]
	Not reported	Not reported	Not reported		[45]
	DB17	From 200 °C to 280 °C (5 °C/min), held 14 min	170 (M^+), 141, 115		[38]
HBP	DB1	From 50 to 310 (10 °C/min)	Not reported	Structural determination	[36]
	SE-54	Not reported	154 (M^+), 76, 115		[31]
2-MBP	SE-54	Not reported	184 (M^+), 169, 141, 115	Structural determination	[31]
	DB17	From 200 °C to 280 °C (5 °C/min), held 14 min	Not reported		[18]
4,6-Dimethyl DBT	DB5	Not reported	Not reported	Structural determination	[30]
	DB1	From 50 to 310 (10 °C/min)	Not reported		[36]
	DB17	250 °C	Not reported		[37]
4,6-Dimethyl HBP	DB1	from 50 to 310 (10 °C/min)	Not reported	Structural determination	[36]
	Not reported	Not reported	Not reported		[45]
	DB17	250 °C			[39]
Metabolites from 4,6-dimethyl DBT	DB5	Not reported	Not reported	Structural determination	[30]
4,6-Diethyl DBT	DB5	Not reported	Not reported	Structural determination	[30]
	DB17	250 °C			[37]
4,6-diethyl HBP	DB17	250 °C	Not reported	Structural determination	[39]
Metabolites from 4,6-diethyl DBT	DB5	Not reported	Not reported	Structural determination	[30]
4,6-dipropyl DBT	DB5	Not reported	Not reported	Structural determination	[30]
	DB17	250 °C	Not reported		[37]
	DB17	From 200 °C to 280 °C (5 °C/min), held 14 min	268, 240, 268		[47]

Table 2 (*Continued*)

Compound	Column	Temperature program	Ions (*m/z*)	Purpose	Reference
4,6-Diprophyl HBP	DB17	250 °C	Not reported	Structural determination	[39]
2-Metabolites from 4,6-dipropyl DBT	DB5	Not reported	Not reported	Structural determination	[30]
4, 6-Dipropyl DBT sulfone	DB17	From 200 °C to 280 °C (5 °C/min), held 14 min	300, 285, 272	Structural determination	[47]
2-Hidroxy-3,3′-dirpropylbiphenyl.	DB17	From 200 °C to 280 °C (5 °C/min), held 14 min	254, 226, 183	Structural determination	[47]
4,6-Dibutyl DBT	DB5	Not reported	Not reported	Structural determination	[30]
	DB17	From 200 °C to 280 °C (5 °C/min), held 14 min			[47]
4,6-Dibupyl DBT sulfone	DB17	From 200 °C to 280 °C (5 °C/min), held 14 min	244, 299, 328	Structural determination	[47]
2-Hidroxy-3,3′-dibutylbiphenyl	DB17	From 200 °C to 280 °C (5 °C/min), held 14 min	239, 282	Structural determination	[47]
Metabolites from 4,6-dibutyl DBT	DB5	Not reported	Not reported	Structural determination	[30]
4,6-Dipentyl DBT	DB17	From 200 °C to 280 °C (5 °C/min), held 14 min	324, 267, 211	Structural determination	[47]
2-Hydrxy-3,3′-dipentylbiphenyl	DB17	From 200 °C to 280 °C (5 °C/min), held 14 min	310, 254	Structural determination	[47]
1-Methyl DBT	Shimadzu GC-17A	Not reported	Not reported	Identification of its metabolites	[28]
6-Methyl 2-HBP	Shimadzu GC-17A	Not reported	Not reported	Identification	[28]
2′-Methyl 2-HBP	Shimadzu GC-17A	Not reported	Not reported	Identification	[28]
2-Methyl DBT	Shimadzu GC-17A	Not reported	Not reported	Identification of its metabolites	[28]
5-Methyl 2-HBP	Shimadzu GC-17A	Not reported	184 (M^+) (*100%*), 183 ($[M-1]^+$) (*45%*), 169 ($[M-15]^+$) (*80%*)	Identification	[28]
3′-Methyl 2-HBP	Shimadzu GC-17A	Not reported	184 (M^+) (*100%*), 183 ($[M-1]^+$) (*50%*), 169 ($[M-15]^+$) (*10%*)	Identification	[28]
3-Methyl DBT	Shimadzu GC-17A	Not reported	Not reported	Identification of metabolites	[28]
4-Methyl 2-HBP	Shimadzu GC-17A	Not reported	Not reported	Identification	[28]
4′-Methyl 2-HBP	Shimadzu GC-17A	Not reported	Not reported	Identification	[28]
4-Methyl DBT	Shimadzu GC-17A	Not reported	Not reported	Identification of its metabolites	[28]
3-Methyl 2-HBP	Shimadzu GC-17A	Not reported	Not reported	Identification	[28]
3′-Methyl 2-HBP	Shimadzu GC-17A	Not reported	Not reported	Identification	[28]

Gas chromatography (GC) coupled with mass selective detection (MSD) is widely used for separation and determination of such volatile PASHs as DBTs. The ionisation mode used to determine these compounds is electron impact ionisation at 70 eV. Qualitative analysis is often limited to classification based on the mass to charge ratio and therefore only gives the number of carbon atoms present in the substituents. Definitive chemical structures cannot be obtained through mass spectrometry data in the electron ionisation mode because of the almost identical spectra of isomers when a mixture of unknown alkylated DBT's are elucidated. Chemical ionisation is an efficient alternative, since the molecular mass of the compounds could be determined [18], but this technique has not been used until now to determine these kinds of compounds. Nevertheless, mass spectrometry in electron impact ionisation may help distinguish between dibenzothiophenes, which only contain methyl groups or carry longer alkyl side chains [49]. It has been found that for DBTs carrying only methyl groups, the base peak in the mass spectrum is defined by the molecular ion, but that longer alkyl chains give rise to fragmentation and therefore the molecular ion is no longer the base peak. These results for mono-and dialkylated DBTs (with methyl, *n*-alkyl and branched alkyl substituents) also apply to multiply alkylated DBTs [48].

High performance liquid chromatography coupled with UV detection has been employed in order to determine compound such as 4,6-dimethyl-DBT [29,36,45], in these applications C18 columns were used to separate the compounds chromatographically from the matrix. Different mobile phases have been used (see Table 1), and different wavelengths have been selected for the detection of these compounds: 254 nm [29], 232 nm [36] and 280 nm [45].

3.3. Bezothiophene, naphtothiophene

Naftho [2,1-*b*] thiophene (NTH) (see structure in Fig. 1), which includes a benzothiophene (BTH) structure (see structure

Table 3
Gas chromatography–flame photometric detection based method applied in the analysis parents compounds (in bold) in biodesulfurization processes and its degradation products

Compound	Column	Temperature program	Purpose	Reference
NTH	DB5	Not reported	Quantification	[30]
$NTHO_2$	DB5	Not reported	Quantification	[30]
HNE	DB5	Not reported	Quantification	[30]
NFU	DB5	Not reported	Quantification	[30]
BTH	DB5	Not reported	Quantification	[24]
	DB 17	250 °C		[39]
$BTHO_2$	DB5	Not reported	Quantification	[30]
BFU	DB5	Not reported	Quantification	[30]
DBT	DB5	Not reported	Quantification	[30]
	DB 17	250 °C		[39]
$DBTO_2$	DB5	Not reported	Quantification	[30]
2-HBP	DB5	Not reported	Quantification	[30]
4,6-Dimethyl DBT	DB5	Not reported	Quantification	[30]
	DB 17	250 °C		[39]
4,6-Diethyl DBT	DB5	Not reported	Quantification	[30]
	DB 17	250 °C		[39]
4,6-Dipropyl DBT	DB5	Not reported	Quantification	[30]
	DB 17	250 °C		[39]
4,6-Dibutyl DBT	DB5	Not reported	Quantification	[30]

in Fig. 1), is an asymmetric structural isomer of DBT. Recently it has become apparent that in addition to DBT derivatives, NTH derivatives can also be detected in diesel oil following HDS treatment, although NTH derivatives are minor components in comparison to DBT derivatives.

Therefore, NTH may also be a model target compound for deeper desulfurization [29,30]. Fewer applications have been published concerning the biodesulfurization of benzothiphene and naphtothiophene compared with dibenzothiophene.

Recently, there is confirmation that alkyl-substituted derivatives of naphtha [2,1-*b*] thiophene (NTH) and benzo [b] thiophene (BTH) may be detected in diesel oil, in addition to DBT derivatives [50].

Gas chromatography coupled to mass spectrometry [29,30,32], FPD [30,39] and flame ion detection [30] has been used to determine these compounds in biodesulfurization process. The columns employed are 5% phenyl, 95% dimethylpolysiloxane (e.g. HP-5, DB-5).

The mass spectrum of NTH and BTH in the electron impact ionisation mode (see Table 2) show the molecular ions at *m*/*z* 184 [29,30] and *m*/*z* 134 [29,32] respectively. The mass spectrum of NTH shows a fragment at *m*/*z* 135. More fragmentation is achieved for BTH, three fragment ions have been reported at *m*/*z* 89, 67 and 63.

Liquid chromatography coupled to UV detection has also been used to determine NTH and BTH in biodesulfurization processes [29]. The wavelength selected to analyse both compounds is 254 nm, and a C18 analytical column has been used in order to separate these compounds from the matrix. AcN:water (1:1) or AcN:THF:water (1:1:3) has been employed as mobile phase (see Table 1).

4. Transformation products

Gas chromatography–mass spectrometry (GC–MS) is by far the most frequent analysis tool for identifying transformation products. Important advantages of the GC–MS based methods are: (i) the high amount of structural information yielded and the possibility of using commercial libraries which make the identification of unknown transformation products feasible; (ii) the ruggedness and reliability of the GC–MS interface; and (iii) the high sensitivity and separation efficiency which avoid the overlapping of compounds with similar structures.

Electron impact ionization is the most popular since its spectra are highly reproducible, which mean that mass spectral libraries can be used for the identification of unknowns. Compound identification is currently performed by comparing an unknown electron ionisation MS spectrum with collections of references spectra. The identification process is based on search algorithms which compare the obtained spectra with those of a library, and which are generally implemented in the GC–MS instrument. A spectral match and fit factor defines the certainty of the identification. Although library searches are a powerful tool for the identification of unknowns, for this purpose, a series of conditions must be met: the compound must be included in the library; the MS conditions at which both spectra have been obtained must be similar; and finally, the GC separation must be sufficiently efficient to obtain a clean mass spectrum.

However, GC–MS methods have important drawbacks as a consequence of their low capacity for analyzing very polar, less volatile and thermally unstable compounds.

Identification of transformation products is usually carried out on the basis of their EI mass spectra, mainly because

Table 4
Gas chromatography–flame ion detection based method applied in the analysis of parents compounds (in bold) in biodesulfurization processes and its degradation products

Compound	Column	Temperature program	Purpose	Reference
NTH	DB5	Not reported	Quantification	[30]
$NTHO_2$	DB5	Not reported	Quantification	[30]
HNE	DB5	Not reported	Quantification	[30]
NFU	DB5	Not reported	Quantification	[30]
BTH	DB5	Not reported	Quantification	[30]
$BTHO_2$	DB5	Not reported	Quantification	[30]
BFU	DB5	Not reported	Quantification	[30]
DBT	DB5	Not reported		[30]
	WCOT FUSED SILICA	From 100 °C to 280 °C (20 °C/min)		[35] (solo compuesto de partida)
	SE-54	Not reported	Quantification	[31]
	DB17	250 °C		[37,40]
	DB1	250 °C		[33]
	DB17	From 200 °C to 280 °C (5 °C/min), held 14 min		[38]
	OV17	From 120 °C (5 min) to 250 °C (3 °C/min)		[26]
DBT sulfone	DB1	250 °C		[33]
	DB5	Not reported	Quantification	[30]
	OV17	From 120 °C (5 min) to 250 °C (3 °C/min)		[26]
2-HBP	DB5	Not reported		[30]
	SE-54	Not reported		[31]
	DB17	250 °C	Quantification	[40]
	DB17	From 200 °C to 280 °C (5 °C/min), held 14 min		[38]
	OV17	From 120 °C (5 min) to 250 °C (3 °C/min)		[25]
HBP	SE-54	Not reported	Quantification	[31]
	DB1	250		[33]
2-MBP	SE-54	Not reported	Quantification	[31]
	DB17	From 200 °C to 280 °C (5 °C/min), held 14 min		[38]
4,6-Dimethyl DBT	DB5	Not reported		[30]
	DB17	250 °C	Quantification	[37]
	DB1	250 °C		[33]
4,6-Dimethyl DBT sulfone	DBI	250 °C	Quantification	[33]
4,6-Diethyl DBT	DB5	Not reported		[30]
	DB17	250 °C	Quantification	[37]
	DB1	250 °C		[33]
4,6-Diethyl DBT sulfone	DB1	250 °C		[27]
4,6-Dipropyl DBT	DB5	Not reported		[30]
	DB17	250 °C	Quantification	[37]
	DB1	250° C		[33]
4,6-Dipropyl DBT sulfone	DB1	250 °C	Quantification	[33]
4,6-Dibutyl DBT	DB5	Not reported	Quantification	[30]
	DB1	250 °C		[33]
4,6-Dibutyl DBT sulfone	DB1	250 °C	Quantification	[33]
4,6-dipentyL DBT	DB1	250 °C	Quantification	[33]
4,6-Dipentyl DBT sulfone	DB1	250 °C	Quantification	[28]
1-Methyl DBT	Shimadzu GC-17A	Not reported	Quantification and following the process	[28]
Degradation products	Shimadzu GC-17A	Not reported	Following the process	[28]
2-Methyl DBT	Shimadzu GC-17A	Not reported	Quantification and following the process	[28]
Degradation products	Shimadzu GC-17A	Not reported	Following the process	[28]
3-Methyl DBT	Shimadzu GC-17A	Not reported	Quantification and following the process	[28]
Degradation products	Shimadzu GC-17A	Not reported	Following the process	[28]
4-Methyl DBT	Shimadzu GC-17A	Not reported	Quantification and following the process	[28]
Degradation products	Shimadzu GC-17A	Not reported	Following the process	[28]

structural elucidation can easily be achieved by comparing the spectrum of the unknown compound with published spectra either from data bases or from research papers.

Throughout the last decade GC–MS techniques have been used to elucidate the metabolisme pathway of DBT studied with different microorganisms, this review focuses only on microorganisms which follow the 4S pathway.

As has been mentioned in the introduction part, BDS is studied with model compounds such as *DBT*, the most usual of all. There are many reports concerning different microorganisms which are able to metabolise DBT via a hydrocarbon degradative pathway (with destruction of carbon–carbon bonds), but only a small number of microorganisms, mainly *Rhodococcus*, *Bacillus*, *Corynebacterium* and *Anthrobacter* species, are able to remove sulphur from DBT via sulphur-specific pathway, selectively cleaving sulphur from DBT without ring degradation [23,51,52]. This desulfurisation pathway has been named as 4S route, because the molecule of DBT is transformed into 2-hdroxibiphenyl (HBP) [53,54]. According to a reaction scheme formed by four consecutive reactions or steps as shown in Fig. 2 DBT is first oxidized to DBTO (DBT sulfoxide). DBTO is then transformed to DBT sulfone ($DBTO_2$) and to sulfinate (HBPS), followed by hydrolytic cleavage to 2-HBP and subsequent release of sulfite or sulphate. This pathway is regarded as preferable and promising, because the sulfur of DBT is selectively removed without destroying the hydrocarbon skeleton so that the thermal value of fuels is not decreased [5].

All these degradation products of DBT and analogous from biodesulfurization of other parents compounds that we are reviewing in this work have been identified by different analytical techniques mentioned before in this review and have been summarized in Tables 1–4. But special attention is required for the GC–MS technique, since it is the technique which provides more structural information when a pathway has to be elucidated. For this reason, in this section, more specific comments of published data concerning this technique are included.

In biodesulfurization studies of DBT, 2-HBP [30,31,38,45] is the most detected degradation product, due to the fact that it is the final product in the process and owing to its concentration is, normally, high enough to be determined with the analytical techniques applied. However intermediate compounds, which are typically at lower concentrations, have not been detected in all biodesulfurization studies, and a hypothesis of their presence has been adopted to explain the 4S pathway, Samir et al. [36] could not detect HBPS, even when the formation of this compound is the limiting step in the 4S route [55], GC analysis of the methylene chlorine extracted compounds did not reveal any intermediary metabolite (only 2-HBP was detected), any transient accumulation of sulfinate was not detected. Authors considered that this was due to the fact that this water soluble compound was not extracted using methylene chloride as extractant solvent. In the same study attempts to detect HBPS in the aqueous phase by HPLC–UV were neither possible. Because the HBP concentration determined by GC and HPLC were similar, authors suggested that the concentration of HBP-sulfinate accumulated was low.

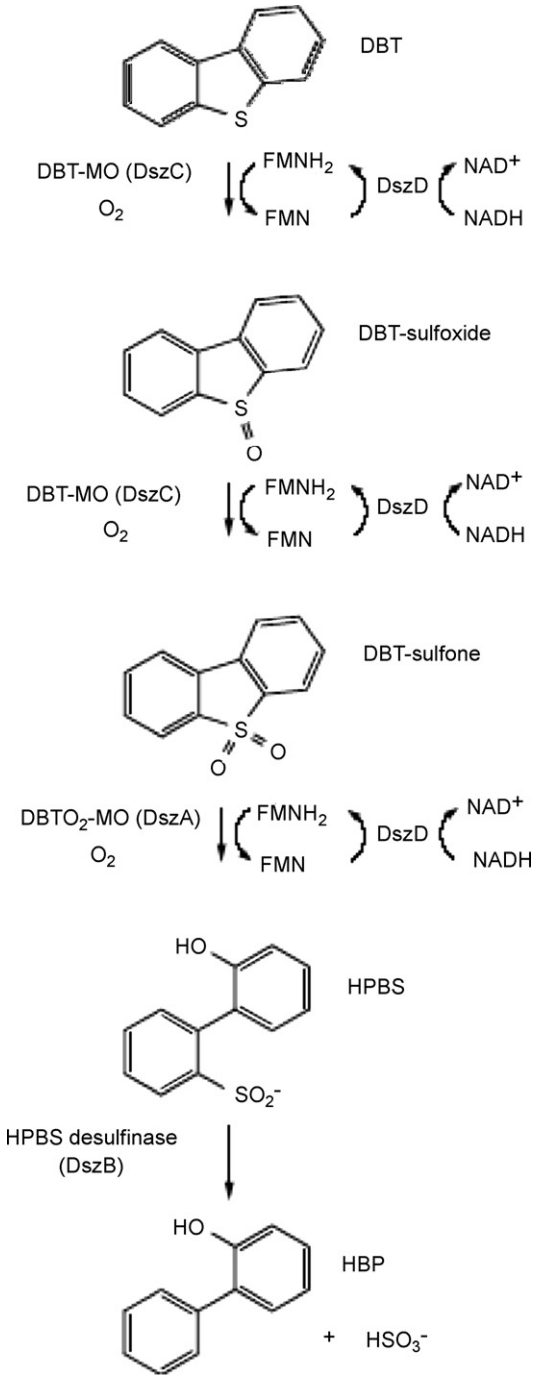

Fig. 2. Scheme of 4S biodesulfurization route of dibenzothiophene.

Although 2-HBP is the final product in a biodesulfurization process, this compound can lead in to other degradation products HBP [31,36] and 2-methoxybiphenyl (2-MBP) [31,38]. 2-HBP has been analysed by GC–MS in the electron impact mode [30,31,38,45], the mass spectrum show the molecular ion at *m*/*z* 170 and also two fragments at *m*/*z* 141 and 115. HBP which is the dehydroxilated 2-HBP, has been analysed as well by GC–MS in electron impact mode [31,36], the mass spectrum show the molecular ion at *m*/*z* 154 and two fragment ions at *m*/*z* 76 and 115 [31]. 2-MBP which is formed by the methylation of the hydroxyl group of 2-HBP [56], show a mass spectrum

in electron impact mode with the molecular ion at *m/z* 184 and three fragments at *m/z* 169, 141 and 115. These three compounds have been analysed by GC–FID [30,31,33,38,40] and GC–FPD [30]. The analytical columns employed in gas chromatography for the analysis of these compounds are DB-1, DB-5, DB-17 and SE-54, see Tables 2–4.

DBTO2, one of the intermediates in the 4s pathway, which has been detected more than others, has been analysed by GC–MS, GC–FPD [30] and GC–FID [26,30,33].

Liquid chromatography coupled with UV detection has been used, also to the determination of 2-HBP [26,42,44,46], DBTO2 [26,29] and HBP [36].

Biodesulfurization of *alkilated DBTs* occur by the analogous pathway of DBT degradation, see Tables 1–4. In these tables, we collect the analytical techniques employed to analyse degradation products of alkilated DBT's, such as for other compounds already discussed in this review. GC–MS in electron impact mode is the analytical technique which gives more information on the structure of the transformation products. By analogy of the microbial conversion of DBT to 2-HBP, 2-MDBT (e.g.) is expected to be transformed into the hydroxilated desulfurization product, 5-methyl-2-hydroxybiphenyl (5-MHBP) or 3′-methyl-2-hydroxy-biphenyl (3′-MHBP) in the course of biodesulfurization. The mass spectrum obtained for 5-MHBP and 3′-MHBP [28] (see Table 2) shows an ion at *m/z* 184 corresponding to the molecular mass of these methyl hidroxybiphenyls. The peak intensities of some of their fragment ions, specially *m/z* 183 and *m/z* 169 corresponding to each of the H ($[M-1]^+$) and CH_3 ($[M-15]^+$) elimination from the molecular ions are different from each other. The difference between peak intensities of these fragment ions (*m/z* 183 and 169) is estimated by the authors [28] to determine the differences in their chemical structures, although both fragment ion peaks in the low-mass ion series less than *m/z* 141, exhibited the same spectral pattern.

As happens with DBT, when the degradation of methylated DBTs is performed, the hydroxylated product is the most frequently analysed [28,36,45,47], data of the identification of intermediates are not frequently reported, some authors don't even specify which transformation products have been formed throuhout the biodesulfurization process [30].

GC–FID have been used to the quantitative determination of microbial transformation products (see Table 4) such as 4,6-dibutyl DBT sulfone, 4,6-dimethyl DBT sulfone, 4,6-diethyl DBT sulfone, 4,6-dipropyl DBT sulfone, 4,6-dipenthyl DBT sulfone [33] and others which authors do not specify [28]. GC–AED has been used to detect sulphur atoms in transformation products [57]. This technique is a powerful method to simultaneously detect multiple elements of which a given compound is composed [18,19]. In an atomic emission detector, excited atoms are generated in a microwave–induced electrical discharge plasma. Upon deactivation, excited states generate light quanta which produce an elemental emission spectrum [58].

Intermediates from biodesulfurization of *NTH and BTH* have been analysed by the analytical techniques already exposed in this review, the only one which gives structural information is the GC–MS technique, as previously mentioned. By this technique, in electron impact ionization mode, three intermediates

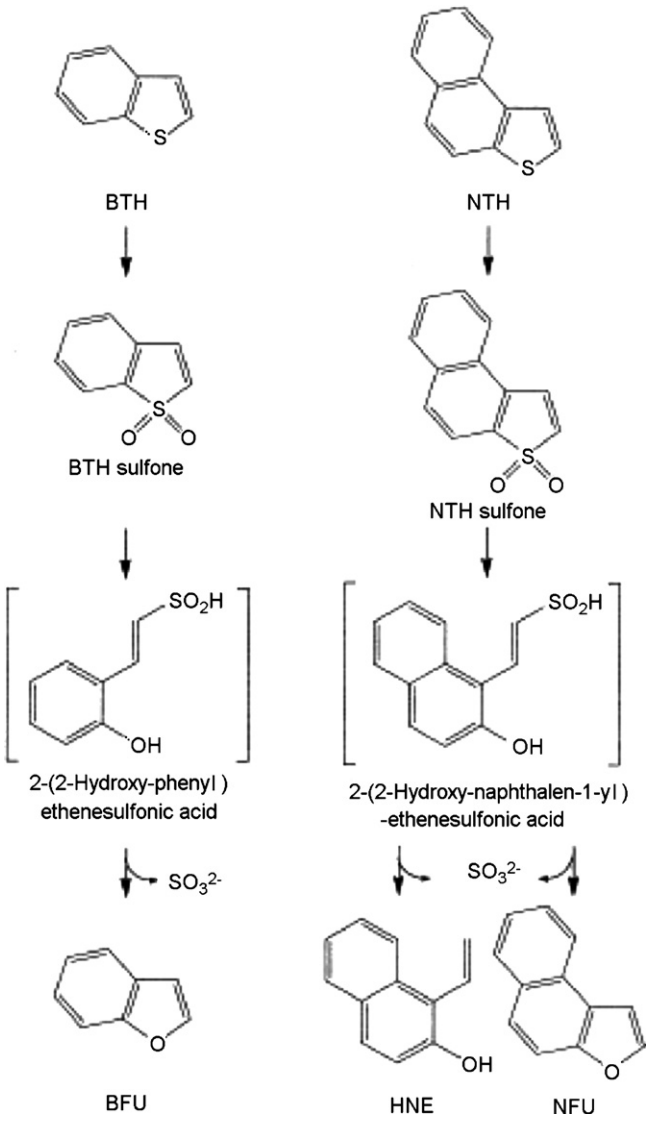

Fig. 3. Scheme of 4S biodesulfurization route of benzothiophene and naftothiophene.

have been identified for NTH and six for BTH [29,30]. The chromatographic conditions and the ions reported are shown in Table 2, and the structures of some of the degradation products are shown in Fig. 3. When the biodesulfurization of NTH has been performed, three degradation products were identified. One metabolite has been identified as $NTHO_2$ (M^+, *m/z* 160) since its MS spectrum was identical to that of authentic $NTHO_2$. The other metabolites were considered to include no sulphur atom in their molecular structures. One have been identified as 2′-hydroxynaphthylethene (HNE) (M^+, *m/z* 170), the fragment ion at *m/z* 141 corresponds to loss of the vinyl group from the molecular ion. Other degradation products has been identified as naphto [2,1-*b*] furan (NFU), since its mass spectrum was identical to that of authentic NFU.

In the biodesulfurization of BTH six degradation products have been identified [29,30,32] whose ions (*m/z*) obtained by mass spectrometry in electron impact mode ionisation are shown in Table 2. These six metabolites have been identified as BTH

sulfone ($BTHO_2$) (M^+, *m/z* 166), benzo [*c*] (1,2) oxathiin s-oxide (BcOTO) (M^+, *m/z* 166), benzo [*c*] (1,2) oxathiin S, S-dioxide ($BcOTO_2$) (M^+ *m/z* 182), *o*-hydroxystyrene (M^+, *m/z* 120), 2-(2′-hydroxyphenyl)ethan-1-al (HPEal) (M^+, *m/z* 136), and BFU (M^+, *m/z* 118).

5. Final remarks

The extraction method employed before chromatographic analysis involve a simple liquid–liquid extraction for the aqueous phase and a solid phase extraction for the organic phase. This second procedure is not always performed, since some authors inject the organic phase directly into GC systems. However, detailed recovery studies of these extraction procedures are not usually reported in the reviewed bibliography. Only Onaka et al. [28] perform a study of solid phase extraction applied to biodesulfurization processes.

In general, HPLC–UV and GC–FID are used by most of authors, in order to follow degradation processes and to quantify the pattern compound as well as the final product. GC–MS is normally used to identify intermediates.

The sensibility of analytical techniques traditionally used in biodesulfurization processes seems to be enough (although no data on the limits of detection are reported by any authors) to detect the initial compound and final products, but in some cases these techniques are not adequate in the detection of intermediate products [36].

A conclusion of this review is that very simple and accessible analytical techniques, such as HPLC–UV and GC–FID, are enough to monitor a biodesulfurization global process. In contrast, it is not always possible to confirm the identification of degradation products extensively, that can represent a very important factor in the process evaluation [45].

Acknowledgements

M. Mezcua acknowledges the “Juan de la Cierva” research contract from the Spanish Ministry of Science and Technology.

The work has been supported by the Spanish Ministry of Science and Technology Project number CTQ2004/06553-C02-02: Biodesulfuración de fracciones petrolíferas: Condiciones y formas de operación.

References

[1] M. Blumer, W. Youngblood, Science 188 (1975) 53.
[2] G. Grimmer, J. Jacob, K.W. Naujak, Fresenius Anal. Chem. 314 (1983) 29.
[3] F. Berthou, V. Vignier, Int. J. Environ. Anal. Chem. 27 (1986) 81.
[4] J.J. Kilbane, Trends Biotechnol. 7 (1989) 97.
[5] D.J. Monticello, Curr. Opin. Biotechnol. 11 (2000) 540.
[6] European standard for gasoline EN 228/1999 and for diesel EN 590/1999.
[7] C.Y. Jiang, R. Wang, H.Z. Liu, J.R. Chen, J. Chin, Process Eng. 1 (2001) 80.
[8] Y. Tanaka, T. Matsui, J. Konishi, K. Maruhashi, R. Kurane, Appl. Microbiol. Biotechnol. 59 (2002) 325.
[9] J.H. Chang, Y.K. Chang, H.W. Ryu, H.N. Chang, FEMS Microbiol. Lett. 182 (2000) 309.
[10] T. Onaka, J. Kinishi, Y. Ishii, K. Maruhashi, J. Biosci. Bioeng. 92 (2001) 193.
[11] S. Maghsoudi, M. Vossughi, A. Kheirolomoom, E. Tanaka, S. Katoh, Biochem. Eng. J. 8 (2001) 151.
[12] F.L. Li, P. Xu, C.Q. Ma, L.L. Luo, X.S. Wang, FEMS Microbiol. Lett. 223 (2003) 301.
[13] N. Gupta, P.K. Roychoudhury, J.K. Deb, Appl. Microbiol. Biotechnol. 66 (2005) 356.
[14] J. Kilbane II, Curr. Opin. Biotechnol. 17 (2006) 305.
[15] B. Yu, P. Xu, Q. Shi, C. Ma, Appl. Environ. Microbiol. 72 (2006) 54.
[16] F. Tao, B. Yu, P. Xu, C.Q. Ma, Appl. Environ. Microbiol. 72 (2006) 4604.
[17] B. Yu, C. Ma, W. Zhou, Y. Wang, X. Cai, F. Tao, Q. Zhang, M. Tong, J. Qu, P. Xu, FEMS Microbiol. Lett. 258 (2006) 284.
[18] S. Malato, J. Cáceres, A. Agüera, M. Mezcua, D. Hernando, J. Vial, A.R. Fernández-Alba, Environ. Sci. Tehcnol. 35 (2001) 4359.
[19] A. Agüera, M. Mezcua, D. Hernando, S. Malato, J. Cáceres, A.R. Fernández-Alba, Int. J. Environ. Anal. Chem. 84 (2004) 149.
[20] M. Mezcua, I. Ferrer, M.D. Hernando, A.R. Fernández-Alba, Food Addit. Contam. 23 (2006) 1242.
[21] M. Mezcua, M.J. Gómez, I. Ferrer, A. Agüera, M.D. Hernando, A.R. Fernández-Alba, Anal. Chim. Acta 524 (2004) 241.
[22] I. Ferrer, M. Mezcua, M.J. Gómez, E.M. Thurman, A. Agüera, M.D. Hernando, A.R. Fernández-Alba, Rapid Commun. Mass Spectrom. 18 (2004) 443.
[23] Y. Izumi, T. Ohshiro, H. Ogino, Y. Hine, M. Shimao, Appl. Environ. Microbiol. 60 (1994) 109.
[24] T. Onaka, M. Kobayashi, Y. Ishii, J. Konnishi, K. Maruhashi, J. Biosc. Bioeng. 92 (2001) 80.
[25] J.R. Gallegher, E.S. Olson, C. Stanley, F.E.M.S. Microbiol, Letters 107 (1993) 31.
[26] S. Maghsoudi, A. Kheirolomoom, M. Vossoughi, E. Tanaka, S. Katoh, Biochem. Eng. J. 5 (2000) 11.
[27] T. Onaka, K. Okamura, M. Suzuki, J. Chromatogr. Sci. 35 (1997) 417.
[28] T. Onaka, M. Kobayashi, Y. Ishii, K. Okumura, M. Suzuki, J. Chromatogr. A 903 (2000) 193.
[29] K. Kirimura, T. Furuya, R. Sato, Y. Ishii, K. Kino, S. Usami, Appl. Environ. Microbiol. (2002) 3867.
[30] Y. Ishii, S. Kozaki, T. Furuya, K. Kino, K. Kirimura, Curr. Microbiol. 50 (2005) 63.
[31] W. Li, Y. Zhang, M.D. Wang, Y. Shi, FEMS Microbil. Lett. 247 (2005) 45.
[32] F. Li, P. Xu, J. Feng, L. Meng, Y. Zheng, L. Luo, C. Ma, Appl. Environ. Microbiol. (2005) 276.
[33] N. Nomura, M. Takada, H. Okada, Y. Shinohara, T. Nakajima, K. Tadaatsu, N. Hiroo, J. Biosc. Bioeng. 100 (2005) 398.
[34] S. Maghsoudi, M. Vossoughi, A. Kheirolomoon, Emiko Tanaka, Shigeo Katoh, Biochem. Eng. J. 8 (2001) 151.
[35] Y. Hou, Y. Kong, J. Yang, J. Zhang, D. Shi, W. Xin, Fuel 84 (2005) 1975.
[36] S. Abbad-Andaloussi, C. Lagnel, M. Warzywoda, F. Monot, Enzyme Microbe Technol. 32 (2003) 446.
[37] K.I. Noda, K. Watanabe, K. Maruhashi, J. Biosci. Bioeng. 95 (2003) 354.
[38] H. Okada, N. Nomura, T. Nakahara, K. Maruhashi, J. Biosci. Bioeng. 93 (2002) 491.
[39] I. Bagus, W. Guanam, Y. Yaku, M. Hirano, K. Yamamura, F. Tomita, T. Sone, K. Asano, J. Biosci. Bioeng. 101 (2006) 322.
[40] K.I. Noda, K. Watanabe, K. Maruhashi, J. Biosci. Bioeng. 95 (2003) 504.
[41] T. Holm, J. Chromatogr. A 842 (1999) 221.
[42] K. Kirimura, T. Furuya, Y. Nishii, Y. Ishii, K. Kino, S. Usami, J. Biosci. Bioeng. 91 (2001) 262.
[43] M. Rashchi, G.H. Mohebali, M.M. Akbarnejad, J. Towfighi, B. Rasekh, A. Keytash, Biochem. Eng. J. 29 (2006) 169.
[44] C.H. del Olmo, V.E. Santos, A. Alcon, F. García-Ochoa, Biochem. Eng. J. 22 (2005) 229.
[45] M.F. Luo, J.M. Xing, Z.X. Gou, S. Li, H.Z. Liu, Biochem. Eng. J. 13 (2003) 1.
[46] S. Guobin, Z. Huaiying, X. Jianmin, C. Guo, L. Wangliang, L. Huizhou, Biochem. Eng. J. 27 (2006) 305.
[47] H. Okada, N. Nomura, T. Nakahara, K. Maruhashi, J. Biosci. Bioeng. 93 (2002) 228.
[48] T. Schade, J.T. Anderson, J. Chromatogr. A 1117 (2006) 206.
[49] F. Borbeg, W. Bruns, D. Muhoff, Erdölf Kohle Erdgas 47 (1994) 56.

[50] J. Chen, Z. Ring, Fuel 83 (2004) 305.
[51] M. Constantini, J. Giralt, A. Bordons, World J. Microbiol. Biotechnol 10 (1994) 510.
[52] P. Wang, S. Kraviec, Arch. Microbiol. 161 (1994) 266.
[53] B.L. McFarland, D.J. Boron, W. Deever, J.A. Meyer, A.R. Johnson, R.M. Atlas, Crit. Rev. Microbiol. 24 (1998) 99.
[54] B.L. McFarlang, Biodesulfurirzation, Curr. Opin. Microbiol. 2 (1999) 257.
[55] K.A. Gray, O.S. Pogrebinsky, G.T. Mrachko, L. Xi, D.J. Monticello, C.H. Squires, Nat. Biotchnol. 14 (1996) 1705.
[56] F.L. Li, P. Xu, C.Q. Ma, L.L. Luo, X.S. Wang, FEMS Microbial. Lett. 23 (2003) 301.
[57] T. Onaka, J. Konishi, Y. Ishii, K. Maruhashi, J. Biosci. Bioeng. 92 (2001) 193.
[58] P.C. Uden, J. Chromatogr. A 703 (1995) 393.

Available online at www.sciencedirect.com
ScienceDirect
Talanta 73 (2007) 81–86
Talanta
www.elsevier.com/locate/talanta

Study on simultaneous speciation of arsenic and antimony by HPLC–ICP-MS

Yukitoki Morita [a,*], Teppei Kobayashi [a], Takayoshi Kuroiwa [b], Tomohiro Narukawa [b]

[a] *Department of Materials and Applied Chemistry, College of Science and Technology, Nihon University, 1-8 Kanda-Surugadai, Chiyoda-ku, Tokyo 101-8308, Japan*
[b] *National Metrology Institute of Japan (NMIJ), National Institute of Advanced Industrial Science and Technology (AIST), 1-1-1 Umezono, Tsukuba, Ibaraki 305-8563, Japan*

Received 22 December 2006; received in revised form 6 March 2007; accepted 6 March 2007
Available online 12 March 2007

Abstract

A method was developed for the simultaneous speciation of arsenic and antimony with HPLC–ICP-MS using C30 reversed phase column. Eight kinds of arsenic compounds (As(III), As(V), monomethylarsonic acid (MMAA), dimethylarsinic acid (DMAA), arsenobetaine (AB), arsenocholine (AsC), trimethylarsine oxide (TMAO) and tetramethylarsonium (TeMA)), Sb(III) and Sb(V) were simultaneously separated by the special mobile phase containing ammonium tartrate. Especially for the species of organic As, a C30 column was better than a C18 column in the effect of separation. Limits of detection (LOD) for these elements were 0.2 ng ml^{-1} for the species of each As, and 0.5 ng ml^{-1} for the species of each Sb, when a 10 μl of sample was injected, respectively. The proposed method was applied to a hot spring water and a fish sample.

Keywords: Simultaneous speciation; As; Sb; HPLC–ICP-MS

1. Introduction

Chemical species of elements in biological and environmental samples are of importance to understand toxicity, metabolism and transport properties of elements. Therefore, speciation analysis [1–4] becomes an increasing active-research field in recent years. Arsenic (As) is essential element for human body, and is a base of many chemical species in environmental samples. In addition, there are different toxicity with corresponding the species of As to human body and environments. Consequently, speciation analysis of As (As speciation) are reported with various analytical techniques, such as HPLC–HG-AAS and HPLC–ICP-MS, etc. [5]. HPLC–ICP-MS is widely applied to As speciation due to the advantages of excellent separation and high sensitivity. So far, the methods using a reversed phase column and ion exchange column coupled with ICP-MS are much used. As known, As species in environments are mainly in presence of As(III), As(V) and monomethylarsonic acid (MMAA) and dimethylarsinic acid (DMAA). Therefore, these anions species of As can be separated with ion exchange column using a simple composition of eluent. However, it is difficult to use the eluent in separating the other species of organic As. On the other hand, C18 reversed phase column packing octadecyl group (ODS), with high resolution factor and excellent ability of separation for many As species, is often used for biological samples.

The importance of Sb determination is reflected by the fact that Environmental Protection Agency (EPA) considers it a priority pollutant. The species of antimony (Sb) in environments are in presence of Sb(III) and Sb(V). Analysis and risk evaluation for Sb species are important from the view of toxicity. However, owing to the absence of standards of organic Sb species, speciation analysis for Sb species in biological and environmental samples is not enough.

As known, simultaneous multi-element determination is an important feature of ICP-MS. Nevertheless, speciation analysis is mainly performed for a single element in present methods using the detector. The reason is that the optimum composition of eluent is different for each element. Although there are a few reports [6–9] on speciation analysis of simultaneous multi-

* Corresponding author. Tel.: +81 3 3259 0820; fax: +81 3 3293 7572.
E-mail address: morita@chem.cst.nihon-u.ac.jp (Y. Morita).

0039-9140/$ – see front matter © 2007 Elsevier B.V. All rights reserved.
doi:10.1016/j.talanta.2007.03.005

element, it is not found that the species of Sb and eight kinds of As are simultaneously separated using reversed phase column.

In this study, the simultaneous speciation of As and Sb by HPLC–ICP-MS with C30 reversed phase column was investigated. The optimum chromatographic conditions, concerning the composition of eluent and the pH of simultaneous separation of As and Sb species, were examined. The proposed method has been applied to a hot spring water and a fish sample.

2. Experimental

2.1. Reagent

All reagents were of analytical grade. Ultra-pure water was prepared by a Milli-Q system (Elix-3 and Milli-Q gradient, Millipore, Tokyo, Japan).

2.1.1. Arsenic standard solutions

Stock solutions of arsenic species (1000 mg l^{-1} for As) were prepared by dissolving the follow compounds: sodium metaarsenite (As(III)), disodium hydrogen arsenate heptahydrate (As(V)), monomethylarsonic acid, dimethylarsinic acid, arsenobetaine (AB), arsenocholine bromide (AsC), trimethylarsine oxide (TMAO), and tetramethylarsonium iodide (TeMA). As(III), As(V) and DMAA were obtained from Wako pure Chemical Ind., Ltd. (Osaka, Japan). MMAA, AB, AsC, TMAO, and TeMA were purchased from Tri Chemical Laboratories Inc. (Yamanashi, Japan). The standard solutions of arsenic species were used by diluting the corresponding stock solutions.

2.1.2. Antimony standard solutions

Stock solutions of antimony species (1000 mg l^{-1} for Sb) were prepared by dissolving diantimonate dipotassium trihydrate (Sb(III)) and potassium hexahydroxoantimonate (Sb(V)) from Wako Pure Chemical Ind. Ltd. The standard solutions of antimony species were used by diluting the corresponding stock solutions.

2.1.3. Eluent

Malonic acid, 1-butanesulfonic acid sodium salt, ammonium tartrate, diammonium hydrogen citrate, 15% tetramethylammonium hydroxide and methanol were gained from Wako Pure Chemical Ind. Ltd. Eluent comprised the above regents according to the different ratio.

2.2. Instrumentations

An ICP-MS, Agilent 7500c, was used from Yokogawa Analytical Systems (Tokyo, Japan). A C30 reversed phase column packing triaconcyl group, DEVELOSIL C30-UG-5 (particle size 5 μm, 4.6 mm i.d. × 250 mm), was employed from Nomura Chemical Co., Ltd. (Aichi, Japan). A C18 reversed phase column, Inertsil ODS-3 (particle size 3 μm, 4.6 mm i.d. × 250 mm) was utilized from GL Science (Tokyo, Japan). A anion exchange column, CHEMCOSORB 7SAX (particle size 5 μm, 4.6 mm i.d. × 250 mm) was obtained from Chemco Scientific Co., Ltd. (Tokyo, Japan). A HPLC and an ICP-MS were connected with PEEK tube. All of measurements were performed under the operating conditions given in Table 1.

Table 1
Instrumental operating conditions of HPLC–ICP-MS

ICP-MS conditions
Incident Rf power: 1.5 kW
Reflected power: <2 W
Outer gas flow rate: Ar 15 l min^{-1}
Intermediate gas flow rate: Ar 0.9 l min^{-1}
Carrier gas flow rate: Ar 0.8 l min^{-1}
Make-up gas flow rate: Ar 0.4 l min^{-1}
Nebulier: Micro mist
Spray chamber: Scott type
Sampling depth: 7 mm from work coil
Reaction mode: He 2.0 ml min^{-1}
Measured *m/z*: As: 75, Sb: 121
Chromatographic conditions
Column: Develosil C30-UG-5 (4.6 mm i.d. × 250 mm)
Eluent: 10 mmol l^{-1} sodium butanesulfonate/4 mmol l^{-1} malonic acid/4 mmol l^{-1} tetramethylammonium hydroxide/0.1 (v/v)% methanol/20 mmol l^{-1} ammonium tartrate (pH 2.0) mixed solution
Flow rate: 0.75 ml min^{-1}
Injection volume: 10 μl
Column temperature: room temperature

2.3. Procedure

2.3.1. Preparation of mixed standard solution

A mixed standard solution were prepared by diluting stock solutions of As and Sb species.

2.3.2. Composition of eluent

An eluent (1 l) was composed of 10 mM 1-butanesulfonic acid, 4 mM malonic acid, 4 mM tetramethylammonium hydroxide, 0.1 (v/v)% methanol, and 20 mM ammonium tartrate. The malonic acid was used for buffer, and 1-butanesulfonic acid and tetramethylammonium hydroxide was used for ion pair reagent.

2.3.3. Sample preparation

A hot spring water marketed as a drinking water was filtered with membrane filter (pore size, 0.45 μm) and then was determined. A fish sample solution was prepared as follows: a 0.5 g of fish sample was placed into a 50 ml centrifugal tube, and then a 10.0 ml of ultra-pure water was added. After being placed in an ultrasonication (W-113MK,) for 1 h, the solution was filtered with membrane filter. The species of As and Sb in the obtained solution were separated and measured by HPLC–ICP-MS.

3. Results and discussion

3.1. Selection of column

Column plays an important role in separating the species of As and Sb. Therefore, it is of importance to select a column of excellent ability of separation. In this study, a C30, a C18 and an anion exchange column were used to perform the investigation.

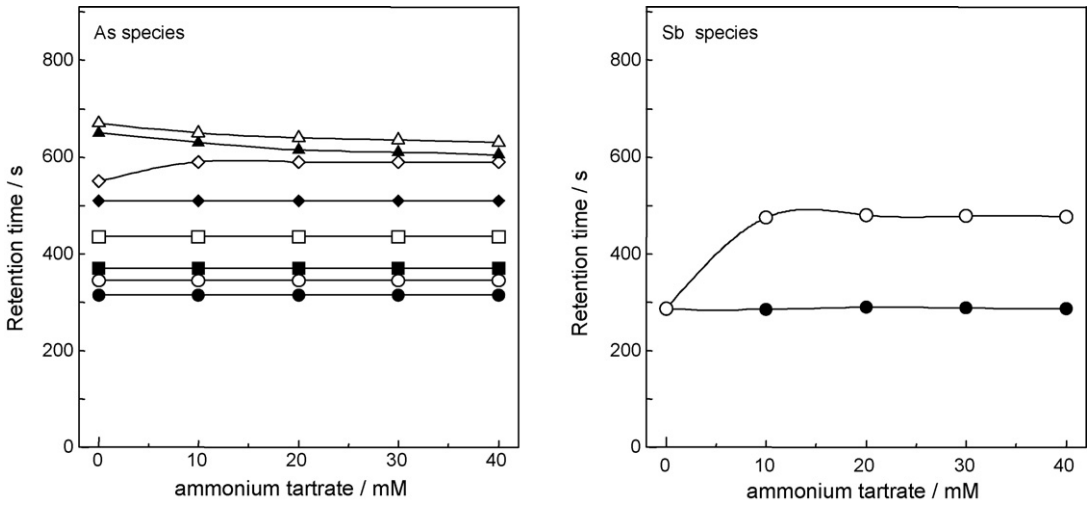

Fig. 1. Effect of the concentration of ammonium tartrate. As species: (◯) As(III), (●) As(V), (■) MMAA, (□) DMAA, (□) AB, (□) TMAO, (▲) TeMA, (□) AsC; Sb species: (◯) Sb(III), (●) Sb(V). Concentration of each species: 20 ng ml^{-1}.

The inorganic species of As(III), As(V), Sb(III), and Sb(V) were separated with the anion exchange column using mobile phase (50 mM ammonium tartrate, pH 2.5 by sulfuric acid). However, under above conditions, broad half-width and small signal intensity were observed for the chromatograms, thus it was difficult to separate the species of organic As (TMAO, TeMA and AsC) by the column.

We tried to simultaneously separate the species of As and Sb by the mentioned reversed phase columns with the eluent reported by Kamidate et al. [10] (10 mM 1-butanesulfonic acid/4 mM malonic acid/4 mM tetramethylammonium hydroxide/0.1 (v/v)% methanol). For the two columns, eight kinds of As species were simultaneously separated within the retention time of 700 and 800 s, but it was difficult in separating the species of Sb. In addition, the separation of TMAO and TeMA was incomplete with the C18 column. Compared with a C18 column, a C30 column was more suitable for being used in separating eight kinds of As species. The subsequent investigations were performed with the C30 column.

3.2. Simultaneous separation of As and Sb species

The above investigations show that a C30 column was proper to separate As species. Thus, it is necessary to investigate the composition of eluent so as to apply to Sb species by the C30 column.

3.2.1. Effect of concentration of chelating agent

The speciation analysis of Sb was examined by using the same eluent as that of As. As discussed above, the speciation analysis of Sb was difficult when the eluent was utilized. Chelating agents are often used in eluent to form complex, and make the species of Sb retained in the C30 column. Tartaric acid [11], diammonium citrate, and citric acid [12] have been reported as chelating agents. Different from the above chelating agents, an ammonium tartrate was used in the study. The effect of the concentration of the ammonium tartrate was investigated. The obtained results (Fig. 1) show that two species of Sb were separated using the new eluent containing the ammonium tartrate. Moreover, with increasing the concentration of the ammonium tartrate, retention time decreased for TeMA and AsC, but retention time increased for TMAO. In addition, TeMA, TMAO and AsC could not be separated completely over a 30 mM of the ammonium tartrate. Therefore, a 20 mM of the ammonium tartrate was applied in the subsequent experiments.

3.2.2. Effect of pH

In order to simultaneously separate the species of As and Sb, the effect of pH in eluent on retention time was investigated. As known, Sb(III) and Sb(V) are strongly hydrolyzed, and easily form precipitate. When hydrochloric acid, nitric acid and acetic acid were used to adjust pH, precipitate occurred in the new eluent. However, there was not the phenomenon when sulfuric acid was used. Therefore, sulfuric acid was used to adjust the pH of the new eluent. When the pH was changed in the range 2.0–8.0, retention time for the species of As and Sb was examined in the column. The obtained results (Fig. 2) indicate that retention time was smallness dependence of pH for As(III) and As(V); but for AB and TMAO, the effect of pH was large. In addition, the retention time of TeMA and AsC increased with increasing the pH, but it decreased for other species. On the other hand, the retention time of Sb(III) was unaltered when the pH was changed; the retention time of Sb(V) decreased with increasing the pH. Therefore, considering simultaneous separation for each species of As and Sb and the application of real samples, pH 2.0 is adjusted for the subsequent work.

3.2.3. Effect of methanol concentration

The separation of hydrophobic species is influenced by solvents such as methanol, ethanol and acetonitrile in eluent with HPLC. In addition, methanol has an impact on the stability of plasma during determination with ICP-MS. The effect of the concentration of methanol was investigated. Fig. 3 shows that the retention time of inorganic species of As and Sb were not

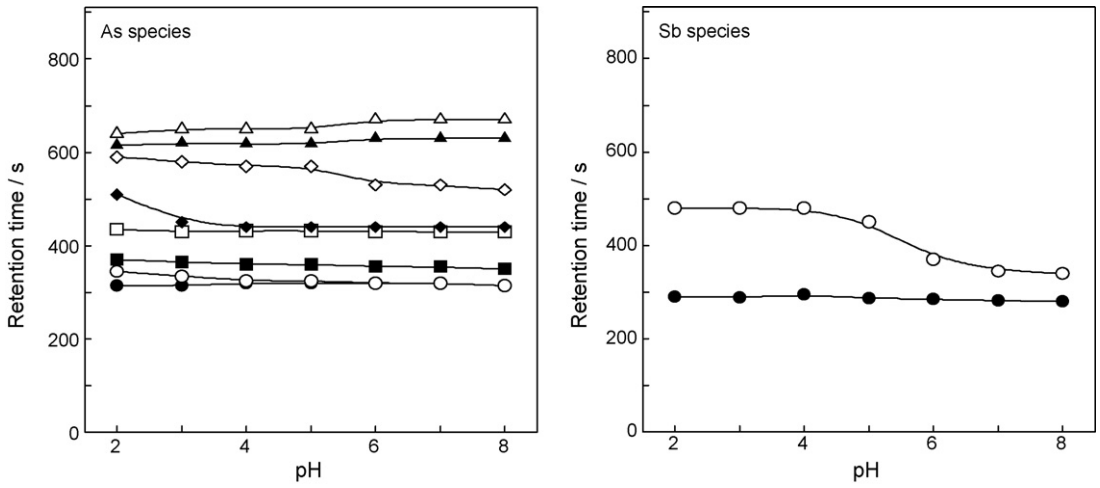

Fig. 2. Effect of pH on retention time. As species: (◯) As(III), (●) As(V), (■) MMAA, (□) DMAA, (□) AB, (□) TMAO, (▲) TeMA, (□) AsC; Sb species: (◯) Sb(III), (●) Sb(V). Concentration of each species: 20 ng ml^{-1}.

influenced with increasing the concentration of methanol. For the species of the organic As, retention time decreased with increasing the concentration of methanol due to the effect of hydrophobic interaction of the methanol. Therefore, the concentration of methanol in the new eluent was chosen at 0.1 (v/v)%.

3.2.4. Chromatograms for As and Sb species and precision

A mixed standard solution (20 ng ml^{-1} for each species) was applied under the above optimum operating conditions, and chromatograms for the species of As and Sb were shown in Fig. 4. The results indicate that Sb(III), Sb(V) and eight kinds of As species were simultaneously separated within 700 s.

The calibration curves for eight kinds of As species were linear in concentration range 0.2–400 ng ml^{-1}; The calibration curves for Sb species were linear in concentration range 0.5–200 ng ml^{-1}. Limit of detection (LOD) were about 0.2 for As and 0.5 ng ml^{-1} for Sb, respectively, with a 10 μl of injection volume. The R.S.D.% were less than 2 and 3% for As and Sb when six replicated measurements with a sample spiked 10 ng ml^{-1} of each species, respectively. Due to the absence of the proper certified reference material containing the above As and Sb species, the evaluation of the validation of the method for simultaneous speciation of As, and Sb is difficult. NMIJ CRM 7901-a (Arsenobetaine solution, National Metrology Institute of Japan, Tsukuba, Japan) and NMIJ CRM 7402-a (Trace Elements, Arsenobetaine and Methylmercury in Cod Fish Tissue) were used to determine the concentration of arsenobetaine. The determined value (32.4 ± 0.5 mg kg^{-1}) of arsenobetaine for CRM 7402-a by the present method was in good agreement with the certified value (33.1 ± 1.5 mg kg^{-1}).

3.3. Application for real samples

The proposed method was applied to a hot spring water and a fish sample solution. The species of As and Sb in real samples were identified by the obtained retention time of each species in mixed standard solution. Fig. 5 indicates that As(III) and As(V) were found in the hot spring water with the present method, but the other species of As and Sb could not be detected. Fig. 6 shows that AB in the fish sample solution was found.

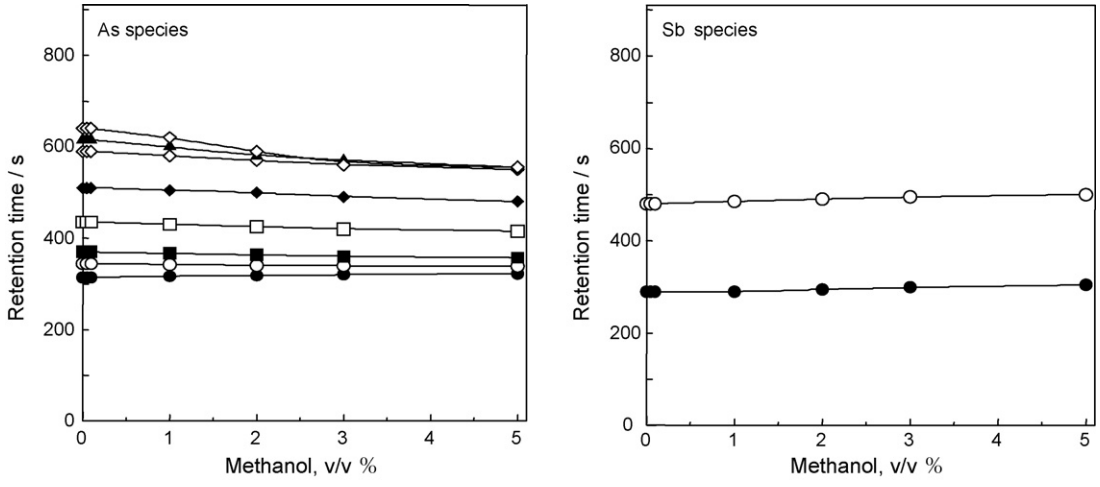

Fig. 3. Effect of concentration of methanol. As species: (◯) As(III), (●) As(V), (■) MMAA, (□) DMAA, (□) AB, (□) TMAO, (▲) TeMA, (□) AsC; Sb species: (◯) Sb(III), (●) Sb(V). Concentration of each species: 20 ng ml^{-1}.

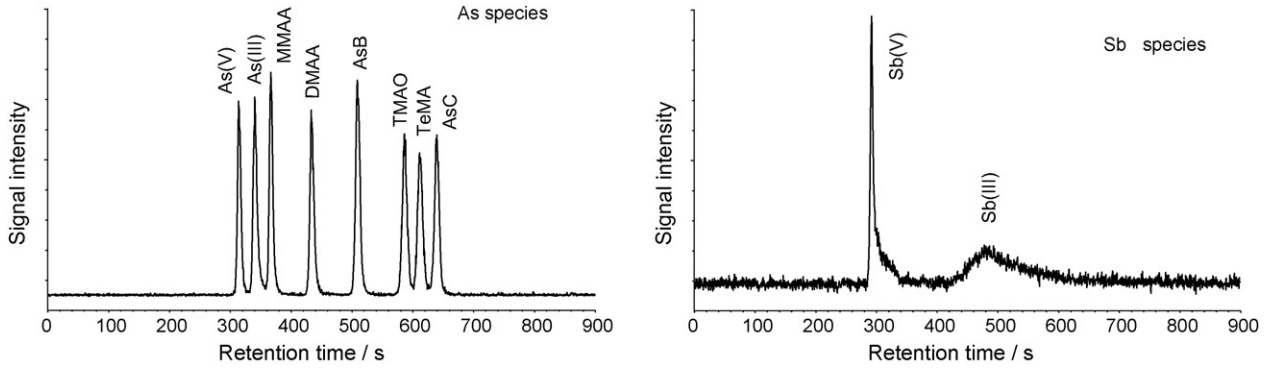

Fig. 4. Chromatograms of As and Sb species by HPLC–ICP-MS. Chromatograms of As and Sb species in standard solution by separation on C30 reversed phase column. Concentration of each species: 20 ng ml^{-1}, flow rate: 0.75 ml min^{-1}, sample loop size: 10 μl.

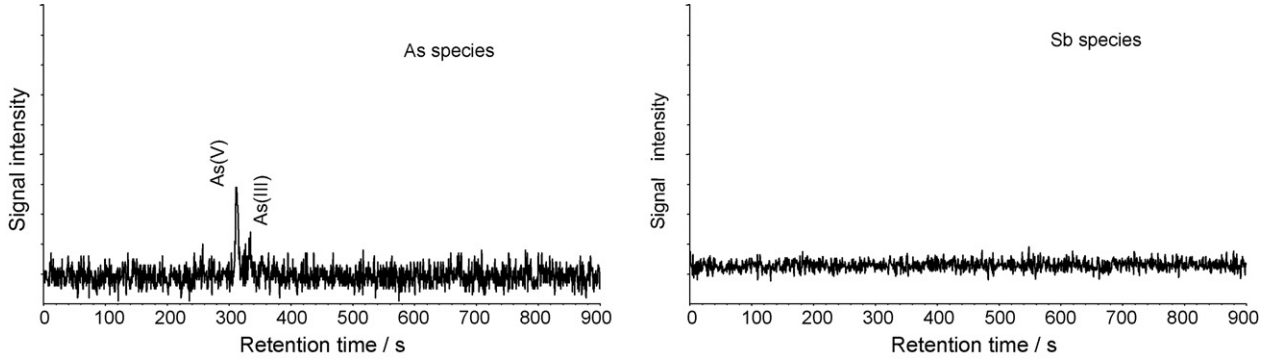

Fig. 5. Chromatograms of As and Sb species in hot spring water sample. Column: C30 reversed phase column, flow rate: 0.75 ml min^{-1}, sample loop size: 10 μl.

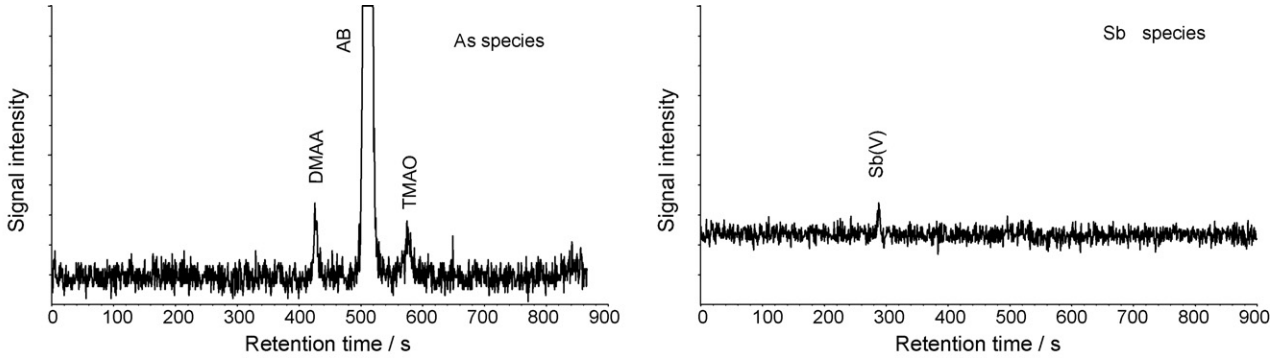

Fig. 6. Chromatograms of leachability As and Sb species in fish sample. Extract: water, column: C30 reversed phase column, flow rate: 0.75 ml min^{-1}, sample loop size: 10 μl.

The DMAA, TMAO and Sb(V) were estimated according to signal intensity at 420, 580 and 280 s, respectively. However, because the determined values of DMAA, TMAO and Sb(V) were near limit of detection, poor reproducibility was found. Those quantitative analysis results were shown in Table 2. The proposed method can be applied to similar matrix samples.

4. Conclusion

A method for simultaneous speciation of As and Sb species with HPLC–ICP-MS was established. The composition of the eluent was optimized and discussed in detail. It was possible to simultaneously separate eight kinds of As species, Sb(III) and

Table 2
Analytical results for real samples by the proposed method

	As(V)	As(III)	DMAA	AB	TMAO	Sb(III)	Sb(V)
Hot spring water (ng ml^{-1})	1.6 ± 0.3	0.4 ± 0.1	–	–	–	–	–
Fish (mg kg^{-1})	–	–	0.004 ± 0.002	18.3 ± 0.5	0.004 ± 0.002	_	0.010 ± 0.004

n = 6, average ± S.D., –: not detected.

Sb(V) with a C30 column using the new eluent. The proposed method was applied for a hot spring water and a fish sample. In the course of the studies, the simultaneous quantitative analysis of As and Sb species will then be studied.

References

[1] H. Tao, Bunseki Kagaku 46 (1997) 239.
[2] T. Sakai, Y. Date, Y. Inoue, Biomed. Res. Trace Elem. 12 (2001) 33.
[3] K.A. Francesconi, D. Kuehnelt, Analyst 129 (2004) 373.
[4] A.L. Rosen, G.M. Hiefije, Spectrochim. Acta Part B 59 (2004) 135.
[5] T. Guerin, A. Astruc, M. Astruc, Talanta 50 (1999) 1.
[6] T. Guerin, M. Astruc, A. Batel, M. Borsier, Talanta 44 (1997) 2201.
[7] X.C. Le, X.-F. Li, V. Lai, M. Ma, S. Yalcin, J. Feldmann, Spectrochim. Acta Part B 53 (1998) 899.
[8] Y. Martínez-Bravo, A.F. Roig-Navarro, F.J. Lóez, F. Hernández, J. Chromatogr. A 926 (2001) 265.
[9] Z. Zhang, S. Chen, H. Yu, M. Sun, W. Liu, Anal. Chim. Acta 513 (2004) 417.
[10] Y. Kamidate, M. Yamada, Y. Furusho, T. Kuroiwa, T. Kaise, K. Fujiwara, Biomed. Res. Trace Elem. 11 (2000) 443.
[11] M. Krachler, H. Emons, J. Anal. At. Spectrom. 16 (2001) 20.
[12] J. Zheng, A. Iijima, N. Furuta:, J. Anal. At. Spectrom. 16 (2001) 812.

Available online at www.sciencedirect.com
ScienceDirect
Talanta 73 (2007) 157–165
Talanta
www.elsevier.com/locate/talanta

Mechanism of sensitivity difference between trivalent inorganic As species [As(III)] and pentavalent species [As(V)] with inductively coupled plasma spectrometry

Tomohiro Narukawa *, Takayoshi Kuroiwa, Koichi Chiba

Inorganic Analytical Chemistry Division, National Metrology Institute of Japan (NMIJ), National Institute of Advanced Industrial Science and Technology (AIST), Tsukuba Central 3, 1-1-1 Umezono, Tsukuba, Ibaraki, 305-8563, Japan

Received 14 February 2007; received in revised form 14 March 2007; accepted 14 March 2007
Available online 23 March 2007

Abstract

The pentavalent inorganic arsenic (As) species [As(V)] is found to be 4% more sensitive than the trivalent species [As(III)] with inductively coupled plasma mass spectrometry (ICP-MS) and inductively coupled plasma optical emission spectrometry (ICP-OES). Although there was no sensitivity difference between As(III) and As(V) with atomic absorption spectrometry (AAS), electrothermal atomization atomic absorption spectrometry (ETAAS), X-ray fluorescence (XRF), and neutron activation analysis (NAA). The calibration solutions of As(III) and As(V) were gravimetrically prepared from the unique mother standard solution of JCSS As standard solution which is certified by Japan Calibration Service System (JCSS). Since it is essential to use the calibration solutions with exactly the same concentration of As in order to accurately compare the sensitivities between As(III) and As(V). The mechanisms of this sensitivity difference between them were investigated by ICP-MS and ICP-OES, and it elucidated that the formation rates of hydride polyatomic species of As were definitively different between As(III) and As(V) species in the plasma. This phenomenon directly affected their sensitivities with ICP-MS and ICP-OES.

Keywords: Arsenic species; Analytical sensitivity; ICP-MS; ICP-OES; Hydride polyatomic species

1. Introduction

Arsenic (As) is widely distributed in the natural environment such as ground water, river water, and sediment and in organisms such as seaweeds and fish tissues. It is well known that As is a toxic element [1–4]. The major chemical forms of As are arsenite [As(III)] and arsenate [As(V)] in environment, although organoarsenic species such as arsenobetaine, methylated As compounds, and arsenosuger compounds are mainly found in organisms. Many countries set maximum permissible concentration values for As in drinking water and food. The World Health Organization (WHO) is currently conducting the guidelines for drinking water and environmental water [5].

There are great demands to determine not only the total concentration of As in environment but also the concentration of individual chemical forms of As compounds for scientific interests as well as for implementing regulations. In particular, the speciation determination of As(III) and As(V) is stringently required in order to measure the most toxic As compound, As(III), concentration in samples. Until now, many analytical techniques have been reported for the determination of the total concentration of As as well as the speciation determination of individual arsenic species [6]. The atomic spectrometric methods such as electrothermal atomization atomic absorption spectrometry (ETAAS), inductively coupled plasma optical emission spectrometry (ICP-OES) and inductively coupled plasma mass spectrometry (ICP-MS) are widely employed for the determination of trace amount of As because of their high sensitivity, good precision and wide availability. Furthermore, combinations with hydride generation (HG), gas chromatography (GC) and/or liquid chromatography (LC) can be applied for speciation determination of arsenic compounds.

Creed et al. reported that the As(III) response was suppressed approximately 20% relative to As(V) standard when they were determined by ICP-OES with an ultrasonic nebulizer (USN) [7]. No response deference was observed by ICP-OES with

* Corresponding author. Tel.: +81 29 861 6889; fax: +81 29 861 6889.
E-mail address: tomohiro-narukawa@aist.go.jp (T. Narukawa).

0039-9140/$ – see front matter © 2007 Elsevier B.V. All rights reserved.
doi:10.1016/j.talanta.2007.03.021

a pneumatic nebulizer. They concluded that the response deference was caused by oxidization of As(III) to As(V) during the ultrasonic nebulization and desolvation process. Yu et al. reported that As(V) was about 8% more sensitive than As(III) with ICP-OES installed even with a pneumatic nebulizer [8]. The difference in sensitivity of As in atomic spectrometric analysis has been reported by other groups, too [9–12]. They also concluded that the phenomenon occurs in the injection and transportation systems and named it "desolvation effect", "speciation effect" or "transportation effect". Although they did not explain the mechanism resulting in the sensitivity deference between As(III) and As(V), they suggested that the sensitivity deference phenomenon occurred before the atomization step, that is, before introduction into plasma.

The authors have studied on As analysis in environmental and biological samples and have also been developing analytical techniques for total determination of As as well as speciation determination of As species [13–15]. The authors reported the sensitivity deference between As(III) and As(V) with ICP-OES and ICP-MS but not with ETAAS in 1999 [16], and informed their excitation and ionization behaviors in plasma in 2005 [17]. The calibration solutions with the exactly correct concentrations of both As(III) and As(V) are essential to discuss the sensitivity deference, so it is very important to prepare the standard solutions whose oxidation state is guaranteed. The JCSS As standard solution, which is traceable to the national standard, allows us to establish traceability of the As concentration in measurement. The concentration is characterized by titrimetry, which is one of the primary methods. Almost all the As atoms are in the trivalent oxidation state As(III) in JCSS standard, since the standard solution is made from highly pure As_2O_3, but JCSS does not guarantee the oxidation state of As in their standard. Thus, the authors always validated the content level of As(V) in JCSS standard solution before use, and decided that it was low enough not to effect the experiment. On the contrary, there is no commercially available As(V) base standard solution. Standard solutions of As(V) have usually been prepared by using Na_2HAsO_4 as a source material, however, evaluation of its purity and moisture content has rarely been carried out. Therefore, the authors used the JCSS As standard solution as a unique mother standard solution for preparation of both As(III) and As(V) calibration solutions, where As(V) standard solution was prepared by oxidizing the JCSS standard.

In this work, mechanism of sensitivity difference between As(III) and As(V) with ICP-OES and ICP-MS was investigated using the As(III) and As(V) calibration solutions prepared from the unique mother source of the standard solution. It was elucidated that the formation rates of hydride polyatomic species of As were definitively different between As(III) and As(V) species in the plasma. We propose a mechanism based on the oxidation states of atoms of this phenomenon, and define it as "the Incoherent Molecular Formation (IMF) effect".

2. Experiment

2.1. Apparatus

An ICP-OES Optima 4300DV (Perkin-Elmer Co. Ltd., Yokohama, Japan) equipped with a concentric nebulizer and a cyclonic spray chamber was used. An ICP-MS 7500c (Agilent Co. Ltd., Tokyo, Japan) and an ICP-high resolution MS Quest Element 2 (Thermo Co. Ltd., Yokohama, Japan) equipped with a micromist nebulizer and a Scott spray chamber, and an ICP-MS ELAN DRC II (Perkin-Elmer Co. Ltd.) equipped with a micromist nebulizer and a cyclonic spray chamber were also used. Operating conditions for ICP-OES and ICP-MS are summarized in Table 1.

Table 1
Instrument conditions of ICP-OES, ICP-MS and GFAAS

Plasma	ICP-OES	ICP-MS	
Conditions			
Incident Rf power	1.3–1.5	1.3–1.5	kW
Outer gas flow rate	Ar 15	Ar 15	$l\,min^{-1}$
Intermediate gas flow rate	Ar 0.2	Ar 0.9	$l\,min^{-1}$
Carrier gas flow rate	Ar 0.8	Ar 0.8	$l\,min^{-1}$
Make-up or shear gas	N_2 18	Ar 0.4	$l\,min^{-1}$
Sampling conditions			
Nebulizaer	Concentric (glass)	Micro mist (glass or PFA)	
Spray chamber	Cyclonic	Scott or cyclonic	
Sample injection	Peristaltic pumping	Peristaltic pumping natural aspirate	
GFAAS			
Wavelength	As 193.7	nm	
Lump current	380	mA	
Lump	EDL		
Slit width	0.5	nm	
Dry	130	°C	
Pyrolysis	1000	°C	
Atomize	2400	°C	
Chemical modifier	100 ppm Pd + 50 ppm $Mg(NO_3)_2$		

The hyphenated system of liquid chromatography and ICP-MS 7500c (LC–ICP-MS) was used in order to determine the chemical species of As(III) and As(V) individually. The liquid chromatographic system consisted of a CAPCELL PAC MG S3 column (length 150 mm × ID 4.6 mm, Shiseido Co. Ltd., Tokyo, Japan), metal-free six-port injection valves (Sanuki Co. Ltd., Tokyo, Japan) with a PEEK 10 μl sample loop, and a MODEL325DI instrument with a CH-2-D HPLC pump (Chemco Scientific, Osaka, Japan). It was connected to the nebulizer of ICP-MS with PEEK tubes. A metal-free syringe with a PEEK needle (Ito Co. Ltd., Shizuoka, Japan) was used for sample injection.

An AAnalyst800 atomic absorption spectrometer (AAS, Perkin-Elmer Co. Ltd.) equipped with an EDL lamp was used for flame AAS. The AAS was equipped with a Transverse Heated Graphite Atomizer (THGA) to heat the graphite tube and a Zeeman background correction system for graphite furnace AAS (GFAAS). The instrument operating parameters are also shown in Table 1.

2.2. Reagents

The Japan Calibration Service System (JCSS) As standard solution was used as the source standard solution for the preparation of all calibration solutions. Its elemental concentration is traceable to the national standard (SI unit) and allows us to establish traceability of the As concentration in measurement. 1000 mg l^{-1} of As JCSS standard solution was purchased from Kanto Chemical Industries, Ltd. It is made from highly pure As_2O_3.

The mobile phase for liquid chromatography contained 10 mmol l^{-1} sodium butanesulfonate, 4 mmol l^{-1} tetramethylammonium hydroxide, 4 mmol l^{-1} malonic acid, and 0.05% (v/v) methanol (pH 3.0).

All the acids used were of ultra-pure grade (Kanto). Ultrapure water purified with a Milli Q-Labo filter (Nippon Millipore, Ltd., Tokyo, Japan) was used throughout the experiment.

2.3. Procedures

2.3.1. Preparation of As(III) calibration solution

The JCSS As standard solution (As: 1005 mg l^{-1} ± 0.6%) was diluted to prepare 100 mg kg^{-1} of the As(III) standard solution with water. The As(III) standard solution was gravimetrically diluted to prepare As(III) calibration solutions with water, 1% HNO_3 or 1% HCl.

2.3.2. Preparation of As(V) calibration solution

There is no As(V) base standard solution available that is certified to the concentration of As(V). Five gram of 1005 mg l^{-1} JCSS As standard solution [As(III)] was precisely weighed and poured into a Teflon vessel, to which 3 g of HNO_3 was added. The vessel was placed on a hot plate (plate surface temperature: 140 °C) and the sample solution was evaporated to dryness. The resulting residue was dissolved in water and made up to 50 g. This solution was used as the 100 mg kg^{-1} As(V) standard solution. In addition, blank tests of the preparation procedure were performed using pure water instead of JCSS As standard solution under the same conditions, and no As contamination was detected. The As(V) standard solution was diluted to prepare As(V) calibration solutions with water, 1% HNO_3 or 1% HCl.

2.3.3. Preparation of calibration solution for each measurement method

The calibration solutions for ICP-OES were first prepared from the As(III) and As(V) standard solutions. Then, those for ICP-MS and GFAAS were prepared by further dilution.

Yttrium (Y), Re, Rh, Tl and Yb were added to the calibration solutions for ICP-OES and ICP-MS as internal standard elements, which were monitored in order to compensate fluctuation of the signal intensities or counts of As. For all the preparation in this work, a gravimetric preparation method was employed.

Before the calibration solutions were used for measurements, all the calibration solutions were analyzed by LC–ICP-MS in order to confirm the oxidation states [15,18,19].

3. Results and discussion

3.1. The chemical forms of As and their stability in the standard solutions

Speciation for As(III) and As(V) in the standard solutions were carried out using LC–ICP-MS and the results are shown in Fig. 1. The main chemical form detected in the JCSS As standard solution was As(III), and approximately 0.5% of As(V) was found. The amount of As(V) in JCSS standard solution is negligibly small. Only As(V) was detected in the As(V) standard solution, which was prepared by oxidization of JCSS As solution with HNO_3. Every As(III) and As(V) calibration solution was also analyzed by LC–ICP-MS to confirm the oxidation states. It was found that the oxidation states of As in the calibration solutions did not change through the dilution process. The oxidation states of As in the calibration solutions are stable for at least 2 weeks even at room temperature.

3.2. Measurement of As(III) and As(V) by ICP-OES

The As(III) and As(V) calibration solutions were measured by ICP-OES at the wavelengths of 188.98 nm and 193.70 nm. Yttrium (Y), Re, Rh, Tl, and Yb were used as internal standard elements in this measurement. The analytical results are shown in Fig. 2. The As(V) is always more sensitive than As(III). Moreover, there is no analytical wavelength dependency for As measurement by ICP-OES, even when the different internal standard elements were used.

As a result, Y was used as an internal standard element throughout the following experiment.

3.2.1. Influence of matrix (acid of solution) on measurement of As(III) and As(V)

The effect of the matrix (acid of solution) on the As sensitivity was investigated. The calibration curves for As(III) and As(V) were made with calibration solutions which were prepared by diluting the standard solutions with water, 1%HNO_3

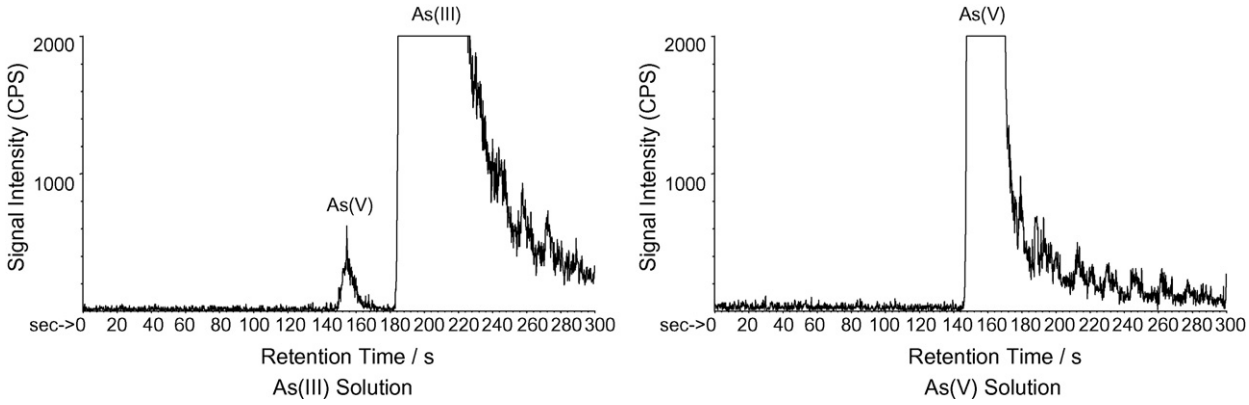

Fig. 1. Chemical forms of arsenic in As(III) and As(V) standard solution by LC–ICP-MS. Concentration of As, 20 mg kg^{-1}; Sample injection volume, 10 μl.

and 1%HCl. The analytical results are shown in Fig. 3. In all the cases, the sensitivities of As(V) were greater than those for As(III), and sensitivity differences were approximately 4%, 3% and 11% for water, 1% HNO_3 and 1% HCl solutions, respectively. The greater effect of HCl solution is probably due to partial As–Cl_3 formation [20]. When the analytical uncertainty related to the dilution of solutions and the measurements were estimated, the extended uncertainty ($k = 2$) was 0.6% [21]. The determination results were compared to the concentration of JCSS standard solution, so the concentration of As(V) standard solution was then calculated according to the calibration curves obtained with As(III) calibration solutions. As can be seen in Fig. 4, the calculated concentrations of As(V) in water solution were about 4% greater than that of the JCSS solution. The sensitivity differences between As(III) and As(V) are considerably greater than the analytical uncertainties, thus the differences are significant.

3.2.2. *Effect of plasma operating conditions*

The plasma operating conditions such as RF power (1300–1500 W), plasma gas flow rate (10–20 l min^{-1}) and carrier gas flow rate (0.3–1.0 l min^{-1}) were varied and the signal intensities of As(III) and As(V) were measured. The sensitivities of As(V) are still greater than those of As(III) under all the conditions examined, although the observed signal intensities changed according to the analytical conditions. The ICP-OES measurements were carried out through the axial and the radial observations of the plasma. The difference in sensitivity between As(III) and As(V) was recorded in both cases. When the radial observation position was changed from 5 to 25 mm above the coil, the sensitivity difference was measured at every setting.

The effects of sample introduction processes were investigated using both a peristaltic pump and a natural aspiration device. In addition, Scott and cyclonic type spray chambers were combined with both of them. As a result, the analytical sensitivity of As(V) is always greater than that of As(III) regardless of sample introduction systems used. These experimental results indicated that the sample introduction system including nebulization and transportation did not cause the sensitivity difference between As(III) and As(V).

3.3. *Measurement of As(III) and As(V) by ICP-MS/calibration curves for As(III) and As(V) solutions*

Calibration curves of As(III) and As(V) are shown in Fig. 5. The calibration solutions were prepared by using water and 1%HNO_3 solutions. HCl solution was not used since it causes the severe interference of $^{40}Ar^{35}Cl^{+}$ on As measurement at *m/z* 75.

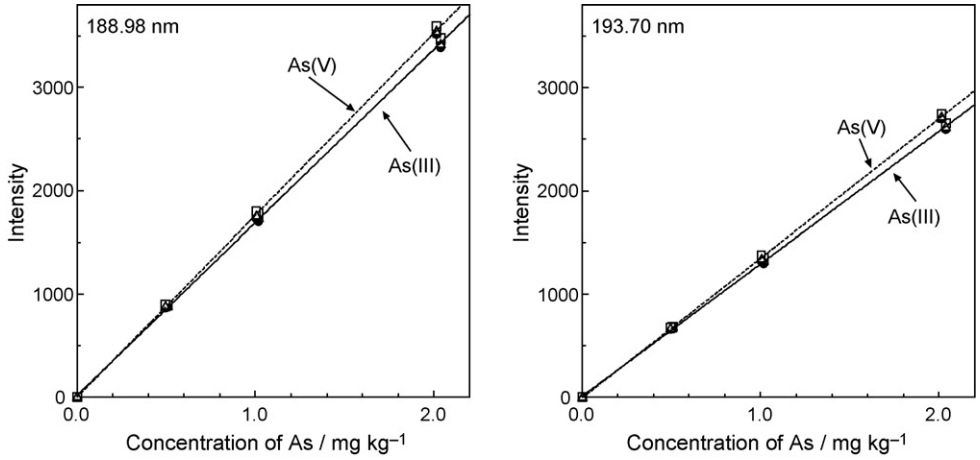

Fig. 2. Calibration curves of As(III) and As(V) by ICP-OES. Wavelength 188.98 nm (Left) and 193.70 nm (Right). Internal standard element: (●) Non, (◯) Re, (■) Rh, (□) Tl, (▲) Y, (□) Yb. The replicate error bars on measurements are within the plots.

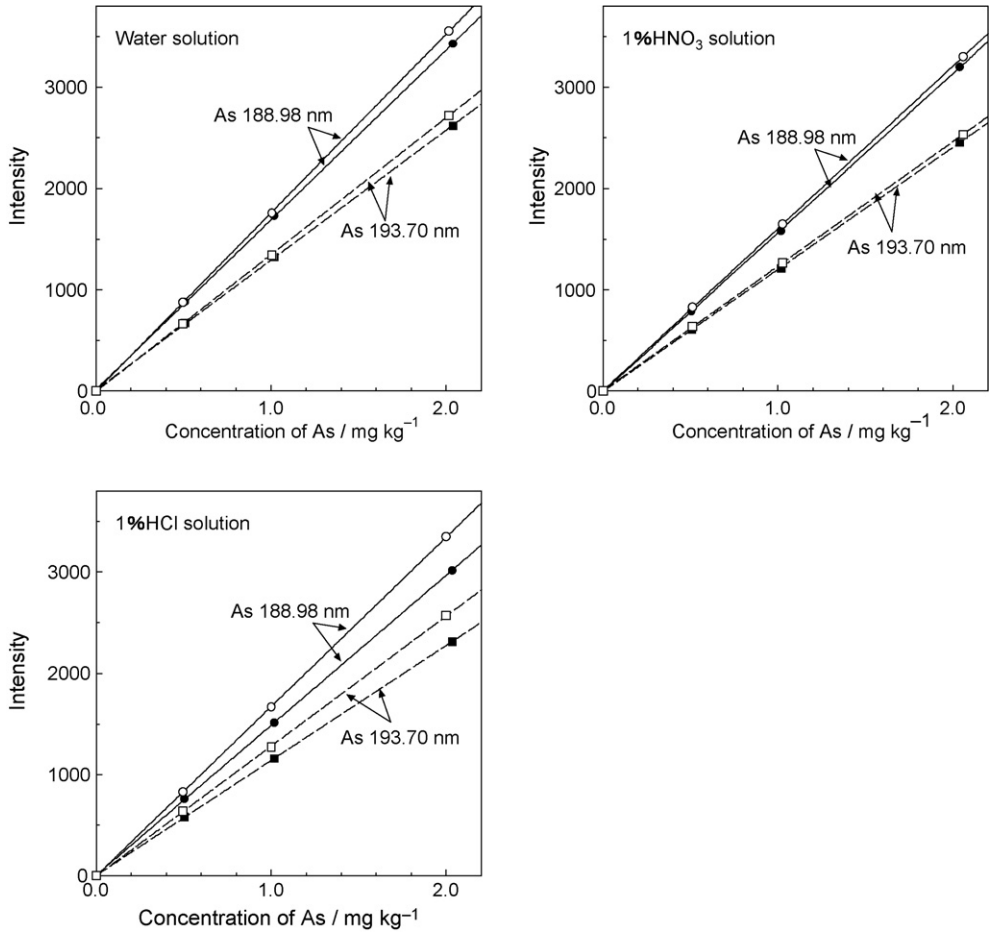

Fig. 3. Effect of matrix (acid solution) on As(III) and As(V) sensitivities by ICP-OES. (●), (■) As(III) solution; (◯), (□) As(V) solution, internal standard element Y. The replicate error bars on measurements are within the plots.

The As(V) solution was still approximately 4% more sensitive than the As(III) solution in all the cases. Analytical sensitivity of both As(III) and As(V) by ICP-MS was investigated under the various operating conditions such as RF power (1300–1500 W), plasma gas flow rate (10–20 l min^{-1}) and carrier gas flow rate (0.3–1.0 l min^{-1}) were varied. The analytical sensitivity of As(V) is always higher than that of As(III) under every experimental condition examined, although the observed signal counts (CPS) changed according to the analytical conditions. Moreover, the effect of the ICP-MS operation mode such as normal conditions and non-gas mode, the types of nebulizers (including material: glass and PFA), the types of spray chambers (Scott and cyclonic types), and materials of sampling cone (Pt and Ni) were investigated in their various combinations. The analytical sensitivity difference between As(V) and As(III) always remained under the all the measurement conditions examined, although the observed signal counts differed according to the instruments used.

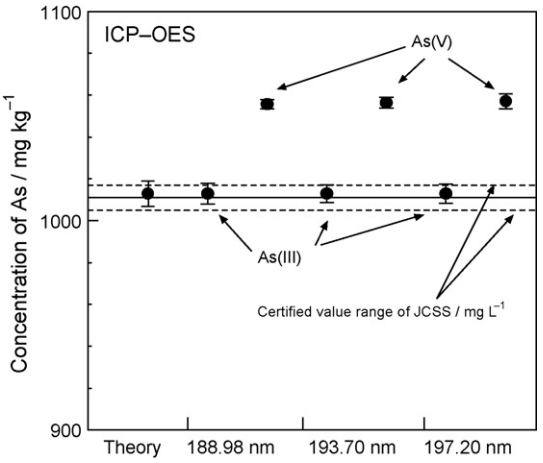

Fig. 4. Sensitivity difference between As(III) and As(V) by ICP-OES. The results were obtained using the diluting standard solution with water.

These observations were very similar to those observed in ICP-OES although the detection principles are quite different. Therefore, these results suggest that the analytical sensitivity difference between As(III) and As(V) by ICP measurements neither depends on the instrumental detection system nor on the sample injection and transport system.

3.4. Measurement of As(III) and As(V) by NAA, EDXRF and AAS

In order to investigate the effect of oxidation states of As on analytical sensitivity in other spectrometry, As(III) and

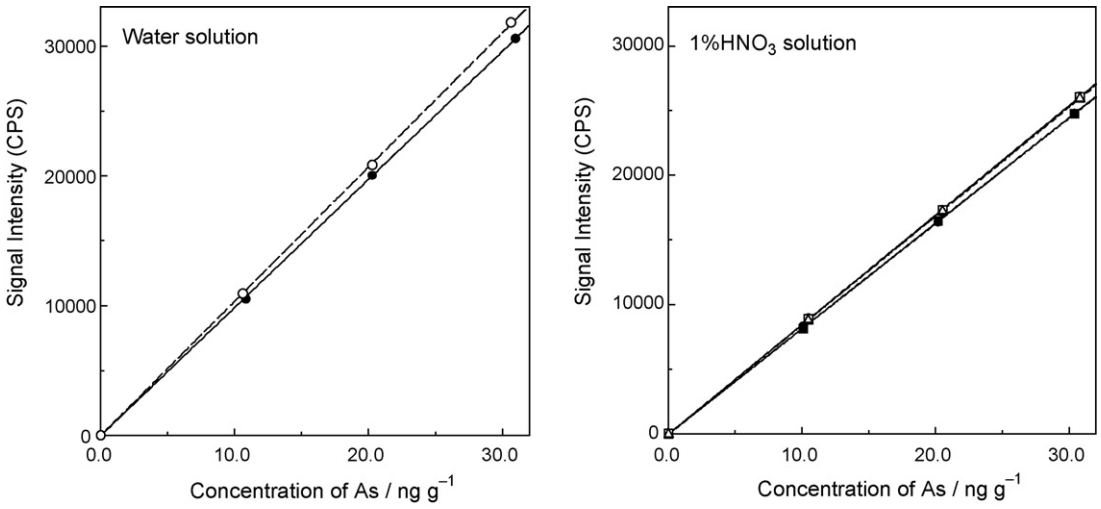

Fig. 5. Calibration curve of As(III) and As(V) by ICP-MS. (●), (■), (▲) As(III) solution, (◯), (□), (□) As(V) solution, $m/z = 75$. Internal standard element: (●), (◯) Non; (■), (□) Y; (▲) (□) Rh. The replicate error bars on measurements are within the plots.

As(V) calibration solutions were measured by neutron activation analysis (NAA), energy dispersive X-ray fluorescent analysis (EDXRF) and AAS. The 20 mg kg^{-1} As(III) and As(V) standard solutions were determined by NAA and EDXRF. A drop of the As(III) and As(V) standard solutions was placed onto a filter paper, and they were put into polyethylene bags. Neutron irradiation was carried out on the prepared samples using JRR-3M PN-1 (Japan Atomic Energy Agency research reactor, Neutron flux: 5.2×10^{17} m^{-2} s^{-1}) for 20 min. After, gamma ray of ^{76}As (559 keV) was measured using Ge semiconductor detector. For EDXRF, the standard solutions were poured into plastic vessels, which equipped with prolene film (Chemplex Industries Inc., FL, USA), and the vessels were set in the EDXRF instrument and As spectrum was measured.

The results are shown in Table 2. The As concentrations of the As(III) and As(V) standard solutions measured by both NAA and EDXRF were in concordance with each other within the determination error. Also, they were in good agreement with the theoretical values calculated by the gravimetric preparation method.

No differences in analytical sensitivities between As(III) and As(V) have been reported for electrothermal atomic absorption spectrometry [13]. Thus, sensitivities of As(III) and As(V) standard solutions were measured by GFAAS and Flame AAS (FAAS). The results are shown in Fig. 6. The concentration of As(III) and As(V) were measured again in good agreement with each other, and they agree with the theoretical values within the uncertainty range of the JCSS standard solution. As a result, no sensitivity difference between As(III) and As(V) is observed in AAS measurement. Particularly in FAAS measurement which has a similar pneumatic sample nebulization system. These results suggest that a sample injection and transportation system does not cause the sensitivity difference observed between As(III) and As(V) in ICP methods.

Table 2
Results of arsenic concentration in As(III) and As(V) solution

	Theory[a] ± uncertainty (mg kg^{-1})	NAA[b] (mg kg^{-1})	EDXRF[b] (mg kg^{-1})
As(III)	20.42 ± 0.12	20.1 ± 1.2	20.6 ± 0.3
As(V)	20.41 ± 0.12	19.9 ± 1.2	20.5 ± 0.3

[a] Calculated gravimetrically prepared value.
[b] Mean ± S.D. ($n = 6$).

3.5. Mechanism of difference in sensitivity between As(III) and As(V) in ICP

The analytical sensitivities of As(III) and As(V) are significantly different, when As is measured by ICP-OES and ICP-MS. The results suggest that neither the excitation of outer shell electron of As nor the ionization of As atom to As$^+$ in the plasma does not occur to cause the sensitivity difference between As(III) and As(V) in ICP spectrometry.

In general, the ionization rate of As atom to As$^+$ ion in the plasma is approximately 49% [22], therefore, all As atoms were not ionized. The formation of polyatomic species can

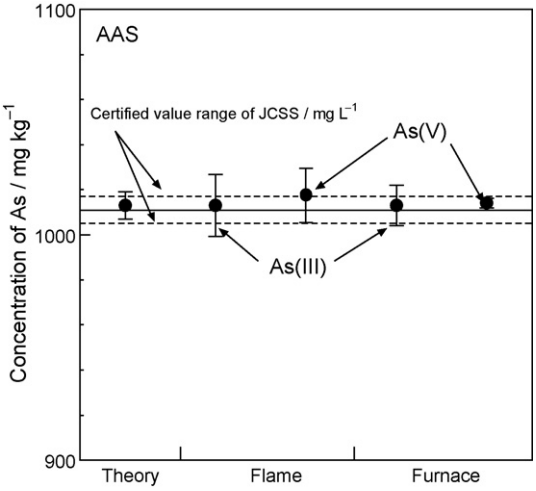

Fig. 6. Sensitivity difference between As(III) and As(V) by AAS. The results were obtained using the diluting standard solution with water.

Table 3
Signal intensities on the measurement by ICP-HRMS

Non gas	As(III)/counts (CPS)	As(V)/counts (CPS)	As(V)/As(III) ratio (%)
As	506000 (91%)	527000 (94%)	104
AsH	7500 (1.3%)	0 (0%)	0
AsH_3	40000 (7.2%)	30000 (5.3%)	75
AsO	420 (0.1%)	460 (0.1%)	110
AsO_3	670 (0.1%)	860 (0.2%)	128
Total counts	555000 (100%)	558000 (100%)	100.5

As: 20 ng g^{-1}.

affect the atomization efficiency in the plasma. Thus, a high-resolution ICP-MS was employed to investigate the polyatomic ions of As. The hydrogenated species (AsH_x^+: $x = 1$–5), the oxygenated species (AsO_x^+: $x = 1$–5), the As molecule (As–As), and the halogenated compounds [(ex) $AsCl_x^+$: $x = 1$–5] were all observed along with other possible molecular compounds. The calibration solutions diluted with water were used in the experiment, and the analytical results are shown in Table 3. In this experiment, ionic species of As^+ ($m/z = 75$), AsH^+ (76), AsH_3^+ (78), AsO^+ (91) and AsO_3^+ (123) were measured. The signal counts of As^+ for As(V) was 4% more than those of As(III), when the same concentration of As calibration solutions were measured. Moreover, there were large differences in signal counts of hydrogenated and oxygenated species between As(III) and As(V). For the As(III) solution, rather large amounts of AsH_x^+ ($x = 1$ or 3) was recorded and its signal intensity was corresponding to about 8% of the total counts. On the contrary, the signal counts of AsH_x^+ generated from the As(V) solution was lower than As(III), approximately 5% of the total.

The oxygenated species was also observed in the As(III) and As(V) calibration solutions, but their quantities were too low (less than 0.2% of total counts) to compare the formation efficiency between As(III) and As(V). Their contribution to sensitivity difference between the As(III) and As(V) solutions is negligible. The results indicate that As(III) and As(V) behave in different manner in the plasma even under the same analysis conditions.

When the ion signal counts at $m/z = 75$ (As^+), 76 (AsH^+), 78 (AsH_3^+), 91 (AsO^+) and 123 (AsO_3^+) for the As(III) and As(V) solutions were summed up respectively, their total signal counts (CPS) were almost equivalent with the relative difference of less than 1%, although the signal counts of $As(V)^+$ was still approximately 4% more than those of $As(III)^+$.

On the other hand, AsH_x^+ ($x = 2$, 4, 5) and AsO_x^+ ($x = 2$, 4, 5) were not observed in the measurements of both As(III) and As(V) calibration solutions, probably because the generation energies of H_2 and O_2 are low. The difference in behavior of halogenated arsenic compounds was not observed between the As(III) and As(V) solutions.

Thus, the differences in sensitivity between As(III) and As(V) by ICP spectrometry arose from differences in the formation efficiency of As atoms and the corresponding polyatomic species between As(III) and As(V) in the plasma, since the emission from excited As atoms was measured in ICP-OES and As^+ ionized from As atom was monitored at $m/z = 75$ in ICP-MS. We propose to call these kinds of phenomenon "the Incoherent Molecular Formation (IMF) effect" based on the oxidation states of atoms.

3.6. Measurement of As(III) and As(V) by collision/reaction cell ICP-MS

Collision and reaction cells have widely been used for precise determination of arsenic by ICP-MS [23–29], since they can

Table 4
Signal intensities on the measurement by ICP-collision-MS

	As(III)/counts (CPS)	As(V)/counts (CPS)	As(V)/As(III) ratio, %
He Gas			
As	15548 (93%)	16997 (95%)	109%
AsH	641 (2%)	0 (0%)	0%
AsH_3	9779 (38%)	8143 (32%)	83%
AsO	12 (0%)	13 (0%)	111%
AsO_3	28 (0%)	23 (0%)	84%
Total counts	16630	17848	107%
H_2 Gas			
As	3210 (77%)	3451 (79%)	108%
AsH	19 (0%)	7 (0%)	34%
AsH_3	914 (22%)	899 (20%)	98%
AsO	8 (0%)	8 (0%)	108%
AsO_3	28 (1%)	29 (1%)	104%
Total counts	4179	4393	105%

Table 5
Signal intensities on the measurement by ICP-DRC-MS

	As(III)/Counts (CPS)	As(V)/Counts (CPS)	As(V)/As(III) ratio, %
CH_4 Gas			
As	19394 (95%)	19521 (98%)	101%
AsH	633 (3%)	100 (1%)	16%
AsH_3	166 (1%)	119 (1%)	71%
AsO	142 (1%)	90 (0%)	64%
AsO_3	122 (1%)	105 (1%)	86%
Total counts	20457	19934	97%
NH_3 Gas			
As	11610 (77%)	11851 (87%)	102%
AsH	496 (3%)	164 (1%)	33%
AsH_3	1410 (9%)	455 (3%)	32%
AsO	722 (5%)	762 (6%)	106%
AsO_3	927 (6%)	400 (3%)	43%
Total counts	15166	13633	90%
O_2 Gas			
As	8708 (14%)	9660 (18%)	111%
AsH	5859 (0%)	1942 (4%)	33%
AsH_3	16104 (26%)	4905 (9%)	30%
AsO	28409 (47%)	36777 (68%)	129%
AsO_3	1913 (3%)	775 (1%)	41%
Total counts	60993	54058	89%

remove the polyatomic species interfering with As^+ monitoring at $m/z = 75$. Thus, the effect of the collision/reaction cells on As(III) and As(V) measurement sensitivities was investigated using He, H_2, NH_3, CH_4 and O_2 as cell gases.

When He (2 ml min^{-1}) and H_2 (2 ml min^{-1}) gases were used as collision cell gas, As(V) was 9% and 8% more sensitive than As(III), respectively (Table 4). When NH_3 (0.6 ml min^{-1}), CH_4 (0.6 ml min^{-1}) and O_2 (0.6 ml min^{-1}) were used as reaction cell gas, As(V) was 2%, 1%, and 11% more sensitive than As(III), respectively (Table 5). The differences in sensitivity were negligible when NH_3 gas and CH_4 gas were used as a reaction gas. However, the analytical sensitivity difference between As(III) and As(V) changed according to the gas flow rate of CH_4 in the range from 0.1 to 1.0 ml min^{-1}. When CH_4 gas flow rate was less than 0.3 ml min^{-1}, the analytical sensitivity of As(V) was higher than that of As(III). There was almost no difference (less than 1%) in sensitivity between them when the CH_4 gas flow rate was from 0.3 to 0.8 ml min^{-1}. In contrast, the analytical sensitivity of As(III) became slightly higher than that of As(V) when CH_4 gas flow rate was between 0.8 and 1.0 ml min^{-1}.

On the other hand, when O_2 was used as reaction gas, the major ionic species observed was AsO^+, the amount was about half of the total As species ions. That is because that AsO^+ was generated by the reaction of As and O_2 in the cell. Therefore, O_2 is ill suited as a reaction gas in As measurement.

Moreover, these results prove that sensitivity difference is not attributed to transportation efficiency and memory effect in ICP spectrometry. Also, it is clear that reaction gases can enhance or depress the sensitivity difference between As(III) and As(V).

4. Conclusions

There are significant differences in analytical sensitivity between As(III) and As(V) with ICP-OES and ICP-MS. The difference is significantly greater than the uncertainty resulted from the sample preparation and the measurement. The sensitivity difference is caused by complex formations of As atomic and polyatomic molecular species in the plasma. From the observation by a high resolution ICP-MS, it was found that the formation rates of AsH_x^+ in the plasma are the essential factors for the sensitivity difference between As(III) and As(V) in ICP spectrometry. The phenomenon was named "the Incoherent Molecular Formation (IMF) effect" from the study.

Moreover, the sensitivity difference between As(III) and As(V) can be enhanced or depressed using a reaction cell system with various kinds of gases.

References

[1] National Research Council, Arsenic in Drinking Water, National Academy Press, Washington DC, 1999.
[2] Material Safety Data Sheet, National Institute of Standards and Technology, MSDS Number 3103a, 2006.
[3] J.S. Petrick, F. Ayala-Fierro, W.R. Cullen, D.E. Carter, H.V. Aposhian, Toxicol. Appl. Pharmacol. 163 (2000) 203.
[4] M. Delnomdedieu, M.M. Basti, M. Styblo, J.D. Otvos, D.J. Thomas, Chem. Res. Toxicol. 7 (1994) 621.
[5] Environmental Health Criteria 224 Arsenic and Arsenic Compounds, second ed., World Health Organisation, Geneva, 2001, pp. 168–345.
[6] S.J. Hill, T.A. Arowolo, O.T. Butler, J.M. Cook, M.S. Cresser, C. Harrington, D.L. Miles, J. Anal. At. Spectrom. 19 (2004) 301.
[7] J.T. Creed, T.D. Martin, C.A. Brockhoff, J. Anal. At. Spectrom. 10 (1995) 443.

[8] L.L. Yu, T.A. Butler, G.C. Turk, Anal. Chem. 78 (2006) 1651.
[9] B. Budič, J. Anal. At. Spectrom. 16 (2001) 129.
[10] B. Gammelgaard, O. Jøns, J. Anal. At. Spectrom. 15 (2000) 499.
[11] E.H. Larson, S. Sturup, J. Anal. At. Spectrom. 9 (1994) 1099.
[12] F. Vanhaecke, R. Dams, C. Vandecasteele, J. Anal. At. Spectrom. 8 (1993) 433.
[13] T. Narukawa, W. Yoshimura, A. Uzawa, Bull. Chem. Soc. Jpn. 72 (1999) 701.
[14] T. Narukawa, T. Kuroiwa, K. Inagaki, A. Takatsu, K. Chiba, Appl. Organomet. Chem. 19 (2005) 239.
[15] T. Narukawa, A. Takatsu, K. Chiba, K.W. Riley, D.H. French, J. Environ. Monit. 7 (2005) 1342.
[16] T. Narukawa, CITAC'99 Japan Symposium on Practical Realization of Metrology in Chemistry for the 21st Century, 1999 (Abstract).
[17] T. Narukawa, T. Kuroiwa, K. Inagaki, K.T. Yarita, K. Chiba, 54th Japan society for analytical chemistry conference, 2005 (Abstract).
[18] T. Narukawa, T. Kuroiwa, T. Yarita, K. Chiba, Appl. Organomet. Chem. 20 (2006) 565.
[19] Y. Shibata, M. Morita, Anal. Sci. 5 (1989) 107.
[20] Z. Mester, R. Sturgeon, J. Anal. At. Spectrom. 16 (2001) 470.
[21] International Organization for Standardization, Guide to the Expression of Uncertainty in Measurements, ISO, Geneva, Switzerland, 1993.
[22] G. Horlick, S.H. Tan, M.A. Vaughan, V. Shao, in: A. Montaser, D.W. Golightly (Eds.), Inductively Coupled Plasma in Analytical Atomic Spectroscopy, VCH Pub. Inc., New York, 1987.
[23] J.W. Olesik, D.R. Jones, J. Anal. At. Spectrom. 21 (2006) 141.
[24] D.W. Koppenaal, G.C. Eiden, C.J. Barinaga, J. Anal. At. Spectrom. 19 (2004) 561.
[25] R.K. Marcus, J. Anal. At. Spectrom. 19 (2004) 591.
[26] E. McCurdy, G.J. Woods, J. Anal. At. Spectrom. 19 (2004) 607.
[27] D.E. Nixon, K.R. Neubauer, S.J. Eckdahl, J.A. Butz, M.F. Burritt, Spectrochim. Acta. Part B 59 (2004) 1377.
[28] R.J.C. Brown, R.E. Yardley, A.S. Brown, M.J.T. Milton, J Anal. At. Spectrom. 19 (2004) 703.
[29] M. Niemelä, P. Perämäki, H. Kola, J. Piispanen, Anal. Chim. Acta 493 (2003) 3.

Available online at www.sciencedirect.com
ScienceDirect
Talanta 73 (2007) 178–184
Talanta
www.elsevier.com/locate/talanta

Short communication

Speciation of chromium in Australian fly ash

Tomohiro Narukawa [a,*], Kenneth W. Riley [b], David H. French [b], Koichi Chiba [a]

[a] *Inorganic Analytical Chemistry Division, National Metrology Institute of Japan, National Institute of Advanced Industrial Science and Technology, Tsukuba Central 3, 1-1-1 Umezono, Tsukuba, Ibaraki 305-8563, Japan*
[b] *CSIRO Energy Technology, Lucas Heights Science and Technology Centre, PMB 7 Bangor, NSW 2234, Australia*

Received 16 January 2007; received in revised form 5 March 2007; accepted 6 March 2007
Available online 12 March 2007

Abstract

The concentrations of chromium (III) and (VI) in fly ash from nine Australian coal fired power stations were determined. Cr(VI) was completely leached by extraction with 0.01 M NaOH solution and the concentration was determined by inductively coupled plasma atomic emission spectrometry (ICP-AES). This was confirmed by determining Cr(III) and Cr(VI) in the extracts of fly ash that had been spiked with chromium salts. These analytical measurements were done using a combination of ion-exchange chromatography and ICP-AES. The elutant was 0.05 M HNO_3 containing 0.5%-CH_3OH. When the column was operated at a flow rate of 1.2 ml min^{-1} and samples were injected by use of a sample loop with a volume of 100 μl, Cr(III) and Cr(VI) in sample solution was exclusively separated within approximately 10 min. The detection limits (3σ) were 5 ng for Cr(III) (0.050 mg l^{-1}) and 9 ng for Cr(VI) (0.090 mg l^{-1}), respectively. A relative standard deviation of 1.9% ($n=6$) was obtained for the determination by IC–ICP–AES of 0.25 mg l^{-1} Cr(III) and Cr(VI).

Keywords: Chromium speciation; Coal fly ash; ICP-AES; IC–ICP–AES; Alkaline extraction

1. Introduction

Chromium compounds are widely distributed in nature and are commonly used in industry. Generally, the chemical species of naturally occurring chromium is Cr(III) although anthropogenic Cr(VI) can be found in recent sediments. While Cr(III) is essential for metabolic processes, Cr(VI) is toxic and carcinogenic. Accordingly, the environmental concentration of Cr(VI) or total Cr is strictly regulated. Therefore, it is important to not only accurately determine the amount of total Cr in environmental samples, but also the proportions of Cr(III) and Cr(VI). A number of procedures for the determination of total Cr as well as Cr(III) and Cr(VI) in environmental samples have been reported. These include solvent extraction [1], coprecipitation [2], activated alumina in combination with flame atomic absorption spectrometry [3], electrospray mass spectrometry [4], ion-exchange [5], pretreatment-flame atomic absorption spectrometry or electrothermal atomic absorption spectrometry [6–10]. Recently, methods that couple liquid chromatography (LC) or ion chromatography (IC) to inductively coupled atomic emission spectrometry (ICP-AES) or inductively coupled mass spectrometry (ICP-MS) have been reported [11–19]. The methods adopted for the disposal of fly ash from power stations and industrial incinerators have environmental significance as fly ash is a significant anthropogenic source in the environmental circulation of trace elements in nature and there have been several studies of trace elements (including Cr) in fly ash, coal, soil and related materials [20–32]. However, in many cases, the total leached Cr is reported and not the actual concentrations of Cr(III) and Cr(VI). There are exceptions, fly ash has been leached with $CaCl_2$ solution and the Cr species determined. [25,26] Leaching with Na_2CO_3–NaOH for Cr(VI) in soil samples has been used [33]. An IC–ICP–MS technique to determine Cr(III) and Cr(VI) in fly ash has been reported [34].

In this work, Cr in fly ash was leached with 0.01 M NaOH. The concentrations of total Cr leached were measured using ICP-AES. As well, IC–ICP–AES was used to confirm the speciation of the Cr present in the extracting solution.

* Corresponding author. Tel.: +81 29 861 6889; fax: +81 29 861 6889.
E-mail address: tomohiro-narukawa@aist.go.jp (T. Narukawa).

0039-9140/$ – see front matter © 2007 Elsevier B.V. All rights reserved.
doi:10.1016/j.talanta.2007.03.003

2. Experimental

2.1. Reagents

High purity acids and water (Milli Q) as well as analytical grade (or better) reagents were used throughout this study.

2.1.1. Cr(III) and Cr(VI) standard solutions

There were prepared by diluting Cr(III) (1000 mg l^{-1}, $Cr(NO_3)_3{\cdot}9H_2O$ in 2–5% HNO_3, or Cr(VI) (1000 mg l^{-1}, $(NH_4)_2Cr_2O_7$ in H_2O.

2.1.2. 0.01 M-NaOH solution for extract

0.40 g of NaOH was dissolved in 1000 ml water, and the resulting solution was used for extraction.

2.1.3. 0.05 M-HNO_3/0.5%-CH_3OH elution solution

This was prepared as follows: 3.46 ml of HNO_3 was diluted with 995 ml water, and the resulting solution was degassed prior to the addition of 5 g CH_3OH to make up the solution, which was used in the elution experiments.

2.2. Apparatus

A Spectro CIROS CCD ICP-AES instrument equipped with a concentric nebulizer and a Scott chamber was used for the determination of major, minor elements and total Cr in the fly ash samples. A SPS 4000 ICP-AES instrument equipped with a concentric nebulizer and a cyclone chamber was used for monitoring chromium signals on speciation of Cr(III) and Cr(VI). A TSK gel – IC–Anion – PW_{XL} PEEK column (diameter 4.6 mm × length 75 mm,), packed with anion exchange resin ($-Et_2Me^+$ groups) with a particle size of 6 μm (30 ± 3 meq l^{-1}) was used for separating Cr(III) and Cr(VI). The metal free six port injection valves combined 100 μl sample loop (PEEK tubing) and MODEL325DI&CH-2-D HPLC pump were used in the experiments. The chromatographic system was connected to the nebulizer with PEEK tubing. A metal free syringe with PEEK needle was used for sample injection.

A domestic microwave oven (maximum power 1200 W) was used in the sample dissolution procedure.

2.3. Samples

Fly ash samples (A–I) were obtained from nine coal-fired power stations in Australia. The stations were in Queensland, New South Wales and Western Australia and all burn local bituminous coal. The ash yields of the coals vary from less than 10% to greater than 30%. Generally a small proportion of the ash (0–20%) is identified as being effectively utilised; most is deposited in landfill or in wet ash dams [35]. The major and minor elements concentrations in the fly ash samples are shown in Table 1. These were prepared using the procedure described below, and the analyses completed using a Specto CIROS CCD ICP-AES. The optimized analytical conditions are shown in Table 2. NIST–SRM 1633b (Coal Fly Ash) was used as the certified reference material to validate the analytical procedures.

Table 1
Concentration of major and minor elements in fly ash samples

Sample	Mean (%)							
	Al	Ba	Ca	Fe	Mg	P	Si	Ti
A	12.7	0.352	0.90	6.07	0.425	0.736	24.2	0.924
B	10.8	0.065	2.14	4.83	0.605	0.065	26.2	0.493
C	12.1	0.039	0.63	1.99	0.361	0.096	28.9	0.543
D	14.0	0.077	0.81	1.14	0.595	0.042	26.5	0.984
E	13.4	0.039	0.26	0.71	0.171	0.072	28.3	0.709
F	14.7	0.119	2.74	9.09	0.887	0.376	18.8	1.030
G	10.8	0.016	0.04	0.28	0.068	0.024	31.1	0.750
H	16.4	0.023	0.98	8.40	0.600	0.023	23.2	1.140
I	14.6	0.091	0.26	1.82	0.061	0.173	27.2	0.738
NIST 1633b	15.05	0.0707	1.53	7.76	0.481	0.239	22.99	0.793
Certificate[a]	15.05	0.0709	1.51	7.78	0.482	0.230[b]	23.02	0.791

Results of acid decomposition in microwave oven.
[a] Certified value.
[b] Non-certified.

2.4. Procedure

2.4.1. Sample preparation for measurement of major, minor elements and total Cr

A precisely weighed 30 mg sub-sample of fly ash was transferred into a polycarbonate container to which 0.50 ml of HCl, 0.50 ml of HF and 0.25 ml of HNO_3 were added. The container was placed in a screw top jar in a microwave oven; the sample and acids were heated at 20% power for 5 min and 10% power for 15 min to complete the decomposition. After cooling, the digest was made up to 30 ml with water. The resulting solution was used for major, minor elements and total Cr measurements by ICP-AES.

Table 2
Instrumental operating parameters

Specto CTROS CCD ICP-AES	
Wavelength	Al 167.08 nm
	Ba 455.40 nm
	Ca 317.93 nm
	Fe 259.94 nm
	Mg 279.08 nm
	P 178.29 nm
	Si 251.61 nm
	Ti 334.94 nm
	Cr 267.72 nm
RF power	1.4 kW
Carrier gas flow rate	0.85 l min^{-1}
Plasma gas flow rate	14 l min^{-1}
Coolant gas flow rate	1.0 l min^{-1}
Seiko SPS4000 ICP-AES	
Wavelength	283.56 nm (Cr, Ionic line)
RF power	1.3 kW
Observation height	9.0 mm
Carrier gas flow rate	0.80 l min^{-1}
Plasma gas flow rate	16 l min^{-1}
Coolant gas flow rate	0.50 l min^{-1}

Table 3
Concentrations of Cr in fly ash samples

Sample	Concentration of Cr (mg kg^{-1})			%Cr(VI)
	Total Cr acid decomposition	Cr(VI)[a] alkaline leaching	Cr(III)[b]	
A	130.0	0.041	129.96	0.03
B	18.0	1.041	16.96	5.78
C	45.2	0.386	44.81	0.85
D	26.5	0.296	26.24	1.12
E	49.6	0.293	49.31	0.59
F	69.2	0.130	69.07	0.19
G	34.0	0.630	33.37	1.85
H	90.0	0.090	89.91	0.10
I	59.7	1.280	58.42	2.14
NIST 1633b	198.2	N.D	198.20	0.00
Certified Value[c]	198.2 ± 4.7			

[a] Relative standard deviation (R.S.D.) of replication measurements ($n = 6$): ±5%.
[b] Concentration of Cr(III) = total Cr − Cr(VI).
[c] NIST 1633b certified value.

Table 4
Leaching test on fly ash unspiked and spiked with solutions of Cr(III) and Cr(VI)

Sample	pH	Form of spiked Cr	Concentration of Cr (ppm[a])	Found Cr (mgl^{-1}[b])	Concentration of Cr in FA (mg kg^{-1})	Recovery of spiked Cr (%)
	12.08	–	–	0.0051		
A	12l19	Cr(III)	0.25	0.0049	0.041	<0.05
	12.58	Cr(VI)	0.25	0.2583		101
	12.56	–	–	0.1301		
B	12.37	Cr(III)	0.25	0.1349	1.041	<0.05
	12.18	Cr(VI)	0.25	0.3811		100
	12.37	–	–	0.0484		
C	12.05	Cr(III)	0.25	0.0501	0.386	<0.05
	12.57	Cr(VI)	0.25	0.2980		100
	12.27	–	–	0.0371		
D	12.18	Cr(III)	0.25	0.0407	0.296	<0.05
	12.05	Cr(VI)	0.25	0.2881		100
	12.14-	–	–	0.0367		
E	12.03	Cr(III)	0.25	0.0365	0.293	<0.05
	12.15	Cr(VI)	0.25	0.2859		100
	12.25	–	–	0.0162		
F	11.81	Cr(III)	0.25	0.0158	0.130	<0.05
	12.24	Cr(VI)	0.25	0.2822		106
	12.66	–	–	0.0784		
G	12.87	Cr(III)	0.25	0.0812	0.627	<0.05
	12.81	Cr(VI)	0.25	0.3228		98
	12.90	–	–	0.0118		
H	12.92	Cr(III)	0.25	0.0120	0.090	<0.05
	12.21	Cr(VI)	0.25	0.2593		99
	12.32	–	–	0.1598		
I	12.12	Cr(III)	0.25	0.1538	1.280	<0.05
	12.19	Cr(VI)	0.25	0.4188		104
	12.80	–	–	ND		
NIST 1633b	12.83	Cr(III)	0.25	<0.0001	ND	<0.05
	12.84	Cr(VI)	0.25	0.2492		100

Sample weight: 5.00 g; extract volume: 40.0 ml.
[a] The concentration is spiked Cr(III) or Cr(VI). It was spiked as a solution. The value shows the concentration of Cr in 40 ml of extract.
[b] The value shows the concentration of Cr in the extract on the determination.

2.4.2. Extraction and measurement of leachable Cr

Leachable Cr in each fly ash was extracted with 0.01 M NaOH solution. A precisely weighed 5.0 g sub-sample of fly ash was transferred to a 100 ml polycarbonate container, to which 40 ml of 0.01 M-NaOH were added. The container was placed on a shaker (50 r.p.m) for 6 h to leach Cr(VI). After shaking, the solution was filtered through a cellulose nitrate filter (pore size 0.45 μm)). Total leachable Cr in this filtered extract was determined by ICP-AES. Leachable Cr(III) and Cr(VI) were determined by IC–ICP–AES.

2.4.3. Assessment of analytical validity

To assess the validity of the leaching and measurement procedures, known amounts of Cr(III) and Cr(VI) in solution as well as solid salts were added as spikes prior to leaching. The solutions of Cr(III) and Cr(VI) were added to determine whether there was evidence of any oxidation of the soluble Cr(III) to Cr(VI) and also to assess the overall solubilibily of the Cr(III) in the NaOH extractant. The use of the solid salts was to assess the extractability of the Cr(III) and Cr(VI) compounds.

3. Results and discussion

3.1. Measurement of total Cr and Cr(VI) and estimation of Cr(III)

The total Cr and NaOH-leachable Cr(VI) together with the calculated Cr(III) in the fly ash samples are listed in Table 3.

The effectiveness of the leaching procedure in preferentially leaching Cr(VI) in the presence of Cr(III) is evident in the results obtained on both the samples spiked leaching solutions and those spiked with solid salts. The actual concentrations in the extracts of solutions that were unspiked, spiked with solutions of Cr(III) or Cr(VI) are listed in Table 4. The spiked amounts of both Cr(III) and Cr(VI) were equivalent to 0.25 mg l^{-1} in the final extract. When 0.01 M NaOH solution as an extract is used, Cr(VI) was completely leached and the recovery of spiked Cr(VI) is 100% at pH above 12. No leaching of Cr(III) was observed at this high pH. Also, the negligible solubility of Cr(III) in the NaOH solution suggests that there was no oxidation of Cr(III) to produce Cr(VI). The obtained results from the extraction of powdered compounds of Cr were added to fly ash samples are shown in Table 5. When large amounts of powdered Cr(III) as Cr_2O_3 were added to the fly ash samples, the concentrations of Cr in the extract did not change, i.e. Cr(III) was not observed at the high pH of the extract. Conversely, when powdered Cr(VI) as chromate compound is added, the recovery of Cr(VI) ranged from 94 to 106%. It needs to be pointed out that very small masses of the chromate were added and this increases the potential error in the determination.

The leaching of fly ash samples with 0.01 M NaOH solution and determination of the total chromium in the extract has been shown to give a reliable estimate of Cr(VI). Assuming that the Cr(VI) is totally soluble, the proportion of Cr(VI) and Cr(III) in the fly ash can also be estimated. However, the results from the ICP-AES are for total soluble Cr. It is an assumption that the soluble species in the NaOH leachate is Cr(VI). This assumption was tested by determining the species of Cr in solution by IC–ICP–AES (see below).

Table 5
Leaching test on flyash unspiked and spiked with salts of Cr(III) and Cr(VI)

Sample	pH	Form of spiked Cr	Concentration of Cr (ppm[a])	Found Cr (mgl^{-1}[b])	Recovery of spiked Cr (%)
A	12.84	Cr(III)	0.5132	0.0019	<0.05
	12.59	Cr(VI)	2.1662	2.1759	100
B	12.88	Cr(III)	0.4288	0.0519	<0.05
	12.91	Cr(V)	1.3330	1.3830	94
C	12.91	Cr(III)	2.2237	0.0191	<0.05
	12.03	Cr(VI)	1.2775	1.2990	98
D	12.88	Cr(III)	3.4210	0.0149	<0.05
	12.76	Cr(VI)	1.8885	1.8754	97
E	12.22	Cr(III)	2.5658	0.0148	<0.05
	12.89	Cr(VI)	1.3330	1.3426	98
F	12.81	Cr(III)	19.4998	0.0067	<0.05
	12.84	Cr(VI)	2.6106	2.6461	101
G	12.92	Cr(III)	2.53125	0.0926	<0.05
	12.01	Cr(VI)	2.6106	2.6906	100
H	12.09	Cr(III)	1.5820	0.0124	<0.05
	12.03	Cr(VI)	2.1108	2.1202	100
I	12.01	Cr(III)	1.8960	0.1477	<0.05
	12.08	Cr(VI)	1.4442	1.6001	100

Sample weight: 5.00 g; extract volume: 40.0 ml.

[a] The concentration is spiked Cr(III) or Cr(VI). It was spiked as a powder reagent. Used chemical forms of powdered Cr(III) and Cr(VI) are Cr_2O_3 and $Na_2CrO_4{\cdot}4H_2O$, respectively. The value shows the concentration of Cr in 40 ml of extract.

[b] The value shows the concentration of Cr in the extract on the determination.

3.2. Optimisation of IC–ICP–AES procedure for determination of Cr(III) and Cr(VI)

A speciation method using IC–ICP–AES was developed to confirm the species of Cr present in the NaOH extracting solution. Operating parameters on ICP-AES instruments are generally optimised to obtain a maximium signal/background ratio. But, in this work, the strongest Cr signal was sought, as the target element was separated from matrix elements with the IC column and no spectral interference was possible. The effect of wavelength on 0.25 mg l^{-1} Cr(III) and Cr(VI) solution was studied when the other parameters were held constant. The results indicate the largest absolute emission intensity was observed at 283.56 nm (ionic line) and the highest S/B ratio was observed at 205.56 nm (ionic line), therefore, we selected 283.56 nm for Cr analysis. As well, the effect of emission intensity on the other parameters were studied when the wavelength was set at 283.56 nm and the carrier gas flow rate was varied from 0.5 to 1.2 l min^{-1}, the RF power was varied from 0.8 to 1.5 kW and the observation height was varied from 0 to 30 mm (above coil). The optimized operating parameters with the results obtained are shown Table 2. In this work, the signal intensity varied with the elution of the Cr species from the chromatograph. Therefore, measurement of Cr required estimation of peak area of the Cr spectrum. The detection limits (3σ) were 5 ng for Cr(III) (0.050 mg l^{-1}: 100 μl loop) and 9 ng for Cr(VI) (0.090 mg l^{-1}: 100 μl loop), respectively. The relative standard deviations using 0.25 mg l^{-1} (100 μl loop) of Cr(III) and Cr(VI) using the optimized IC–ICP–AES were 1.9% (n = 6).

Calibration curves were obtained using 0.01 M-NaOH solution containing Cr(III) and Cr(VI). The results indicate that the calibration curves were linear up to 1 μg for both Cr(III) and Cr(VI) (10 mg l^{-1}: 100 μl loop). The slopes of the two calibration curves of Cr(III) and Cr(VI) differ as a consequence of the different peak shapes of the eluted Cr(III) and Cr(VI). Thus, individual calibration curves are necessary and were prepared for the Cr(III) and Cr(VI).

The choice of column and chromatograph are based on the following considerations. The column must be used with an elute at lower pH values because Cr(III) was not removed from a column at the higher pH. The aim was to retain Cr(VI) on the column and retard its elution. As Cr(III) and Cr(VI) exist as cation and anion, respectively in solution, these species can be relatively easily separated with chromatography. However, care must be taken to prevent the oxidation of Cr(III) or the reduction of Cr(VI) during the elution. In this work, a TSK gel – IC–Anion – PW_{XL} PEEK column was employed. With this anion column, Cr(III) is not significantly retained, however Cr(VI) is effectively retained and can be accurately determined.

The most important factor for optimization of the analysis is the value of pH and the composition of the eluent. The optimisation of the eluent was investigated using several solutions: HNO_3 solution, HCl solution, phosphoric system buffer and oxalic acid system buffer. The results indicate that HNO_3 solution was the most effective. The efficiency of separation and the retention times of Cr(III) and Cr(VI) were determined with various concentrations from 0.01 to 1.0 M HNO_3 as the elution. Fig. 1 shows

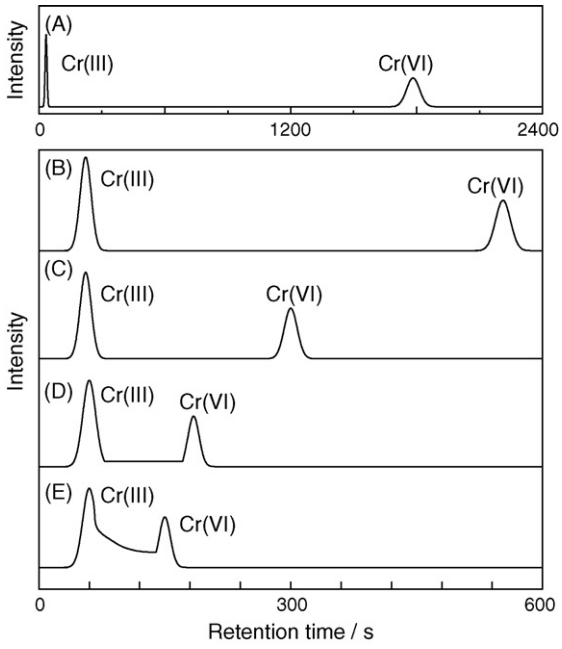

Fig. 1. Retention of Cr(III) and Cr(VI) with varying concentrations of HNO_3 in the elution. (A) 0.01 M-HNO_3; (B) 0.05 M-HNO_3; (C) 0.10 M-HNO_3; (D) 0.50 M-HNO_3; (E) 1.0 M-HNO_3. Flow rate 1.2 ml min^{-1}, concentration of Cr(III) and Cr(VI) 0.25 mg l^{-1}, sample loop 100 μl.

the results. When 0.01 M-HNO_3 solution was used, the retention time of Cr(VI) was approximately 30 min, and a broad peak was obtained. Conversely, when 1.0 M-HNO_3 solution was used, retention time was approximately 3 min; however, the peaks of Cr(III) and Cr(VI) were not separated perfectly. When 0.10 M-HNO_3 solution was used as elution, the retention time was about 5 min and complete separation was achieved As column life is shortened by strong acids, slightly weaker 0.05 M-HNO_3 solution was employed for the elution. However, it was found that if HNO_3 alone was used, the separation efficiency and retention

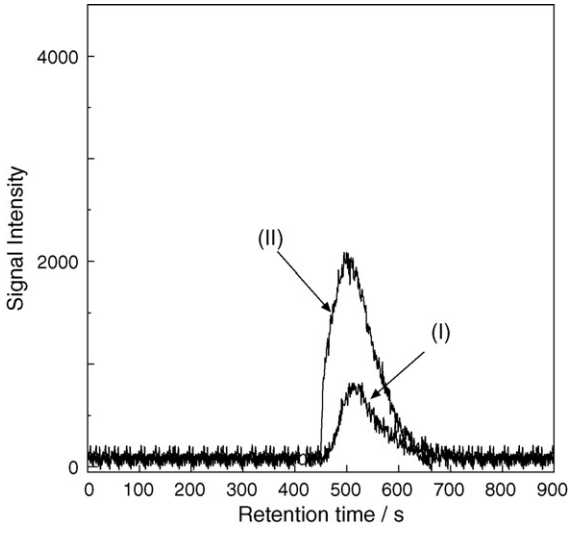

Fig. 2. Speciation of leachability Cr from fly ash by using IC–ICP–AES. (I) 0.01 M NaOH solution; (II) 0.01 M NaOH solution containing 0.25 mg l^{-1} Cr(VI). Elution 0.05 M HNO_3/0.5% CH_3OH, Flow rate 1.2 ml min^{-1}, sample loop 100 μl, fly ash sample 5 g, extract 40 ml.

Table 6
Concentrations and speciation of Cr in fly ash samples

Sample	pH	Found (mg^{-1}[a])		Leachable Cr in ash ($mg\,kg^{-1}$)		Leachable Cr % of total[b]
		Cr(III)	Cr(VI)	Cr(III)	Cr(VI)	
A	12.0	ND	0.0053	0.000	0.042	0.03
B	12.4	ND	0.1323	0.000	1.058	5.88
C	12.0	ND	0.0485	0.000	0.388	0.86
D	12.9	ND	0.0368	0.000	0.294	1.11
E	12.2	ND	0.0368	0.000	0.294	0.59
F	12.7	ND	0.0169	0.000	0.135	0.20
G	12.0	ND	0.0760	0.000	0.608	1.79
H	12.8	ND	0.0126	0.000	0.101	0.11
I	12.9	ND	0.1580	0.000	1.264	2.12

Samples weight 5.00 g.
[a] Relative standard deviation (R.S.D.) of replication measurements ($n = 6$): ±2%.
[b] (Cr(III) + Cr(VI)/total Cr) × 100, ND: not detected. Note: leachable Cr is Cr(VI).

time decreased over time due to a decrease in the anion exchange function of the column. This was corrected by the addition of CH_3OH to 0.5% in the eluent. In the metal free chromatographic system, there was no evidence of any contamination with Cr.

3.3. Speciation of leachable Cr in fly ash samples

The results of the determination by IC–ICP–AES of Cr species leached from the fly ash samples are given in Table 6. These results are in good agreement with the results obtained by ICP-AES (Table 3). When 0.01 M NaOH was used for the extraction of Cr in fly ash samples, there was no evidence of Cr(III) present in the chromatograms (Fig. 2).

4. Conclusions

A speciation method of Cr was developed using IC–ICP–AES. The procedure is very useful for the determination of Cr(III) and Cr(VI) in fly ash. Importantly, the results confirm that it is possible to determine the concentration of Cr(VI) in fly ash by simply using a NaOH-leach/ICP-AES method. This latter technique offers a very simple procedure for the determination of the environmentally important Cr(VI) in a material, which is widely disposed of in landfills, worldwide. Based on the analysis of the nine fly ash samples from power stations burning bituminous coals from Queensland, New South Wales and Western Australia, it is apparent that the concentration of the Cr(VI) in Australian fly ash is generally very low and the soluble Cr(VI) is unlikely to pose an environmental or health risk when the ash is utilised (e.g. in the manufacture of concrete or disposed of in landfill or ash dams. The very low proportion of the total Cr occurring as soluble Cr(VI) in fly ash from Australian coal is consistent with the findings of others [36].

Acknowledgments

This work had been supported by CSIRO's personnel in Australia; Owen Farrell, Steve Lavrencic, Rob Rowland, Jan Chipperfield, Brett Warden, Rosemary Wood and David Jacyna are thanked for their contributions.

References

[1] M. Sugiyama, O. Fujino, S. Kihara, M. Matsui, Anal. Chim. Acta 181 (1986) 159.
[2] C.-R. Lan, C.-L. Tseng, M.-H. Yang, Z.B. Alfassi, Analyst 116 (1991) 35.
[3] M. Sperling, S. Xu, B. Welz, Anal. Chem. 64 (1992) 3101.
[4] A.B. Gwizdala III, S.K. Johnson, S. Mollah, R.S. Houk, J. Anal. At. Spectrom. 12 (1997) 503.
[5] C.A. Johnosn, Anal. Chim. Acta 238 (1990) 273.
[6] I. Kubrakova, T. Kudinova, A. Formanovsky, N. Kuz'min, G. Tsysin, Y. Zolotov, Analyst 119 (1994) 2477.
[7] A. Gáspár, J. Posta, Anal. Chim. Acta 354 (1997) 151.
[8] M.E. Soares, M.L. Bastos, M.A. Ferrira, J. Anal. At. Spectrom. 9 (1994) 1269.
[9] K. Ndung'u, N.-K. Djane, F. Malcus, L. Mathiasson, Analyst 124 (1999) 1367.
[10] M.J. Marués, A. Salvador, A. Morales-Rubio, M. de la Guardia, Fresenius J. Anal. Chem. 367 (2000) 601.
[11] A.G. Coedo, T. Dorado, I. Padilla, F.J. Alguacil, J. Anal. At. Spectrom. 15 (2000) 1564.
[12] C. Barnowski, N. Jakubowski, D. Stuewer, J.A.C. Broekaert, J. Anal. At. Spectrom. 12 (1997) 1155.
[13] M.J. Tomlinson, J. Wang, J.A. Caruso, J. Anal. At. Spectrom. 9 (1994) 957.
[14] N. Jakubowski, B. Jepkens, D. Stuewer, H. Berndt, J. Anal. At. Spectrom. 9 (1994) 193.
[15] M.j. Powell, D.W. Boomer, D.R. Wiederin, Anal. Chem. 67 (1995) 2474.
[16] F.A. Byrdy, L.K. Olson, N.P. Vela, J.A. Caruso, J. Chromatogr. A 712 (1995) 311.
[17] Y. Inoue, T. Sakai, H. Kumagai, J. Chromatogr. A 706 (1995) 127.
[18] H. Gürleyük, D. Wallschläger, J. Anal. At. Spectrom. 16 (2001) 926.
[19] R.A. Sabty-Daily, K.K. Luk, J.R. Froines, Analyst 127 (2002) 852.
[20] K. Furtmann, D. Seifert, Fresenius J. Anal. Chem. 338 (1990) 73.
[21] C. Bloomfield, G. Pruden, Environ. Pollut. A 23 (1980) 103.
[22] R.A. Griffin, A.K. Au, R.R. Frost, J. Environ. Sci. Health A 12 (1977) 431.
[23] R.J. Bartlett, J.M. Kimble, J. Environ. Qual. 5 (1976) 379.
[24] M. Kersten, B. Schulz-Dobrick, T. Lichtensteiger, C.A. Johnson, Environ. Sci. Technol. 32 (1998) 1398.
[25] V.J.G. Houba, I. Novozamsky, A.W.M. Huybregts, J.J. Van Der Lee, Plant Soil 96 (1986) 433.
[26] J. Prikisch, S.A. Katz, B. Kovacs, Z. Györi, J. Chromatogr. A 774 (1997) 363.
[27] E. Fujimori, R. Shiozawa, S. Iwata, K. Chiba, H. Haraguchi, Bull. Chem. Soc. Jpn. 75 (2002) 1205.
[28] F.A. Chmilenko, N.M. Smityuk, A.N. Baklanov, J. Anal. Chem. 57 (2002) 313.
[29] A. Carlosena, P. López-Mahía, S. Muniategui, E. Fernandez, D. Prade, J. Anal. At. Spectrom. 13 (1998) 1361.

[30] A.S. Hursthouse, J. Environ. Monit. 3 (2001) 49.
[31] F. Goodarzi, F.E. Huggins, J. Environ. Monit. 3 (2001) 1.
[32] K. Ashley, R.N. Andrews, L. Cavazos, M. Demange, J. Anal. At. Spectrom. 16 (2001) 1147.
[33] R.J. Vitale, G.R. Mussoline, J.C. Petura, B.R. James, J. Environ. Qual. 23 (1994) 1249.
[34] K. Tirez, W. Brusten, A. Cluyts, J. Patyn, N.D. Brucker, Anal. At. Spectrom. 18 (2003) 922.
[35] S.J. Day and K.W. Waste Streams in Black Coal Mining and Coal Fired Power Stations, Research Report 42, Cooperative Research Centre for Coal in Sustainable Development, Pullenvale, Qld, Australia (2004).
[36] F.E. Huggins, M. Najih, G.P. Huffman, Fuel 78 (1999) 233.

Available online at www.sciencedirect.com
ScienceDirect
Talanta 73 (2007) 54–61
Talanta
www.elsevier.com/locate/talanta

Fast Fourier transformation with continuous cyclic voltammetry at an Au microelectrode for the determination of morphine in a flow injection system

Parviz Norouzi [a,*], Mohammad Reza Ganjali [a], Ali Akbar Moosavi-movahedi [b], Bagher Larijani [c]

[a] *Center of Excellence in Electrochemistry, University of Tehran, Tehran, Iran*
[b] *Institute of Biochemistry & Biophysics, University of Tehran, Tehran, Iran*
[c] *Endocrinology & Metabolism Research Center, Tehran University of Medical Science, Tehran, Iran*

Received 29 November 2006; received in revised form 25 February 2007; accepted 25 February 2007
Available online 1 March 2007

Abstract

For the fast morphine monitoring in flow injection systems a highly sensitive method is being introduced in this work. The fast Fourier transformation with continuous cyclic voltammetry (FFTCV) in a flowing solution as a detection system was applied for the prompt morphine monitoring. Here it should be stressed that this technique is simple, precise, accurate, time saving and economical. This research includes the observation of the effects of various parameters on the sensitivity of the detection system. Eventually, it was concluded that the best condition was obtained within the pH value of 2, scan rate value of 40 V s^{-1}, accumulation potential of 400 mV and accumulation time of 0.6 s.

In detail, the noteworthy advantages which this method illustrates in comparison with other reported methods are the following; no necessity for the oxygen removal from the test solution, a sub-nano molar detection limit and the fast determination of any such compound in a wide variety of chromatographic methods.

The method proved to be linear over the concentration range of 285–305,300 pg mL^{-1} ($r = 0.999$) with a detection limit and a quantitation limit of 95.5 and 285 pg mL^{-1}, respectively. Consequently, the method illustrates the requisite accuracy, sensitivity, precision and selectivity to assay morphine in its tablets and biological fluids.

Keywords: Morphine; Fast Fourier transformation; Continuous cyclic voltammetry; Ultra microelectrode

1. Introduction

Morphine, a well-known potent narcotic analgesic and the active metabolite derived from heroin (3,6-diacecylmorphine), has been reported to influence various immune functions. In fact, morphine is an alkaloid and a common drug often offered to patients for pain relief from surgical procedure or carcinomatosis. Morphine (MOR) is a μ-opioid agonist traditionally used for the treatment of moderate or severe pain [1]. It is extensively metabolized to its morphine-3-gluc-uronide (M3G), with normorphine (NM) and morphine-6-glucuronide (M6G) as minor metabolites, irrespective of the species or administration route [2–4].

Different methods have been developed for the detection and determination of opiate derivatives, including GC–MS [5–7], high performance liquid chromatography (HPLC) [8–11], chemiluminescence [12,13], direct fluorimetric [14], capillary electrophoresis [15,16] and ion mobility spectrometry (IMS) [17,18] and electrochemical methods [19]. Ion mobility spectrometry is a well-known technique, which offers low detection limit, fast response, simplicity and portability. Gas chromatography–mass spectrometry (GC–MS) is still the most widely used reference method but liquid chromatography coupled with single-stage or tandem mass spectrometry (LC–MS, LC–MS–MS) is becoming increasingly important for the identification and quantification of the analytes [20–23], especially for

* Corresponding author. Tel.: +98 21 61112788.
E-mail address: norouzi@khayam.ut.ac.ir (P. Norouzi).

0039-9140/$ – see front matter © 2007 Published by Elsevier B.V.
doi:10.1016/j.talanta.2007.02.029

the more polar, thermo labile or low-dosed drugs, as indicated by Maurer [24].

Regarding the pharmacokinetic studies, various assay methods have been developed. Radio-immunoassay methods [25] present high sensitivity but, at the same time, they may demonstrate low specificity owing to the cross-reactivity among morphine, M-3-G and M-6-G. Furthermore, high performance liquid chromatography methods are vastly applied and allow simultaneous analysis of morphine and its glucuronides, detected by ultraviolet (UV) detection [26–29], fluorescence (FL) detection [30,31], combined electrochemical detection (ECD)–UV detection [32–34] and combined ECD–FL detection [35,36]. Nevertheless, UV and FL detection were not sensitive enough for morphine and its glucuronides in biological samples. Therefore, these compounds could be precisely detected by ECD. However, combined chromatographic ECD consumes long time to determine. Finally, mass spectrometric methods [37–41] have achieved the desired sensitivity and selectivity.

As far as voltammetric techniques are considered, they are generally rapid and economical in the determination of some organic and inorganic compounds in aqueous systems with a sensitivity range of parts-per-billion. Indeed, because of the selective detector, voltammetric techniques are useful for the samples. In addition, owing to the movement of the analyte zone in an electrochemical flow cell for flowing solutions, the application of these techniques requires fast analyte accumulation and fast potential sweeping (which is not appropriate for large electrodes) [42,43]. The use of voltammetric techniques have been further stimulated by the advent of UMEs, due to their steady state currents, higher sensitivity, increased mass transport and their ability to be used in electroanalysis in solutions with high resistance [44,45]. UMEs, for instance, have been applied as sensors in various techniques such as flow injection analysis [46–47], cardiovascular monitoring and organic compounds analysis [48,49]. Here, this research describes a new electrochemical method, based on FIA and FFT Cyclic voltammetry, for the determination of morphine.

The instrumentation that we used in the previously reported papers was not able to determine this drug at this LOD level. For this work, we used the highly developed version of an old electrochemical system (the computer program is more advanced in the algorithm for integration and filtering). As a consequence, the noise level was less, resulting in a better S/N. Fortunately; it was feasible to determine morphine at a detection limit lower than those of other reported methods.

Furthermore, it should be noted that this novel electrochemical method has many advantages over the classical methods. For example, one of its most important abilities is the monitoring of several surface active compounds in a very short time. It means that 60 samples per hour can be determined. Currently, we are trying to explore its capability in new areas for the determination of significant compounds, which cannot be measured at very low concentrations by other methods. For instance, the method can be used in the indirect mode for the detection and determination of components of electroactive and non-electroactive substances.

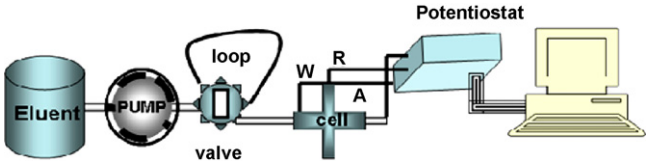

Fig. 1. Diagram of the flow injection setup.

2. Experimental

2.1. Flow injection setup

A 10-roller peristaltic pump (UltrateckLabs Co., Iran) and a four-way injection valve (Supelco Rheodyne Model 5020) with a 50-μL sample injection loop consisted of the necessary equipment for the flow injection analysis. The schematic of flow injection setup has shown in Fig. 1. Flow rate of the pump was set at 3 mL min^{-1} during an experimental run. The solutions were introduced into the sample loop by a plastic syringe. After, opening the loop in the way of eluent flow, the sample can pass over the working electrode. The potentiostate applies a potential in the range of gold oxidation in acidic media (Eq. (1)) and the potential waveform was shown in Fig. 3. The special program on computer can monitor the cyclic voltammograms online and every change on current or charge will be shown in program. In Fig. 2, the electrochemical cell of the flow injection analysis was shown in detail.

2.2. Reagents

For the experimental part of the research, the analytical grade reagents and the reagents for the preparation of the eluent solution for the flow injection analysis (0.05 mol L^{-1} H_3PO_4) and 1 mol L^{-1} NaOH (for the pH eluent adjustment), were obtained from the Merck Chemicals. The Drug Quality Control Center (Tehran, Iran) provided morphine kindly as a gift. Also, morphine tablets with a label of 15 mg morphine sulfate were purchased from a local pharmacy.

All solutions were prepared in doubly distilled deionized water, filled with the background electrolyte solution and they were used without the removal of the dissolved oxygen.

2.3. Background electrolyte (BGE)

The running buffer or BGE was made by phosphoric acid (85%, w/v) with the addition of 8.7 mL into a 1000 mL volumet-

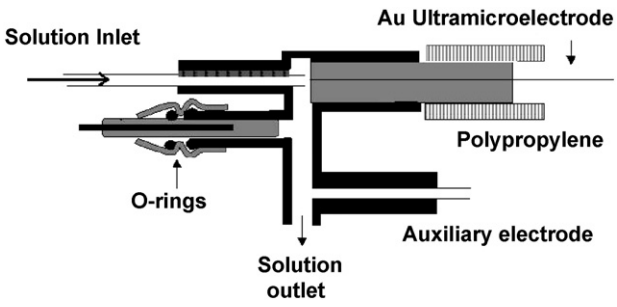

Fig. 2. Diagram of the electrochemical cell.

ric flask and dilution to a constant volume with distilled water. The pH was adjusted to the value of 2 with sodium hydroxide. The solutions were freshly prepared and filtered, using a Millipore filter (0.45 μm) each day.

2.3.1. Standards and sample solutions

For the preparation of the standard stock solutions, a morphine standard stock solution (1 mg mL^{-1}) was made by distilled water. This solution was light-protected using foil and stored at 4 °C for 5 days. It was found to be stable during this period.

Also, for the preparation of the standard solutions for FIA, aliquots of the standard stock morphine solution were dispensed into 10 mL volumetric flasks. These flasks were filled up with the running buffer to give final concentrations range of (285–305,300 pg mL^{-1}).

2.3.2. Assay of sample preparation

Twenty tablets were weighed, finely powdered and portions equivalent to 15 mg morphine were transferred into a 100 mL volumetric flask; 50 mL of distilled water were added, shaken thoroughly to dissolve, filled up and mixed well. Suitable solution aliquots were filtered through a Millipore filter (0.45 μm). One milliliter of the filtered solution was diluted with distilled water in a 100 mL volumetric flask. Then, 1 mL of the resulting solution was added to a 100 mL volumetric flask and filled up with 0.05 M phosphoric acid, reaching an initial concentration of (15,000 pg mL^{-1}).

2.3.3. Sample preparation of human urine and plasma

Drug free human plasma was obtained from the Iranian blood transfusion service (Tehran, Iran) and stored at (−20 °C), until its use after gentle thawing. Urine was also collected from healthy volunteers (males, around 35 years old).

For the determination of morphine in human urine, 1 mL of untreated urine containing 6 ng mL^{-1} morphine was placed into a 20 mL volumetric flask and diluted with a pH 2 buffer solution to the mark. Then, 50 μL of the aliquot were injected into the FIA system. For the determination of morphine in plasma, 100 μL of aqueous morphine solutions (1 ng mL^{-1}) were added to 100 μL of untreated plasma. The mixture was vortexed for 30 s. In order to precipitate the plasma proteins, the plasma samples were treated with 20 μL of perchloric acid $HClO_4$ 20%. After that, the mixture was vortexed for further 30 s and then centrifuged at 6000 rpm for 5 min. Eventually, 50 μL aliquot of the obtained supernatant were injected into the FIA system. The voltammograms were recorded according to the above recommended procedure. The voltammograms of the samples without morphine did not show any signal that could interfere with the direct determination. Therefore, external calibration could be used.

2.4. Electrode preparation

The construction of the gold UMEs (12.5 μm in radius) involved the metal micro-wires (Good fellow Metals Ltd., UK) sealing into a soft glass capillary. Then, the capillary was cut perpendicularly to its length to expose the wire. Silver epoxy (Johnson Matthey Ltd., UK) was used for the electrical contacts. Previous to the initiation of any experiment, the electrode surface was polished for 1 min using extra fine carborundum paper and, afterwards, for 10 min with 0.3 μm alumina. Prior to being placed in the cell, the electrode was washed with water. In all measurements, an Ag (s)|AgCl (s)|KCl (aq, 1 mol L^{-1}) reference electrode was used. The auxiliary electrode was made of a Pt wire, 1 cm in length and 0.5 mm in diameter.

3. Results and discussions

3.1. Data acquisition and processing

For the data acquisition, a setup of a PC PIV Pentium 900 MHz microcomputer, equipped with a data acquisition board (PCL-818HG, Advantech. Co.) and a custom made potentiostat, was used. All data acquisition and data processing programs were developed in Delphi 6® program environment. In Fig. 3, the applied waveform potential diagram during the cyclic voltammetric measurements is shown. The potential waveform consists of three parts; (a) Potential steps, E_{c1} and E_{c2} (which are used for the oxidation and reduction of the electrode surface, respectively), during which the electrochemical cleaning of the electrode surface takes place, (b) E_c, where the analyte accumulation takes place and (c) the potential ramp, where the current measurements occur.

In this method, the signal calculation is measured by the integration of the net current changes over the scanned potential range. It must be noted that, in this case, the current changes (result of the injected analyte) at the voltammogram can be caused by various processes, which happen on the electrode surface. Those processes include: (a) oxidation and reduction of the adsorbed analyte and (b) oxidation and reduction inhibition of the electrode surface by the adsorbed analyte. Indeed, in order to observe the influence of the adsorbed analyte on the oxidation and reduction peaks of the gold surface, the scan rate must be set at high rates (e.g. >20 V s^{-1}).

However, during the scan, some of the adsorbed analyte molecules are desorbed. Depending on the rate of those processes and the scan rate, the amount of the desorption analyte molecules (during the scan) can be changed. The important point

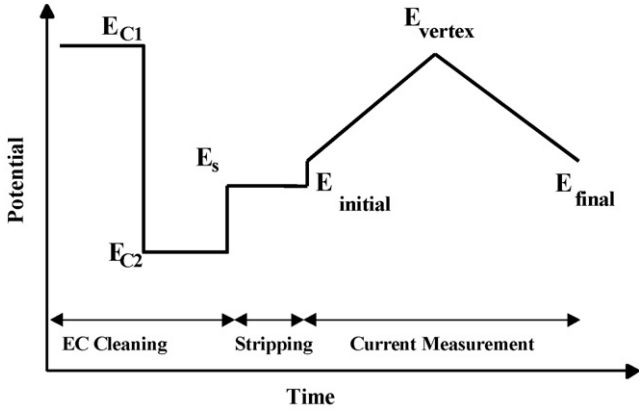

Fig. 3. The diagram of the applied potential waveform.

here is that part of the adsorbed analyte molecules still remain on the electrode surface, inhibiting the red/ox process of the electrode surface. In this technique, ΔQ is calculated according with the all current changes at the CVs [50–54]. Nonetheless, the selectivity and sensitivity of the analyte response, expressed in terms of ΔQ, strongly depends on the selection of the integration limits.

One of the considerable aspects of this method is the application of a special digital filtration, which is applied during the measurement. At first, an electrode CV was recorded and then by applying FFT on the collected data, the existing high frequency noises were indicated. With the aid of this information, the cutoff frequency of the analog filter was set at a certain value (where the noises were removed from the CV).

Since the crystal structure of a polycrystalline gold electrode is greatly affected by the condition of the applied potential waveform [45], different potential waveforms were examined in order to obtain a reproducible electrode surface (or a stable background signal). In fact, the application of cyclic voltammetry for the determination of electroactive compounds mainly faces low stability of the background signal, due to the changes taking place in the surface crystal structure during the oxidation and reduction of the electrode in each potential cycle. After the examination of various potential waveforms, the best potential waveform, providing a stable background during the measurement, was the waveform depicted in Fig. 2. As mentioned above, the potential waveform was continuously applied during an experiment run where the collected data were filtered by the FFT method before their use in the signal calculation.

The electrochemical oxidation process of the gold surface starts with the hydroxyl ion electrosorption, which at more positive potentials results in the gold oxide formation, undergoing structural rearrangement [55]. Also, the surface oxidation can be initiated by the water molecule adsorption and, at a more positive potential, AuOH is formed leading to a two-dimensional phase formation of the gold oxide;

$$2Au + 3H_2O \rightarrow Au_2O_3 + 6e + 6H^+ \quad (1)$$

An example of the recorded CVs is demonstrated in Fig. 4 (a and b). Fig. 3a shows a CV sequence recorded during the flow analysis for the drug determination. The injection volume was 50 μL of (5.0×10^{-6} mol L^{-1}) morphine (in 0.05 mol L^{-1} H_3PO_4) into the eluent solution, containing 0.05 mol L^{-1} H_3PO_4. The time axis of the graph represents the time of the flow injection experiment. In the absence of morphine, the shape of the CV curves is typical for a polycrystalline gold electrode in acidic media [56]. Fig. 4b illustrates the absolute current changes in the CVs curves, after subtracting the average background of 4 CVs (in the absence of the analyte). Evidently, this way of presenting the electrode response gives more details about the adsorbed ion effect on the CV currents. As a matter of fact, the curves show that the current changes mainly take place at the potential regions of the oxidation and reduction of gold. When the electrode-solution interface is exposed to morphine, which can be adsorbed on the electrode, the oxide formation process

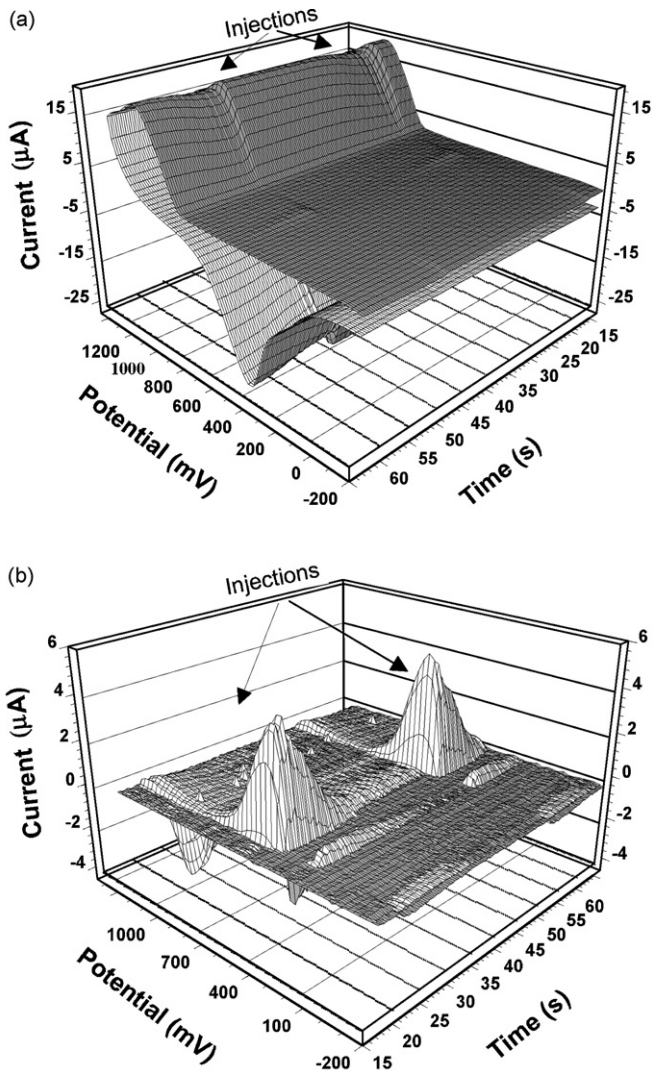

Fig. 4. (a) Cyclic voltammogram at a 12.5 μm Au ultramicroelectrode recorded during a flow injection experiment. The eluent was 0.05 M H_3PO_4, the flow rate was 100 μL s^{-1} and the sweep rate was 40 V s^{-1}. Each scan was preceded by 100 ms (at 1600 mV) and 100 ms (at 300 mV) conditioning, respectively. The accumulation time was 400 ms at 300 mV. The injected solution (50 μL) contained 50×10^{-6} mol L^{-1} morphine in 0.05 M H_3PO_4. (b) Curves result from the subtraction of the CVs average (in the absence of the analyte) from the test of the CVs in (a).

becomes severely inhibited. In detail, the surface process inhibition causes significant change in the currents at the potential region and, as a consequence, the profound changes in the shape of the CVs take place. In chromatographic analysis, where a mixture of compounds presents in the sample, the universality of the detector is beneficial.

Theoretically, the analyte response can be affected by the thermodynamic and kinetic parameters of adsorption, the mass transport rate and the electrochemical behavior of the adsorbed species. The free energy and the adsorption rate depend on the electrode potential, the electrode material and, to some extent, on the choice of the concentration and the type of the supporting electrolyte. By taking these points into consideration, for the achievement of the detector maximum performance, the effect of the experimental parameters (such as the pH of the supporting

electrolyte, the potential, the accumulation time and the potential scan rate) must be examined and optimized [57–63].

3.2. Experimental parameter optimization

The pH effect of the eluent on the detector performance was examined additionally. The corresponding results were shown that the best S/N ratio was obtained between the pH values of 2–3. Moreover, it is illustrated that, at pH values higher than 9, the noise level in the baseline (ΔQ versus Time), is higher up to 12%, compared with that of the acidic solution.

Also, for the investigation of the scan rates influence and the eluent flow rate on the sensitivity of the detector response, solutions having a concentration of (2.0×10^{-7} mol L^{-1}) in morphine were injected. At different scan rates (from 10 to 200 V s^{-1}) and eluent flow, the detector responses to the injected sample were recorded. These results are presented in Fig. 5. As it is clear from Fig. 5, the detector exhibits the maximum sensitivity at the scan rate of (40 V s^{-1}) and flow rate of (3 mL min^{-1}). The sweep rate effects on the detection performance can be considered in three different aspects: firstly, speed in data acquisition; secondly, kinetic factors of the morphine adsorption and, finally, the eluent flow rate which controls the time window of the solution zone in the detector. The main reason for the application of high scan rates is the desorption prevention of the adsorbed morphine during the potential scanning (because under this condition, the inhibition outcome of the adsorbed morphine on the oxidation process can take place).

It is a fact that the employment of high scan rates is required for the use of this detection method in conjunction with fast separation techniques such as capillary electrophoresis. From this point of view, it is necessary to check how the method sensitivity is affected by the sweep rate. Therefore, high sweep rates must be employed to detect the amount of the adsorbed analyte on the electrode surface, so that the potential scanning step is short in comparison with the accumulation period. An important point to be taken into consideration is the time when the morphine accumulation occurs at a potential that is greater or smaller than E_i, However, the sensitivity of the detection system mainly depends on the potential sweep rate, mostly because of the adsorption kinetic factors and the instrumental limitations.

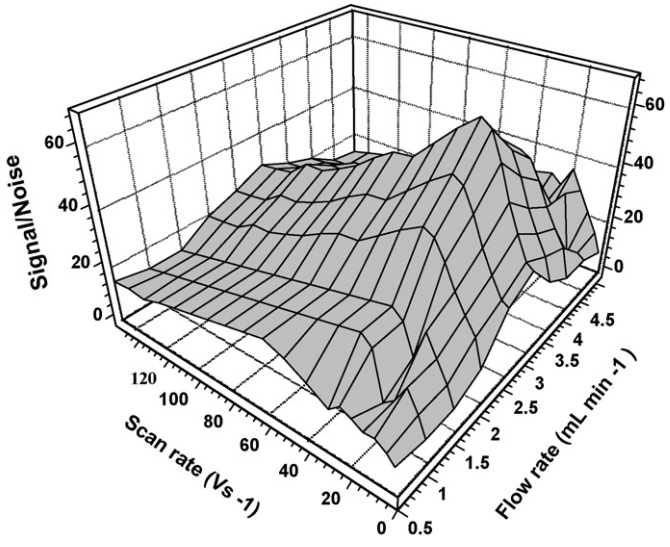

Fig. 5. The effect of the sweep rate on the response of the Au electrode (with a radius of 12.5 μm) to injections of 2.0×10^{-7} mol L^{-1} in 0.05 mol L^{-1} H_3PO_4 and the effect of the flow rate.

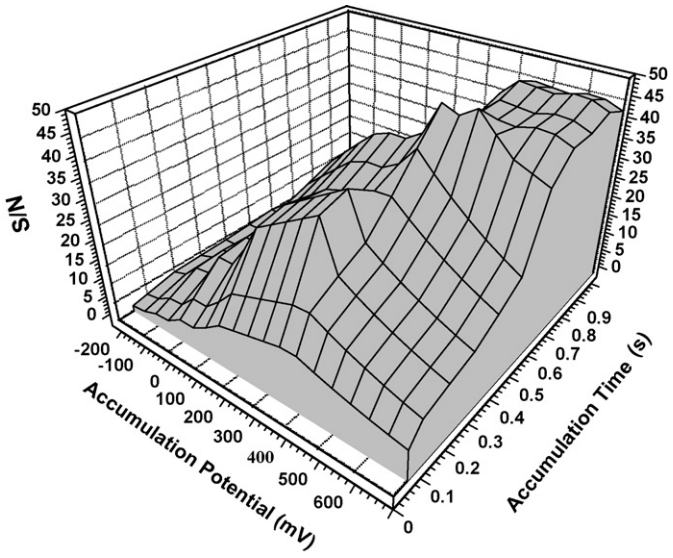

Fig. 6. The effect of the accumulation potential and the effect of the accumulation time on the electrode response to injections of 2.0×10^{-7} mol L^{-1} morphine in 0.05 mol L^{-1} H_3PO_4.

Notably, any changes in the parameters, related to the adsorption process and affecting the applied potential, the time and the potential of accumulation, severely influence the sensitivity of the measurement. For that reason, the influence of the accumulation potential and time on the response of the method for the injection of a solution of (2.0×10^{-7} mol L^{-1}) morphine, in 0.05 mol L^{-1} H_3PO_4, was studied. Fig. 6 shows the detector response over the accumulation potential ranges from (−300 to 700 mV) and the accumulation time range from (0.05 to 1.0 s). From this figure derives the conclusion that the optimum conditions to be chosen are accumulation potential of (400 mV) and accumulation time of (600 ms), on the grounds that the electrode surface becomes morphine saturated within a (600 ms) time window.

On the electrode, the morphine accumulation takes place during the accumulation step (assuming that an appropriate potential is selected). In fact, the difference in the saturation time of the various compounds can be related to the existing differences in their kinetics of the electron transfer and mass transport. As mentioned above, the surface of the gold ultra microelectrode is small and in a short time the electrode surface can be saturated.

3.3. Validation

The method was validated in terms of linearity, limit of quantitation (LOQ), limit of detection (LOD), precision, accuracy, ruggedness/robustness, recovery and selectivity [64–67].

The linearity was evaluated by linear regression analysis, which was calculated by the least square regression method

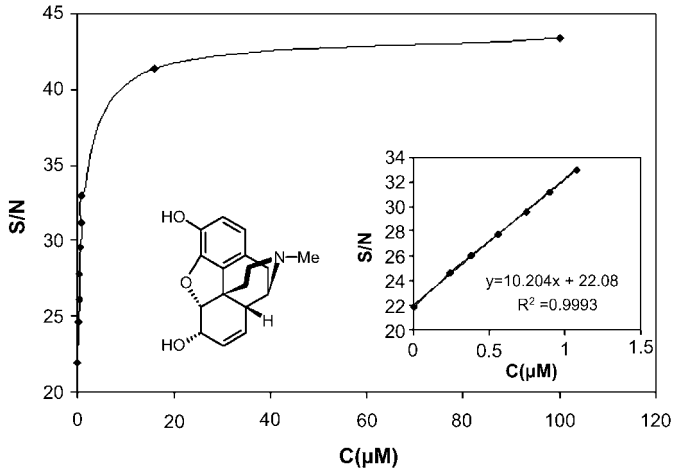

Fig. 7. Calibration curves obtained for morphine on the Au electrode in 0.05 mol L^{-1} H_3PO_4.

[68,69]. The calibration curves, constructed for morphine, were linear over the concentration range of (285–305,300 pg mL^{-1}). The peak areas of morphine were plotted versus its concentration and, then, linear regression analysis was carried out on the resultant curve. After this analysis, a correlation coefficient of $R = 0.999$ and %R.S.D. values, ranging from 0.18 to 3.85% across the studied concentration range, were obtained. Typically, the regression equation for the calibration curve was found to be $Y = 10.204X + 22.08$. Fig. 7 depicts the calibration graph that resulted from the monitoring of morphine in a 0.05 mol L^{-1} H_3PO_4.

Concerning the LOD value, it was measured as the lowest analyte amount that may be detected to produce a response, which is significantly different from that of a blank one. The limit of detection was approved by calculations, based on the standard deviation of the response (δ) and the slope (S) of the calibration curve, at the levels approaching the limits according to the equation LOD = 3.3 (δ/S) [70]. The LOD for morphine was found to be (95.5 pg mL^{-1}).

On the other hand, the LOQ was measured as the lowest analyte amount that can be reproducibly quantified above the baseline noise, for which triplicated injections resulted in an R.S.D. ≤1.49%. A practical LOQ, giving a good precision and acceptable accuracy, was equivalent to (285 pg mL^{-1}).

The precision of the assay was investigated with respect to both repeatability and reproducibility. The repeatability was investigated by injecting nine replicate samples of each of the (285, 10,000 and 305,300 pg mL^{-1}) standards, where the mean concentrations were found to be (293, 10,134 and 304,296) with associated %R.S.D. values of 3.84, 1.11 and 0.34, respectively. Additionally, the inter-day precision was assessed by injecting the same three concentrations over 3 consecutive days, resulting in mean morphine concentrations of (297, 10,137 and 304,293 pg mL^{-1}) and associated %R.S.D. of 3.65, 2.31 and 1.13%, respectively.

Regarding the accuracy of the assay, it was determined by the interpolation of replicate ($n = 6$) peak areas of three accuracy standards (285, 10,000 and 305,300 pg mL^{-1}) from a calibration curve prepared as previously described. In each case, the relevant error percentage and the accuracy was calculated. The resultant concentrations were (296 ± 11.12 pg mL^{-1}), (10,130 ± 165 pg mL^{-1}) and (304,300 ± 987 pg mL^{-1}) with relevant error percentage of 3.83, 1.34 and 0.3%, respectively.

Table 1
Influence of the changes in the experimental conditions on the performance of the FIA system

Parameter	Modification	Morphine (% recovery)
pH	1.8	101.5
	2	100.8
	2.3	101.2
	3.0	100.4
Flow rate (mL min^{-1})	2.8	101.6
	3.0	101.3
	3.2	99.9
Buffer composition (M)	0.04	99.8
	0.05	100.5
	0.06	101.4
Laboratory temperature (°C)	20	100.4
	25	99.6
	30	100.2

The ruggedness of the method was calculated by the comparison of the intra- and inter-day assay results for morphine undertaken by two analysts. The %R.S.D. values for intra- and inter-day assays of morphine in the cited formulations, performed in the same laboratory by the two analysts, did not exceed 4%; thus, indicating the ruggedness of the method. Also, the robustness of the method was investigated under a variety of conditions such as small changes in the pH of the eluent, in the flow rate, in the buffer composition and in the laboratory temperature [71]. As it can be seen in Table 1, the morphine recovery percentages were good under most conditions, not demonstrating any significant change when the critical parameters were modified.

A known amount of morphine standard powder was added to the samples of the tablets, which was then extracted, diluted and analyzed as previously described. The final nominal concentration of morphine was found to be (15996.3 pg mL^{-1}). The examination was repeated ($n = 9$) for 3 consecutive days to obtain intermediate precision data. The resultant %R.S.D. value for this study was found to be 2.13% with a corresponding recovery percentage value of 99.97%.

The method selectivity was checked by the monitoring of the morphine standard solutions in the presence of the formulation components. The responses were not different from that obtained in the calibration. Hence, the determination of morphine in this formulation was considered to be free from component formulation.

3.4. Assay of tablets

The developed method in the present study was applied for the determination of morphine in tablets from the Iranian market. The respective results illustrated a recovery percentage of 99.93% and an R.S.D. value of 1.37%.

Table 2
Application of the proposed method to the determination of morphine in spiked human plasma and urine

Added (ng mL^{-1})	Interpolated concentration	R.S.D. (%)	R.E. (%)
1 (Plasma)	0.96 ± 0.03	3.13	4.05
6 (Urine)	5.82 ± 0.13	2.20	3.10

Data obtained from five replicates at each concentration. Interpolated concentration data expressed as mean ± S.D.

Table 3
Comparison between the detection limit of the proposed method with those of other reported methods

Method	DL	Reference no.
Ion mobility spectrometry	5.6×10^{-11} g	[17,18]
HPLC/UV	0.003 nmol mL^{-1}	[9]
LC (direct fluorimetric)	140 pg mL^{-1}	[14]
Capillary electrophoresis	40 ng mL^{-1}	[16]
FFTCV	95.5 pg mL^{-1}	This work

3.5. Determination of morphine in real samples

The proposed method was also applied to the determination of morphine in spiked urine and plasma samples. The results of analysis of spiked human plasma ($n = 5$) and urine ($n = 5$) is shown in Table 2. The results were satisfactory, accurate and precise. No interference was noticed from the urine content, exactly after the dilution with the supporting electrolyte as well as after the plasma samples treatment. The major advantage of the method as applied to plasma and urine is that no prior extraction step is required.

3.6. Sensitivity comparison of the suggested method with other previously reported methods

Table 3 compares the detection limit of the proposed method with those of the other reported methods. As it is immediately evident, the sensitivity of this method is superior to all the respective previously reported sensitivity values. The data in Table 3 reveal that the detection limit of the method is about 14.5 times lower than the detection limit of the most sensitive reported method.

References

[1] World Health Organization, Cancer Pain Relief, second ed., World Health Organization, Geneva, 1986.
[2] R.W. Milne, R.L. Nation, A.A. Somogyi, Drug Metab. Rev. 28 (1996) 345.
[3] S.Y. Yeh, C.W. Gorodetzky, J. Pharm. Sci. 66 (1977) 1288.
[4] S.Y. Yeh, H.A. Krebs, C.W. Gorodetzky, J. Pharm. Sci. 68 (1979) 133.
[5] U. Hofmann, S. Seefried, E. Schweizer, T. Ebner, G. Mikus, M. Eichelbaum, J. Chromatogr. B 727 (1999) 81.
[6] E. Marengo, M. Aceto, V. Maurino, J. Chromatogr. A 943 (2001) 123.
[7] C. Meadway, S. George, R. Braithwaite, Forensic Sci. Int. 127 (2002) 136.
[8] C. Yin, C. Tang, X. Wu, J. Pharm. Biomed. Anal. 33 (2003) 39.
[9] J.A. Gunn, C. Shelley, S.W. Lewis, T. Toop, M. Archer, J. Anal. Toxicol. 30 (2006) 519.
[10] Q.C. Meng, M.S. Cepeda, T. Kramer, H. Zou, D.J. Matoka, J. Farrar, J. Chromatogr. B 724 (2000) 115.
[11] L. Shehong, H. Chiyang, G. Fei, L. Daobing, C. Zheng, L. Huwei, L. Kean, L. Feng, Talanta (2006), in press.
[12] Y. Zhuang, X. Cai, J. Yu, H. Ju, J. Photochem. Photobiol. A 162 (2004) 457.
[13] G.M. Greenway, L.J. Nelstrop, S.N. Port, Anal. Chim. Acta 405 (2000) 43.
[14] S. Hara, S. Mochinaga, M. Fukuzawa, N. Ono, T. Kuroda, Anal. Chim. Acta 378 (1999) 121.
[15] I.S. Lurie, S. Panicker, P.A. Hays, A.D. Garcia, B.L. Geer, J. Chromatogr. A 984 (2003) 109.
[16] X. Zhang, J. Li, J. Gao, L. Sun, W. Chang, J. Chromatogr. A 895 (2000) 1.
[17] L.M. Matz, H.H. Hill, Anal. Chem. 73 (2001) 1664.
[18] M.A. McCooeye, B. Ells, D.A. Barnett, R.W. Purves, R. Guevremont, J. Anal. Toxicol. 25 (2001) 81.
[19] A. Salimi, R. Hallaj, G.R. Khayatian, Electroanalysis 17 (2005) 873.
[20] H.H. Maurer, Comb. Chem. High Throughput Screen 3 (2000) 461.
[21] J.F. Van Bocxlaer, K.M. Clauwaert, W.E. Lambert, D.L. Deforce, E.G. Van Eeckhout, A.P. De-Leenheer, Mass Spectrom. Rev. 19 (2000) 165.
[22] P. Marquet, Ther. Drug Monit. 24 (2002) 225.
[23] H.H. Maurer, Clin. Chem. Lab. Med. 42 (2004) 1310.
[24] H.H. Maurer, Anal. Bioanal. Chem. 381 (2005) 110.
[25] J.W. Lee, J.E. Pederson, T.L. Moravetz, A.M. Dzerk, A.D. Mundt, K.V. Shepard, J. Pharm. Sci. 80 (1991) 284.
[26] K. Otter, C. Mignat, D. Heber, A. Ziegler, Biomed. Chromatogr. 14 (2000) 327.
[27] O. Beck, I. Ohman, H.K. Nordgren, Ther. Drug Monit. 28 (2006) 603.
[28] S. Emara, I. Darwish, D. Youssef, T. Masujima, Biomed. Chromatogr. 18 (2004) 21.
[29] M. Freiermuth, J.C. Plasse, J. Pharm. Biomed. Anal. 15 (1997) 759.
[30] R.F. Venn, A. Michalkienwicz, J. Chromatogr. 525 (1990) 379.
[31] J. Huwyler, S. Rufer, E. Kuters, J. Drewe, J. Chromatogr. A 674 (1995) 57.
[32] J.O. Svensson, J. Chromatogr. 375 (1986) 174.
[33] M. Konishi, H. Hashimoto, J. Pharm. Sci. 79 (1990) 379.
[34] P.P. Rop, F. Grimoldi, J. Burle, M.N. De SaintLeger, A. Viala, J. Chromatogr. B 661 (1994) 245.
[35] M. Pawula, D.A. Barrett, P.N. Shaw, J. Pharm. Biomed. Anal. 11 (1993) 401.
[36] Y. Rotshteyn, B. Weingarten, Ther. Drug Monit. 18 (1996) 179.
[37] D. Hummel, D. Loffler, G. Fink, T.A. Ternes, Environ. Sci. Technol. 40 (2006) 7321.
[38] N. Tyrefors, B. Hyllbrant, L. Ekman, M. Johansson, B. Langstrom, J. Chromatogr. A 279 (1996) 279.
[39] M.J. Bogusz, R.D. Maier, M. Erkens, S. Driessen, J. Chromatogr. B 703 (1997) 115.
[40] G. Schanzle, S. Li, G. Mikus, U. Hofmann, J. Chromatogr. B 721 (1999) 55.
[41] A.D. Nagy, L. River, C. Giroud, M. Augsburger, P. Mangin, J. Chromatogr. A 854 (1999) 109.
[42] L. Kristoffersen, A. Bugge, E. Lundanes, L. Slørdal, J. Chromatogr. B 734 (1999) 229.
[43] P.T. Kissinger, W.R. Heineman, Laboratory Techniques in Electroanalytical Chemistry, Marcel Dekker, New York, 1984.
[44] S.F.Y. Li, Capillary Electrophoresis, Principles Practice and Applications, Elsevier, Amsterdam, 1992.
[45] R.M. Wightman, D.O. Wipf, in: A.J. Bard (Ed.), Electroanalytical Chemistry, vol. 15, Marcel Dekker, New York, 1989.
[46] M. Paeschke, F. Dietrich, A. Ulig, R. Hintsche, Electroanalysis 8 (1996) 891.
[47] T. Dimitrakopoulos, P.W. Alexander, D.B. Hibbert, Electroanalysis 8 (1996) 438.
[48] V. Cosofret, M. Erdosy, T.A. Johnson, R.P. Buck, R.B. Ash, M.R. Neuman, Anal. Chem. 67 (1995) 1647.
[49] R. Hintsche, M. Paeschke, U. Wollenberger, U. Schnakenberg, B. Wagner, T. Lisec, Biosens. Bioelectron. 9 (1994) 697.
[50] P. Norouzi, M.R. Ganjali, P. Matloobi, Electrochem. Commun. 7 (2005) 33.
[51] P. Norouzi, G.R. Nabi Bidhendi, M.R. Ganjali, A. Sepehri, M. Ghorbani, Microchim. Acta 152 (2005) 123.
[52] M.R. Ganjali, P. Norouzi, M. Ghorbani, A. Sepehri, Talanta 66 (2005) 1225.

[53] P. Norouzi, M.R. Ganjali, M. Ghorbani, A. Sepehri, Sens. Actuators B 110 (2005) 239.
[54] P. Norouzi, M.R. Ganjali, T. Alizadeh, P. Daneshgar, Electroanalysis 18 (2006) 947.
[55] J. Lipkowski, L. Stolberg, Adsorption of Molecules at Metal Electrodes, VCH, New York, 1992.
[56] J.O.M. Bockris, B.E. Conway, E. Yeager, Comprehensive Treatise of Electrochemistry, Plenum, New York, London, 1980.
[57] P. Norouzi, M.R. Ganjali, S. Shirvani-Arani, A. Mohammadi, J. Pharm. Sci. 96 (2007) 893.
[58] P. Norouzi, S. Shirvani-Arani, P. Daneshgar, M.R. Ganjali, Biosens. Bioelectron. 22 (2007) 1068.
[59] P. Norouzi, P. daneshgar, M.R. Ganjali, A.A. Moosavi-Movahedi, J. Brazilian Chem. Soc. 18 (2007) 231.
[60] P. Norouzi, M.R. Ganjali, P. Daneshgar, Anal. Lett. 40 (2007) 547.
[61] P. Norouzi, M.R. Ganjali, L. Hajiaghababaei, Anal. Lett. 39 (2006) 1941.
[62] P. Norouzi, M.R.Ganjali, S. Labbafi, A. Mohammadi, Anal. Lett., 2007.
[63] P. Norouzi, M.R. Ganjali, P. Daneshgar, J. Pharm. Toxicol. Method 55 (2007) 289.
[64] A. Mohammadi, I. Haririan, N. Rezanour, L. Ghiasi, R.B. Walker, J. Chromatogr. A 1116 (2006) 153.
[65] A. Mohammadi, I. Kanfer, V. Sewram, R.B. Walker, J. Chromatogr. B 824 (2005) 148.
[66] A. Mohammadi, N. Rezanour, M. Ansari Dogaheh, F. Ghorbani Bidkorbeh, M. Hashem, R.B. Walker, J. Chromatogr. B 846 (2007) 215.
[67] United States Pharmacopoeia 28-NF 23, United States Pharmacopeial Convention, INC., M.D. Rockville, 2748, 2005.
[68] J.C. Miller, J.N. Miller, Statistics for Analytical Chemistry, vol. 22, Ellis Horwood, Chichester, 1984, p. 82.
[69] Z. Al-Kurdi, T. Al-Jallad, A. Badwanamd, A.M.Y. Jaber, Talanta 50 (1999) 1089.
[70] International Conference on Harmonization (ICH) Topic Q2 B: Validation of Analytical Procedures: Methodology, The European Agency for the Evaluation of Medicinal Products, Geneva, 1996.
[71] Y.V. Heyden, A. Nijhuis, J. Smeyers-Verbeke, B.G.M. Vandeginste, D.L. Massaret, J. Pharm. Biomed. Anal. 24 (2001) 723.

Available online at www.sciencedirect.com
ScienceDirect
Talanta 73 (2007) 189–193
Talanta
www.elsevier.com/locate/talanta

Short communication

Silver(I) ions-enhanced electrochemiluminescence of tris(2,2-bipyridyl)ruthenium(II)

Lei Qian [a,b], Xiurong Yang [a,*]

[a] *State Key Laboratory of Electroanalytical Chemistry, Changchun Institute of Applied Chemistry, Chinese Academy of Sciences, Changchun, Jilin 130022, China*
[b] *Graduate School of the Chinese Academy of Sciences, Beijing 100039, China*

Received 1 February 2007; received in revised form 1 March 2007; accepted 9 March 2007
Available online 19 March 2007

Abstract

In this paper, we demonstrate an electrochemiluminescence (ECL) enhancement of tris(2,2-bipyridyl)ruthenium(II) ($Ru(bpy)_3^{2+}$) by the addition of silver(I) ions. The maximum enhancement factor of about 5 was obtained on a glassy carbon electrode in the absence of co-reactant. The enhancement of ECL intensity was possibly attributed to the unique catalytic activity of Ag^+ for reactions between $Ru(bpy)_3^{3+}$ with OH. The higher enhancement was observed in phosphate buffer solutions compared with that from borate buffer solutions. This resulted from the fact that formation of nanoparticles with large surface area in the phosphate buffer solution exhibited high catalytic activity. The amount of Ag^+, solution pH and working electrode materials played important roles for the ECL enhancement. We also studied the effects of Ag^+ on $Ru(bpy)_3^{2+}$/tripropylamine and $Ru(bpy)_3^{2+}/C_2O_4^{2-}$ ECL systems.

Keywords: Ag^+; $Ru(bpy)_3^{2+}$; ECL

1. Introduction

Electrochemiluminescence (ECL) has received much attention and become an important detection method in analytical chemistry. ECL advantages include high selectivity, sensitivity and simple operation process. Tris(2,2-bipyridyl)ruthenium(II) ($Ru(bpy)_3^{2+}$) and luminol are usually used as ECL substrates due to their high quantum yields and stable signals. A large amount of analytes can be detected by $Ru(bpy)_3^{2+}$-ECL, including alkylamine, oxalate and amino acids [1–4]. Based on $Ru(bpy)_3Cl_2$ as a label, this method is also used in immunoassay and DNA analysis [5,6]. The ECL of luminol has been used to determine hydrogen peroxide and glucose [7,8].

Metallic nanoparticles have unique optical, catalytic properties and have been widely used in many fields. Au and Ag nanoparticles have recently been used to enhance or quench fluorescence of dyes and semiconductor nanoparticles. The enhancement of luminescence intensity is dependent on size, and shapes of nanostructures and distance between fluorophore and nanostructures [9–11]. Through efficient coupling between excitation or emission bands of semiconductor nanoparticles and surface plasmon resonance of nanostructures, the strong luminescence enhancement of semiconductor nanoparticles can be achieved [11]. Pompa et al. [11] have reported that fluorescence of CdSe/ZnS nanocrystals was enhanced on an ordered array of gold nanostructures. Five-fold fluorescence enhancement of CdTe nanoparticles has also been observed on the silver island films [12]. Deposition of silver nanoparticles onto dye monolayer film has also increased photoluminescence of dyes [13]. Fluorescence enhancement of dyes can be obtained from metal-core/silica-shell nanoparticles [14]. Cheng and Xu [15] have reported that fluorescence enhancement of fluorescein isothiocyanate could be adjusted by the distance between Ag nanoparticles and dyes. Metallic nanoparticles are also used to increase ECL intensity. ECL intensity of $Ru(bpy)_3^{2+}$/pentoxyverine has been enhanced by the introduction of gold nanoparticles [16]. It has been reported that strong luminol ECL can be observed on a gold nanoparticle modified gold electrode in neutral conditions [17]. However, these enhancements of the ECL intensity are obtained by metallic

* Corresponding author. Tel.: +86 431 5689711; fax: +86 431 5689711.
E-mail address: xryang@ciac.jl.cn (X. Yang).

0039-9140/$ – see front matter © 2007 Elsevier B.V. All rights reserved.
doi:10.1016/j.talanta.2007.03.016

nanoparticles and there are few papers about ECL enhancement of $Ru(bpy)_3^{2+}$ via metallic ions. In this paper, an enhancement of ECL signals of $Ru(bpy)_3^{2+}$ by the addition of Ag^+ into the phosphate buffer solutions was reported. The maximum enhancement of five times was obtained from 0.1 mM $Ru(bpy)_3^{2+}$ and 1 mM $AgNO_3$ in 50 mM phosphate buffer solution (pH 7.5) without co-reactant on a glassy carbon electrode (GCE). The enhancement was also observed on a gold electrode and no enhancement was observed on an indium tin oxide electrode. Between pH 7.0 and 7.5, the optimal relative ECL intensity was obtained. At last, the effect of Ag^+ on ECL of $Ru(bpy)_3^{2+}$ in the presence of tripropylamine (TPA) or $C_2O_4^{2-}$ was also examined.

2. Experimental

2.1. Chemicals and reagents

$Ru(bpy)_3Cl_2{\cdot}6H_2O$ was obtained from Aldrich. $AgNO_3$, $HAuCl_4$, H_2PtCl_6 and tripropylamine (TPA) were purchased from ACROS. $H_2C_2O_4{\cdot}2H_2O$ was obtained from Beijing Chemical Factory. All chemicals and reagents were of analytical grade. All solutions were prepared with distilled water.

2.2. Apparatus and procedures

ECL signal was obtained from on MPI-A chemiluminescence analyzer (Xi'An Remax Science & Technology Company, Xi'An, China) and ECL experiments were carried out in 1 ml of 50 mM buffer solution (pH 7.5) containing 0.1 mM $Ru(bpy)_3^{2+}$. Electrochemical experiments were carried out with a CHI 660B (Shanghai, China). A three-electrode system was used with a glassy carbon electrode as the working electrode. The reference electrode was an Ag/AgCl (saturated potassium chloride solution) electrode, and the counter electrode was a platinum plate. The GCE was polished with α-Al_2O_3 powder (followed by 1.0, 0.3 and 0.05 μm), and sonicated in distilled water and dried by nitrogen.

Sixty microlitres of 10 mM $AgNO_3$ was added into 1 ml of 50 mM phosphate solution (pH 7.5) containing 0.1 mM $Ru(bpy)_3^{2+}$ and the mixed solution became buff and turbid. The mixture was centrifuged three times with washing by water and the precipitates were obtained. Morphologies were characterized by field-emission scanning electron microscopy (FE-SEM). The images were obtained from PHILIPS XL-30 ESEM with an accelerating voltage of 20 kV. The compositions were characterized by energy-dispersive spectroscopy (EDS).

3. Results and discussion

Fig. 1 gives cyclic voltammograms from 0.1 mM $Ru(bpy)_3^{2+}$ on the GCE in 50 mM phosphate buffer solution (pH 7.5) without (a) and with 0.6 mM $AgNO_3$ (b) at a scan rate of 100 mV s^{-1}. A couple of redox peaks at about 1.1 V corresponding to the redox process of $Ru(bpy)_3^{2+}$ was observed from curve a. However, the peak currents obviously increased with the addition of 0.6 mM $AgNO_3$ (curve b). This indicated that Ag^+ ions could affect the redox reaction of $Ru(bpy)_3^{2+}$ on the electrode surface. We also

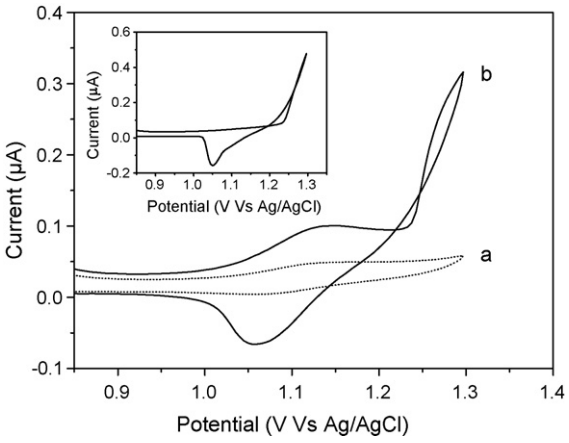

Fig. 1. Cyclic voltammograms from 0.1 mM $Ru(bpy)_3^{2+}$ on the GCE in 50 mM phosphate buffer solution (pH 7.5) without (a) and with 0.6 mM $AgNO_3$ (b). Inset: cyclic voltammogram of the GCE in 50 mM phosphate buffer solution with 0.6 mM $AgNO_3$. Scan rate, 100 mV s^{-1}.

studied the electrochemical properties of silver ions on the GCE and the corresponding cyclic voltammogram is shown in the inset of Fig. 1. As shown in the inset, only an obvious reductive peak at about 1.05 V was observed. Thus, the large oxidative peak of curve b arose from the oxidation of $Ru(bpy)_3^{2+}$. This also showed that Ag^+ ions were in favor of the oxidation of $Ru(bpy)_3^{2+}$ on the electrode surface.

ECL behavior of $Ru(bpy)_3Cl_2$ in the presence of $AgNO_3$ was also investigated. Fig. 2A corresponds to the ECL–potential profile from 0.1 mM $Ru(bpy)_3^{2+}$ on the GCE in 50 mM phosphate buffer solution (pH 7.5) without (a) and with 0.6 mM $AgNO_3$ (b). The maximum ECL signal appeared for curve a at about 1.2 V, resulting from oxidation of $Ru(bpy)_3^{2+}$. In the absence of co-reactant, $Ru(bpy)_3^{2+}$ was firstly oxidized to $Ru(bpy)_3^{3+}$ on electrodes, then $Ru(bpy)_3^{3+}$ reacted with OH and produced $Ru(bpy)_3^{2+*}$, which decayed to the ground state with luminescence [18]. However, higher ECL intensity was observed with the addition of Ag^+ (curve b). It was found that the ECL enhancement with Ag^+ was approximately four-fold the ECL without silver nitrate. There was no ECL signal for 50 mM buffer solution only containing 0.6 mM $AgNO_3$. Thus, the luminescence signal was from $Ru(bpy)_3^{2+}$. No enhancement was observed with the addition of $NaNO_3$ into the phosphate buffer solution containing $Ru(bpy)_3^{2+}$ (Fig. 2B). This showed that the ECL enhancement resulted from Ag^+. We thought that the enhancement of ECL was possibly attributed to the catalytic activity of Ag^+ towards the reactions between OH and $Ru(bpy)_3^{3+}$. This increased the reaction rate and led to the formation of more $Ru(bpy)_3^{2+*}$. We observed that the solution became turbid after the addition of $AgNO_3$ into the phosphate buffer solution containing $Ru(bpy)_3^{2+}$. The precipitates were obtained by centrifugation and were characterized by FE-SEM. Fig. 3 gives the image and composition analysis of these precipitates. As shown in Fig. 3a, the precipitates consisted of many nanoparticles and most of them exhibited spherical shapes. The signals of O, Cl, P and Ag elements were observed from the results of EDS (Fig. 3b). The ECL enhancement was also observed in borate buffer solutions, but the maximum enhancement factor was low compared

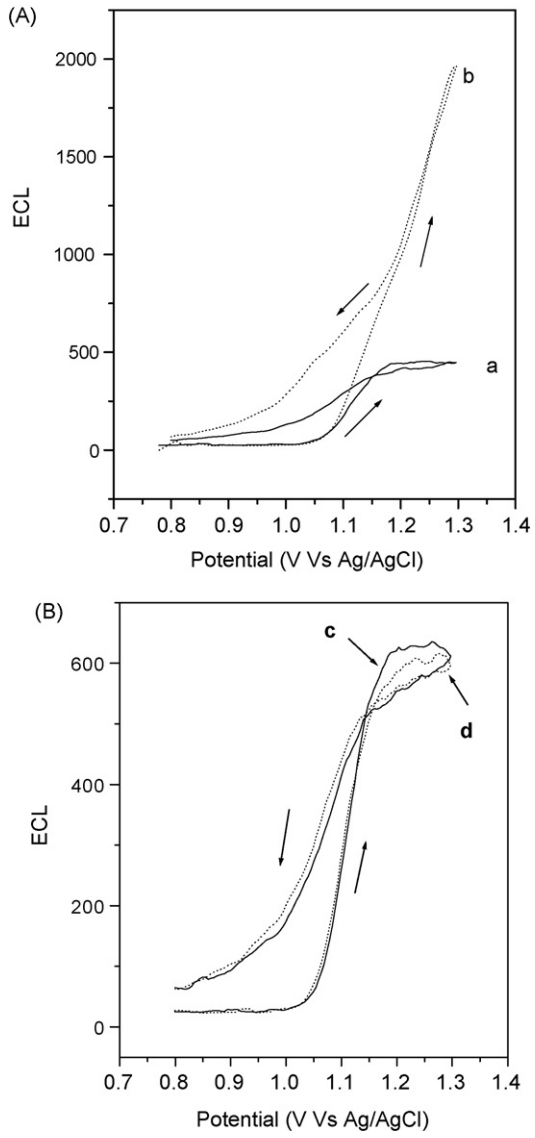

Fig. 2. (A) ECL-profile from 0.1 mM $Ru(bpy)_3^{2+}$ on the GCE in 50 mM phosphate buffer solution (pH 7.5) without (a) and with 0.6 mM $AgNO_3$ (b) and (B) ECL-profile from 0.1 mM $Ru(bpy)_3^{2+}$ on the GCE in 50 mM phosphate buffer solution (pH 7.5) without (c) and with 0.6 mM $NaNO_3$ (d). Scan rate, 100 mV s^{-1}; PMT, biased at 900 V. The arrows show the potential scan direction.

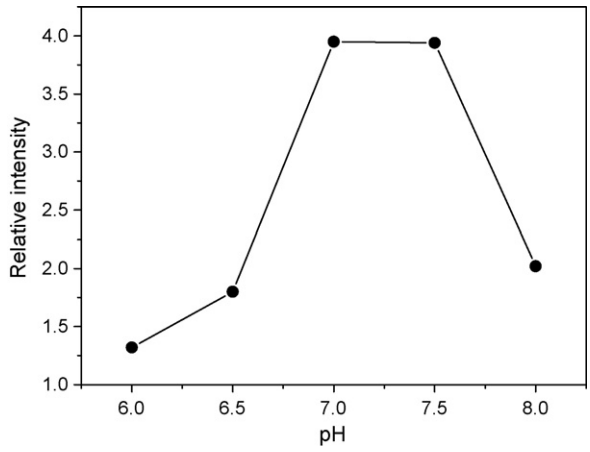

Fig. 4. Effect of pH on the relative ECL intensity. Conditions: $Ru(bpy)_3^{2+}$, 0.1 mM; $AgNO_3$, 0.6 mM; scan rate, 100 mV s^{-1}; PMT, biased at 900 V.

with that from phosphate buffer solutions. No precipitates were observed, when $AgNO_3$ solution was mixed with the borate buffer solution. The better enhancement in phosphate buffer solution was possibly attributed to formation of nanoparticles, which exhibited large surface area and this resulted in higher catalytic activity.

The relative ECL intensity was dependent on the solution pH. As shown in Fig. 4, the maximum relative ECL intensity appeared between pH 7.0 and 7.5. At pH < 7.0, the amount of OH was small in the solution. The reactions between OH and $Ru(bpy)_3^{3+}$ were affected and less $Ru(bpy)_3^{2+*}$ appeared. Thus, the low ECL intensity was observed. When the solution pH was above 7.5, large amounts of OH were easily oxidized to oxygen on the electrode surface [18]. It is well known that oxygen can quench the luminescence of $Ru(bpy)_3^{2+}$. This resulted in low ECL signals. Fig. 5A shows the relationship between the ECL intensity and the amount of $AgNO_3$ on a GCE (a), gold electrode (b) and indium tin oxide electrode (c). For the GCE and gold electrodes, the ECL intensity increased with the addition of more $AgNO_3$. When the content was more than 0.8 mM, the ECL intensity did not obviously increase. The maximum enhancement factor was about 5 and 4 for the GCE and gold electrode, respectively. No ECL enhancement was observed on an indium tin oxide electrode (curve c). This indicated that different work-

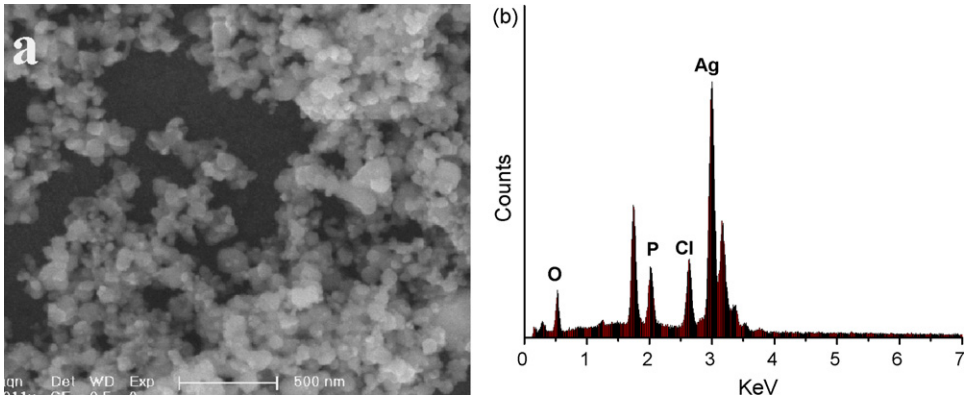

Fig. 3. The FE-SEM image of the mixtures of $Ru(bpy)_3Cl_2$ and $AgNO_3$ in the phosphate buffer solution (a) and the corresponding EDS spectrum (b).

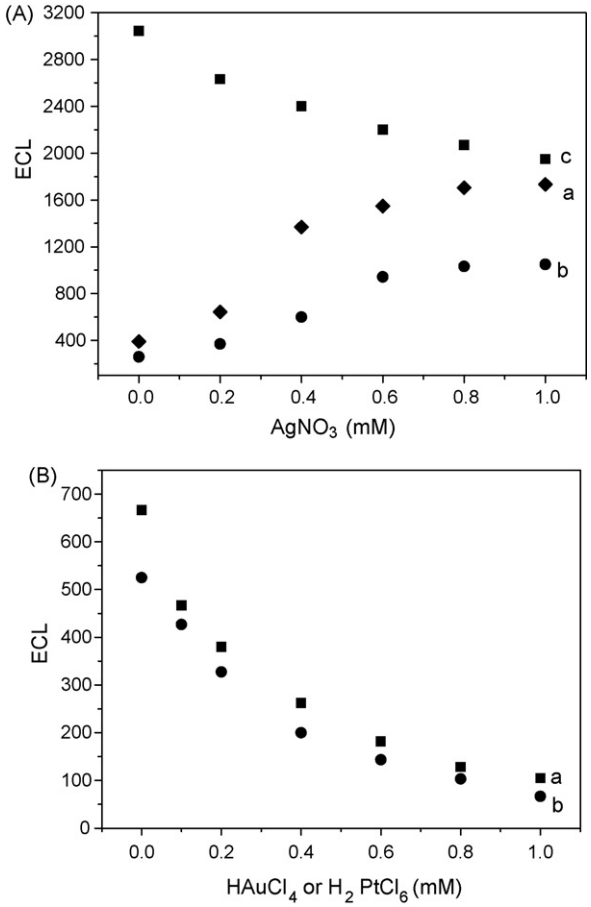

Fig. 5. (A) The relationship between the ECL intensity and the content of $AgNO_3$ on a GCE (a), gold electrode (b) and indium tin oxide electrode (c) and (B) the relationship between the ECL intensity and the content of $HAuCl_4$ (a) and H_2PtCl_6 (b). Conditions: $Ru(bpy)_3^{2+}$, 0.1 mM; pH 7.5; scan rate, 100 mV s^{-1}; PMT, biased at 900 V.

ing electrodes also affected the enhancement of ECL intensity. $HAuCl_4$ and H_2PtCl_6 were also used to study their effects on the ECL intensity of $Ru(bpy)_3^{2+}$. Fig. 5B gives the relationship between the ECL intensity and the content of $HAuCl_4$ (a) and H_2PtCl_6 (b). We found that the ECL intensity decreased with the increase in the amount of $HAuCl_4$ or H_2PtCl_6. This showed that both $HAuCl_4$ and H_2PtCl_6 could not increase the ECL intensity of $Ru(bpy)_3^{2+}$.

$Ru(bpy)_3^{2+}$/TPA and $Ru(bpy)_3^{2+}/C_2O_4^{2-}$ systems have been usually used in analytical ECL applications due to their high ECL efficiency. We also examined the effect of Ag^+ on these systems. Fig. 6 gives the corresponding ECL signal from 0.1 mM $Ru(bpy)_3^{2+}$ and 1 mM $H_2C_2O_4$ in the 50 mM phosphate buffer solution (pH 7.5) without (a) and with 0.6 mM $AgNO_3$ (b). It was found that the ECL intensity obtained in the presence of $AgNO_3$ was about two times that from 0.1 mM $Ru(bpy)_3^{2+}$ without $AgNO_3$. This indicated that Ag^+ also enhanced the ECL intensity of $Ru(bpy)_3^{2+}/C_2O_4^{2-}$ system. The ECL mechanism could be described by the following steps [19]:

$$Ru(bpy)_3^{2+} \rightarrow Ru(bpy)_3^{3+} \quad (1)$$

$$Ru(bpy)_3^{3+} + C_2O_4^{2-} \rightarrow Ru(bpy)_3^{2+} + CO_2^{\bullet -} + CO_2 \quad (2)$$

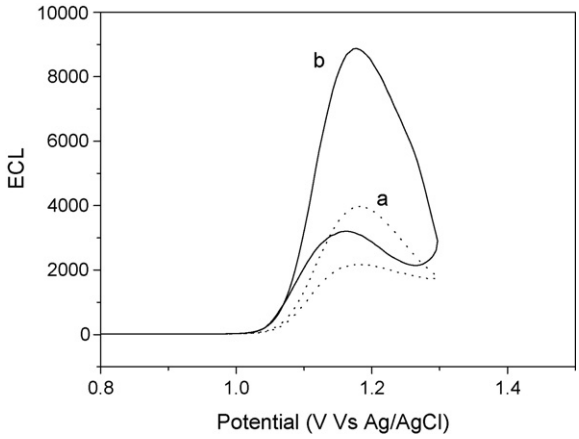

Fig. 6. The ECL curve of 0.1 mM $Ru(bpy)_3^{2+}$ and 1 mM $H_2C_2O_4$ on the GCE in 50 mM phosphate buffer solution (pH 7.5) without (a) and with 0.6 mM $AgNO_3$ (b). Scan rate, 100 mV s^{-1}; PMT, biased at 600 V.

$$CO_2^{\bullet -} + Ru(bpy)_3^{3+} \rightarrow Ru(bpy)_3^{2+*} + CO_2 \quad (3)$$

During the preparation of this paper, Barnett and coworkers [20] reported that the chemiluminescence response from $Ru(bpy)_3^{2+}$, cerium(IV) and citrate was enhanced by catalytic activity of silver(I) citrate complex and initiation of silver nanoparticles. In addition, Ag^+ could catalyze the oxidation of carboxylic acids with cerium(IV) through the formation of Ag^+ and carboxylic acids complex [21]. Here, the enhancement possibly resulted from the catalytic activity of silver(I) and oxalic acid complex for step (2). In addition, the formation of nanoparticles also increased the catalytic efficiency. This directly resulted in large amounts of $CO_2^{\bullet -}$ and more light-emitted species, $Ru(bpy)_3^{2+*}$ formed by step (3). However, no enhancement was observed for the $Ru(bpy)_3^{2+}$/TPA system.

4. Conclusion

In summary, ECL enhancement of $Ru(bpy)_3^{2+}$ with Ag^+ has been demonstrated. The maximum enhancement factor was about 5 in the phosphate buffer solution (pH 7.5) from the GCE without co-reactant. The enhancement was possibly attributed to the unique catalytic activity of Ag^+ towards the reactions of $Ru(bpy)_3^{3+}$ and OH. This resulted in the formation of more $Ru(bpy)_3^{2+*}$ and the ECL intensity was enhanced. We carefully studied the effects of the amount of silver ions, solution pH and electrode materials. At last, it was found that Ag^+ also enhanced ECL of $Ru(bpy)_3^{2+}/C_2O_4^{2-}$ system, but showed no enhancement for $Ru(bpy)_3^{2+}$/TPA system. The interesting enhancement will be useful for analysis and detection based on $Ru(bpy)_3^{2+}$-ECL methods.

Acknowledgements

This work was supported by the National Nature Science Foundation of China with the Grant (No. 20475052) and the National Key Basic Research Development Project Research on Human Major Disease Proteomics (No. 2001CB5102).

References

[1] I. Rubinstein, A.J. Bard, Anal. Chem. 55 (1983) 1580.
[2] S.N. Brune, D.R. Bobbitt, Talanta 38 (1991) 419.
[3] A.J. Bard, Electrogenerated Chemiluminescence, Marcel Dekker, New York, 2004.
[4] M.M. Richter, Chem. Rev. 104 (2004) 3003.
[5] S.J. Miller, P. McCord, A.J. Bard, Langmuir 7 (1991) 2781.
[6] W. Cao, J.P. Ferrance, J. Demas, J.P. Landers, J. Am. Chem. Soc. 128 (2006) 7572.
[7] B. Leca, L.J. Blum, Analyst 125 (2000) 789.
[8] L.D. Zhu, Y.X. Li, F.M. Tian, B. Xu, G.Y. Zhu, Sens. Actuators, B 84 (2002) 265.
[9] J.R. Lakowicz, Anal. Biochem. 337 (2005) 171.
[10] J.R. Lakowicz, Anal. Biochem. 298 (2001) 1.
[11] P.P. Pompa, L. Martiradonna, A.D. torre, F.D. Sala, L. Manna, M. de Vittorio, F. Calabi, R. Cingolan, R. Rinaldi, Nat. Nanotechnol. 1 (2006) 126.
[12] K. Ray, R. Badugu, J.R. Lakowicz, J. Am. Chem. Soc. 128 (2006) 8988.
[13] S. Pan, Z. Wang, L.J. Rothberg, J. Phys. Chem. B 110 (2006) 17383.
[14] O.G. Tovmachenko, C. Graf, D.J. van den Heuvel, A. van Blaaderen, H.C. Gerritsen, Adv. Mater. 18 (2006) 91.
[15] D.M. Cheng, Q.H. Xu, Chem. Commun. 3 (2007) 248.
[16] Y. Liu, W. Pan, Q. Liu, S. Yao, Electrophoresis 16 (2005) 4468.
[17] H. Cui, Y. Xu, Z.F. Zhang, Anal. Chem. 76 (2004) 4002.
[18] W. Cao, J. Jia, X. Yang, S. Dong, E. Wang, Electrophoresis 23 (2002) 3692.
[19] H.S. White, A.J. Bard, J. Am. Chem. Soc. 104 (1982) 6891.
[20] B.A. Gorman, P.S. Francis, D.E. Dunstan, N.W. Barnett, Chem. Commun. 4 (2007) 395.
[21] A.K. Das, Coord. Rev. 213 (2001) 307.

Available online at www.sciencedirect.com
ScienceDirect
Talanta 73 (2007) 12–22
Talanta
www.elsevier.com/locate/talanta

Review

Application of atomic force microscopy to characterize liposomes as drug and gene carriers

Barbara Ruozi, Giovanni Tosi, Eliana Leo, Maria Angela Vandelli *

Department of Pharmaceutical Sciences, University of Modena and Reggio Emilia, Via Campi 183, 41100 Modena, Italy

Received 13 November 2006; received in revised form 7 March 2007; accepted 15 March 2007
Available online 24 March 2007

Abstract

At present, liposomes play a significant role as drug delivery vehicles being considered very promising for gene therapeutics. The *in vivo* application of these drug delivery systems widely depends on their physico-chemical and technological characteristics such as the structure, the shape, the size distribution, the surface modification and the drug interaction. To describe the liposomes, different analytical techniques were used. In this paper, we reviewed the application of the atomic force microscopy (AFM), one of the most commonly applied scanning probe microscopy (SPM) techniques, in the description of liposome. The advantages and limitations of these techniques are discussed comparing the reported data with those referred to other well-know microscopical and spectroscopical techniques such as transmission electron microscopy (TEM) and photon correlation spectroscopy (PCS). A detailed description of the application of AFM to evaluate the formation and the geometry of liposomes/DNA complexes is presented.

Keywords: Liposomes; AFM; Characterization; Surface modification; Liposome/DNA complexes

Contents

1. Introduction

Modern drug carrier systems such as micro-nanoparticles, liposomes, solid lipid nanoparticles and polymeric micelles play an important role in controlled delivery of the active agent to the desired site of action, limiting the side effects at non-target site [1–3]. In particular, in the past decade, liposomes were extensively used in research, analytical and therapeutic applications [4].

Liposomes are micro- or nano-particulate vesicles formed by self-assembly of natural (phospholipids, cholesterol, etc.) or synthetic amphiphiles in aqueous environment. They are formed by concentric lipid bilayer surrounding aqueous compartments [5]. First described by Bangham et al. [6] on the basis of size, liposomes are well-known as small unilamellar vesicles (SUV;

* Corresponding author. Tel.: +39 059 205 5149; fax: +39 059 360113.
E-mail address: vandelli.mariaangela@unimo.it (M.A. Vandelli).

0039-9140/$ – see front matter © 2007 Elsevier B.V. All rights reserved.
doi:10.1016/j.talanta.2007.03.031

20–100 nm), large unilamellar vesicles (LUV; 50–400 nm) and multilamellar vesicles (MLV; 400–5000 nm). Frequently prepared using non-toxic phospholipids and cholesterol, they are biodegradable, biocompatible and non-immunogenic [7]. Considering the drug nature and the liposomal composition, both hydrophilic and hydrophobic compounds can interact with liposomes in different ways; they can be incorporated into the bilayer membrane, adsorbed on the surface, anchored at the polar head group region or entrapped in the aqueous core [8].

Liposomes can be designed for specific and selective applications by controlling the lipid composition or by modifications of the surface meaning conjugation with antibody or peptides [9]. To stabilize against the opsonization, hydrophilic long chain polymers such as polyethylene glycols can be incorporated in the bilayer [10]. The improvement in liposome technology, their versatility but also their safety have given rise to the growing success of liposomes as carriers for diagnostic agents [11,12] and pharmaceuticals [13–15]. In gene therapy, negatively charged DNA can neutralize cationic liposomes resulting in an aggregation and continuous fusion with time while DNA is entrapped during this process [16]. Cationic liposomes have also proven to be useful tools for the delivery of genetic materials into cells [17,18]. More recently, other important applications of liposomes have been reported; for example, in the vaccine field, virosomes, i.e. liposome formulations including viral envelope proteins anchored in the lipid membrane [19,20]. In the near future, many more liposome based-drug formulations can be expected both for the delivery of conventional drugs and for the new biotechnology therapeutics such as enzymes, recombinant proteins and cloned genes [21].

The rapid development of these colloidal systems required a rational characterization approach. Parameters having critical importance on the *in vivo* performance of liposomes such as morphology, size, polydispersity index, number of lamellae, charge, bilayer fluidity, lipid composition, encapsulation efficiency, liposome-gene interaction and chemical stability must be assessed. Various analytical techniques have been applied; dynamic light scattering (DLS, also known as photon correlation spectroscopy, PCS) is frequently used in the determination of liposome size distribution [22,23], just as the nuclear magnetic resonance (NMR) and the electron paramagnetic resonance (EPR) have been described to investigate the lamellarity, the permeability of the bilayer and the influence of liposome size on the substance transport [24,25]. The zeta potential, that describes the charge on the liposomal surface and indicates the tendency of the vesicles to fuse and to aggregate, can be determined by measuring the mobility of the liposomes in an electrical field.

The microscopical approach is commonly used to characterize the liposomal structure. Electron microscopy techniques have been widely used to measure the liposomal size and the size distribution [26]. In particular, transmission electron microscope (TEM) provides information on the size distribution and shape of vesicles. Unfortunately, liposomes can suffer of a structure perturbations triggered by the high vacuum conditions and the staining process. In the last years, besides the progress in sample preparation, other microscopical techniques have gained the attention. Atomic force microscopy (AFM), one of the techniques owing to the family of scanning probe microscopes with dimensional resolution approaching 1 Å, has changed the manner to look the sample [27,28]; developed in 1986, the AFM was applied for imaging different material surfaces including ceramics [29], metals [30], but also biological [31] and pharmaceuticals preparations [32,33]. The AFM ability to explore samples under variety of environmental conditions, including biological specimens in an aqueous environment or in air at room temperature, makes it a very versatile characterization technique. Unlike the electron microscopical methods, that often require sophisticated sample preparation procedures, the sample preparation for AFM is easy and fast and it allows the material to be preserved in its native state.

The atomic force microscope utilises a tip (probe) attached to the flexible cantilever of a specific spring constant. The cantilever deflects in z-direction due to the surface topography during the tip scanning of the sample surface. A photodiode detects the deflection of the cantilever through a laser beam focused on and reflected from the back of the cantilever. As AFM generally measures the vertical deflection of the cantilever with picometer resolution, even its little deflection causes the shift of the laser beam on photodiode; consequently, the amount of light received by every segment of the detector changes. The photo-current outgoing to the photodiode is transmitted to the differential amplificatory. Usually, during the scanning, a constant force between the tip and the sample is kept through a feedback circuit that adjusts the movement of piezoelectric tube scanner in z-direction. The movement in z-direction directly provides the topography of the sample surface. Considering the tip approach and the deflection way, AFM can operate in different modalities that can be referable as repulsive (contact) mode and attractive (non-contact) mode (for detailed information see [34–37]). In the contact mode, the tip is in constant close contact to the surface of the sample; this approach can be used to detect hard samples such as silicone matrices, polyurethane pads, carbon surface, etc. [38–40]. In the non-contact mode, a stiff cantilever oscillates in the attractive regime, meaning that the tip is quite close to the sample, but not touching it (hence "non-contact"). The forces between the tip and the samples are quite low. The evaluation of the shifts of the natural resonant frequency or the amplitude and the phase of the cantilever is frequently used to amplify the small signal detected used soft biomaterials [41,42]. A possible variation of this approach is the acquisition obtained by intermittent contact (tapping mode). The intermittent contact motion of the tip eliminates lateral or shear forces which would deform or scrape the sample [43].

In addition to topographic imaging and especially considering the versatility of the operation mode (for example using of the additional measurement mode such as lateral force mode, LFM, and force modulation mode, FFM) [44,45], AFM can also provide information of micro-mechanical properties such as surface and adhesive forces [46,47].

This review focused on the AFM applications used to characterize liposomes as drug delivery systems. In this paper, we discussed the AFM application in evaluating the physico-chemical and technological properties of liposomes by comparing the published results with those obtained using well-

known techniques, such as TEM in detecting liposomes and their interaction with nucleic acids or PCS in evaluating liposome size distribution. In order to evaluate the liposome morphology (i.e. structure, shape, diameter and size distribution, characterization of surface modifications) along with the interaction between these lipid vesicles and drugs or genes, we examined the recent applications of this versatile microscopical technique.

2. Physico-chemical characterization

For a productive development of liposomes as drug carriers, it is essential to characterize these systems as particles. The evaluation of liposome morphology includes the characterization of shape, structure, surface morphology and size measurement of these carriers. Evaluation of liposome size distribution is important not only to study the physico-chemical properties and the stability of preparations but also to identify the *in vivo* kinetics of these systems and in particular their ability to cross vessel walls and to be accumulated in tumours in order to exert the desired targeting [48–50].

2.1. Shape and size measurement

To study liposomes as drug delivery systems, the geometry, the size and the size distribution are key parameters to evaluate both *in vitro* and *in vivo* stability, encapsulation efficiency, and finally their applicability in the pharmaceutical field. A wide variety of techniques, including microscopical and various kinds of spectroscopical methods, have been used to characterize liposomes. Usually, transmission electron microscopy (TEM), able both to image liposomes and to provide information about their size, is currently applied on vesicles morphology characterization. Techniques such as negative staining, freeze fracture electron microscopy (FFEM) and cryo-transmission electron microscopy (Cryo-TEM), provide detailed information about liposomes, but the sample preparation is complex and frequently it requires a long time [51]. Also the environmental scanning electron microscopy (ESEM), an evolution of the scanning electron microscopy able to be applied to the observation of hydrated samples, has been recently used to investigate the relationship between the morphology and stability of free or incorporating ibuprofen multilamellar liposomes (MLV) [52]. To achieve a good resolution, wet delicate sample can be imaged using both lower magnification and electron dose; but, in the nano-structures characterization, this technique presents different instrumental limitations actually restricting the field of application [53]. Dynamic light scattering (DLS or PCS) is the most important spectroscopical technique used to measure both size and size distribution; although only for monodisperse systems, Z-Average diameter, a mean peculiar to the dynamic light scattering, compares correctly with many other methods. With polydisperse systems, the Z-Average must be used in a relative sense. The PCS analysis of multimodal suspension (with polydispersity index value lower than 0.7) is by far complicated but possible. Besides, the aggregation of vesicles cannot be evaluated because the vesicle aggregates are identified as a single particle.

In this context, AFM can be used to directly image and measure the size of liposomes adsorbed onto a surface (mica, silicon wafers, etc.). It is well-known that liposomes adsorbed onto solid substrate generally modify the shape. Compressed or flattened spheroidal shapes are frequently related to AFM technique limitations. In fact, to correctly evaluate the shape and to measure the size of the adsorbed vesicles, it is necessary to pay attention to the different factors that could affect the topographical changes including the type of liposomes, the time of analysis, along with the vertical and the lateral forces applied by the tip on the liposome during the scanning procedure.

In the last years, different papers have extensively demonstrated that many factors influence the absorption of liposomes and their morphological modifications: in particular, the lipid and the buffer composition, the liposome concentration, the electrostatic interaction with the support and the elapsed time between the liposome deposition and the observation could strongly affect the liposome characteristics [54–58]. As well, the topography of the vesicles could be influenced by the tip effect close correlated to the mode of analysis. Frequently, liposomes have been imaged in tapping mode AFM. The periodic contact between the probing tip and the sample surface reduces the frictional lateral destructive forces and the tip convolution effect thus affecting, in particular, the measure of the liposomal size. The non-contact mode has less probability in damaging the samples than the tapping mode, owing to the elimination of the possible dragging of liposomes when the tip moves across the vesicles. In fact, Paclet et al. [59] established that accurate height information of liposomes deposed on the substrate could be obtained in the non-contact mode.

Nevertheless, also using non-contact and tapping mode and operating in aqueous solution, liposomes absorbed on mica surface can change their shape. The interaction between the sample and the substrate, as well as the continuous movement of the tip, can induce a liposome deformation [60,61]. Recently, we have compared the size of liposomes measured by AFM image sectional analysis and the PCS data. Operating in non-contact mode, liposome diameters remain comparable to the heights of the vesicles and in a spherical defined shape within the first 10 min after deposition. The AFM data were in agreement with PCS ones also considering that in the AFM measures liposomes are adsorbed on solid surface while the PCS evaluated liposomes in suspension. Ten minutes after deposition, liposomes showed a progressive tendency to turn into an asymmetrical and flattened structure described as planar vesicles (Fig. 1). Liposomes with different compositions have a different tendency to change their structure after mica adsorption: the elastic properties of the lipid constituting liposomes influence the interaction with the tip [62]. In particular, during the continuous scanning of Egg phosphatidilcoline (EggPC) liposomes, we observed the same changing described by Liang et al. [63] on EggPC liposomes imaged using the tapping-mode tip approach. In particular, after 2 h scanning, the liposomes showed "concave shape" characterized by a depressed central portion and a higher outline (Fig. 2). The diameter of these structures was approximately 260 ± 28 nm and the height 4.1 ± 0.6 nm. These data represent the confirmation that, after a long time,

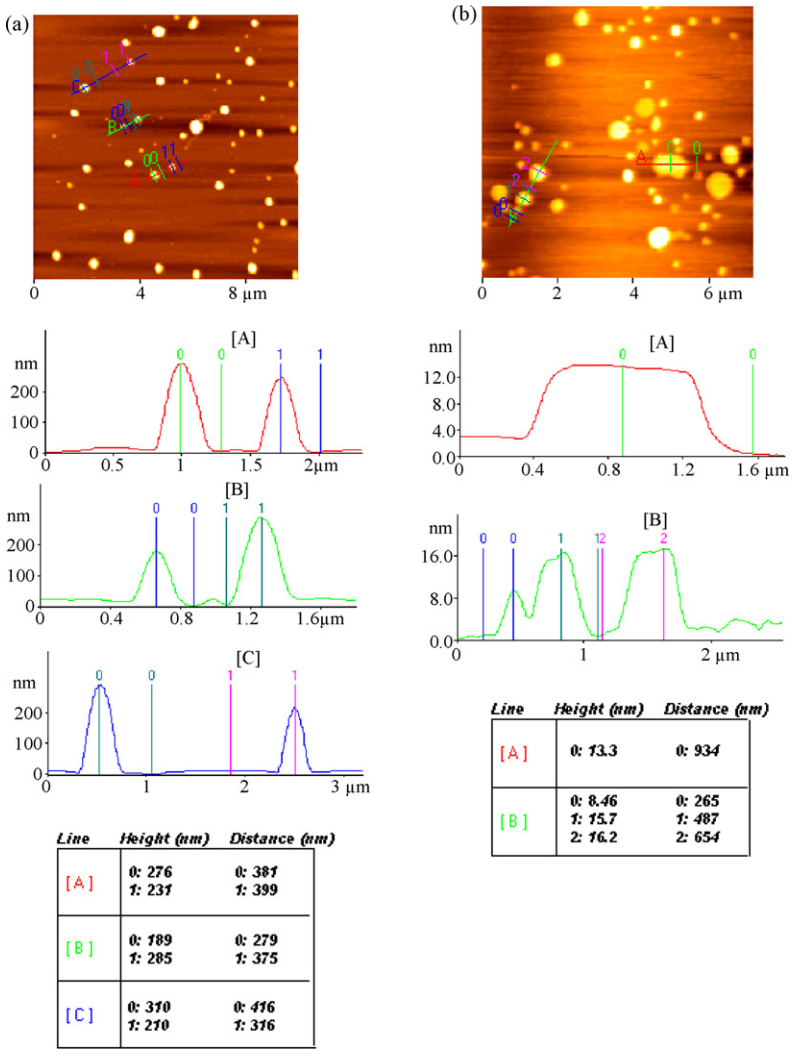

Fig. 1. AFM images of liposomes under water obtained (a) 5 min and (b) 20 min after the deposition on mica support. The profiles were obtained from the height images.

the vertical force of tip damages the soft samples also using non-contact mode. Liposome absorption on mica surface represents one of the possible approaches used to form supported lipid bilayers, which are the main biomimetic membranes used for the current studies. The information obtained with AFM analysis about the nanoscopic domains, the modulation and the microscopic phase behaviours of the supported membrane bilayers are useful toward understanding the native biological membranes [64–66]. Using modified-liposomes (lipid vesicles formed with phospholipid incorporating transmembrane proteins), Kanno et al. [67] demonstrated that also when the vesicles were adsorbed on mica support and collapsed thus changing the structure, the diameter acquired by AFM measuring could be compared with the size obtained using PCS analysis. In fact, evaluating the differences between the diameters and the height of liposomes deposed on mica supports, the AFM diameters of flattened structures could be elaborated and then compared to spheres or hemispheres. These re-calculated diameters were in agreement with those obtained by the PCS technique. These studies suggest that AFM technique can be used in association or alternatively to PCS analysis in order to measure the liposomal size. Nowadays, considering the size distribution obtained by PCS analysis, different authors compare the diameters of liposomes acquired measuring the cross-section of vesicles on AFM images. For example, Tavares et al. [68], operating in tapping mode and at fixed time, imaged liposomes on solid support and demonstrated that AFM-derived liposomal size measurement was in agreement with the result obtained by PCS analysis. Using a similar approach, Wang et al. [69], well-characterized submicron unilamellar liposomes prepared by a new method described as freeze-drying double emulsions (FDE) procedure.

Few articles examine the size distribution of liposomes elaborating the AFM images obtained by contact AFM. In this context, the results obtained by Storrs et al. [70] studying the paramagnetic polymerised liposomes (PPL) with AFM are worthy of attention. The authors visualized PPL using both AFM and TEM approaches; the size distribution obtained using the two microscopical approaches was similar, but the AFM topographies appeared more detailed compared to the TEM ones. In

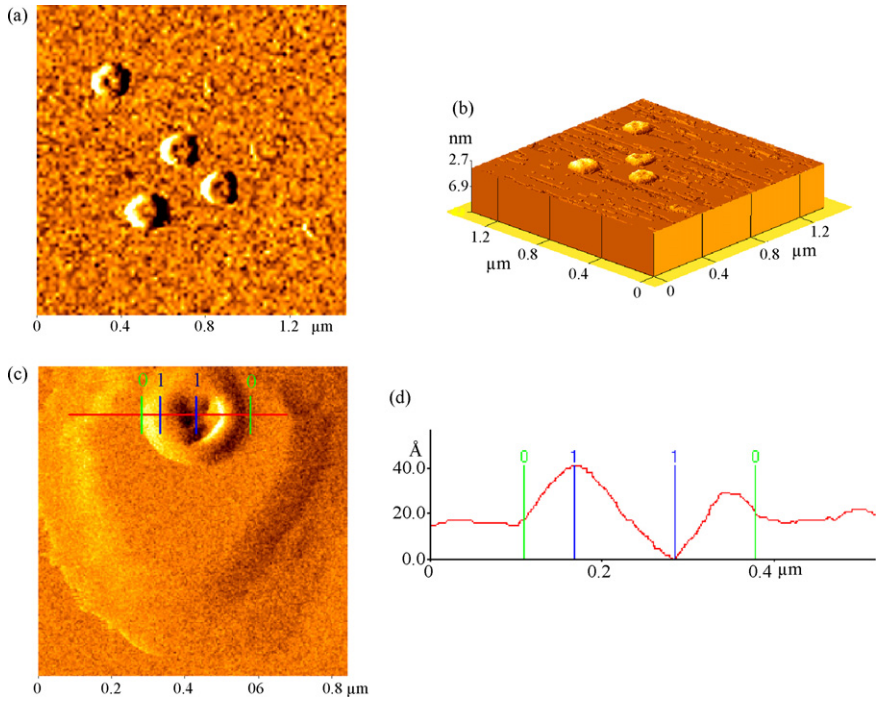

Fig. 2. AFM image under water by non-contact mode of EggPC obtained 2 h after the sample deposition on mica support: (a) topography, (b) 3D-view, (c) magnification and (d) profiles from the height image. Long time analysis produce the liposome collapse and the formation of concave structure with the central part compressed.

fact, near the ellipsoids structures referable to liposomes, greater abundance of particles on the lower end of the size spectrum was recorded in AFM images. Analysing liposomes with different lipid composition, but also more stiff polymeric nanoparticles, different authors demonstrated incongruence or difficulties in comparing the particle size with data obtained using other analytical techniques [71,72]. It is clear that AFM contact mode is not easily applicable for the exact particle size determination when the carriers are soft or flexible, while it is very appreciable to characterize elasticity, flexibility and adhesion properties of liposomes providing the force mapping (force-distance-curves).

2.2. *Surface morphology; protein and polymer modification*

Liposomes used in pharmaceutical applications are often modified in the surface properties. In order to improve the *in vivo* stability, functionalised liposomes have been formulated by different polymers. Since the early 1990s, long circulation liposomes have been designed; these liposomes were sterically stabilized by coating the surface with polyethylene glycol (PEG) derivatives. The PEG chains create a sterical barrier that allows the liposomes to evade the phagocytic uptake, extending their circulation half time and increasing the possibility for targeting [73]. Moreover, site-directing moieties and ligands can be incorporated into liposome membrane surface to further enhance the selectivity of liposomal drug delivery [74–77]. These modifications change the structure and, in particular, the surface morphology of liposomes; all information about the disposition and the spatial conformation of protein or polymer networks anchored on liposomal surface are important to clarify the possible development of these stable and targeted drug carriers.

Besides the ability to investigate the surface structural details, AFM, through the force measurements, could provide information about the mechanical and chemical properties of sample surface. A force curve (force versus distance curve) indicates the force felt by the cantilever as the probe tip is brought vertically towards the sample surface and then retracts away. Force measurement can provide information about the elastic and adhesive properties of liposomes. Recently, Mao et al. [78] described this technique and its application on liposomes.

Considering the large number of research papers published on the functionalized liposomes, only few recent studies apply the AFM technique to characterize the liposomal surface modifications.

Bendas et al. [79] applied AFM approach with the aim of illustrating antibodies at the liposomal membrane surface, an application never described before. Considering the AFM images of immunoglubulin G (IgG) available on literature, Fritz et al. [80] compared the magnification of the liposome images in order to demonstrate the presence of a different density of antibody coupled between the cyanur-PEG-PE immunoliposomes obtained attaching monoclonal antibody via a new membrane anchor (PEG 2000 functionalised with cyanuric chloride) and the well-studied *N*-glutaryl-PE immunoliposomes. These findings were important to evaluate the changes in the liposomal surface and in protein mobility produced by the type of antibody conjugation and to correlate the surface differences between the two different immunoliposomes population with their targetability. Recently, comparing the tapping mode AFM images of different formulations of targeted sterically stabilized pH-

sensitive liposomes, Fonseca et al. [81] investigated the ability of new covalent coupling procedures. In particular the authors investigated whether the thiolated transferrin (choose as target ligand) was coupled to the distal malaimide end of PEG chains or non-specifically bound to the liposomal lipid bilayer. The different location of the proteins observed on the lipid bilayer after deposition of two different modified liposomal formulations suggests the importance of malaimide groups in the covalent linkage of transferrin. The AFM studies correlated with the cellular experiments were crucial to demonstrate the targetability of these structures.

As mentioned before, in order to characterize liposomes morphology, TEM approach is often used. If it is true that this electronic microscopical technique ensures the complete structural analysis, the artefacts due to the staining process and the alteration caused by the exposition of the samples to vacuum condition could provide a wrong interpretations.

In this context, Stauch et al. [82] combined AFM and TEM analysis to clarify the effects of photopolymerization on liposomal encapsulated NIPAM (N-isopropylacrylamide) and TEGDM (tetraethylene glycol dimethacrylate) monomers and the interaction between the formed polymer and the lipid vesicles. The AFM analysis, performed both in tapping mode/height mode and in tapping mode/phase mode of the ultra-thin sections of liposomes, was carried out both to describe the morphology of the carrier and to confirm the data of TEM, excluding that possible staining artefacts can distort the images. Comparing TEM and AFM analysis of ultra-thin section, the architecture of the polymer inside the vesicles was clarified assuming a key role in the development of these new formulations as drug delivery systems. In an other study, analysing the AFM images, Moutardier et al. [83] described the interaction between a liposome formulation and a polymeric network used to prepare new liposomes with a polymeric core (LSP). The corresponding pictures showed the presence of polymer on the external surface of liposomes and, considering also the shape assumed after deposition of LSP on the support, the authors elucidated the localization and the morphology of these modified drug delivery carriers.

AFM and TEM enhanced the understanding of the modified-liposomes obtained conjugating a selective ligand (transferrin) to liposomes [84]. In fact, AFM and TEM were able to detect transferrin at the liposomal surface at the molecular level in a fast and reproducible way. Even though both microscopic techniques can provide information on liposome surface (in particular on the protein-modification of these lipid drug carriers), the study showed some important differences suggesting and strengthening their complementarily; for example, the maximum resolution is obtained using AFM, but the contrast and the contour of the images are better understood using TEM**.** The complementarily of these techniques was confirmed in our recently studies. Fig. 3 shown the TEM and AFM images of the modified-liposomes (prepared using *N*-[1-(2,3-dioleoyloxy)propyl]-*N*,*N*,*N*-trimethylammonium chloride salt (DOTAP) and ursodeoxycholic acid (UDCA)). In TEM image (negative-stain electron microscopy), the more electron transparent lipid vesicles appear as bright areas defined by a concentric lipid layer with a free internal structure. On the contrary, the homogeneity of the liposomal surface was better described in the AFM image.

Liang et al. [85] have recently reported an interesting approach. The authors, using the AFM, investigated the morphology of egg yolk phosphatidylcholine liposomes (EggPC) modified with Pluronic copolymer (poly(oxyethylene)-poly(oxypropylene)-poly(oxyethylene) [PEO-PPO-PEO]). They observed some significant morphological changes and different topography of liposomes upon incorporating the Pluronic copolymer. These results do not agree with those obtained by previous study carried out using cryo-TEM [86]: the experimental condition, the mode of analysis and the different physical state of liposomes (analysed in dilute aqueous solution directly by cryo-TEM and upon absorption using AFM) could properly justify this incongruence. The paper was important because using AFM force-curve, the researchers provided important information about the stability and the transitions occurring from vesicles to bilayers owing to the length of PEO and PPO chains; considering these results, the authors proposed a membrane-spanning model which can help to select the appropriate Pluronic copolymer to ensure the steric stabilized vesicles with the suitable lipid membrane stiffness.

3. Technological characterization

The localization and the way by which liposomes interact with the active substance are very important to obtain a good *in vivo* applicability. In particular, in the field of gene therapy, the characterization of liposome/DNA interaction is necessary to effectively improve the carriers' ability in gene transfer.

3.1. Liposomes/drug interaction

Currently, TEM is the most used microscopical approach to obtain information about the liposomes–drug interaction. In the last years, different TEM techniques were well-developed to analyse the internal structure and in particular the drug-loaded liposomes. At the present, FFEM and Cryo-TEM are the most used approaches to visible describe the entrapment of drug into the liposomes [87–90]. As previously described, the sample preparation remains expensive and very laborious. Negative staining is an easy and classical method used to characterize liposomes–drug interaction [91–93] but, also in this case, the staining processes and the analysis conditions (particularly the drying procedures) can produce artifacts.

A relative number of papers describes the use of AFM in the study of the interaction between the drug and the lipid membranes; the aim of these researches is mainly to understand the properties of biomembranes and the correlated processes such as cell adhesion, membrane fusion and drug membrane-interaction [94–96]. In these papers, the AFM was the essential tool to clarify the re-organization occurring in the lipid bilayer after the interaction of the active compound. Besides the utility in pharmacology and biological field, the effect induced by the drug on the permeability and on the fluidity of lipid bilayer has certainly provided useful information for the encapsulation efficiency and stability of the liposomal formulation, suggesting

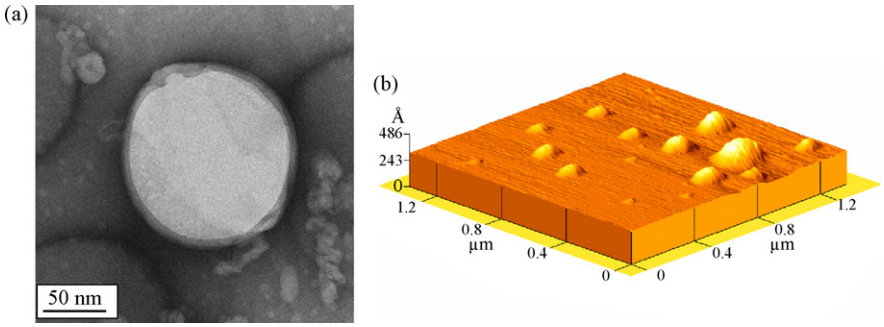

Fig. 3. Images of modified-liposomes (DOTAP/UDCA mixed vesicles); (a) negative stain electron microscopy and (b) a 3D-view of AFM topography.

the possible application of AFM in the pharmaceutical liposomal technological characterization. For this aim, Ramachandran et al. [97] used the AFM to study the physico-chemical characteristics of cisplatin-encapsulated liposomes. In particular, the information about the liposome-drug formulation was obtained using AFM height mode image (tapping mode) and analysing the AFM force mapping (in particular the force-curves). In fact, AFM force curves made possible a semiquantitative estimation of cisplatin encapsulation and showed that the cisplatin-loaded liposomes were stiffer than unloaded ones. These data provided important details about the stability of the liposomal formulation and demonstrated the versatility of AFM to characterize liposome-drug formulation.

3.2. *Liposomes as gene carriers*

During the past 20 years, more than 400 clinical studies in gene therapy have been described. Gene therapy is identified with the procedures used to insert the exogenous genetic material (DNA, mRNA, oligonucleotides) into cells or tissues to cure a disease or to improve associated symptoms [98]. Really, the gene therapy starts with the choice of therapeutic gene but the most critical objective is the success in the gene transfer to the target tissue. Liposomes, in particular the cationic ones, have become one of the most studied non-viral vectors frequently used in human gene therapy studies [99–102]. The ability of cationic liposomes to mediate transfection was attributed to the intrinsic properties of these systems, like a spontaneous electrostatic interaction between the positively charged vesicles and the negatively charged plasmid DNA (and oligonucleotides) that ensures an efficient condensation of the nucleic acids. Modifying the lipid composition, the formed liposomes/nucleic acid complex can exhibit an appropriate charge that enhance the possibility of cellular uptake; in the case of cationic liposomes both fusion and endocytosis have been proposed as mechanisms for the DNA or oligo uptake [103]. To efficaciously use these systems for *in vivo* gene transfer, the aspect and the physico-chemical properties of the liposomes/DNA complex must be clarified.

Liposomes/DNA complexes are usually called lipoplexes. Several studies indicated that the formation of these lipoplexes extensively depends on factors such as the lipid composition, the molar ratio between liposomes and gene materials, [also described as charge (+/−)], the time of contact, the concentration, the temperature and the environment of reaction [104–107].

Several biophysical approaches have been used to elucidate the ultra-structure of the lipoplexes. In addition, in this case, FFEM and Cryo-TEM were applied to evaluate the lipoplex formation. In the last twenty years, several structures were discussed; fluorescent analysis, X-ray diffraction studies and small-angle X-ray scattering measurements (SAXS) suggested that during the liposome/DNA interaction, DNA can be surrounded by lipid bilayer or more fused liposomes organized in structures called “bead on string” [108], “spaghetti meatball complex” [109], “rod-shaped” assembly [110]. In particular, cryo-TEM reveals the formation of new re-organized multilamellar structures [111–113]. Recently, the application of AFM gave a relevant contribution to the knowledge of the complex formation. Firstly, to correctly evaluate the morphology of lipoplex, liposomes and plasmid DNA must be separately examined. In the last years, cryo-TEM was used to visualize the plasmid DNA. The main drawback in the cryo-TEM analysis on nucleic acid seems to be the manifest tendency of these molecules in avoiding thin areas of the solution film. A thin layer of the solution is required for the satisfactory visualization of DNA [114]. AFM provides excellent possibilities of deeply describing the structure of nucleic acid at a high resolution level [115–117]. To examine the lipoplex formation, Oberle at al. [118] visualized the structural state of the plasmid DNA: considering the appearance of plasmid, they can exactly describe the condensing effect of amphiphilic lipid, excluding that the observed structure could be ascribed to the plasmid ones. To visualize the distinct steps involved in the amphiphile/plasmid complex formation, the authors carried out the experiments under equilibrium conditions, using a film balance approach (monolayer experiment). With this original approach, the identified mechanism of complex formation was described by observing the most studied amphiphilic vesicles/plasmid interaction. They demonstrated that, firstly amphiphile/plasmid complexes involved the interaction between plasmid and lipid monolayer; only subsequently, lipids surrounded single plasmid. These structures were instable and tended to aggregate in larger fused complexes.

Also van Groll et al. [119] using AFM described the importance of DNA topology in gene transfer. They evaluated the efficiency of a commercial liposome mediating transfection by circular and linear DNA. Liposome/DNA complexes, visualized using AFM, showed different organizations that account for the disparity in the ability of gene transfer. AFM images of liposome/circular DNA complexes described compact aggre-

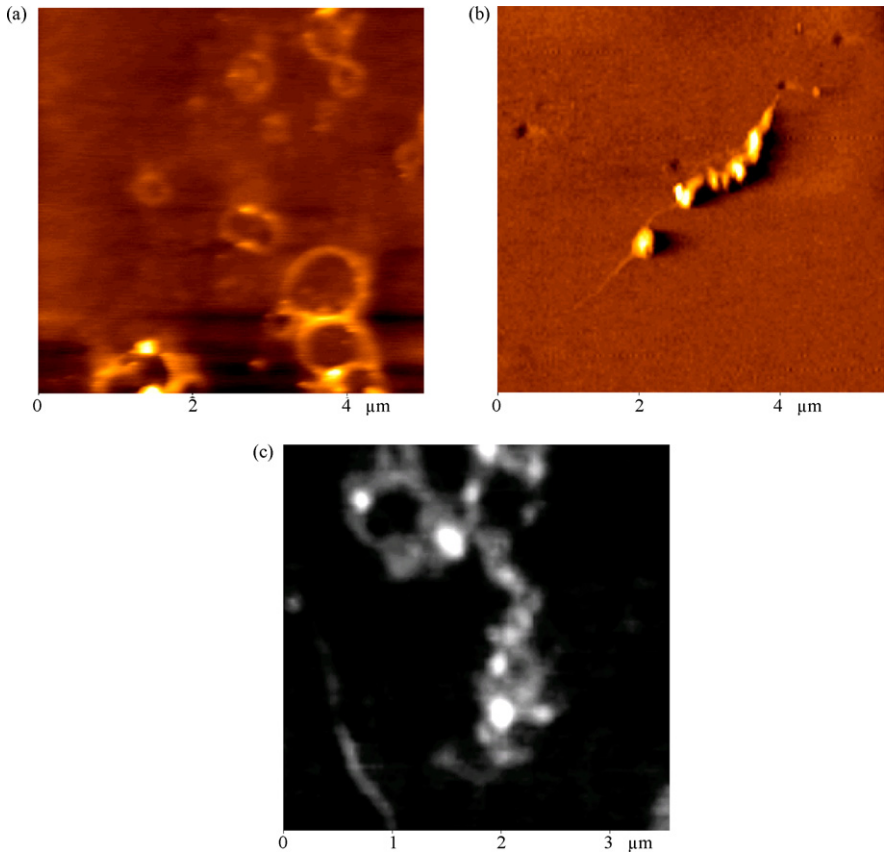

Fig. 4. AFM images under water and by non-contact mode of (a) DNA (plasmid pCMVβ), (b) PC/DDAB liposome/plasmid pCMVβ complexes and (c) PC/DDAB/DOPE liposome/plasmid pCMVβ complexes at ratio 10:1 (nmol of lipid: μg of DNA). For the abbreviations see text.

gates that were very efficient of transfecting the Vero cells. On the contrary, using linear DNA, the necklace-like structures that exhibit low transfection efficiency were observed.

Besides, AFM has proven to be useful in imaging and clarifying how the factors such as composition, liposome/DNA molar ratio, size, etc. can affect the assembly and the geometry of the lipoplex and the relative gene transfection ability.

In the last 5 years, our research group studied the formation mechanism of lipoplexes and also of liposome/oligo complexes using the non-contact AFM approach. First, we studied how the liposome composition influences the packing and the organization of liposomes/DNA complexes and then their transfection efficiency [120]. An example of AFM images of plasmid pCMVβ and well-characterize complexes with liposomes prepared using phosphatidilcoline (PC), dimethyldioctadecylammonium bromide (DDAB) and/or 1,2-dioleoyl-sn-glycero-3 phosphatidylethanolamine (DOPE) at ratio 10:1 (nmol of lipid:μg of DNA) was reported in Fig. 4. At this complex ratio, PC/DDAB liposomes coated DNA forming the necklace-like structure while the complex formed between PC/DDAB/DOPE liposomes and the plasmid appeared more large and compacted. These particular lipoplex morphology and size were correlated with the optimal DNA transfer ability showed by commonly cationic liposomes prepared in presence of a co-lipid (DOPE). More recently, using AFM, we have well-imaged a new formulation proposed for gene transfer and the related complex with oligonucleotides [121]. Not only the AFM images supported the HR MAS NMR data describing the structure and the stability of new formulation, but provided the information about the oligo interaction showing the formation of large clusters not referable both to liposomes or oligos previously described [122].

Also Wangerek et al. [123] using the AFM approach clarified the role in gene transfer of the type of cationic lipid commonly used in liposomal formulations. The starting point of this research was the evidence that high transfection efficiencies in neuronal immortalized cell lines were achieved especially with multivalent cationic liposomes, while monovalent cationic liposomes optimally transfected primary neuronal cell. The AFM images of lipoplexes obtained by four different commercial liposomal formulation and plasmid DNA demonstrated that more compact globular structures were formed by multivalent cationic liposomes than by monovalent liposomes. These data confirmed that a strong correlation between the geometry of complex and the mechanism of cellular uptake exists.

Different authors correlated the complex morphologies obtained mixing cationic liposomes and DNA at different molar ratio with their ability in gene transfection. Using AFM, Kawaura et al. [124] demonstrated that not all the structures observed mixing liposomes prepared with new cationic cholesterol derivatives and DNA at different molar ratio were suitable for gene transfection. In a following study, the authors correlated the size of complexes and the gene transfer in order to demon-

strate that only the complexes with a moderate average diameter were more efficient for gene transfection by endocytosis [125]. In a related study, Noguchi et al. [126] evaluated the difference between liposome/DNA and liposome/protamine/DNA complexes. Elaborating the AFM images, they demonstrated that the diminished size of the complex produced by protamine facilitated the endocytosic uptake and also the nuclear translocation of gene. Sakurai et al. [127] confirmed that an optimal liposome/DNA molar ratio for efficiently gene transfer exists: at this ratio, the AFM images showed that the plasmid DNA was completely covered by the liposomes that fused or aggregated in structures with large size. Using similar approach Almofti et al. [128] confirmed the ability of DNA to induce liposome-liposome fusion, which involved the formation of large lipid structures able to transfer the nucleic acid. On this basis, the authors hypothized that large lipoplexes cannot follow this route without a previous fusion with the cell membrane, although the endocytosis pathway is the main way for lipoplex entry into the cells.

The AFM approach was recently used to correlate the geometry of lipoplexes with a kinetic parameter such as the incubation time of DNA with liposomes [129]. The paper well-describes the type of lipoplexes observed incubating liposomes and DNA at different molar ratio and their change during the incubation time. Also the composition of medium plays an important role on lipoplexes stability. In a recent study, the AFM images of lipoplexes in different medium help to clarify their stability and ability in gene transfection [130].

In addition, the less studied anionic liposomes/DNA complexes were imaged with AFM. In particular, Mozafari et al. [131] described the complexation obtained between anionic multilamellar liposomes and DNA by the mediation of divalent cation Ca^{2+}. The presence of Ca^{2+} was necessary for the charge neutralization of DNA that subsequently collapsed into packed form leading fusion of phospholipid vesicles [132,133]. Using AFM, the authors visualized the aggregated/semifused vesicles formed when the complexation occurs in the presence of Ca^{2+}, confirming the fusogenic action of DNA/Ca^{2+} complex.

4. Conclusion

Owing to the safety properties and the efficacy as drug vehicle, liposomes are considered one of the most important nanocarriers which can be use to protect, formulate and selectively deliver the drugs to the target cells. The liposome characterization was the first step in the evaluation of the present and coming applications. Particularly, the microscopical approach provides more information about the morphology, the size distribution and the superficial properties affecting the interaction with drugs, genetic materials, imaging agents, etc. In this context, AFM has recently become an essential tool in liposome and liposome-drug or liposome/DNA evaluation. Using this microscopical technique and, in particular, the tapping and the non-contact mode approach, liposomes are well-imaged in air, at room temperature, without any sample manipulation. Initially AFM was applied to describe liposome morphology. Currently, the AFM application in liposome characterization remains an innovative and rapidly growing field of research, as the last recently reported citations demonstrated. Imaging liposomes in three-dimensional resolution, AFM was sufficiently able to provide important information concerning the surface modifications. Thus, this microscopical technique describes both the density and the spatial distribution of ligands such as polymer, peptides, and antibody anchored to liposome and able to exert a site-specific delivery. Additionally, AFM has the capability to explain the interaction between the lipid carriers and the active substances. In particular, this technique was applied to investigate the nature of liposome/DNA interaction and to clarify the properties of lipoplexes affecting the transfection ability, such as the morphology, the size distribution and the stability. The rapid and continuous evolution of the AFM procedure in biological and biomedical field will allow the current applications to be optimised and new approaches to be developed. Force measurement, for example, is an interesting approach able to provide important information about the elastic, chemical and adhesion properties of liposomes.

Acknowledgements

The author would like to thank C.I.G.S. (Centro Interdipartimentale Grandi Strumenti, University of Modena and Reggio Emilia) and particularly Dr. M. Tonelli for the fruitful collaboration and the use of atomic force microscopy.

References

[1] R.H. Müller, K. Mäder, S. Golha, Eur. J. Pharm. Biopharm. 50 (2000) 161.
[2] N. Nishiyama, K. Kataoka, Pharmacol. Therapeutics 112 (2006) 630.
[3] V. Torchilin, Adv. Drug Deliv. Rev. 58 (2006) 1532.
[4] K.A. Edwards, A.J. Baeumner, Talanta 68 (2006) 1421.
[5] S. Chatterjee, D.K. Banerjee, Meth. Mol. Biol. 199 (2002) 3.
[6] A.D. Bangham, M.M. Standish, J.C. Watkins, J. Mol. Biol. 13 (1965) 238.
[7] M. Voinea, M. Simionescu, J. Cell. Mol. Med. 6 (2002) 465.
[8] C. Grabielle-Madelmont, S. Lesieur, M. Ollivon, J. Biochem. Biophys. Meth. 56 (2003) 189.
[9] T.M. Allen, P. Sapra, E. Moase, J. Moreira, D. Iden, J. Liposome Res. 12 (2002) 5.
[10] E. Roux, C. Passirani, S. Scheffold, J.P. Benoit, J.C. Leroux, J. Control. Rel. 94 (2004) 447.
[11] W. Krause, Adv. Drug. Del. Rev. 37 (1999) 159.
[12] V.P. Torchilin, Mol. Med. Today 2 (1996) 242.
[13] R.L. Juliano, D. Layton, in: R.L. Juliano (Ed.), Drug delivery systems: characteristics and biomedical applications, Oxford University Press, New York, 1980, pp. 189–236.
[14] T. Lian, R.J.Y. Ho, J. Pharm. Sci. 90 (2001) 667.
[15] D. Felnerova, J. Viret, R. Gluck, C. Moser, Curr. Opin. Biotechnol. 15 (2004) 518.
[16] A. El Aneed, J. Control. Rel. 94 (2004) 1.
[17] I. Lebedeva, L. Benimetskaya, C.A. Stein, M. Vilenchik, Eur. J. Pharm. Biopharm. 50 (2000) 101.
[18] S. Simões, V. Slepushkin, R. Gaspar, M.C. Pedroso de Lima, N. Düzgüne, Gene Ther. 5 (1998) 955.
[19] R. Mischler, I.C. Metcalfe, Vaccine 20 (2002) B17–B23.
[20] R. Zurbriggen, I. Novak-Hofer, A. Seelig, R. Gluck, Prog. Lipid Res. 39 (2000) 3.
[21] P. Goyal, K. Goyal, S.G. Vijaya Kumar, A. Singh, O.P. Katare, D.N. Mishra, Acta Pharm. 55 (2005) 1.

[22] A. Kim, M.O. Yun, Y.K. Oh, W.S. Ahn, C.K. Kim, Int. J. Pharm. 180 (1999) 75.
[23] N. Venkatesan, S.P. Vyas, Int. J. Pharm. 203 (2000) 169.
[24] G. Puglisi, M. Fresta, G. Mazzone, P.M. Furieri, G. Tempera, Int. J. Pharm. 118 (1995) 65.
[25] W.W. Sulkowski, D. Pentak, K. Nowak, A. Sulkowska, J. Mol. Struct. 793 (2006) 257.
[26] G.V. Betageri, S.A. Jenkins, D.L. Parsons, Lancaster (1993) 27–44.
[27] M. Miles, Science 277 (1997) 1845.
[28] J.W. Cross, SPM-Scanning Probe Microscopy Website, http://www.mobot.org/jwcross/spm.
[29] B. Baretzky, B. Reinsch, U. Taffner, G. Schneider, M. Rhule, Z. Metallk. 87 (1996) 332.
[30] S. Orisaka, T. Minobe, T. Uchihashi, Y. Sugawara, S. Morita, Appl. Surf. Sci. 140 (1999) 243.
[31] C.J.P. Boonaert, V. Toniazzo, C. Mustin, Y.F. Dufrêne, P.G. Rouxhet, Coll. Surf. B-Biointerfaces 23 (2002) 201.
[32] A. zur Mühlen, E. zur Mühlen, H. Niehus, W. Mehnert, Pharm. Res. 13 (1996) 1411.
[33] A.L. Martin, M.C. Davies, B.J. Rackstraw, C.J. Roberts, S. Stolnik, S.J.B. Tendler, P.M. Williams, Proc. 27th Int. Symp. Control. Rel. Bioact. Mater, 2000, p. no. 7319, pp. 852–853.
[34] D.A. Bonnell, Scanning Tunneling Microscopy and Spectroscopy: Theory Techniques and Applications, VCH, New York, 1993.
[35] R. Wiesendanger, Scanning Probe Microscopy and Spectroscopy: Methods and Applications, Cambridge University Press, Cambridge, 1994.
[36] G.J. Leggett, in: J.C. Vickerman (Ed.), Surface Analysis: The Principal Techniques, John Wiley and Sons, Chichester, 1997, pp. 393–449.
[37] T. Sakurai, Y. Watanabe, Advances in Scanning Probe Microscopy (Advances in Materials Research), Springer Verlag, London, 2000.
[38] A. Adenier, N. Barré, E. Cabet-Deliry, A. Chaussé, S. Griveau, F. Mercier, J. Pinson, C. Vautrin-Ul, Surf. Sci. 600 (2006) 4801.
[39] I. Sokolov, Q.K. Ong, H. Shodiev, N. Chechik, D. James, M. Oliver, J. Coll. Interface Sci. 300 (2006) 475.
[40] M. Zielecka, E. Bujnowska, Prog. Org. Coat. 55 (2006) 160.
[41] E. Meyer, H. Heinzelmann, in: R. Wiesendanger, H.J. Guntherodt (Eds.), Scanning Tunneling Microscopy II, Springer, Berlin, 1992, pp. 99–149.
[42] K.D. Jandt, Surf. Sci. 491 (2001) 303.
[43] J. Legleiter, T. Kowalewski, Drug Discov. Today: Technol. 1 (2004) 163.
[44] J. Colchero, H. Bielefeldt, A. Ruf, M. Hipp, O. Marti, J. Mlynek, Phys. Status Solidi A – Appl. Mat. 131 (1992) 73.
[45] D.F. Ogletree, R.W. Carpick, M. Salmeron, Rev. Sci. Instrum. 67 (1996) 3298.
[46] W.R. Bowen, N. Hilal, R.W. Lovitt, C.J. Wright, Coll. Surf. A – Physicochem. Eng. Asp. 136 (1998) 231.
[47] B. Cappella, G. Dietler, Surf. Sci. Rep. 34 (1999) 1.
[48] D. Papahadjopoulos, T.M. Allen, E. Gabizon, E. Mayhew, K. Matthay, S.K. Huang, K.D. Lee, M.C. Woodle, D.D. Lasic, C. Redemann, F.J. Martin, Proc. Natl. Acad. Sci. U.S.A. 88 (1991) 11460.
[49] F. Yuan, M. Leunig, S.K. Huang, D.A. Berk, D. Papahadjopoulos, R.K. Jain, Cancer Res. 54 (1994) 3352.
[50] K. Uchiyama, A. Nagayasu, Y. Yamagiwa, T. Nishida, H. Harashima, H. Kiwada, Int. J. Pharm. 121 (1995) 195.
[51] P.M. Frederik, M.C.A. Stuart, P.H.H. Bomans, D.D. Lasic, in: D.D. Lasic, Y. Barenholz (Eds.), Nonmedical Applications of Liposomes, CRC Press, 1996, pp. 309–322.
[52] A.R. Mohammed, N. Weston, A.G.A. Coombes, M. Fitgerald, Y. Perrie, Int. J. Pharm. 285 (2004) 23–34.
[53] A.M. Donald, Nat. Mater. 2 (2003) 511.
[54] H. Egawa, K. Furusawa, Langmuir 15 (1999) 1660.
[55] N.H. Thomson, I. Collin, M.C. Davies, K. Palin, D. Parkins, C.J. Roberts, S.J.B. Tendler, P.M. Williams, Langmuir 16 (2000) 4813.
[56] I. Reviakine, A. Brisson, Langmuir 16 (2000) 1806.
[57] A.S. Muresan, K.Y.C. Lee, J. Phys. Chem. B 105 (2001) 852.
[58] E.F. Souza, O. Teschke, Rev. Adv. Mater. Sci. 5 (2003) 34.
[59] M.H. Paclet, A.W. Coleman, S. Vergnand, F. Morel, Biochemistry 39 (2000) 9302.
[60] D. Keller, C. Bustamante, Biophys. J. 64 (1993) 896.
[61] J. Jass, T. Tjärnhage, G. Puu, Biophys. J. 79 (2000) 3153.
[62] B. Ruozi, G. Tosi, F. Forni, M. Fresta, M.A. Vandelli, Eur. J. Pharm. Sci. 25 (2005) 81.
[63] X. Liang, G. Mao, K.Y.S. Ng, Coll. Surf. B – Biointerfaces 34 (2004) 42.
[64] G.W. Feigenson, J.T. Buboltz, Biophys. J. 80 (2001) 2775.
[65] F. Tokumasu, A.J. Jin, J.A. Dvorak, J. Electron. Microsc. 51 (2002) 1.
[66] F. Tokumasu, A.J. Jin, G.W. Feigenson, J.A. Dvorak, Ultramicroscopy 97 (2003) 217.
[67] T. Kanno, T. Yamada, H. Iwabuki, H. Tanaka, S. Kuroda, K. Tanizawa, T. Kawai, Anal. Biochem. 309 (2002) 196.
[68] G.D. Tavares, C.M. Viana, J.G.V.C. Araújo, G.A. Ramaldes, W.S. Carvalho, J.L. Pesquero, J.M.C. Vilela, M.S. Andrade, M.C. de Oliveira, Chem. Phys. Lett. 429 (2006) 507.
[69] T. Wang, Y. Deng, Y. Geng, Z. Gao, J. Zou, Z. Wang, Biochim. Biophys. Acta 1758 (2006) 222.
[70] W.R. Storrs, F.D. Tropper, H.Y. Li, C.K. Song, J.K. Kuniyoshi, D.A. Sipkins, K.C.P. Li, M.D. Bednarski, J. Am. Chem. Soc. 117 (1995) 7301.
[71] T. Shibata-Seki, J. Masai, T. Tagawa, T. Sorin, S. Kondo, Thin Solid Film 273 (1996) 297.
[72] B.A. Yegin, A. Lamprecht, Int. J. Pharm. 320 (2006) 165.
[73] M.C. Woodle, D.D. Lasic, Biochim. Biophys. Acta 1113 (1992) 171.
[74] E. Forssen, M. Willis, Adv. Drug Deliv. Rev. 29 (1998) 249.
[75] R.M. Schiffelers, G. Molema, T.L.M. ten Hagen, A. Janssen, A.J. Schraa, R.J. Kok, G.A. Koning, G. Storm, J. Liposome Res. 12 (2002) 129.
[76] A. Schnyder, J. Huwyler, NeuroRX 2 (2005) 99.
[77] P. Sapra, P. Tyagi, T.M. Allen, Curr. Drug Deliv. 2 (2005) 369.
[78] G. Mao, X. Liang, K.Y.S. Ng, in: J.A. Schwarz, C.I. Contescu, K. Putyera (Eds.), Encyclopedia of Nanoscience and Nanotechnology, Marcel Dekker, New York, 2004, pp. 933–942.
[79] G. Bendas, A. Krause, U. Bakowsky, J. Vogel, U. Rothe, Int. J. Pharm. 181 (1999) 79.
[80] J. Fritz, D. Anselmetti, J. Jarchow, X. Fernandez-Busquets, J. Struct. Biol. 119 (1997) 165.
[81] C. Fonseca, J.N. Moreira, C.J. Ciudad, M.C. Pedroso de Lima, S. Simões, Eur. J. Pharm. Biopharm. 59 (2005) 359.
[82] O. Stauch, T. Uhlmann, M. Frolich, R. Thomann, M. El Badry, Y.K. Kim, R. Schubert, Biomacromolecules 3 (2002) 324.
[83] V. Moutardier, F. Tosini, P. Vlieghe, L. Cara, J.R. Delpero, T. Clerc, Int. J. Pharm. 260 (2003) 23.
[84] S. Anabousi, M. Laue, C.M. Lehr, U. Bakowsky, C. Ehrhardt, Eur. J. Pharm. Biopharm. 60 (2005) 295.
[85] X. Liang, G. Mao, K.Y.S. Ng, J. Coll. Interface Sci. 285 (2005) 360.
[86] M. Johnsson, M. Silvander, G. Karlsson, K. Edwards, Langmuir 15 (1999) 6314.
[87] I.V. Zhigaltsev, N. Maurer, K.F. Wong, P.R. Cullis, Biochim. Biophys. Acta 1565 (2002) 129.
[88] M. Müller, S. Mackeben, C.C. Müller-Goymann, Int. J Pharm. 274 (2004) 139.
[89] A.S. Taggar, J. Alnajim, M. Anantha, A. Thomas, M. Webb, E. Ramsay, M.B. Bally, J. Control. Rel. 114 (2006) 78.
[90] I.V. Zhigaltsev, N. Maurer, K. Edwards, G. Karlsson, P.R. Cullis, J. Control. Rel. 110 (2006) 378.
[91] A. Manosroi, K. Podjanasoonthon, J. Manosroi, Int. J. Pharm. 235 (2002) 61.
[92] B. Ruozi, G. Tosi, F. Forni, M.A. Vandelli, J. Liposome Res. 15 (2005) 175.
[93] J.A. Zhang, G. Anyarambhatla, L. Ma, S. Ugwu, T. Xuan, T. Sardone, I. Ahmad, Eur. J. Pharm. Biopharm. 59 (2005) 177.
[94] S. Merino, O. Domenech, I. Diez, F. Sanz, M. Vinas, M.T. Montero, J. Hernandez-Borrell, Langmuir 19 (2003) 6922.
[95] A. Berquand, N. Fa, Y.F. Dufrêne, M.P. Mingeot-Leclercq, Pharm. Res. 22 (2005) 465.
[96] L. Zhao, S.S. Feng, J. Coll. Interface Sci. 300 (2006) 314.
[97] S. Ramachandran, A.P. Quist, S. Kumar, R. Lal, Langmuir 12 (2006) 8156.
[98] R.C. Mulligan, Science 260 (1993) 926.
[99] X. Gao, L. Huang, Gene Ther. 2 (1995) 710.

[100] Y. Liu, D. Liggitt, W. Zhong, G. Tu, K. Gaensler, R. Debs, J. Biol. Chem. 270 (1995) 24864.
[101] C.R. Dass, T.L. Walker, E.E. DeCruz, M.A. Burton, Drug Deliv. 4 (1997) 151.
[102] R. Ramesh, T. Saeki, N.S. Templeton, L. Ji, L.C. Stephens, I. Ito, D.R. Wilson, Z. Wu, C.D. Branch, J.D. Minna, J.A. Roth, Mol. Ther. 3 (2001) 1.
[103] M.C. Pedroso de Lima, S. Simões, P. Pires, H. Faneca, N. Düzgüne, Adv. Drug Deliv. Rev. 47 (2001) 277.
[104] I. Koltover, T. Salditt, C.R. Safinya, Biophys. J. 77 (1999) 915.
[105] J.A. Heyes, D. Niculescu-Duvaz, R.G. Cooper, C.J. Springer, J. Med. Chem. 45 (2002) 99.
[106] J. Rejman, V. Oberle, I.S. Zuhorn, D. Hoekstra, Biochem. J. 377 (2004) 150.
[107] A. Elouahabi, J.M. Ruysschaert, Mol. Ther. 11 (2005) 336.
[108] P.L. Felgner, T.R. Gadek, M. Holm, R. Roman, H.W. Chan, M. Wenz, J.P. Northrop, G.M. Ringold, M. Danielsen, Proc. Natl. Acad. Sci. U.S.A. 84 (1987) 7413.
[109] B. Sternberg, F.L. Sorgi, L. Huang, FEBS Lett. 356 (1994) 361.
[110] H. Gershon, S. Ghirlando, S.B. Guttman, A. Minsky, Biochemistry 32 (1993) 7143.
[111] D.D. Lasic, H. Strey, M.C.A. Stuart, R. Podgornik, P.M. Frederik, J. Am. Chem. Soc. 119 (1997) 832.
[112] S. Huebner, B.J. Battersby, R. Grimm, G. Cevc, Biophys. J. 76 (1999) 3158.
[113] Y.S. Mel'nikova, S.M. Mel'nikov, J.E. Löfroth, Biophys. Chem. 81 (1999) 125.
[114] J. Gustafsson, G. Arvidson, G. Karlsson, M. Almgren, Biochim. Biopys. Acta – Biomembr. 1235 (1995) 305.
[115] T.W. Jing, A.M. Jeffrey, J.A. DeRose, Y.L. Lyubchenko, L.S. Shlyakhtenko, R.E. Harrington, E. Appella, J. Larsen, A. Vaught, D. Rekesh, F.X. Lu, S.M. Lindsay, Proc. Natl. Acad. Sci. U.S.A. 90 (1993) 8934.
[116] M.H. Zareie, M.R. Mozafari, V. Hasirci, E. Piskin, J. Liposome Res. 7 (1997) 491.
[117] H.D. Wang, Z.Y. Tang, Z. Li, E.K. Wang, Surf. Sci. 480 (2001) L389–L394.
[118] V. Oberle, U. Bakowsky, I.S. Zuhorn, D. Hoekstra, Biophys. J. 79 (2000) 1447.
[119] A. van Groll, Y. Levin, M.C. Barbosa, A.P. Ravazzolo, Biotechnol. Prog. 22 (2006) 1220.
[120] B. Ruozi, F. Forni, R. Battini, M.A. Vandelli, J. Drug Targ. 11 (2003) 407.
[121] B. Ruozi, R. Battini, G. Tosi, F. Forni, M.A. Vandelli, J. Drug Targ. 13 (2005) 295.
[122] B. Ruozi, R. Battini, A. Mucci, L. Schenetti, G. Tosi, F. Forni, M.A. Vandelli, 15th Symposium on Microencapsulation, Parma, Italy, 2005, p. 207.
[123] L.A. Wangerek, H.H. Dahl, T.J. Senden, J.B. Carlin, D.A. Jans, D.E. Dunstan, P.A. Ioannou, R. Williamson, S.M. Forrest, J. Gene Med. 3 (2001) 72.
[124] C. Kawaura, T. Furuno, M. Nakanishi, Bioimages 5 (1997) 121.
[125] C. Kawaura, A. Noguchi, T. Furuno, M. Nakanishi, FEBS Lett. 421 (1998) 69.
[126] A. Noguchi, N. Hirashima, M. Nakanishi, Pharm. Res. 19 (2002) 933.
[127] F. Sakurai, R. Inoue, Y. Nishino, A. Okuda, O. Matsumoto, T. Taga, F. Yamashita, Y. Takakura, M. Hashida, J. Control. Rel. 66 (2000) 255.
[128] M.R. Almofti, H. Harashima, Y. Shinohara, A. Almofti, Y. Baba, H. Kiwada, Arch. Biochem. Biophys. 410 (2003) 246.
[129] A. Elkady, V.P. Tychinsky, T.V. Vyshenskaja, Y.L. Sebyakin, I.V. Yaminskii, R.I. Zhdanov, A.R. Khokhlov, Dokl. Biochem. Biophys. 396 (2004) 161.
[130] K. Tabatt, C. Kneuer, M. Sameti, C. Olbrich, R.H. Muller, C.M. Lehr, U. Bakowsky, J. Control. Rel. 97 (2004) 321.
[131] M.R. Mozafari, C.J. Reed, C. Rostron, D.S. Martin, 6th International Conference-Liposome Advances: Progress in Drug and Vaccine Delivery, London, England, 2003, p. 114.
[132] M.R. Mozafari, V. Hasirci, J. Microencapsul. 15 (1998) 55.
[133] G.S. Manning, Biopolymers 19 (1980) 37.

Available online at www.sciencedirect.com
ScienceDirect
Talanta 73 (2007) 185–188
Talanta
www.elsevier.com/locate/talanta

Short communication

Bioassay (CALUX) measurements of 2,3,7,8-TCDD and PCB 126: Interference effects

Hermes Sanctorum, Marc Elskens, Willy Baeyens *

Department of Analytical and Environmental Chemistry, Vrije Universiteit Brussel, Pleinlaan 2, 1050-Brussels, Belgium

Received 14 July 2006; received in revised form 22 February 2007; accepted 7 March 2007
Available online 14 March 2007

Abstract

Interference effects in CALUX measurements were studied. 2,3,7,8-TCDD and PCB 126 solutions were added, according to an experimental design, to the genetically modified cells. CALUX responses were measured for pure solutions of each of these pollutants, for their mixtures and for successive additions where the first added pollutant is removed after 4 h and replaced by medium solution, the same pollutant or the other one. It appeared that in cases where the cells were exposed to TCDD and PCB 126 in series, additivity was obeyed. This was not the case when the pollutants were added to the cells simultaneously as these results show antagonistic effects.

Keywords: 2,3,7,8-TCDD; PCB 126; CALUX; Antagonism

1. Introduction

Chemical activated luciferase gene expression (CALUX) is a method based on the reactivity of dioxins, dioxin-like compounds (such as coplanar PCBs) and PAHs (not considered as dioxin-like compounds) with the Aryl hydrocarbon Receptor (AhR) and afterwards of that substrate–receptor complex with the dioxin response elements (DRE) in the cell nucleus (e.g. Refs. [1–3]). It is well-known that at the same concentration, the different dioxin and PCB congeners have a different CALUX response according to their relative equivalent potency (REP). The quantification of those compounds is therefore expressed in CALUX-TEQ values being a number of 2,3,7,8,-TCDD equivalents, since the calibration is performed relative to 2,3,7,8,-TCDD.

When complex mixtures of dioxins and PCBs are measured with a CALUX method, the overall result is often not the sum of the individual responses but lower (antagonistic effects) or higher (synergetic effects) [4]. In fact, previous studies have indicated that the ligand binding to the AhR is rather irreversible [5]. This means that once a ligand has bound to the receptor, it is generally not replaced by another one. Hence, kinetic effects are more important than equilibrium effects on the time scale of CALUX experiments, observation that Brown et al. [5] also reported.

Non-additive effects are naturally very important regarding the analysis of a sample containing a large spectrum of dioxins and dioxin-like compounds [6,7]. Until now appropriate sample clean-up procedures, including silica, alumina and/or carbon columns, are applied to quantify the amounts of dioxins and dioxin-like PCBs in a given sample [6]. However, the significance of the global dioxin-like activity of a sample measured by CALUX (the global TEQ-value of a sample extract added to the genetically modified cells without any clean-up), versus the sum of the various individual AhR ligand activities (sum of TEQ-values of the various clean-up fractions such as the dioxins and dioxin-like PCB fractions) is still a matter of debate. Since there are not yet many studies dealing with this problem, we compared the CALUX responses obtained when TCDD or PCB 126 are added simultaneously with those obtained when one of both is added with some delay. Delayed spiking, which means adding the different clean-up fractions of a sample to the cells with some time interval, may eventually reduce the interferences and will also help us to better understand the potential activity of a sample.

* Corresponding author. Tel.: +32 2 629 32 63; fax: +32 2 629 32 74.
E-mail address: wbaeyens@vub.ac.be (W. Baeyens).

0039-9140/$ – see front matter © 2007 Elsevier B.V. All rights reserved.
doi:10.1016/j.talanta.2007.03.009

2. Methods and materials

2.1. Preparation of the cells for CALUX analysis

The mouse hepatoma cell line (H1L6.1c3) that had been stably transfected with the AhR-responsive firefly luciferase reporter plasmid pGudLuc 6.1, was supplied by Xenobiotic Detection Systems Inc. (USA). Cells were cultured in a medium of phosphate buffered saline with L-Glutamine (Gibco, UK), supplemented by 8% fetal bovine serum (Hyclone Laboratories, Utah, USA), 45.5 units/mL of penicillin and 45.5 units/mL streptomycin (Gibco, UK), at 37 °C and 5% CO_2 in an atmosphere saturated with water. For the CALUX bioassay, 96-well culture plates were seeded with 200 μL of cell suspension at a density of 8.10^4 cells/mL. For further details, see Windal et al. [6].

2.2. Dosing the cells

After 20–24 h of incubation, the medium of the cell suspension was removed from each well of the dosing plate and replaced with 200 μL medium containing 2 μl of each added pollutant (TCDD or PCB 126 in DMSO). At the same time TCDD in DMSO (25,000, 12,500, 6250, 3125, 1562, 781, 391, 195, 98 and 49 fg TCDD/μL in DMSO) were analyzed to generate the calibration curve (Fig. 1). A concentration of 781 fg TCDD/μL DMSO is used as verification standard solution. For further details we refer to Windal et al. [6].

2.3. Experimental design

Concentrations of 10^{-7} M and 10^{-8} M PCB 126 and 2.43×10^{-9} M TCDD in DMSO were added to the cells. As in each well 2 μL of the DMSO solution was added to 200 μL medium, the cells were exposed to 10^{-9} and 10^{-10} M PCB 126 and 2.43×10^{-11} M TCDD. These concentrations were chosen because (1) below 10^{-8} M PCB 126 in DMSO no result or influence on TCDD was observed; (2) above 10^{-7} M PCB 126 in DMSO the obtained signals were too high and became irregular and (3) the dioxin-like activity of 10^{-7} M PCB 126 in DMSO is almost equal to that of 2.43 10^{-9} M TCDD (it is the same as the verification standard solution).

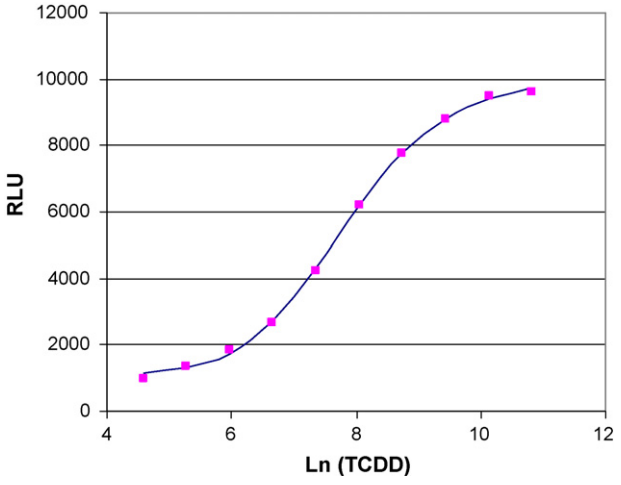

Fig. 1. Calibration curve of standard solutions of 2,3,7,8-TCDD. Relative light units (RLU) vs. the logarithm of the 2,3,7,8-TCDD concentration.

Four series of experiments were carried out. The first series (experiments 1–5 and 13) were carried out according following sequence: one or a mixture of pollutants were added to the wells of the incubation plate and the cells were incubated for 4 h, then all solutions were removed from the wells and medium solution, the same or the other pollutant were added and incubation continued up to 24 h; in the second series (experiments 6, 9 and 10) one or a mixture of pollutants were added to the wells of the incubation plate and the cells were incubated for 24 h; in the third series (experiments 7 and 8) one pollutant (double concentration in half of the normal volume) was added to the wells of the incubation plate and the cells were incubated for 4 h, then the other pollutant (also double concentration in half of the normal volume) was added (after the addition, both pollutants were again at their normal concentrations) and incubation continued up to 24 h; in the fourth series (experiments 11 and 12), medium solution was first added to the wells of the incubation plate and the cells were incubated for 4 h, then this solution was removed from the wells and one pollutant was added and incubation continued up to 24 h.

3. Results and discussion

The results obtained from the CALUX experiments (a summary is shown in Table 1) with the higher PCB 126 concentration ($C = 10^{-7}$ M in DMSO) allow us to make the following observations:

3.1. Only one compound is incubated

The signal observed when PCB 126 was incubated for 4 h (experiment 1), is significantly lower at the 1 and 5% level than when PCB 126 is incubated for 24 h (experiment 6); *t*-test $p = 0.001$. The same is true when TCDD was incubated instead of PCB 126 (experiments 5 versus 10; *t*-test $p < 0.001$).

3.2. During incubation one compound is replaced by the other one

When first PCB 126 was incubated for 4 h and then removed, followed by an addition of TCDD (experiment 2), the signal is statistically not different from that obtained when first TCDD was incubated for 4 h and then replaced by PCB 126 (experiment 3; *t*-test $p = 0.182$).

When first PCB 126 was incubated for 4 h and then removed, followed by an addition of TCDD (experiment 2), the result does not statistically differ from the sum of the signals of PCB 126 after 4 h of incubation (experiment 1) and TCDD after 20 h incubation (experiment 12; *t*-test $p = 0.095$). The same conclusion can be drawn when comparing the response of experiment 3 with those of experiments 5 and 11 (*t*-test $p = 0.189$). This suggests that when TCDD and PCB 126 were not present as

Table 1
Overview of the CALUX experiments

0 h	4 h	24 h	*n*	*m*	pg CALUX-TEQ	CI
(1) Add PCB	Remove PCB, add medium	Measure	2	4	PCB-7:0.89	0.06
			2	4	PCB-8:0	
(2) Add PCB	Remove PCB, add TCDD	Measure	2	4	PCB-7: 2.33	0.16
			2	4	PCB-8: 1.62	0.83
(3) Add TCDD	Remove TCDD, add PCB	Measure	2	4	PCB-7: 2.12	0.30
			2	4	PCB-8: 1.03	0.16
(4) Add PCB and TCDD	remove PCB and TCDD, add medium	Measure	3	6	PCB-7: 1.63	0.48
			3	6	PCB-8: 1.04	0.10
(5) Add TCDD	Remove TCDD, add medium	Measure	2	4	0.78	0.02
(6) Add PCB		Measure	4	8	PCB-7: 1.67	0.15
			2	4	PCB-8: 0.37	0.08
(7) Add PCB (in half of medium)	Add TCDD (in half of medium)	Measure	5	10	PCB-7: 1.14	0.22
			5	10	PCB-8: 0.92	0.10
(8) Add TCDD (in half of medium)	Add PCB (in half of medium)	Measure	4	8	PCB-7: 1.24	0.24
			5	10	PCB-8: 0.98	0.22
(9) Add PCB and TCDD		Measure	3	6	PCB-7: 1.21	0.12
			3	6	PCB-8: 1.01	0.40
(10) Add TCDD		Measure	8	16	1.45	0.07
(11) Add medium	Remove medium, add PCB	Measure	2	4	PCB-7: 1.53	0.10
			2	4	PCB-8: 0.31	0.14
(12) Add medium	Remove medium, add TCDD	Measure	4	8	1.58	0.07
(13) Add TCDD	Remove TCDD, add TCDD	Measure	4	8	2.42	0.15

PCB-7 (PCB-8) is a solution of 10^{-7} M (10^{-8} M) PCB 126 in DMSO. The results in pg CALUX-TEQ are mean values, *n* is the number of independent experiments, *m* is the number of repeated measurements per experiment and CI is the 95% confidence interval of the mean

mixtures but removed and replaced, the signals are similar to the addition of the individual pollutant responses.

When TCDD was incubated for 4 h and then removed, followed by an addition of TCDD again (experiment 13), the response does not significantly differ from the one observed when TCDD was replaced by PCB 126 in one of the procedure steps (experiments 2 and 3; one way ANOVA $p = 0.077$). This supports that there is no interference effect caused by TCDD or PCB 126 when one pollutant solution is removed and replaced by the other one.

3.3. Mixtures are incubated

When we consider mixtures of pollutants, the responses are much more complex to understand. When PCB 126 and TCDD were added simultaneously and removed after 4 h (experiment 4), the signal is not statistically different than when this mixture of pollutants was incubated for 24 h (experiment 9; *t*-test $p = 0.092$). When PCB 126 and TCDD were added with 4 h difference and were not removed (experiments 7 and 8), the responses are similar (*t*-test $p = 0.504$). When a mixture of pollutants was added at the start of the experiment (experiment 9) or if both pollutants were added with a delay of 4 h, hence no pollutant was removed after 4 h (experiments 7 and 8), similar results are observed (one way ANOVA $p = 0.759$).

More remarkable are the low signals observed: there is no additivity noticeable and the responses are always lower at the 1 and 5% level than for successive additions when the first added pollutant is removed after 4 h and replaced by the other one (experiment 9 compared to experiments 2 and 3) but even in case when only one of the individual pollutants was added (experiment 9 compared to experiments 6 and 10; one way ANOVA $p < 0.001$). This means that important antagonistic effects occur when there was no removal step of TCDD and/or PCB 126 (Pairwise Multiple Comparison Procedure Holm–Sidak method: group 6 versus 9 $p < 0.01$; group 6 versus 10 $p < 0.001$; group 9 versus 10 $p = 0.007$).

3.4. Replacing the cell medium during incubation

To be sure that deleting the cell medium after 4 h of incubation and replacing it by a new cell medium had no adverse effect on the cell culture, experiments 11 and 12 were carried out. Cell medium was added to the cells and removed after 4 h of incubation. Then either PCB 126 or TCDD were added and the incubation continued up to 24 h. Comparing these results to the results observed for pure solutions of PCB 126 or TCDD incubated during 24 h show no statistical differences (experiment 6 *versus* 11; *t*-test $p = 0.230$ and experiment 10 versus 12 *t*-test $p = 0.051$), although in the latter case, the *p* value is borderline significant.

3.5. Experiments with the lower PCB 126 concentration

A more limited number of experiments with the lower PCB 126 concentration (10^{-8} M in DMSO) were carried out. These experiments confirm the result observed with the higher PCB 126 concentration:

(1) The lower PCB 126 concentration yielded low CALUX activity, but there is still a difference between 4 and 24 h incubation (not measurable for a 4 h incubation—experiment 1, and 0.37 pg CALUX-TEQ for a 24 h incubation—experiment 6);
(2) there is no significant difference between 20 and 24 h incubations (experiment 6 versus experiment 11);
(3) incubations of mixtures of TCDD and the lower PCB 126 concentration for 20–24 h (experiments 7, 8 and 9) yield similar results as the incubation of the same mixture for 4 h (experiment 4) and the incubation of TCDD for 4 h and its replacement by the lower PCB 126 concentration up to 24 h (experiment 3);
(4) only experiment 2 when first the lower PCB 126 concentration was incubated for 4 h and then replaced by TCDD for the next 20 h (experiment 2), shows a result which is significantly higher than all the other ones involving the lower PCB 126 concentration. In all experiments with the lower PCB concentration and where TCDD was incubated for at least 20 h, the results were significantly higher when successive additions were applied (experiment 2) than for mixtures of TCDD and PCB 126 (experiments 7, 8 and 9).

It is clear that in the experiments where one compound is replaced by another one, additivity is observed. Moreover, as kinetic effects are more important than equilibrium effects and these pollutants bind irreversibly to the receptor [5], it is only the pollutant fraction remaining in the medium that is removed after 4 h. When the second pollutant is added to the cells, there is no or minimal interaction with the first compound which is irreversibly bound. When a mixture of pollutants is present in the medium, the compounds seem to interact, causing antagonistic effects.

4. Conclusion

In all experiments where no mixture of pollutants in the medium solution was present, additive effects are observed. This is also valid for experiments where the initially added pollutant was removed after 4 h of exposure to the cells and replaced by the other one. In all these cases the order of addition of PCB 126 and TCDD was of no importance. When a mixture of pollutants of PCB 126 and TCDD was added to the cells, the signals are more complex and show antagonism.

The results of these experiments show that delayed spiking can be helpful in analyzing mixtures of dioxins and dioxin-like substances and eventually may reduce antagonistic effects. This aspect should be further investigated on real samples.

Acknowledgements

The authors are grateful to the members of the Department of Pharmacology and Bromatology of the Scientific Institute of Public Health involved with the CALUX Bio-assay (L.G., I.W., I.V.O., N.V.W., S.C.) for offering access to the cell lines.

References

[1] M. Cooke, G.C. Clark, L. Goeyens, W. Baeyens, Today's Chemist at Work 9 (2000) 34–39.
[2] I. Van Overmeire, G.C. Clark, D.J. Brown, M.D. Chu, M. Cooke, M.S. Denison, W. Baeyens, S. Srebrnik, L. Goeyens, Env. Sci. Pol. 4 (2001) 345–357.
[3] M.S. Denison, B. Zhao, D.S. Baston, G.C. Clark, H. Murata, D. Han, Talanta 63 (2004) 1123–1133.
[4] C. Schroijen, I. Windal, L. Goeyens, W. Baeyens, Talanta 63 (2004) 1261–1268.
[5] M.M. Brown, U.A. Schneider, J.R. Petrulis, N.J. Bunce, Toxicol. Appl. Pharmacol. 129 (1994) 243–251.
[6] I. Windal, N. Van Wouwe, G. Eppe, C. Xhrouet, V. Debacker, W. Baeyens, E. De Pauw, L. Goeyens, Environ. Sci. Technol. 39 (2005) 1741–1748.
[7] H. Sanctorum, I. Windal, V. Hanot, L. Goeyens, W. Baeyens, Arch. Environm. Cont. Toxicol. 52 (2007) 317–325.

Available online at www.sciencedirect.com
ScienceDirect
Talanta 73 (2007) 127–133
Talanta
www.elsevier.com/locate/talanta

Investigation of the chromatographic behaviour of some selenium species—Comparison with their octanol–water partitioning

Fotios Tsopelas [a], Anna Tsantili-Kakoulidou [b], Maria Ochsenkühn-Petropoulou [a,*]

[a] *Laboratory of Inorganic and Analytical Chemistry, School of Chemical Engineering, National Technical University of Athens, Iroon Polytechniou 9, 157 73 Athens, Greece*
[b] *Department of Pharmacy, Division of Pharmaceutical Chemistry, University of Athens, Panepistimiopolis, Zografou, 157 71 Athens, Greece*

Received 30 November 2006; received in revised form 7 March 2007; accepted 7 March 2007
Available online 14 March 2007

Abstract

The retention behaviour of selenites (Se(IV)), selenates (Se(VI)), seleno-DL-methionine (Se-Met), selenocystine (Se-Cyst), selenocystamine (Se-CM) and selenourea (Se-U) was investigated using a Discovery end-capped reversed-phase column as stationary phase and different mobile phase conditions. Extrapolated to 100% aqueous mobile phase retention factors ($\log k_w$) of the investigated Se species, determined using different methanol fractions (φ) as organic modifier, were compared with the corresponding actual values. The proper operation of this column even at 100% aqueous phase proved to be valuable for the accurate determination of $\log k_w$ values of Se-CM and Se-Cyst, presenting a convex curvature $\log k = f(\varphi)$ at low MeOH fractions, often neglected in the extrapolation procedure. The effect of the presence of *n*-decylamine as well as saturation of the mobile phase with *n*-octanol was also studied. For ampholytic Se-Met and Se-Cyst the effect of *n*-decylamine in retention reflected the predominance of zwitterionic nature in the case of Se-Met in contrary to the non-zwitterionic species found in the case of Se-Cyst, in accordance with our previous findings concerning partitioning experiments in the *n*-octanol/water system. Finally, an attempt was made to correlate $\log k_w$ values with the logarithm of *n*-octanol/water distribution coefficient, $\log D$, of the investigated Se species and an indicative $\log D$ value of Se-U was derived.

Keywords: Lipophilicity; Extrapolated retention factors $\log k_w$; Reversed-phase liquid chromatography; Mobile phase additives; Logarithm of distribution coefficient $\log D$; Selenium speciation

1. Introduction

The importance of selenium to human health has been well established [1–3]. As an anti-cancer agent, Se has become the subject of great research in recent years [3–7]. Anti-oxidative activity as well as cancer chemoprevention have been associated mainly with organoselenium compounds, among others selenoaminoacids, such as selenomethionine (Se-Met) and selenocystine (Se-Cyst), while inorganic selenium salts, selenites (Se(IV)) and selenates (Se(VI)) have also been tested [3–7]. The dietary considerations of Se along with the cancer preventative considerations have led to a widespread use of commercially available Se supplements [3,8,9]. However, despite the great efforts for Se speciation in Se supplements and foods [10,11], the chemical form of Se which can achieve best nutritional effect still remains an open question [12]. As bioavailability, toxicity and chemopreventive activity of selenium is species-dependant, each selenium compound is absorbed differently by the human body and has a different bioaccumulation tendency.

Lipophilicity, as expressed by the logarithm of octanol/water partition or distribution coefficient, $\log P$ or $\log D$, respectively, is of paramount importance in several absorption, distribution, metabolism and elimination (ADME) aspects, influencing bioaccumulation tendency, bioavailability, pharmacological activity and toxicological profile [13–15]. From an environmental point of view, lipophilicity influences to a great extent issues concerning risk assessment and the fate of chemicals

* Corresponding author. Tel.: +30 210 7723094; fax: +30 210 7724039.
E-mail addresses: tsantili@pharm.uoa.gr (A. Tsantili-Kakoulidou), oxenki@central.ntua.gr (M. Ochsenkühn-Petropoulou).

0039-9140/$ – see front matter © 2007 Elsevier B.V. All rights reserved.
doi:10.1016/j.talanta.2007.03.006

in the environment [16]. Furthermore, the Physical Chemistry Expert Group of the Organization for Economic Cooperation and Development (OECD) has drawn up a test guideline for the determination of lipophilicity of new chemicals, as part of a minimum pre-marketing set of data (MPD) [17]. However, very few relevant experimental data are available for Se species [18]. Consequently, the value of Se as atom type or fragment is not incorporated in most software programmes used in drug design, which predict log P of chemical compounds as a sum of lipophilicity of their individual atoms or fragments, respectively, and when Se is included the predictions are rather unreliable [18]. Furthermore, the traditional shaking flask method for direct partitioning experiments is tedious, time-consuming and it cannot be applied in case of compounds undergoing degradation. Partition chromatography techniques offer a popular alternative for measuring lipophilicity, combining insensitivity to impurities, wide dynamic range and possibility of automation, while they are compound sparing [19–29]. The obtained retention factors, $\log k_w$, directly measured or extrapolated to 0% concentration of the organic modifier used in the mobile phase, can be directly correlated to log P or log D via Collander type of equations [21]. However, the chromatographic conditions used need to be further standardized in order the obtained chromatographic indices for each species to be converted into biomimetic partition coefficients. Some special problems, depending on the nature of the investigated compounds, can occur, such as silanophilic interactions in the partition mechanism especially in the case of basic compounds [21,25,26]. The problem is partially faced by using stationary phases with reduced silanol sites, such as end-capped base deactivated silica gel (BDS) [26] or polar embedded RP-Amide with improved performance towards acids, bases and zwitterions, widely known as ABZ columns [21], instead of classical octadecyl silica (ODS) columns. Other alternative stationary phases involve Discovery end-capped columns which have been used for lipophilicity studies as well [25]. The addition of masking agents, such as n-decylamine, in the mobile phase is a popular way to reduce silanophilic interactions [21,26]. More recently, the use of n-octanol as mobile phase additive is also recommended by some authors, although its role has not been fully understood. One assumption is that during equilibration it associates with stationary phase as a lipophilic component providing additional masking of the free silanols and an octanol-like character in respect to hydrogen bonding capability of the stationary phase [21,25,26].

In this work, the retention behaviour of selenites (Se(IV)), selenates (Se(VI)), seleno-DL-methionine (Se-Met), selenocystine (Se-Cyst), selenocystamine (Se-CM) and selenourea (Se-U) was investigated by using a Discovery end-capped BIO Wide Pore RP-18 reversed-phase column as stationary phase. The effect of MeOH as organic modifier, ionic strength and the presence of n-decylamine and n-octanol as mobile additives in the retention of the investigated Se species were also studied. Finally, the retention factors of the six investigated Se species were compared with the corresponding octanol–water log D values determined in our previous study [18] and an indicative value of log D of Se-U was proposed.

2. Experimental

2.1. Instrumentation

The investigation of the retention behaviour of the investigated Se species was performed using a high performance liquid chromatography (HPLC) system, including a Knauer K-1001 HPLC gradient pump with K-1500 degasser and solvent organizer (Model Wellchrom) and a Knauer K-2501 UV–Vis detector (180–800 nm). As stationary phase, a Discovery end-capped BIO Wide Pore RP-18 (Supelco, USA, 150 mm × 4.6 mm i.d., 3 μm particle size) column was used. The flow rate was adjusted at 0.8 ml min^{-1} and an injection loop of 100 μl was selected. The investigated Se species were detected at 205 nm, while the detection of $KMnO_4$ was performed at 530 nm. For the selection of the appropriate wavelength for the UV detector of the HPLC system, the scanning of the UV spectra of the individual Se species into each eluent was carried out with the Cary 1 E spectrophotometer (Varian). Chromatographic data were processed with the software Eurochrom 2000 Version 2.05 (Knauer). High purity water (HPW) for the preparation of eluents was obtained using a Millipore Simplicity system.

2.2. Reagents

All reagents were of analytical grade. KH_2PO_4, $KMnO_4$, NaCl and KCl were purchased by Merck, Na_2HPO_4 by Carlo-Erba and concentrated H_3PO_4 (85%) by Riedel de Haen. Working solutions in the range of 10–30 mg Se l^{-1} of sodium selenite, Na_2SeO_3 (Riedel de Haen), sodium selenate, Na_2SeO_4 (≥98%, Fluka Chemika), seleno-DL-methionine (≥99%, Fluka Chemika), L-selenocystine (98%, Acros Organics), selenocystamine dichloride (Sigma) and selenourea (≥99%, Aldrich) were daily prepared by dissolving the necessary amount of each compound in each eluent used in the chromatographic system. As mobile additives, n-decylamine (≥99.5%, Fluka Chemika) and n-octanol (≥99.5%, Fluka Chemica) were used. All reagents were supplied from Chemilab (Athens, Greece), except for L-selenocystine, which was bought from Tech-line (Athens, Greece).

2.3. Analytical procedure

Mobile phases consisted of the following buffer or methanol buffer mixtures:

A. 0.13 M KH_2PO_4/Na_2HPO_4 + 0–22% MeOH, pH 7.0;
B. 0.13 M KH_2PO_4/Na_2HPO_4 + 0.027 M KCl + 0.137 M NaCl, pH 7.0;
C. 0.13 M KH_2PO_4/Na_2HPO_4 + 0.20% n-decylamine, pH 7.0;
D. 0.13 M KH_2PO_4/Na_2HPO_4 saturated in n-octanol + 0.15% n-decylamine, pH 7.0.

The saturation with n-octanol was achieved by gentle mixture of the mobile phase with n-octanol in a separation funnel and overnight allowance. The pH value of all buffers was adjusted at

7.0 using H_3PO_4, if necessary and mobile phases were filtered through a 0.45 μm filter.

Retention factors were determined at least in triplicate for each sample and converted to $\log k$ values by means of the Eq. (1):

$$\log k = \log\left(\frac{t_r - t_0}{t_0}\right) \quad (1)$$

where t_r is the elution time of each investigated Se species and t_0 the column dead time being measured using $KMnO_4$.

2.4. Statistical analysis

Linear regression analysis was performed using SPSS Version 10.0 for Windows and the following statistical data were provided for the obtained regression equations: n is the number of data points, s the standard deviation, R the correlation coefficient and F is the Fisher test calculated for a significance level of $\alpha = 0.05$.

3. Results and discussion

In our previous work concerning lipophilicity study of Se species by the shaking flask method, phosphate buffer, pH 7.0, had been used as aqueous phase [18]. Therefore, the same buffer was also selected for this investigation in order the obtained chromatographic indices to be comparable with the previously determined $\log D$ values [18]. On the other hand, methanol is the most widely used organic modifier for lipophilicity assessment by reversed-phase liquid chromatography [21–29]. In the present work, six different concentrations of methanol in the range of 1–22% were used to measure isocratic retention. Measurements were also performed without organic modifier since the Discovery BIO Wide Pore RP-18 column can work properly even at 100% aqueous mobile phase [30], showing good reproducibility and shape of peaks in our previous work [31].

In the case of Se-U, a secondary small chromatographic peak, having lower retention time than the main peak, was observed for water rich mobile phases with MeOH fraction up to 5%. This peak presented in Fig. 1(a) should be attributed to the degradation of Se-U in the aqueous environment [32,33]. For higher MeOH fractions, at which Se-U eluted close to the dead time, the two peaks overlapped and they were observed as one non-symmetrical peak as shown in Fig. 1(b). It should be mentioned that due to this degradation, direct partitioning experiments for the determination of $\log D$ of Se-U could not be performed.

3.1. Effect of methanol in retention

According to the Schoenmaker's model [22,26], the relationship between $\log k$ values and MeOH fraction in the mobile phase, φ, is expressed by Eq. (2):

$$\log k = A \cdot \varphi + B \cdot \varphi^2 + E\sqrt{\varphi} + \log k_w \quad (2)$$

where A, B and E are the fitting coefficients and $\log k_w$ is the intercept which corresponds to 100% aqueous phase. The B φ^2 term accounts for a curvature at higher organic modifier concentrations and the term $\sqrt{\varphi}$ accounts for a, usually convex, curvature observed at low, up to 3%, fractions of the organic modifier. Using MeOH as organic modifier, for a certain concentration range, a linear relationship $\log k = f(\varphi)$ can be expected for most organic compounds [21–29], following the Snyder's linear solvent strength model [22,24–26], expressed by Eq. (3):

$$\log k = -S \cdot \varphi + \log k_w \quad (3)$$

Eq. (3) permits the calculation of $\log k_w$ values, which correspond to 100% aqueous phase and they are considered as lipophilicity indices, associated with $\log D$. The slope S of the Eq. (3) is considered to be related to the specific hydrophobic area of the solutes and depends on the chromatographic system as well.

The effect of MeOH fraction to the retention factors, $\log k$, of Se(IV), Se(VI), Se-Met, Se-Cyst, Se-CM and Se-U is presented in Fig. 2. In general, by increasing the concentration of MeOH, the retention factors of all the investigated Se species decreased. This decrease is linear in the case of Se-Met and Se-U up to 10% and for Se(IV) up to 8% MeOH fraction. For higher MeOH fractions, a curvature was observed for Se-Met, Se-CM

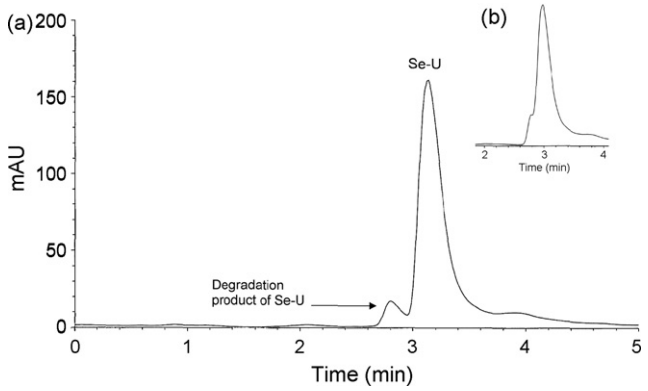

Fig. 1. (a) Presence of degradation product of Se-U in its chromatogram (concentration of Se-U: 30 μg Se ml^{-1}) using as mobile phase 0.13 M KH_2PO_4/Na_2HPO_4 + 1% MeOH, pH 7.0. The two peaks overlapped (b) by increasing the MeOH fraction to 8%. Detection was carried out using UV spectrometry at the wavelength of 205 nm.

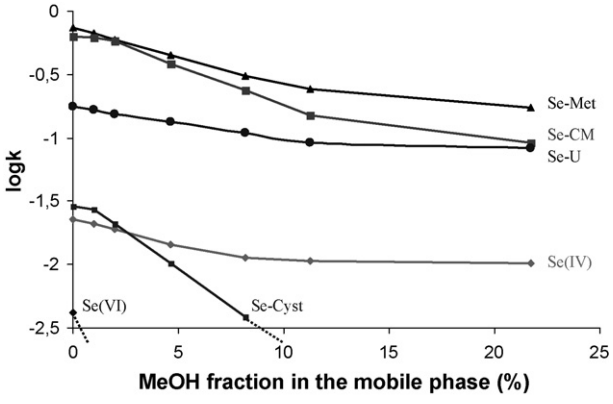

Fig. 2. Effect of the addition of MeOH in the mobile phase to the final retention outcome of the six investigated Se species.

Table 1
Retention factors log k_w extrapolated to 0% MeOH and the corresponding slopes S of the investigated Se species in comparison with the corresponding actual log k_w values determined using 100% aqueous phase

Se species	Extrapolated log k_w	Slope (-S)	Actual log k_w values	Difference (extrapolated-actual)
Se(IV)	-1.65 ± 0.11	0.04 ± 0.03	-1.64 ± 0.09	-0.01
Se(VI)	–	–	-2.38 ± 0.25	–
Se-Met	-0.14 ± 0.03	0.05 ± 0.01	-0.13 ± 0.02	-0.01
Se-Cyst	-1.45 ± 0.10	0.12 ± 0.03	-1.54 ± 0.09	+0.09
Se-CM	-0.13 ± 0.03	0.06 ± 0.01	-0.20 ± 0.02	+0.07
Se-U	-0.76 ± 0.05	0.03 ± 0.01	-0.75 ± 0.03	-0.01

and Se-U, which should be partly attributed to silanophilic interactions of the solutes with the stationary phase, behaviour often observed in the case of protonated amines. It should be noted that silanophilic interactions are less significant at water rich mobile phases, since water molecules may hydrate silanol sites, acting as masking agent themselves [34]. For Se-Cyst and Se-CM, an additional convex curvature was observed at low MeOH fractions, due possibly to stationary phase solvation problems [22]. It should be mentioned that the latter curvature is often neglected in the extrapolation procedure performed using retention factors obtained at water rich mobile phases and, therefore, it may be a source of error for the calculation of log k_w values. In order to evaluate this error, extrapolated log k_w values were calculated using data for MeOH fractions from 1 up to 10%. In Table 1, the extrapolated retention factors log k_w with their standard deviation and the corresponding slopes S of the investigated Se species along with their statistics are presented. In all cases, the correlation coefficients R were found to be very high, from 0.997 to 1. In the same Table, actual log k_w values with their standard deviation determined in absence of MeOH are also included along with the difference between extrapolated and actual log k_w values. In the case of Se(VI), only actual log k_w could be determined since addition of even 1% MeOH led to its elution within the dead time. As shown in Table 1, an excellent agreement between extrapolated and actual log k_w values for Se(IV), Se-Met and Se-U was obtained, while a small positive difference for Se-CM and Se-Cyst was found as a result of the aforementioned curvature in the log k/φ relationship.

Slopes, S, of Eq. (3) may correlate with log k_w values if retention is governed by a uniform mechanism for all solutes. In the case of the investigated Se species, no correlation between S and log k_w was observed, indicating that besides partition mechanism, retention is affected by secondary interactions (mainly concerning hydrogen-bonding or silanophilic interactions) which may differ among the different functional groups present in their molecule [35]. It should be noted that the slopes obtained for Se(IV), Se-Met and Se-U are low and fairly parallel. On the contrary, in the case of Se-Cyst and Se-CM, unexpectedly higher slopes were obtained.

3.2. Effect of the increasing of the ionic strength of the mobile phase

The investigation of the influence of mobile phase ionic strength to the retention factors, log k, of the investigated Se species, was performed using phosphate buffer saline (PBS), being prepared by addition of 0.137 M NaCl/0.027 M KCl into the phosphate buffer. No significant difference in retention was observed for Se species in the present of electrolytes except for Se-CM, which exists as doubly protonated species, $^{+}H_3NCH_2CH_2Se–SeCH_2CH_2NH_3^{+}$. The slight increase of log k_w of Se-CM in the presence of NaCl/KCl (-0.16 ± 0.02 compared with -0.20 ± 0.02 in the absence of electrolytes) could be attributed to potential ion pair formation in accordance with its corresponding behaviour observed in the n-octanol/water system [18]. It should be noted that in our previous work [18], the presence of electrolytes in partition experiments led to an increase of log D in the case of the acidic solutes Se(IV) and Se(VI), as a result of salting out effect.

3.3. Effect of the addition of n-decylamine and n-octanol in the mobile phase

In Table 2, the log k_w factors of the six Se species, obtained in the presence of n-decylamine and n-decylamine plus n-octanol saturated buffer, are compared with those obtained in the absence of the two organic additives. Decylamine is considered to act as masking agent, suppressing silanophilic interactions, while in combination with n-octanol, it is assumed to provide a more octanol like character to the stationary phase, so that log D values are better reproduced [21,26]. Generally, the presence of these mobile phase additives leads to a decrease of retention in the case of basic and neutral compounds. In fact, the presence of n-decylamine increased substantially the retention values of the anionic inorganic species Se(VI) ($pK_{a2} = 1.7$) [36] and Se(IV) ($pK_{a1} = 2.46$, $pK_{a2} = 7.31$) [36], which exist as SeO_4^{2-} and mainly as $HSeO_3^{-}$, respectively, at pH 7.0. This can be explained as acidic species may form ion-pairs with protonated n-decylamine with more favourable partition in the hydrophobic stationary phase, which leads to an increase of their retention. This is more evident in the case of dianion SeO_4^{2-}. The saturation of the mobile phase with n-octanol does not seem to have any further significant impact on the retention of these Se species. The most interesting observation is the opposite behaviour of the two ampholytic selenoaminoacids, Se-Met and Se-Cyst by the addition of n-decylamine with or without saturation of the buffer with n-octanol. Se-Met has two dissociation constants ($pK_1 = 2.19$, $pK_2 = 9.05$), while Se-Cyst has four corresponding values ($pK_{a1} = 1.68$, $pK_{a2} = 2.15$, $pK_{a3} = 8.07$, $pK_{a4} = 8.94$) [36]. In general, the retention behaviour of ampholytes may be

Table 2
Comparison of actual log k_w values of the investigated Se species using as mobile phase aqueous solutions of (a) KH_2PO_4/Na_2HPO_4, pH 7.0, (b) KH_2PO_4/Na_2HPO_4, pH 7.0 + 0.2% *n*-decylamine and (c) saturated with *n*-octanol KH_2PO_4/Na_2HPO_4 + 0.15% *n*-decylamine, pH 7.0, with the corresponding log *D* values in the octanol–water system obtained in our previous work [18]

Se species	Actual log k_w values			log D[a] [18]
	Phosphate buffer	Phosphate buffer + 0.2% *n*-decylamine	Saturated in *n*-octanol phosphate buffer + 0.15% *n*-decylamine	
Se(IV)	−1.64 ± 0.09	−1.28 ± 0.06	−1.21 ± 0.06	−1.81 ± 0.15
Se(VI)	−2.38 ± 0.25	−1.15 ± 0.06	−1.20 ± 0.06	−2.60 ± 0.20
Se-Met	−0.13 ± 0.02	−0.37 ± 0.02	−0.40 ± 0.02	−1.70 ± 0.05
Se-Cyst	−1.54 ± 0.09	−1.19 ± 0.06	−1.14 ± 0.05	−2.38 ± 0.17
Se-CM	−0.20 ± 0.02	−0.36 ± 0.02	−0.34 ± 0.02	−2.08 ± 0.10
Se-U	−0.75 ± 0.03	−0.93 ± 0.04	−1.05 ± 0.04	–

[a] Mean values obtained by ICP-AES and polarography.

governed by the degree of exposure of their positively or negatively charged group. The log k_w value of Se-Met decreased significantly in the presence of the mobile phase additives, in contrast with the corresponding substantial increase in the case of Se-Cyst. This chromatographic behaviour can be explained on the basis of our previous findings concerning the log *D*/pH relationship of the two ampholytes [18]. Especially, log *D*/pH relationship of Se-Met was found [18] to follow the bell-shaped curve with maximum lipophilicity close to its iso-electrical point [37,38], implying presence of intramolecular interaction between the charged centres $–COO^-$ and $–NH_3^+$. On the contrary, the U-shaped curve of Se-Cyst with a minimum lipophilicity close to its iso-electrical points [18], indicates absence of such interactions, due perhaps to stereochemical reasons [37,38]. Consequently, the charged anionic $–COO^-$ centres of Se-Cyst are exposed to form hydrophobic ion pairs with protonated *n*-decylamine, leading to the observed increase of its retention factor log k_w. On the other hand, protonated *n*-decylamine could not form ion-pairs with zwitterionic species of Se-Met. In this case, it exerted its effect on the stationary phase acting as a masking agent of the free silanols, leading to a decrease in retention. Analogous decrease in retention was observed in the case of the basic Se-CM and Se-U. The dissociation constants of these species are not available in literature, but in the case of Se-CM indicative values ($pK_{a1} = 8.07$, $pK_{a2} = 8.98$) were estimated using ACD Labs software in our previous work [18]. However, the saturation of the buffer with *n*-octanol in combination with *n*-decylamine had no considerable further effect in retention.

3.4. Comparison of log k_w with log *D* values

The retention factors, log k_w, of the investigated Se species, measured under different conditions, were compared with their corresponding octanol/water log *D* values, determined in our previous work [18], which are also included in Table 2. For Se(VI) an approximate log *D* value of −2.6 was considered. This value is justified by the fact that it was found to be slightly below −2.50, at the limit of accuracy for the shaking flask method, while it was increased to −2.45 in the presence of electrolytes [18]. In the case of Se-U no log *D* data are available, due to its gradual degradation [32,33], which did not permit direct partitioning experiments. As observed from the data of Table 2 the log k_w values of inorganic selenium species are consistent with their corresponding log *D* values. By contrast, log k_w values of organoselenium species are considerably higher than their corresponding log *D* ones. In Fig. 3(a), the plot of log *D* versus log k_w values of Se species in absence of any mobile phase additive is illustrated. The change of the corresponding log k_w values in the presence of *n*-decylamine is also depicted in the same Fig-

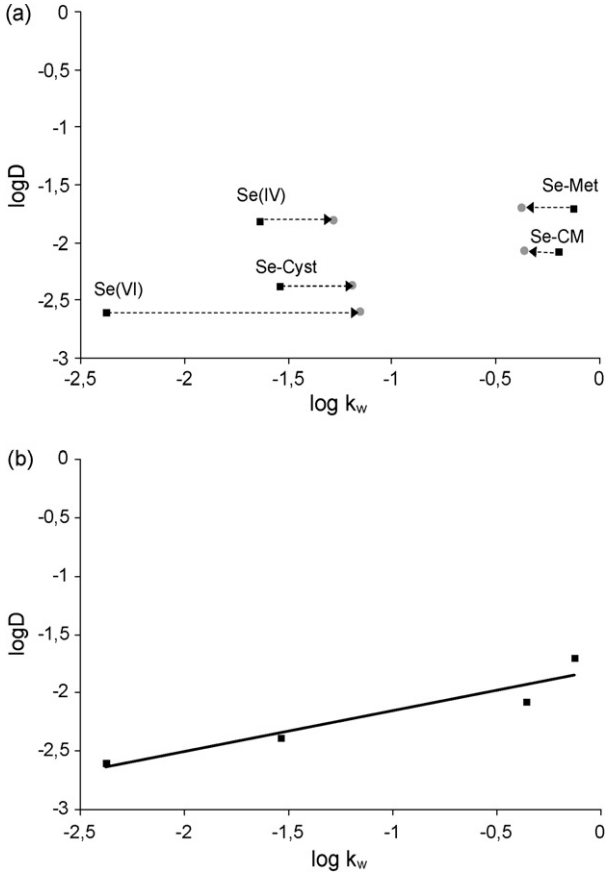

Fig. 3. (a) Plot of log *D* vs. log k_w values measured in phosphate buffer (■) and the effect of *n*-decylamine in the retention factors of the investigated Se species (●). (b) Regression analysis of log *D* = *f*(log k_w) data of Se(VI), Se-Met, Se-Cyst and Se-CM (retention factors of Se(VI), Se-Met and Se-Cyst were measured using phosphate buffer as mobile phase, while log k_w value of Se-CM was measured using phosphate buffer + 0.2% *n*-decylamine).

ure with dashed lines. This profile leads to an unsatisfactory data correlation ($R = 0.679$, $s = 0.320$, $F = 2.570$). However, if Se(IV) is not included, an Eq. (4) with satisfactory statistics is obtained, associating actual retention factors determined using phosphate buffer as mobile phase and $\log D$ values.

$$\log D = 0.33(\pm 0.10) \cdot \log k_w - 1.84(\pm 0.14)$$
$$n = 4,\ R = 0.926,\ s = 0.181,\ F = 11.96 \quad (4)$$

Therefore, using Eq. (4) and setting as $\log k_w = -0.75$, the octanol–water distribution coefficient of Se-U was calculated to be $\log D = -2.09$. Taking into account that the presence of *n*-decylamine leads to a better simulation of partition mechanism for basic compounds [21,26], such as Se-CM and Se-U, the regression analysis was repeated, replacing $\log k_w$ value of the weak base Se-CM with those measured in presence of *n*-decylamine. It should be noted that the addition of *n*-decylamine is a necessary condition in standard procedures used to determine $\log k_w$ values for basic compounds [21,26] and Se-CM was the only base of the four Se species used for this correlation. Indeed, the obtained Eq. (5) is similar to Eq. (4), but it is accompanied with better correlation coefficient.

$$\log D = 0.35(\pm 0.08) \cdot \log k_w - 1.80(\pm 0.12)$$
$$n = 4,\ R = 0.946,\ s = 0.154,\ F = 17.18 \quad (5)$$

The corresponding plot of $\log D/\log k_w$ data correlation obtained by Eq. (5) is illustrated in Fig. 3(b). Using the more "appropriate" value $\log k_w = -0.93$ of Se-U, measured in presence of *n*-decylamine, its lipophilicity, calculated according to Eq. (5), was found to be $\log D = -2.13$. Considering only the three organoselenium compounds, Se-Met, Se-Cyst and Se-CM, a further similar equation to Eqs. (4) and (5) was obtained and a value of $\log D = -2.16$ for Se-U, close to the previous ones, was derived. It should be mentioned that the calculated $\log D$ values of Se-U are only indicative since the relevant regression equations are based on 3 to 4 data points. However, to the best of our knowledge, this is the first study concerning the determination of chromatographic indices and their correlation with $\log D$ data for the investigation of lipophilicity of Se species. It is interesting that the three Se species with the common property of possessing multiple free charges, Se(VI), Se-Cyst and Se-CM provide an excellent $\log D = f(\log k_w)$ correlation with $R = 0.9999$. These findings support a common retention mechanism for these Se compounds, despite their opposite charges.

4. Conclusions

A stationary phase permitting good operation in 100% aqueous phase, such as the Discovery end-capped BIO Wide Pore RP-18 column, is useful for the accurate determination of $\log k_w$ factors, especially in the case of compounds, presenting a convex curvature at low organic modifier fractions, as found for Se-Cyst and Se-CM. The effect of *n*-decylamine depends on the ionizable centre present in the molecule, leading to an increase in retention in the case for anionic centres and a decrease for basic species. For ampholytic Se-Met and Se-Cyst the effect of *n*-decylamine in retention reflects the predominance of zwitterionic/non-zwitterionic species in accordance with our previous findings concerning the corresponding $\log D$ nature. Finally, a $\log D$ indicative value in the range of -2.09 to -2.16 in the case of Se-U can be suggested based on the relationship between $\log D$ and $\log k_w$ values obtained from some selenium species.

Acknowledgment

Financial support for this work given by the "Alexandros S. Onasis" foundation, as a scholarship for the Ph.D. thesis of Mr. F. Tsopelas, is gratefully acknowledged.

References

[1] M.R. Calomme, K. Van den Branden, D.A. Vanden Berghe, J. Appl. Bacteriol. 79 (1995) 331.
[2] P. Whanger, J. Trace Elem. Exp. Med. 13 (2001) 367.
[3] C. B'Hymer, J.A. Caruso, J. Chromatogr. A 1114 (2006) 1.
[4] F. Fernandez-Banares, E. Cabre, M. Esteve, M.D. Mingorance, A. Abad-Lacruz, M. Lachica, A. Gil, M.A. Gassull, Am. J. Gastroenterol. 97 (2002) 2103.
[5] E. Klein, I. Thompson, S. Lippman, P. Goodman, D. Albanes, P. Taylor, C. Coltman, Urol. Oncol. 21 (2003) 59.
[6] P.J. Limburg, W. Wei, D.J. Ahnen, Y. Qiao, E.T. Hawk, G. Wang, C.A. Giffen, G. Wang, M.J. Roth, N. Lu, E.L. Korn, Y. Ma, K.L. Caldwell, Z. Dong, P.R. Taylor, S.M. Dawsey, Gastroenterology 129 (2005) 863.
[7] H. Hu, C. Jiang, T. Schuster, G.X. Li, P.T. Daniel, J. Lu, Mol. Cancer Ther. 5 (2006) 1873.
[8] L.C. Clark, J.G. Combs, B.W. Turnbill, E.H. Slate, D.K. Chalker, J. Chow, K.S. Davis, R.A. Glover, G.F. Graham, E.G. Gross, A. Krongrad, J.L. Lesher, K. Park, B.B. Sanders, C.L. Smoth, J.R. Taylor, J. Am. Med. Assoc. 276 (1996) 1957.
[9] J.W. Finley, Nutr. Rev. 63 (2005) 196.
[10] B. Michalke, P. Schramel, Biol. Trace Elem. Res. 59 (1997) 45.
[11] L. Liang, S. Mo, P. Zhang, Y. Cai, S. Mai, G. Jiang, M. Wen, J. Chromatogr. A 1118 (2006) 139.
[12] J. Zheng, M. Ohata, N. Furuta, Talanta 59 (2003) 27.
[13] C. Hansch, Drug Dev. Res. 1 (1981) 267.
[14] H. Van de Waterbeemd, B. Testa, in: B. Testa (Ed.), Advances in Drug Research, vol. 16, Academic, New York, 1987, pp. 85–227.
[15] B. Testa, P. Crivori, M. Reist, P.A. Carrupt, Perspect. Drug Discov. 17 (2000) 179.
[16] R.V. Thomann, Environ. Health Perspect. 5 (1995) 53.
[17] OECD, Guideline for Testing of Chemicals 107, Partition Coefficient (*n*-octanol/water)-Flask Shaking Method, OECD, Paris, 1981.
[18] F. Tsopelas, M. Ochsenkühn-Petropoulou, A. Tsantili-Kakoulidou, K.M. Ochsenkühn, Anal. Bioanal. Chem. 381 (2005) 420.
[19] J.G. Dorsey, M.G. Khaledi, J. Chromatogr. A 656 (1993) 485.
[20] A. Tsantili-Kakoulidou, E. Filippatos, O. Todoulou, A. Papadaki-Valiraki, J. Chromatogr. A 654 (1993) 43.
[21] F. Lombardo, M.Y. Shalaeva, K.A. Tupper, F. Gao, J. Med. Chem. 44 (2001) 2490.
[22] P.A. Tate, J.G. Dorsey, J. Chromatogr. A 1042 (2004) 37.
[23] L.R. Snyder, J.W. Dolan, P.W. Carr, J. Chromatogr. A 1060 (2004) 77.
[24] K. Valko, J. Chromatogr. A 1037 (2004) 299.
[25] X. Liu, H. Tanaka, A. Yamauchi, B. Testa, H. Chuman, J. Chromatogr. A 1091 (2005) 51.
[26] C. Giaginis, S. Theocharis, A. Tsantili-Kakoulidou, Anal. Chim. Acta 573–574 (2006) 311.
[27] J. Matysiak, A. Niewiadomy, B. Senczyna, A. Zabinska, J.K. Rozyto, J. AOAC Int. 87 (2004) 579.
[28] F. Hollosy, J. Seprodi, L. Orfi, D. Eros, G. Keri, M. Idei, J. Chromatogr. B 780 (2002) 355.

[29] E.H. Kerns, L. Di, S. Petusky, T. Kleintop, D. Huryn, O. Mc Conell, G. Carter, J. Chromatogr. B 791 (2003) 381.
[30] http://www.sigmaaldrich.com.
[31] F. Tsopelas, M. Ochsenkühn-Petropoulou, I. Mergias, L. Tsakanika, Anal. Chim. Acta 539 (2005) 327.
[32] R. Badiello, D. Di Maggio, M. Quintiliani, O. Sapora, Int. J. Radiat. Biol. 20 (1971) 61.
[33] S.H. Yu, L. Shu, J. Yang, Z.H. Han, Y.T. Qian, Y.H. Zhang, J. Mater. Res. 14 (1999) 4157.
[34] A. Bechalany, A. Tsantili-Kakoulidou, N. El Tayar, B. Testa, J. Chromatogr. 541 (1991) 221.
[35] C. Horvath, W. Melander, I. Molnar, J. Chromatogr. 125 (1976) 129.
[36] J. Zheng, M. Ohata, N. Furuta, W. Kosmus, J. Chromatogr. A 874 (2000) 55–64.
[37] A. Pagliara, P.A. Carrupt, G. Caron, P. Gaillard, B. Testa, Chem. Rev. 97 (1997) 3385.
[38] H. Van de Waterbeemd, H. Karajiannis, N. El Tayar, Amino Acids 7 (1994) 129.

Available online at www.sciencedirect.com
ScienceDirect
Talanta 73 (2007) 87–94
Talanta
www.elsevier.com/locate/talanta

Development of a novel colorimetric indicator pad for detecting aldehydes

Evanly Vo [a,*], David K. Murray [b], Tricia L. Scott [c], A.J. Attar [d]

[a] Department of Health and Human Services, CDC/National Institute for Occupational Safety and Health, National Personal Protective Technology Laboratory, 626 Cochrans Mill Road, Pittsburgh, PA 15236, USA
[b] National Institute for Occupational Safety and Health, HELD, 1095 Willowdale Road, Morgantown, WV 26505, USA
[c] Department of Chemistry, West Virginia University, Morgantown, WV 26505, USA
[d] Appealing Products Inc., 3400 Swift Dr, Raleigh, NC 27606, USA

Received 3 January 2007; received in revised form 6 March 2007; accepted 6 March 2007
Available online 15 March 2007

Abstract

A colorimetric indicator was developed and a colorimetric indicator pad was fabricated for the rapid detection of aldehydes. The detection pad has two sides: an observation side on top and a barrier on the bottom. The top side contains a reagent which reacts directly with aldehydes to produce a color change, while the bottom side is coated with a double-sided plastic tape barrier to prevent the escape of chemicals. Sensitivity of the indicator pads was determined using the vapor sensitive ASTM F739 technique with the presence of the indicator. A significant indicator color change (yellow to red) occurred about 5 min before the infrared analyzer response of the ASTM method. The chemical principle and reaction characterization of the test are described. The stability and potential interferences of the indicator pad were also examined by directly spiking aldehydes and compounds with other functional groups, respectively, onto the indicator pads. The newly developed aldehyde indicator pad should find utility in detecting aldehydes in both liquid and vapor phases and in collecting aldehyde permeation through PPE for further study.
Published by Elsevier B.V.

Keywords: Health and safety; Skin chemical exposure; Development of colorimetric indicator; Aldehyde detector

1. Introduction

Glutaraldehyde is used widely in a variety of industries. In the chemical industry, glutaraldehyde is used as an intermediate agent in pesticide synthesis, to tan soft leathers, and to produce adhesives for electrical products [1]. In the healthcare industry, glutaraldehyde is used as a cold disinfectant, to process X-ray film, and to fix tissues in microscopy [1,2]. Aldehydes are strongly irritating to the nose, eyes, and skin, and can cause allergic contact dermatitis from occasional or incidental occupational exposure [1–3]. The 1995 ACGIH (American Conference of Government Industrial Hygienists) short-term exposure limit (STEL)/ceiling for glutaraldehyde is 0.2 ppm (0.82 mg/m^3), as its recommended exposure limit [4].

Personal protective equipment (PPE), such as chemical-resistant gloves and protective clothing, is routinely employed to prevent skin exposure to toxic chemicals in the workplace [5–7]. Chemical-resistant gloves are typically selected based on manufacturers' recommendations. However, many workplace variables influence glove performance, including flexing, increased temperature, mixtures of two or more chemicals, and differences among glove manufacturers [8–10]. Limited laboratory test data cannot address all these variables [8–11].

There is a pressing need for sensors or indicators that can be worn inside or beneath the PPE barrier to warn the user that a chemical breakthrough has occurred and the user needs to change the PPE. These sensors or indicators would also be valuable training tools for users and provide information to industrial hygienists on proper glove selection. However, very few technologies exist that are amenable to this application. Most methods used for the detection of aldehydes do not have the required sensitivity or are too bulky to wear underneath gloves or protective clothing. Chemically sensitive indicator pads have shown potential for this application [12–17]. Other promising technologies include fiber optic sensors and conducting polymer electrodes sewn into protective clothing [18,19]. Regardless of what detection methodology is used, a chemically sensitive layer is required and additional research in this area is needed.

* Corresponding author. Tel.: + 1 412 386 5201; fax: +1 412 386 5250.
E-mail address: Eav8@cdc.gov (E. Vo).

0039-9140/$ – see front matter. Published by Elsevier B.V.
doi:10.1016/j.talanta.2007.03.014

Several aldehyde indicator compounds have been developed, using Jones oxidation [Cr(VI)] [20], Schiff's reagent (p-rosanaline hydrochloride) [21], 2,4-dinitrophenylhydrazine reagent [20,22], and sodium sulfite (Serim™ Research Corp, Elkhart, IN and Comply™ 3 M Health Care, St. Paul, MN). These compounds provide aldehyde classification tests in the liquid rather than the vapor phase [20–22]. In addition, chromium(VI) has a history as a cancer suspect agent [23] while 2,4-dinitrophenylhydrazine needs a few minutes to develop a color characteristic in the detection system [20]. On exposure to aldehydes, Schiff's reagent changes color from dark-purple to light-blue, so it is hard to distinguish the color change of the indicator pad in the vapor phase. We report here a new development of a colorimetric indicator to detect and collect glutaraldehyde and alkaline glutaraldehyde in both liquid and vapor phases.

2. Experimental methods

2.1. Chemicals, pad materials, and other apparatuses

Unless otherwise specified, the starting glutaraldehyde, methanol, glycerol, methyl red, alkaline glutaraldehyde solutions, sodium hydroxide, and other solvents used for this study were obtained from a commercial supplier (Aldrich Chemical, Milwaukee, WI) and used as neat standard chemicals without further purification. The pad material (Whatman Benchkote Plus, Catalog No.: 2301-6150) was purchased from Fisher Scientific (Pittsburgh, PA). A Miran-IA (Miniature Infrared Analyzer) closed-loop configuration (Fig. 1), which consisted of a metal bellows pump (Model MB-41, Metal Bellows, Sharon, MA), a 2.5-cm chemical permeation cell (2.5 cm in diameter, AMK Glass Company, Vineland, NJ), and the Miran (Foxboro, Norwalk, CT), was used to evaluate the indicator pad.

2.2. Colorimetric indicator

2.2.1. Aldehyde indicator solution preparation

A magnetic stirring bar, 500 mL of water, and 420 mL of methanol were placed into a 2-L Erlenmeyer flask, and a stirrer immediately started. After stirring for 10 min, 0.35 g of methyl red {2-[4-(dimethylamino) phenylazo]benzoic acid, sodium salt, $(CH_3)_2NC_6H_4N=NC_6H_4CO_2Na$}, was added to the solution with continuous stirring for 1 h. The solution immediately adopted a yellow colored appearance. Glycerine (80 mL) was slowly added into the solution to a final volume of 1 L [a final concentration of $(CH_3)_2NC_6H_4N=NC_6H_4CO_2Na$ is 1.2 mM]. The dissolution process was allowed to proceed at room temperature with continuous stirring for an additional 1 h. Once the solution had become completely homogenous, the color of the solution changed from yellow to orange. Then, pellets of sodium hydroxide were added to the solution to a final concentration of 0.7 mM, and the solution immediately changed from orange to a yellow color. The crude solution was purified by vacuum filtration on the Hirsch funnel, and the filtrate was collected. This filtrate was used as the final indicator solution for making the indicator pads.

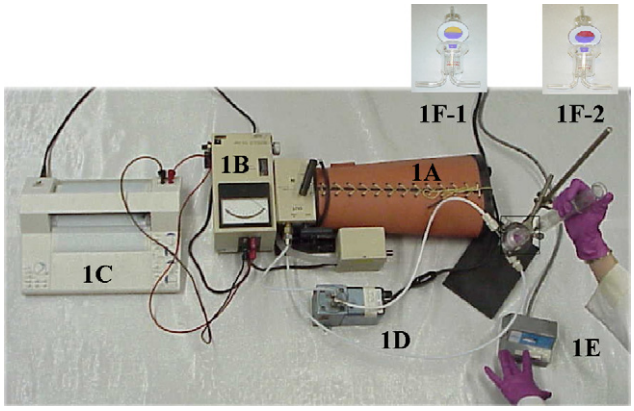

Fig. 1. A Miran (Miniature Infrared Analyzer) closed-loop configuration: Miran (A) with its IR detector (B); a chart recorder (C); metal bellows pump (D); timer (E); and a 2.5-cm chemical permeation cell (indicator sensor pad with a yellow color (F-1); on exposure to glutaraldehyde, the pad changed color to red color (F-2).

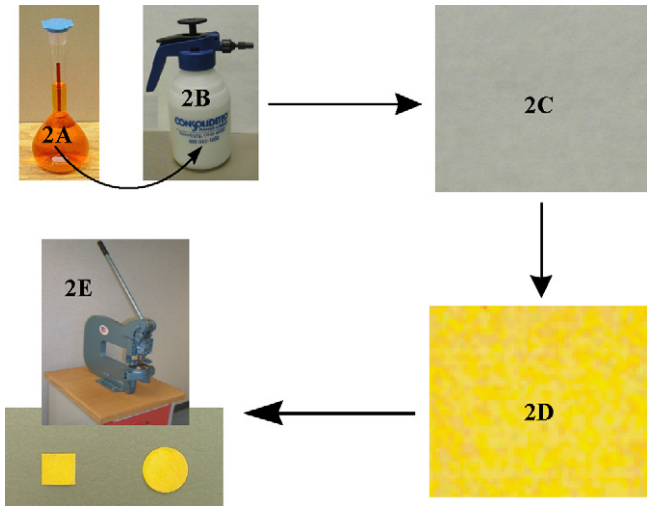

Fig. 2. Aldehyde indicator in the solid phase: aldehyde indicator (A); a hand-operated sprayer (B); the pad material sheet (C); the indicator sheet (D); a hand operated puncher (E).

2.2.2. Indicator pad fabrication

The aldehyde indicator solution (Fig. 2A) was applied at a concentration of 27 μg/cm^2 onto the absorbency side of the new pad materials (cellulose) either by using a hand-operated sprayer (Fig. 2B) or by dipping the pad-material sheet (Fig. 2C) into the indicator solution. The wet pad materials, containing an aldehyde indicator (referred to as indicator sheets), were dried under a hood at room temperature for 24 h. Then, the indicator sheets (Fig. 2D), were dried at 65 °C for 6 h using an Isotemp Oven to remove residual water and methanol from the indicator sheets. The polyethylene in the backing side of the indicator sheet was then taken off and the indicator sheets were dried at 65 °C for another 2 h before being used for pad fabrication. The backing side of the indicator sheet was then coated with a double-sided plastic tape (www.DuckProducts.com, Cat. #: DT-75-1.88 in. ×75 ft) to produce the sheets suitable for fabricating the indicator pads. These indicator sheets were cut using a hand-operated puncher (Fig. 2E) and attached to a nonsterile adhesive

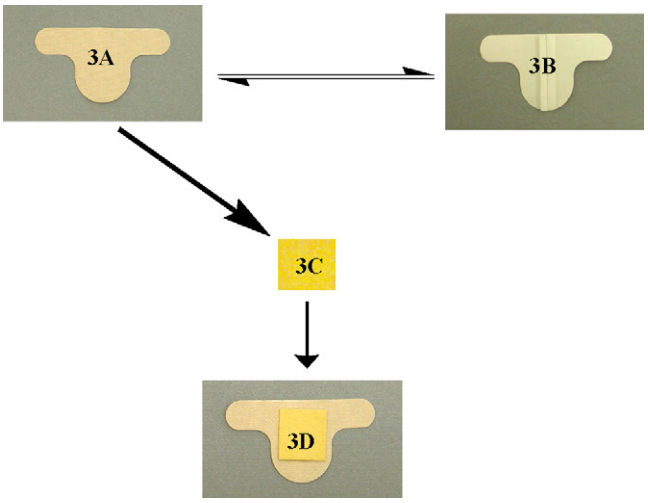

Fig. 3. Design and fabricate new aldehyde indicator pads: top side of adhesive strip (A); bottom peel-pouch side of strip (B); aldehyde indicator sensor (C); a complete aldehyde indicator pad (D).

bandage (Fig. 3, www.buymed.com, BEI00801) before being used.

2.3. The sensitivity study for aldehyde indicator pads

2.3.1. Testing the indicator with liquid aldehydes

The sensitivity of the indicator pads for aldehydes in the liquid phase was conducted by spiking chemicals directly onto the surface of the indicator pads. The amount of aldehydes required to produce a noticeable color change was determined by spiking a known standard aldehyde directly to the surface of the indicator pads using a calibrated syringe. A timer was immediately started upon the application of the spike.

2.3.2. Testing the indicator with vapor aldehydes

A sensitivity assessment of the indicator pads for aldehydes in the vapor phase was run according to the modified ASTM F739 method [24]. The Miran-IA instrumental settings were as follows: slit, 1.0 mm; wavelength, 3.7 μm; pathlength, 20.25 m; and minimum detectable concentration, 1 ppm for glutaraldehyde [25]. The 2.5-cm permeation cell is divided into a liquid phase "challenge side" which contains 50% glutaraldehyde in water, and a vapor phase "collection side" which contains the sweep gas (house air in a closed loop; flow rate, 11.328 L min^{-1}). A glove membrane (sections from the palm of the gloves) separated the two sides of the permeation cell, with the outer surface toward the challenge side of the permeation cell. A half circle of an indicator pad (Fig. 1F-1) was attached to half of the inner surface of the glove section and covered with clear plastic tape. The other half of the glove section was left unobstructed so that permeating glutaraldehyde could reach the analyzer detector. This system was operated in the closed-loop mode and the experiment was conducted at room temperature (22 ± 1 °C). 15 mL of 50% glutaraldehyde solution was injected into the challenge side of the cell using a 30-mL glass syringe, and a timer and a metal circulation pump were immediately started. Permeation of glutaraldehyde through the glove was collected and subsequently detected by either the change in color of the pads or the infrared analyzer response.

2.4. Chemical principle and characterization of the test

The chemical reaction, interaction mechanism and its relationships to color change were characterized using pH data, absorption spectroscopy, and nuclear magnetic resonance (NMR) spectroscopy.

2.4.1. The relationships between color-formation and pH

The color and the pH relationships of indicator solutions and products of glutaraldehyde solutions and indicators (referred to as reaction products) were characterized visually and using a pH meter. The color change of indicator pads was also characterized by spiking glutaraldehyde, alkaline glutaraldehyde, and non-alpha hydrogen aldehyde solutions (1.0–3.0 μL) in the pH range from 4.55 to 8.63 onto the surface of the indicator pads using a syringe.

2.4.2. Absorbance spectroscopy

The UV–vis (ultraviolet visible) spectra of the indicator and the reaction product in deionized H_2O were obtained at room temperature using an U-3010 module spectrophotometer (Model UV–Vis 3010, Hitachi, www.hii.hitachi.com).

2.4.3. NMR spectroscopy

All NMR sample concentrations were the same as stock samples as described in the "Aldehyde indicator solution preparation" section without the presence of methanol. All NMR indicator samples contained 1.2 mM indicator in 0.5 mL of 90% D_2O and 10% H_2O/glycerine. The NMR reaction product samples contained 1.2 mM indicator in the presence of glutaraldehyde (the ratio of glutaraldehyde/indicator = 1/1 to 2/1 in mole) in 0.5 mL of 90% D_2O and 10% H_2O/glycerine. The samples in D_2O were prepared by lyophilization of the water samples and resuspension in D_2O. ^1H NMR spectra were recorded at 599.672 MHz on a Varian INOVA 600 spectrometer at 298 K. Data were processed using Varian software (MSI). Water suppression was achieved through presaturation of the H_2O signal during the relaxation delay. TPPI (time proportional phase incrementation) was used for performing phase-sensitive 1D and 2D NMR experiments. All spectra were referenced to the chemical shift of the residual HDO signal at 4.85 ppm (relative to TMS). In general, 64 transients were recorded with a relaxation delay of 2–3 s and a spectral width of 8.1 kHz. 512 increments of 2 K data points were collected in each 2D COSY experiment and were zero filled so that spectra with 2 k × 2 k data points were obtained.

2.5. The interference study for aldehyde indicator pads

Volumes of 1.0–3.0 μL of chemicals containing different functional groups were spiked directly onto the surface of the indicator pads using a syringe. A timer was immediately started upon the application of the spike. Based on the indicator structure, some chemical groups were selected for testing

for chemical interference, including organic and inorganic acids (HCl, H_2SO_4, acetic acid, and acrylic acid), organic and inorganic bases (NH_4OH, NaOH, KOH, and butyl amine), alcohols (ethanol and 1-octanol), and ketones (acetone and 2-butanone).

3. Results

An aldehyde indicator was developed and a new indicator pad was fabricated for detecting aldehyde exposures (Fig. 3D). It was shown that the indicator pad was sensitive enough to detect 5 μg of glutaraldehyde (0.5 μL of 1% glutaraldehyde in water) spiked onto the pad. Glutaraldehyde caused the pads to change from yellow to red immediately (within a second). The aldehyde pad which carries thereon a predetermined reagent was designed to be responsive to contact by an aldehyde or aldehydes to produce a visible color indication; therefore, the reuse of this indicator pad is not recommended. The minimum detectable concentration of glutaraldehyde required to produce a noticeable color change was also determined and found that when ≤0.5 μg of glutaraldehyde (0.5 μL of 0.1% glutaraldehyde in water) was spiked directly to the surface of the pads, the color of the pads changed from yellow to orange-red, but it disappeared within a minute. With the ASTM F739 permeation method, a significant visible color change from yellow to red occurred on the pad about 5 min before the infrared analyzer responded. Therefore, the determination of the breakthrough time of glutaraldehyde through the gloves was highly dependent on the sensitivity of the indicator detection method with the indicator pad response being faster than the vapor phase infrared analyzer.

It was also shown that the indicator pad was sensitive to detect alkaline glutaraldehyde and non-alpha hydrogen aldehyde solutions. The aldehyde indicator formed a red or orange-red color in contact with alkaline glutaraldehyde solutions in the pH range from 4.55 to 8.06 (Table 1). However, alkaline glutaraldehyde solutions with pH > 8.06 remained yellow (Table 1). The aldehyde indicator also formed a red color in contact with formaldehyde and benzaldehyde solutions (≥8% formaldehyde solution in water and ≥5% benzaldehyde solution in cyclohexane).

Methanol was determined by a gas chromatography (GC) analysis following the solvent extraction process as described by Vo [14]. The indicator showed the absence of the methanol peak on a GC chromatogram when a new aldehyde indicator pad (1.8 cm square pad, Fig. 3C) has been extracted in 300 μL of distilled water, and volumes of 5 μL of extracted samples were injected into the GC column using a syringe. This result indicates that the methanol used to spread glycerine on the surface of the pad materials was removed from indicator pads. The indicator color was very stable in the solid phase of the pad (without glycerine, the indicator color was not stable at room temperature, as it changed from yellow to black). The thermal stability of the indicator pad was also monitored at 65 °C for 8 h (Note: these pads were tested with glutaraldehyde after storing them inside an aluminum bag at room temperature for 1 year, and changed color from yellow to red, and thus the pads are expected to have a minimum of 1 year of shelf-life).

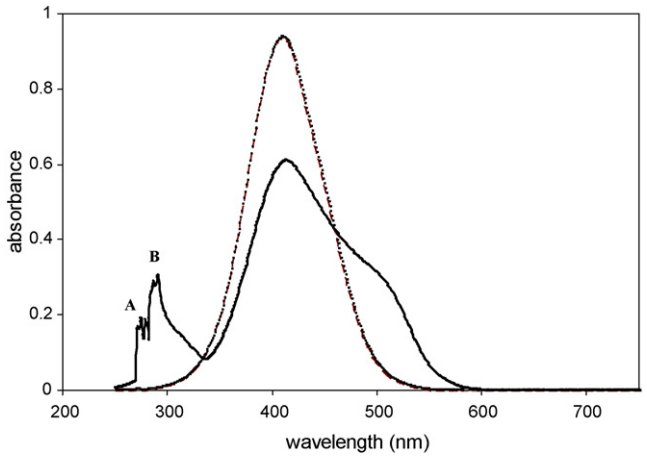

Fig. 4. Absorbance spectra of indicator (dashed line) and the reaction product between glutaraldehyde and the indicator (solid line) at room temperature.

The color and pH changes occurring with the reaction between glutaraldehyde and the indicator were characterized. The orange-red color of the reaction product formed when adding 0.15 mL of glutaraldehyde into the 500-mL indicator at pH = 7.85. With sufficient glutaraldehyde added into the indicator (≥0.2 mL of glutaraldehyde per 500 mL of the indicator solution), the reaction product changed to a red color and its pH decreased to the neutral pH.

The UV–vis spectrum of the reaction product (Fig. 4, solid line) was essentially identical to that of the indicator in the UV–vis region of 300–520 nm (Fig. 4, dashed line). The absorbance bands in the UV–vis region of 300–520 nm indicated a significant complex structure of 2-[4-dimethylamino)phenylazo]benzoate anion. Furthermore, the spectrum of the reaction product with two additional bands (a weak band in the region of 270–320 nm and a strong shoulder band in the region of 460–570 nm) was distinct from that of the indicator. A weak band (containing 2 peaks: A and B; Fig. 4) in the ultraviolet region, ranging from 270–320 nm with λ_{max} at

Table 1
The color-formation data of the reaction between glutaraldehyde solutions and indicators

Testing glutaraldehyde solutions	Amount of glutaraldehyde in solutions (spiking volumes to pad)	The pH of glutaraldehyde solutions	Positive detection (original indicator color: yellow)	Negative detection
Glutaraldehyde	2.0% glutaraldehyde in water (1 μL)	4.55	Red color was formed	
Wavicide®	2.65% glutaraldehyde in inert ingredients (1 μL)	6.20	Red color was formed	
Metricide®	2.5% glutaraldehyde in other ingredients (2 μL)	7.92	Red color was formed	
Procide-D®	2.5% glutaraldehyde in other ingredients (3 μL)	8.06	Orange-red color was formed	
Cidex®	2.4% glutaraldehyde in other ingredients (3 μL)	8.63		No color was formed

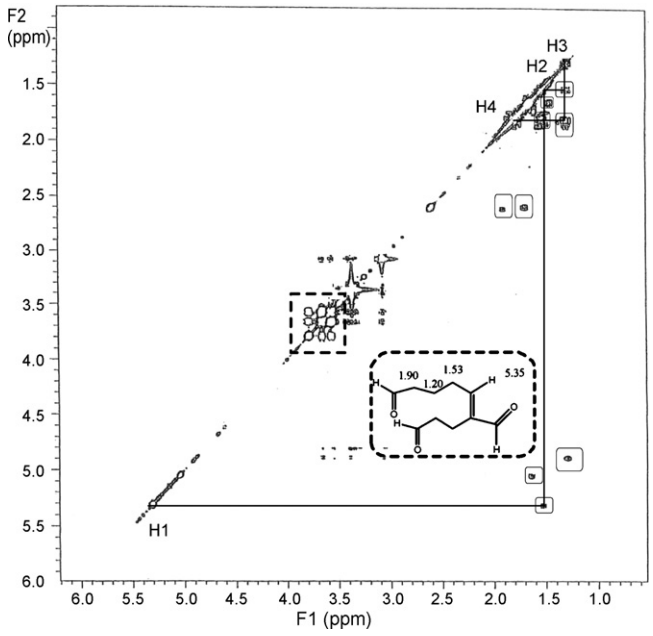

Fig. 5. Two-dimensional DQF-COSY spectra of indicator (above diagonal) and the reaction product (below diagonal) taken at 298 K. The samples of both spectra were 0.5 mL of 1.2 mM of indicator and the reaction product in 90% D_2O and 10% H_2O/glycerine. Identical cross peaks of the indicator and the reaction product spectra in the region of the 3.5–3.8 ppm are boxed (dashed line box). New cross peaks that were detectable in the reaction product spectrum in the region of 1.20–5.35 ppm are boxed (solid line box) and labeled according to sequential assignment.

275 and 290 nm, indicated non-conjugated and conjugated aldehyde groups, respectively. A strong shoulder band in the visible region, ranging from 460–570 nm, is related to the extended conjugation with a delocalized positive charge in the azo complex structure which is suggestive of the observed color change from yellow to red [26,27].

The structural features of the reaction product were assessed by NMR spectroscopy. All ^1H–^1H cross peaks in the COSY spectra of the reaction product had a counterpart at an essentially identical position in the spectra of the indicator in the region of the 3.5–3.8 ppm (Fig. 5) and 6.8–8.0 ppm. The signals in the region of the 3.5–3.8 ppm were assigned to glycerol protons while the signals in the region of the 6.8–8.0 ppm were assigned to phenyl protons of 2-[4-dimethylamino)phenylazo]benzoate anion. Several differences in the appearance of the spectra of the indicator and the reaction product, however, were apparent. The reaction product spectrum displayed some additional resonances of aldehyde functional groups in the region of 9.6–9.9 ppm and the glutaraldehyde polymer main-chain peaks in the region of the 1.20–5.35 ppm (Fig. 5). Convincing evidence for the presence of the glutaraldehyde oligomer in the reaction product was obtained from the COSY spectrum (Fig. 5). The sequential assignment for the glutaraldehyde oligomer was started by searching for alkenyl protons ($R_2C=CHR$), and found three correlation peaks with roughly equivalent intensities at 5.35, 5.05, and 4.90 ppm (Fig. 5). The sequential assignment was continued from each proton peak and a next aliphatic alkyl proton ($R_2C=CH–CH_2R$). A detailed example of the sequential assignment for the glutaraldehyde dimer segment was started from a proton at 5.35 ppm (H1 of $R_2C=CHR$, Fig. 5). This proton peak correlated to a next aliphatic proton at 1.53 ppm (H2 of $R_2C=CH–CH_2R$, Fig. 5). The aliphatic H2-proton peak correlated to a H3 proton at 1.20 ppm ($R_2C=CHCH_2CH_2R$, Fig. 5). This sequential assignment was ended at a H4-proton adjacent to a carbonyl of aldehyde group at 1.92 ppm ($R_2C=CHCH_2CH_2CH_2COH$).

The interference tests were performed for organic/inorganic acids, organic/inorganic bases, alcohols, and ketones. The results indicated that only acids interfered with the aldehyde indicator, while none of the organic/inorganic bases, alcohols, and ketones formed color when used neat or in solution.

4. Discussion

The indicator-glycerine complex in the cellulose pad material afforded a stable product that would incorporate hydrogen-bond elements between the indicator-glyceryl complex and the polysaccharide of the pad materials. The slowly exchanging NH and OHs which were believed to be possibly involved in hydrogen bonds will be further investigated in our future study using the same methods of Vo et al. [28] and Mino et al. [29]. Indicator solutions applied to pads have a very low vapor pressure and low concentration (about 27 $\mu g/cm^2$). The methyl red reagent was tested by NIOSH's Health Effects Laboratory using the Local Lymph Node Assay and phenotypic analysis and was found to be a contact sensitizer [30]. To protect against skin exposure, the reverse side of the indicator pad is covered with an impermeable double-side plastic tape.

The indicator was sensitive enough to detect 5 μg of glutaraldehyde applied to the pads. In the vapor phase, glutaraldehyde and glutaraldehyde solutions were detected by the change in the color of the indicator pad before the infrared analyzer responded.

The UV–vis spectrum of the reaction product revealed the conjugated aldehyde group and the extended conjugation with a delocalized positive charge in the azo complex structure. The extended conjugation of the azo complex structure would yield a longer wavelength of visible light and the observed color change from yellow to red.

The structural features of the indicator and the reaction product were assessed by NMR spectroscopy. The COSY spectrum of the reaction product displayed new peaks of aldehyde functional groups in the region of 9.6–9.9 ppm and the main chain of the glutaraldehyde polymer in the region of the 1.20–5.35 ppm. The sequential assignment for the glutaraldehyde polymer was convincing evidence that the oligomer was formed.

Under the basic conditions employed, glutaraldehyde would rapidly form an enolate ion which acted as a nucleophilic carbon to attack the carbonyl group of another molecule of glutaraldehyde. This self-aldol condensation resulted in the formation of glutaraldehyde oligomers (Scheme 1, Path a). When the pH of the reaction product decreased to about neutral pH, the 2-[4-dimethylamino)phenylazo]benzoate anion with two electron-donating methyl groups at the terminal amino group in the *para* position was able to delocalize the lone pair of elec-

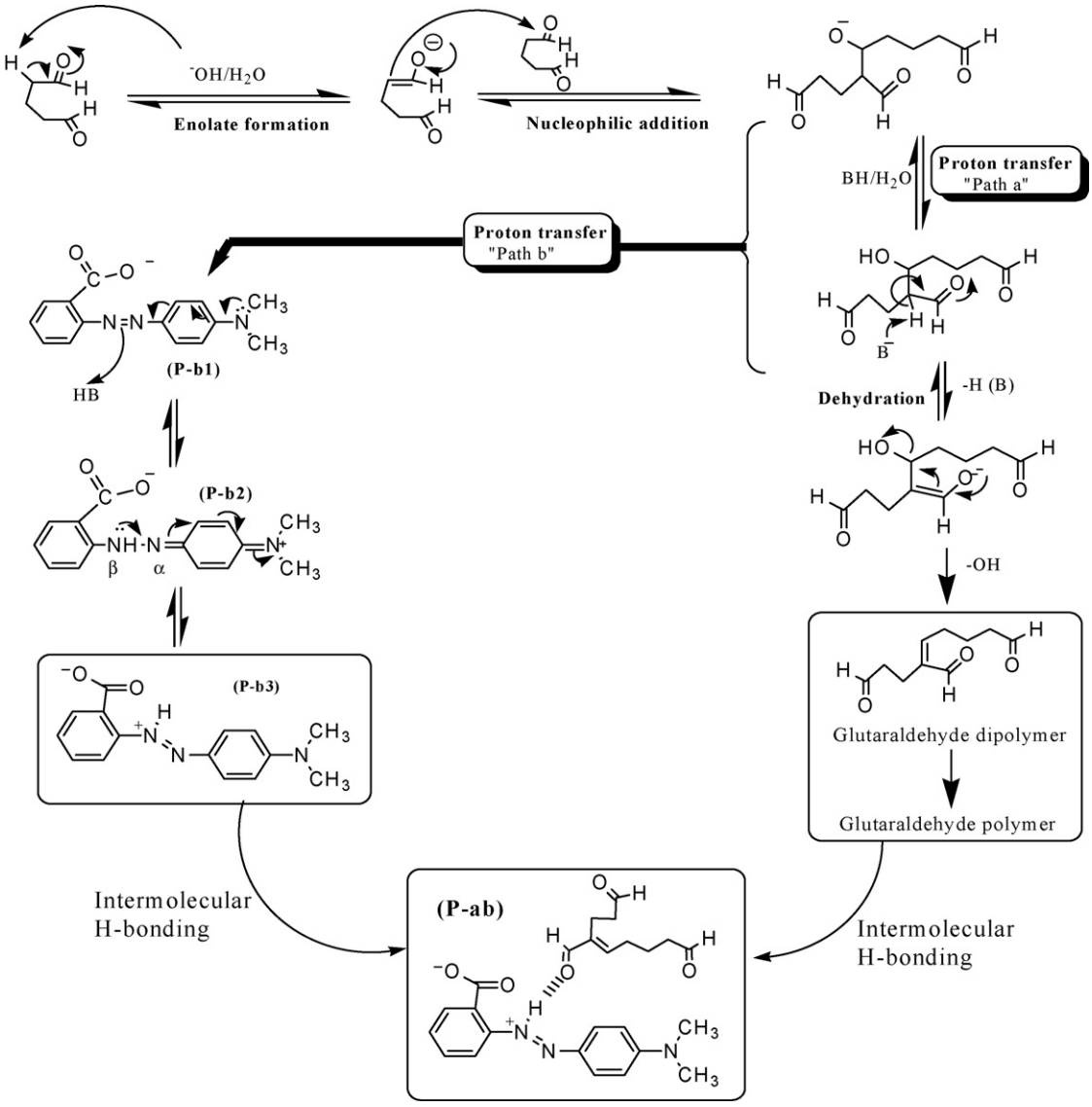

Scheme 1. Chemical reaction and mechanism between glutaraldehyde and the indicator under a base-catalyzed condition.

trons into the π-system (P-b1 in "Path b", Scheme 1). Therefore, the protonation of the 2-[4-dimethylamino)phenylazo]benzoate anion occurred to a greater extent on the β-nitrogen atom of the azo group (P-b3 in "Path b", Scheme 1) to yield the azonium tautomer with both cationic and anionic groups (P-b3 in "Path b", Scheme 1). This tautomer contained a delocalized positive charge (P-b2 ↔ P-b3) [26,31]. The azo proton in the azonium tautomer (P-b3) would form a hydrogen bond to the carbonyl group of conjugated aldehyde in the azo-complex compound (P-ab) or to the oxygen in the anionic group to form a 6-membered chelate ring [26] to increase the exceptional stability of the azo-complex compound. The azo-complex compound containing a delocalized positive charge form caused the color change in the indicator from yellow to red [26,27].

In solution studies, glutaraldehyde would undergo self-aldol condensation to yield the glutaraldehyde oligomers, and the orange-red color of the reaction product formed at pH = 7.85 suggests this is due to the color of the indicator glyceryl complex. It is probable that with the low aldehyde concentration, the pH of the indicator decreased to the range of $7.0 < pH \leq 8.06$, and the orange-red color appeared due to the significant van der Waals forces between indicator and glycerine. These forces in the aldehyde indicator are not as strong as H-bond forces, but they play an important role in the physical properties, such as boiling point, solubility, and color of the indicator-glyceryl complex compound. With sufficient glutaraldehyde added into the indicator, the reaction product changed to a red color and the pH decreased to a neutral pH. A possible explanation for the decreased pH would be the acidic nature of glutaraldehyde and a significant amount of Cannizarro reaction [32] forming a carboxylate salt and an alcohol from two glutaraldehydes. At about neutral pH, the protonation of the 2-[4-dimethylamino)phenylazo]benzoate anion occurred to a greater extent on the β-nitrogen atom of the azo group to yield the azonium tautomer with both the β-nitrogen cationic and carbonyl anionic groups. The azo proton in the azonium tautomer would form a hydrogen bond to the carbonyl

group of conjugated aldehyde in the azo-complex compound to increase the exceptional stability of the azo-complex compound. The azo-complex compound containing a delocalized positive charge form caused the color change in the indicator from yellow to red [26,27]. However, when the pH of the indicator solution decreased to pH < 7.0, the protonation of the 2-[4-dimethylamino)phenylazo]benzoate anion occurred both on the β-nitrogen atom and carbonyl anionic groups to form an acid. Even though this azonium tautomer contained both cationic groups, it would have the same color characteristic as the azonium tautomer (P-ab, Scheme 1) because the positive charge on β-nitrogen atom only contributed a delocalized positive charge in the conjugated indicator system.

Non-alpha hydrogen aldehydes, such as formaldehyde (≥8% formaldehyde solution) and benzaldehyde (≥5% benzaldehyde solution) also changed the color of the indicator pad from yellow to red, but the indicator pads were less sensitive to their detection compared with glutaraldehyde solutions (1% glutaraldehyde solution). A possible explanation for the low response for these non-alpha hydrogen aldehydes is that these aldehydes would only undergo of Cannizarro reaction forming a carboxylate salt and an alcohol from two non-alpha hydrogen aldehydes to decrease pH in the indicator pads; however, these aldehydes did not undego self-aldol condensation to yield the aldehyde oligomers which would contribute an extended conjugation in the azo-complex compound.

The indicator formed a red or orange-red color in contact with glutaraldehyde solutions in the pH range from 4.55 to 8.0. Interestingly, a 2-[4-dimethylamino)phenylazo]benzoic acid, sodium-salt, reagent in alcoholic solutions or in water is associated with a change in pH [the change in color of methyl red is associated with a change in pH in alcoholic solutions at pH 4.4 (pink-red) and at 6.2 (yellow) as described in *Aldrich Catalog*, 2003/04, p. 1287]. Therefore, the new aldehyde indicator forming a red or orange-red color in contact with glutaraldehyde solutions at 4.40 < pH < 8.06 appears to be uniquely associated with the reaction of aldehydes and the indicator to detect aldehydes outside the range of the normal use of the 2-[4-dimethylamino)phenylazo]benzoic acid, sodium salt, reagent as a pH indicator.

5. Conclusion

An indicator pad was developed for detecting aldehydes. It was shown that the new indicator pad responded to glutaraldehyde with a visible color change from yellow to red about 5 min before the infrared analyzer responded. This indicator pad can be used to determine glove permeation to glutaraldehyde and alkaline glutaraldehyde solutions. The color formation of the indicator in contact with glutaraldehyde solutions over the range 4.40 < pH < 8.06 appears to be associated with the reaction and interaction of aldehydes and the indicator. The aldehyde indicator should find utility in detecting aldehyde solutions in the pH range from 4.40 to 8.06, in which the normal pH indicator of 2-[4-dimethylamino)phenylazo]benzoic acid reagent does not respond.

Acknowledgement

This work was conducted as part of the National Occupational Research Agenda (NORA) Dermal Exposure Research Program. The authors thank Dr. Randolph P. Thummel (University of Houston, Houston, Texas), Dr. Bjorn Soderberg (WVU, Morgantown, WV), and Mr. Dennis Viscusi for their valuable assistance in the preparation of the manuscript. The authors also express their sincere appreciation to Quynh-Giao Nguyen, Jennifer Nguyen Vo, and Elaine Nguyen Vo for their valuable support.

Disclaimer: The findings and conclusions in this paper are those of the authors and do not necessarily represent the views of the National Institute for Occupational Safety and Health.

References

[1] S. Goncalo, M. Brandao, M. Pecegueiro, A. Moreno, I. Sousa, Contact Dermatitis 10 (1984) 183–184.
[2] G.J. Hathaway, N.H. Proctor, J.P. Hughes, Proctor and Hughes' Chemical Hazards of the Workplace, fourth ed., Wiley, New York, 1996, 320 pp.
[3] K.S. Hansen, Contact Dermat. 9 (1983) 81–82.
[4] G.J. Hathaway, N.H. Proctor, J.P. Hughes, Proctor and Hughes' Chemical Hazards of the Workplace, fourth ed., Wiley, New York, 1996, 321 pp.
[5] OSHA, U.S. Occupational Health and Safety Administration: Personal Protective Equipment for General Industry, Final Rule. CFR 59, No. 66, 1994, pp. 16334–16364.
[6] M. Boeniger, T. Klingner, Appl. Occup. Environ. Hyg. 17 (2002) 368–378.
[7] T. Klingner, M. Boeniger, Appl. Occup. Environ. Hyg. 17 (2002) 360–367.
[8] D. Ehntholt, I. Bodek, J.R. Valentine, in: J.L. Perkins, J.O. Stull (Eds.), Chemical Protective Clothing Performance in Chemical Emergency Response, ASTM STP 1037, American Society of Testing and Materials, Philadelphia, PA, 1989.
[9] E. Zellers, R. Sulewski, Am. Ind. Hyg. Assoc. J. 54 (1993) 465–479.
[10] J.L. Perkins, K. Vesical, Appl. Occup. Environ. Hyg. 12 (1997) 206–210.
[11] J.L. Perkins, B. Pool, Am. Ind. Hyg. Assoc. J. 58 (1997) 474–479.
[12] E. Vo, S. Berardinelli, J. Environ. Monit. 1 (1999) 545–548.
[13] E. Vo, S. Berardinelli, R. Hall, N. Ayouby, Am. Ind. Hyg. Assoc. J. 61 (2000) 837–841.
[14] E. Vo, Analyst 127 (2002) 178–182.
[15] E. Vo, J. Nicholson, P. Gao, Z. Zhuang, S. Berardinelli, Am. Ind. Hyg. Assoc. J. 64 (2003) 771–776.
[16] E. Vo, J. Occup. Environ. Hyg. 1 (2004) 799–805.
[17] T. Klingner, US Patent No. 5967881 (November 1999).
[18] M.A. El-Sherif, J. Yuan, A. MacDiarmid, J. Intell. Mater. Syst. Struct. 11 (2000) 407–414.
[19] G.E. Collins, L.J. Buckley, Synth. Met. 78 (1996) 93–101.
[20] K.L. Williamson, Microscale Organic Experiments, D.C. Heath and Company, Lexington, Masssachusetts, 1987, 513 pp.
[21] K.L. Williamson, Microscale Organic Experiments, D.C. Heath and Company, Lexington, Masssachusetts, 1987, 275 pp.
[22] S.K. Shannon, G. Barany, J. Combinatorial Chem. 6 (2004) 165–170.
[23] G.J. Hathaway, N.H. Proctor, J.P. Hughes, Proctor and Hughes' Chemical Hazards of the Workplace, fourth ed., Wiley, New York, 1996, 157 pp.
[24] S. Berardinelli, E. Moyer, Am. Ind. Assoc. J. 48 (1987) 324–329.
[25] OSHA, U.S. Occupational Health and Safety Administration: Concentration Limits for Gases, 29 CFR 1910, 1990.
[26] P.F. Gordon, P. Gregory, Organic Chemistry in Colour, Springer-Verlag, Berlin, Heidelberg, New York, London, Paris, Tokyo, 1983, pp. 112–115.
[27] L. Antonov, S. Stoyanov, Appl. Spectrosc. 47 (1993) 1030.

[28] E. Vo, H. Wang, J.P. Germanas, J. Am. Chem. Soc. 119 (1997) 1934–1940.
[29] Y. Mino, T.L. Loehr, K. Wade, H. Matsubara, S. Loehr, J. Biochem. 26 (1987) 8059.
[30] S. Azadi, B. Meade, Evaluation of the Sensitization Potential of Two Chemicals, Methyl Red and Basic Fuchsin, with Potential Use in indicator Pads; American Industrial Hygiene Conference and Exposition, May 8–13, 2004, Atlanta, GA. (www.aiha.org/abs04/ps403.htm).
[31] L. Antonov, S. Stoyanov, Anal. Chim. Acta 314 (1995) 225–232.
[32] S. Margel, A. Rembaum, Macromolecules 13 (1980) 19–24.

Available online at www.sciencedirect.com
ScienceDirect
Talanta 73 (2007) 30–36
Talanta
www.elsevier.com/locate/talanta

Second-order standard addition for deconvolution and quantification of fatty acids of fish oil using GC–MS

Maryam Vosough [a,*], Amir Salemi [b]

[a] *Chemistry and Chemical Engineering Research Center of Iran, P.O. Box 14335-186, Tehran, Iran*
[b] *Environmental Sciences Research Institute, Shahid Beheshti University, Tehran, Iran*

Received 11 December 2006; received in revised form 18 February 2007; accepted 18 February 2007
Available online 23 February 2007

Abstract

In the present work two second-order calibration methods, generalized rank annihilation method (GRAM) and multivariate curve resolution-alternating least square (MCR-ALS) have been applied on standard addition data matrices obtained by gas chromatography–mass spectrometry (GC–MS) to characterize and quantify four unsaturated fatty acids *cis*-9-hexadecenoic acid (C16:1ω7c), *cis*-9-octadecenoic acid (C18:1ω9c), *cis*-11-eicosenoic acid (C20:1ω9) and *cis*-13-docosenoic acid (C22:1ω9) in fish oil considering matrix interferences. With these methods, the area does not need to be directly measured and predictions are more accurate. Because of non-trilinear conditions of GC–MS data matrices, at first MCR-ALS and GRAM have been used on uncorrected data matrices. In comparison to MCR-ALS, biased and imprecise concentrations (%R.S.D. = 27.3) were obtained using GRAM without correcting the retention time-shift. As trilinearity is the essential requirement for implementing GRAM, the data need to be corrected. Multivariate rank alignment objectively corrects the run-to-run retention time variations between sample GC–MS data matrix and a standard addition GC–MS data matrix. Then, two second-order algorithms have been compared with each other. The above algorithms provided similar mean predictions, pure concentrations and spectral profiles. The results validated using standard mass spectra of target compounds. In addition, some of the quantification results were compared with the concentration values obtained using the selected mass chromatograms. As in the case of strong peak-overlap and the matrix effect, the classical univariate method of determination of the area of the peaks of the analytes will fail, the "second-order advantage" has solved this problem successfully.

Keywords: Second-order calibration; GRAM; MCR-ALS; Fatty acid analysis; Matrix effect

1. Introduction

The quantification of fatty acids (FAs) in different matrices is of concern because of their important roles as metabolites and intermediates in biological processes [1]. Among the different oils, fish oil because of the low amount of erucic acid (22:1), the factor responsible for cardiac lesion [2], and also as a rich source of "good fatty acids" or ω3 fatty acids, such as eicosapentaenoic acid (20:5 EPA) and docosahexaenoic acid (22:6 DHA) needs special attention.

Gas chromatography with mass spectrometric detection is commonly used for the quantification and characterization of the various kinds of saturated, mono and poly-unsaturated fatty acids (PUFAs) in foods and biological samples [3–6]. In many cases derivatization to fatty acid methyl esters (FAMEs) and liquid–liquid extraction (LLE) have been used to extract acids into an organic medium prior to GC analysis. The analysis of fatty acids in complex multicomponent matrices can result in incomplete separations and overlapped peaks. There are some commercially available polar stationary phases that provide excellent separation of FAMEs, even when these compounds are being analyzed in biological samples. However, the disadvantage of such columns is their restricted maximum operation temperature, due to low thermal stability. This leads to a limited temperature programming and also longer run times. On the other hand, non-polar stationary phases have a much greater thermal stability, wide range of operating temperature and chemical inertness, but inferior resolution [2]. With respect to these advantages, non-polar phases can be applied effectively in the analysis of fatty acids with higher molecular masses. In spite of the low resolution for such columns, the combination of different multivariate curve resolution methods in chemometrics with

* Corresponding author. Tel.: +98 21 44580720; fax: +98 21 44580762.
E-mail address: vosough@ccerci.ac.ir (M. Vosough).

0039-9140/$ – see front matter © 2007 Elsevier B.V. All rights reserved.
doi:10.1016/j.talanta.2007.02.025

hyphenated chromatographic systems can be used effectively for resolving (qualitatively and quantitatively) the complex mixtures of natural compounds.

Different multivariate curve resolution methods like evolving factor analysis (EFA) [7], heuristic evolving latent projections (HELP) [8], iterative target transformation factor analysis (ITTFA) [9] and many others have been used for the analysis of two-way hyphenated chromatographic data. In many cases the selectivity is a necessary requirement for unambiguous resolution and quantification of analytes in the complex mixtures. Three-way data analysis methods, which handle two or multiple matrices simultaneously are more robust, in addition to the fact that the relative concentration of the analytes in the standard to the sample can be obtained properly [10].

The data produced with a GC–MS system are of second-order; the data points represent intensity as a function of both retention time and *m/z* ratio. For example, Fig. 1 shows a three-dimensional representation of a set of augmented data matrices. Each data matrix has been obtained by recording mass spectra at several retention times. Complete resolution and quantification information can be attained by second-order calibration methods. There are different three-way data analysis methods to resolve analyte profiles in each order of measurements and also to predict the analyte concentration in a non-resolved peak cluster [11–14]. In GC–MS studies, the data can be separated into mass spectra, GC elution profiles and the concentration of the solutes in the sample. Second-order calibration methods exploit "second-order advantage" which implies the calibration and determination of analytes in the presence of non-calibrated and unknown interferences [15]. These methods have been successfully applied for analyzing compounds in the complex matrices using GC × GC [16–19], GC–MS [20,21], HPLC-DAD [22–26], HPLC-DAD/MS [27] and LC–MS [28].

In the present work generalized rank annihilation method (GRAM) [11] and multivariate curve resolution-alternating least squares (MCR-ALS) [13] have been used as second-order calibration methods for characterization and determination of four unresolved mono-unsaturated fatty acids *cis*-9-hexadecenoic acid (C16:1ω7c), *cis*-9-octadecenoic acid (C18:1ω9c), *cis*-11-eicosenoic acid (C20:1ω9), and *cis*-13-docosenoic acid (C22:1ω9) in fish oil and in presence of matrix effect by GC–MS. Standard addition method was used in a second-order way to make different relative concentration of analytes into unknown interferents. In case study, co-eluted positional isomers of fatty acids are considered as interferents, too. Because of retention time variation in GC–MS data sets during different runs (due to imprecision of injection timing, variation of flow rate and temperature fluctuations) which may cause non-trilinear condition, the first attempt was the analysis of data set without considering the corrections. At the next step multivariate rank alignment has been used for making trilinear data and the data analysis has been repeated for the corrected data sets. The resolved spectra and concentration profiles have been compared with each other and with the reference profiles. Finally, some of the quantification results were validated with the concentration values obtained using the selected mass chromatograms.

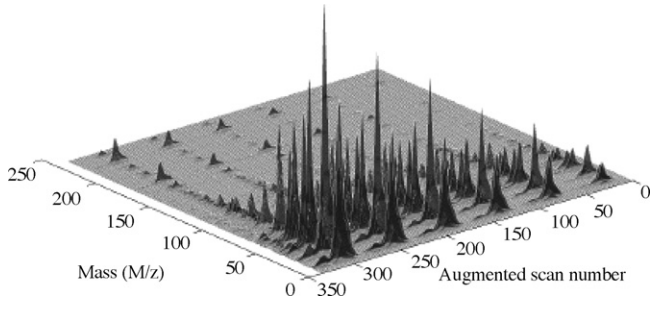

Fig. 1. A subsection of second-order standard addition data as mesh plot, resulting from GC–MS analysis of eicosenoic acid (C20:1n9) in fish oil extract.

2. Experimental

2.1. Materials and reagents

Boron trifluoride–methanol complex for synthesis, sodium hydroxide, HPLC-grade methanol and sodium chloride, used in sample preparation and *n*-hexane for extraction step, were all of analytical reagent quality and were from Merck (Darmstadt, Germany). Two methyl ester standard mixtures in which the identity and quantity of components is known, PUFA, No. 1 with marine source and grain fatty acid methyl ester were purchased from Supelco (Bellefonte, PA, USA). The real sample was commercial fish oil and obtained from a local market in Iran.

2.2. Sample preparation

The AOCS official method as a standard method was used for esterification of fatty acids (FAMEs) [30]. Briefly, the fatty acids were split off by saponification with methanolic sodium hydroxide, and then methylated with boron trifluoride-methanol reagent (containing butylated hydroxytoluene (BHT) as an antioxidant) under nitrogen atmosphere. The corresponding FAMEs were extracted with hexane by adding salt solution for complete recovery [3]. Here the standard addition method was used for deconvolution and quantification of four methyl ester fatty acids of *cis*-9-hexadecenoic acid, *cis*-9-octadecenoic acid, *cis*-11-eicosenoic acid, and *cis*-13-docosenoic acid. So, different amounts of pure FAMEs standard were added into a definite aliquot of the extracted sample. The sample and the standard addition solutions were injected to the GC column. The standard addition was done in linear range of calibration curve of each single analyte and for each analyte four standard addition solutions were obtained. The standard addition procedure was replicated so that the repeatability of the methods could be calculated. Variations of injected volumes, were corrected based on the area of one of the sample solution constitutes. So 1,4,8-dodecatriene is considered as internal standard (IS) and the ratio of areas between the analytes and this compound is used for quantification. The standard addition curves have been obtained using relative area (with respect to IS) of deconvoluted GC peaks of the mentioned methyl esters originated from unresolved signals.

2.3. GC–MS analysis

The analyses were carried out using a Hewlett-Packard 6890 series gas chromatograph interfaced to a Hewlett-Packard 5973 mass spectrometer. A HP ChemStation G1701 CA version C.00.0021 was used for data collection and conversion to ASCII format.

Separation was performed on a HP-5 capillary column (30 m × 0.25 mm i.d.) and oven temperature programming was as follow: column temperature was set at 130 °C for 1 min and then raised from 130 to 250 °C at a rate of 5 °C min^{-1} and was kept constant for 5 min. Inlet temperature was kept at 260 °C. A split mode injector with split ratio of 1/20 was applied. Helium as carrier gas was used at a constant flow rate of 1 mL min^{-1}. In the mass spectrometer, electron impact (EI^+) mass spectra were recorded (70 eV ionization energy) in full scan mode (mass range 35–300 *m/z*) with 0.2 s $scan^{-1}$. The ionization source temperature was set at 230 °C. The total chromatographic run time was 30 min; however, a subset between 300 and 1060 s was used for the analysis of the mentioned FAMEs.

2.4. Chemometric analysis

Two second-order calibration methods, GRAM and MCR-ALS, as a trilinear and a non-trilinear algorithm, respectively, were considered for the analysis. The other characteristics of two algorithms are as follows: GRAM uses only two data matrices while in MCR-ALS more than two data matrix can handle with each other, GRAM has a unique solution but MCR-ALS may produce a range of feasible solutions in case of lack of selectivity constraint [36] and finally the methods work, respectively, in a non-iterative and iterative way, so the second algorithm needs initial estimates. The results of each algorithm regardless of their differences would be the resolved pure profiles in each dimension of measurement, i.e. chromatographic profiles and their corresponding mass spectra. As calibration sample is included in the data sets, the relative concentration of components can be obtained. The algorithms will not be further described here; the details can be found in the other publications [11,13].

Before applying any of the above-mentioned algorithms, the number of chemical components in the data matrices has to be known. In addition to inspection of singular values, there are many statistical methods for determination of pseudorank of a data matrix [31]. The number of chemical components in the present work was known using fixed size moving window evolving factor analysis (FSMW/EFA), which is a local rank analysis method [29]. Because of a relatively high background signal that must be considered as an additional component, a linear background correction was performed on every data set before using any of the above methods.

For GRAM analysis as a trilinear algorithm, some corrections need to be met usually for chromatographic data sets. Actually the retention time shift and the different shape of the peaks between different chromatographic runs are the common factors that cause lack of trilinearity. As in GC analysis the peak profiles are quite reproducible, the variation of retention time shift is the only factor responsible for non-trilinearity conditions. So the time shift correction is usually enough in GC because of reproducibility of peak shape, but it does not work alone in LC data. Anyway using standard addition method has strong effect to make the different matrix composition the same and to reduce non-trilinearity.

Here, the second-order chromatographic standardization algorithm [32] was used for the rank alignment of the sample and standard data matrices. In this algorithm, sample and standard data matrices are row-wise augmented (retention time axis). Then, the sample data matrix is shifted along the GC column axis relative to standard matrix and the procedure is repeated. The percent residual variance of the augmented matrices is determined through singular value decomposition (SVD). The shift producing a minimum percent residual variance is the shift along the GC column axis for the sample matrix, which indicates the correct alignment of the two data sets. In this way the calibration matrix window should be selected in a wider range relative to the sample. The percent residual variance is based on the estimated pseudorank of the sample data. After trilinearity correction, GRAM was used properly for qualitative and quantitative analysis of target FAMEs in the sample GC–MS data matrix.

MCR-ALS was applied to resolve the column-wise augmented matrices into individual chromatographic and spectral profiles, in an iterative way. Evolving factor analysis [33] was used to make an estimate of initial chromatographic profiles. The improvement of the solutions was carried out using constraints such as non-negativity of all profiles and the unimodality of concentration profiles.

All calculations were performed using a Pentium 3 GHz with 512 MB RAM personal computer. GC–MS data files exported as Microsoft Excel format using ChemStation software. Data handling algorithms containing linear background correction and multivariate rank alignment for shift correction were coded as in house subroutines for MATLAB (version 6.0.0.88 R12, The Mathworks, Natick, MA). The GRAM routine belonged to PLS-toolbox (v.2) of Wise and Gallagher was applied on all raw and preprocessed data matrices [34]. The MCR-ALS routine belonged to the MCR toolbox of Tauler and de Juan was downloaded from their websites [35].

3. Result and discussion

Four clusters A, B, C and D as sub-matrices which included four FAME analytes were selected from each of full data matrices and were analyzed. In these clusters the numbers of two, two, four and four compounds were co-eluted together with a slopping baseline, respectively. Providing four calibration solutions in addition to the sample solution, five data matrices were obtained totally for each analyte, which repeated twice. Avoiding any erroneous result, the standard addition method was used to make the calibration solutions. The selected retention time range for the analysis of FAMEs in both sample and calibration matrices, has been shown in Table 1. Fig. 2 shows the total ion chromatograms (TICs) of the sample and the calibration solutions, which have been used for the chemometric analysis. Four sub-sections of the chromatograms used in the second-

Table 1
Different retention time regions selected for each analyte

Analyte	Cluster name	Initial time (s)		Final time (s)	
		Sample	Calibration	Sample	Calibration
C16:1n7	A	342.4	340.4	358.3	360.3
C18:1n9	B	571.1	569.8	581.0	582.2
C20:1n9	C	780.3	778.3	793.0	795.0
C22:1n9	D	975.2	972.7	996.2	998.2

The time range is selected in a wider window for calibration sets, so that the sample matrix can shift along the retention time within the calibration matrices.

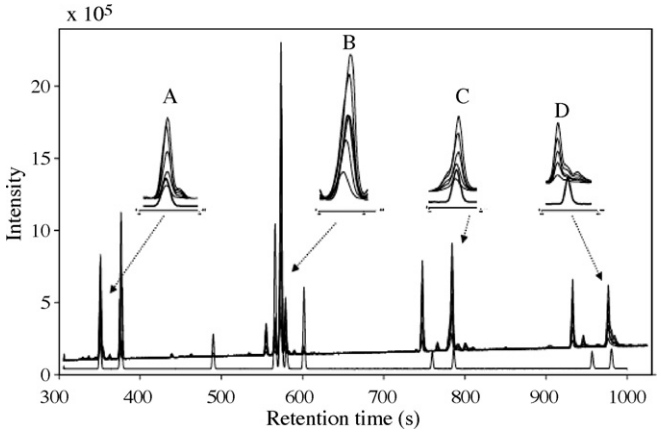

Fig. 2. TIC curves of mixture of standards, sample extract and standard addition solutions of fatty acid methyl esters in one set of measurements. The four peak clusters of interest are enlarged as A, B, C and D clusters.

order calibration have been enlarged for indicating the co-elution problems. The TIC of the standard FAMEs has been depicted, too, which clearly shows the retention time region of each eluted analyte. Deconvolution and determination of single target FAME was considered in each of four clusters using pure standards. It is worth noting that in two clusters of the TIC (B and D), two positional isomers of mono-unsaturated fatty acids eluted close together and so the commercial GC–MS softwares would fail to resolve it. This is due to the fact that the deconvolution basis of these softwares is to find at least one pure variable (unique *m*/*z*) for each component while in the case of positional isomers with similar mass spectral pattern, this mentioned requirement is rarely met.

At the first step MCR-ALS and GRAM were applied on non-trilinear data sets. Simultaneous analysis of five data matrices using MCR-ALS was performed on an augmented matrix of one test sample and four standard addition sample matrices, which was arranged by setting one matrix on top of

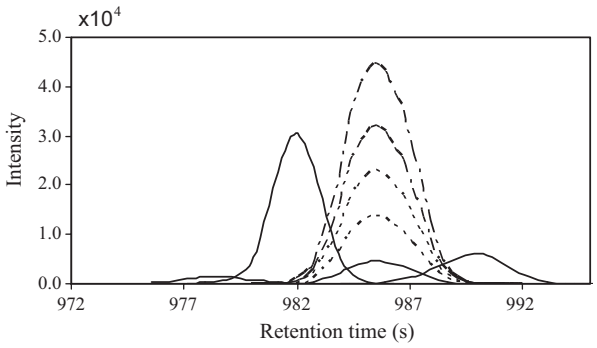

Fig. 3. Representation of standard addition of erucic acid as a target analyte in the presence of some interferences. The resolved patterns have been obtained through MCR-ALS analysis of cluster D using five augmented GC–MS data matrices.

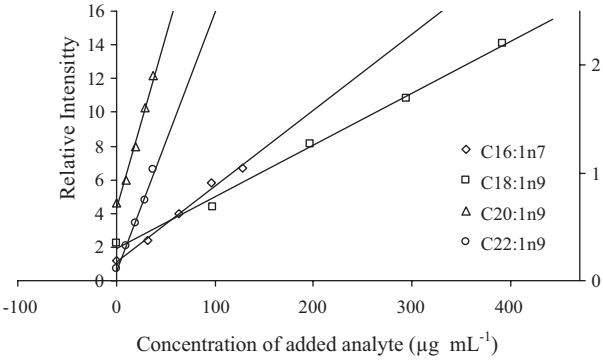

Fig. 4. Calibration graphs using the standard addition method in the determination of four FAME extracts of fish oil, replicate1. Solid lines indicate the regression line.

the other and keeping the common mass spectra in the same column. The unfolded data matrices were obtained with the dimensions of $(5 \times 40) \times 230$, $(5 \times 23) \times 230$, $(5 \times 35) \times 230$ and $(5 \times 55) \times 230$ for C16:1ω7c, C18:1ω9c, C20:1ω9 and C22:1ω9, respectively. As an example, in Fig. 3 the standard addition process has been shown for deconvolution of erucic acid (C22:1ω9). The analysis was replicated for each analyte. Using relative peak area recovered for each analyte in different standard addition levels, a calibration graph could be drawn. Fig. 4 depicts a standard addition plot for the quantification of C16:1ω7, C18:1ω9, C20:1ω9 and C22:1ω9 FAMEs in the sample (first replicate) using the corresponding standard additions. The intercept of the calibration line with the abscissa gave the concentration of the selected FAMEs in the sample. Similar graphs were obtained for the other analyzed replicate. Predicted concentrations of the analytes are shown in Table 2.

Table 2
Mean predicted concentrations in FAME extracts ($\mu g\,mL^{-1}$) and their R.S.D. using GRAM and MCR-ALS on non-trilinear data (before rank alignment)

Analyte	Retention time	GRAM						MCR-ALS		
		Std-addn1	Std-addn2	Std-addn3	Std-addn4	Grand mean	R.S.D. (%)	Mean value	R^2	R.S.D. (%)
C16:1n7	351.13	26.57	22.73	26.95	19.77	24.00	13.8	25.09	0.991	5.2
C18:1n9	577.05	52.17	53.88	59.89	54.72	55.17	10.8	61.37	0.995	3.8
C20:1n9	789.03	24.09	20.35	21.68	22.78	22.22	7.2	21.14	0.994	4.3
C22:1n9	985.51	4.07	3.65	6.55	4.55	4.70	27.3	3.78	0.995	6.5

Table 3
Mean predicted concentrations in FAME extracts ($\mu g\,mL^{-1}$) and their R.S.D. using GRAM on trilinear data (after rank alignment)

Analyte	Retention time	GRAM					
		Std-addn1	Std-addn2	Std-addn3	Std-addn4	Grand mean	R.S.D. (%)
C16:1n7	351.13	22.70	26.45	25.12	23.80	24.52	6.62
C18:1n9	577.05	61.34	55.78	60.05	63.91	60.27	5.63
C20:1n9	789.03	20.20	21.37	19.61	18.72	19.98	5.56
C22:1n9	985.51	3.43	4.33	4.27	4.00	4.01	10.18

Then, GRAM was run with only two matrices, i.e. test and calibration samples. Here, any of the mentioned standard addition samples were considered as a calibration sample, so four models were built for each analyte in each replicate. According to relative concentration of each target in two data matrices and implementing the concentration of added standard analytes, the concentration values of target FAMEs in the test solution were calculated in different replicates. Mean concentration values in different standard addition levels; have been shown in Table 2, too. When the retention time shift was not corrected, the concentration predictions of two methods were relatively different (especially for C18:1ω9) and the relative standard deviations of predicted values (%) were pretty high. This shows the dissimilarity of predicted values and the reason is the non-trilinearity of the data matrices. In other word, the most important requirement of GRAM has not been met. This is not the case for MCR-ALS, because trilinearity is not an essential requirement, so the reasonable R.S.D.s (%) have been obtained. Table 2 also shows the values of correlation coefficients (R^2) between MCR-ALS resolved elution peak area for each target FAME and their concentrations in the standard addition calibration curve. Linear relationships between resolved peak areas in a second-order way and concentrations has led to good R^2-values for all standard addition curves.

After correcting the retention time shift, the predicted concentrations through GRAM were more similar with each other and also were closer to MCR-ALS method, so R.S.D. values were improved significantly. The results have been shown in Table 3 for four analytes at different standard addition levels, as mean of two replicates. For MCR-ALS analysis, in spite of making data trilinear, the prediction results and R.S.D. (%) values were very similar. Also R^2-values were not improved significantly, so these values have not been included in Table 3, as it was preferred to compare the GRAM results obtained from trilinear data with MCR-ALS results obtained from non-trilinear data. It is worth noting that in all cases the highest R.S.D. values obtained for the smallest peak area, as it was expected. In Table 4 the mean areas of the recovered peaks in all clusters have been shown. In all cases, peak area of the analytes in different matrices followed a suite linear relationship with the relative concentration of the standards in the standard addition samples ($R^2 > 0.99$). GRAM and ALS decomposition with one to three interferences were capable to provide good estimates of the area of the four ana-

Table 4
Recovered peak areas of selected FAMEs using GRAM and MCR-ALS methods as average values

Analyte	Mean area of recovered peaks	
	MCR-ALS	GRAM
C16:1n7	8.61E+04	8.42E+04
C18:1n9	1.93E+05	1.89E+05
C20:1n9	7.61E+04	7.19E+04
C22:1n9	1.22E+04	1.29E+04

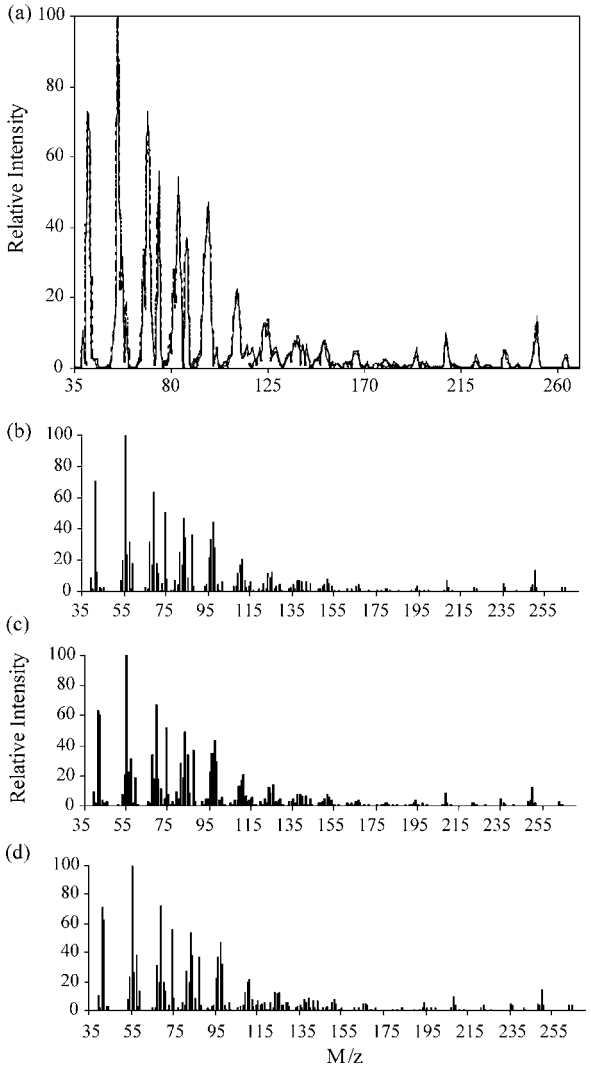

Fig. 5. Superimposed resolved spectra of eicosenoic acid (C20:1n9) in cluster C using GRAM (dot line) and MCR-ALS (dash dot) superimposed on standard mass spectrum (solid line) (a). The resolved spectra are shown, respectively, using bar graphs in (b)–(d) for better comparison.

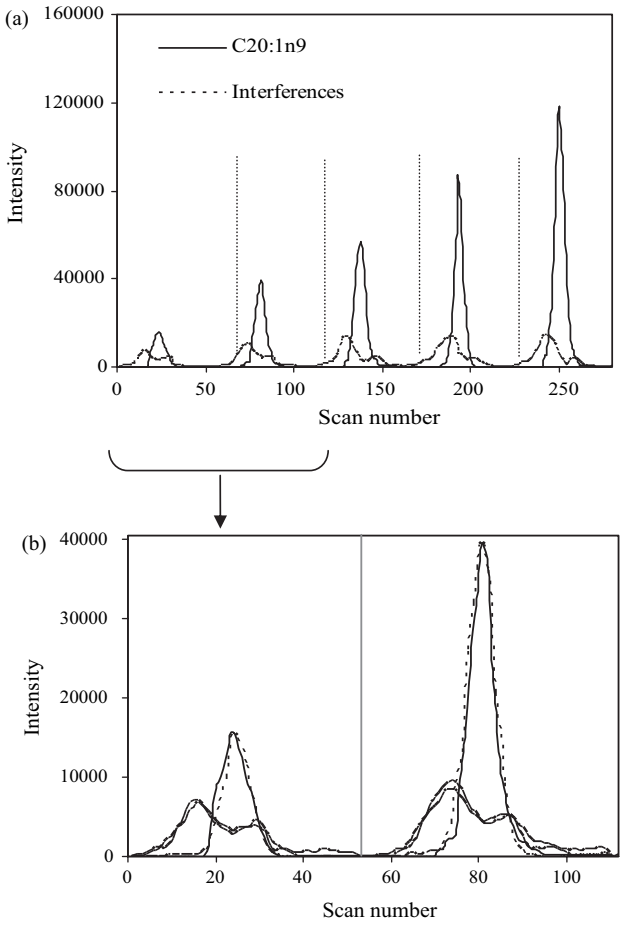

Fig. 6. (a) Resolved chromatographic profiles of eicosenoic acid (C20:1n9) as a target analyte (solid line) in augmented data matrices of cluster C using MCR-ALS. The profiles of interferences (dash line) added to each other to make one profile, which has been shown, too. (b) The superimposed results of recovered eicosenoic acid elution profile using MCR-ALS (solid line) and GRAM (dash line) on the first two data matrices as the sample and standard solution, respectively. The profiles of interferences MCR-ALS (- · -), GRAM (- ·· -) are depicted, too.

lytes and their spectral profiles despite their heavily overlapped and unknown interferents.

Among the results obtained from the mentioned algorithms, the resolved mass spectra with GRAM and MCR-ALS were considered at first to study the reliability of the results. Recovered mass spectra using two second-order algorithms were very similar together (correlation coefficients > 0.999) and also similar to the ones measured with the pure analyte standards. Fig. 5 as an example shows the mass spectra resolved for C20:1ω9 (cluster C) using GRAM, MCR-ALS and the reference mass spectrum. In Fig. 6(a) the results of MCR-ALS analysis on augmented five data matrices containing C20:1ω9 FAME has been displayed. Ascending elution profiles of the analyte evidently show the standard addition strategy for the analysis. The concentration profiles of interferences were added to each other to make a whole interfering profile. The results of GRAM and MCR-ALS analysis for the first two data matrices in Fig. 6(b) have been depicted for comparison of the two algorithms. As it is clear, the recovered concentration profiles of the corresponding analyte are pretty matched with each other. The results have been obtained after correcting the retention time shift between different runs and strongly supported each other. Similar results have been obtained for the other matrices containing recovered elution and mass spectral profiles.

It was also possible comparing the results obtained using combination of GRAM and MCR-ALS approaches and GC–MS data in TIC mode with the results obtained using selected pure mass chromatograms of the analytes. Because of having no unique mass fragment in case of positional isomers C18:1n11 and C18:1n9 and also C22:1n11 and C22:1n9, quantification using some selected mass chromatograms was only possible for C16:1n7 and C20:1n9. The concentration values of the above analytes in the extracted solutions were 26.74 and 21.53 $\mu g\,mL^{-1}$, respectively. A *t*-test was used to compare these results with the ones obtained by different methods in Table 3. For a confidence interval of 95%, it was found the similarity of the results obtained by GC–MS in the scan mode and second-order calibration approaches with the results obtained using MS strategy based on selected mass chromatograms, so the second-order results can be validated in this respect.

Considering the above results, any of two mentioned algorithms can be applied in second-order calibration, but the MCR-ALS has the advantage that no shift correction is necessary; however, GRAM is a fast and non-iterative method and no need for estimating a reasonable initial estimate.

4. Conclusion

In the present work two second-order calibration methods, GRAM and MCR-ALS were used as powerful chemometric tools for characterization and quantification of some target FAMEs in the presence of interfering components such as fatty acid positional isomers and also non-fatty acid constituents in fish oil sample. Unlike MCR-ALS, which can handle non-trilinear data sets, for GRAM as a trilinear algorithm a retention time shift correction is necessary on GC profiles. So, applying second-order chromatographic standardization, an improvement in calibration accuracy was observed with GRAM. The resolved mass spectral patterns of all targets pretty matched with each other and also with the standard mass spectra. The results illustrated the potential of extending the standard addition method on GC–MS data into three-way curve resolution algorithms as an efficient way for solving the matrix effect. Using this strategy, detection and quantification of each analyte is allowed with advantages of saving time and chemical resources.

References

[1] E. Fogelqvist, B. Josefsson, C. Roos, J. High Resolut. Chromatogr. Chromatogr. Commun. 3 (1980) 568.
[2] H.J.D. Geus, I. Aidos, J.D. Boer, J.B. Luten, U.A.Th. Brinkman, J. Chromatogr. A 910 (2001) 95.
[3] K. Eder, J. Chromatogr. B 671 (1995) 113.
[4] R.P. Evershed, J. Am. Soc. Mass Spectrom. 7 (1996) 350.
[5] R.G. Ackman, Anal. Chim. Acta 465 (2002) 175.
[6] I. Brondz, Anal. Chim. Acta 465 (2002) 1.
[7] M. Maeder, A.D. Zuberbuhler, Anal. Chim. Acta 181 (1986) 287.

[8] O.M. Kvalheim, Y.Z. Liang, Chemometr. Intell. Lab. Syst. 45 (1999) 171.
[9] B.G.M. Vandeginste, W. Derks, G. Kateman, Anal. Chim. Acta 173 (1985) 253.
[10] R. Tauler, A.A. Smilde, B.R. Kowalski, J. Chemometr. 9 (1995) 31.
[11] E. Sanchez, B.R. Kowalski, Anal. Chem. 58 (1986) 496.
[12] R. Bro, Chemometr. Intell. Lab. Syst. 38 (1997) 149.
[13] R. Tauler, Chemometr. Intell. Lab. Syst. 30 (1995) 133.
[14] N.M. Faber, R. Bro, P.K. Hopke, Chemometr. Intell. Lab. Syst. 65 (2003) 119.
[15] K.S. Booksh, B.R. Kowalski, Anal. Chem. 66 (1994) A782.
[16] B.J. Prazen, C.A. Bruckner, R.E. Synovec, B.R. Kowalski, J. Microcolumn Sep. 11 (1999) 97.
[17] C.G. Fraga, B.J. Prazen, R.E. Synovec, Anal. Chem. 72 (2000) 4154.
[18] C.G. Fraga, C.A. Bruckner, R.E. Synovec, Anal. Chem. 73 (2001) 675.
[19] L.L. Xie, P.J. Marriot, M. Adams, Anal. Chim. Acta 500 (2003) 211.
[20] C.G. Fraga, J. Chromatogr. A 1019 (2003) 31.
[21] M. Jalali-Heravi, M. Vosough, Anal. Chim. Acta 537 (2005) 89.
[22] R.A. Gimeno, E. Comas, R.M. Marcé, J. Ferré, F.X. Rius, F. Borrull, Anal. Chim. Acta 498 (2003) 47.
[23] E. Comas, R.A. Gimeno, J. Ferré, R.M. Marcé, F. Borrull, F.X. Rius, J. Chromatogr. A 988 (2003) 277.
[24] E. Comas, R.A. Gimeno, J. Ferré, R.M. Marcé, F. Borrull, F.X. Rius, J. Chromatogr. A 1035 (2004) 195.
[25] M.J. Rodríguez-Cuesta, R. Boqué, F.X. Rius, J.L.M. Vidal, A.G. Frenich, Chemometr. Intell. Lab. Syst. 77 (2005) 251.
[26] Y. Zhang, H.L. Wu, Y.J. Ding, A.L. Xia, H. Cui, R.Q. Yu, J. Chromatogr. B 840 (2006) 116.
[27] E. Peré-Trepat, R. Tauler, J. Chromatogr. A 1131 (2006) 85.
[28] J.S. Salau, M. Honing, R. Tauler, D. Barcelo, J. Chromatogr. A 795 (1998) 3.
[29] M. Jalali-Heravi, M. Vosough, J. Chromatogr. A 1024 (2004) 165.
[30] AOCS, Official Methods and Recommended Practices of the American Oil Chemists' Society, 5th ed., American Oil Chemist's Society, Champaign, IL, 1998.
[31] E.R. Malinowski, Factor Analysis in Chemistry, 3rd ed., Wiley, New York, 2002.
[32] B.J. Prazen, R.E. Synovec, B.R. Kowalski, Anal. Chem. 70 (1998) 218.
[33] A. de Juan, R. Tauler, Anal. Chim. Acta 500 (2003) 195.
[34] B.M. Wise, N.B. Callagher, PLS-toolbox Version 2.0, Eigenvector Research, Manson, WA, 1998.
[35] R. Tauler, A. de Juan, MATLAB program MCR-ALS, http://www.ub.es/gesq/mcr/mcr.htm.
[36] R. Tauler, J. Chemometr. 15 (2001) 627.

Available online at www.sciencedirect.com
ScienceDirect
Talanta 73 (2007) 147–156
Talanta
www.elsevier.com/locate/talanta

Prediction of surface tension for common compounds based on novel methods using heuristic method and support vector machine

Jie Wang [a], Hongying Du [a], Huanxiang Liu [a], Xiaojun Yao [a], Zhide Hu [a,*], Botao Fan [b]

[a] *Department of Chemistry, Lanzhou University, Lanzhou 730000, China*
[b] *Université Paris 7-Denis Diderot, ITODYS-CNRS UMR 7086, 1 rue Guy de la Brosse, 75005 Paris, France*

Received 24 November 2006; received in revised form 14 March 2007; accepted 14 March 2007
Available online 24 March 2007

Abstract

As a novel type of learning machine method a support vector machine (SVM) was first used to develop a quantitative structure–property relationship (QSPR) model for the latest surface tension data of common diversity liquid compounds. Each compound was represented by structural descriptors, which were calculated from the molecular structure by the CODESSA program. The heuristic method (HM) was used to search the descriptor space, select the descriptors responsible for surface tension, and give the best linear regression model using the selected descriptors. Using the same descriptors, the non-linear regression model was built based on the support vector machine. Comparing the results of the two methods, the non-linear regression model gave a better prediction result than the heuristic method. Some insights into the factors that were likely to govern the surface tension of the diversity compounds could be gained by interpreting the molecular descriptors, which were selected by the heuristic model. This paper proposes a new effective way of researching interface chemistry, and can be very helpful to industry.

Keywords: Surface tension; Quantitative structure–property relationship; Support vector machine; Heuristic method

1. Introduction

Surface tension (ST) is an important property in the study of physics, chemistry and applications. The surface tension is a function of molecular structure. Such data are important to scientists, engineers, and reactor engineering, flow and transport through porous media, materials selection and engineering, biomedical engineering, etc. ST has also been identified as a key property in seeking the "greener" cleaning agents [1].

Based on the importance of surface tension, it is very important to study the relationship between molecular structure and ST property. Although surface tension data can be attained from experimentation, the material of interest may be in short supply, or the experimental procedure itself may be too time consuming or expensive to be performed for more than just a few compounds. Therefore, it is of interest to find a new method to obtain the surface tension of compounds.

In previous papers some researchers have proposed theoretical methods of calculating ST based on thermodynamics [2,3]. These theoretical methods may be complex and require additional chemical properties and simplifying assumptions to complete the calculations.

Alternatively, quantitative structure–property relationship (QSPR) provides a promising method for predicting the surface tension. This method is based on the molecular descriptors which are calculated solely form the molecular structure to fit the experimental data. The advantage of this approach over other methods lies in the fact that it requires only the knowledge of chemical structure and is slightly dependent on experiment properties [4–6].

Several quantitative structure–property relationships (QSPRs) have been derived for the prediction of physical properties, such as refraction index [7,8], boiling point [9,10], surface tension [11–14], etc. Stanton and Jurs [11] used three multivariate linear regression models to predict alkane, ester, and alcohol datasets, and got promising results. Each model

* Corresponding author. Tel.: +86 931 891 2540; fax: +86 931 891 2582.
E-mail addresses: wangjie04@lzu.cn (J. Wang), hu_zhide@yahoo.com.cn (Z. Hu).

0039-9140/$ – see front matter © 2007 Elsevier B.V. All rights reserved.
doi:10.1016/j.talanta.2007.03.037

was useful to predict the surface tension of the unique variety compound. James [12] proposed a method for predicting surface tension, which works best for compounds not containing OH, COOH, or a CHO groups, Egemen et al. [13] proposed a group contribution method to predict the surface tension of liquid organic solvents. For this model, the experimental surface tension values and the predicted values by this method agreed well with $R^2 = 0.75$ and $R^2 = 0.89$, for the training set and the external test set, respectively. Kauffman and Jurs [14] used multiple linear regression and computational neural network to predict surface tension and got promising results.

In the present investigation, for the first time, SVM and HM were used to predict the surface tension of 196 various compounds using the descriptors calculated by the software CODESSA as inputs. The aim of this work was to seek the structural factor affecting their surface tension, and to build a new quantitative structure–property model to predict surface tension. The prediction results agreed with the experimental data in both the training set and test set compounds. This proved that SVM was a useful tool in predicting the surface tension.

2. Experimental section

2.1. Data set

The data set of this investigation consisted of a diverse set of 196 compounds. The initial pool of substances is taken from the latest database [15,16]. It included hydrocarbons, halogenated aliphatics, aromatics, alcohols, ethers, esters, ketones, amines, etc. with cyclic, saturated, and unsaturated structures. The surface tension values of 196 compounds ranged from 0 to 50 dyn/cm. A complete list of the compounds' name and its corresponding surface tension was shown in Table A1. The data set was randomly divided into two subsets: a training set of 157 compounds and a test set of 39 compounds. The training set was used to build HM and SVM models, and the test set was used to evaluate their prediction ability for both methods.

2.2. Molecular descriptor generation

The calculation process of the molecular descriptors was described as below: The software ISIS DRAW 2.3 was used to draw the two-dimensional structures of the researched molecules. All of the structures were transferred into HYPERCHEM 7.0 program and pre-optimized using the MM+ molecular mechanics force field. A more precise optimization was done using the semi-empirical PM3 method in MOPAC. The MOPAC and HYPERCHEM output files were transferred into the CODESSA software [17,18] to calculate five kinds of molecular descriptors: constitutional (number of various types of atoms and bonds, number of rings, molecular weight, etc.); topological (Wiener index, Randic indices, Kier–Hall shape indices, etc.); geometrical (moments of inertia, molecular volume, molecular surface area, etc.); electrostatic (minimum and maximum partial charges, polarity parameter, charged partial surface area descriptors, etc.); quantum chemical (reactivity indices, dipole moment, HOMO, LUMO energies, etc.) [19].

2.3. Selection of the descriptors on the basis of the heuristic method

Once molecular descriptors were generated, the heuristic method in CODESSA was used to select the main molecular descriptors and build a linear regression model. Using this method, all descriptors were checked to ensure (a) that values of each descriptor were available for each structure and (b) that there was a variation in these values. The descriptors which were not in agreement with the two rules would be discarded. Thereafter, the one-parameter correlation equations for each descriptor were calculated. The following criteria were applied to further reduce the number of the molecular descriptors: (1) the F-test's value for the one-parameter correlation with the descriptor was below 1.0, (2) the squared correlation coefficient of the one-parameter equation was less than $R^2_{\min}$, and (3) the parameter's t-value was less than t_1 (where $R^2_{\min}$ and t_1 were user specified values).

In the next step, HM calculated the pair-correlation regression models and further reduced the descriptors by eliminating highly correlated descriptors. All two-descriptor regression models with remaining descriptors were developed and ranked by the regression correlation coefficient, R^2. The final result listed the highest squared correlation coefficient and the 10 correlations found with the highest F-value are generated. The optimal correlation was defined that with the highest square correlation coefficient among the 10 best according to the F-value.

Then, HM did the multi-correlation regression models using the same method. The HM procedure correlations are usually 2–5 times faster than other methods with comparable quality [20]. The rapidity of calculations from the HM renders it the first method of choice in practical research. Thus, in our research, we used this method to select the main descriptors and build the linear model.

2.4. Support vector machine (SVM)

The foundation Support Vector Machine (SVM) was developed by Vapnik, and is gaining popularity due to its many attractive features and promising empirical performance [21,23]. Compared with traditional neural networks, SVM possesses prominent advantages: (1) strong theoretical background provides SVM with high generalization capability and can avoid local minima. (2) SVM always has a solution, which can be quickly obtained by a standard algorithm (quadratic programming). (3) SVM need not determine network topology in advance, which can be automatically obtained when training process ends. (4) SVM builds a result based on a sparse subset of training samples, which reduce the workload [24].

Originally, SVM was developed for pattern recognition problems. Now, with the introduction of ε-insensitive loss function, SVM has been extended to solve non-linear regression problems and time series prediction [25]. Theories of support vector classification and SRM can be found in the tutorials for SVM [22]. For this reason, we will only briefly describe the main idea of SRM here.

SVM can be applied to regression problems by the introduction of an alternative loss function. In support vector regression (SVR), the input **x** (descriptor) is first mapped into a higher dimensional feature space using kernel function. Thus, a non-linear feature mapping will allow the treatment of non-linear problems in a linear space. The prediction or approximation function used by a basic SVM is:

$$f(x) = \sum_{i=1}^{l} \alpha_i K(\mathbf{x}, \mathbf{x}_i) + b$$

where $\mathbf{x}_i$ is a feature vector corresponding to a training object, $K(\mathbf{x}, \mathbf{x}_i)$ is a kernel function and α_i is some real value. The component of vector α and the constant b represent the hypothesis and are optimized during the training. $K(\mathbf{x}, \mathbf{x}_i)$ is a kernel function, which value is equal to the inner product of two vectors **x** and $\mathbf{x}_i$ in the feature space $\Phi(\mathbf{x})$ and $\Phi(\mathbf{x}_i)$. That is $K(\mathbf{x}, \mathbf{x}_i) = \Phi(\mathbf{x}) \cdot \Phi(\mathbf{x}_i)$. The elegance of using kernel function lies in the fact that one can deal with feature spaces arbitrary dimensionality without having to compute the map $\Phi(\mathbf{x})$ explicitly, and it may be useful to think of the kernel, $K(\mathbf{x}, \mathbf{x}_i)$ as comparing patterns or as evaluating the proximity of objects in their feature space. Thus, a test point is evaluated by comparing it to all training points. Training points with non-zero weight α_i are called *support vectors*.

For a given dataset, only the kernel function and the regularity parameter C must be selected to specify one SVM. Any function that satisfies Mercer's condition can be used as the kernel function. In support vector regression, the Gaussian kernel $K(u, v) = \exp(-\gamma^* |u - v|^2)$is most commonly used.

All calculation programs implementing SVM were written in R-file based on R script for SVM. All scripts were compiled using R 1.7.1 compiler running operating system on a Pentium IV with 512MB RAM.

2.5. A Factor of error (FE)

In this dataset, the values of the 196 compounds ranged from 0 to 50 dyn/cm. It had a large range, so it is useful to find a better method to qualify the model. In our method, the factor of error (FE) was introduced. It was defined as the ratio of the calculation values to the experimental values; if the value of the ratio was less than one, the inverse value was used. So it can be described as follow:

$$\mathrm{FE} = \frac{\max(\mathrm{ST}_{\mathrm{exp}}, \mathrm{ST}_{\mathrm{pre}})}{\min(\mathrm{ST}_{\mathrm{exp}}, \mathrm{ST}_{\mathrm{pre}})}$$

where $\mathrm{ST}_{\mathrm{exp}}$ was the experimental value of the surface tension for the compound and $\mathrm{ST}_{\mathrm{pre}}$ was the predicted value of the surface tension for the compound.

If the value of FE was less than 1.25, it could be proved that the predicted value was in general agreement with the experimental value; if the value of FE was larger than 1.5, the fitting error was unacceptable. So the value of FE was used to evaluate the quantity of the predicting model [2,13].

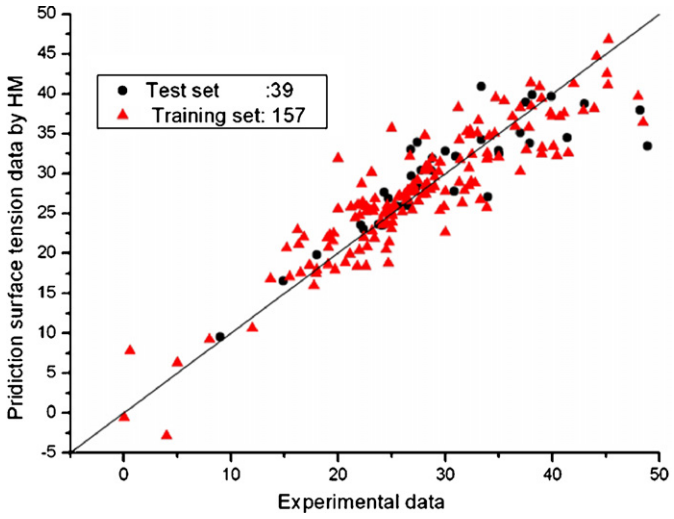

Fig. 1. Predicted vs. experimental surface tension (ST) by HM.

3. Results and discussion

3.1. The results of HM

Using the software, about 600 descriptors were calculated for all the compounds. Using the method HM, the pool of the descriptors was reduced. A variety of subset sizes were investigated to determine the optimum number of the descriptor in a model. When adding another descriptor it did not improve the statistics of the model significantly, it was proved that the optimum model was found. In order to avoid the "over-parametrization" of the model, an increase of the R^2-value of less than 0.02 was chosen as the breakpoint criterion.

Based on the selected descriptors, a linear regression model was constructed for the training set. The predicted values of the surface tension by HM method were given in Table A1. The statistical analysis results of the eight-parameter model and the involved molecular descriptors as well as the corresponding meaning were summarized in Table A2. The correlation matrix of the selected eight descriptors was shown in Table A3. It could be concluded that the correlation coefficient was less than 0.85, which meant that the descriptors were independent of each other.

The fitting error was unacceptably large with $\mathrm{FE} \geq 1.5$ for 3 compounds of the 157 (1.9% of the training set) and $1.5 > \mathrm{FE} \geq 1.25$ for 17 compounds of the 157 (10.8% of the training set). The values of the FE were all acceptable for the test set, which indicated that the model was acceptable. The overall average factors of the errors (AFE) were 1.31, 1.10, and 1.27 for the training set, test set, and all data.

In eight-parameter model, there were two constitutional descriptors, four electrostatic descriptors, and two quantum chemical descriptors. Fig. 1 showed the experimental versus the predicted surface tension using HM.

3.2. The results of SVM

In order to get more accurate prediction models, SVM was used to develop non-linear models based on the same descriptors.

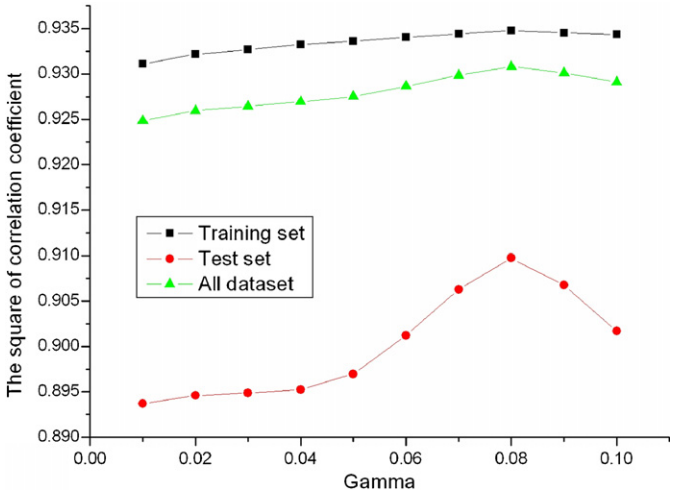

Fig. 2. Gamma vs. square correlation coefficient for the training set, test set, and all data set ($C = 100$ and $\gamma = 0.08$).

Similar to other statistical methods, the performance of SVM for regression depend on the combination of several parameters. They are capacity parameter C, ε-insensitive loss function, the kernel type K, and its corresponding parameters. C is a regularization parameter that controls the tradeoff between maximizing the margin and minimizing the training error. If C is too small, insufficient stress will be placed on fitting the training data. If C is too large, the algorithm will overfit the training data. However, Ref. [26] indicated that the prediction error was scarcely influenced by C. To make the learning process stable, a large value should be set up for C ($C = 100$).

The kernel type is another important parameter. For regression tasks, the Gaussian kernel is commonly used. The form of the Gaussian function is as follows:

$$K(x_i, x) = \exp\{-\gamma|x - x_i|\}^2$$

where γ is a constant, the parameter of the kernel; x and x_i are two independent variables; γ controls the amplitude of the Gaussian function, therefore, controls the generalization ability of SVM. So it is very important to find an optimum value for γ.

In our research, we used the grid research to find the optimum value for γ and ε. Figs. 2 and 3 show γ and ε influencing the square of the correlation coefficient for the training set, test set, and all data set. It can be clearly seen that the optimum values for γ and ε are 0.08 and 0.04, respectively.

Using the optimum value, we get a better non-linear regression model. The results of this model are shown in Table A1 and Fig. 4. The square correlation coefficient for the training set, test set, and all the data set are 0.9348, 0.9097, and 0.9308, respectively. The number of unacceptable values of FE (FE $\geq$ 1.5) for the compound is 2 (1.3%), 0 (0.0%), 2 (1.0%) for training set, test set and all data set, respectively. The exact values of ST for the two compounds 195 and 196 are 0.03 and 0.574. The relative differences between the experimental and predicted values are 0.70 and 0.706, it can be concluded that the predicted values for them are in agreement with the experimental values. The overall average factors of errors, AFE, are acceptable 1.22, 1.07, and 1.19 for the training set, test set, and all data set. If the values

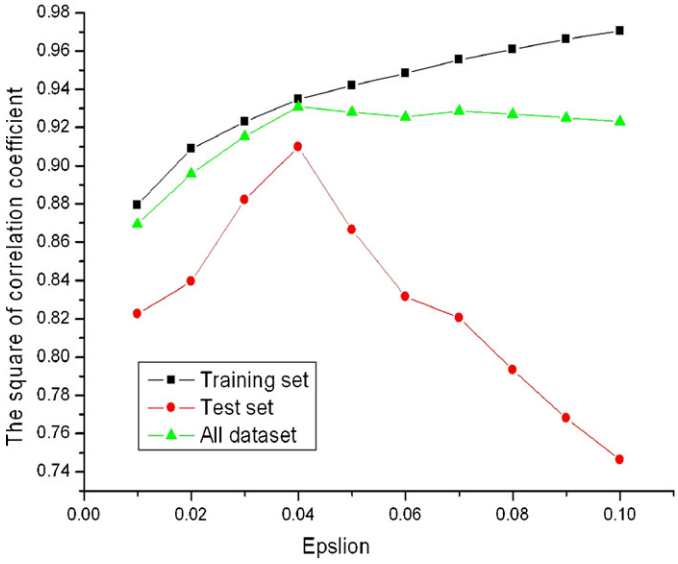

Fig. 3. Epsilon vs. square correlation coefficient for the training set, test set, and all data set ($C = 100$ and $\gamma = 0.04$).

of FE for compounds 195 and 196 are not included, AFE will be changed to 1.06, 1.07, and 1.06 for the training set, test set, and all data set. From the above discussion, the obtained SVM results indicated that the model we proposed correctly represents structural–property relationships of these compounds, and the molecular descriptors calculated solely from structures can represent the structural features for these compounds.

Comparing the correlation models and the predictive surface tension's values obtained by HM and SVM, it can be concluded seen that the performance of SVM is better than HM. However, HM can find the most important factors which influence surface tension significantly. So this investigation provides a new method to investigate and predict the surface tension. To further test the suitability of the QSPR approach constructed in our study, the variety of compounds which involved in our research is more than Refs. [11,12] and the square of correlated

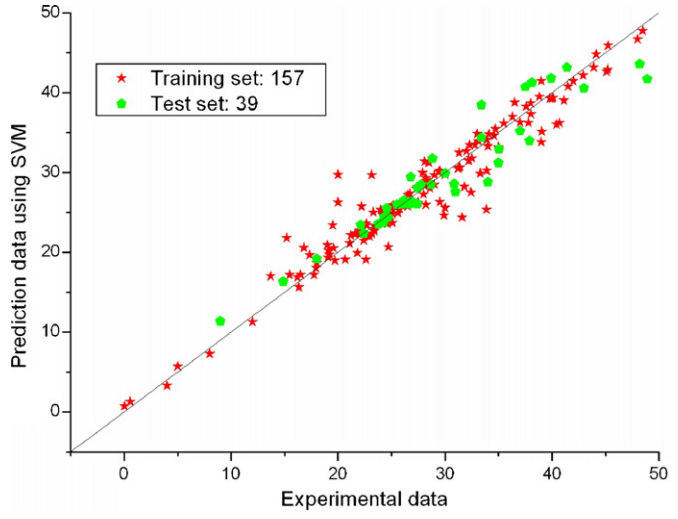

Fig. 4. Predicted vs. experimental surface tension (ST) by SVM ($C = 100$, $\gamma = 0.08$, and $\varepsilon = 0.04$).

regression is little higher than Ref. [13]. It implies that this approach is suitable and an alternative method.

3.3. Discussion of the results

Generally, surface tension of different compounds has been interpreted by macroscopical compounds feathers, such as density, acceleration due to gravity, etc. In general, the higher the density, the bigger the surface tension is. In this research, we provide another way to interpret surface tension by analyzing the microscopical structures. At the end of the research, the main factors which play important roles in surface tension are obtained.

In the two regression models, there are eight descriptors involved. By interpreting the descriptors in the model, it is possible to gain some insight into factors that influence the surface tension of the compounds.

According to the *t*-test values of the eight descriptors, it is obvious that the more relevant descriptors are five descriptors which play more important roles in deciding the values of surface tension for compounds. They are *DPSA-3 Difference in CPSAs (PPSA3-PNSA3) [Zefirov's PC]*, *HA dependent HDCA-2/TMSA [Quantum-Chemical PC]*, *Number of rings*, *Relative number of F atoms*, *FPSA-3 Fractional PPSA (PPSA-3/TMSA) [Quantum-Chemical PC]* (orderd by *t*-test value). Among the five descriptors, there are three electrostatic ones, *DPSA-3 Difference in CPSAs (PPSA3-PNSA3) [Zefirov's PC]* and *FPSA-3 Fractional PPSA (PPSA-3/TMSA) [Quantum-Chemical PC]* were belong to CPSA (charged partial surface area) descriptors. The descriptor, *DPSA-3 Difference in CPSAs (PPSA3-PNSA3) [Zefirov's PC]* [27] is the difference between PPSA3 (atom charged weighted partial positive surface area) and PNSA3 (atom charged weighted partial negative surface area), which is related to the positive and negative charge distribution and the respective surface and encodes information about polar features of the compounds and polar interactions between the molecules. The second one is fractional partial positive surface area descriptors [28]. It is defined as the ratio of the atomic charge weighted practical positive surface area (PPSA3), which was obtained by the summation of the products of the individual atomic partial charges, the atomic solvent-accessible surface areas, and the total molecular surface area (TMSA). The last electrostatic descriptor, *HA dependent HDCA-2/TMSA [Quantum-Chemical PC]*, describes the hydrogen donor charged solvent-accessible surface area, and represents the sum of solvent-accessible surface area of the H-bonding donor atoms. This descriptor describes the hydrogen bonding acceptor properties of the compounds. Formation of the hydrogen bonds could be linked with the power between the molecules strength. All of these three descriptors were encode the hybrid descriptors from discussing the meaning of the descriptors. The positive values of *t* in the linear model indicate that hydrogen bonding is favored for the strength of the compounds. The other two descriptors were all constitutional descriptors. *The number of rings* is the same as the number of aromatic rings in this investigation. The number of rings encodes the hydrophobicity of the compound, thus, an increase in this descriptor strengthens the hydrophobicity of the molecule and thus, strengthens the ST of the compound. The other constitutional descriptor, *Relative number of F atoms*, is related to the polarizability of the compounds. It will affect the number of C–F bond. The more the number is, the smaller the retention is [29]. The negative value of *t*-test in the linear model indicates that relative number of F atoms is disfavored for surface tension.

From the above discussion, it can be concluded that hydrogen bonds interactions, hydrophobicity, and polarizability (number of C–F bond) of the molecule are likely major factors controlling the surface tension of the compounds. All the descriptors involved in the model, which have explicit physical meaning, may account for the structural features responsible for the surface tension of these compounds.

3.4. Application

From our work, it can be concluded that surface tension for solvent is relevant to the property of the molecules, hydrogen bonds interactions, hydrophobicity, and polarizability (number of C–F bonds), etc. In industrial work, reactor engineering, flow and transport through porous media, materials selection and engineering, biomedical engineering, etc. these molecular properties can be very beneficial for selecting a solvent which has good surface tension. This will lead us to selecting proper solvents before experiments theoretically. This method combining HM and SVM also gives another way to research interface chemistry, and provide another efficient way to select better solvents for industrial work.

4. Conclusions

QSPR models for the prediction of surface tension of diversity of compounds using the heuristic method and support vector machine based on descriptors calculated from molecular structure alone have been developed. We have attained satisfactory results using the proposed model. It will give some insight into the factors that influence surface tension of these diverse compounds by discussing the descriptors selected by HM. Using the same set of descriptors, non-linear regression model is constructed, which better shows predictive activity than the linear regression model HM. Our investigation first used SVM to research the relationship between structural descriptors and surface tension, and obtained a promising result. This investigation provides a new and effective method to predict the surface tension for diversity of compounds. Furthermore, the proposed method can also be extended to other investigations into the property of the compounds and the interface chemistry.

Acknowledgement

The authors would like to express their gratitude to Lanzhou University foreign teacher Allan Grey who thoroughly corrected the English in the paper for us.

Appendix A

See Tables A1–A4.

Table A1
Experimental and calculated surface tension for the 196 compounds

Number	Compounds	EXP	HM	FE	SVM	FE
1[a]	Ethanolamine	48.89	33.44	1.46	41.75	1.17
2	Ethylene glycol	48.49	36.39	1.33	47.79	1.01
3[a]	Diethylene glycol	48.18	37.96	1.27	43.62	1.10
4	Diethanolamine	48.00	39.67	1.21	46.74	1.03
5	Triethanolamine	45.24	46.80	1.03	45.94	1.02
6	Triethylene glycol	45.20	41.07	1.10	42.94	1.05
7	Benzophenone	45.10	42.52	1.06	42.66	1.06
8	Tetraethylene glycol	44.13	44.67	1.01	44.83	1.02
9	Nitrobenzene	43.90	38.15	1.15	43.20	1.02
10[a]	Dimethyl sulfoxide	42.98	38.73	1.11	40.62	1.06
11	Aniline	42.90	37.87	1.13	42.20	1.02
12	Ethylene glycol monophenyl ether	42.00	41.25	1.02	41.48	1.01
13	Bromoform	41.50	32.55	1.27	40.80	1.02
14[a]	Propylene carbonate	41.39	34.50	1.20	43.18	1.04
15	Furfural	41.10	37.54	1.09	39.05	1.05
16	*N*-Methylpyrrolidone	40.70	37.13	1.10	36.24	1.12
17	γ-Butyrolactone	40.43	32.21	1.26	36.05	1.12
18	Dimethyl sulfate	40.10	33.40	1.20	39.39	1.02
19	Benzaldehyde	40.00	37.19	1.08	39.30	1.02
20[a]	Phenol	39.90	39.66	1.01	41.83	1.05
21	Acetophenone	39.80	37.54	1.06	39.30	1.01
22	Benzonitrile	39.05	33.19	1.18	35.14	1.11
23	Benzyl alcohol	39.00	39.42	1.01	41.50	1.06
24	Lactic acid, methyl ester	39.00	32.46	1.20	33.84	1.15
25	Diphenyl ether	38.82	40.87	1.05	39.52	1.02
26[a]	Propylene glycol monophenyl ether	38.10	39.87	1.05	41.29	1.08
27	Benzotrichloride	38.03	38.42	1.01	37.33	1.02
28	Furfuryl alcohol	38.00	41.36	1.09	38.70	1.02
29[a]	Di-(2-chloroethyl)ether	37.90	33.83	1.12	34.00	1.11
30	1,3-Butanediol	37.80	35.75	1.06	36.25	1.04
31	Formic acid	37.58	32.96	1.14	38.28	1.02
32[a]	Diethyl phthalate	37.50	38.95	1.04	40.76	1.09
33	*o*-Dichlorobenzene	37.00	38.27	1.03	36.30	1.02
34	Nitromethane	37.00	30.28	1.22	36.30	1.02
35[a]	Tetrahydrofurfuryl alcohol	37.00	35.11	1.05	35.20	1.05
36	1,2-Propylene glycol	36.51	35.90	1.02	38.80	1.06
37	Benzoyl chloride	36.30	37.11	1.02	37.00	1.02
38	Sulfolane	35.50	39.10	1.10	36.20	1.02
39[a]	Cyclohexanone	35.05	32.53	1.08	32.93	1.06
40[a]	Lactic acid, butyl ester	35.00	32.86	1.07	31.23	1.12
41	Methoxybenzene	35.00	32.02	1.09	33.18	1.05
42	1,4-Dichlorobenzene	34.70	39.51	1.14	35.47	1.02
43	*p*-Chlorotoluene	34.60	35.02	1.01	34.63	1.00
44	Tetrahydropyran-2-methanol	34.10	34.67	1.02	34.80	1.02
45[a]	Ethylene glycol methyl ether acetate	34.00	27.04	1.26	28.81	1.18
46	Lactic acid, ethyl ester	34.00	32.07	1.06	33.30	1.02
47	Cyclohexanol	33.91	32.55	1.04	34.13	1.01
48	1,3-Dichloropropane	33.90	31.77	1.07	30.24	1.12
49	Methyl propyl ketone	33.87	25.74	1.32	25.38	1.33
50[a]	*o*-Chlorotoluene	33.40	34.25	1.03	34.39	1.03
51[a]	Dibutyl phthalate	33.40	40.91	1.22	38.49	1.15
52	Bromochloromethane	33.30	26.67	1.25	29.90	1.11
53	Hexylene glycol	33.10	36.63	1.11	33.96	1.03
54	Chlorobenzene	33.00	35.05	1.06	34.87	1.06
55	1,4-Dioxane	32.80	28.78	1.14	33.50	1.02
56	1,1,2-Trichloroethane	32.50	32.36	1.00	31.80	1.02
57	*N*,*N*-Dimethylacetamide	32.43	28.93	1.12	27.51	1.18
58	Benzyl bromide	32.30	34.84	1.08	33.48	1.04
59	Isophorone	32.30	35.39	1.10	33.44	1.04
60	Diethyl oxalate	32.22	30.67	1.05	31.52	1.02
61	1,3-Pentanediamine	32.20	28.42	1.13	31.50	1.02
62	Carbon disulfide	32.00	35.20	1.10	32.70	1.02
63	2-Ethoxyethyl acetate	31.80	27.86	1.14	28.25	1.13

Table A1 (*Continued*)

Number	Compounds	EXP	HM	FE	SVM	FE
64	α-Terpineol	31.60	26.29	1.20	24.39	1.30
65	Diethylene glycol monoethyl ether acetate	31.40	31.73	1.01	30.70	1.02
66	Nitroethane	31.30	28.87	1.08	32.50	1.04
67	1,1,2,2-Tetrachloroethylene	31.30	34.20	1.09	30.60	1.02
68	Acetyl acetone	31.20	38.25	1.23	30.50	1.02
69[a]	Diacetone alcohol	31.00	32.14	1.04	27.56	1.12
70[a]	2-Methoxyethanol	30.84	27.75	1.11	28.55	1.08
71	Chloromethyl methyl ether	30.00	22.61	1.33	25.59	1.17
72[a]	Diethylene glycol monobutyl ether acetate	30.00	32.79	1.09	29.89	1.00
73	2-Nitropropane	30.00	27.72	1.08	29.75	1.01
74	Butyraldehyde	29.90	25.81	1.16	24.64	1.21
75	Diethylene glycol monoethyl ether	29.53	31.40	1.06	30.23	1.02
76	Diethylene glycol dimethyl ether	29.50	25.32	1.17	26.33	1.12
77	Triethylene glycol dimethyl ether	29.40	30.22	1.03	30.10	1.02
78	1,1-Dichloropropane	29.00	28.33	1.02	28.51	1.02
79	1,2-Dichloropropane	29.00	29.54	1.02	29.70	1.02
80	Dipropylene glycol monomethyl ether	28.80	31.86	1.11	31.76	1.10
81[a]	1,1,2-Trichloroethylene	28.80	31.86	1.11	31.76	1.10
82[a]	Xylene	28.70	30.42	1.06	28.50	1.01
83	Dipropylene glycol monomethyl ether acetate	28.60	28.00	1.02	28.08	1.02
84	Toluene	28.60	30.55	1.07	28.74	1.00
85	Diethylene glycol monomethyl ether	28.49	30.84	1.08	31.24	1.10
86	Ethylbenzene	28.48	30.84	1.08	31.24	1.10
87	Dimethylethanolamine	28.30	28.71	1.01	29.00	1.02
88	Benzene	28.20	30.58	1.08	28.90	1.02
89	2-Ethoxyethanol	28.20	27.41	1.03	25.97	1.09
90	Isopropylbenzene	28.20	30.83	1.09	29.31	1.04
91	Acrylic acid	28.10	34.75	1.24	31.40	1.12
92	*m*-Xylene	28.10	30.36	1.08	28.56	1.02
93	Methyl isobutenyl ketone	28.09	28.41	1.01	28.35	1.01
94	Propylene glycol monomethyl ether	28.00	27.41	1.02	27.29	1.03
95	Dichloromethane	27.89	27.34	1.02	29.97	1.07
96[a]	*p*-Xylene	27.76	30.42	1.10	28.50	1.03
97	Ethyl chloroformate	27.50	26.51	1.04	26.25	1.05
98[a]	Acetic acid	27.42	33.92	1.24	28.13	1.03
99[a]	2-Butoxyethanol	27.40	28.34	1.03	26.10	1.05
100	Ethylene glycol monobutyl ether acetate	27.40	29.13	1.06	28.21	1.03
101	Acrylonitrile	27.30	27.61	1.01	28.00	1.03
102	Diethylene glycol dibutyl ether	27.00	28.53	1.06	26.30	1.03
103	Carbon tetrachloride	26.92	25.43	1.06	26.22	1.03
104	1-Octanol	26.92	27.61	1.03	26.36	1.02
105[a]	D-Limonene	26.87	29.65	1.10	26.42	1.02
106[a]	Butyric acid	26.80	33.02	1.23	29.46	1.10
107	Acetyl chloride	26.70	32.16	1.20	27.40	1.03
108[a]	Diethylene glycol diethyl ether	26.68	25.95	1.03	26.07	1.02
109	Chloroform	26.53	27.89	1.05	27.23	1.03
110	Dimethyl sulfide	26.50	26.81	1.01	25.80	1.03
111	Tetrahydrofuran	26.40	26.58	1.01	25.96	1.02
112	2-Octanol	26.38	26.58	1.01	25.96	1.02
113	1-Heptanol	26.20	27.37	1.04	26.02	1.01
114[a]	Methyl amyl ketone	26.17	25.96	1.01	26.51	1.01
115[a]	*n*-Hexyl acetate	26.00	25.91	1.00	26.09	1.00
116	Propylene glycol monomethyl ether acetate	26.00	25.16	1.03	26.33	1.01
117	1-Hexanol	25.73	27.16	1.06	25.44	1.01
118	1-Pentanol	25.60	27.02	1.06	24.95	1.03
119[a]	Methyl *n*-butyl ketone	25.50	25.87	1.01	26.01	1.02
120	Methyl isoamyl ketone	25.33	25.84	1.02	25.69	1.01
121	*n*-Amyl acetate	25.13	25.90	1.03	25.90	1.03
122	Acetic acid, *sec*-butyl ester	25.09	23.88	1.05	23.71	1.06
123	*n*-Butyl acetate	25.09	24.73	1.01	24.82	1.01
124	*p*-Chlorobenzotrifluoride	25.00	35.66	1.43	25.70	1.03
125	Methyl amyl acetate	25.00	25.13	1.01	25.59	1.02
126	Methyl formate	25.00	23.04	1.09	25.70	1.03

Table A1 (*Continued*)

Number	Compounds	EXP	HM	FE	SVM	FE
127	Diamyl ether	24.76	21.36	1.16	24.06	1.03
128[a]	*n*-Nonane	24.70	18.72	1.32	20.68	1.19
129	1-Butanol	24.67	26.91	1.09	24.39	1.01
130	Methyl isopropyl ketone	24.61	25.10	1.02	23.61	1.04
131	Methyl ethyl ketone	24.60	25.97	1.06	24.94	1.01
132[a]	Diisobutyl ketone	24.54	25.22	1.03	25.54	1.04
133	Bromomethane	24.50	20.49	1.20	23.80	1.03
134	Ethyl butyrate	24.50	23.93	1.02	24.00	1.02
135	Butyric acid, methyl ester	24.46	23.72	1.03	24.16	1.01
136[a]	Ethylene oxide	24.30	27.63	1.14	24.41	1.00
137	*n*-Propyl acetate	24.28	24.93	1.03	24.79	1.02
138[a]	Ethyl propionate	24.27	23.58	1.03	23.72	1.02
139	Methyl acrylate	24.20	23.57	1.03	24.67	1.02
140[a]	Methyl acetate	24.10	23.50	1.03	23.79	1.01
141	Ethyl formate	24.00	23.99	1.00	25.34	1.06
142[a]	Ethyl acetate	23.75	23.60	1.01	23.54	1.01
143	1-Propanol	23.45	26.82	1.14	23.31	1.01
144	Ammonia	23.40	21.85	1.07	22.92	1.02
145	2-Butanol	23.37	25.70	1.10	22.67	1.03
146	Methyl isobutyl ketone	23.29	25.20	1.08	25.02	1.07
147	*n*-Butylamine	23.17	22.77	1.02	22.33	1.04
148	Acrolein	23.14	30.11	1.30	29.71	1.28
149	Isobutanol	22.98	25.40	1.11	22.02	1.04
150	1,1,2,2-Tetrachlorodifluoroethane	22.73	20.78	1.09	22.03	1.03
151	Acetone	22.68	25.81	1.14	23.38	1.03
152	4-Methyl-2-pentanol	22.63	25.16	1.11	23.60	1.04
153	*tert*-Amyl methyl ether	22.60	18.39	1.23	19.11	1.18
154[a]	1-Aminopropane	22.40	23.02	1.03	22.38	1.00
155	*sec*-Butylamine	22.40	21.96	1.02	21.48	1.04
156	Methanol	22.30	26.36	1.18	23.00	1.03
157	Propylene oxide	22.20	28.70	1.29	25.77	1.16
158[a]	Acetic acid, isopropyl ester	22.10	23.52	1.06	23.42	1.06
159	Isobutyraldehyde	22.00	24.72	1.12	22.79	1.04
160	Dibutyl ether	21.99	20.36	1.08	22.52	1.02
161	Ethanol (anhydrous)	21.99	25.98	1.18	22.31	1.01
162	*n*-Octane	21.80	18.35	1.19	19.93	1.09
163	Isopropyl alcohol	21.79	25.99	1.19	22.40	1.03
164	Methylcyclopentane	21.60	24.40	1.13	22.30	1.03
165	Acetaldehyde	21.20	25.80	1.22	22.15	1.04
166	Dimethoxymethane	21.10	19.86	1.06	21.13	1.00
167	Triethylamine	20.66	18.80	1.10	19.11	1.08
168	*n*-Butyl acrylate	20.00	25.51	1.28	26.26	1.31
169	Ethylene glycol diacetate	20.00	31.83	1.59	29.72	1.49
170	*n*-Heptane	19.70	17.93	1.10	19.00	1.04
171	Ethylamine	19.58	22.48	1.15	20.53	1.05
172	Chloroethane	19.50	21.53	1.10	23.40	1.20
173	Methylamine	19.19	22.28	1.16	19.73	1.03
174	Diisopropylamine	19.11	20.68	1.08	20.25	1.06
175	Methyl *tert*-butyl ether	19.07	18.55	1.03	19.39	1.02
176	*tert*-Butylamine	19.00	21.88	1.15	20.92	1.10
177[a]	Dichlorofluoromethane	18.00	19.80	1.10	19.21	1.07
178	Trichlorofluoromethane	18.00	17.94	1.00	18.70	1.04
179	*n*-Hexane	17.94	17.47	1.03	18.04	1.01
180	1,1,2-Trichlorotrifluoroethane	17.75	15.96	1.11	17.18	1.03
181	Diisopropyl ether	17.34	18.48	1.07	19.66	1.13
182	Isopropylamine	16.80	21.99	1.31	20.58	1.22
183	Diethyl ether	16.50	17.53	1.06	17.20	1.04
184	Dimethylamine	16.33	21.06	1.29	15.63	1.04
185	Carbon dioxide	16.20	22.91	1.41	16.90	1.04
186	*n*-Pentane	15.48	17.08	1.10	17.18	1.11
187	Chloromethane	15.19	20.64	1.36	21.82	1.44
188[a]	Butane	14.87	16.59	1.12	16.34	1.10
189	2-Methylbutane	13.70	16.82	1.23	17.02	1.24

Table A1 (*Continued*)

Number	Compounds	EXP	HM	FE	SVM	FE
190	1,2-Dichlorotetrafluoroethane	12.00	10.64	1.13	11.30	1.06
191[a]	Dichlorodifluoromethane	9.00	9.51	1.06	11.40	1.27
192	Chlorodifluoromethane	8.00	9.20	1.15	7.30	1.10
193	Chloropentafluoroethane	5.00	6.26	1.25	5.70	1.14
194	Tetrafluoromethane	4.00	−2.90	−1.38	3.30	1.21
195	Chlorotrifluoromethane	0.57	7.79	13.57	1.28	2.22
196	Trifluoromethane	0.03	−0.57	−19.00	0.73	24.46
	AFE			1.27		1.19

[a] Test set.

Table A2
The involved parameters and the statistical of the HM model

Descriptors	Meaning	*B*	Standard error	*t*
	(Constant)	16.22	1.57	10.33
FHFA	Final heat of formation/no. of atoms	0.11	0.10	1.03
PPSA-3/PNSA-3	DPSA-3 Difference in CPSAs (PPSA3-PNSA3) [Zefirov's PC]	0.89	0.08	10.63
NOR	Number of rings	6.89	0.75	9.17
PPSA-3/TMSA(QC)	FPSA-3 Fractional PPSA (PPSA-3/TMSA) [Quantum-Chemical PC]	85.72	14.39	5.96
HDCA-2/TMSA(QC)	HA dependent HDCA-2/TMSA [Quantum-Chemical PC]	1539.90	163.52	9.42
LUMO + 1	LUMO + 1 energy	−1.26	0.30	−4.23
RNFA	Relative number of F atoms	−34.67	4.79	−7.24
PPSA-3/TMSA(ZFC)	FPSA-3 Fractional PPSA (PPSA-3/TMSA) [Zefirov's PC]	−317.30	73.70	−4.31

$R^2 = 0.8055$; $q^2 = 0.7632$; $F = 96.79$.

Table A3
Correlation matrix of the eight descriptors used in HM model

	PPSA-3/TMSA	NOR	RNFA	PPSA-3/TMSA(QC)	HDCA-2/TMSA(QC)	LUMO + 1	PPSA-3/TMSA(ZFC)	FHFA
PPSA-3/TMSA	1.0000							
NOR	−0.2377	1.0000						
RNFA	0.3471	−0.1331	1.0000					
PPSA-3/TMSA(QC)	−0.2329	0.0323	−0.1750	1.0000				
HDCA-2/TMSA(QC)	−0.5767	0.1568	0.1252	−0.1737	1.0000			
LUMO + 1	−0.5374	0.4013	0.1125	−0.2428	0.5704	1.0000		
PPSA-3/TMSA(ZFC)	−0.7055	0.1359	0.0384	0.0236	0.5387	0.4621	1.0000	
FHFA	0.4984	−0.3213	0.7932	−0.2257	0.1075	−0.0822	−0.2145	1.0000

Table A4
Statistical results using SVM HM and SVM

Data	AFE		Error (FE > 1.5)		Acceptable (FE > 1.25)		R^2	
	HM	SVM	HM (%)	SVM (%)	HM (%)	SVM (%)	HM	SVM
Training set	1.31	1.22	1.9	1.3	10.8	3.8	0.8166	0.9348
Test set	1.10	1.07	0.0	0.0	10.3	2.6	0.7366	0.9097
All data set	1.27	1.19	1.5	1.0	10.7	3.6	0.7834	0.9308

References

[1] C. Trevizo, C. Daniel, N. Nirmalakhandan, Environ. Sci. Technol. 34 (2000) 2587.
[2] R. Defay, L. Prigogine, Surface Tension and Adsorption, John Wiley & Sons, New York, 1966.
[3] C.R. Reid, T.K. Sherwood, The Properties of Gases and Liquids, McGraw-Hill, New York, 1966.
[4] H.X. Liu, X.J. Yao, M.C. Liu, Z.D. Hu, B.T. Fan, Talanta 71 (2007) 258.
[5] Y.P. Zhou, J.H. Jiang, W.Q. Lin, L. Xu, H.L. Wu, G.L. Shen, R.Q. Yu, Talanta 71 (2007) 848.
[6] K. Yu, Y.Y. Cheng, Talanta 71 (2007) 676.
[7] W.Q. Liu, P.G. Yi, Z.L. Tang, QSAR Comb. Sci. 25 (2006) 936.
[8] A.R. Katritzky, S. Sild, M. Karelson, J. Chem. Inf. Comput. Sci. 38 (1998) 840.
[9] B. Ehresmann, M.J. de Groot, A. Alex, T. Clark, J. Chem. Inf. Comput. Sci. 44 (2004) 658.
[10] Z.Y. Ha, Z. Ring, S.J. Liu, Energy Fuels 19 (2005) 152.
[11] D.T. Stanton, P.C. Jurs, J. Chem. Inf. Comput. Sci. 32 (1992) 109.
[12] K.C. James, Solubility and Related properties, Marcel Dekker, New York, 1986.
[13] E. Egemen, N. Nirmalakhandan, C. Trevizo, Environ. Sci. Technol. 34 (2000) 2596.

[14] G.W. Kauffman, P.C. Jurs, J. Chem. Inf. Comput. Sci. 41 (2001) 408.
[15] G. Wypych, Knovel Solvents—A Properties Database, ChemTec Publishing, 2000.
[16] Online version available at: http://www.knovel.com/knovel2/Toc.jsp?BookID=635&VerticalID=0.
[17] A.R. Katritzky, V.S. Lobanov, M. Karelson, CODESSA: Training Manual, University of Florida, Gainesville, Florida, 1995.
[18] A.R. Katritzky, V.S. Lobanov, M. Karelson, CODESSA: Reference Manual, University of Florida, Gainesville, Florida, 1994.
[19] A.R. Katritzky, V.S. Lobanov, M. Karelson, Comprehensive Descriptors for Structural and Statistical Analysis, Reference Manual, Version 2.0, 1994.
[20] A.R. Katritzky, R. Petrukhin, R. Jain, M. Karelson, J. Chem. Inf. Comput. Sci. 41 (2001) 1521.
[21] C.J.C. Burges, Data Min. Knowl. Disc. 2 (1998) 121.
[22] V.N. Vapnik, Statistical Learning Theory, Wiley, New York, 1998.
[23] N. Cristianini, J. Shawe-Taylor, An Introduction to Support Vector Machines, Cambridge University Press, Cambridge, UK, 2000.
[24] S.R. Gunn, M. Brown, K.M. Bossley, Lect. Notes Comput. Sci. 1280 (1997) 313.
[25] H.X. Liu, R.J. Hu, R.S. Zhang, X.J. Yao, M.C. Liu, Z.D. Hu, B.T. Fan, J. Comput. Aid. Mol. Des. 19 (2005) 33.
[26] W.J. Wang, Z.B. Xu, W.Z. Lu, X.Y. Zhang, Neurocomputing 55 (2003) 643.
[27] A.R. Katritzky, D.B. Tatham, U. Maran, J. Chem. Inf. Comput. Sci. 41 (2001) 1162.
[28] R. Bosque, J. Sales, J. Chem. Inf. Comput. Sci. 43 (2003) 637.
[29] B.Y. Zhu, Z.G. Zhao, Interface Chemistry Foundation, Chemical Industry Press, Beijing, China, 1999, p. 78.

Available online at www.sciencedirect.com
ScienceDirect
Talanta 73 (2007) 68–75
Talanta
www.elsevier.com/locate/talanta

Artificial neural networks based on principal component analysis input selection for clinical pattern recognition analysis

Ya Xiong Zhang

School of Chemistry and Material Science, Shanxi Normal University, Linfen 041004, China

Received 14 April 2006; received in revised form 9 August 2006; accepted 26 February 2007
Available online 1 March 2007

Abstract

Two clinical data sets were applied for pattern recognition in order to discover the correlation between urinary nucleoside profiles and tumours. One data set contains 168 clinical urinary samples, of which 84 specimens are from female thyroid cancer patients (malignant tumour group), and the other samples were collected from healthy women (normal group). However, 168 clinical urinary samples comprised the second data set, too. In all the specimens, each number of the samples for both uterine cervical cancer patients (malignant tumour group) and healthy females (normal group) is 60, and the other 48 samples were collected from uterine myoma patients (benign tumour group). For the two data sets, the separation and quantitative determination of the clinical urinary nucleosides were performed by capillary electrophoresis (CE). The pattern recognition was achieved applying multiple layer perceptron artificial neural networks (MLP ANN) based on conjugate gradient descent training algorithm. Moreover, applying the proposed principal component analysis (PCA) input selection scheme to MLP ANN, the accuracy rate of the pattern recognition was improved to some extent (or without any deterioration) even by much simpler structure of MLP ANN. The study showed that MLP ANN based on PCA input selection was a promising tool for pattern recognition.

Keywords: Clinical urinary nucleosides; Tumour; Pattern recognition; MLP ANN; PCA

1. Introduction

Nucleosides in human urine are often used as biomedical markers for cancer diagnosis and therapy [1–3]. It has been discovered that the nucleosides are excreted abnormally in the urine of cancer patients [4,5]. Therefore, urinary nucleosides have been applied as biomedical markers in the clinical studies of different kinds of cancers [6–11]. In the clinical researches of urinary nucleosides, reversed phase high performance liquid chromatography (RP-HPLC) [5,6] and immunoassays [12,13] were commonly available instrumental methods. Moreover, capillary electrophoresis (CE) methods have also been applied successfully in the separation and quantitative analysis of clinical urinary nucleosides [7,8,10,11,14].

To perform the multivariate classifications in a complex metabolic system, pattern recognition methods based on chemometrics are required [15,16]. Therefore, multivariate statistical techniques such as PCA [8], partial least squares (PLS) [16], stepwise discriminant analysis (SDA) and canonical discriminant analysis (CDA) [10,11] have been reported in the corresponding pattern recognition studies. Linear discriminant analysis [17,18] and cluster analysis were also investigated [19,20]. Artificial neural network (ANN) is a branch of chemometrics to resolve the regression or classification problems. The applications of ANN in separation science and chemistry have been reported widely [21–26]. For pattern recognition analysis in clinical study, ANN was also proved to be a powerful method [8].

The paper focuses on employing MLP ANN based on PCA input selection to perform the pattern recognition of clinical urinary nucleosides as tumour markers. Although ANN based on PCA input selection has been applied for quantification in different analytical methods [27–30], as far as we are aware, the application of MLP ANN based on PCA input selection in pattern recognition for clinical CE data has not yet been reported. Hence, the proposed PCA input selection scheme in combination with MLP ANN for pattern recognition of clinical CE data was developed in this paper. For the first data set, binary values were used to represent the two groups of samples, "1"

E-mail address: zhangyx@sxnu.edu.cn.

0039-9140/$ – see front matter © 2007 Elsevier B.V. All rights reserved.
doi:10.1016/j.talanta.2007.02.030

for healthy person and "−1"for thyroid cancer patients. For the second data set, "1" and "−1" represent the normal and uterine cervical cancer samples, respectively, and the samples from uterine myoma patients were indicated by "0". According to the results of this study, when the input selection scheme based on PCA was applied to MLP ANN, some improvements were generated in the accuracy rate of pattern recognition for the two data sets even with much simpler structures of MLP ANN, or the same accuracy rate can be acquired even by simplified structures of MLP ANN. It was proved that MLP ANN based on PCA input selection was an effective method for pattern recognition in this work.

2. Theory

2.1. Artificial neural networks

Details of the theory concerning ANN has been described in several papers [31–33] and books [34,35]. Although many training algorithms of MLP ANN have been developed, a frequently used one is called conjugate gradient descent (CGD) algorithm [36,37]. In this paper, MLP ANN based on CGD algorithm was applied to perform the clinical pattern recognition analysis.

2.2. Principal component analysis

Principal component analysis (PCA) is an unsupervised statistic technique to extract information from multivariate data sets. This is achieved by identifying principal components (PC), which are the linear combinations of original variables. The maximum variability of the original multivariate data set is represented by the first principal component, and the second one explains the maximum variances of the residual data set. Then, the third one will describe the most important variability of the next residual data set, and so forth. According to the theory of least squares, the eigenvectors of all principal components are orthogonal each other in multidimension data space. Generally speaking, p principal components can account for the most variance of an m-dimensional data set, where p is the number of important principal components, and m means the number of all the principal components. Obviously, p is less than m. So PCA is generally regarded as a data reduction technique, i.e., PCA can be applied to produce a lower-dimensionality version of the original data set retaining most of the information in the data set. Statheropoulos et al. [38] and Dong and McAvoy [39] described the algorithm of PCA in detail in their papers.

The selection of input variables to ANN is necessary to avoid "over fitting" [40] in the case of many input parameters available. As a linear technique for dimensionality reduction, PCA can transform the input data set from its original form (points in m-dimensional space) to its new form (points in p-dimensional space), where p is smaller than m. Using the projected input data set in a lower dimension, smaller MLP ANN is applied in the performance of pattern recognition analysis. Since PCA is a linear technique in this work, we performed the transformation of input data set by linear ANN, which has the same number of input and output nodes. PCA produces a linear transformation, which rotates the training sample data into a new coordinate system. The system formed from the eigenvectors of the autocorrelation matrix of the training data. The autocorrelation matrix of the training data can be defined as

$$A = \sum_{p} (X_p - \bar{X})^{\mathrm{T}} (X_p - \bar{X}) \quad (1)$$

In the formula, X_p is the training sample denoted by p.

The eigenvalues for each eigenvector indicate how much variability of the data is represented by that eigenvector. The computer program for calculation in this study can sort the eigenvectors and their corresponding eigenvalues in descending order. The eigenvalues and the eigenvectors were identified using the method of householder reduction to tri-diagonal form, followed by application of QL algorithm.

2.3. PCA input selection scheme

In this paper, many input variables (the corresponding concentrations of urinary nucleosides) were adopted in different MLP ANN to perform the clinical pattern recognition. For this method, problem of data analysis may be induced. If the number of weights in neural networks is larger than that of samples for the training of ANN to some extent, "over fitting" may be caused [40]. In the case of a high number of input variables, irrelevant, redundant, and noisy variables might be included in the data set, simultaneously, meaningful variables could be hidden [41]. For large number of input variables, the probability of chance correlation also increases [42]. Moreover, high number of input variables may prevent ANN from finding optimized models [43]. Therefore, PCA input selection is necessary in order to improve the accuracy rate of pattern recognition analysis with different MLP ANN.

After the performance of PCA pre-processing procedure to the input variables, all the principal components of a training data set can be acquired. Then, the principal components were input to the corresponding MLP ANN in sequence, i.e., the largest principal component was applied as the input variable of the corresponding MLP ANN at first, and then the largest and the second largest one were employed as MLP ANN input data set. In third step, the third largest one was also included in the input data set of MLP ANN, and so forth. The processes continued until all the principal components represented nearly all the variability of the training data set were included in the input data set. For all of the MLP ANN with different number of input principal components, the architecture of the corresponding MLP ANN was experimentally determined by ANN program package based on simulated annealing [44] and conjugate gradient descent algorithm [36,37]. The structures of the corresponding MLP ANN giving the best pattern recognition results were adopted to perform the classification.

3. Experimental

3.1. Data

In this paper, the first group of clinical data was from Ref. [11], and the second one was cited from Ref. [10]. The concentrations of some nucleosides not detected by the CE method in Ref. [11] were assumed to be zero. In the first clinical data set, the concentrations of 14 kinds of urinary nucleosides were used as the descriptive variables for each clinical urinary sample. For the second data set, the same kinds of nucleosides were also applied to describe each clinical urinary sample. However, due to the incomplete resolution of N^2-methylguanosine and N^2,N^2-dimethylguanosine in the proposed CE analytical conditions of Ref. [11], the summation of the concentrations of the two kinds of nucleosides was used as one descriptive variable for each clinical urinary sample. Therefore, totally, 13 variables were applied to define the corresponding clinical urinary samples.

3.2. Calculations and data analysis

All the calculations of different MLP ANN and the performance of PCA input selections were carried out using ANN program package programmed in MATLAB computing language on a lenovo Pentium IV personal computer.

4. Results and discussion

4.1. Pattern recognition for the simulated data set

The validity of MLP ANN based on PCA input selection to be applied in pattern recognition was first investigated on simulated data set. In this work, a 168 × 14 normally distributed data matrix $\boldsymbol{A}$ and a coefficient vector $\boldsymbol{B}$ with 14 elements were generated applying a library function of MATLAB 6.5. Then, a simulated nonlinear function was constructed by the following formula:

$$f(i) = \sum_{j=1}^{j=14} B(j)A(i, j)^{7-j} \quad (2)$$

If $f(i)$ is smaller than 0.5 but larger than −0.5, the target value of $f(i)$ was regarded as 0. For $f(i)$ larger than (or equal to) 0.5, its target value was assigned as 1, and for $f(i)$ smaller than (or equal to) −0.5, the target value was then assigned as −1, i.e., each row of matrix $\boldsymbol{A}$ can be regarded as a data point in multidimensional data space or a sample belonging to a certain category. Then, all the elements in each row of matrix $\boldsymbol{A}$ were used as input variables to corresponding MLP ANN designed automatically in 1000 iteration times with unit penalty 0.01, and the target output values of MLP ANN were those of $f(i)$ calculated according to formula (2). In all the 168 samples for training and designing of MLP ANN, 28 of them selected randomly were used as verification samples. So the training process of the corresponding MLP ANN could be monitored and controlled. In addition, the ANN program package performing the calculations in this work can search for the best iterative times automatically. Therefore, "over training" of the corresponding MLP ANN can be avoided conveniently. Then, the automatic network design was performed. However, for the initial weights of MLP ANN are set randomly, different runs of MLP ANN often result in different calculated results. Therefore, the procedure of the automatic network design was performed for 10 parallel runs as the same performance parameters as above. The average correct rate of the classification for all the samples by "modeling network" in this work was 84.2% with R.S.D. (relative standard deviation) = 12.2%. In order to investigate the pattern recognition ability and the robustness of the proposed MLP ANN model, leave-one-out cross validation [45] was also carried out, i.e., only the sample to be classified was not included in the data set for the training of MLP ANN. The MLP ANN employed to perform the classification were also designed automatically in 1000 iteration times with unit penalty 0.01. The correct classification rate of leave-one-out cross validation was only 41.7% with poor selectivity and specificity. In order to improve the accuracy rate of the pattern recognition by a simpler structure of MLP ANN, PCA input selection scheme was introduced. According to the PCA scheme, eight principal components accounting for 88.1% variability of the data set were suitable for the designing of the corresponding "modeling" MLP ANN to give the best classification results (R.S.D. = 5.0). Moreover, in leave-one-out cross validation process, when 10 important principal components were applied to design the corresponding MLP ANN, the best correct classification rate can also be acquired. Furthermore, the selectivity and the specificity parameters for the corresponding simulated clinical samples under this condition were also the best among all the predicted results. The PCA input selection process for modeling network and leave-one-out cross validation is shown in Fig. 1. From the results of the pattern recognition of the simulated data set, it is shown that PCA input selection

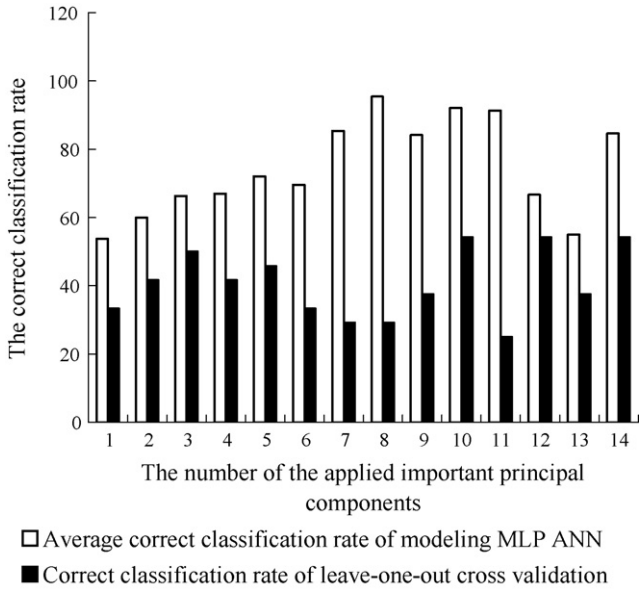

Fig. 1. The PCA input selection process in the pattern recognition for the simulated data set. (□) Average correct classification rate of modeling MLP ANN; (■) correct classification rate of leave-one-out cross validation.

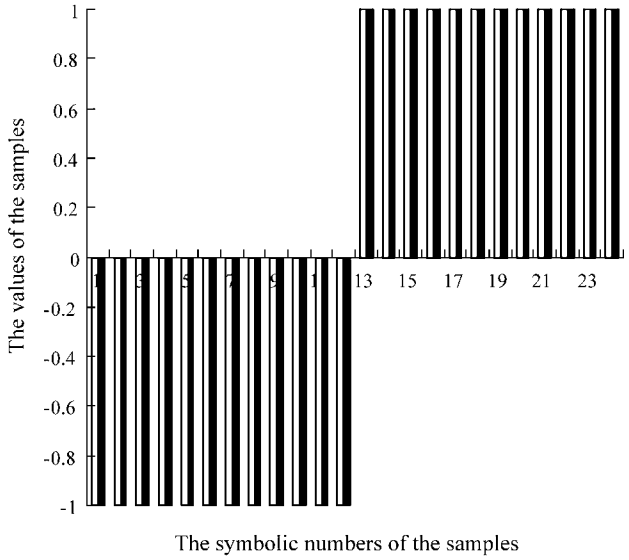

Fig. 2. The comparison between (■) the target and (□) the predicted values of MLP ANN for the corresponding samples in the first data set.

can improve the ability of MLP ANN for pattern recognition either for modeling MLP ANN or in leave-one-out cross validation process. Hence, PCA input selection may also be applied in MLP ANN to improve the results of pattern recognition for real-world data.

4.2. Pattern recognition for the first data set

In this data set, 168 urinary samples were investigated. Of all the specimens, 84 samples were from healthy women, and the others were collected from female thyroid cancer patients. The calculated values larger than or equal to 0.5 were regarded as healthy samples and those smaller than or equal to −0.5 were treated as cancer samples. If the values are smaller than 0.5 but larger than −0.5, the classifications of the corresponding samples were uncertain. The visual comparison between the target and the predicted values of some samples calculated by an automatically designed MLP ANN is given in Fig. 2. It is shown that the ANN predicted values are in good consistent with the target ones. Hence, the threshold used to classify the corresponding samples is suitable. The concentrations of the 14 kinds of nucleosides for each sample were used as the multiple input variables to the corresponding MLP ANN. Moreover, in all the 168 samples, 24 of them selected randomly were included in the verification set, and the others were training samples. After 1000 iteration times with unit penalty 0.01, a 14:1:1 MLP ANN was designed automatically. The automatically designed network could give 100% success recognition rate. Furthermore, all of the 10 parallel performances proposed 14:1:1 architecture of MLP ANN. Each of the modeling MLP ANN can perform the pattern recognition with 100% accuracy rate (R.S.D. = 0.0%). In order to investigate the pattern recognition ability and the robustness of the proposed MLP ANN model, leave-one-out cross validation was also performed. The MLP ANN employed to perform the discrimination were also designed automatically

Table 1
The classification results of the MLP ANN for the first data set

	The number of input variables	Relative standard deviation (R.S.D.) (%)	Selectivity of healthy samples (%)	Specificity of healthy samples (%)	Selectivity of cancer samples (%)	Specificity of cancer samples (%)	Correct classification rate of modeling ANN (%)	Correct classification rate in leave-one-out cross validation (%)	Percent of variance explained
One PC	1	1.8	58.3	91.7	66.7	83.3	67.5	62.5	84.1
Two PC	2	0.0	75.0	83.3	75.0	83.3	91.7	75.0	93.1
Three PC[a]	3	0.0	75.0	91.7	91.7	75.0	100.0	83.3	96.1
Four PC	4	0.0	83.3	91.7	91.7	83.3	100.0	87.5	98.2
Five PC[b]	5	0.0	100.0	100.0	100.0	100.0	100.0	100.0	98.8
Original input variables	14	0.0	100.0	100.0	100.0	100.0	100.0	100.0	

[a] The modeling MLP ANN giving the best correct classification rate (with corresponding R.S.D.).
[b] The MLP ANN giving the best selectivity and specificity in leave-one-out cross validation.

in 1000 iteration times with unit penalty 0.01. All the samples in this data set were classified correctly. Moreover, both selectivity and specificity parameters for the two kinds of samples in leave-one-out cross validation were 100%. However, in order to perform the pattern recognition using a simpler architecture of MLP ANN, PCA input selection was also introduced to the data set. According to the PCA procedure, three important principal components accounting for 96.1% of the total information in the original data set can give 100% success classification rate applying the automatically designed MLP ANN (modeling network) in 1000 iteration times with unit penalty 0.01. Further more, all the samples can be classified correctly in 10 parallel runs of the automatically designed MLP ANN by the same performance parameters as above (R.S.D. = 0.0%). It is shown that the proposed MLP ANN model was robust and appropriate for the classification in this data set. However, although applying the three important principal components in the automatically designed MLP ANN can classify the corresponding samples correctly, not all samples can be assigned to their own classifications correctly in leave-one-out cross validation scheme. Therefore, both the specificity and the selectivity parameters for the two kinds of samples were less than 100%. However, when the five important principal components were applied to design the corresponding networks, the 100% success classification rate can be acquired for both all the samples in the data set and those to be classified in the leave-one-out cross validation strategy. The R.S.D. of the classification results calculated by the 10-times-parallel-designed modeling MLP ANN is also 0.0%. Moreover, both selectivity and specificity parameters of the network for the two kinds of clinical samples were 100%. The calculated results in this section were given in Table 1. According to the study, the conclusion can be drawn that 100% success classification rate with 100% selectivity and specificity parameters can be achieved even using much simpler structure of MLP ANN models. Moreover, the classification results of the corresponding modeling MLP ANN showed their good repeatability.

4.3. Pattern recognition for the second data set

The second data set investigated in this study also included 168 samples. Among all the samples, 60 samples were from healthy women, 48 samples were collected from uterine myoma patients, and the others were uterine cervical cancer samples. If the calculated results of the corresponding MLP ANN for the samples were between −0.5 and 0.5 (larger than −0.5 but smaller than 0.5), the samples were regarded as belonging to uterine myoma patients. However, the calculated results by MLP ANN for the corresponding samples larger than or equal to 0.5 were considered to be from healthy samples, and those smaller than or equal to −0.5 were judged to be the symbol of uterine cervical cancer samples. Fig. 3 proves the validity of the threshold applied to classify the corresponding samples, i.e., some target values are also consistent with the MLP ANN predicted ones well. The study for the pattern recognition of this data set was divided into four cases.

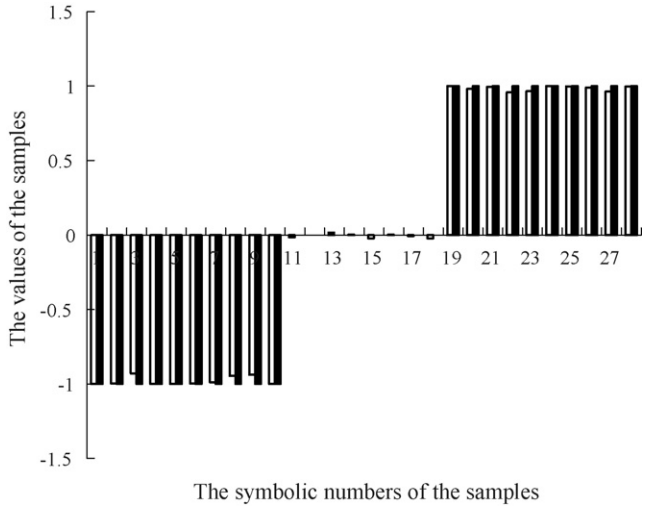

Fig. 3. The comparison between (■) the target and (□) the predicted values of MLP ANN for the corresponding samples in the second data set Case I.

4.3.1. Case I

In this case, the three kinds of clinical samples were applied to construct the training data set for the corresponding MLP ANN. The average correct rate of the classification in modeling ANN for all the samples was 100.0% with R.S.D. = 0.0%. However, the correct classification rate for all the samples was only 42.9% in leave-one-out cross validation scheme. Moreover, for all the three kinds of clinical samples, the corresponding selectivity and specificity parameters were also poor. In order to improve the accuracy rate of the pattern recognition in leave-one-out cross validation and simplify the structure of the modeling MLP ANN without any deterioration in classification results, PCA input selection for this data set was also investigated. After the PCA input selection, it was shown that when seven important principal components were applied to design the MLP ANN, the average correct rate of the pattern recognition by the corresponding modeling ANN designed in 10 parallel runs was also 100.0% (R.S.D. = 0.0). The input selection process for the modeling network in this section is given in Fig. 4. Obviously, after using the PCA input selection scheme, the pattern recognition results were also the best even with much simpler architecture of MLP ANN. The leave-one-out cross validation was also investigated. When six important principal components were applied to construct the corresponding MLP ANN, the correct classification rate for all the samples was 67.9%, which is the best result in this section. At the same time, both the selectivity and the specificity for the classification in leave-one-out cross validation were also improved to some extent. The input selection process was also given in Fig. 4. Comparing the leave-one-out cross validation classification results from MLP ANN of original input variables, it is shown that the PCA input selection scheme can improve the classification results even a much simpler structure of MLP ANN was applied.

4.3.2. Case II

From the calculated results in Case I, it can be seen that the discrimination ability of the proposed MLP ANN model was

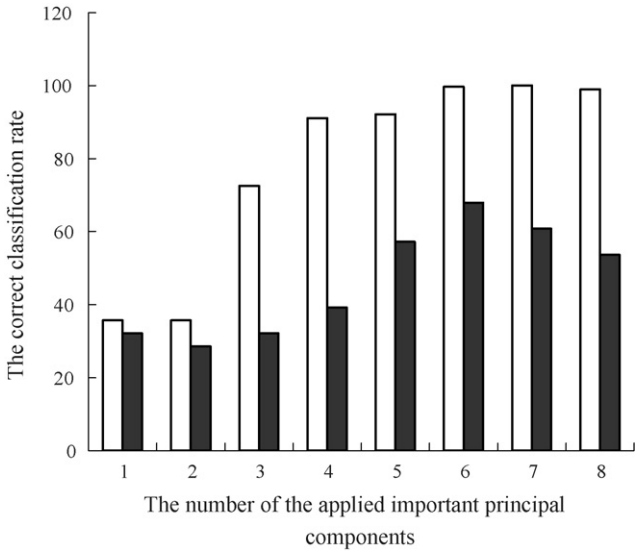

Fig. 4. The PCA input selection process in the pattern recognition for the second data set Case I. (□) Average correct classification rate of modeling MLP ANN; (■) correct classification rate of leave-one-out cross validation.

poor in the case of leave-one-out cross validation scheme. In order to improve the success classification rate, only two kinds of samples were included in the data set, i.e., the samples from the healthy women and the uterine cervical cancer patients. If the original input variables were employed directly to construct the corresponding MLP ANN, all the samples can be classified correctly in 10 parallel runs of the automatically designed networks (R.S.D. = 0.0%). However, for leave-one-out cross validation scheme, the success classification rate was only 70.0%. The corresponding calculated results in this part are shown in Table 2.

4.3.3. Case III

The data set including the samples from the healthy women and the uterine myoma patients was also studied. When the 13 original input variables were adopted to design the corresponding MLP ANN, all the samples can be classified correctly in 10 parallel-designed "modeling" neural networks (R.S.D. = 0.0%). However, not all samples can be classified correctly in the leave-one-out cross validation scheme (the correct classification rate is 94.4%). The calculated results in this section are given in Table 3.

4.3.4. Case IV

The pattern recognition for the clinical data from the uterine myoma and the uterine cervical cancer patients was also performed. Without the input selection scheme based on PCA, the modeling MLP ANN can give 100.0% average success classification rate in 10 parallel runs with R.S.D. = 0.0%. However, only 61.1% of all the samples were classified correctly in the leave-one-out cross validation scheme. Moreover, the corresponding parameters of selectivity and specificity for the two kinds of samples were poor. The calculated results of this section are listed in Table 4.

From the results of the pattern recognition in this paper, an interesting phenomenon has been discovered, i.e., although

Table 2
The classification results of the MLP ANN for the second data set in Case II

	The number of input variables	Relative standard deviation (R.S.D.) (%)	Selectivity of cancer samples (%)	Specificity of cancer samples (%)	Selectivity of healthy samples (%)	Specificity of healthy samples (%)	Correct classification rate of modeling ANN (%)	Correct classification rate in leave-one-out cross validation (%)	Percent of variance explained
One PC	1	3.2	10.0	90.0	0.0	100.0	9.0	5.0	99.80
Two PC	2	17.4	20.0	90.0	0.0	90.0	15.5	10.0	99.94
Three PC[a]	3	0.0	70.0	80.0	80.0	70.0	100.0	75.0	99.96
Four PC	4	0.0	70.0	90.0	90.0	70.0	100.0	80.0	99.97
Five PC[b]	5	0.0	90.0	90.0	90.0	90.0	100.0	90.0	99.99
Six PC	6	0.0	80.0	90.0	90.0	80.0	100.0	85.0	99.99
Seven PC	7	0.0	60.0	80.0	80.0	60.0	100.0	70.0	100.00
Original input variables	13	0.0	60.0	80.0	80.0	60.0	100.0	70.0	

[a] The modeling MLP ANN giving the best correct classification rate (with corresponding R.S.D.).
[b] The MLP ANN giving the best selectivity and specificity in leave-one-out cross validation.

Table 3
The classification results of the MLP ANN for the second data set in Case III

	The number of input variables	Relative standard deviation (R.S.D.) (%)	Selectivity of healthy samples (%)	Specificity of healthy samples (%)	Selectivity of benign tumour samples (%)	Specificity of benign tumour samples (%)	Correct classification rate of modeling ANN (%)	Correct classification rate in leave-one-out cross validation (%)	Percent of variance explained
One PC	1	0.0	90.0	0.0	0.0	90.0	55.6	50.0	96.87
Two PC	2	2.5	70.0	37.5	37.5	70.0	95.6	55.6	99.31
Three PC[a]	3	0.0	60.0	37.5	37.5	60.0	100.0	50.0	99.69
Four PC	4	0.0	80.0	62.5	62.5	80.0	100.0	72.2	99.87
Five PC	5	0.0	70.0	75.0	75.0	70.0	100.0	72.2	99.93
Six PC	6	0.0	80.0	62.5	62.5	80.0	100.0	72.2	99.95
Seven PC	7	0.0	70.0	62.5	62.5	70.0	100.0	66.7	99.97
Eight PC	8	0.0	80.0	62.5	62.5	80.0	100.0	72.2	99.98
Nine PC[b]	9	0.0	100.0	100.0	100.0	100.0	100.0	100.0	99.99
Ten PC	10	0.0	90.0	75.0	75.0	90.0	100.0	83.3	100.00
Original input variables	13	0.0	100.0	87.5	87.5	100.0	100.0	94.4	

[a] The modeling MLP ANN giving the best correct classification rate (with corresponding R.S.D.).
[b] The MLP ANN giving the best selectivity and specificity in leave-one-out cross validation.

Table 4
The classification results of the MLP ANN for the second data set in Case IV

	The number of input variables	Relative standard deviation (R.S.D.) (%)	Selectivity of benign tumour samples (%)	Specificity of benign tumour samples (%)	Selectivity of cancer samples (%)	Specificity of cancer samples (%)	Correct classification rate of modeling ANN (%)	Correct classification rate in leave-one-out cross validation (%)	Percent of variance explained
One PC	1	3.8	0.0	100.0	100.0	0.0	57.2	55.6	99.75
Two PC	2	2.9	75.0	70.0	70.0	75.0	80.6	72.2	99.93
Three PC[a]	3	0.0	37.5	80.0	80.0	37.5	100.0	61.1	99.96
Four PC	4	2.9	62.5	60.0	60.0	62.5	96.7	61.1	99.98
Five PC	5	0.0	37.5	50.0	50.0	37.5	100.0	44.4	99.99
Six PC[b]	6	0.0	75.0	80.0	80.0	75.0	100.0	77.8	99.99
Seven PC	7	0.0	62.5	80.0	80.0	62.5	100.0	72.2	100.00
Original input variables	13	0.0	62.5	60.0	60.0	62.5	100.0	61.1	

[a] The modeling MLP ANN giving the best correct classification rate (with corresponding R.S.D.).
[b] The MLP ANN giving the best selectivity and specificity in leave-one-out cross validation.

modeling MLP ANN can give the best classification results for the training and verification samples, however, in leave-one-out cross validation process, the classification results of the "best" modeling MLP ANN were not always the best. That is to say, "best" modeling MLP ANN cannot always show their best predictive ability for unknown samples for its limited number of training and verification samples although the relationship between the ANNs' structures and their corresponding numbers of the training patterns in this work was limited to the rule of Haykin [46]. This opinion is also supported by statistical learning theory (SLT) and support vector machine (SVM) algorithm devised by Vapnik [47].

5. Conclusions

The proposed MLP ANN method based on PCA input selection scheme was suitable for the pattern recognition of the clinical urine samples from female tumour patients and the simulated data set. In the group of the clinical data from Ref. [11], when the PCA input selection was introduced to the MLP ANN for pattern recognition, the 100% success classification rate can also be acquired in both the modeling MLP ANN and the leave-one-out cross validation procedure even employing much simpler structures of neural networks. Moreover, the selectivity and the specificity parameters for the two kinds of samples were also 100.0%. In the second group of the clinical urine samples collected from uterine tumour patients and healthy women cited from Ref. [10], the PCA input selection scheme could also be applied in the corresponding MLP ANN to improve the results of pattern recognition by simplified structure of networks in this study. Moreover, the results of the pattern recognition in this paper also suggested that the classification results for two kinds of samples were much better than those for three kinds of samples, i.e., MLP ANN method is more suitable for the pattern recognition in dual pattern system.

Acknowledgement

The corresponding scientific research fund from Shanxi Normal University, China (No. YZ06004) financially supported the work. It was gratefully acknowledged.

References

[1] A. Apffel, J.A. Chakel, S. Fisher, K. Lichtenwalter, W.S. Hancock, Anal. Chem. 69 (1997) 1320.
[2] A.S. Cohen, S. Terabe, J.A. Smith, B.L. Karger, Anal. Chem. 59 (1987) 1021.
[3] H.J. Gaus, S.R. Owens, M. Winniman, S. Cooper, L.L. Cummins, Anal. Chem. 69 (1997) 313.
[4] T.P. Waalkes, M.D. Abeloff, D.S. Ettinger, K.B. Woo, C.W. Gehrke, K.C. Kuo, E. Borek, Cancer 50 (1982) 2457.
[5] R.W. Trewyn, R. Glaser, D.R. Kelly, D.G. Jakoson, W.P. Graham, C.E. Speicher, Cancer 49 (1982) 2513.
[6] H.M. Liebich, C. Di Stefano, A. Wixforth, H.R. Schmid, J. Chromatogr. A 763 (1997) 193.
[7] H.M. Liebich, G. Xu, C. Di Stefano, R.J. Lehmann, J. Chromatogr. A 793 (1998) 341.
[8] R. Zhao, G. Xu, B. Yue, H.M. Liebich, Y. Zhang, J. Chromatogr. A 828 (1998) 489.
[9] G. Xu, C. Di Stefano, H.M. Liebich, Y. Zhang, P. Lu, J. Chromatogr. B 732 (1999) 307.
[10] K.R. Kim, S. La, A. Kim, J.H. Kim, H.M. Liebich, J. Chromatogr. B 754 (2001) 97.
[11] S. La, J.H. Cho, J.H. Kim, K.R. Kim, Anal. Chim. Acta 486 (2003) 171.
[12] M. Masuda, T. Nishihira, K. Itoh, M. Mizugaki, N. Ishida, S. Mori, Cancer 72 (1993) 3571.
[13] C. Reynaud, C. Bruno, P. Boullanger, J. Grange, S. Barbesti, A. Niveleau, Cancer Lett. 61 (3) (1992) 255.
[14] H.M. Liebich, G. Xu, C. Di Stefano, R. Lehmann, H.U. Hãring, P. Lu, Y. Zhang, Chromatographia 45 (1997) 396.
[15] G. Rhodes, M. Miller, M.L. McConnell, M. Novotny, Clin. Chem. 27 (1981) 580.
[16] E. Jellum, M. Harboe, G. Bjune, S. Wold, J. Pharm. Biomed. Anal. 9 (1991) 663.
[17] K. Chan, T.W. Lee, P.A. Sample, M.H. Goldbaum, R.N. Weinreb, T.J. Sejnowski, IEEE. Trans. Biomed. Eng. 49 (2002) 963.
[18] S.E. Seltzer, D.J. Getty, R.M. Pickett, J.A. Swets, G. Sica, J. Brown, S. Saini, R.F. Mattrey, B. Harmon, I.R. Francis, J. Chezmar, M.O. Schnall, E.S. Siegelman, R. Ballerini, S. Bhat, Acad. Radial. 9 (2002) 256.
[19] R.J. Marshall, R. Turner, H. Yu, E.H. Cooper, J. Chromatogr. A 297 (1984) 235.
[20] K. Birkenkamp-Demtroder, L.L. Christensen, S.H. Olesen, C.M. Frederiksen, P. Laiho, L.A. Aaltonen, S. Laurberg, F.B. Sorensen, R. Hagemann, T.F. Orntoft, Cancer Res. 62 (2002) 4352.
[21] G. Bocaz-Beneventi, R. Latorre, M. Farková, J. Havel, Anal. Chim. Acta 452 (2002) 47.
[22] J. Havel, J.E. Madden, P.R. Haddad, Chromatographia 49 (1999) 481.
[23] L.L. Yannis, J. Chromatogr. A 904 (2000) 119.
[24] Y. Zhang, H. Li, A. Hou, J. Havel, Talanta 65 (2005) 118.
[25] Y.X. Zhang, H. Li, J. Havel, Talanta 65 (2005) 853.
[26] H. Li, Y.X. Zhang, L. Xu, Talanta 67 (2005) 741.
[27] M. Kompany-Zareh, A. Massoumi, Sh. Pezeshk-Zadeh, Talanta 48 (1999) 283.
[28] T. Khayamian, A. Ensafi, M. Atabati, Microchem. J. 65 (2000) 347.
[29] W. Wu, D.L. Massart, Chem. Intell. Lab. Syst. 35 (1996) 127.
[30] J. Brezmes, B. Ferreras, E. Llobet, X. Vilanova, X. Correig, Anal. Chim. Acta 348 (1997) 503.
[31] J. Zupan, J. Gasteiger, Anal. Chim. Acta 248 (1991) 1.
[32] B.G. Sumpter, C. Gettino, D.W. Noid, Annu. Rev. Phys. Chem. 45 (1994) 439.
[33] B.G. Sumpter, D.W. Noid, Annu. Rev. Mater. Sci. 26 (1996) 223.
[34] J. Zupan, J. Gasteiger, Neural Networks for Chemists: An Introduction, VCH, Verlaggesellschaft, Weinheim, 1993.
[35] R.Q. Yu, Introduction to Chemometrics, Hunan Education Publishing House, Changsha, 1991 (in Chinese).
[36] J.A. Kinsella, Network 3 (1992) 27.
[37] R. Bulirsch, J. Stoer, The Conjugate-Gradient Method of Hestenes and Stiefel, § 8.7 in Introduction to Numerical Analysis, Springer-Verlag, New York, 1991.
[38] M. Statheropoulos, A. Pappa, P. Karamertzanis, H.L.C. Meuzelaar, Anal. Chim. Acta 401 (1999) 35.
[39] D. Dong, T.J. McAvoy, Comput. Chem. Eng. 20 (1996) 65.
[40] I.V. Tetko, A.I. Luik, G.I. Poda, J. Med. Chem. 36 (1993) 811.
[41] M.B. Seasholtz, B. Kowalski, Anal. Chim. Acta 277 (1993) 165.
[42] D.J. Livingstone, D.T. Manallack, J. Med. Chem. 36 (1993) 65.
[43] D. Broadhurst, R. Goodacre, A. Jones, J.J. Rowland, B. Kell, Anal. Chim. Acta 348 (1997) 71.
[44] S. Kirkpatrick, C.D. Gelatt Jr., M.P. Vecchi, Science 220 (1983) 671.
[45] S. Courtois, R. Phan-Tan-Luu, Analysis 26 (1998) 304.
[46] S. Haykin, Neural Networks: A Comprehensive Foundation, Macmillan, New York, 1994.
[47] V.N. Vapnik, The Nature of Statistical Learning Theory, Springer, Berlin, 1995.

Available online at www.sciencedirect.com
ScienceDirect
Talanta 73 (2007) 142–146
Talanta
www.elsevier.com/locate/talanta

Determination of levodopa by capillary electrophoresis with chemiluminescence detection

Shulin Zhao *, Wenling Bai, Bing Wang, Min He

College of Chemistry and Chemical Engineering, Guangxi Normal University, Guilin 541004, China

Received 4 October 2006; received in revised form 6 March 2007; accepted 14 March 2007
Available online 20 March 2007

Abstract

A rapid and simple method using capillary electrophoresis (CE) with chemiluminescence (CL) detection was developed for the determination of levodopa. This method was based on enhance effect of levodopa on the CL reaction between luminol and potassium hexacyanoferrate(III) ($K_3[Fe(CN)_6]$) in alkaline aqueous solution. CL detection employed a lab-built reaction flow cell and a photon counter. The optimized conditions for the CL detection were 1.0×10^{-5} M luminol added to the CE running buffer and 5.0×10^{-5} M $K_3[Fe(CN)_6]$ in 0.6 M NaOH solution introduced postcolumn. Under the optimal conditions, a linear range from 5.0×10^{-8} to 2.5×10^{-6} M ($r = 9991$), and a detection limit of 2.0×10^{-8} M (signal/noise = 3) for levodopa were achieved. The precision (R.S.D.) on peak area (at 5.0×10^{-7} M of levodopa, $n = 11$) was 4.1%. The applicability of the method for the analysis of pharmaceutical and human plasma samples was examined.

Keywords: Chemiluminescence; Capillary electrophoresis; Levodopa

1. Introduction

Levodopa [3-(3,4-dihydroxyphenyl)-lalanine], a precursor of the neurotransmitter dopamine, is the most widely prescribed drug in the treatment of Parkinson's disease. People with Parkinson's disease have depleted levels of dopamine, which causes tremor, muscle stiffness or rigidity, slowness of movement (bradykinesia) and loss of balance. Dopamine cannot be administered directly because it does not cross the blood brain barrier readily, while its precursor levodopa is given orally and is easily absorbed through the bowel and converted into dopamine by decarboxylase. Then, levodopa is used to increase dopamine in the brain, which reduces the symptoms of Parkinson's disease. Nevertheless, elevated levels of dopamine also cause adverse reactions such as nausea, vomiting and cardiac arrhythmias [1,2]. Therefore, in order to achieve a better curative effect and a lower toxicity, it is very important to rapidly control the content of levodopa and its inhibitors and impurities in biological fluids and pharmaceutical formulations.

Several techniques have been reported in the literature for the determination of levodopa such as spectrophotometry [3–9], spectrofluorimetry [10], ion-selective electrode [11,12], NMR spectroscopy [13], flow injection analysis (FIA) [14–20], high performance liquid chromatography (HPLC) [21–31] and gas chromatography (GC) [32]. Nevertheless, each technique has often suffered from diverse disadvantages with regard to cost and selectivity, the use of organic solvents, complex sample preparation procedures or long analysis time [33].

Capillary electrophoresis (CE) is a microanalytical technique, which provides advantages in term of simplicity, high efficiency, low cost and short analysis time. CE with electrochemical detection or UV detection has been applied for determination of levodopa in tablets and beans [33,34]. Major drawback of CE with UV detection is its sensitivity. Chemiluminescence (CL) detection has been proven to be one of the most sensitive detection technologies, and the costs of the instrumental setup for CL detection are relatively low [35–37]. Therefore, CL detection has become an attractive detection scheme for sensitive detection in CE [38–40].

In this work, a CE/direct CL detection method was developed for the determination of levodopa. To our knowledge, such procedures have not been reported previously for the determination of levodopa. The method employs a

* Corresponding author. Tel.: +86 773 5849646; fax: +86 773 5845973.
E-mail address: zhaoshulin001@163.com (S. Zhao).

0039-9140/$ – see front matter © 2007 Elsevier B.V. All rights reserved.
doi:10.1016/j.talanta.2007.03.023

new CE system with CL detector, which was setup in our laboratory [41], and was applied for the determination of the levodopa in pharmaceutical preparations and biological fluids.

2. Experimental

2.1. Chemicals and reagents

Luminol was purchased from Fluka (Buchs, Switzerland). Levodopa was supplied by Sigma (St. Louis, MO, USA). Levodopa drugs were obtained from Guangxi Hefong pharmaceutical company (Guangxi, China). All the other chemicals and organic solvents used in this work were of analytical grade. Milli-Q water was used throughout. All solutions were filtered through a 0.45 μm membrane filter.

The 0.1 M sodium borate stock solution was prepared by dissolving 3.814 g $Na_2B_4O_7{\cdot}10\ H_2O$ in 100 mL water; 0.01 M luminol solution was prepared by dissolving 0.0177 g luminol in 2 mL of 0.1 M NaOH solution, and diluting to 10 mL with water. The 0.1 M potassium hexacyanoferrate(III) ($K_3[Fe(CN)_6]$) stock solution was prepared in water. The running buffer solution was prepared by mixing 7.5 mL of 0.1 M sodium borate solution and 25 μL of 0.01 M luminol solution, adjusting the pH value to 9.4 with a 0.1 M NaOH solution, and then diluting to 25 mL with water. The oxidizer solution was prepared by dissolving 12.5 μL of 0.1 M $K_3[Fe(CN)_6]$ stock solution in 25 mL of 0.6 M NaOH solution. The levodopa standard solution was prepared by dissolving 0.50 mg levodopa in 100 mL of 0.1 M HCl solution. An aliquot of 10.0 μL was transferred into 50 mL volumetric flask and volume was completed with water as working solution.

2.2. CE–CL apparatus

The basic design of the CE–CL system has been previously described [41]. Briefly, a high-voltage supply (0–30 kV, Beijing Cailu Science Instrument Company, Beijing, China) was used to drive the electrophoresis. A 50 cm × 75 μm i.d. uncoated fused-silica capillaries (Hebei Optical Fiber, China) was used for the separation. The polyimide on 2.5 cm end section of the capillary was burned and removed. After etching with HF for 1 h, this end of capillary was inserted into the reaction capillary, which was 320 μm i.d. (Hebei Optical Fiber, China). A four-way plexiglass joint held a separation capillary and a reaction capillary in place. The CL solution was siphoned into a tee. The grounding electrode was put in one joint of the tee. The CL solution flowed down to the detection window, which was made by burning 1 cm of the polyimide of the reaction capillary and was placed in front of the photo multiplier tube (PMT, R374 equipped with a C1556-50 DA-type socket assembly, Hamamatsu, Shizuoka, Japan). CL emission was collected by a PMT, and recorded and processed with an IBM compatible computer using in-house written software.

2.3. Sample preparation

One tablet of levodopa drug (containing 250 mg of levodopa) was smashed and dissolved in 10 mL of 0.1 M HCl solution. The solution was centrifuged at 2000 rpm for 10 min, and the supernatant was transferred into 250 mL volumetric flask and volume was completed with water.

The plasma sample was prepared as described in Ref. [42]. A 0.5 mL of plasma sample was deproteinized by adding 0.5 mL of acetonitrile. After centrifugation at 12,000 rpm for 15 min, 90 μL of the supernatant liquid was spiked with 10 μL of levodopa. Plasma samples of various levodopa contents were similarly prepared by spiking the plasma with the desired amount of levodopa.

2.4. CE conditions

The new capillary was preconditioned by flushing with 1 M NaOH for 30 min before first use. Between two consecutive injections, the capillary was rinsed sequentially with 0.1 M NaOH, water and running buffer for 3 min each. Samples were injected into the capillary by hydrodynamic flow at a height differential of 20 cm for 10 s. Running voltages was 16 kV. Electrophoresis electrolyte was 1.0×10^{-5} M luminol in 0.03 M borate buffer (pH 9.4). The oxidizer solution was 5.0×10^{-5} M $K_3[Fe(CN)_6]$ in 0.6 M NaOH solution.

3. Results and discussions

3.1. CL reaction between luminol and $K_3[Fe(CN)_6]$ in the presence of levodopa

It was found that levodopa could enhance the CL reaction between luminol and $K_3[Fe(CN)_6]$ (see Fig. 1). To maximize

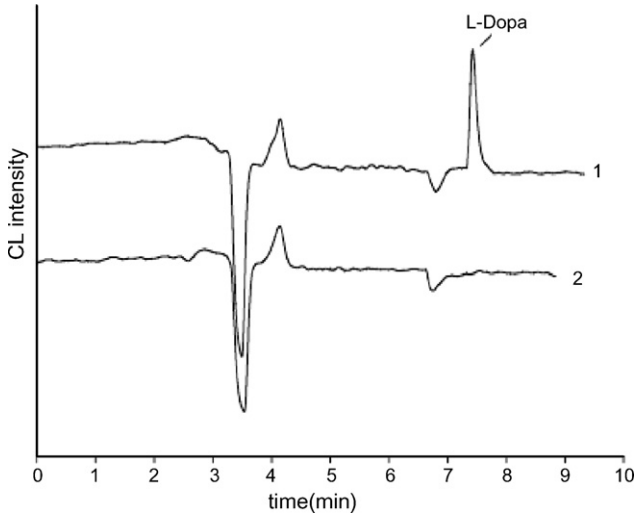

Fig. 1. Electropherograms obtained from a standard solution of levodopa at 1.0×10^{-6} M (trace 1) and a blank solution (trace 2). Electrophoresis electrolyte was 1.0×10^{-5} M luminol in 0.03 M borate buffer (pH 9.4). The oxidizer solution was 5.0×10^{-5} M $K_3[Fe(CN)_6]$ in 0.6 M NaOH solution. Capillary was 75 μm i.d. × 50 cm effective length. Applied voltage was 16 kV.

the sensitivity of CL detection, the signal to noise ratio for levodopa determination was used to compare and examine the effects of luminol, $K_3[Fe(CN)_6]$, borate and NaOH concentration on the CL intensity. In these experiments, a 1.0×10^{-6} M of levodopa solution was injected into the CE–CL system, and the CL intensity (peak height or peak area) was recorded.

3.1.1. Effect of luminol concentration

The influence of luminol concentration (from 5.0×10^{-6} to 1.0×10^{-4} M) on the CL intensity was studied in a system keeping $K_3[Fe(CN)_6]$ concentration at 5.0×10^{-5} M, the borate concentration at 0.03 M and NaOH concentration at 0.6 M. The results indicate that higher the concentration of luminol is, the higher the light emission that can be obtained, but a larger baseline noise was observed when the concentration was higher than 1.0×10^{-5} M, which lead to low the signal to noise ratio. So a concentration of 1.0×10^{-5} M luminol was chosen for further experiments.

3.1.2. Effect of $K_3[Fe(CN)_6]$ concentration

The effect of $K_3[Fe(CN)_6]$ concentration on the CL reaction was investigated over the concentration range 1.0×10^{-5} to 5.0×10^{-4} M. It is found that the signal to noise ratio first increased and then decreased with the increase in $K_3[Fe(CN)_6]$ concentration. The maximum signal to noise ratio was obtained when the concentration was at 5.0×10^{-5} M. Then a 5.0×10^{-5} M of $K_3[Fe(CN)_6]$ concentration was selected and used for the following experiments.

3.1.3. Effect of NaOH concentration

Owing to luminol reacts with $K_3[Fe(CN)_6]$ to produces CL in alkaline condition, therefore, the NaOH solution was selected as the reaction medium, and the effect of NaOH concentration on the determination sensitivity of levodopa was studied by varying the concentration from 0.1 to 1.0 M. The signal to noise ratio increased gradually with increasing NaOH concentration up to 0.6 M, where maximum signal to noise ratio was reached and further increasing the NaOH concentration result in a decrease in signal to noise ratio. According to the result, a NaOH concentration of 0.6 M was chosen for optimum.

3.1.4. Effect of borate concentration

In the CE–CL detection system, levodopa migrated in the separation capillary, where it mixed with luminol included in the running buffer. The running buffer (borate buffer) concentration affects directly the migration rate of levodopa and luminol in capillary, which cause the change of CL intensity. To examine the change, several borate solutions concentration ranges from 0.02 to 0.04 M were tested. The results indicate that the effect is similar with the effect of $K_3[Fe(CN)_6]$ concentration, i.e. the signal to noise ratio first increased tremendously and then decreased slightly with the increase in borate concentration. The maximum signal to noise ratio was obtained when the concentration was 0.03 M. So the 0.03 M borate buffer (pH 9.4) was carried out for further studies.

3.1.5. Effect of the applied voltage

Applied voltage affects directly the migration rate of levodopa and luminol in capillary, which lead also to the change of CL intensity. Generally, higher CL intensity can be obtained when higher applied voltage was used. However, higher applied voltage should cause large Joule heating, which result in large baseline noise and low signal to noise ratio. Dependence of signal to noise ratio on applied voltage was examined over the voltage ranges 12–20 kV. It was found that the applied voltage of 16 kV is the optimal one to obtain higher CL intensity.

3.2. Analytical figures of merit

The CE–LC method was evaluated in terms of the response linearity, limit of detection and reproducibility (precision). To test the CL response linearity, a series of levodopa standard solutions were tested to determine the linearity between the levodopa concentration and CL intensity. Linear regression analysis of the results yielded the following equation: $A = 2.4872 \times 10^6 C + 0.1976$, $r = 0.9991$, where A is the peak area (mV s) and C is the concentration of levodopa in M. The calibration curve was linear over the concentrations range of from 5.0×10^{-8} to 2.5×10^{-6} M. The limit of detection (signal/noise = 3) for levodopa was estimated to be 2.0×10^{-8} M.

The reproducibility was investigated by injecting a 5.0×10^{-7} M levodopa standard solution 11 times and recording the peak areas. The reproducibility of the method was demonstrated by the mean relative standard deviation (R.S.D.). The result obtained indicates that the R.S.D. was 4.1%.

3.3. Sample analysis

The present method was applied to the determination of levodopa in commercial levodopa drug. The results (average of three determinations) were compared with those declared on the tablets label, i.e. the amount declared was 250 mg/tablet, and the amounts found were between 248 and 258 mg/tablet. The recoveries of added levodopa in different samples were ranged between 92% and 106% (see Table 1).

In order to demonstrate the applicability of the CE–CL method for the determination of levodopa in complex biological sample, the proposed method was used for the analysis of human plasma. First, a blank plasma sample from healthy volunteer was analyzed to examine the interference from endogenous compounds in human plasma. Fig. 2 illustrates the electropherograms without and with the addition of the standard levodopa solution, which made it possible to identify levodopa in the sam-

Table 1
Assay results for commercial sample of levodopa tablet

Labeled (mg/slice)	Found[a] (mg/slice)	Added (mg/slice)	Total found[a] (mg/slice)	Recovery (%)
250.0	258.0	312.5	587.5	105
250.0	248.5	312.5	536.4	92
250.0	249.5	312.5	581.3	106

[a] Average of three determinations.

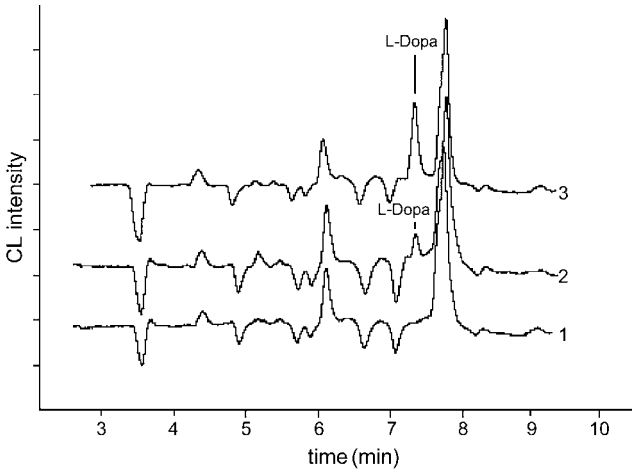

Fig. 2. Electropherograms of human plasma samples: (1) plasma blank; (2) plasma spiked with 1.0×10^{-7} M levodopa; (3) plasma spiked with 5.0×10^{-7} M levodopa. CE and CL conditions were as in Fig. 1.

Table 2
Precision and recovery for the determination of levodopa spiked in plasma samples

Added (M)	Found[a] (M)	Precision (R.S.D., %)	Recovery (%)
1.0×10^{-7}	9.7×10^{-8}	4.3	97
2.0×10^{-7}	1.9×10^{-7}	4.2	95
3.0×10^{-7}	3.2×10^{-7}	3.2	107
4.0×10^{-7}	4.2×10^{-7}	3.7	105
5.0×10^{-7}	5.1×10^{-7}	2.8	102

[a] Average of four determinations.

ple and to evaluate its concentration. As can be seen from Fig. 2, there is not the peak observed across the migration time of levodopa in the electropherogram of blank plasma (trace 1). After the plasma samples were spiked with levodopa at 1.0×10^{-7} and 5.0×10^{-7} M, the plasma samples were analyzed again. It was found that a peak for the determination of levadopa was observed in the electropherogram of plasma spiked with levadopa (trace 2, 3), which indicates that none of endogenous compounds in human plasma would interfere with the determination of levodopa. The results obtained are summarized in Table 2. As can be seen, good detection accuracy was obtained. The recovery was ranged between 95% and 107%. According to the report in literature [29], for 1 year old, healthy male Beagle dog, the concentrations of levodopa in plasma are in the range of 0.05–2.25 μg/mL within 0.5–6 h after a single 250 mg levodopa oral dose. In our experiments, the concentrations of levodopa spiked in human plasma samples are in the range of 0.1–0.5 μM (0.02–0.1 μg/mL). If the concentration is higher than 0.1 μg/mL, it can also be analyzed by diluting the sample solution. Therefore, the presented method fulfilled completely the requirements for the pharmacokinetic study of levodopa.

4. Conclusion

A CE–CL detection method was developed for the determination of levodopa. Quantitative measurements of levodopa in tablets and human plasma have been demonstrated. In comparison with other possible methods such as spectrophotometry, spectrofluorimetry and FIA, the proposed procedure is selective. The simple direct determination of levodopa is a good alternative to existing HPLC methods giving a short analysis time, low cost and minimal organic waste. Comparing to CE with UV and electrochemical detection, the developed CE–CL detection method given higher detection sensitivity, which is well suited for the use in pharmacokinetic study and therapeutic monitoring of levodopa.

Acknowledgments

Financial support from National Natural Science foundation of China (No. 20665002) and Guangxi Natural Science Foundation, China (No. 0575045) are gratefully acknowledged.

References

[1] D.B. Clane, N. Engl. J. Med. 329 (1993) 1021–1028.
[2] D.G. Standaert, A.B. Young, in: J.G. Hardman, L.E. Limbird, P.B. Molinoff, R.W. Ruddon, A.G. Gilman (Eds.), Goodman and Gilman's, The Pharmacological Basis of Therapeutics, 9th ed., McGraw-Hill, New York, 1996, p. 503.
[3] G.A. Davidson, J. Pharm. Sci. 73 (1984) 1582–1584.
[4] S.T. Hassib, Anal. Lett. 23 (1990) 2195–2214.
[5] M.I.H. Helaleh, N. Rahman, E.S.M. Abu-Nameh, Anal. Sci. 13 (1997) 1007–1010.
[6] P. Nagaraja, K.C.S. Murthy, K.S. Rangappa, N.M.M. Gowda, Talanta 46 (1998) 39–44.
[7] M.I.H. Helaleh, E.S.M. Abu-Named, Chem. Anal. 43 (1998) 225–230.
[8] P.C. Damiani, A.C. Moschetti, A.J. Rovetto, F. Benavente, A.C. Olivieri, Anal. Chim. Acta 543 (2005) 192–198.
[9] J. Coello, S. Maspoch, N. Villegas, Talanta 53 (2000) 627–637.
[10] S. Honda, Y. Araki, M. Takahashi, K. Kakehi, Anal. Chim. Acta 149 (1983) 297–303.
[11] S.S. Badawy, Y.M. Issa, A.S. Tag-Eldin, Electroanalysis 8 (1996) 1060–1064.
[12] M.F. Bergamini, A.L. Santos, N.R. Stradiotto, M.V.B. Zanoni, J. Pharm. Biomed. Anal. 39 (2005) 54–59.
[13] Z. Talebpour, S. Haghgoob, M. Shamsipur, Anal. Chim. Acta 506 (2004) 97–104.
[14] T.N. Deftereos, C.A. Calokerines, E.C. Efstathiou, Analyst 118 (1993) 627–632.
[15] A.C. Georgiou, A.M. Koupparis, P.T. Hadjiioannou, Talanta 38 (1991) 689–696.
[16] T. Perez-Ruiz, C. Martinez-lozano, V. Tomas, O. Val, Talanta 40 (1993) 1625–1630.
[17] B.A. Hassan, K.D. Khalaf, M. de la Guardia, Talanta 42 (1995) 627–633.
[18] L.H. Marcolino-Juĭnior, M.F.S. Teixeira, A.V. Pereira, O. Fatibello-Filho, J. Pharm. Biomed. Anal. 25 (2001) 393–398.
[19] M. Pistonesi, M.E. Centurion, B.S.F. Band, P.C. Damiani, A.C. Olivieri, J. Pharm. Biomed. Anal. 36 (2004) 541–547.
[20] L.K. Abdulrahman, A.M. Al-Abachi, M.H. Al-Qaissy, Anal. Chim. Acta 538 (2005) 331–335.
[21] M.A. Rihbany, F.D. Michael, J. Chromatogr. 248 (1982) 125–133.
[22] L.A. Rihbany, M.F. Delaney, J. Chromatogr. 248 (1982) 125–133.
[23] E. Nissinen, J. Taskinen, J. Chromatogr. 231 (1982) 459–462.
[24] L.R. Gelber, J.L. Neumeyer, J. Chromatogr. 257 (1983) 317–326.
[25] S. Ting, J. Assoc. Off. Anal. Chem. 69 (1986) 169–173.
[26] S. Ting, J. Assoc. Off. Anal. Chem. 70 (1987) 987–990.
[27] Y. Michotte, M. Moors, D. Deleu, P. Herregodts, G. Ebinger, J. Pharm. Biomed. Anal. 5 (1987) 659–664.

[28] F. Blandini, E. Martignoni, C. Pacchetti, S. Desideri, D. Rivellini, G. Nappi, J. Chromatogr. B 700 (1997) 278–282.
[29] A. Tolokan, I. Klebovich, K. Baloghnemes, G. Horvai, J. Chromatogr. B 698 (1997) 201–207.
[30] M. Dolezalova, M. Tkaczykova, J. Pharm. Biomed. Anal. 19 (1999) 555–567.
[31] K.A. Sagar, M.R. Smyth, J. Pharm. Biomed. Anal. 22 (2000) 613–624.
[32] P.J. Murphy, T.L. William, D.L. Kau, J. Pharmacol. Exp. Ther. 199 (1976) 423–431.
[33] L. Zhang, G. Chenb, Q. Hu, Y. Fang, Anal. Chim. Acta 431 (2001) 287–292.
[34] X. Chen, J. Zhang, H. Zhai, X. Chen, Z. Hu, Food Chem. 92 (2005) 381–386.
[35] C. Kuyper, R. Milofsky, Trends Anal. Chem. 20 (2001) 232–240.
[36] W. Ruengsitagoon, S. Liawruangrath, A. Townshend, Talanta 69 (2006) 976–983.
[37] L. Wang, P. Yang, Y. Li, C. Zhu, Talanta 70 (2006) 219–224.
[38] B.M. Simonet, A. Rios, M. Valcarcel, Trends Anal. Chem. 22 (2003) 605–614.
[39] T.D. Staller, M.J. Sepaniak, Electrophoresis 18 (1997) 2291–2296.
[40] X. Ji, Z. He, X. Ai, H. Yang, C. Xu, Talanta 70 (2006) 353–357.
[41] S.L. Zhao, C. Xie, X. Lu, Y.R. Song, Y.-M. Liu, Electrophoresis 26 (2005) 1745–1750.
[42] S.Y. Chang, W.-C. Lin, J. Chromatogr. B 794 (2003) 17–22.